Textile Macroelectronics: Architecting Sensate and Computational Fabrics across Scales

by

Irmandy Wicaksono

B.Eng., University of Southampton (2014)
M.Sc. ETH., Swiss Federal Institute of Technology Zurich (2016)
S.M., Massachusetts Institute of Technology (2019)

Submitted to the Program in Media Arts and Sciences, School of Architecture and Planning, in partial fulfilment of the requirements for the degree of

Doctor of Philosophy

at the
MASSACHUSETTS INSTITUTE OF TECHNOLOGY
September 2024

Author

……

Irmandy Wicaksono
Program in Media Arts and Sciences
30th August 2024

Certified and Accepted by

……

Joseph A. Paradiso, Ph.D.
Alexander W. Dreyfoos (1954) Professor of Media Arts and Sciences
Advisor and Acting Academic Head, Program in Media Arts and Sciences

Textile Macroelectronics: Architecting Sensate and Computational Fabrics across Scales

by

Irmandy Wicaksono

Submitted to the Program in Media Arts and Sciences, School of Architecture and Planning, in partial fulfilment of the requirements for the degree of

Doctor of Philosophy

Abstract

Textiles are omnipresent and among the oldest forms of art and culture in human civilization. They serve as our protective skin, the interface between our bodies and the environment, and a medium for self-expression and collective experience. As electronics become more compliant, miniaturized, and low-cost, textiles provide an ideal substrate for technology integration, further driving the era of ubiquitous computing. My research fuses recent advances in functional materials, digital fabrication, hardware systems, and immersive technologies to demonstrate *Textile Macroelectronics* architecture and develop sensate and computational fabrics across scales.

In this dissertation, I propose a ubiquitous computational textile framework—a synergy between functional device selection, textile structures, fabrication tools, and system architecture—that integrates a distributed network of sensing and computational elements as primitives or raw materials in the manufacturing process of electronic textile products. In the first part of the dissertation, I present several methods, artifacts, and implementations of sensate textiles using functional fibers and digital machine knitting. I argue that to promote the disruption and adoption of sensate textiles and achieve seamless integration, we require a better hierarchical understanding of textile construction and fiber-fabric properties, as well as ways to integrate electronics and functionalities with industrial textile fabrication processes. By controlling functional and common yarn inputs, along with knitting structures and patterns, I can architect fabric forms and aesthetics while tuning their electrical and mechanical properties. With this approach, I have developed a set of custom proxemic and tactile textile interfaces based on capacitive and piezoresistive sensing for musical expression, human-computer interaction,

activity recognition, and multi-sensory experiences in various forms such as cloth, footwear, mats, carpets, and large-scale architectural facades.

In the second part of the dissertation, I will discuss my work in exploring flexible, stretchable, and soft printed circuit technologies, incorporating multi-modal sensing with distributed computation to address scalability issues inherent in large and dense sensate textiles. These efforts have led to unique power, interconnection, and networking paradigms that allow us to transition from application-specific sensate textiles to generic computational fabrics that can be tailored and programmed for various applications. Finally, through these collective and complementary efforts, I aim to demonstrate an ecosystem of fabric artifacts that will lead us toward an *Electronic Textile Gaia*—a vision where sensing and intelligence are seamlessly interconnected and integrated into the fabric of everyday life, from in-body, on-body, room-scale, to architectural textiles, for applications ranging from physiological and physical activity monitoring to interactive media and built environments.

Thesis Advisor:
Joseph A. Paradiso, Ph.D.
Alexander W. Dreyfoos (1954) Professor of Media Arts and Sciences
Program in Media Arts and Sciences

Textile Macroelectronics: Architecting Sensate and Computational Fabrics across Scales

by

Irmandy Wicaksono

This dissertation has been reviewed and approved by the following committee members:

Thesis Advisor:

……..

Joseph A. Paradiso, Ph.D.

Alexander W. Dreyfoos (1954) Professor of Media Arts and Sciences

Media Lab, Massachusetts Institute of Technology

Thesis Reader:

……

Svetlana Boriskina, Ph.D.

Principal Research Scientist

Department of Mechanical Engineering, Massachusetts Institute of Technology

Thesis Reader:

……

Alexander Stolyarov, Ph.D.

Chief Executive Officer

Advanced Functional Fabrics of America (AFFOA), Manufacturing USA Institute

Acknowledgements

I don't really know where to start. It took me a while to begin writing this section, as the journey that brought me here has been a whirlwind—a roller-coaster ride of intense adventures, discoveries, challenges, and emotions. I find myself overwhelmed with gratitude and awe for the experiences and connections I've had at MIT, especially at the Media Lab. As an engineer, MIT is without a doubt a dream place to build, to fail, and to envision and realize the future. But the MIT Media Lab, in particular—this unique, vibrant, and interdisciplinary space—has kindled a passion within me that goes beyond the bounds of traditional disciplines, merging art and design into the very fabric of my work and being. This place has connected my dots and brought out the best in me in ways I could have never imagined. There has not been a single day that I haven't been excited to work here!

Yet, as daunting as the journey of a PhD may seem, I am incredibly fortunate and privileged to have had a special community, a safety net behind me. It's like a place to train and recover; whenever I stumbled or fell on an adventure out there in the wild, this net was there to catch me and bounce me back onto my path. *With all my heart*, I know that I couldn't have accomplished this work without the unwavering love and support I've received from so many people. Specifically, I extend my deepest gratitude to:

To **Prof. Joe Paradiso**—you opened the door to this world for me, introducing me to this wonderful place with endless possibilities. Your encouragement and freedom have allowed me to truly push the boundaries of my work. You grounded me in technical rigor while giving me the space to take risks, discover, and explore my other passion for design and the arts. Your mentorship has been invaluable, and I aspire to be as sharp, wise, and kind as you someday.

To **Dr. Svetlana Boriskina and Dr. Alexander Stolyarov**—thank you for all of the conversations, the insightful feedback, and for being integral members of my PhD committee. Watching the MIT

textiles community grow has been a source of great excitement, and your involvement has only fueled my passion for this field. I eagerly look forward to our future collaborations.

To **Prof. Dava Newman, Prof. Pattie Maes, Prof. Tod Machover, and Dr. Joi Ito**—you have not only been mentors but also caretakers of this magical space that nurtures innovation, creativity, and expression. Thank you for truly listening to and caring for the students at the Media Lab, even in the most challenging times. You have shown me what it means to be a community person, and for that, I am deeply grateful. To **Prof. Dava Newman, Gui Trotti, and Prof. Hiroshi Ishii**—thank you for taking the time to learn about my work, to be critical, and for helping me find my path.

To the **Lexus Design Community**—Paola Antonelli, Gong Dong, Greg Lynn, Simon Humphries, Sabine Marcelis, Mariam Kamara, Sputniko!, and Joe Doucet—you have offered me perspectives from beyond the walls of academia, and your mentorship has been transformative in my journey as a designer. Thank you for believing in me and my vision, for helping me elevate my prototypes, and for encouraging me in mastering my craft.

To my **collaborators**—Dr. Don Derek Haddad, Mike Jiang, Jordan Rudess, Loni Landon, Nina Gentile, Lancelot Blanchard, Manaswi Mishra, Pichet Klunchun Dance Company—it's been such an honor to work with people across disciplines, connecting electronics, textiles, and performing arts. Those intense moments when the performance surpassed my expectations still give me shivers. Thank you for your magic, for making these projects come alive in ways I could have only dreamed of. To my **textile partners**—Dr. Juliana Cherston, thank you for listening to my weekly TED talk about e-textiles and for crafting the Gaia vision, Dr. Wei Yan, Cedric Honnet—for the constant conversations and collaborations. To the **hardware gurus**—Dr. Artem Dementyev, Dr. Brian Mayton, Dr. Mark Feldmeier, Fangzheng Liu—thank you for sharing your knowledge and giving me all of the tips and tricks on how to debug almost anything.

To the **Living Knitwork Pavilion core team**—Alfonso Parra Rubio, Judy Cichoka, Gabriela Advincula, Sam Chin, Erik Stand, Nicole Bakker, Age van der Mei—what an unforgettable adventure we have had! Thank you for your collaboration, for taking a leap of faith on this ambitious project, for enduring the tight schedules, and the thrills of building in the dust and dancing in the rain. We have shared so many incredible moments—under the magical Playa sunrise and sunset. I owe you all a great debt of gratitude.

To **Burning Man Arts**—Katie Hazard and Marc Scheff—thank you for your excitement and support of the Living Knitwork vision, for helping me navigate the countless challenges of creating art in the Black Rock Desert. I am really glad to have found another special home. To

Phage/the Institute—Daniel Alvarez Gavela, Daniel Hernandez, Matt Brand, Amy Brand, Ben Carter, Joel Shor, Valerie Kong, Sydney Staehle, Chris Moloney, Ladan Amouzegar—thank you for welcoming us, the LKP team with open arms and making us feel at home in Black Rock City. Building art in such an environment was an experience like no other, and I am deeply thankful for your help and support during those exhilarating and intense times. Witnessing the Pavilion gradually take shape was an incredible and humbling experience. The outpouring of support and enthusiasm from our friends here deeply touched us — as numerous hands were involved in realizing this community art. To the people who made our **MIT Saxon Lawn** exhibition possible— Dean Hashim Sarkis, James Harrington, Elena Sajno, Samantha Chan, Phil Cherner, Cayden Pierce, Selena Liu, and many others—thank you for helping us bring our vision to life, and for sparking the Burning Man principles of immediacy and communal effort at MIT.

To **my Shenzhen family**—Gavin Zhao, Jie Qi, Bunnie Huang, Jifei Ou, Angela Chen, Andy Su, Jordi Montaner, Shifu Yu—thank you for introducing me to a place where everything is possible, where ideas come to life at lightning speed. Some of you taught me the ins and outs of operating and fixing knitting machines, a process that has demanded—and taught me—immense patience.

To the rest of the **Responsive Environments Group**—Patrick Chwalek, David Ramsay, Perry Nascek, Nathan Perry, Ali Shtarbanov, Marie Kuronaga, Dr. Devora Najjar, Dr. Spencer Russel, Dr. Ishwarya Ananthabhotla, Dr. Caroline Jaffe, Elena Kodama, Dr. Gershon Dublon, Dr. Valentina Sumini, Prof. Katia Vega, Dr. Nan Zhao, Severin Meyer—you are truly some of the kindest, most remarkable, and selfless people I've ever met. I've had so much fun working and sharing space with you all. I will cherish all the moments (and the late-nights!) we shared. To **Space Exploration Initiative**—Dr. Ariel Ekblaw, Sean Auffinger, Maggie Coblentz—thank you for providing me with the space and resources to realize the Spacesuit dream, triggering my interests in space-tech, and for the extraordinary experience of floating in zero-gravity.

To my amazing **UROPs**—Allison Serio, Samir Droubi, Peter Hwang, Franny Xi Wu, Angelica Zhuang, Marissa Liu, Tongge Yu, Jing Tan, Xavier Sanchez, Cristian Colon, Tananya Prankprakma, Sophia Xin, Esha Ranade, and Andrea Leang—your energy, enthusiasm, and capability have been a constant source of a boost. You are also the reason I wake up earlier than usual (becoming a morning person at times) and keep going, day after day.

To **Arts at MIT**—Andres Volpe, Lydia Broshanan, Sarah Hirzel—thank you for giving this collective work a platform within the MIT and broader community. To **Artura ICAD**— it was truly a profound experience to be back and introduce my work to my roots. Thank you for inviting me to my first exhibition back home, in the place that has shaped me and my understanding of textiles, as I strive to fuse the traditional with the modern.

To the **MIT Media Lab community**—Pat Pataranutaporn and Ziv Epstein, we had a great time together at the ML SEA Forum; every time I talk to you both, I come back energized. Thank you for being my oracle and embodying the true Media Lab spirit. Phil Tan and David Kong**,** thank you for introducing me to the world of DJ and spinning, I will truly miss the ML99F. Angela Vujic, , Camilo Rojas, Valdemar Danry, Oceane Boulais, Cathy Fang, Eyal Perry, Vik Parth, Rubez Chong, Matt Groh, Ken Nakagaki, Judith Amores, Matt Carney, Luis Alonso, Joanne Leong, Abhinandan Jain, Belen Saldias, Zoe Fang, Mark Weber—thank you for the friendship and adventures, both inside and outside the Lab! I will forever be grateful for the time we've spent together. Mirei Rioux, Jimmy Day, Amna Carreiro, Xan Foote, Kevin Davis, Cornelle King, Candido Monteiro, Dr. Mahy El-Kouedi, Sarra Shubart, Sarah Beckmann, Chia Evers, Alexandra Kahn—we wouldn't be here without all of you. Thank you for helping me documenting and exhibiting my projects and navigating through life as an MAS student. With all of the troublemakers at the Media Lab, you've somehow managed to keep the Lab running smoothly.

To **Indonesia@MIT**—the Association of Indonesian Students at MIT—thank you for being my second family here, for all of the laughter, and for sharing our love for our food. Your friendship has made this journey all the more meaningful. I am so proud that during my time here, we have grown from a handful of students to almost three dozen now. It has also been a joy to share the beauty of our culture with the MIT community, through teaching Javanese Batik at the ML Festival of Learning (thank you Alice Hong) and performing with MIT Gamelan Galaktika. To **Boston and Camberville** community—to all the sweet, precious people in this area, thank you for lifting me up and understanding me. Living here has felt like being in a Barbieland, where friends are just within walking distances, and there's always something happening every week. You've reminded me to take breaks, to enjoy and live a life, and to find balance in my PhD journey. Ohh, I have at least two dozen names in my mind… you know who you are, and I'm looking forward to celebrating life with all of you!. Finally, to **my family**—thank you for always being there no matter what, for your unwavering patience and support as I pursue my study and career abroad. I miss you, and I look forward to seeing you soon.

As I reflect on this journey, I am reminded of Steve Jobs' words: "You can't connect the dots looking forward; you can only connect them looking backwards. So you have to trust that the dots will somehow connect in your future." My life has indeed been a journey of connecting the dots, and this dissertation is no different. It is about finding and making connections—between micro and macro, wires and fibers, electronics and textiles, dance and music, digital and physical, art and technology, and between human ingenuity and the humble yet powerful materials that have shaped our world and will continue to do so. As I look ahead, I am filled with excitement for what the future holds!.

Cambridge, 8/30/24

Table of Contents

List of Abbreviations

ACK	Acknowledgment
ADC	Analog to Digital Converter
AI	Artificial Intelligence
AC	Alternating Current
AOI	Automated Optical Inspection
AR	Augmented Reality
BLE	Bluetooth Low Energy
CAD	Computer-Aided Design
CAM	Computer-Aided Manufacturing
CB	Curved Beam
CCD	Charge-Coupled Device
CMOS	Complementary Metal-Oxide-Semiconductor
CNC	Computer Numerical Control
CNN	Convolutional Neural Network
CNT	Carbon Nanotube
CRC	Cyclic Redundancy Check
CTS	Cellular Temperature Sensing
DC	Direct Current
DFM	Design for Manufacturing
ECG	Electrocardiography
EEG	Electroencephalography
EMG	Electromyography
ENIG	Electroless Nickel Immersion Gold

FFC	Flat Flexible Cable
GUI	Graphical User Interface
HVAC	Heating, Ventilation, and Air Conditioning
I2C	Inter-Integrated Circuit
IC	Integrated Circuit
IO	Input-Output
IMU	Inertial Measurement Unit
IoT	Internet of Things
JTAG	Joint Test Action Group
LED	Light Emitting Diode
MEMS	Micro-Electro-Mechanical Systems
MIDI	Musical Instrument Digital Interface
MOSFET	Metal-Oxide-Semiconductor Field-Effect Transistor
NACK	Not Acknowledged
NFC	Near Field Communication
OSC	Open Sound Control
P2P	Peer to Peer
PC	Personal Computer
PCB	Printed Circuit Board
PDMS	Polydimethylsiloxane
PEC	Packet Error Code
PET	Polyethylene Terephthalate
PI	Polyimide
PPy	Polypyrrole
PTFE	Polytetrafluoroethylene
PU	Polyurethane
ROM	Read-Only Memory
SCL	Serial Clock Line
SDA	Serial Data Line
SEM	Scanning Electron Microscope
SMA	Shape Memory Alloy
SMP	Shape Memory Polymer
SoC	System on Chip
SPDT	Single-Pole Double-Throw
SPI	Serial Peripheral Interface
TPU	Thermoplastic Polyurethane
UART	Universal Asynchronous Receiver-Transmitter
UDP	User Datagram Protocol

USB	Universal Serial Bus
UV	Ultra-violet
VOC	Volatile Organic Compound
VR	Virtual Reality
XR	Extended Reality
ZIF	Zero Insertion Force

List of Figures

List of Tables

Abstract

Textiles are omnipresent and among the oldest forms of art and culture in human civilization. They serve as our protective skin, the interface between our bodies and the environment, and a medium for self-expression and collective experience. As electronics become more compliant, miniaturized, and low-cost, textiles provide an ideal substrate for technology integration, further driving the era of ubiquitous computing. My research fuses recent advances in functional materials, digital fabrication, hardware systems, and immersive technologies to demonstrate *Textile Macroelectronics* architecture and develop sensate and computational fabrics across scales.

In this dissertation, I propose a ubiquitous computational textile framework—a synergy between functional device selection, textile structures, fabrication tools, and system architecture—that integrates a distributed network of sensing and computational elements as primitives or raw materials in the manufacturing process of electronic textile products. In the first part of the dissertation, I present several methods, artifacts, and implementations of sensate textiles using functional fibers and digital machine knitting. I argue that to promote the disruption and adoption of sensate textiles and achieve seamless integration, we require a better hierarchical understanding of textile construction and fiber-fabric properties, as well as ways to integrate electronics and functionalities with industrial textile fabrication processes. By controlling functional and common yarn inputs, along with knitting structures and patterns, I can architect fabric forms and aesthetics while tuning their electrical and mechanical properties. With this approach, I have developed a set of custom proxemic and tactile textile interfaces based on capacitive and piezoresistive sensing for musical expression, human-computer interaction, activity recognition, and multi-sensory experiences in various forms such as cloth, footwear, mats, carpets, and large-scale architectural facades.

In the second part of the dissertation, I will discuss my work in exploring flexible, stretchable, and soft printed circuit technologies, incorporating multi-modal sensing with distributed computation to address scalability issues inherent in large and dense sensate textiles. These efforts have led to unique power, interconnection, and networking paradigms that allow us to transition from application-specific sensate textiles to generic computational fabrics that can be tailored and programmed for various applications. Finally, through these collective and complementary efforts, I aim to demonstrate an ecosystem of fabric artifacts that will lead us toward an *Electronic Textile Gaia*—a vision where sensing and intelligence are seamlessly interconnected and integrated into the fabric of everyday life, from in-body, on-body, room-scale, to architectural textiles, for applications ranging from physiological and physical activity monitoring to interactive media and built environments.

Chapter 1: Introduction

"It's not an idea until you write it down."
Ivan Sutherland

Preface

Textiles have played a crucial role in our lives, from clothing that gives us warmth to the intricate tapestry that reflects social status and cultural identity. They are are not only products of cultural significance but also drivers of technological progress. The complex craftsmanship, material, and structure of textiles have continued to inspire and stimulate many innovations, particularly in the field of digital fabrication and computing technology. In hindsight, the relationship between textiles and digital electronics has a long history dating back to the early days of computing. Punch cards, initially used in the textile industry to control and automate weaving processes, marked the beginning of the rise of computing technology. These cards, instrumental in the development of early computing concepts similar to those used in the Jacquard loom, enabled precise control over intricate patterns, laying the groundwork for modern programming

Frequently among the most precious goods, textiles have also played a crucial role in shaping trade networks and influencing economic systems. [1]. The Silk Road, for instance, facilitated not only the exchange of silk but also the flow of ideas, technologies, and cultures between East and West. In modern times, the use of computer numerical control (CNC) machines in textiles has continued to evolve and expand, enabling computer-aided design and manufacturing of various textile structures, including braiding, weaving, and knitting. Digital fabrication techniques,

inspired by traditional textile methods, have led to the creation of smart fabrics and wearable technology, seamlessly integrating computing capabilities into our daily lives. From the looms of ancient civilizations to the digital knitting machines of today, the evolution of textiles continues to weave together the threads of culture, technology, and innovation.

Although research and development of smart fabrics and electronic textiles have advanced in interactive media and wearable technology, challenges remain in their integration, scaling, and application to everyday products and surfaces. Designers typically consider electronic systems to be additional tools that they leverage to help maximize efficiency, add functionalities, or induce behaviors. Electronics are rarely incorporated or integrated in the early fabrication process of building or product materials. Computational design tools (i.e., 3D CAD/CAM and Devices/Materials Library) exist in the individual Architecture, Material Science, and Electrical Engineering fields, and there is a disconnection that makes it challenging to fuse electronic devices and circuits and computational intelligence into the natural and the built environments and create a hybrid-material ecosystem that allow them to become ubiquitous and interconnected as a "physical-digital nervous system." Such a system would necessitate a paradigm shift towards distributed intelligence, where sensing and computation happen locally and seamlessly within materials themselves, rather than depending on external or centralized elements.

In order to realize this concept, these distributed systems must also be able to communicate with each other, mirroring the complexity and interactivity of biological neural networks, as an example. Achieving this would require significant innovation not only in the domains of materials and architectural design but also in electrical engineering and computer science. Therefore, it becomes imperative to fuse these disciplines to explore new devices, tools, and system architectures that would not be possible without deep collaboration and intersection between these traditionally disparate fields. Using textile as a language and substrate for ubiquitous computing, my research proposes the synergy between digital craft/fabrication, microelectronic devices, and functional fibers. Together with distributed and spatiotemporal systems, my framework and approach veer toward Mark Weiser's vision of the *Computer for the 21st Century* [2]. The boundaries between physical and digital materials will dissolve, creating products ingrained with functional, sensing, and computational elements.

Specifically, I demonstrate that through the digital knitting of functional yarns, we can develop seamless sensate textiles with intrinsically tunable electromechanical properties, enabling large-scale production of e-textiles with highly customized aesthetics. I also propose modular and distributed processing principles that allow us to move away from highly customized and microfabricated electronic skin to highly scalable computing substrates, enabling us to shift from an application-specific to a general-purpose paradigm. Finally, through various application

spaces and the integration of data processing, artificial intelligence, and immersive technologies, I hope to showcase the versatility of these sensate and computational artifacts in various applications, including wireless physical and physiological monitoring, biomechanics, human-computer interaction, interactive media, environmental sensing, and telepresence.

Thesis Statement

"Any sufficiently advanced technology is indistinguishable from magic"
Arthur Clarke

With electronic devices becoming more miniaturized and low-cost, the vision of ubiquitous computing, where technology would be seamlessly woven into our everyday lives, is also becoming a reality. However, most of the research pursuit in this area focuses on novel sensing materials and techniques with limited spatial coverage or modality and methods for controlling and understanding large computation networks. Electronic devices are rarely treated as a part of an object's intrinsic structure or fabricated in a large-scale, flexible, or stretchable form. To overcome this barrier, I am interested in integrating electronic devices and systems in the fabrication of everyday hybrid materials, focusing on textiles as they are soft and provide a rich structural, textural, and geometrical language for ***Textile Macroelectronics***. Furthermore, they can be found everywhere, from clothing and upholstery to architectural formwork, providing a unique real estate to incorporate sensors that could better understand our physiology and physical interaction with the environment. As a whole, this dissertation proposes a framework to design and develop:

1. **Sensate textiles** with tailored forms and functions by employing distributed functional fibers with digital manufacturing techniques of machine knitting
2. **Computational fabrics** with multimodal sensing and distributed processing by leveraging soft printed circuits with microelectronic devices and novel system architecture.

In the first part of the dissertation, I present a design methodology for developing sensate textiles starting from electronics or functionalities at the primitive fiber-level and toward their integration into large-scale multi-layer textiles with digital machine knitting [3]. Digital machine knitting is an established textile manufacturing technique that has been pervasive in the garment and technical fabrics industry. With the growing areas of digital fabrication and computer-aided design, a new generation of knitting machines now enable users to personalize and rapidly

develop their textile design through a specialized visual programming environment and various types of functional, electronic, and common yarns. Compared to weaving, knitting has several advantages, including the ability to create intricate forms, patterns, and structures from two to three-dimensional fabrics, socks, or garments. By developing electronic textiles through knit configurations and constructions of functional and non-functional fibers, yarns, and fabrics, we can design the aesthetic, engineer active area and resolution, and tune e-textile mechanical properties, such as stretchability and conformability to match the substrate of interest and satisfy a physical and functionality requirement.

With this seamless and scalable approach, I have developed four knitted sensate textile artifacts and demonstrated their practical applications, including:

1) **KnittedKeyboard**, a soft and tactile piano-patterned cloth with 60 capacitive-based proximity and touch-sensing keys and integrated with piezoresistive pressure and strain-sensing layers for musical performance.
2) **3DKnITS**, a set of spatiotemporal piezoresistive pressure-imaging intelligent textile mat and shoe with 265 and 96 sensing pixels, respectively for applications in biomechanics, activity recognition, and gaming interfaces.
3) **Tapis Magique**, a large-area pressure-sensitive carpet with 1800 sensing pixels that generates 3D sensor date based on body gestures, movements, and location and drives an immersive sonic environment in real time for interactive dance.
4) **Living Knitwork Pavilion,** an architectural-scale e-textile shade structure integrated with 24 transmitter and receiver knitted antennas for distributed electrical field sensing. The Pavilion, accompanied with its virtual environment (*KnitworkVR*), acts as an immersive space that controls an integrated audio and lighting system based on movements and crowd activity in the physical environment and audiovisual experience in a virtual environment for collective experience and telepresence.

The previous approach demonstrates a tailored and application-specific methodology in designing sensate textiles. In the second part of my dissertation, I leverage soft, flexible, and stretchable printed circuit technologies to demonstrate multimodal, miniaturized sensor and processing nodes that can be densely integrated into a textile substrate to create a programmable, generic computational fabric called **Networked Electronic Textile Skin/System (*NETS*).** *NETS* can be cut, tailored, and reconfigured for a wide variety of applications, enabling designers and developers to construct smart garments or interior fabrics directly from raw computational fabrics, with the flexibility to program and customize their own applications.

I also aim to address the bandwidth, robustness, and scalability issues associated with multiplexed and centralized sensate textiles by employing distributed processing and

networking capabilities on each node. The development of *NETS* is inspired by the human skin and somatosensory network. It represents the first realization of a multifunctional computational fabric, where sensor stimuli are processed within the network, and multimodal data and controls are routed through a common backbone or peer-to-peer channels to a main processing module, allowing for self-configuring, event-driven, and low-power networks. Finally, I propose interaction design spaces, use cases, and several applications of such distributed computational fabrics in wearable computing, robotics, interactive objects, and environmental sensing.

Through this work, I hope to demonstrate the potential of sensate and computational fabrics across scales and context. Future augmented textiles would serve as an aesthetic tool to express our ideas and identities, as a mesh between the tactile-physical and the immersive-digital, as well as a second skin to protect and improve our health and well-being. These elements, inspired by our deep relationship with textiles and their current technological advances, highlight the importance of textile arts, culture, and craftsmanship into our never-ending quest for human connection, experience, and survival on Earth and beyond.

1.3 Thesis Contribution

My thesis aims to contribute to the electronic textiles, digital fabrication, sensor networks, ubiquitous computing, and human-computer interaction fields by:

1) Proposing a design methodology and framework for the development of sensate textiles that considers the materials or devices, textile structures and forms, and digital knitting techniques.
2) Introducing several project instances that demonstrate the design methodology to fabricate sensate textiles across scales, from wearable, room-scale, to architectural textiles.
3) Introducing another layer into the design methodology and framework and leveraging distributed system principles and soft flexible printed circuit fabrication to move from application-specific sensate textiles to general-purpose computational fabrics.
4) Developing hardware systems and infrastructure to interface with these sensate textiles and computational fabrics and demonstrate several applications, as well as discussing challenges and findings of the proposed methods and implementations in detail.
5) Designing and demonstrating novel interaction paradigms and application space for such sensate textiles and computational fabrics through thinking across scales and contexts, as well as through multi-disciplinary collaborations.

1.4 Outline

In this dissertation, I have started with an Introduction (Chapter 1), outlining the thesis statement, contributions, and common terminology used throughout the research. This provides a clear framework and understanding of the key concepts and goals of *Textile Macroelectronics*.

Following the introduction, I will delve into the background and state-of-the-art (Chapter 2). This chapter will be divided into three main sections. First, I will explore Moore's and Bell's Law as a driver of ubiquitous computing, discussing the challenges in realizing electronic textiles and introducing new paradigms in digital-material design. Next, I will trace the history of textiles and computation, covering manufacturing and materials from fibers to systems, and examining early examples of e-textiles. Finally, I will review efforts and applications of computational fabrics, building on various research areas such as electronic skin and *sensate media*.

Chapter 3 will explain in detail the fundamentals of knit fabrics and machine knitting, including various types of machine-knitting and knit architectures. This knowledge is crucial as it enables the control of electrical and mechanical properties through yarn inputs and structural changes in the fabric, facilitating the creation of textile-based interconnects, electrodes, and sensors. Building on this foundation, Chapter 4 will introduce the first major contribution of this dissertation: the digital knitting of sensate textiles across scales. This chapter will present several projects, ranging from object-scale to architectural-scale applications, including *KnittedKeyboard, 3DKnITS, Tapis Magique*, and the *Living Knitwork Pavilion*. Each subsection will discuss the design, development, and applications of these works, demonstrating the diverse potential of sensate textiles.

Next, I will introduce and discuss the second major contribution of this dissertation: efforts toward general-purpose computational fabrics. This involves combining soft and stretchable printed circuit technologies, as proposed in Chapter 5, with distributed local processing, multi-modal sensors, and a novel system architecture, as described in Chapter 6. I will delve deeper into this concept by demonstrating how our bioinspired framework (Chapter 6.1 and 6.2) enables scalable and multi-modal design (Chapter 6.3 and 6.4), self-configuration (Chapter 6.5), power management (Chapter 6.6 and 6.7), and broad applications for computational fabrics (Chapter 6.8).

In Chapter 7, I will explore future work and research opportunities for both research thrusts within an interdisciplinary context, addressing potentials and challenges related to materials, manufacturing, ecosystems, and implications. I will present my vision of *Electronic Textile Gaia* and other computational material substrates, highlighting future possibilities and the impact of our research on the integration of electronic materials into everyday life, which will redefine the

arts, sciences, and culture of making. Finally, I will conclude the dissertation by summarizing my research contributions (Chapter 8).

1.5 Terminology

This dissertation places a particular emphasis on the development and integration of sensing and processing systems within sensate textiles and computational fabrics. To define the broader terms utilized throughout this dissertation, the following clarifications are essential:

Textile is a general term that encompasses a broad category of fiber-based materials and interlaced fibers, including fibers, yarns, threads, and fabrics. On the other hand, **fabrics** are made by intersecting, winding, or joining fiber-based materials through weaving, knitting, stitching, sewing, *et cetera*, including non-woven material (which is not typically considered textiles**).**

Fabrics are materials specifically produced by weaving, knitting, or bonding yarns or fibers. They are typically used to make garments and clothing, while textiles can refer to a wider range of products. Fabrics are also a subset of textiles, usually referring to the finished raw materials that is ready for use in making textile products.

Functional textiles are textiles produced or engineered with certain functionality to cater requirements on top of their basic purpose. The functional properties can be incorporated into the textile or fiber-based material at different stages of production, such as fiber, yarn fabric, or garment stage. These textiles can be antibacterial, ultraviolet (UV)-protecting, water-repellent, self-cleaning, phase-changing, shape-changing, and electrically-active. They can also be called passive smart textiles.

Electronic textiles, also known as e-textiles, are a type of functional textiles that incorporate electronic devices into their design. These devices could include things like sensors, actuators, circuits, interconnects, or batteries, and they allow the fabric to have sensing, actuation, or processing capabilities. Computational, intelligent, or active smart textiles are fabrics that have been designed to have some level of intelligence or computational capability through the incorporation of a microprocessor or sensor-actuator feedback, allowing it to not only sense, but also respond to stimuli or perform specific tasks.

Sensate textiles refers to textiles or fabrics embedded with sensory and interactive capabilities. These textiles integrate sensors, actuators, and potentially other electronic components, enabling

them to detect and respond to various stimuli, such as pressure, temperature, moisture, or even electrical signals.

Computational fabrics are fabrics that can process data and make decisions, through the incorporation of not only sensors, but also microprocessor, memory, and other elements. Both sensate and computational fabrics are a subset of e-textiles since they both incorporate electronic devices

Macroelectronics are flexible electronics that cover a large surface area. They are fabricated through cost-effective and mass-manufacturing approaches, such as roll-to-roll printing.

Chapter 2: Background Research

"The most profound technologies are those that disappear. They weave themselves into the fabric of everyday life until they are indistinguishable from it."
Mark Weiser

2.1 Integrating Electronics into Everyday Materials

2.1.1 A Ubiquitous Computing Era

Moore's Law, articulated by Gordon Moore in 1965 (Figure 2.1), has been the cornerstone of microelectronics, predicting that the number of transistors on a microchip doubles approximately every 18 to 24 months [4]. This principle has propelled astonishing advancements in computing power and miniaturization. For instance, a state-of-the-art microprocessor in 2020, such as Apple's A14 Bionic, featured 11.8 billion transistors with a 5-nanometer pitch [5]. The A14 Bionic marked a significant leap in performance and efficiency for mobile devices, integrating a neural engine capable of performing 11 trillion operations per second, which enhanced capabilities in machine learning, augmented reality (AR), and high-efficiency computing. In comparison, the state-of-the-art microprocessor in 2010 had around 1.17 billion transistors with a 32-nanometer pitch. This dramatic increase in transistor count and reduction in pitch size over a decade underscores the relentless march of technological progress. Continuing this trend, the industry is approaching the physical limits of silicon-based technology, with researchers and manufacturers working towards achieving pitches close to 1 nanometer in the next decade.

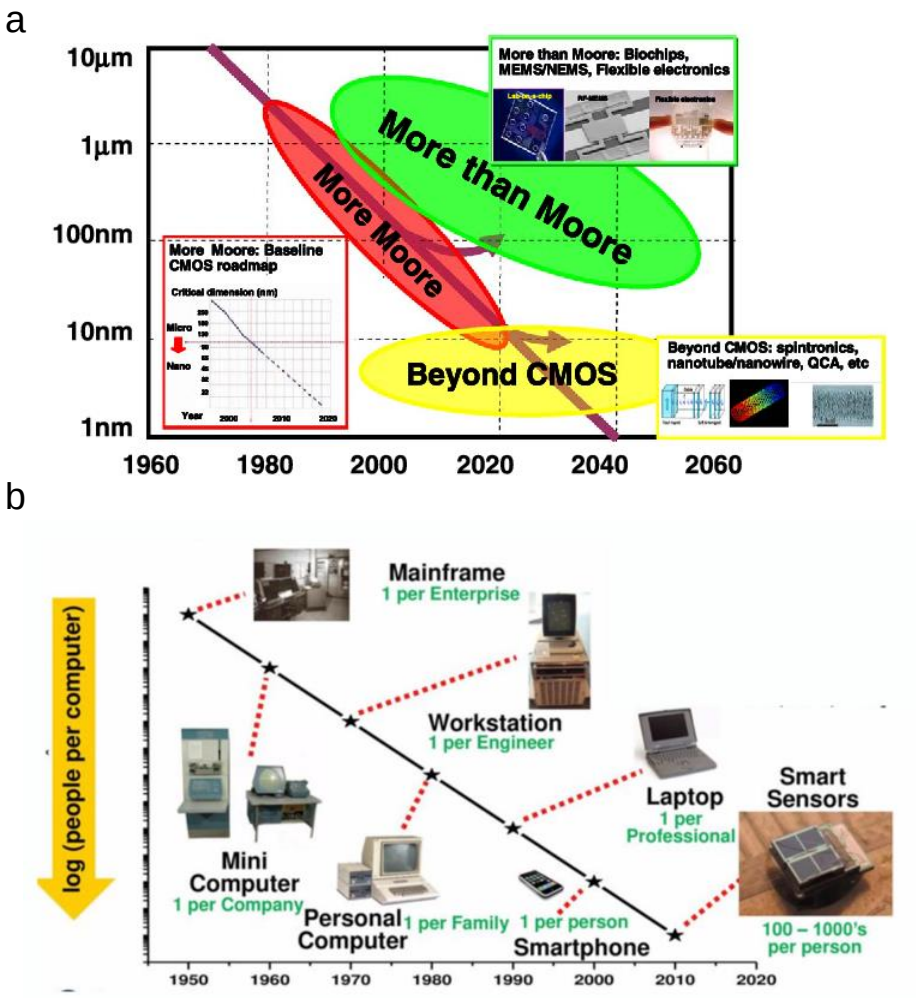

Figure 2.1: IC scaling roadmap: a) from More Moore to More than Moore and b) Bell's law of computer classes, which posits a new class of computers every other decade, resulting in new markets and industries (right) (reprinted from[6], [7]) .

Bell's Law, proposed by Gordon Bell in 1972, complements Moore's Law by highlighting paradigm shifts in computing approximately every decade. As shown in Figure 2.1, these shifts have led us from mainframes to minicomputers, personal computers, smartphones, and now to the era of ubiquitous computing and the Internet of Things (IoT) [7]. In 2000, it was common for people to have one connected device, such as a mobile phone. However, this number has increased significantly over time. By 2020, there were about 4.3 connected devices per person globally, with a total of 33 billion connected devices [8]. The trend continues to grow, with

projections suggesting that the number of connected devices per person could reach as high as 13.24 by 2030 largely driven by the increasing prevalence of IoT devices [9]. Looking toward the future, it is anticipated that we could see a hundred or even thousands of connected devices per person, as we approach scenarios predicted by Bell's Law. This explosion of connectivity can involve advanced computing capabilities in everyday objects and surfaces, transforming our environments into smart, interconnected systems.

As traditional scaling reaches its physical and economic limits, the focus is shifting towards "More-than-Moore" technologies and 3D packaging. "More-than-Moore" enhances silicon-based devices by integrating non-digital functionalities like RF communication, power management, and sensors directly onto chips [6]. Simultaneously, 3D packaging stacks multiple chip layers, improving performance and reducing latency through shorter interconnects (Smith et al., 2018). These innovations are crucial for sustaining performance gains beyond the limitations of conventional scaling. Microelectromechanical systems (MEMS) are at the forefront of "More-than-Moore" innovations, with applications in healthcare and environmental monitoring. Notable examples include Smart Dust, started in a 1997 by researchers from UC Berkeley, which aims to create wireless sensor nodes as small as a cubic millimeter [10]. These nodes integrate various sensors, such as accelerometers, temperature sensors, pressure sensors, and humidity sensors, enabling them to monitor environmental conditions with unprecedented granularity. Another recent commercial example is Bosch's BMA530 and BMA580 accelerometers, measuring just 1.2 x 0.8 x 0.55 mm^3. These accelerometers are among the world's smallest, designed for compact devices like wearables and toys [11].

Additionally, in 2018, researchers from the University of Michigan developed the Cellular Temperature Sensing (CTS) system, a wireless sensor node for accurate cellular temperature measurement (Figure 2.2). This system includes a fully programmable Cortex-M0+ processor, custom SRAM, optical energy harvesting, 2-way communication, and a subthreshold temperature sensor [12]. The CTS, with a volume of just 0.04 mm^3 (approximately 500 times smaller than a grain of rice), represents a significant advancement in MEMS technology for precise temperature sensing.

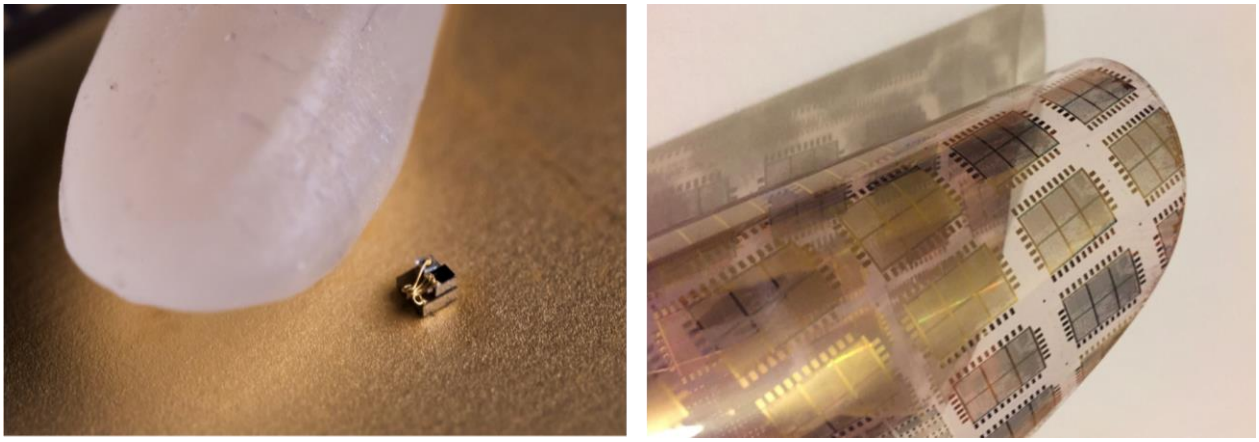

Figure 2.2: Programmable Cellular Temperature Sensing System, –500 × smaller than rice with Integrated Cortex-M0+ Processor (left) and ARM Cortex-M CPU Metal-oxide TFT on flexible polyimide by PragmatIC (right) (reprinted from [12], [13]).

This proliferation of technology miniaturization and integration align well with Mark Weiser's vision of ubiquitous computing, where technology becomes seamlessly integrated into our daily lives. Weiser foresaw a future where computing is embedded everywhere, making technology unobtrusive and omnipresent. Several user interface technologies have become mature and widespread, such as the mouse and keypad for controlling graphical user interfaces (GUIs) in personal computers, and touch-sensitive devices that have become the default controls of today's tablets and smartphones. Wearables now actively respond to users' activities or physiological states.

Continuous innovation in sensing, display, hardware processing, and software developments have also triggered advances in technologies for immersive sensory experiences, such as virtual and augmented reality. Through haptic feedback, gesture-sensing, voice-recognition devices, virtual assistants, and head-mounted displays, these technologies aim to radically change the way users perceive and interact with digital information, either by immersing them in a computer-simulated reality or overlaying digital information onto the physical world. Real-world examples such as smart homes, wearable devices like smartwatches, and smart shirts for physiological monitoring illustrate this vision. Smart home systems like Google Home optimize and automate household functions through AI-driven (artificial intelligence) decision-making, while smartwatches monitor health metrics continuously. Smart shirts, embedded with sensors, provide detailed physiological data, enhancing health and fitness monitoring.

Microprocessors are integral to all modern electronic devices, including smartphones, tablets, laptops, routers, servers, cars, and increasingly, smart objects within the Internet of Things. Despite the prevalence of conventional silicon-based microprocessors, their high costs and lack

of physical flexibility hinder their integration into everyday objects like bottles, food packages, garments, and wearable patches. PlasticARM, a natively flexible 32-bit microprocessor, represents a significant advancement in this area, built using metal-oxide thin-film transistor technology on a flexible substrate [13]. This technology offers an ultrathin solution suitable for mass production, enabling the seamless embedding of billions of microprocessors into various everyday items. The use of metal-oxide TFTs on polyimide substrates ensures that these flexible microprocessors can be scaled down for large-scale integration, overcoming the limitations of traditional silicon technology. These advancements illustrate the realization of a world where ubiquitous computing enhances human interactions with the environment, providing context-aware, personalized experiences that anticipate and respond to individual needs.

2.1.2 From Micro to Macroelectronics

As revolutionary as microelectronics has been over the last few decades, there are significant challenges associated with incorporating them into everyday products. According to Reuss, Hopper, and Park, "Applications requiring control, communications, computing, and sensing over a large area are difficult or cost-prohibitive to achieve because of the material incompatibilities of traditional integrated circuits (ICs) with structures, materials, and manufacturing technology" [14]. This highlights the limitations of microelectronics when it comes to applications that need to span larger surfaces or volumes, where standard IC manufacturing may not be practical or economical.

Microfabrication, for example, is constrained by the size of the wafers used, typically ranging from 6 to 12 inches in diameter. This limitation not only restricts the size of the individual devices but also increases the cost and complexity of manufacturing when scaling up. For instance, the cost of a state-of-the-art 300mm (12-inch) wafer fabrication facility can exceed $10 billion , making large-scale applications prohibitively expensive [15]. Additionally, integrating rigid ICs into flexible and irregular surfaces is inherently challenging, leading to issues with material compatibility and long-term durability.

Macroelectronics, a rarely used term referring to flexible electronics that can cover large areas, offers potential solutions to these challenges. As shown in Figure 2.3, its commercial applications have so far been limited but successful in areas such as rollable solar cells and flexible light-emitting diode (LED) displays. Rollable solar cells, for instance, have succeeded due to their lightweight, flexibility, and ability to be deployed over large areas where traditional rigid solar panels would be impractical [16]. These flexible solar cells can be rolled out onto rooftops,

integrated into building facades, or even used in portable applications. Industries have developed thin-film photovoltaic technologies that allow for such flexibility while maintaining efficiency and reducing installation costs. Similarly, flexible LED displays have found commercial success due to their adaptability and durability [17]. These displays can be curved, folded, or rolled without damage, making them ideal for innovative applications such as foldable smartphones, wearable devices, and large-scale advertising screens.

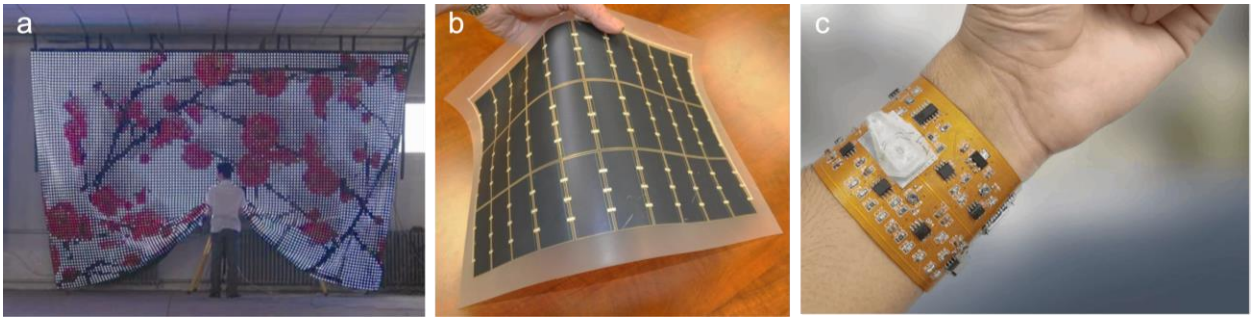

Figure 2.3: a) Flexible LED display system by Eurolite, b) Flexible solar sheet consisting of an array of 30 interconnected, large-area GaAs solar cells, c) Flexible printed circuit technology for wearable impedance cytometry (reprinted from [16]–[18]).

Other enabling advances include the development of flexible printed circuits based on polyimide. Polyimide-based flexible circuits have become low-cost and highly accessible, especially since the early 2000s. These circuits offer high performance with exceptional mechanical flexibility, enabling their use in a wide range of applications, from consumer electronics to medical devices. They can achieve great accuracy and fine pitch comparable to traditional microfabrication techniques, with line widths as small as 10 micrometers and spacing down to 20 micrometers, making them suitable for high-density electronic applications while maintaining flexibility and durability.

My research addresses this gap in adoption and applications by focusing on the integration of electronic devices and systems into the fabrication of everyday hybrid materials, particularly textiles through the use of industrial manufacturing technologies of digital knitting and soft printed circuits. Fiber and fabrics are ubiquitous and offer a rich structural, textural, and geometrical language, making them ideal candidates for *Textile Macroelectronics* architecture and *Ubiquitous Computing* substrate [3].

2.1.3 New Paradigm in Product Design through Smart Electronic Materials

The Ashby Plot, illustrated in Figure 2.4, is a foundational tool in materials science, providing a graphical representation of the trade-offs between various material properties such as stiffness versus tensile strength [19]. This plot is instrumental in helping engineers and designers select materials based on their mechanical properties and performance criteria. It typically plots materials on a two-dimensional graph, allowing for the comparison of natural and engineering materials. For instance, metals like steel and aluminum show high Young's modulus and tensile strength, while polymers are generally softer and less stiff but can be engineered for flexibility and other properties.

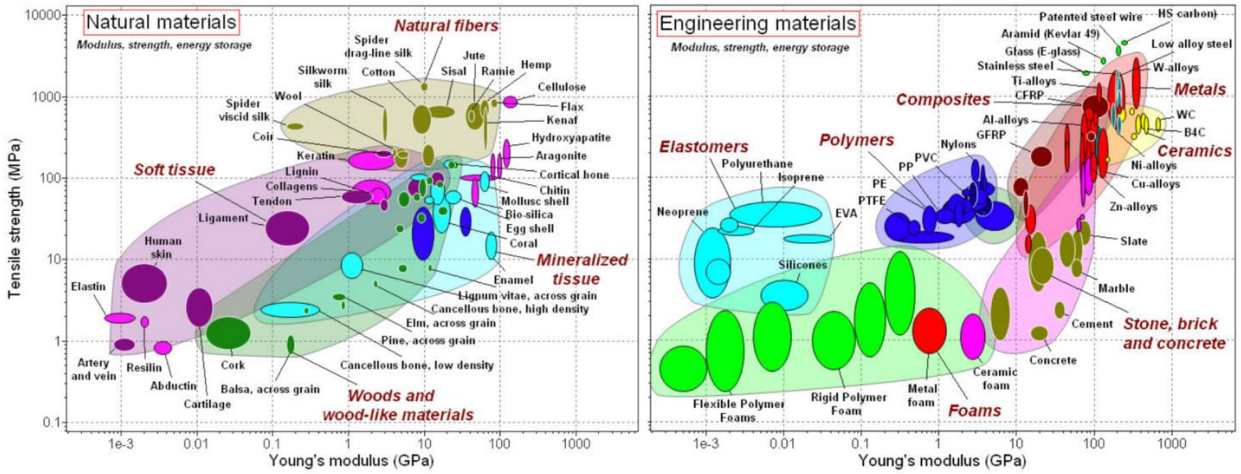

Figure 2.4: Ashby's plot for engineering and natural materials (reprinted from [20])

However, as we advance into the realm of electronic and hybrid materials, the traditional Ashby Plot requires augmentation to address the unique challenges posed by integrating electronic materials with conventional substrates. One significant challenge is bridging the substantial differences in mechanical properties between materials like semiconductors and polymers. For example, silicon, a common electronic material, has a Young's modulus of approximately 130 GPa, whereas polyimide, a widely used polymer substrate, has a modulus in the range of 2-4 GPa [21], [22]. This disparity necessitates the development of composite materials (Figure 2.5b) that can accommodate these differences and meet specific application requirements.

To address the challenges of integrating electronic materials with conventional substrates, various e-materials and e-composites have been developed, leveraging textiles or polymers, for example, as an intriguing substrate due to their network of interlaced fibers that act as natural composites [23]. Significant efforts have been made to integrate functional devices in fiber-format

within these textiles, creating innovative solutions such as segmented IC chips, particulate composites with soft polymers, and multi-layered structures combining conductive and non-conductive materials. Segmented IC chips embedded in textiles enable the creation of flexible, durable electronic fabrics that maintain the mechanical properties of textiles while incorporating advanced electronic functionalities like sensing and signal processing [24], [25]. Particulate composites, where electronic components are embedded within soft polymers, offer the dual benefits of flexibility and robustness against mechanical deformation, making them ideal for applications in stretchable electronics and flexible sensors [26], [27]. Furthermore, multi-layered conductive-non-conductive sandwich structures are designed to function as pressure or stretch sensors [28]. These structures employ a sandwich-like arrangement where conductive layers are separated by insulating layers, making them particularly suitable for applications such as wearable sensing and interactive textiles.

Furthermore, drawing inspiration from biological and natural systems can significantly enhance the hierarchical incorporation of functionalities. Extensive scientific research has shown that natural material systems exhibit exceptional mechanical properties that are not yet replicated in common synthetic materials. The human body and its muscle structure are prime examples of this complexity. Muscle fibers, known as myofibrils, are the fundamental units that contract to produce movement [29]. These myofibrils are bundled together to form muscle fibers or muscle cells, which are then grouped into larger units called fascicles (Figure 2.5a). Fascicles are further assembled to create whole muscles, which are connected to bones via tendons. Tendons themselves are composed of collagen fibers that are both strong and flexible, providing a seamless integration between the soft tissue of muscles and the hard structure of bones. This hierarchical arrangement allows for an efficient transfer of force and movement, optimizing both strength and flexibility within the body.

In contrast, synthetic materials often do not utilize such intricate hierarchical design strategies. For example, a typical sport shoe may use various layers of synthetic polymers and foams to achieve the desired combination of support and comfort. However, these layers are often separately manufactured and then assembled, lacking the integrated hierarchy found in natural systems. Similarly, in automotive engineering, the dashboard might combine hard plastic for structural integrity with additional layers of softer materials to achieve tactile comfort. Synthetic materials generally lack the intermediate design opportunities found in natural systems, such as the layered structure of spider silk, which combines strength and elasticity.

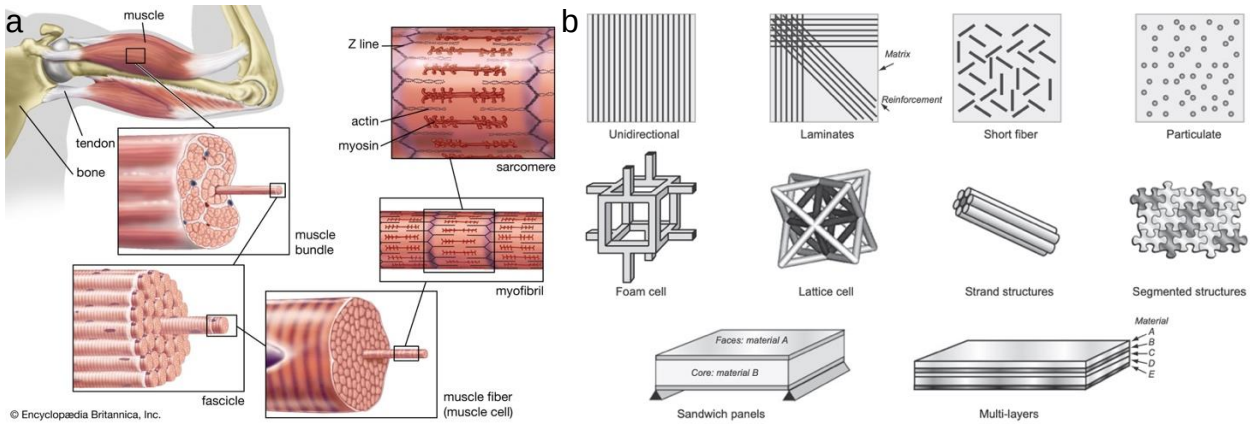

Figure 2.5: a) Skeletal muscles anatomy, attached to the bones by tendon. b) Different types of Architectured or "hybrid" materials. Hybrid materials are combinations of two or more materials, or of materials and space, assembled in such a way as to have the attributes not offered by any one material alone (adapted from [29], [23]).

Textile manufacturing, for example, represents one of the few processes capable of creating hierarchical structures in artificial artifacts. This process ranges from fiber spinning and yarn twisting and braiding to weaving, knitting, and annealing, allowing designers and engineers to finely tune the properties of the end-product by adjusting various manufacturing parameters. This hierarchical capability in textiles mirrors the organization of muscle fibers, highlighting the potential for biomimicry in developing advanced material systems [30].

The analog thinking of the Ashby Plot, applying it to physical-digital or hybrid electronic materials represents a significant shift in material and product design. By integrating sensate and computational capabilities into materials, physical-digital material engineers and designers can create innovative composites that bridge the gap between electronic and substrate materials. By emulating the complex, multi-level organization seen in biological systems, such as the hierarchical structure of muscles or the layered composition of spider silk, we can also enhance the adaptability and efficiency of hybrid electronic materials. This new paradigm in material design not only addresses mechanical and functional requirements but also opens up new possibilities for interaction and programmability through sensate and compute behaviors, transforming how we use and interact with the next generation of everyday materials and products.

2.2.4 Toward New Materiality and Responsive Environments

Digital smart materials are defined as materials that possess sensate or computational capabilities and are fabricated through additive manufacturing techniques [31]. These materials are designed to integrate seamlessly into both physical and digital environments, enabling new forms of interaction and functionality beyond its form. Adding to this paradigm shift, Manuel De Landa's concept of "new materiality" provides a theoretical framework for understanding how material properties can emerge from the interaction of different components and processes [32]. Phillip Beesley extends this discourse by examining the integration of computational design within material science. Beesley's work focuses on the intersection of material properties and digital processes, emphasizing how computational techniques can not only optimize but also fundamentally transform the capabilities and applications of materials [33], [34]. By leveraging computational design, digital materials can be programmed to respond to various stimuli, thus extending their functionality beyond traditional uses. This aligns with De Landa's notion of materials as active agents in reality construction, where the computational layer can add a new dimension of interactivity and adaptability.

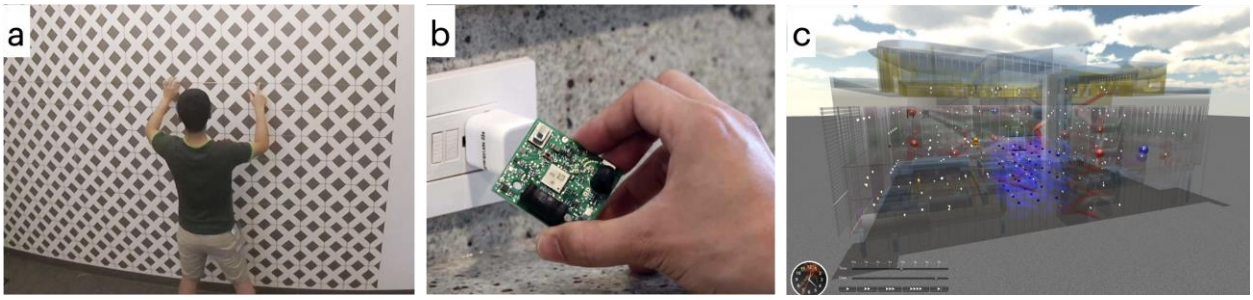

Figure 2.6: a) Wall++ conductive paint spread through the wall as arrays for proxemic sensing. b) Synthetic Sensor that can be plugged to an outlet and gives rich multimodal sensor data for detecting various signal changes and classifying occupant activities in the environments, c) DoppelLab virtual reality browser that connects to large-scale dense sensor network in the MIT Media Lab building. (reprinted from [35-37])

As electronics and sensing capabilities become integrated into everyday objects—from ceramics to walls—we are also moving toward the prevalence of responsive environments [35]. Projects like Wall++, for example, are transforming this role by turning walls into smart infrastructure through conductive paints [36]. These smart walls can track users' touch and gestures, estimate body positions, and detect active appliances by capturing airborne electromagnetic noise, creating robust, room-scale interactive and context-aware applications (Figure 2.6a). The Synthetic Sensors project, as shown in Figure 2.6b, explores general-purpose sensing, which is crucial for realizing smart environments and the IoT that leverage big data and machine learning

[37]. A novel sensor hub was designed to integrate nine physical sensors from illumination to motion sensors and capture in total of twelve distinct parameters. Unlike traditional methods that use specific sensors for specific tasks, general-purpose sensing employs highly capable sensors to monitor large contexts indirectly. This design aims to approach the versatility of camera-based systems without the associated privacy issues.

Furthermore, the DoppelLab project emphasizes the importance of visualizing real-time, mobile, and distributed sensing technologies into various domains, such as homes, offices, and construction sites [38]. These environments are increasingly filled with sensor networks that provide specific data but often remain locked in closed-loop control systems. DoppelLab addresses the challenge of managing and interpreting this data influx by using sensor fusion algorithms to combine different data streams, providing valuable context and making information accessible through a digital twin experience (Figure 2.6c). In summary, integrating electronics and sensing capabilities into everyday objects and spaces through advancements in digital materials, smart infrastructure, and general-purpose sensing can create dynamic, interactive environments. This convergence of smart material and computation heralds a future where the objects and surfaces in our surroundings are not only passive structures but active participants in our daily lives, enhancing the knowledge of our environments and our interaction with the world in new ways.

2.3 Textiles as Technological Substrate

There was a deep historical link between manufacturing processes used in the textile and electronics industries that in some cases continue into the present era: dies draw down both electrical wires and optical fibers; lithography and screen-printing techniques pattern both printed circuit boards and fabric embellishments. Some other examples as shown below in the Electronics and Textile *Industrial Cross-Polination Map* (Figure 2.7) include the connections between embroidery and pick-and-place machines, drill holes and button holes, as well as braiding techniques in both ropes and cabling [39]. It dates back to the punch cards initially developed for the Jacquard loom that triggered the advancement of computing devices and information and communication technology. By interpolating from this historical and ongoing cross-pollination, we can envision a future where the textile and electronic industries work side-by-side or even merge into one, driving innovations in *Textile Macroelectronics.*

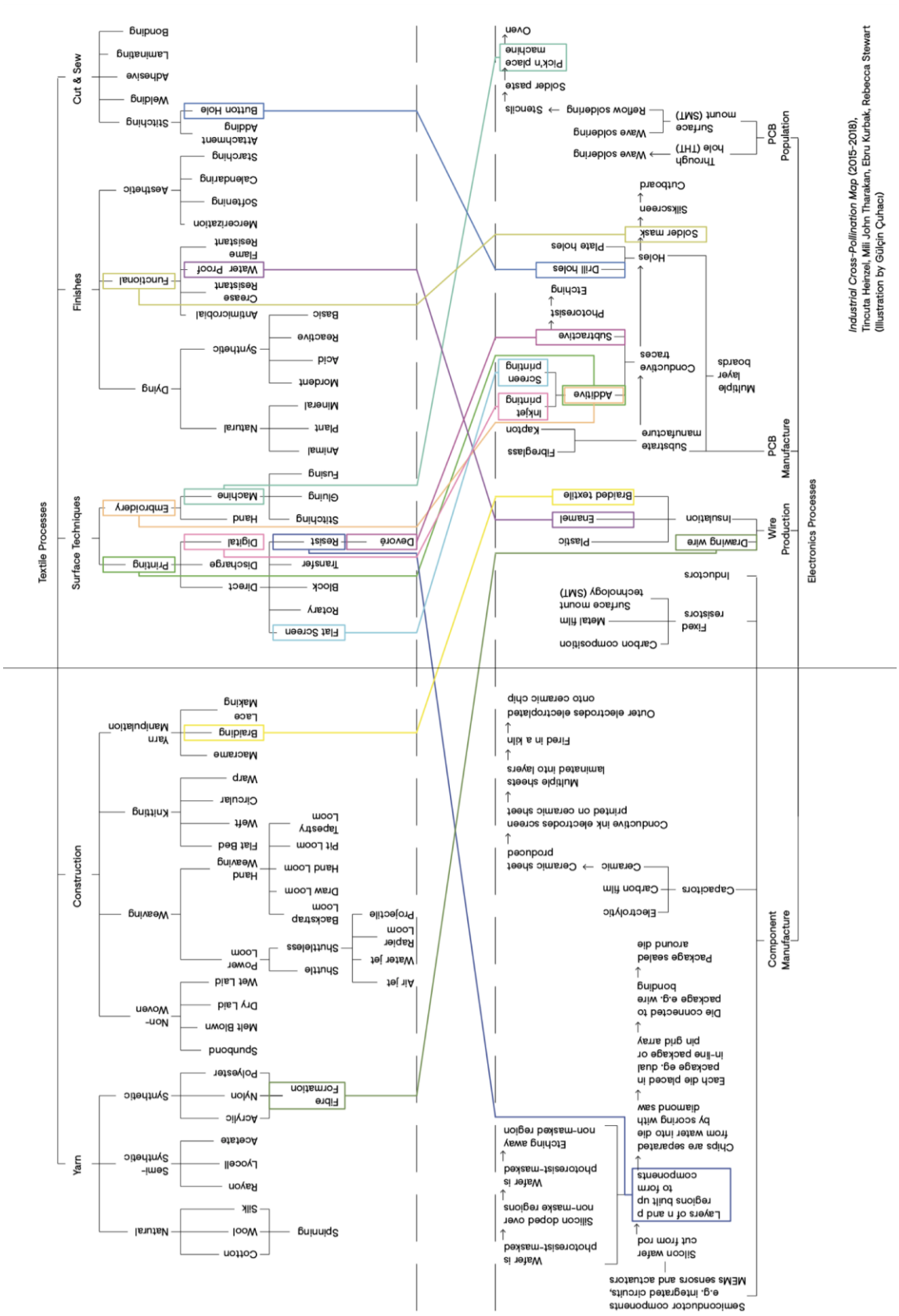

Figure 2.7: Electronics and Textile Industrial Cross-Polination Map (Kurbak, Stitching World [39])

The invention of the Jacquard loom by Joseph Marie Jacquard in 1804 represented a significant technological leap in the textile industry (Figure 2.8a). The loom's use of punched cards to control the weaving of intricate patterns mechanized and revolutionized textile production, allowing for unprecedented complexity and efficiency [40]. This innovation had far-reaching implications beyond textiles, impacting early computational theory and machine design. Charles Babbage, recognizing the potential of the punched card system, conceptualized the Analytical Engine in the 1830s. The Analytical Engine is widely considered the first design for a general-purpose mechanical computer. Babbage's design incorporated key computational concepts such as an arithmetic logic unit, control flow via conditional branching and loops, and memory storage. These features enabled the machine to perform a wide range of calculations and operations, setting the stage for modern computing.

Ada Lovelace, a mathematician and visionary, began to understand the implications of Babbage's Analytical Engine (Figure 2.8b). In her extensive notes on the Engine, she emphasized its potential to go beyond arithmetic calculations to manipulate symbols and create complex patterns, drawing a parallel to the Jacquard loom's weaving of intricate designs. Lovelace's insight into the machine's capabilities anticipated modern concepts of algorithms and programming, earning her recognition as the world's first computer programmer [41]. She articulated the idea that the Analytical Engine could be programmed to execute any series of operations, laying the groundwork for the field of computer science. The design principles of the Analytical Engine had a lasting impact on subsequent computational theory. Alan Turing, in the 1930s, built upon these foundational ideas with his theoretical construct of the Turing Machine. The Turing Machine formalized the concept of computation and algorithms, demonstrating that a machine could simulate any human-computable function. This theoretical framework was instrumental in the development of artificial intelligence (AI), providing a basis for understanding how machines could emulate cognitive tasks traditionally associated with human intelligence.

The transition from punched cards to transistors marked a pivotal shift in the evolution of computing technology. With the invention of the transistor in 1947 by John Bardeen, Walter Brattain, and William Shockley, electronic devices became smaller, faster, and more reliable. Transistors replaced the bulky and less reliable vacuum tubes, leading to the development of integrated circuits. This miniaturization revolutionized computing, making it possible to build more powerful and compact devices. The advent of microprocessors in the 1970s further accelerated this trend, enabling the integration of complex computational capabilities into a single chip [42]. This progression laid the groundwork for the modern digital age, where computing power could be embedded into a myriad of applications, including textiles.

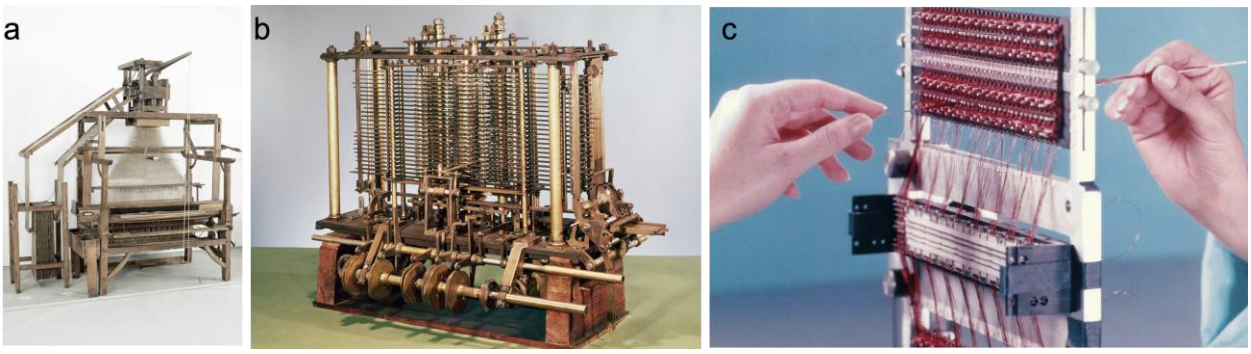

Figure 2.8: a) A loom with punchcards and Jacquard Mechanism (Deutsches Museum, 1805 [43]), b) the Analytical Engine, controlled with punch cards and a programming language with loops and conditional branching [44]. C) During the first Apollo missions, NASA hired skilled women from the local textile industry as well as from the Waltham Watch Company to weave a high-density storage called "core rope memory" (reprinted [45])

In the textile industry, the transition from mechanical systems to electronic control systems paralleled the broader trends in computing. CNC technology emerged, allowing for the precise control of machinery through computer programming. CNC technology revolutionized industrial textiles by enabling the automation of complex manufacturing processes, enhancing precision, and reducing waste.

As demonstrated in Figure 2.8c, another notable instance of textiles and electronics interplay was the weaving of core-rope memory for the Apollo missions. Core-rope memory, an early form of read-only memory (ROM), was essential for the Apollo Guidance Computer. At MIT, this memory was manually woven by skilled workers from a local company, Raytheon. The process involved threading wires through and around tiny magnetic cores. Each core represented a bit of data, with the presence or absence of a wire through the core determining the bit's value. This collaboration highlighted the high precision and reliability required in both textile and electronic manufacturing, and demonstrated how traditional textile techniques could be adapted to meet the needs of advanced technological applications.

The progression from the Jacquard loom to the Analytical Engine, and from the Turing Machine to modern AI, illustrates a continuous trajectory of innovation driven by the constant progress between textile technology and computational theory. The integration of electronics and miniaturization in mechanical systems has transformed industrial textiles into advanced CNC textiles, further fusing computation with textiles. This historical context underscores the transformative impact of early technological innovations on the evolution of computational theory and AI, and highlights the ongoing potential for cross-disciplinary research to yield novel insights and applications in both fields. The future of textiles is poised to be increasingly

intelligent, adaptive, and intertwined with the digital world, continuing the legacy of innovation that began with the Jacquard loom.

2.3.1 History of Textiles Manufacturing

At its origin, textiles were not made for aesthetics and expression, but for functional purposes, such as in clothing, wrappings, or blankets to keep ourselves warm [1]. Though they date back to the ancient time, to more than 100,000 years ago, it is not until 30,000 BC that archeologists discovered early evidence of spun, dyed, and knitted flax fibers and 8,000 BC for domestic flax cultivation to produce linen (Figure 2.9). Early textile and fiber making involves manual and hand-operated techniques, such as hand-weaving with resist-wax printing and patterning, Nalbinding, and wooden wheel-spinning. As time went by, other plants such as cotton and animal skins, furs, and byproducts were harvested and collected to make natural fibers, yarns, and textile artifacts. The importance of textiles circa 200 triggered the Silk Road trade routes that brought Chinese silk to India, Africa, and Europe.

While clothing items were still the dominant types of textile products in these classical and medieval ages, royalties decorated their palaces' walls, floors, and furniture with vibrant and luxurious textiles. The Industrial Revolution in the early modern period starting around 1700, was a defining point for textile manufacturing. With the invention and commercialization of cotton gins, drawing machines, spinning jennies, sewing machines, Jacquard, and power looms, fabric production became more rapid and customizable. Textiles were not just for the wealthy anymore; they were affordable and available to more society. More people could design and produce their own fabrics and clothing in creative ways. Alongside advances in the manufacturing ecosystem, man-made or synthetic fibers and yarns and textile structures were investigated to solve some problems with natural fabrics, such as their lack of elasticity or wrinkling. These fibers are made from synthesized molecules, which come from compounds of chemicals. From the year of 1910 onwards, synthetic fibers such as Rayon, Nylon, Acrylic, Polyester, Spandex, as well as high-performance fibers such as Aramid and Kevlar started to flood factories and markets as garment and technical fabric products due to their respective properties, including moisture-wicking, as well as heat and radiation-resistance [46].

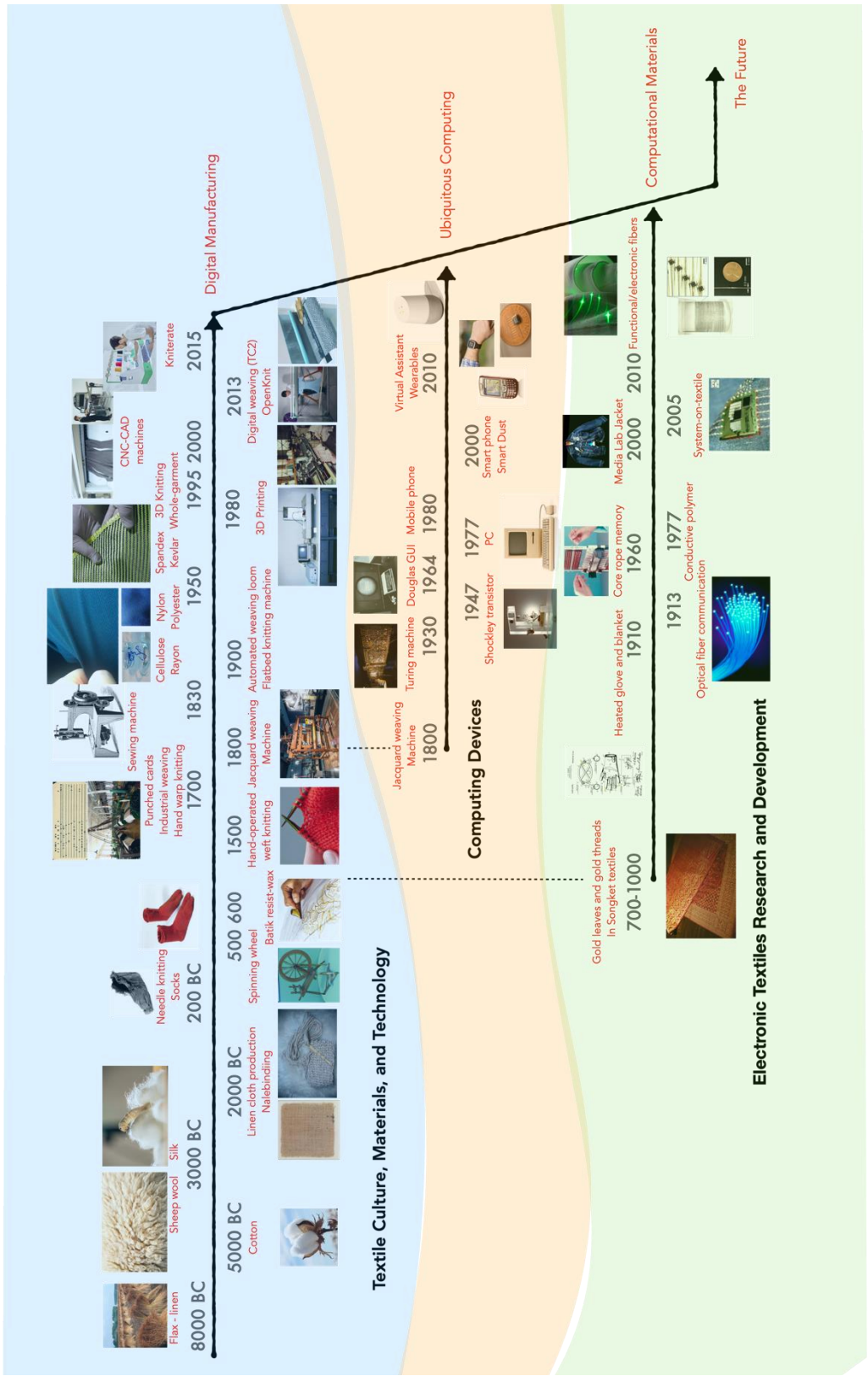

Figure 2.9: Historical timeline of electronic and textile cultural and technological advancement.

In the early 20th, punch-cards and tapes with encoded design patterns in mechanized textile weaving and knitting machines have become much more adopted in factories. However, the miniaturization of mechanical and electronic devices did not immediately disrupt the digitization of these textile manufacturing machines until the mid-90s. After 3D printing was introduced in the 1980s, several industries started exploring the concept of 3D whole-garment knitting and digital weaving, allowing more intricate and customizable textile patterns, structures, and end-products with reduction in raw materials and less human interventions.

Today, CNC systems with integrated GUIs and open-source computer-aided design (CAD) have started to push forward personalized, on-demand, and in-house digital textile design and production [47]. Though their software interfaces are still complex and tailored for industrial, mass-manufacturing processes, these systems will inevitably become more accessible to a wider audience. While CNC and CAD systems for sewing, felting, and embroidery are already widely available and accessible, 3D knitting, braiding, and digital weaving technologies are following in their footsteps, poised to expand into broader, more user-friendly applications.

2.3.2 Electronic Textiles

In recent years, we have developed hundred micron-scale multisensory neural probes and millimeter-scale sensory meshes that can be injected into the body, alongside mesoscale fabrics with sensing, communication, and even locomotive capabilities. E-textiles and functionalized fabrics now touch the full range of scales from microns to kilometers, with active and computational capability achieved at the level of fiber, yarn, fabric, and system.

The history of electronic textiles dates to the early modern period, where gold and silver yarn were woven into tapestries or metallic organza for fashion, interior design, and decorative purposes [48]. However, it was not only after the 20th century that the electrical properties of such textiles were harnessed. Some of the earliest use of conductive fibers in everyday garments can be found in early patents of heating gloves, blankets, and socks between 1910 and 1970 [49].

Generally speaking, there are three main approaches to develop e-textiles, ranging in complexity from highly specialized to widely accessible. The first approach applies common textile art practices such as fusing, embroidery, sewing, weaving or knitting either by hand or machine. In the late 1990s, e-broidery and smart fabrics (Figure 2.10a) [25] incorporating electronics were introduced at the MIT Media Lab and Georgia Tech, with “Washable Computing” [50] and “The Wearable Motherboard” [51] being the some of the first few papers introducing these concepts.

Musical Jackets and Musical Balls [52], [53], for instance, demonstrated the first embroidered touch and pressure-sensitive textile sensors for performing music. One of the first efforts in developing textile circuits is e-broidery by Post et al. [25]. By embroidering steel threads through a special carrier for high-density pins, connections to high-density microprocessors can be achieved. Shortly after that, in Europe, strain-sensing fabrics [54] and conductive textile electrodes in wearable healthcare system (WEALTHY) [55] have also seeded further work and sparked research community in this field.

As shown in Figure 2.10c, Linz et al. developed a customized flexible printed circuit board (PCB) as appendages in which connection to the textile layer is done through looping and sewing conductive threads [56], whereas Buechley and Eisenberg explored do-it-yourself, multi-layer fabric PCB using conductive fabrics, sacrificial films, and iron-on adhesive [57], [58]. Buechley also developed LilyPad in 2007, an e-textile Arduino-enabled platform for sewable electronic components and conductive threads (Figure 2.10b) [59]. As shown in Figure 2.10d, Tao et al. developed a washable electronic system for electrophysiology and activity monitoring [60]. The fabric electrodes were fabricated through the embroidery of conductive threads. Adhesion and encapsulation processes with thermo-plastic polyurethane (TPU) and polydimethylsiloxane (PDMS) electrically and mechanically-protect the processing and communication flexible PCB during washing. The system is connected to textile electrodes and attached to a compression garment.

Locher et al. explored weaving techniques as they created a matrix for the conductive routing of electronic textiles. A wire-grid fabric, named PETEX, is fabricated by weaving common threads with conductive filaments (Figure 2.10e,f) [61]. Interconnects can be realized by cutting intersections by laser ablation and using conductive adhesive and encapsulation. Fusing interposers would then create a bridge to connect this wiregrid with IC pads. Laser ablation defined the direction or the path of the wires, and conductive adhesive, interposers, and encapsulation techniques were used to connect intersections and ICs.

The second technique is to electrically functionalize textiles with solution-based coating or printing at either the fiber or fabric level. This technique can be quickly scaled using existing textile manufacturing and treatment processes. An example by Lee et al. is demonstrated in Figure 2.10g [62]. They built a process to screen-print circuit traces on both sides of a multi-layer fabric PCB and designed an Eyelet metal connector as a via that connects both functional layers.

Last but not least, the third main approach is to grow computational fibers by depositing electronic nanostructures on the surface or embedding them inside the fibers or strips, ultimately treating these functional 1D filaments as raw, basic materials for textile integration. It requires an

advanced fabrication and manufacturing process that integrates microelectronics seamlessly within the 1D fiber structure. Some notable example of these efforts are woven sensing and display fabric by Cherenack et al. [63] (Figure 2.10h) and Komolafe et al. [64] (Figure 2.10j). These teams developed a fabrication process of copper interconnects and inorganic transistors on flexible polyimide strips. The transistors, for example, are used as switching circuits for connection to temperature and humidity sensors, as well as LEDs.

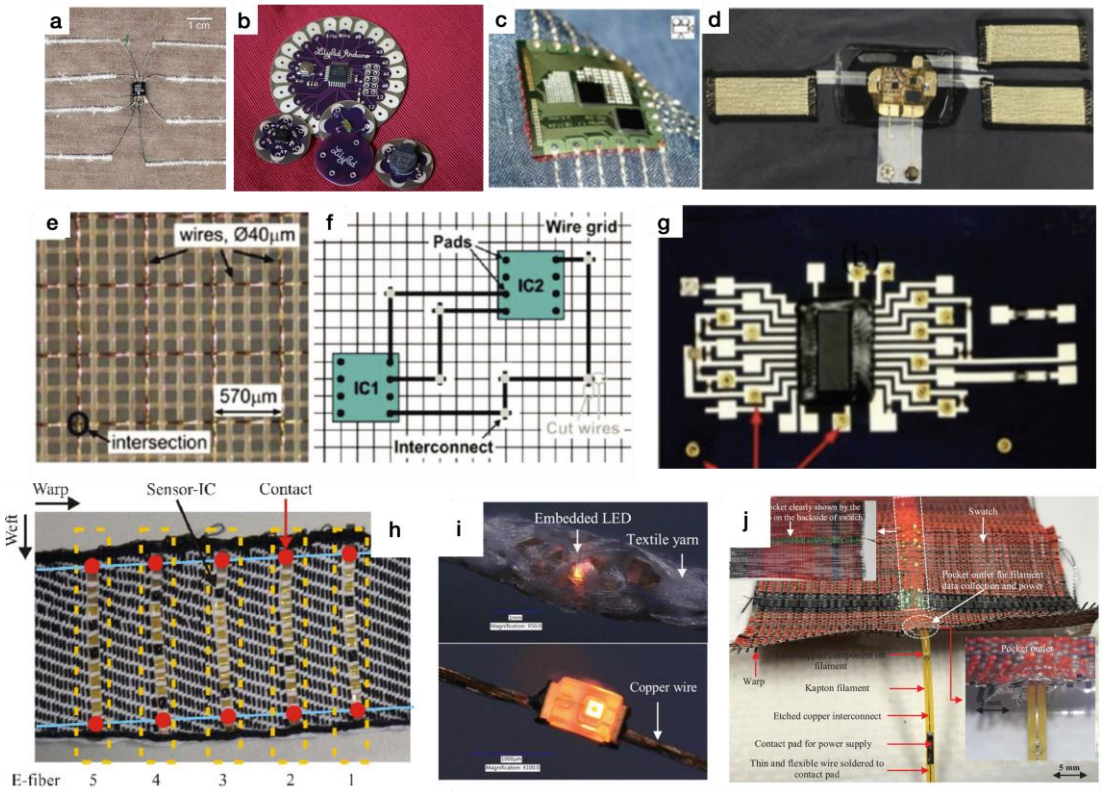

Figure 2.10: Several examples of electronic-textile integration techniques: a) Embroidered conductive threads as interconnects and interfacial socket to ICs [25], b) Sewable Lilypad Arduino [59], c) Flexible PCB connected with sewn conductive yarns [56], d) Textronic system encapsulated and attached on compression garment [60], e-f) Integrating woven wire grid into fabrics with PETEX [61] , g) Multi-layer screen-printed fabric PCB with Eyelet , h,j) Woven fabrics with sensing and display electronics fabricated on top of polyimide filaments [63], [64], and i) insulated sheath mechanism for making die-embedded yarn [65].

A more fiber-like example by Nashed et al. encapsulates LED with long wires in a knitted sheath to create an electronic yarn (Figure 2.10i) [65]. Recent efforts by Fink's group at Fibers@MIT demonstrated an even more complex integration of electronics such as inertial measurement units (IMUs), photodiodes, temperature sensors and memory devices inside a strand of fiber through thermal drawing [66], [67] . These approaches are directing us toward seamless fabrication of

electronic fibers and textiles, making them more invisible, acceptable, and comfortable to wear, as we are giving advanced functionalities without compromising the look and feel of the fabrics.

As illustrated in Figure 2.11, I have classified the functionalization of textiles hierarchically, considering every dimension: through 0D (material), 1D (fiber), 2D (fabric), 3D (complex structures), and finally to the end-product or system [3]. In this section, I will focus on electronic and electrically-active materials, devices, and systems and textile structures as means for integration and functionalization.

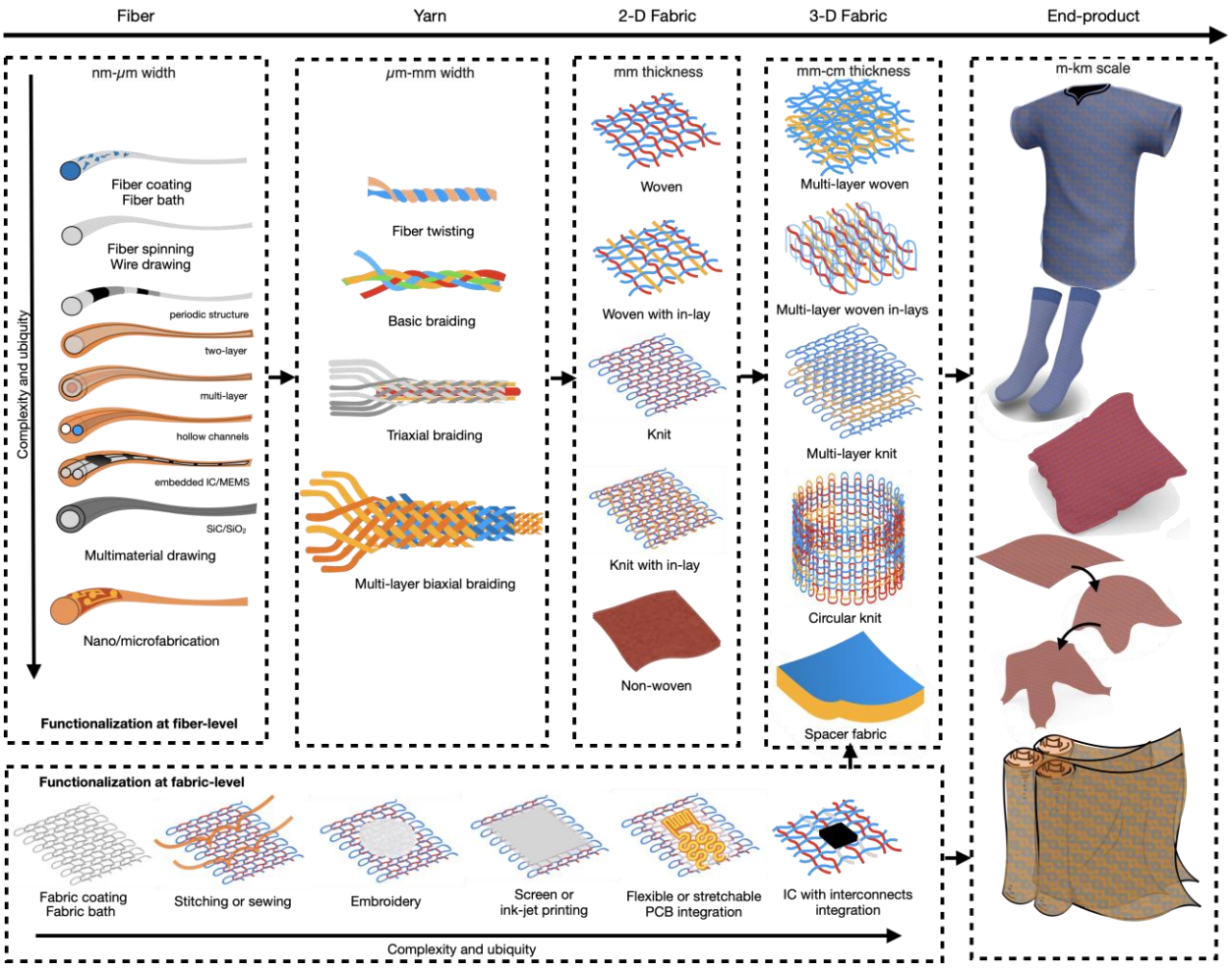

Figure 2.11: Hierarchical architecture and various structures of electronic textiles starting from fiber (1D), yarn (1.5D), fabric (2D), fabric composite (3D), to the end-product. Besides structural functionalization, we also show the material functionalization stage at the fiber or fabric-level.

2.3.2.1 Fibers

Fibres are the most fundamental building block of fabrics. There are two common types of fibres: natural and artificial. Natural fibres come from animal such as wool or silk and plants, such as cotton whereas synthetic fibres can be developed from polymers, rayon or inorganic materials such as glass or ceramic. In e-textiles, the most commonly used materials are the conductive threads. Conductive threads can consist of fully metal filaments, such as silver, gold, copper, or aluminium or a blend between these filaments and base yarns or fibres, such as nylon, cotton, polyester, polyimide. The metal filaments are developed by a mechanical process called wire-drawing [68]. These filaments can be twisted together with the base fibres using a textile spinning machine; this spinning process will result in much more compatible threads for sewing due to its enhanced durability and flexibility. A more straightforward technique to make conductive threads is by coating conductive materials to fibers. The drawback of this technique compared to fully-metal filaments is that the threads will not be able to withstand high temperature and soldering. One example of solderable yarns is insulated copper core twisted with common yarn, as demonstrated by Project Jacquard [69].

Spinning is one of the most frequently applied methods for manufacturing fibers. Raw materials in a fluid state, such as intrinsically conductive polymers, can be added to the spinning precursors. Depending on the spinning process, this base material is then melted or submerged in a chemical bath and pumped under pressure through a spinneret. The spinneret contains many small openings and a cooling mechanism to extrude and harden the polymers into long filaments. The output of this process is synthetic fiber with electrical functionality. Several efforts have blended fiber polymer with silver nanoparticles (AgNP), silicon nanowires (AgNW), carbon black, carbon nanotubes (CNT), graphene, polyaniline, polypyrrole, and poly polystyrene sulfonate (PEDOT:PSS) via wet or dry-spinning methods to develop conductive and resistive fibers as interconnects or sensors [27]. Their functional properties, morphology, and heterogeneity can be engineered to sensitively detect mechanical pressure, strain, temperature, humidity, pH, or specific chemical stimuli.

Electrospinning, another approach that involves high-voltage polarization, has been demonstrated to produce piezoelectric nanogenerators by extrusion and beta enhanced, poled polyvinylidene fluoride (PVDF) fibers. It is also possible to coat conductive polymers onto non-functional, synthetic, or naturally spun fibers using post-spinning processes such as in-situ polymerization, dip-coating, electroless plating, vacuum plasma spraying, and physical vapor deposition [70]. In bundle drawing, a composite wire consisting of thousands of filaments from metal alloys or preforms such as stainless steel, titanium, nickel, ferrous, and aluminum and sacrificial fillers is pulled through a die multiple times until reaching the final desired diameter.

The sacrificial fillers can then be dissolved through a chemical process. Even though metallic fibers (Figure 2.12a,b) have better electrical performance, polymeric fibers (Figure 2.12c) are typically more mechanically robust, lightweight, and flexible than metallic fibers [68].

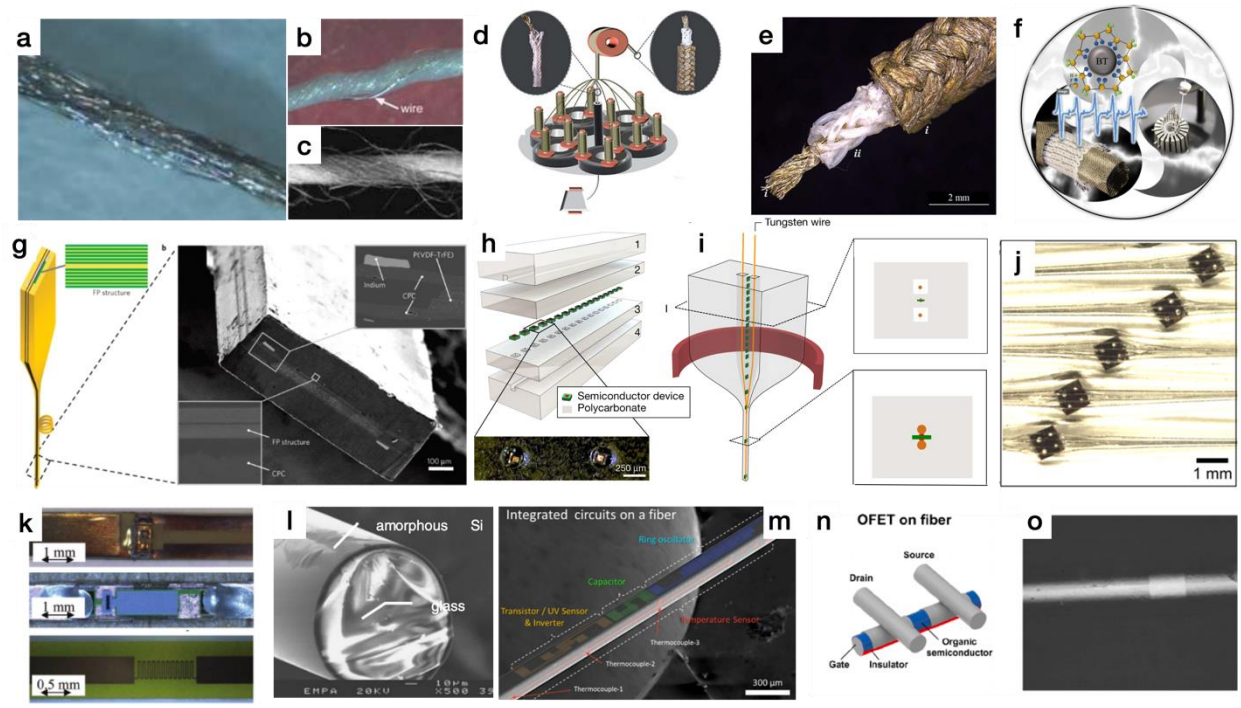

Figure 2.12: Various types of electronic fiber and yarn: a) Common core fiber wrapped with conductive fibers [68], b) Metal wires and non-conductive fibers twisted together, c) Silver coated and common yarns twisted together, d-e) Braiding and f) circular knitting techniques to create multi-layer piezoelectric fibers [71], Thermally-drawn g) thin piezoelectric filament structure [72], h) polycarbonate with embedded LEDs and Tungsten wire, and i-j) temperature and memory I2C devices [66], [67], k) temperature sensor, transistors, and LED fabricated on top of polyimide filaments [63], [73], l) SEM picture of a-Si grown on a glass fiber, m) Scanning electron microscopy (SEM) picture of inorganic, integrated circuits fabrication on a silicon fiber [74], n-o) configuration and SEM image of organic field effect transistor fabricated on a fiber surface [75].

Preform drawing processes have also been explored to develop multi-material and multifunctional electronic fibers (e-fibers) for a broad range of applications [72]. For instance, widely-available copper wires, optical fibers, as well as shape-memory alloy (SMA) wires are each developed using fiber drawing methods. Before becoming advanced electrically-functional fibers, a macroscopic preform is prepared by layering and distributing various polymers, electronic materials, and devices such as low-temperature metals, piezoelectric materials (Figure 2.12g), semiconductor devices (Figure 2.12h), and microchips (Figure 2.12i-j). The preform is then melted and mechanically-drawn through a temperature or laser-controlled drawing device. The

method enables long fiber production with complex cross-sectional architectures for electrical signaling, optical networking, and microfluidic system [76]. This process can also be used to develop length-wise distributed electronic devices such as transistors, diodes, and MEMS together with interconnects using doped semiconductor materials or commercially available complementary metal-oxide-semiconductor (CMOS)-based dies [72].

Finally, researchers have also leveraged nano and microfabrication techniques to fabricate fiber or filament transistors and sensors using either inorganic such as IGZO (Figure 2.12k,m) [63] or organic semiconducting materials (Figure 2.12n,o) [77]. A Si-coated silicon oxide glass and sintered silicon carbide (SiC) fiber has also been fabricated through this fiber extrusion method as a substrate for on-fiber integrated circuits (Figure 2.12l) [74]. Even though the preform drawing method requires precision control of the melt flow and engineering of the preform material's viscosity and thermal expansion, it is more scalable and cost-efficient compared to nano and microfabrication procedures. A synergy between these two methods needs to be further explored to solve some of the technical challenges in developing a dense system-on-fiber.

2.3.2.1 Yarns

We can apply numerous yarn structures on e-fibers to achieve further functionality and mechanical stability before they are integrated into e-textiles. Yarns can be assembled by twisting, twining, and blending (Figure 2.12a-c), as well as braiding (Figure 2.12d,e) many fibers across the axial direction [71], [78]. Twisted electroactive fibers such as CNT, for example, have been demonstrated to produce artificial muscle yarns [79], as well as energy-harvesting yarns that electrochemically [80] or triboelectrically [81] convert torsional to electrical energy.

As a traditional form of cultural practice that has existed for a thousand years, braiding techniques can be used to develop a more complex electronic yarn structure. The most common braiding architecture is a 2D biaxial braid. This biaxial braid can create a textile skin that insulates a core conductive yarn, typically used for e-textile transmission lines. Multiple layers of biaxial braid can also yield a sandwich-type (Figure 2.12f) structure, useful for creating capacitive, piezoelectric, and piezoresistive yarns, with an active or dielectric layer in between two electrode layers. By orienting an additional yarn into the biaxial structure longitudinally, we can also construct a triaxial braid. A biaxial base in a triaxial braid, for instance, can be used as a structural reinforcement for multiple optical or other types of core fibers.

2.3.2.2 Fabrics (with a focus on knitting)

We can apply a solution-based coating and bath, as well as dry fabrication methods, to form an electroactive layer on the surface of a fabric. Solution-based methods such as screen or ink-jet printing of active materials provides a better commercial advantage, since it can be adapted for roll-to-roll (R2R) manufacturing [82]. Another technique is integrating a much more complex system-on-textile by attaching or embedding flexible or stretchable circuit board assemblies on or into fabrics [83], [84]. For hierarchical 1D fiber integration into 2D textile, there are three common types of 2D textile structure: knitted, woven, and non-woven. Non-woven textiles are fabricated by chemical, thermal, or mechanical bonding of staple or long fibers into a single continuous layer, while knit and woven textiles are formed by architecting multiple fibers into a specific structure and pattern. Woven textiles consist of two sets of yarns that are orthogonal and alternately cross-over each other. Weaving generates dense textiles that are mostly found for upholstery, interior fabrics, and protective skins. Its 2D array structure can be employed to develop e-textile sensors and interconnects that benefit a large-array of row-column grids and contacts such as pressure sensors, transistor matrices, or IC routings [61], [69].

Knitted textiles, on the other hand, are constructed through interlocking loops of one continuous strand of yarn. Due to the loop formation and porosity, they are typically more stretchable and breathable than woven textiles. Apparel industries, including medical fabrics and sportswear, rely heavily on knitted textiles. The unique structural characteristics of knitted textiles have been explored in, for example, the design of strain sensors from conductive and piezoresistive yarns, as well as fabric-based actuators from shape-memory polymer (SMP) and muscle yarns. Automatic in-lay techniques in the weft direction have also been leveraged to distribute sensing fibers that are structurally larger than the rest of the fibers in a knitted textile. The in-lay technique is beneficial for larger fibers and fibers with higher modulus as they are either not able to be knitted or caught by the knitting machine needles. In addition, in a technique that is similar to temperature-controlled wire drawing or electrospinning, 3D printing can also be utilized to directly deposit electronics-integrated composites onto various soft 2D to 3D textile structures [85].

Figure 2.13 demonstrates various e-textiles fabricated through a knitting process. Stretchable textile transmission lines and antennas can be knitted in single-jersey layer configuration using highly conductive yarns from purely metal fibers (Figure 2.13a) or silver-coated filaments (Figure 2.13b) [86]. The number of yarn density, as well as loop rows or columns can be decided to tune the overall resistance of the interconnects. Flat-bed knitting machines that produce two-layer configurations can be used to develop multi-layer spacer fabrics. By knitting two conductive layers separately as front and back-knit and having one zig-zag knit inbetween that connects both

layers as insulator or resistive layers, we can develop piezoresistive capacitive, or piezoelectric pressure sensing textiles. Figure 2.13c, for example, presents a sandwich-type capacitive sensor with conductive and non-conductive yarn blend in the top and bottom layers and non-conductive yarn as a spacer, while Figure 2.13d shows a spacer fabric with polyester and silver-coated yarn blend in two top and bottom layers and knitted PVDF spacer layer sandwiched in-between [87].

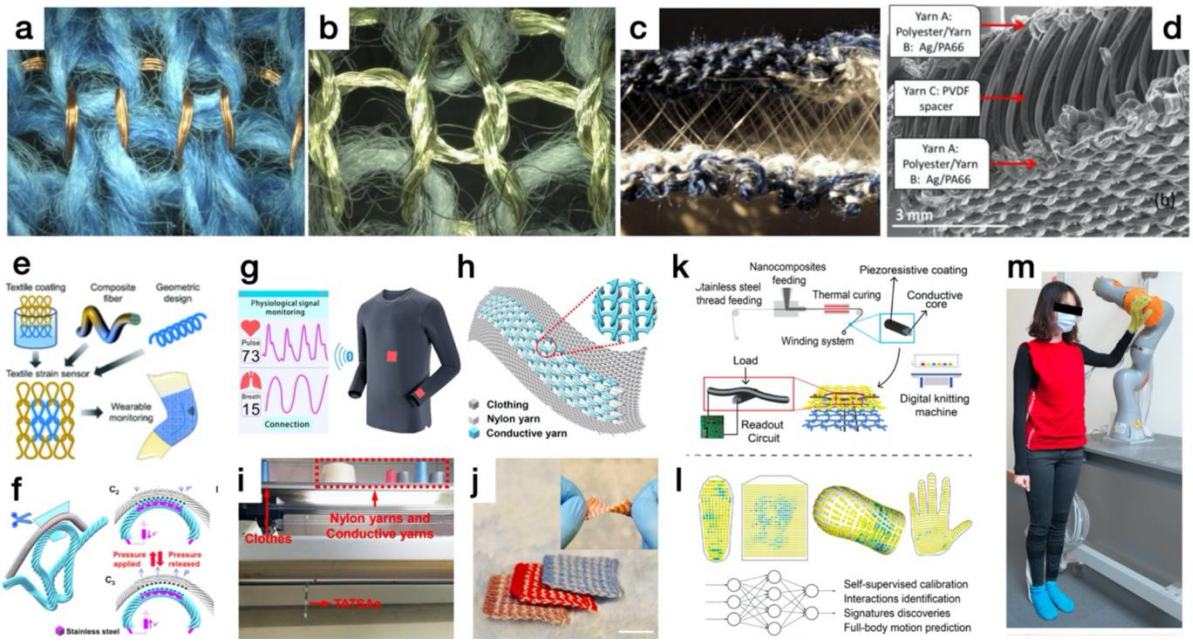

Figure 2.13: Knitted textile sensors and interconnects. a) knitted copper strands and b) silver-coated polyimide filaments as transmission lines [86], c) weft-knitted spacer fabric with conductive (grey) and nonconductive (blue), separated by non-conductive spacer as capacitive pressure sensor, d) cross-sectional SEM of knitted piezoelectric-conductive spacer fabric [87], e) various fabrication methods of knitted textile strain sensor [88], f) working principle of triboelectric knitted textile sensor. g) Triboelectric knitted sensor integrated into a shirt for physiological monitoring [89], showing: h) schematic illustration of the knitted structure and yarn materials, i) computerized flat knitting machine that integrates both conductive and nylon yarns, and j) customization the knitted sensor in various base colors. k) Fabrication process of piezoresistive functional fiber [90], l) machine-learning network applied onto the sensor array data of piezoelectric fabric for activity recognition, m) knitted pressure sensing array in the form of an artificial robotic skin.

The stretchable nature of knitted textiles has been studied in the design of soft strain sensors, as shown in Figure 2.13e. Conductive or resistive threads can be knitted into customized fabrics and geometrical design can be used to specify the active sensing area. Contact resistance in between the conductive loops changes due to the structural adaptation of the fabric upon stretching [91]. Another approach is to develop composite fibers that change resistance or capacitance upon

stretching by coating, drawing, or twisting conductive polymers and then knit or in-lay the fiber onto the textile structure [92]. Coating a common base knitted fabric with conductive polymers or carbonizing it [93]–[95] can also be done to achieve electrical properties and strain sensitivity. The sensing response of the latter two methods is influenced by both the intrinsic electrical property due to the conducting polymer network of the fiber and the interfacial contact resistance due to the structural change of the knitted fabric's loop structure upon stretching. We can also measure textile strain by employing capacitive techniques. A knitted capacitive strain sensor has been developed by fusing a stretchable insulator between two conductive fabrics; the active area and thickness of the sandwich structure change upon stretching and influence the total capacitance of the sensor [96]. Furthermore, conductive yarns that are seamlessly knitted onto medical shirts or undergarments can be utilized as electrophysiological sensing electrodes [97].

Knitted structures have also been studied to harvest triboelectric energy due to slippage, tension, and pressure of conductive-nylon yarn loops (Figure 2.13f) [89]. The result is an all-textile triboelectric knitted sensor that can be seamlessly knitted into clothing for health monitoring and sensitively measure static pressure due to respiration, heart contraction, and blood flow (Figure 2.13g-j). Other applications of wearable knitted sensors are activity recognition and robotic tactile skin. As illustrated in Figure 2.13k, a piezoresistive yarn is developed by coating and thermal curing of graphite and copper nanoparticles in PDMS elastomer on a stainless-steel thread [90]. The piezoresistive yarn is then automatically woven in a knitted fabric with an in-lay technique using digital machine knitting. The configuration of these two-layer fabrics then creates a pressure-sensing matrix that can be used to detect surface interaction and predict full-body motion (Figure 2.13l). The piezoresistive knitted textile can be three-dimensionally designed to form a vest, shoe, glove, and artificial robotic skin (Figure 2.13m). Since textiles are ubiquitous, as they cover most parts of our body and our home and building environments as flooring, beddings, upholstery, and interior and exterior skins, they can be leveraged for various applications from sensing our physiology, physical activity, interaction, to environmental patterns.

2.3.2.3 Scaling and Translation

Most of the current research in e-textiles, as previously discussed, largely explored the fabrication of smart or electronic textiles through methods such as embroidery, stitching, sewing, or attachment or embedding electronics into textile substrates [25], [57]. These boutique or hand-made approaches, while valuable for prototyping and experimental purposes, pose significant limitations in terms of scalability, durability, and integration of electronic functionalities on a

large scale. The inherent challenges in achieving rapid, large-scale, dense, and seamless fabrication have thus hindered the widespread adoption of e-textiles.

Existing products include the MiMu Glove, which incorporates embedded flex sensors and conductive threads to capture and translate hand movements into digital signals for music production [98]. This glove utilizes on-board IMU attached on the textile glove to achieve high precision in gesture recognition. Another example is Ralph Lauren's PoloTech electrocardiography (ECG) shirt, which integrates silver-coated fibers capable of monitoring the wearer's heart rate and transmitting physiological data in real-time [99]. Additionally, Neurable has leveraged fabric-based electroencephalography (EEG) electrodes embedded in headsets, facilitating non-invasive brain-computer interface applications by detecting and interpreting brainwave activity with high fidelity [100].

The realization of commercial e-textile products can be attributed to several factors. Firstly, the integration of electronic components into textiles poses significant challenges in terms of maintaining fabric flexibility, washability, and durability. Traditional electronic materials often lack the mechanical properties required for textile applications, leading to potential failures during use. Secondly, the manufacturing processes for e-textiles are complex and require precise control over the placement and integration of conductive elements, making large-scale production challenging and costly. Thirdly, there is a need for robust and reliable power sources that can be seamlessly integrated into the textile without compromising its aesthetics or comfort. Finally, the market for e-textiles is still emerging, with limited consumer awareness and acceptance, further constraining the commercial viability of such products.

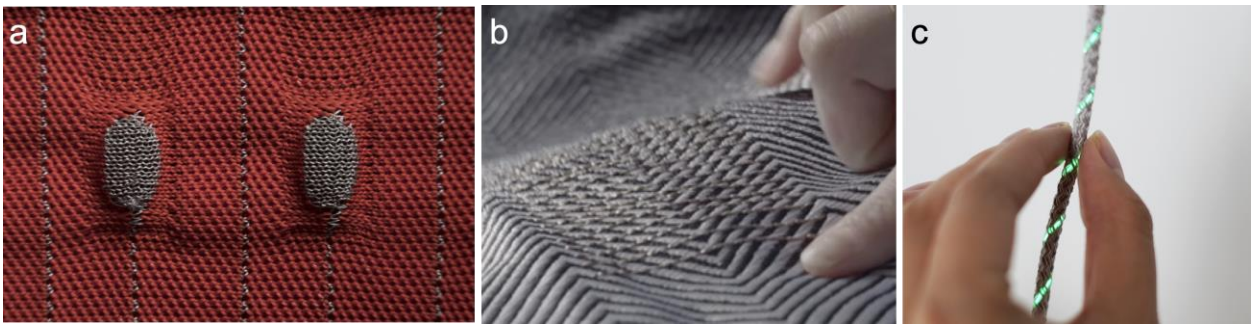

Figure 2.14: a) *SensorKnits* touch buttons machine-knitted from conductive yarns [101], b) conductive threads woven using industrial weaving machine from Google Jacquard multi-touch sensitive jacket [69], c) braided touch-sensitive and optical fibers for interactive cords [102].

To overcome these limitations, several works have leveraged industrial manufacturing techniques to integrate functional fibers and demonstrate the scalability of e-textile products. Project Jacquard [69], for instance, proposes the customization of yarns by twisting thin

conductive wires with common threads, incorporating industrial weaving processes. This approach, combined with the design of custom connectors and pluggable processing and wireless modules, resulted in the Levi's Commuter Jacket, a functional garment capable of physical gesture detection. Similarly, *SensorKnits* [101] utilizes digital fabrication techniques in machine knitting to create dynamic structures of knitted textiles that can sense pressure and strain, functioning as a rheostat through various knitting patterns of conductive and standard yarns. I/O-Braid [102] explores braiding techniques with conductive and optical fibers to develop interactive textile cords with embedded multi-modal sensing and visual feedback capabilities.

Going deeper, researchers are exploring nano/microfabrication technologies to fabricate on-fiber electronic devices [77]or employing industrial fiber extrusion methods such as thermal-drawing or fiber-spinning to develop electrically-conducting yarns [72]. These methods aim to enhance the conductivity, durability, and integration of electronic components into textiles. Additionally, efforts are being made to distribute discrete devices such as temperature ICs and diodes into electronic fibers [66], [67], paving the way for the next generation of e-textiles that combine functionality, scalability, and user comfort.

2.4 From Sensate to Computational Substrates

2.4.1 Soft Electronic Skins

Recent advances in new materials, device designs, and fabrication strategies have established a new form of soft electronics that are biocompatible and can be flexed and stretched to bridge the biological, geometrical, and mechanical mismatch between electronics and the human body [103]. They enable a myriad of novel wearable and implantable applications, from physiological and physical activity sensing (Figure 2.15l), to prosthetics and robotics (Figure 2.15a). Electronics for the human body can be classified into three categories: implantable, on-body, and carry-on electronics [104]. The smartphone is the best example of carry-on electronics. Implantable electronics require invasive techniques to regions under the skin, for instance, to the brain, spinal cord, or organs, such as heart, lung, and diaphragm [3,4]. On-body electronics can be further classified into wearables and on-skin devices. Wearables can show up in the form of clothing or accessories such as electronic textile smart-suits and smartwatches [84], [107], while on-skin devices can be intimately laminated on to the skin and adhered through van der Wall force in epidermis [108], or are attachable in the form of skin bands (Figure 2.15e-f) or stickers (Figure 2.15k-l) [6,7].

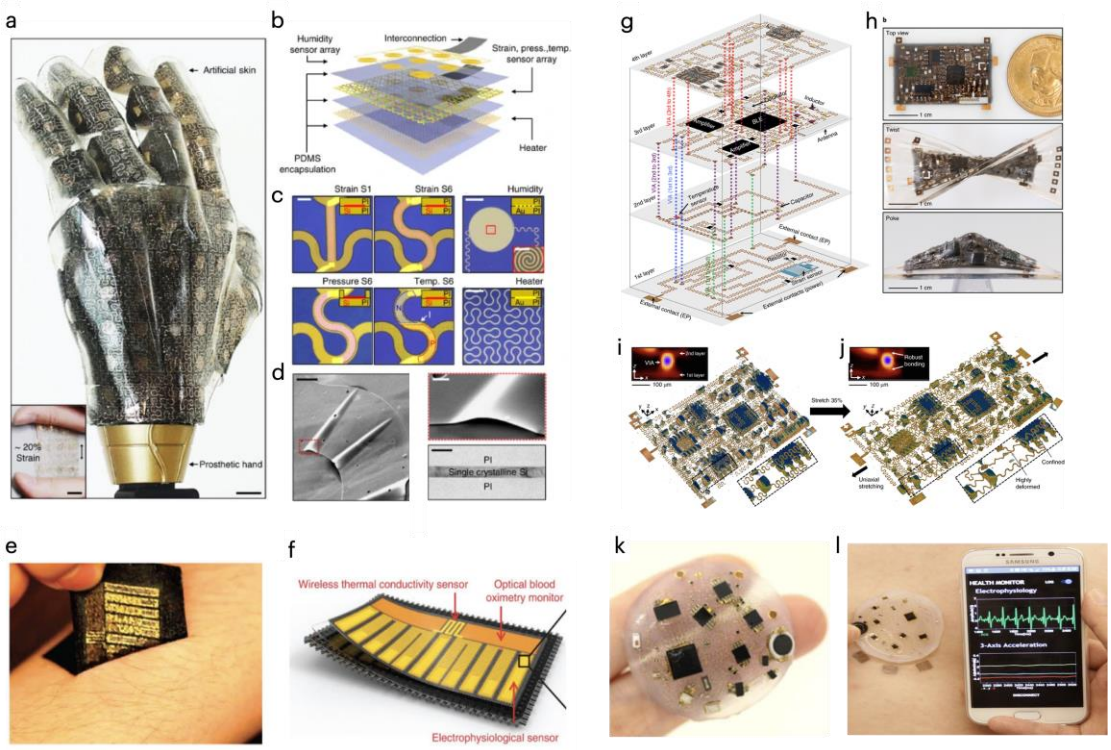

Figure 2.15: Flexible and stretchable electronic devices, a-d) Silicon nanoribbon multimodal sensing arrays for smart prosthetic skin [111], e-f) Breathable electronics on fabric for multi-modal physiological sensing (reprinted from Jang *et al.* [109]), g-j) multi-layer stretchable circuits [112] and k-l) 3D-network of soft and stretchable electronics [113] for wireless physical and physiological monitoring.

The performance and use-cases of flexible and stretchable electronic devices are defined by their material properties, choice of substrates, and fabrication techniques. Most state-of-the-art flexible electronics are developed by fabricating [114] or transfer-printing [115] devices on flexible substrates or by thinning down silicon wafers with methods such as dry etching, wet chemical etching, grinding, chemical-mechanical polishing, and exfoliating [116]. On the other hand, stretchable electronics are realized by developing intrinsically stretchable materials [26], designing serpentine (Figure 2.15g) or helical (Figure 2.15k) interconnect architecture that allows stretching of rigid structures on an elastomeric substrate [117], or leveraging a buckling mechanism by pre-stretching an elastomeric substrate [118]. Even though the most currently used substrates in multi-layer printed circuit manufacturing are rigid and flexible polyimide, new potential substrates such as thermoplastic TPU, PDMS, and Ecoflex have been explored and have great potential in various applications [112], [119]. These materials offer unique advantages in terms of flexibility, stretchability, and biocompatibility, making them suitable for wearable electronics, medical devices, and other applications requiring conformability to complex surfaces (Figure 2.15g-j).

2.4.2 Distributed System-on-Materials

Despite the tremendous amount of research in flexible/stretchable devices and soft electronics over the last two decades, the emphasis has primarily been on specific sensing modalities and novel fabrication technologies with limited spatial coverage. Applications of e-skin have thus been limited to smaller-area wearable physiological and physical activity sensing. These studies, mostly applying row-column addressing and centralized processing, have not yet sufficiently addressed the major challenge of realizing a scalable, customizable, and robust e-skin that could cover a large substrate and handle a significant amount of tactile and environmental information.

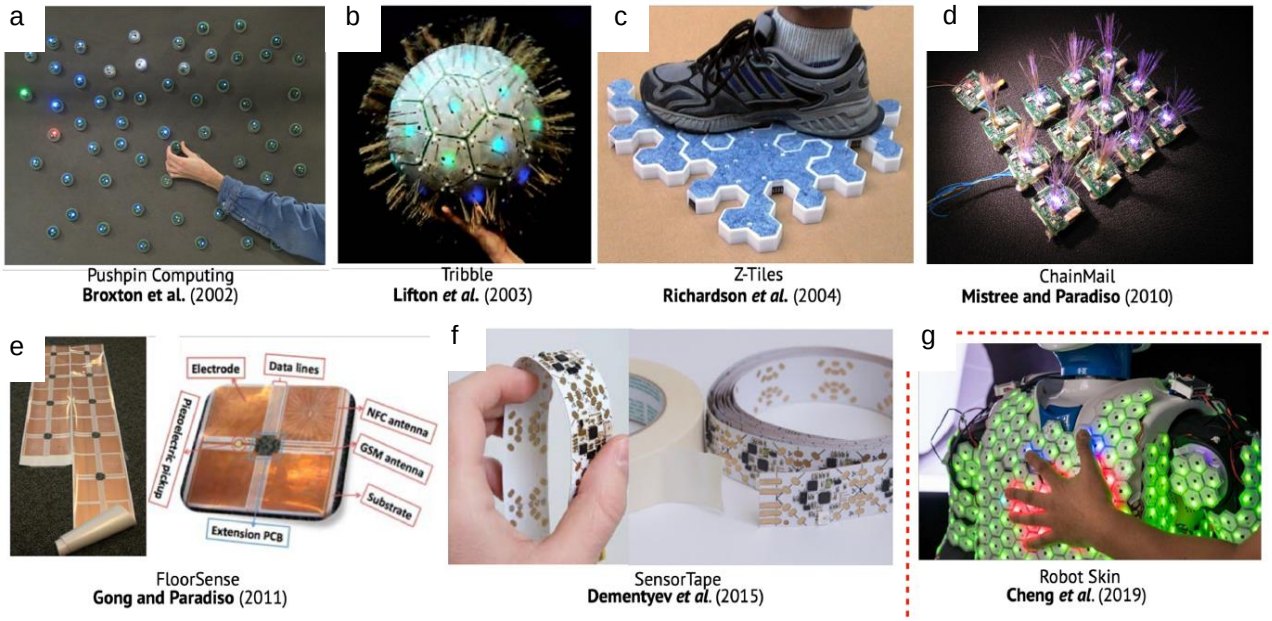

Figure 2.16: Evolution of the *Sensate Media*, from a) *Pushpin Computing*, a planar test-bed for sensor networks that can be inserted and repositioned on a powered substrate board [120], b) Tribble, 32 pieces of tessellated sensor-actuator network [121], c) *Z-Tiles*, modular pressure-sensitive reconfigurable tiles (with 20 pixels per tiles) [122], d) *ChainMail*, a suite of rigid sensorized skin attached to each other through flexible interconnects [123], e) *PrintSense* for the floor, distributed conductive inkjet-printed sensors for contact and proxemic sensing [124], [125], f) *SensorTape*, linear sensor network in the form of a tape, which utilized scalable, flexible PCB technology [126], and g) external work by Cheng et al. which consists of linked rigid PCBs tiles, similar to Tribble or *ChainMail*, but in a significantly higher density [127].

Projects by Hughes and Correll [128] and Cheng et al. [127] tried to apply distributed networking principles in their e-skin systems. However, they lack sensing modality, and their form factors are still rigid, limiting their suitability for dynamic and adaptive surfaces. Efforts in the Responsive Environments Group at the MIT Media Lab, starting from the *Rhythm Tree* [129] and *Pushpin Computing* [120], aimed to realize various rigid, tessellated, and flexible sensor systems by leveraging dense, reconfigurable, peer-to-peer, and multimodal networks that are broadly called the *Sensate Media* (Figure 2.16) [130].

Tribble (Figure 2.16b), for example, consists of 32 tessellated, rigid PCBs with multimodal sensor and actuator networks [121]. Each tile in this truncated icosahedron resembles a coarse patch version of biological skin. We have also explored other mechanisms and circuit fabrication methods to develop these scalable e-skins. *ChainMail* (Figure 2.16d) consists of small (1″ x 1″) PCBs with a suite of sensors, including whisker sensors, attached to each other through flexible interconnects, allowing the entire skin to be bendable for contact and proxemic sensing interactions [123]. Applying this work to Cheng et al.'s robotic skin (Figure 2.16g) [127] would enable conformable, large-area multifunctional skin for various applications, including stroke and tactile sensing, as well as obstacle avoidance. In a flexible format, *PrintSense* is distributed processor that each connects to inkjet printed sensors for large-scale surface sensing on the floor [124], [125], while *SensorTape* (Figure 2.16f) is a programmable, bendable sensor network with integrated ICs on each node that can be cut and rejoined for easy customization [126]. Along with other sensing modalities, the networked IMUs in the *SensorTape* system enable shape-sensing applications as the tape is bent, twisted, or wrapped onto a curved object

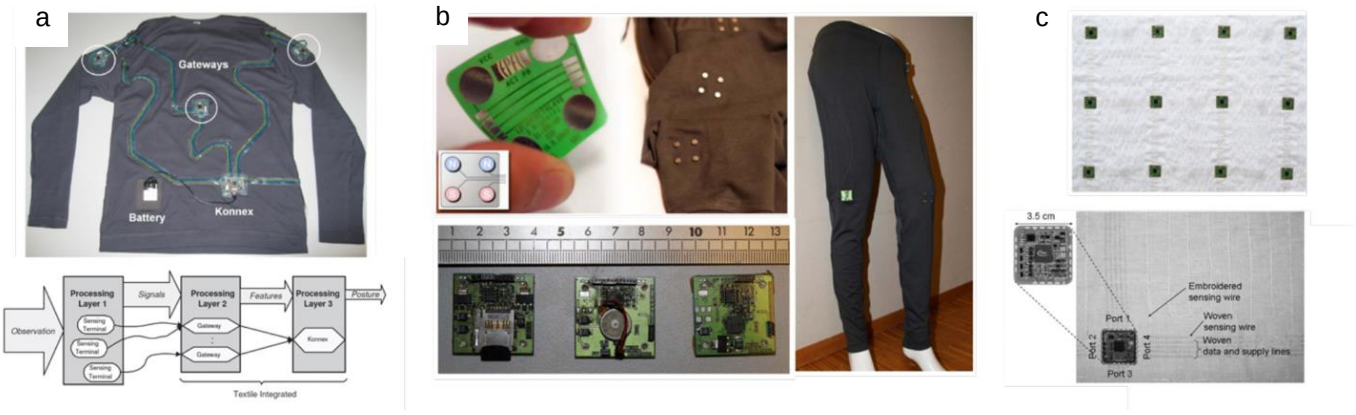

Figure 2.17: Distributed sensor network on textiles: a) multiple accelerometers connected to the main processing module through gateways for posture recognition garment [131], b) magnets as mechanical and electrical connectors to the bus for personalized wearables [132], and c) self-organizing and fault-tolerant distributed sensor network on fabrics based on capacitive conductive fibers [133].

Some forms of distributed processing in an e-textile or soft network exist in research publications; however, as shown in Figure 2.17, they are not dense and stretchable, which restrains them from wearable applications. There is a significant mechanical mismatch between their rigid circuits and the base fabric substrate. Their modalities are also limited, involving either distributed IMU (Harms et al. [131], Righetti and Thalman [132], Zhou et al. [134]) or capacitive sensors (Glaser and Lauterbach [133]). These examples underscore the significant untapped potential and exploration needed in developing distributed systems on textile, soft, and stretchable substrates. By addressing the challenges of scalability, customizability, and robustness, future research can unlock new possibilities for large-area, multifunctional e-textiles and computational substrates.

2.4.3 Paintable and Amorphous Computing

The concept of computational materials has been a significant focus of research and innovation since the Smart Matter program at Xerox PARC in the late 1990s [135]. This vision aims to embed computational capabilities into materials, transforming surfaces and objects in the environment into interactive and intelligent systems. One approach involves printing functional electronic materials onto large surfaces. This method envisions creating extensive arrays of passive sensors that can be manufactured cost-effectively through roll-to-roll processes and laminated onto walls and other surfaces [136]. Such large-area passive sensors can facilitate integrated sensing systems capable of environmental monitoring and interaction.

Another strategy emphasizes miniaturizing sensors and embedding them into materials using microelectromechanical systems (MEMS) and integrated circuit (IC) technology. These tiny sensors can be dispersed throughout a smart surface, akin to raisins in pudding [136]. Advancements in microelectronics have significantly reduced the costs of manufacturing complex logic circuits, sensors, actuators, and communication devices. According to Abelson et al., these integrated particles can be mixed with bulk materials such as paints, gels, and concrete, converting them into intelligent, responsive surfaces capable of sophisticated interactions [137].

Future advancements in process technology are expected to enable the production of autonomous computing elements that are as small as large sand grains and available at bulk prices. This miniaturization, combined with a reduction in sensor and actuator footprints, will transform personal computing. As these computing elements become more resilient to environmental stress, they will migrate from expensive, precision-engineered motherboards into everyday objects such as building materials, furniture, and clothing, making intelligent systems ubiquitous. This shift will change the perception and handling of computation, transitioning from discrete devices, such as smart dust [10] to bulk materials.

Paintable computers represent a revolutionary approach to programming computational materials based on amorphous computing manifesto [138]. The particles are distributed pseudo-randomly and communicate locally with their immediate neighbors. Upon initialization, they form a network by enumerating their neighbors without hardware support for distance or orientation estimation. This localized interaction model allows particles to perform complex sensing and computational tasks collectively, despite being blind to the world beyond their immediate communication radius. In conclusion, the realization of computational materials is driven by advancements in both large-area sensor printing and miniaturized embedded sensors. Whether through the deployment of extensive sensor networks on surfaces or the integration of compact computing elements into materials, the future promises a world where intelligent systems are embedded into every aspect of our environment.

Chapter 3: Fundamental of Machine Knitting and Conductive Textiles

"Whenever Nell's clothes got too small for her,
Harv would pitch them into the deke bin and then have the M.C. make new ones.
Sometimes, if Tequila was going to take Nell someplace …
she'd use the M.C. to make Nell a special dress with lace and ribbons"
Neal Stephenson, Diamond Age (1995)

As illustrated in Figure 3.1, there are three common types of 2D textile structures: woven, weft knit, and warp knit. Each of these structures has distinct characteristics and methods of construction. Woven textiles consist of two sets of yarns, the warp and the weft, that are interlaced at right angles to each other. The warp yarns run vertically while the weft yarns run horizontally. The weaving process involves interlacing the warp and weft yarns on a loom. The warp yarns are held under tension while the weft yarns are passed over and under the warp yarns in a specific pattern. This orthogonal arrangement results in a fabric that is generally stable and durable with limited stretch. Woven textiles can vary in density and pattern depending on the weaving technique used, such as plain weave, twill weave, or satin weave.

Knit textiles, in contrast, are constructed from a single yarn that forms loops either horizontally or vertically. In weft knitting, the yarn is looped back and forth across the fabric width, forming interconnected horizontal loops. This method can create a variety of patterns and textures. Due to their loop formation and porosity, knitted textiles are typically more stretchable and breathable than woven textiles, making them suitable for apparel, including medical fabrics and sportswear. In warp knitting, multiple yarns form loops vertically, creating a fabric with increased stability and reduced elasticity compared to weft knits.

In knitting, the direction of the loops plays a crucial role in defining the fabric's properties. The horizontal direction in weft knitting is known as the course direction, while the vertical direction in warp knitting is referred to as the wale direction. The course direction influences the fabric's widthwise stretch and flexibility, whereas the wale direction affects the fabric's lengthwise stability and strength. Understanding these directional characteristics is essential for optimizing the performance and application of knitted textiles.

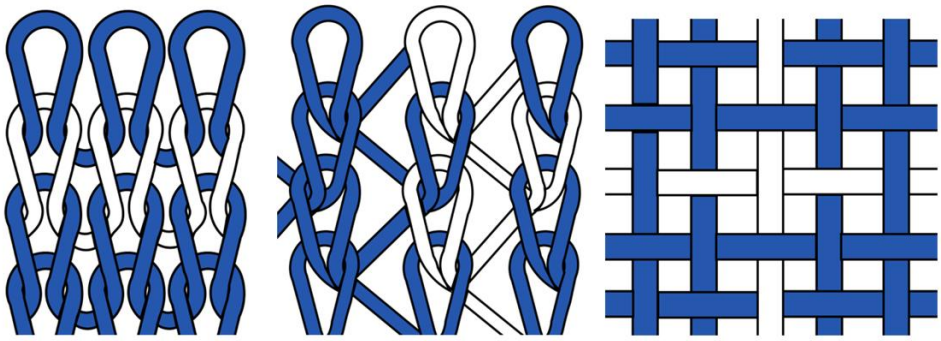

Figure 3.1: Structural difference between weft knit, warp knit, and woven fabrics.

In this section, we will discuss in depth digital knitting techniques, knitting structures, and how we can leverage knit electromechanical properties to develop knitted interconnects and sensors. Knitting techniques can be classified based on the direction of loop formation, the configuration of the needle bed, and the number of yarns used. When loops are created horizontally, known as courses, with the carriage passing usually a single yarn, the textile is termed weft knit. In contrast, when loops are formed vertically in columns by separate yarns, it is referred to as warp knit. In this dissertation, we will concentrate solely on weft knitting.

3.1 Digital Knitting

In recent years, advances in mechatronics, computer-aided design, and knitting technologies have pushed forward utilization of digital machine knitting and led a diverse range of knit textile and knitwear on the market, from high-quality apparel to technical fabrics [139]. The unique and

versatile architecture of knitting enable us to engineer various geometrical, textural, and mechanical properties of textiles, from soft, stretchable, and breathable to rigid and firm structural textiles. The components of a knitting machine include the needle-bed equipped with needles, which are crucial for holding the loops of yarn; the yarn carriage, which slides and controls the movement of these needles; yarn carriers or guides that accompany the carriage to deliver the yarn precisely where it is needed; sinkers for laying in yarns; and a roller or take-down system responsible for rolling and pulling down the formed textile.

Digital knitting is a computer-aided, automatic process of building interlocked loops from multiple strands of yarns (Figure 3.2b). It employs an array of needles or hooks that goes up and down to catch the yarns based on an instruction file. Each yarn is fed to the machine from a cone, passing through a tensioning mechanism towards a yarn carrier. With a knitting machine, it is possible to simultaneously or sequentially knit multiple yarns. These yarn carriers move sideways as the needles grab the yarn to form new loops. The number of needles used in the machine and the yarn carrier number of movements will then define the final width and length of the knit fabric. The process starts with a needle raising up until the latch goes over the loop. New yarn is then transferred through, and the needle then goes down to catch the yarn. Afterward, the latch is knocked over by the previous loop, closed the needle, and a new loop is formed as the fabric is rolled down automatically per new weft. The needle is then ready to repeat the process and form the next loop. Since digital knitting is an additive manufacturing process, it is a rapid fabrication technique that overall creates less waste since we do not need any post fabrication such as manual cutting and sewing.

The needles hold the loops of yarn and are thus one of the key components of the knitting machine. The two most common modern knitting needle types are the latch needle and the compound (or slide) needle. The latch needle is a type of knitting needle that features a latch, or a small, hinged hook, which closes to catch and hold the yarn during the knitting process. As the needle moves, the latch opens to allow the yarn to enter and then closes to pull the yarn through the existing loop, forming a new stitch. Latch needles are versatile and commonly used in both circular and flat knitting machines due to their ability to handle a wide range of yarn types and thicknesses.

The compound needle, also known as the slide needle, consists of two parts: a hook and a sliding latch that opens and closes to catch the yarn (Figure 3.2a). The hook holds the yarn while the sliding latch moves to secure and release it, creating a stitch. Compound needles are typically used in high-speed knitting machines and can provide greater precision and control, making them suitable for fine gauge and complex fabric structures. In the knitting machine that we use, we employ latch needles.

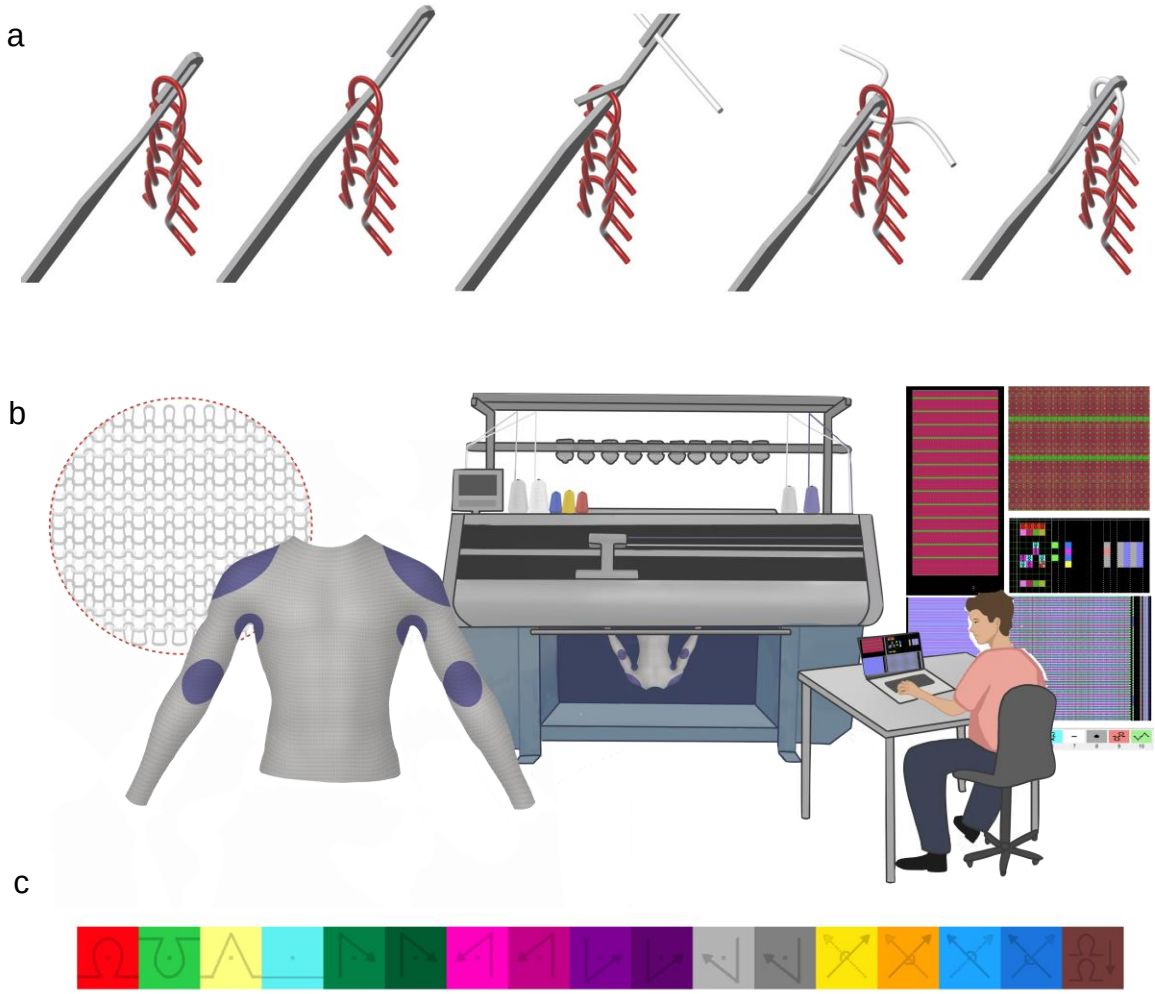

Figure 3.2: a) Knitting action for a loop, from yarn extending out to catch a yarn and sliding back down to close and make the loop, b) Knitting machine outputting a textile product with a user designing a pattern to a visual programming environment, and c) color coding of the common 17 knitting instructions, including knit and purl (front and back stitches), tuck, miss, front, back, left, cross, and stack.

3.1.1 Programming and Package Development

Low-level machine knitting programming entails direct control over the knitting machine's hardware through specific, detailed instructions (Figure 3.2b,c). This process necessitates a deep understanding of both the mechanics of the machine and the desired textile output. The programming focuses on needle selection and manipulation, which determines the operational mode of each needle, such as knitting, purling, tucking, or holding. This precision is vital for creating a variety of stitch patterns. Additionally, it involves managing yarn tension and feed rate to ensure consistent stitch quality and prevent issues such as dropped stitches or yarn breakage.

A prevalent method for representing low-level knitting programs is through time-needle images. In these representations, the x-axis corresponds to the needle positions, while the y-axis going from bottom to the top represents time. Each pixel or color block, referred to as a stitch code, encodes a specific needle operation or a machine state, or sometimes a combination of both. Beyond color and stitch type, color blocks can also denote other critical machine settings, including the activation and location of yarn carriers, tension adjustments, and the speed of the carriage. Machine states are either explicitly encoded in dedicated sections of the time-needle program or implicitly within the stitch codes. This visual format allows for detailed and comprehensive control over the knitting process, ensuring precise execution of complex patterns.

To streamline the transition from high-level designs to machine-executable instructions, package development plays a crucial role in modularizing and abstracting knitting programs. These packages allow designers to work with high-level stitch codes that represent complex knitting patterns and configurations. The packages use pattern matching techniques to associate these high-level color blocks with corresponding low-level instructions, effectively creating an abstraction library of reusable components. This modular approach simplifies the design process by enabling designers to focus on the creative aspects without delving into the intricacies of machine operations. As a result, designers can create intricate and scalable textile patterns more efficiently and with greater ease.

3.2 Types of Machine

3.2.1 Flat-bed Knitting Machine

Flat-bed knitting machines are highly versatile within the knitting industry, particularly due to their configuration with two arrays of needles, known as the back bed and front bed (Figure 3.3). This dual-bed setup facilitates the creation of two layers of single jersey knitted fabric, which can be either joined at the ends to form tubular structures or interlocked at every other loop to produce a single, thicker fabric. Such configurations enable extensive design flexibility, allowing for the fabrication of complex fabric shapes. Continuous lengths of knitted fabric can be produced and subsequently cut to the desired dimensions, with these tubular fabrics being assembled to create garments. The optimization of flat-bed knitting machines involves careful adjustment of several critical parameters and settings.

Gauge: Gauge is defined as the number of needles per inch on the needle bed, directly influencing the fineness of the resultant fabric. Higher gauge machines, with a greater number of needles per

inch, produce finer textiles suitable for delicate applications, while lower gauge machines yield coarser fabrics ideal for more robust uses. For instance, a 12-gauge machine generates a finer knit compared to a 5-gauge machine, which is appropriate for heavier textiles.

Needle Bed Width: The needle bed width is a fundamental parameter that determines the maximum width of the fabric that can be knitted in one piece. Broader needle beds allow for the production of larger fabric panels, which is essential for creating wide garments or textile sheets without the need for seams, thus enhancing both production efficiency and design possibilities.

Stitch Length: This parameter regulates the length of the yarn within each stitch, significantly affecting the fabric's density and elasticity. Shorter stitch lengths result in tighter, denser fabrics with less elasticity but greater stability, whereas longer stitch lengths produce looser, more elastic fabrics, beneficial for applications requiring flexibility.

Stitch Density: Stitch density, influenced by both gauge and stitch length, refers to the number of stitches per unit area. A higher stitch density indicates a greater number of stitches packed into a given area, resulting in heavier and more textured fabrics. Adjusting stitch density is crucial for achieving specific fabric weights, textures, and appearances.

Yarn Tension: Proper yarn tension is crucial for consistent stitch formation and overall fabric quality. The tension of the yarn as it feeds into the machine must be meticulously controlled. Excessive tension can lead to yarn breakage and uneven stitches, while insufficient tension may result in loose and inconsistent stitch formation, thereby compromising fabric integrity.

Carriage Speed: The carriage speed, or the rate at which the carriage traverses the needle bed, impacts both production efficiency and fabric quality. While higher speeds can enhance productivity, they may compromise stitch quality if not properly managed. Therefore, a balance between speed and precision is necessary to maintain high-quality fabric output.

Stitch Cam Setting: The position of the stitch cam governs the depth of needle penetration, influencing stitch size and fabric thickness. Adjusting the stitch cam allows for the creation of various stitch effects and textures, essential for producing fabrics with the desired aesthetic and functional properties.

Take-Down Tension: This parameter refers to the tension applied to the fabric as it is knitted and drawn down from the needle bed. Maintaining consistent take-down tension is vital for ensuring uniform stitch dimensions and fabric quality. Proper take-down tension prevents fabric distortion during the knitting process, ensuring a uniform and high-quality end product.

Sinker Depth: Sinkers assist in holding the fabric in place as the needles move, with the depth of sinker penetration affecting fabric tension and stitch formation. Adjusting the sinker depth is critical for maintaining appropriate tension and ensuring even stitch formation throughout the fabric, preventing issues such as uneven tension or skipped stitches.

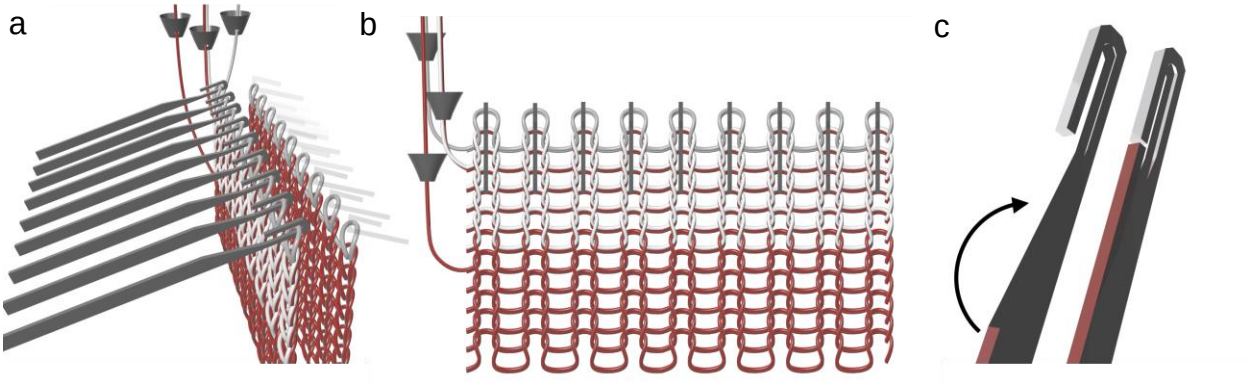

Figure 3.3: a-b) Front and back knit with three yarn carriers, and c) a needle with hook closing mechanism.

3.2.2 Whole-garment Knitting Machine

Whole-garment knitting machine is an improved version of flat-bed typically with double the number of beds (four in total) and the ability to construct and connect several tubes together. It could create a complete garment such as gloves or sweaters in a single production step without any waste materials, eliminating the need for cutting and sewing.

3.2.3 Circular Knitting Machine

Circular knitting machines produce lengths of fabric in the form of a tube rather than panels or panels sizes (Figure 3.4). It dramatically increases productivity because a continuous and faster circular motion replaces the relatively slow reciprocating motion of flat knit machines. Circular knitting is typically used to make various small-sized tubular garments such as socks, shoes, or sleeves. The main disadvantages of circular knitting machines are their limited ability to produce flat panels and the potential for less flexibility in garment design compared to flat-bed knitting machines. Additionally, they may not be as suitable for producing complex, multi-layered fabrics or intricate garment structures that require detailed shaping and patterning.

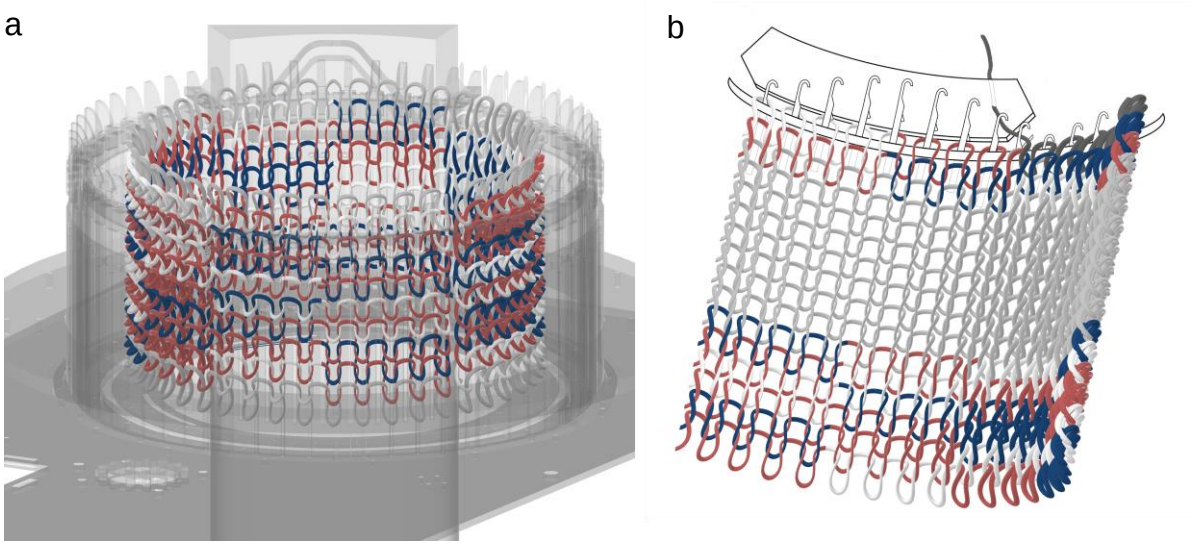

Figure 3.4: a) An illustration of a circular knitting machine with b) rotating motions and needles catching yarn in action.

3.3 Basic Knitting Operations

Machine knitting on a flat-bed (two-bed) knitting machine involves several fundamental operations, each contributing to the complexity and versatility of the knitted fabric. These operations include knitting, rib knitting, tucking, missing (or floating), transferring, increasing, and decreasing (Figure 3.5). Each operation plays a distinct role in the formation and manipulation of the textile structure. For creating holes in the fabric, the miss (float) and transfer operations are particularly effective, allowing for precise control over the placement and size of the openings. Increases and decreases are vital for shaping garments, enabling the creation of curves, contours, and fitted dimensions.

Knit (Plain and Rib). The knit operation is the most basic and essential knitting process. It involves creating a loop through all existing loops on a needle, then dropping the previous loops while holding the newly formed loop. The appearance of the stitch varies significantly depending on which needle bed it is performed on. For instance, stitches formed on the back bed are commonly known as purl or reverse stitches, while those on the front bed are plain knit stitches. Rib knitting is a variation where knit and purl stitches alternate between the front and back beds, creating a fabric with vertical ridges.

Tuck. The tuck operation is used to add texture and bulk to the fabric. In this operation, a new yarn is added to a needle that is either already holding a loop or is empty. This results in the formation of a tuck stitch, where the needle holds multiple loops before knitting them off together. Tucking can create intricate patterns and enhances the fabric's thermal properties and elasticity. It is a critical operation in producing textured and three-dimensional knit fabrics.

Miss (Float). The miss or float operation instructs a needle not to catch the yarn, allowing it to pass laterally without being knitted. This can create float stitches, where the yarn floats across the back of the fabric. When used strategically, missing stitches can create holes in the fabric, as the yarn skips over specific needles, leaving gaps. This technique is particularly useful for creating deliberate holes and openwork patterns, making it a good choice for lace and mesh designs.

Transfer. The transfer operation is crucial for creating complex knit structures. It involves transferring loops from one needle bed to the needle on the opposite bed. By transferring stitches and leaving some needles empty, holes can be formed. This method allows for precise control over the placement and size of the holes. Transfers are often combined with racking (offsetting between needles) to create intricate lace patterns and openwork designs.

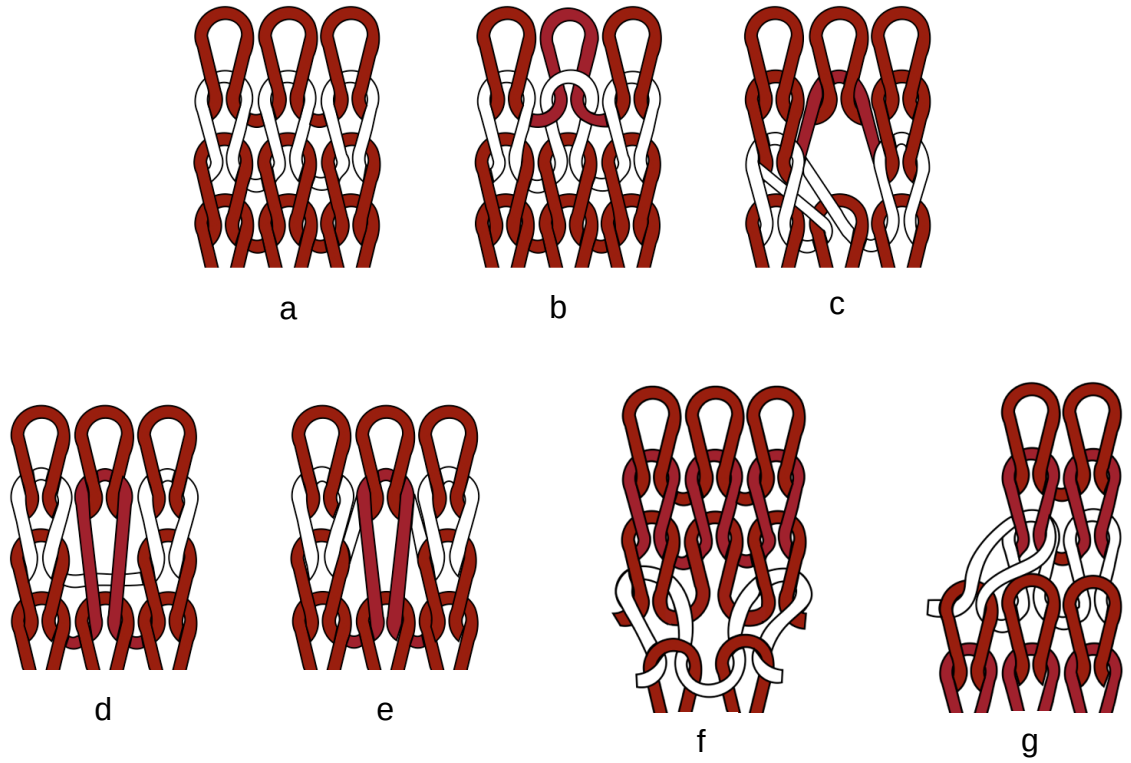

Figure 3.5: Various knitting operations, including a) plain knit, b) rib knit, c) transfer, d) miss or float, e) tuck, f) increase, and g) decrease

Increase. Increasing is a technique used to add extra stitches to the fabric, making it wider. This can be done by either placing new loops on empty needles or creating multiple loops on a single needle. In a flat-bed knitting machine, increases need to be done in a sequential manner to ensure that the yarn can be caught properly by the needles. Jumping too many rows at once can cause the needles to miss the yarn, resulting in dropped stitches and uneven fabric. Increases are essential for shaping garments, allowing for the creation of curves and contours.

Decrease. Decreasing reduces the number of stitches, making the fabric narrower. This can be achieved by transferring loops from one needle to an adjacent needle, thus reducing the total number of active needles. Similar to increases, decreases should be done in a subsequential manner to maintain the integrity of the fabric and ensure that the needles can properly catch the yarn. Abrupt decreases can lead to missed stitches and fabric distortion. Decreases are crucial for shaping garments, enabling the formation of tapers and fitting the fabric to specific dimensions.

3.4 Architecting Knitted Textiles

Weft-knitted textiles can be categorized based on the number of needle beds used and the layering of the fabric produced. Through various architectures, a range of established and innovative strategies for creating these textiles can be explored. These strategies encompass fundamental knitted structure types and loops, options for 3D shaping in surface or tubular forms, surface texturing techniques, and additional functional elements like channels and pockets.

Single Jersey. The simplest form of weft-knitted fabric is the single jersey, which requires only one needle bed. This fabric type has distinct front and back faces, with a smooth side and a more textured side. In single jersey knitting, the yarn is fed from a single yarn carrier to the needles, creating a series of interlocking loops. This interaction is straightforward, as the yarn moves continuously in one direction to form the fabric (Figure 3.6).

A tubular jersey (Figure 3.6b) can be created using a single yarn carrier by knitting continuously in a circular manner on a single needle bed. This technique involves the yarn carrier feeding yarn to the needles in a way that creates a seamless tube. By rotating the fabric and ensuring the loops interlock correctly at both side ends, a tubular structure is formed without side seams. This method is particularly useful for making seamless garments like socks and sleeves.

Double Jersey. Double jersey fabrics are more complex, requiring two needle beds. These fabrics are effectively two layers thick and are created by alternating the direction in which the loops are pulled through the existing loops. The yarn interacts between the two needle beds, being transferred back and forth to form a fabric with identical faces on both sides. This interaction involves precise coordination of the yarn carriers to ensure consistent loop formation on both beds (Figure 2.5c). Double jersey fabrics are often used for garments requiring more structure, such as sweatshirts and dresses.

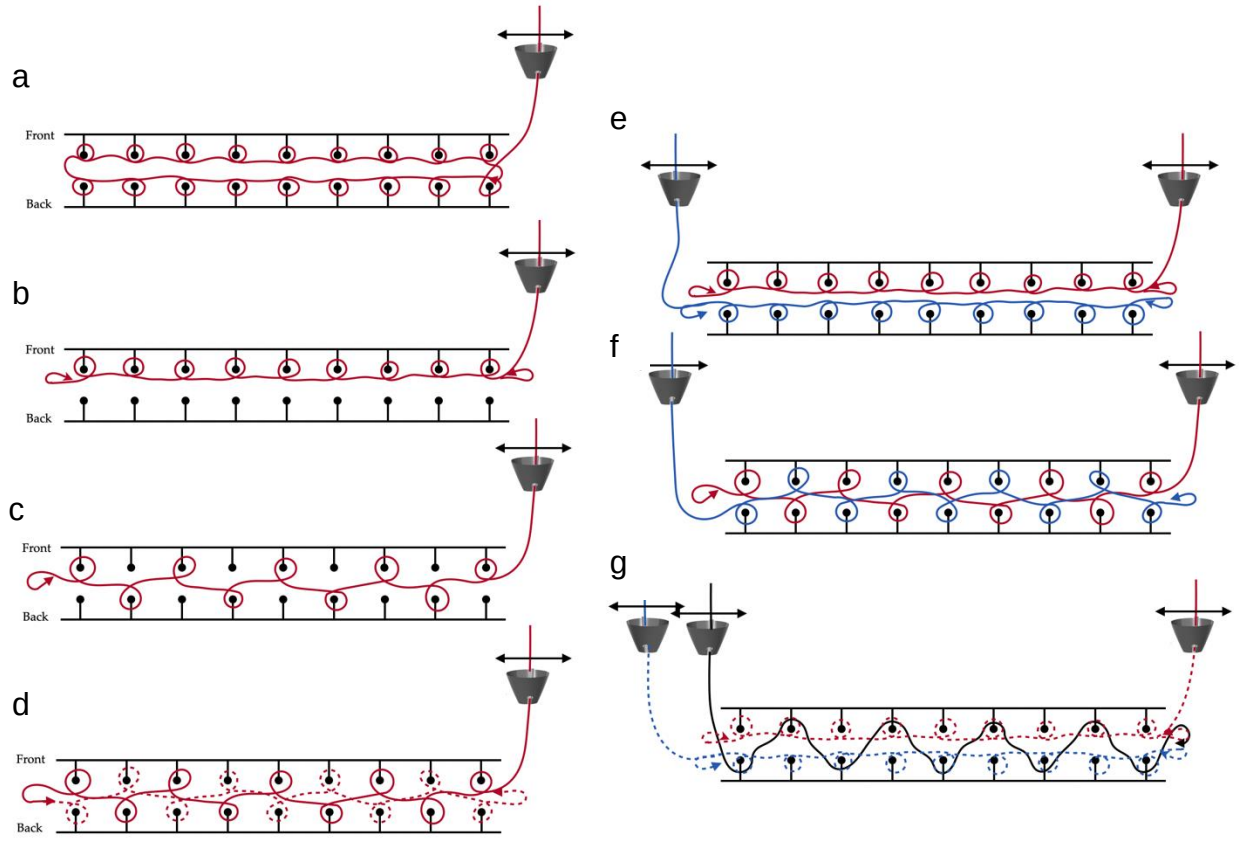

Figure 3.6: Front and back-bed mapping of a) single jersey tubular fabric, b) single jersey in one needle-bed, c) double jersey by alternating between front and back-beds, d) interlock fabric using one carrier, e) two separate single jersey fabrics, f) interlock created by alternating between two yarn carriers, and g) two separate single jersey fabrics connected through spacer yarn.

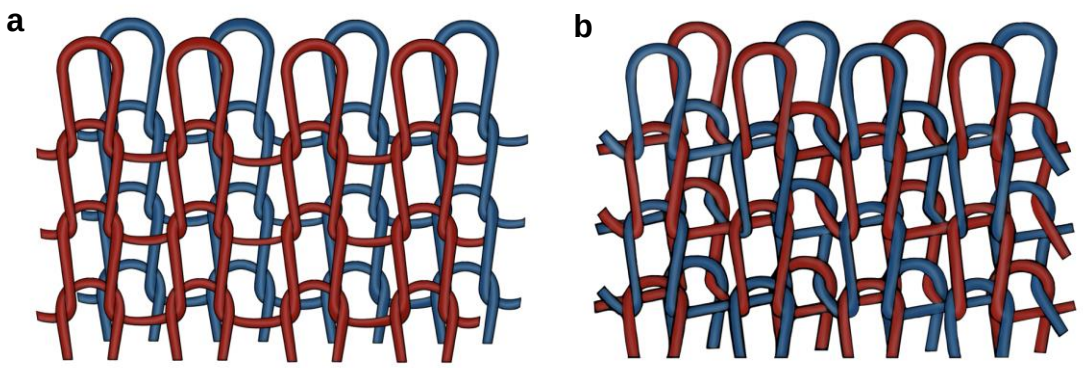

Figure 3.7: Knitting structures of a) separate double jersey fabric and b) interlock fabric.

Interlock Fabric. Interlock fabric is essentially a combination of two double jersey fabrics. This structure also uses two needle beds and produces a fabric with identical faces on both sides (Figure 3.6c). An interlock fabric can be created using a single yarn carrier that moves back and forth between the two needle beds. In this process, the yarn carrier alternately feeds yarn to the front and back needles, creating a tighter and more stable fabric compared to standard double jersey. This technique is highly efficient for producing durable and stretchable fabrics suitable for sportswear and leggings.

Two-Layer Fabric with Two Yarn Carriers. A two-layer fabric can be produced using two yarn carriers, with each layer created independently on separate needle beds and then combined (Figure 3.6e). In this process, one yarn carrier feeds yarn to the needles on the front bed, while the other yarn carrier feeds yarn to the back bed. The yarn carriers interact by ensuring that the layers are connected at specific points, creating a cohesive fabric. This method allows for different types of yarns to be used in each layer, offering versatility in design and functionality. This type of fabric is beneficial for creating reversible garments or items with different properties on each side.

Interlock with Two Yarn Carriers. Interlock fabrics can also be made using two yarn carriers, which allows for more intricate designs and patterns. By using two yarn carriers, each capable of carrying different yarn types or colors, the fabric can achieve a high level of detail and complexity (Figure 3.6f). The yarn carriers work together to feed yarn to alternating needles on both needle beds, creating a synchronized interaction that results in the interlocking structure. This method is particularly useful in creating patterned knitwear and multi-functional textiles.

Spacer Fabric with Multiple Carriers. Spacer fabrics are three-dimensional textile structures that consist of two separate single jersey layers connected by a pile yarn (Figure 3.6g). This connection is made without creating loops, often using a tuck stitch. Spacer fabrics require three yarn carriers: two for the outer layers and one for the pile yarn. The yarn carriers interact by simultaneously feeding yarn to the needles on the front and back beds while the third carrier introduces the pile yarn between these layers. This coordinated interaction ensures that the pile yarn creates a stable connection between the two layers, providing enhanced cushioning and breathability. Spacer fabrics are ideal for applications such as athletic footwear, padded garments, and technical textiles.

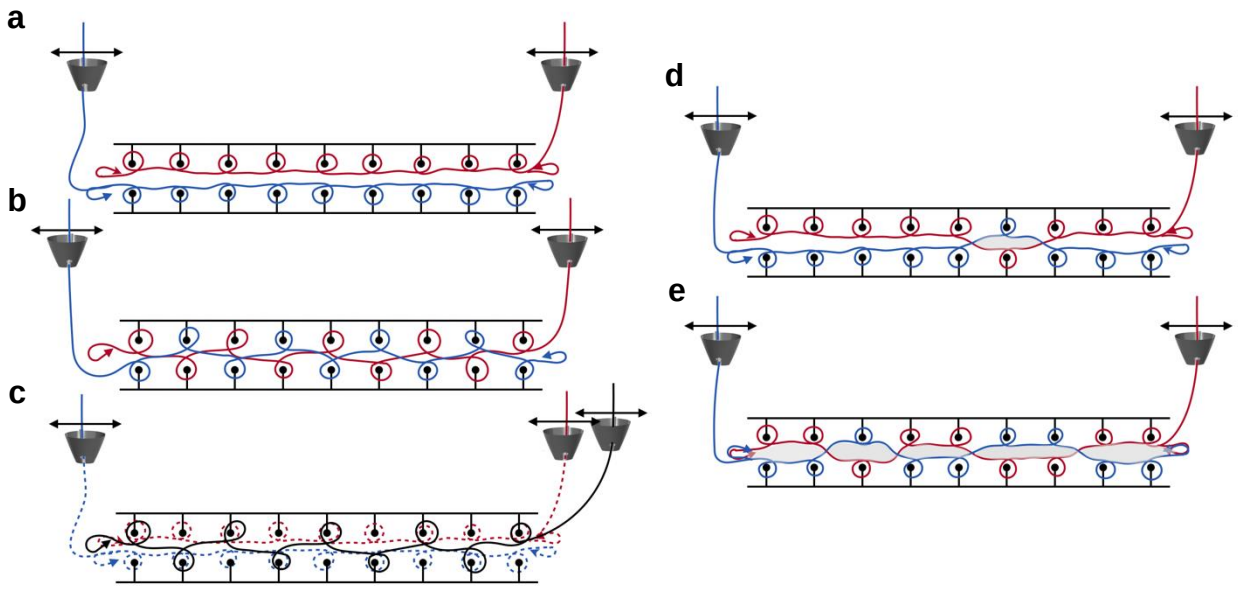

Figure 3.8: Front and back-bed mapping of a) horizontal channels and pockets by knitting a two-side jersey fabric, and then closing it through, b) interlock with the two yarn carriers switching sides, or c) a third yarn carrier closing or creating an interlock between the two beds, d) vertical channels or pockets by switching yarns to create openings, and e) multiple vertical channels by switching yarns from front to back in multiple locations.

Weft-knitted fabrics also offer a wide range of possibilities for creating complex structures, enhancing both their functionality and aesthetic appeal. To create more advanced fabric structures, such as horizontal and vertical channels or pockets, we can manipulate yarn carriers and machine operations.

Horizontal channels and pockets. It involves knitting a two-layer fabric for several rows and then interlocking the two layers (Figure 3.8a-c). To start, two separate layers are knitted

simultaneously on the front and back needle beds, each layer using its respective yarn carrier. By continuing this process for the desired number of rows, the body of the pocket or channel is formed. To secure these layers together and create the horizontal channel, an interlock knitting technique is used. This can be achieved by transferring stitches between the front and back needle beds with the existing yarn carriers or by introducing an additional yarn carrier to feed yarn specifically for the interlocking process. Alternating between knitting separate layers and interlocking them at designated intervals results in a fabric structure with built-in storage or decorative elements.

Vertical channels and pockets. For vertical channels or pockets , we need either yarn switching or transfer between the front and back needle beds. This technique forms vertical separations within the fabric, useful for ventilation, aesthetics, or functional compartments. Starting with a basic weft-knitted fabric using both needle beds, yarn switching is periodically performed, moving the yarn carrier from the front to the back needle bed and vice versa. This action creates a vertical seam or channel (Figure 3.8d,e). Additionally, transfer operations can move stitches between needle beds, creating vertical openings or channels by leaving specific sections unconnected. Reinforcing these channels can be achieved by introducing additional yarn carriers to lay yarn along the edges, providing stability and defining the vertical pockets more clearly. Customizing the frequency and position of yarn switching and transfer operations allows for tailored designs meeting specific functional or aesthetic requirements.

Intarsia. Digital knitting typically operates on an end-to-end basis, where each knitting cycle runs from one edge of the fabric to the other. This process limits the ability to introduce complex patterns in the middle of the fabric without affecting the entire row. The intarsia technique addresses this limitation by allowing for the creation of intricate, localized patterns without disrupting the continuity of the surrounding fabric.

In intarsia, multiple yarn carriers are employed, each dedicated to a specific yarn type. These carriers are precisely controlled by the knitting machine's software, enabling them to insert loops exactly where needed within a row. The process begins with the yarn carriers moving from one end of the fabric to the other, placing the required yarns in the designated areas. Once the pattern section is complete, the carriers return to their starting end, ensuring that each color is correctly positioned without extending across the entire row. Depending on the complexity of the pattern and the number of yarn inputs involved, more yarn carriers may be required to handle different sections of the design within a single line. This targeted approach ensures that complex designs can be integrated seamlessly into the middle of a fabric without necessitating end-to-end pattern repetition.

By combining the methods for creating horizontal and vertical channels, as well as intarsia patterning even more intricate fabric structures can be developed. These advanced knitting techniques demonstrate the versatility and potential of weft-knitted fabrics in textile design. Through precise control of yarn carriers, needle operations, and fabric layering, designers can create complex, multifunctional textiles suitable for a wide range of applications, from wearable to technical textiles.

3.5 Engineering Electrical Properties of Knitted Conductive Textiles

In weft knitting, the fundamental binding and loop element is the stitch (Figure 3.9). A stitch is composed of a head, two legs, and two feet, always including contact or intermeshing points at the head and feet. The geometry of the stitch is defined by its width (b_M) and height (h_M). The length of the yarn in a stitch is termed the stitch length (l_M). For a more comprehensive geometrical models, we can refer to the works of Leaf and Glaskin [140] and Munden [141].

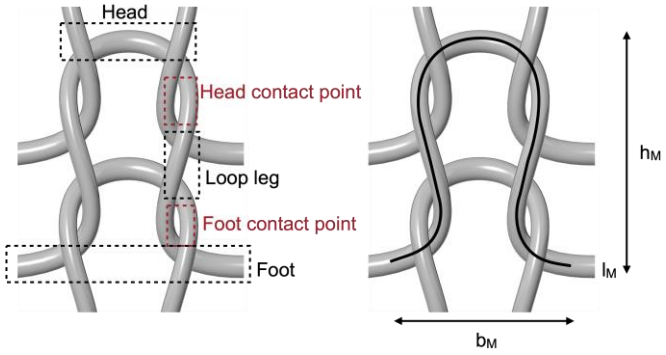

Figure 3.9: Geometry and anatomy of a knit stich

To approximate the length of yarn in one knit loop based on its geometries, we need to consider the fundamental structure of a knit loop. We have defined the key parameters that describe the geometry of the loop. Additionally, we consider the thickness of the yarn (t), which is the diameter of the yarn used.

A single knit loop can be broken down into several distinct segments: the top arc, the bottom arc, and the vertical sides. The top and bottom arcs can each be approximated by a half-circle with a

radius of $\frac{b_M}{2}$. Therefore, the length of the top arc ($l_{M(top)}$ is half the circumference of a circle with radius $\frac{b_M}{2}$. Given by $\frac{\pi b_M}{2}$. Similarly, the length of the bottom arc ($l_{M(bottom)}$) is also $\frac{\pi b_M}{2}$.

Next, we consider the vertical sides of the loop. Each side can be approximated as a straight line of length $h_M - t$, where t accounts for the thickness of the yarn, reducing the effective vertical distance. Thus, the total length for both vertical sides is

$$l_{M(sides)} = 2 \text{ x } (h_M - t) \qquad (3.1)$$

The total length of the yarn in one knit loop l_M is the sum of the lengths of the head arc, foot arc, and legs/vertical sides. This can be expressed mathematically as:

$$l_M = l_{M(top)} + l_{M(bottom} + l_{M(sides)} \qquad (3.2)$$

Substituting the values derived for each segment, we get:

$$l_M = \frac{\pi b_M}{2} + \frac{\pi b_M}{2} + 2 \text{ x } (h_M - t) \qquad (3.3)$$

$$l_M = \pi b_M + 2 \text{ x } (h_M - t) \qquad (3.4)$$

Cuden et al. have estimated the loop length of single jersey knitted fabric for both normal to open and normal to compact knit structures [142]. After fabric relaxation, there is a reduction in wale and course density due to a reduction in loop length, which affects the fabric properties. Therefore, it is useful to find a relation between loop length and courses and wales per unit length, as well as the yarn thickness, because wales and courses per unit length can be easily measured at any state while it is difficult to measure the loop length in knitted fabrics. In their work, estimated equations to calculate the knitted loop length for open to normal structure and for normal to compact structure were developed. By comparing the value of the loop length predicted from their work with other models, they found that the calculated values are very near to the actual values, making the developed equations acceptable.

Peirce proposed that in an open to normal knitted structure, adjacent yarns within the fabric are joined at contact points only [143]. The loop projection onto the fabric plane comprises circular needle and sinker arcs connected by straight lines, forming loop legs. This three-dimensional loop configuration lies on the cylinder surface with a curvature radius (r) and has an axis parallel to the course direction. For a normal structure, the loop length (l_M) is primarily dependent on the yarn thickness (t). For normal to compact structures, the loop legs are more inclined, leading to a reduction in both loop width and height. The loop length for normal to compact structures can

be derived by considering the diagonal distance between the contact points and the reduced height and width of the loop. The Pythagorean theorem can be applied to calculate this diagonal distance, which represents the loop length in a more compact structure

Equation for open to normal structure:

$$l_M = \pi\left(\frac{b_M}{2} + \mathrm{t}\right) + 2\sqrt{h_M^2 + t^2} \qquad (3.5)$$

Equation for normal to compact structure:

$$l_M = \pi(b_M - t) + 2\sqrt{h_M^2 + (\frac{b_M}{2} - t)^2} \qquad (3.6)$$

For normal structures, substituting $b_M = 4t$ and $h_M = 3.46t$ into the equation results in a loop length of $16.63t$. Therefore, for an open structure, the loop length will exceed $16.63t$. In the case of super compact single jersey knitted fabric, where $b_M = 2t$ and $h_M = t$, l_M is calculated as $5.14t$. Ultimately, it is concluded that the existing geometrical loop models for open structures show the best agreement with conventional yarns without elastane [144]. Elasticized structures, however, require different models. Both conventional and elasticized single weft knitted fabrics necessitate specific equations to accurately calculate loop length.

3.5.1 Resistive Network Model

Utilizing the resistive network models described by Zhang et al. [145] and Li et al. [146], we can formulate a systematic method and analytical equation to compute the equivalent resistance of a network of conductive knitting stitches. To measure the resistance of a single loop, it is essential to establish the resistance of the conductive yarn, which depends directly on its length and inversely on its cross-sectional area. This relationship is expressed by the equation:

$$R_M = \rho\frac{l_M}{A^\beta} \qquad (3.7)$$

Here, R represents the resistance, ρ is the resistance coefficient, l is the length, A denotes the cross-sectional area of the conductive yarn, and β is the scaling exponent.

We can imagine a knitting loop serving as a primary structure for current conduction. Within conductive knitting yarns, two types of electrical resistance impact the overall equivalent resistance of the loop: length-related resistance R_l and contact resistance R_c. The contact resistance between two overlapping conductive yarns decreases as the contact force increases. Conductive

yarns are composed of multiple twisted fibers, and as the contact force increases, the contact area between these fibers expands. Based on the configuration of the knitted fabric, a loop might exhibit length resistance or both length-related and contact resistance. As depicted in Figure 3.10c, a single loop modeled with lump resistors illustrates this difference. The length resistances are denoted as R_{l1-l8}, and the contact resistances are shown as R_{c1-c5} . This variation arises from whether the conductive yarns are knitted with other conductive or non-conductive yarns. Just as the basic knitting structure forms the course and wale of textile, this modeling approach can extend to these textile directions.

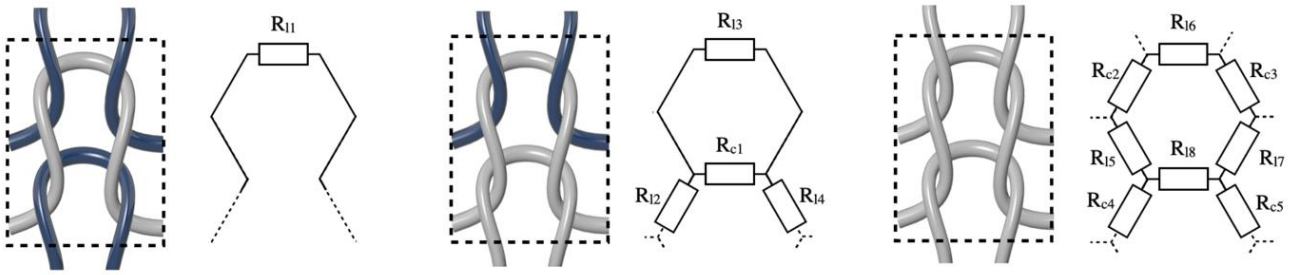

Figure 3.10: Resistance network model of a) a knit stich, b) two neighboring stiches, and c) three neighboring stitches in wale direction.

For different numbers of courses, the conductive knitting loops can be modeled as a resistive network comprising distributed length and contact resistors, shown in Figure 3.10. Assuming a constant unidirectional extensile force along the course direction, all contact resistors R_{c1-c5} can be considered constant and represented as R_c. Using signal flow theory, each contact resistance $R_c$can be divided into four equal parts ($0.25R_c$) and absorbed by the neighboring length-related resistors. Consequently, each length resistance will encounter an additional resistance of $0.5R_c$ at its terminals, meaning the equivalent resistance of a conductive stitch depends solely on the length-related resistors. We will denote the combined resistances depicted in Figure 3.11 using the symbols R_x, R_y, and R_z.

$$\begin{aligned} R_x &= R_{l3} + 0.5R_c \\ R_y &= R_{l6} + 0.5R_c \\ R_z &= R_{l5} + 0.5R_c = R_{l7} + 0.5R_c \end{aligned} \tag{3.8}$$

R_y and $R_z$are the resistances along the course and wale directions, respectively, while R_x represents the external resistance located at the boundary between the conductive yarn and the non-conductive yarn. We substitute R_{l3} and R_{l6}, with R_l and kR_l with R_x as length-related resistor and k ≥ 1 as a scaling factor. Consequently, Equation X and X transform into:

$$\begin{aligned} R_y &= R_l + 0.5R_c \\ R_x &= kR_l + 0.5R_c \end{aligned} \qquad (3.9)$$

For a resistive network with M ≥ 3 wales and N courses (Figure 3.11c), represented by distributive resistors as shown in Figure 3.11d, the parallel resistance $R_{x||y}$ between R_x and R_y is given by:

$$R_{x||y} = \frac{(kR_l^2 + 0.5(k+1)R_cR_l + 0.25R_c^2}{(k+1)R_l + R_c} \qquad (3.10)$$

Since $R_x \neq R_{x||y}$, the bridge resistor R_z needs to be considered. Equal portions Δ of R_x can be transferred to both R_z and $R_{x||y}$ in accordance with signal flow graph theory. The resulting resistive network is illustrated in Figure 5. Given that the current flow in the bridge resistors R2 and R2 + Δ, is negligible, these resistors can be considered open, as depicted in Figure 3.11d.

$$\Delta = \frac{R_x - R_{x||y}}{2} = \frac{(R_l + 0.5R_c)^2}{2[(k+1)R_l + R_c]} \qquad (3.11)$$

$$\frac{R_x - \Delta}{R_{x||y} + \Delta} = \frac{R_{x||y} + \Delta}{R_x - \Delta} \qquad (3.12)$$

$$\begin{aligned} R_{total(m=1)} &= NR \\ R_{total(m=2)} &= 2NR_{x||y} \end{aligned} \qquad (3.13)$$

The analytical equation for the equivalent resistance of a conductive knitting stitch along the course direction with a conductive width of M wales and a conductive length of N courses is provided as follows:

$$R_{total(m>2)} = \frac{2NR_x(R_x + R_{x||y})}{(M+1)R_x + (M-3)R_{x||y}} \qquad (3.14)$$

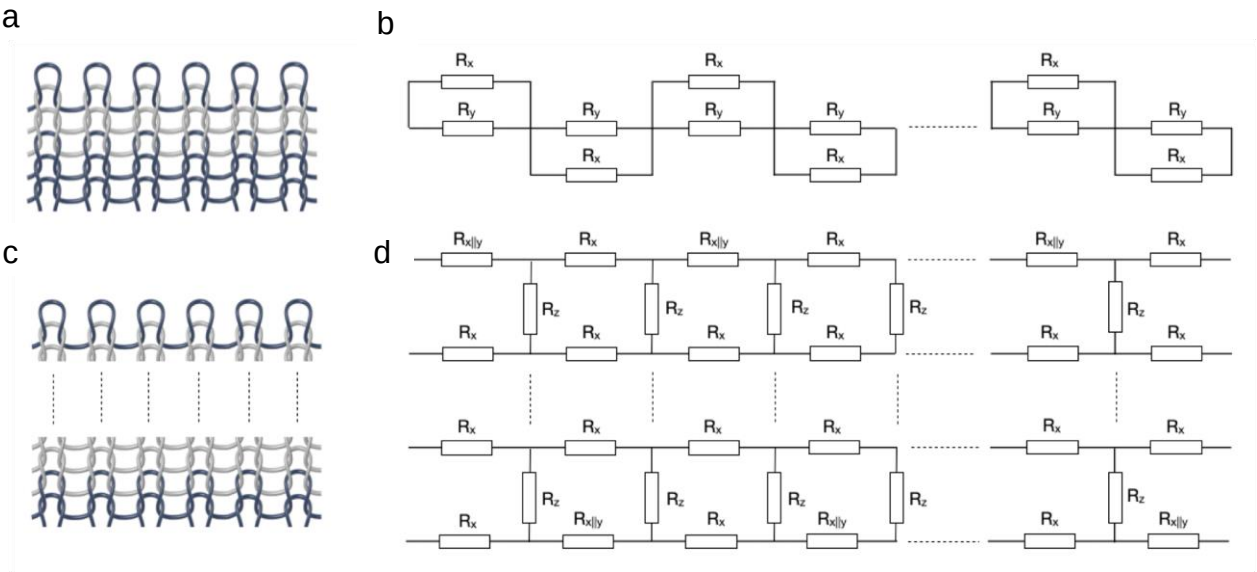

Figure 3.11: Resistance network model of knitting loops in a-b) two and c-d) multiple rows.

3.5.2 Interconnect and Electrodes

To validate our model, we knitted sample conductive-patterned fabrics using polyester base yarns with the specified number of loops. We created samples with various numbers of course and wales knitted conductive loops, producing a 62 cm long sample in the course direction using a knitting machine (Figure 3.12). Each loop was estimated to be 1.25 mm in length and 1 mm in width. We also integrated conductive yarns with different plies—single, double, and three-ply—to vary the resistance. Figure 3.13a shows the resistance for different numbers of loops across various M wales (1, 2, 4, 8, 16, 32 loops) and N courses. Additionally, Figure 3.13b illustrates the relationship between the number of twisted conductive yarns in one carrier and the total resistance. The strong correlation in the experimental results reveals that the derived equations accurately represent the equivalent electrical resistance of conductive knit loops (Equation 13 and 14).

This study introduces a method to measure the resistance of conductive knit loops for interconnects, which is instrumental for tuning to the desired resistance levels. However, in practical applications, knitting stitches with only a few courses or wales are seldom utilized to form a conductive path due to their high resistance, low current capacity, and decreased stability. Our analytical study has demonstrated that doubling the number of wales or rows for the same conductive path length, offers significant advantages by reducing the resistance by more than half. Additionally, using plied yarn can further decrease the length-related resistance, as it provides multiple conductive pathways, thereby enhancing current flow and reducing overall resistance.

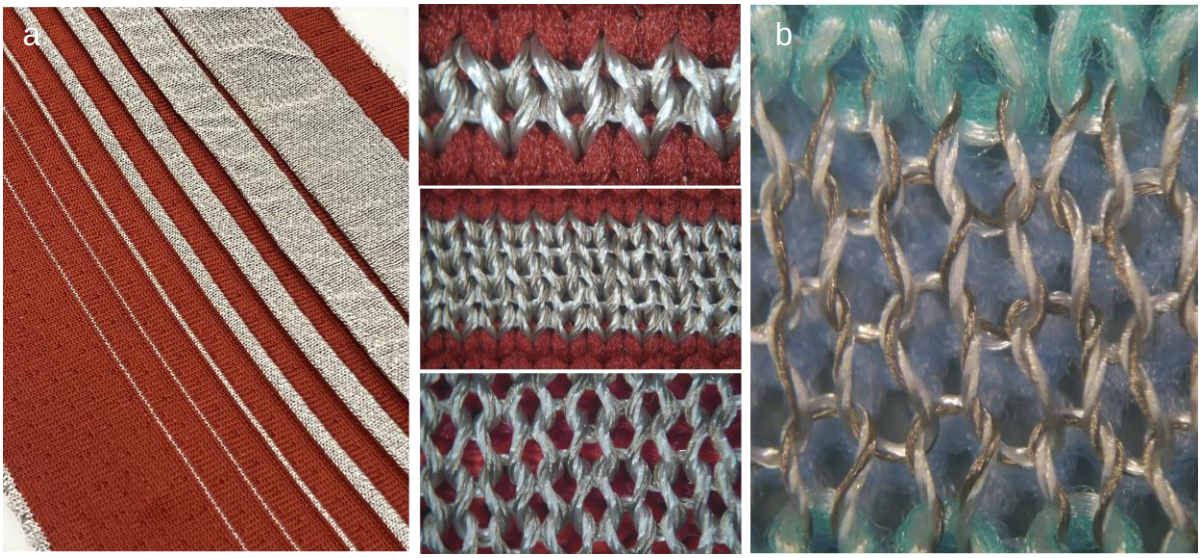

Figure 3.12: Samples of conductive textiles knitted with silver-plated yarns with multiple stich rows (1,2,4,8,16, and 32 rows in wale direction) and their zoomed-in view a) with 2-ply of conductive yarn and b) with 1-ply of conductive yarn.

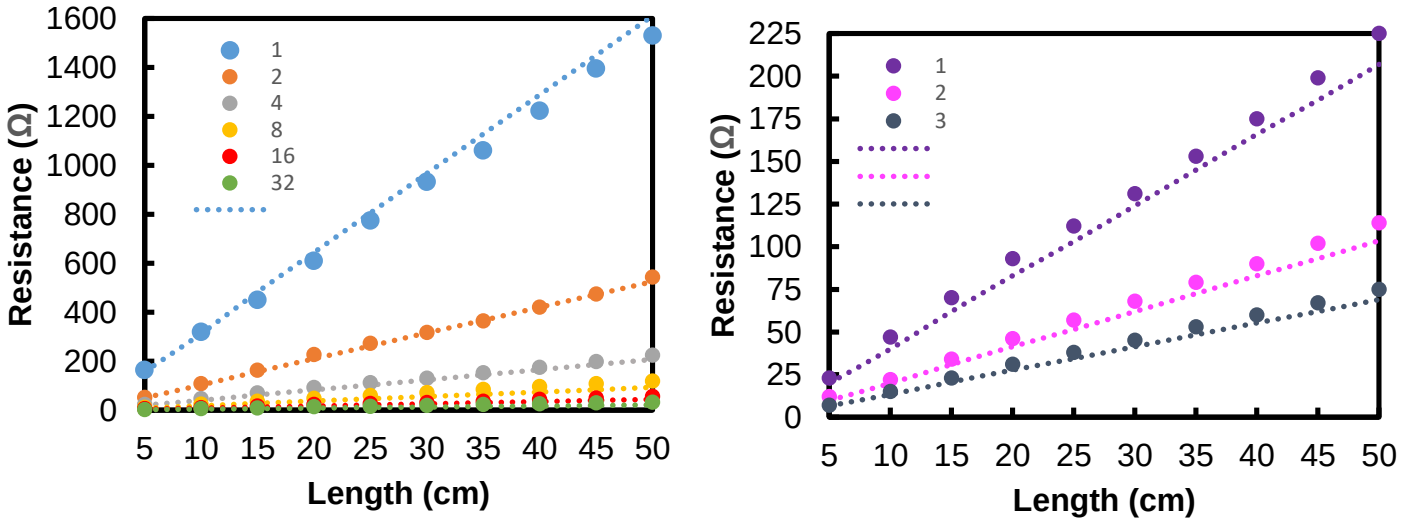

Figure 3.13: Resistance characterization of conductive textiles knitted with silver-plated yarns with multiple stich rows (1,2,4,8,16, and 32 rows in wale direction, length represents the course direction), and multiple yarn twist (1,2, and 3-ply).

3.5.3 Strain Response

Knit conductive textiles exhibit distinct electrical behaviors under strain. Understanding the changes in resistance due to structural movement and molecular interactions within the conductive coating is key to optimizing these materials for pressure and strain sensing. When a knit conductive textile is subjected to strain, the initial change in resistance is primarily attributed to the structural movement of the knit loops. In their relaxed state, the loops form contact points where conductive coatings touch, creating pathways for electrical current. As the textile is stretched, the loops deform, and the contact points between them shift, leading to variations in contact resistance.

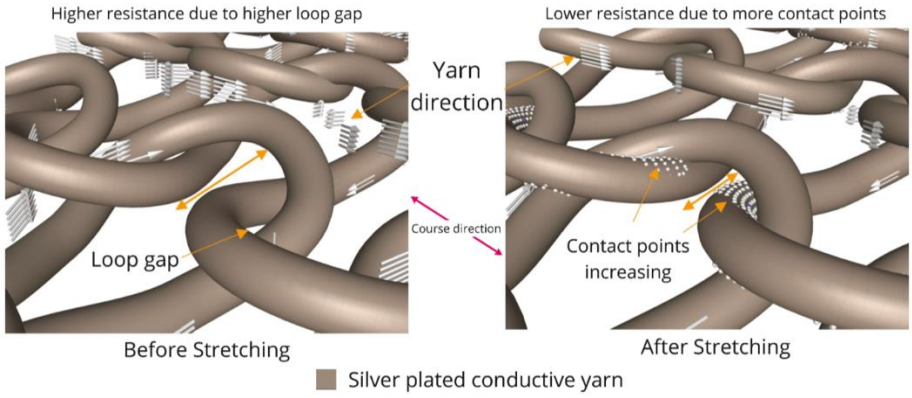

Figure 3.14: Structural change of conductive knits that induces more contact points between the head and the foot, thus the amount of contact points is proportionally related to the strain or stretching [147].

The detection mechanism of the knitted sensor is based on the specific design of the conductive yarn in the fabric structure that enables the sensor to change its electrical resistance with in response to variations in strain. There are two predominant factors which are responsible for change of electrical resistance in response to strain; the resistance changes due to extension of the conductive yarn within the structure, and the contact points between successive knitted loops of conducting yarn are pulled apart and cause the sensor to change its resistance (Figure 3.14). However, the degree of influence of these factors varies with fabric structure, the type of conductive yarn and the applied strain level.

As shown in Figure 3.15, due to the usage of elastomeric yarn in the fabric structure, conductive yarn loops make contact with adjacent loops at their heads and limbs also at their sinker loops which are pressed together and according to Holm`s contact theory [148] where Rc is contact resistance, ϱ represents electrical resistivity, H material hardness, n number of contact points, and p contact pressure. Based on the equation, it is seen that the material hardness and electrical

resistivity are constant for a given conductive yarn but the number of contact areas and the contact pressure change depends on the applied strain Thus, higher contact pressure and an increased number of contact areas between the conductive parts reduce the contact resistance.

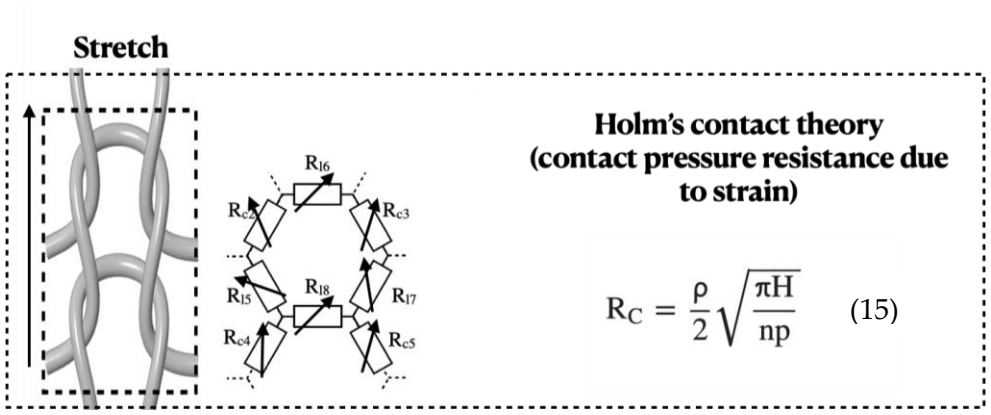

Figure 3.15: Knit stitch resistance modelling under dynamic strain.

In our experimental setup, we tested a 10 cm course direction knitted sample of strain sensors based on two and four rows of knit in the wale direction. Using a tensile testing machine, we measured the resistance of the knitted sensors in response to applied strain. As illustrated in Figure 3.16b and 3.16c, the resistance of the sensor exhibited approximately a 10% change when subjected to a 50% strain, displaying a slight hysteresis response. These results align with the dynamic study of the knit network under tensile strain, suggesting that the reduction in resistance is attributed to the higher contact pressure and the reduced distance between the conductive yarns, as depicted in Figure 3.16a. This behavior corroborates our theoretical understanding that increased contact pressure and an increased number of contact points reduce the overall contact resistance in the knitted sensor structure.

The response of knit conductive textiles to strain also differs based on the direction of stretching, i.e., course direction (horizontal) versus wale direction (vertical) [149]. When stretched in the course direction, the loops elongate horizontally, causing significant changes in contact resistance due to the larger deformations of the loop structure. This direction tends to exhibit more pronounced changes in resistance initially as the contact points are disrupted, followed by a reduction in resistance as the loop legs compress sideways. The horizontal stretching leads to a more substantial architectural shift within the textile, affecting both the contact points and the percolation network of the conductive coating.

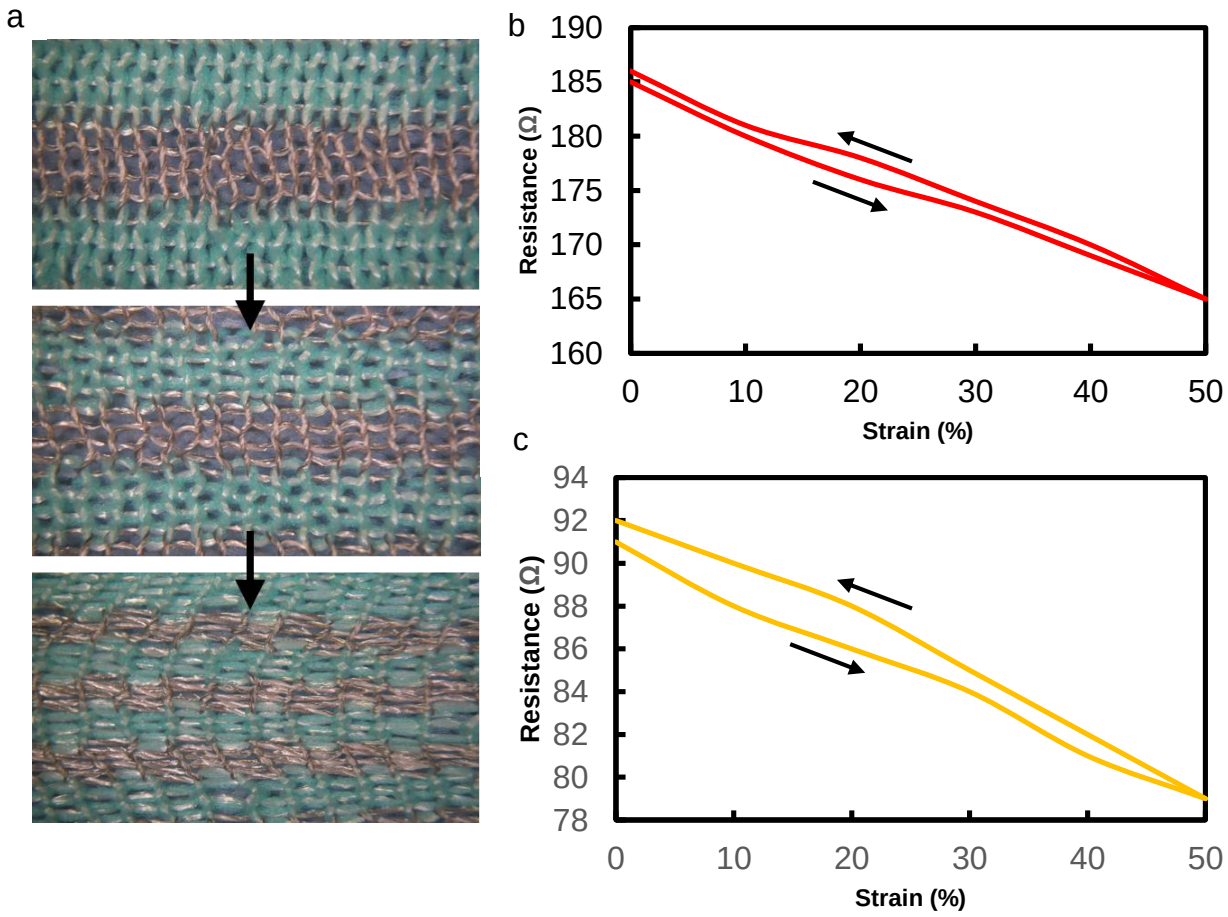

Figure 3.16: a) Conductive knitted textiles being stretched in course/horizontal direction, showing the more dense pathways between the loops. a 10 cm knitted sample of strain sensors tensile characterization based on b) two and c) four rows of knit in the wale/vertical direction.

In contrast, stretching in the wale direction results in vertical elongation of the loops, typically involving less dramatic initial changes in contact resistance. The loops in this direction are more constrained, thus exhibiting less significant shifts in architecture compared to the course direction. However, as strain increases, the compressive effect on the loop legs still occurs, albeit to a lesser extent than in the course direction, leading to a gradual reduction in resistance. This difference in behavior between the two stretching directions underscores the importance of understanding the structural dynamics within knit conductive textiles.

Several studies have analyzed the sensitivity of knit conductive textiles in different stretching directions. It has been observed that silver-plated knit textiles stretched in the course (horizontal) direction tend to be more sensitive than those stretched in the wale (vertical) direction, often

showing gauge factor (GF) performance that is 2 to 8 times higher [149], [150]. The gauge factor GF is given by the equation:

$$GF = \frac{\Delta R/R}{\Delta L/L} \qquad (3.16)$$

Where ΔR is the change in resistance, R is the initial resistance, ΔL is the change in length, and L is the initial length. This equation highlights how more substantial resistance changes in the course direction lead to higher GF values, making textiles stretched in this direction more responsive to strain. The pronounced architectural shifts and greater deformation of the loop structure in the course direction result in significant initial changes in contact resistance and subsequent reductions as the loops compress sideways. Of course, the overall performance depends on several factors such as the choice of base yarns, knitting structure and density, and the coating materials used. For instance, the purl stitch pattern has been shown to perform better than the knit stitch, offering 25% more in dynamic range and approximately 2x higher GF [151].

For functionalized fabric, beyond structural movement, the interactions among the conductive polymer molecules within the fibers are also significant under strain [152], [153]. Initially, as the textile is stretched, the separation between conductive molecules increases, disrupting the percolation network and increasing resistance. However, as the strain progresses and the loop legs compress, the conductive molecules are brought back into closer proximity, enhancing the conductive and intrinsic percolation pathways between the loop contacts and reducing resistance. This dual effect of structural movement and molecular interaction thus creates a complex relationship between strain and electrical resistance in knit piezoresistive textiles [154].

Another approach to textile strain sensing beyond resistive methods is capacitive sensing, which presents distinct advantages when utilizing conductive textiles for improved sensitivity. Capacitive sensors operate by measuring changes in capacitance as a material undergoes deformation, which affects the dielectric layer's thickness and the area of overlap between electrodes. In this setup, two layers of conductive knit fabric serve as electrodes, with a deformable dielectric material in between. The capacitance C of the sensor can be expressed by:

$$C = \frac{\varepsilon A}{d} \qquad (3.17)$$

Where is ε the permittivity of the dielectric material, A is the area of overlap between the two electrodes, and d is the thickness of the dielectric layer. As the textile stretches, the dielectric layer compresses, reducing d, while also potentially changing A due to the stretching fabric, resulting in a detectable change in capacitance. The change in area A is influenced by the Poisson effect,

where the material tends to contract in the perpendicular direction when stretched in one direction. In knitted textiles, this effect results in dimensional changes not only in the thickness of the dielectric but also in the width of the conductive layers, further enhancing the sensitivity of the capacitive sensor.

Atalay et al. has demonstrated promising results in capacitive sensors that use conductive knit fabrics as electrodes with a silicone elastomer serving as the dielectric [96]. Another study explored interdigitated multi-layer structures of conductive and dielectric layers, which improved the sensor's sensitivity [155]. These efforts, enabled by batch manufacturing and laser cutting techniques, allow for the production of large, customizable textile-based strain sensors.

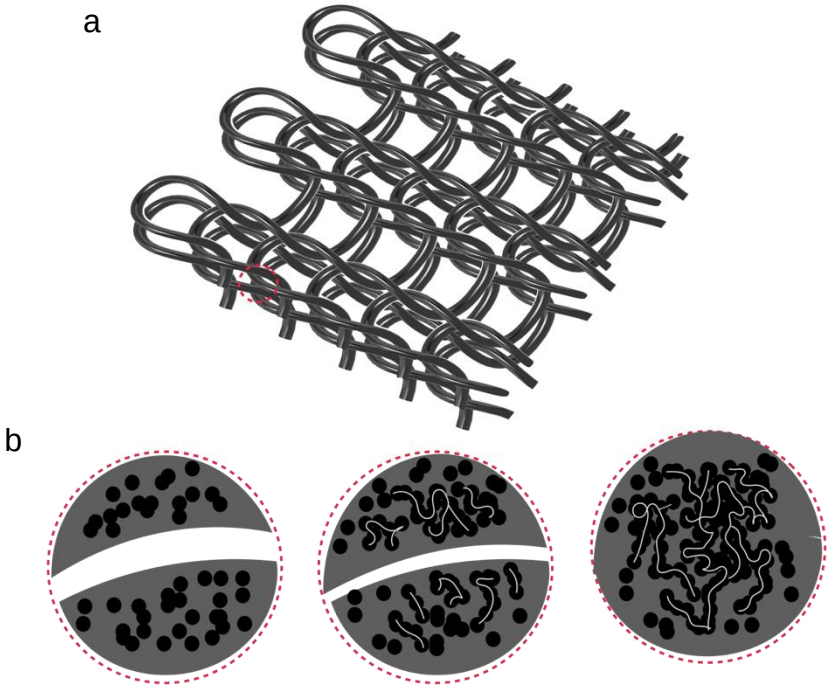

Figure 3.17: a) Multi-layer knit textile with b) conductive molecules in its percolation network between two yarns that interface with each other. The total effective resistance is influenced by both contact resistance between the yarns and the conductive coating of the yarns as the fabric experiences compression.

3.5.4 Pressure Response

Conductive polymers used in coatings respond uniquely to mechanical stress, such as pressure, which can be explained by percolation theory [156], [157]. Initially, conductive polymers form a percolation network within a non-conductive matrix, where a sufficient number of conductive

paths ensure electrical conductivity. When pressure is applied, the yarns in the knit structure compress, causing the conductive polymer molecules to move closer together (Figure 3.17). This compression enhances the percolation network by increasing the number of contact points between conductive particles. The percolation threshold is the critical point at which conductive particles form a continuous path through the matrix. Under pressure, the proximity of conductive particles exceeds this threshold, significantly lowering electrical resistance.

The combination of Holm's contact theory and percolation theory provides a robust framework for optimizing pressure-sensitive knit structures with conductive coatings. The flexibility and compressibility of knit fabrics allow significant deformation under pressure, bringing conductive coatings into closer contact and enhancing both Holm's contact effect and the percolation network simultaneously. Designing textiles with multiple layers or specific knitting patterns can tune sensitivity to pressure, with thicker areas or denser conductive coatings exhibiting more pronounced resistance changes under pressure. Integrating these scientific principles into knit structures for pressure sensing highlights their potential for advanced applications in smart textiles and interactive fabrics. We will revisit and explore pressure sensing principles deeper in our work of piezoresistive, pressure-imaging textiles in Chapter 4.2.

For capacitive-based textile pressure sensing, Meyer et al. used a textile insulator placed between a common electrode fabric and an embroidered array of electrodes to detect activities such as sitting postures on a fabric surface [158]. The sensing principle is similar to the one explained in Equation 3.17. In this work, spacer material was selected to be soft and squishy, enhancing the comfort of the pressure sensor for users. Another research has explored the use of sacrificial particles to create micropores within a dielectric elastomer, improving the compressibility and sensitivity of the sensor by forming air gap [159]s. A combination of conductive knit electrodes and a highly porous dielectric layer resulted in enhanced performance under pressure. These studies highlight the significant potential for capacitive pressure sensors in smart textiles.

However, several challenges remain. Capacitive-sensing circuits are more complex to implement, and the sensors are also prone to parasitic effects from the environment, which can affect performance. Squishy fabric spacers can exhibit hysteresis, leading to fixed pattern noise behavior, which requires adaptation algorithms for reliable measurements. Additionally, mutual crosstalk between pressure and strain poses challenges for precise sensing. One potential solution is using multi-layer structures or novel knit architectures to reduce signal interference. Furthermore, shielding layers can be employed to ground the system and mitigate parasitic effects from the environment, ensuring more stable and accurate sensor performance.

Chapter 4: Digital Knitting of Sensate Textiles across Scales

"There are no boundaries for what can be fabric."
Issey Miyake

This chapter delves deeper into the seamless integration of functionalities within the structure of objects or surfaces, with a particular emphasis on embedding functionalities at the fundamental level of textiles, from fibers to multi-layer fabrics. To demonstrate this, we have leveraged both computational design and digital fabrication techniques, particularly machine knitting, a digital manufacturing technique discussed in Chapter 3, which allows for precise control over the placement and patterns of sensors and interconnects within a textile object or surface. This method enhances the precision, efficiency, and scalability of fabricating complex and multi-functional fabrics. Additionally, the circular or interlock knitting techniques facilitate the transition from 2D to 3D objects, allowing for the creation of not only textile skins but also tubular objects such as sleeves, shoes, and other clothing items.

By leveraging materials such as functional/electronic fibers and yarns, incorporating textile design elements like complex patterns, multi-layer structures, and 2-3D forms, and utilizing fabrication tools of digital knitting, I have devised a framework for the digital knitting of sensate

textiles (Figure 4.1). This framework enables the creation of highly customized textile structures that integrate electronic functionalities directly within the fabric's architecture, resulting in sensate textiles that are both functional and aesthetic. Moreover, functional patterning can also allow discrete or spatial sensing in distributed arrays or matrix formats. Integrating functional devices within textiles can also leverage the inherent properties of fabrics, such as their softness, dynamic movements, and rich mechanical and structural properties to create various types of sensing elements. This approach not only addresses the limitations of current e-textile fabrication methods but also opens new avenues for innovative applications across various scales, from wearable technologies to large-scale architectural installations.

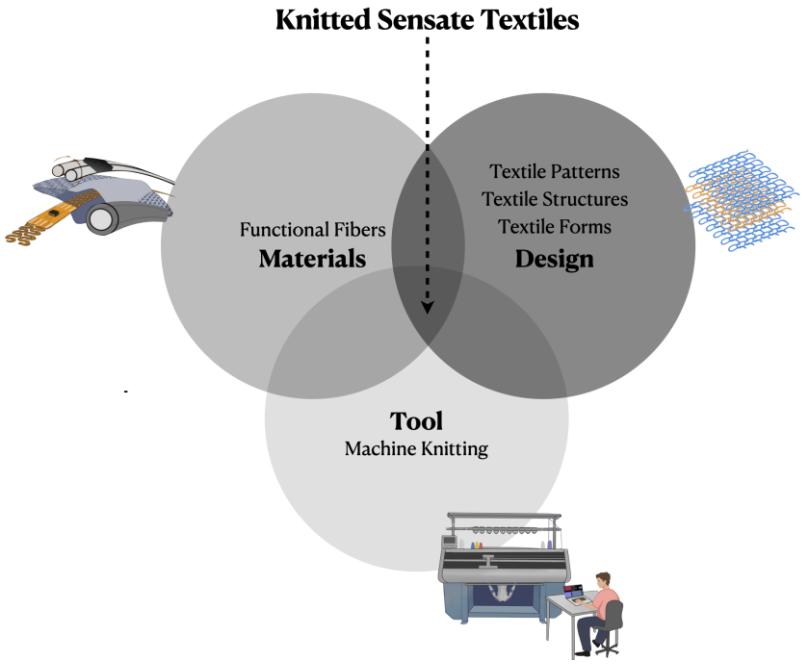

Figure 4.1: Design framework and methodology for architecting knitted sensate textiles.

With this framework and approach, I have developed four knitted sensate fabric artifacts (Figure 4.2) and demonstrated their design rationale, fabrication methods (with a focus on knitting as integration technique, as shown in Figure 4.3), hardware developments, data processing, and practical applications enabled by distributed sensing, these artifacts include:

KnittedKeyboard: A soft and tactile piano-patterned cloth with 60 capacitive-based proximity and touch-sensing keys, integrated with a piezoresistive pressure and strain-sensing layer for musical performance [28], [160]. Key innovations include textile-based multi-modal sensing that combines discrete and continuous controls, enhanced by the custom design of textile pockets

through digital knitting to improve tactile feedback. I collaborated with a sound artist and keyboardist to create a piece that demonstrates the capability of the *KnittedKeyboard*.

3DKnITS: A set of spatiotemporal piezoresistive pressure-imaging intelligent textile mats and shoes with 265 and 96 sensing pixels, respectively, for applications in biomechanics, activity recognition, and gaming interfaces [161]. In addition to flat-bed knitting, we used a circular knitting machine to create tubular e-textiles. We developed custom hardware systems to resolve diffusion and ghosting issues in piezoresistive matrices. Leveraging deep-learning convolutional neural networks on the 2D spatiotemporal pressure-image data, we devised an algorithm to detect posture and activity in real-time for entertainment and sports applications.

Tapis Magique: Expanding the scale of *3DKnITS*, this large-area pressure-sensitive carpet with 1800 parametrically designed sensing pixels generates 3D sensor data based on body gestures, movements, and location, driving an immersive sonic environment in real-time for interactive dance [162]. Collaborating with sound artists and choreographers, we created performances that merge electronic music, interactive textiles, and contemporary dance into cohesive pieces of object and performance.

Living Knitwork Pavilion: An architectural-scale e-textile shade structure integrated with 24 transmitter and receiver knitted antennas for distributed electrical field sensing [163]. Contributions include the design of complex, multi-layer knitted sensate and technical textiles, along with supporting structures for extreme environments. These systems feature distributed active capacitive sensing and integrate audiovisual elements through a spatial array of speakers and motorized lighting. The 'Living Knitwork' incorporates principles and methodologies from fiber/textile arts, material science, digital fabrication, sensing systems, architecture, and structural engineering. As one of the largest *Thereminic* tent structures to date, it operates on an architectural scale, with resolution and sensitivity across multiple bodies or occupants rather than just fine-grained finger measurement. Accompanied by its virtual environment, *KnitworkVR*, designed in Unity, the Pavilion serves as an immersive space that controls integrated audio and lighting systems based on movements and crowd dynamics in the physical environment. This creates a unique experience in both the virtual space and the physical world, offering opportunities for collective interaction as well as co-telepresence.

Through these case studies, I will demonstrate how sensate textiles can revolutionize applications across various scales, from interactive media, wearable technology, to large-scale architectural installations. The insights gained from these projects will underscore the importance of interdisciplinary collaboration and innovation in pushing the boundaries of what is possible with sensate and electronic textiles.

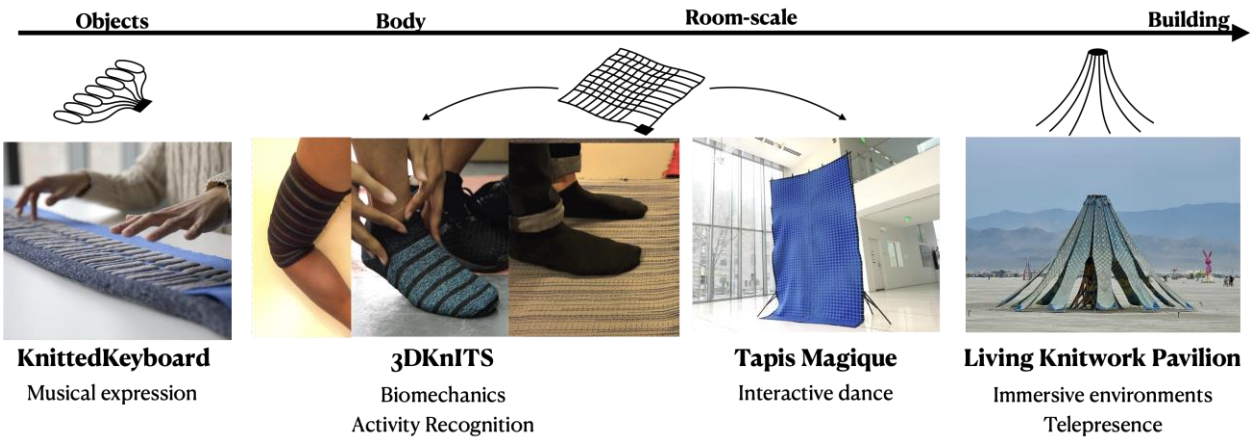

Figure 4.2: Digital knitting of sensate textiles across scales, from the scale of objects to the scale of building.

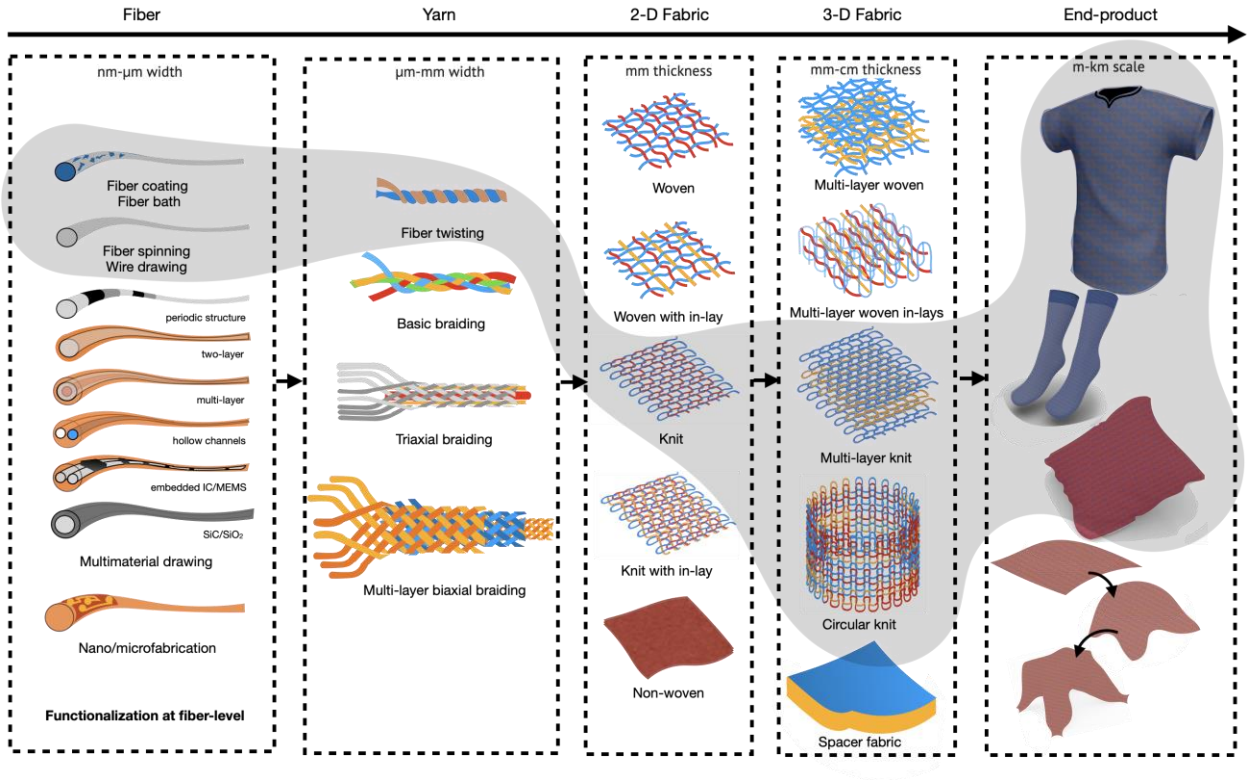

Figure 4.3: Hierarchical architecture and various structures of electronic textiles starting from fiber (1D), yarn (1.5D), fabric (2D), fabric composite (3D), to the end-product. Besides structural functionalization, we also show the material functionalization stage at the fiber or fabric-level. Highlighted region shows yarn types and textile integration techniques used in this chapter.

4.1: KnittedKeyboard

4.1.1: Motivation and Related Work

Spanning from the early Musical Telegraph and Electronic Sackbut to the late EMS Synthi AKS and Moog Synthesizers, electronic music and musical controllers [164], particularly the keyboards, have enabled people from all walks of life and all around the world to produce and manipulate sound as a means of creativity, expression, and shared experience [165]. To leverage hand and finger dexterity in keyboards, Moog and Rhea designed an expressive multimodal sensor layer for discrete and continuous controls in their Multiply-Touch Sensitive Keyboard [166]. Previous work also focused on transforming the key's surface and substrate, from The Continuum, an indiscrete keyboard layout for continuous finger gestures, to the recent Seaboard, a soft, rubbery, and wavy keyboard interface with its signature style polyphonic modulations [167].

Most expressive keyboard interfaces to date rest on a rigid and heavy structure. In contrast, textiles are ubiquitous in our daily life. They are highly formable and palpable materials with a broad spectrum of patterns, structures, and textures, making them excellent candidates for physical interfaces. Early examples like Musical Jackets and Musical Balls demonstrated embroidered touch and pressure-sensitive textile sensors for performing music [52], [53]. MusiCushions, a set of interactive sofa cushions, enable deformable inputs for exploring music interaction at home [168]. Deformable musical controllers, including those involving textiles, have been of growing interest in HCI and musical interfaces community within the last decade. Research led by Troiano et al. explored the impact of deformable interfaces on musicians [169]. Their study demonstrated that musicians perceived a more intimate and direct connection between their movements and the resulting sound with deformable interfaces than with standard controllers. These interfaces gave musicians a direct ability to shape or sculp the sound in their hand and gestures, and many found it simpler to remember the controls compared to traditional interfaces. Additionally, musicians appreciated the tactile and haptic feedback offered by the deformable interfaces.

Figure 4.4: Illustration of the *KnittedKeyboard*.

Sparked by an early proposal of the *ScarfKeyboard* by Paradiso and Borque [170], and a conversation with world-renowned late jazz pianist and composer Lyle Mays, the idea of a keyboard made from fabric emerged. Besides offering new interactions and tactile experiences for musical expression, this fabric keyboard can easily be folded, rolled up, and packed like a pair of socks or a scarf, making it ideal for composing on the road (Figure 4.4). It can also be wearable, extending the functionality of such fabric-based musical controllers, similar to the keyboard tie demonstrated by Laurie Anderson in "Home of the Brave." Inspired by the theremin's expressive controls and the soft and deformable tactile properties of knitted textiles, we have developed an interactive textile-based musical interface with a familiar layout of piano keys.

4.1.2: Evolution from the FabricKeyboard

The transition from the *FabricKeyboard* [28] to the *KnittedKeyboard* [160] (Figure 4.5) represents a significant advancement in the development of textile-based musical interfaces, leveraging digital knitting technology to enhance scalability, functionality, and user experience. The *FabricKeyboard*, constructed using multi-layer fabric sensors sewn onto a stretchable substrate, enabled a unique combination of discrete keystrokes and continuous controls, including pressing, pulling, stretching, twisting, hovering, and waving.

Figure 4.5: Evolution of prototypes *from FabricKeyboard, KnittedKeyboard I,* to *KnittedKeyboard II*

FabricKeyboard (2017)
12 keys/1 octave

- 12 capacitive touch sensing elements,
- 12 proximity sensing elements (1 multiplexed possible)
- 12 pressure sensing elements,
- 1 stretch sensing element across the keys
- 4 stretch sensing elements across the fabric (2 at both ends and 2 below the keys)
- 12 electric field sensing elements (different board)
- Snap-in accessories/add-ons:
  - 2-axis fabric trackpad with proximity and pressure sensing field
  - Fabric ribbon-controller

KnittedKeyboard I (machine-produced, 2020)
60 keys/5 octave

- 60 capacitive touch sensing elements,
- 60 proximity sensing elements (5 multiplexed)
- 1 pressure sensing elements,
- 5 thermochromic color change (per octave)

KnittedKeyboard II (2021, improved design)
60 keys/5 octave

- 60 capacitive touch sensing elements,
- 60 proximity sensing elements (5 multiplexed)
- 1 pressure sensing elements,
- 1 stretch sensing across the keys

The FabricKeyboard featured 12 keys, each equipped with capacitive touch, proximity, and pressure sensing elements. Stretch sensors were integrated across the keys and fabric, while electric field elements were located on a separate board. Additionally, the device includes a 2-axis fabric trackpad with proximity and pressure sensing capabilities, and a fabric ribbon-controller for enhanced interaction that can be snapped at the top and right side of the FabricKeyboard, respectively [28]. The labor-intensive fabrication process, however, limited its efficiency and scalability. Despite its unique design, it faced scalability and robustness challenges due to the manual processes of cutting, hand-stitching, and machine-sewing.

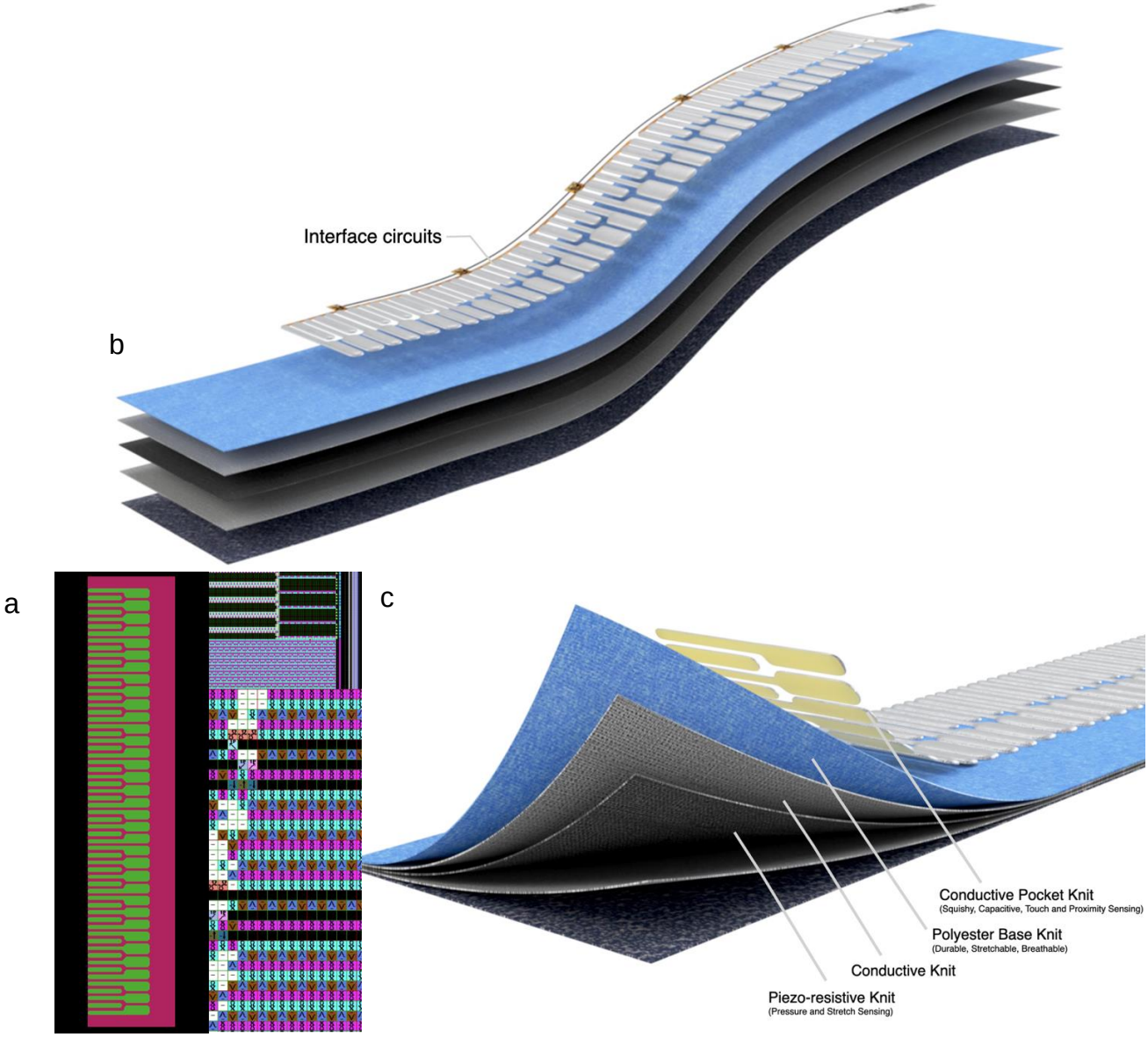

Figure 4.6: a) Digital knitting program and b-c) the exploded view of multi-layer textiles in *KnittedKeyboard II* with its interface circuits.

The *KnittedKeyboard* addresses these limitations by using digital knitting technology to seamlessly integrate functional and non-functional yarns into the textile. This method allows for the creation of intricate patterns and structures with greater precision and reliability. The *KnittedKeyboard* incorporates conductive, thermochromic, and composite yarns alongside high-flex polyester yarns, enabling it to detect touch, proximity, and pressure simultaneously. The use of thermochromic yarns provides visual feedback through color changes, enhancing the interactive experience. Specifically, the *KnittedKeyboard I* [160], machine-produced in 2020, features 60 keys across five octaves, with capacitive touch, multiplexed proximity, and pressure sensing elements. *KnittedKeyboard II* (Figure 4.6) further improves tactile feedback through the knitting of conductive pockets that can be filled with yarns to add a squishy feel (see Appendix A.1). Additionally, it integrates stretch sensors across the keys using piezoresistive fabric. The all textile-based design and digital knitting process facilitate rapid, highly personalized and large-scale production, reducing prototyping time from several weeks to just under two hours.

4.1.3: Digital Knitting Program and Fabrication

For *KnittedKeyboard I*, we utilized a flat two-bed digital knitting machine (Super-NJ 212, Matsuya) and fed it with the following yarns: two cones of silver-plated conductive yarns (150 denier, Weiwei Line Industry), two cones of thermochromic yarns (150 denier, Smarol Technology), and two cones of high-flex polyester yarns (540 denier, 4-ply) combined with melting yarns (150 denier, 1-ply). We fed a cone of silver-plated and thermochromic yarns together on each of the two carriers. Each cone connected to a different yarn carrier, with a total of four carriers used. Intarsia knitting was employed in sections where more than one yarn type was needed, such as in any line where the piano key is plotted. Since it is a two-layer knitting machine, we performed interlock knitting to intersect the front and back fabric layers. It took the machine 1 hour and 40 minutes to knit the entire prototype, which has five octaves of diatonic piano-key patterns. The resulting knitted fabric was steamed at the end to activate the melting yarn, providing structural rigidity to the final prototype.

The single-layer, piano-patterned conductive and thermochromic textile fabricated above could perform touch and proximity sensing, as well as color-changing display when heated. To complement the thermochromic function, we assembled and embedded five textile heaters (one per octave). In order to add pressure sensing capability for modulation, we also developed a fabric pressure sensor that we stacked at the back. It covers the entire active area of the keyboard and consists of a piezoresistive knit fabric (LG-SLPA 20k, Eeonyx) between two conductive knit fabrics (Stretch, LessEMF). In *KnittedKeyboard II*, we eliminated the thermochromic actuation due to the need for external heating elements. Instead, we added strain sensing elements between the keys to provide additional expressive capabilities for the fabric-based musical controller.

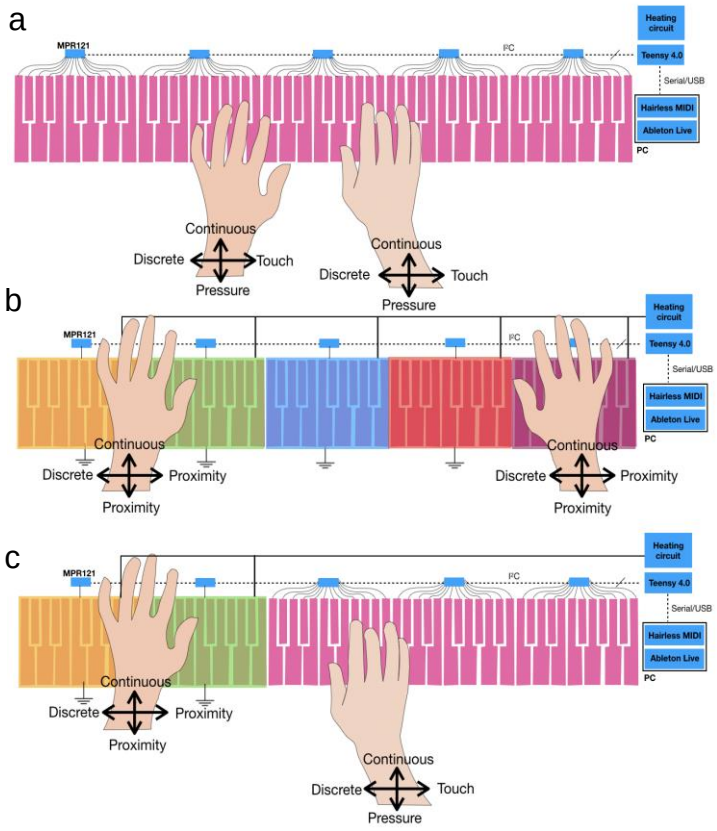

Figure 4.7: System architecture of the KnittedKeyboard I that enables various mode of interactions.

4.1.4: Hardware Design and Development

Figure 4.7 illustrates the various gestural inputs that can be performed on the *KnittedKeyboard* and their corresponding interface circuitry. Each key within an octave is connected to one of twelve printed circuit board pads, which are wired to a capacitive sensing chip (MPR121, NXP Semiconductor) using highly-conductive silver-coated fibers (Liberator 40). The five MPR121 chips are connected to the Teensy 4.0 through 4-wire inter-integrated circuit (I2C) lines. Since an MPR121 can support up to four different addresses (0x5a to 0x5d), we utilized two data (SDA) and clock (SCL) lines in the Teensy 4.0 microcontroller. We developed a flexible PCB with spread-out pads for connection to each key by looping conductive threads (Figure 4.43c). Appendix A.6 and A.7 show the circuit schematic and layout of this PCB with the MPR121. The circuits for the other modalities, such as resistive sensing, were sewn directly onto a breakout board attached to the Teensy 4.0.

The MPR121 performs constant direct-current (DC) charging and discharging for capacitive sensing. By varying the charge current and time, we can adjust the sensitivity of each electrode. It also features a 13th electrode, where all twelve electrodes are multiplexed in-chip to create a large capacitive sensing surface, enabling near-proximity detection across an octave. We found

that setting the charge current to 63 µA and the charge time to 1 µs provided the best dynamic range for large-area proximity sensing, while still reliably detecting touch events. Consequently, the *KnittedKeyboard* has 60 individual touch-sensitive keys that can be programmatically transformed into five proximity-sensing fields.

The MPR121 performs constant direct-current (DC) charging and discharging for capacitive sensing. By varying the charge current and time, we can adjust the sensitivity of each electrode. It also features a 13th electrode, where all twelve electrodes are multiplexed in-chip to create a large capacitive sensing surface, enabling near-proximity detection across an octave. We found that setting the charge current to 63 µA and the charge time to 1 µs provided the best dynamic range for large-area proximity sensing, while still reliably detecting touch events. Consequently, the *KnittedKeyboard* has 60 individual touch-sensitive keys that can be programmatically transformed into five proximity-sensing fields.

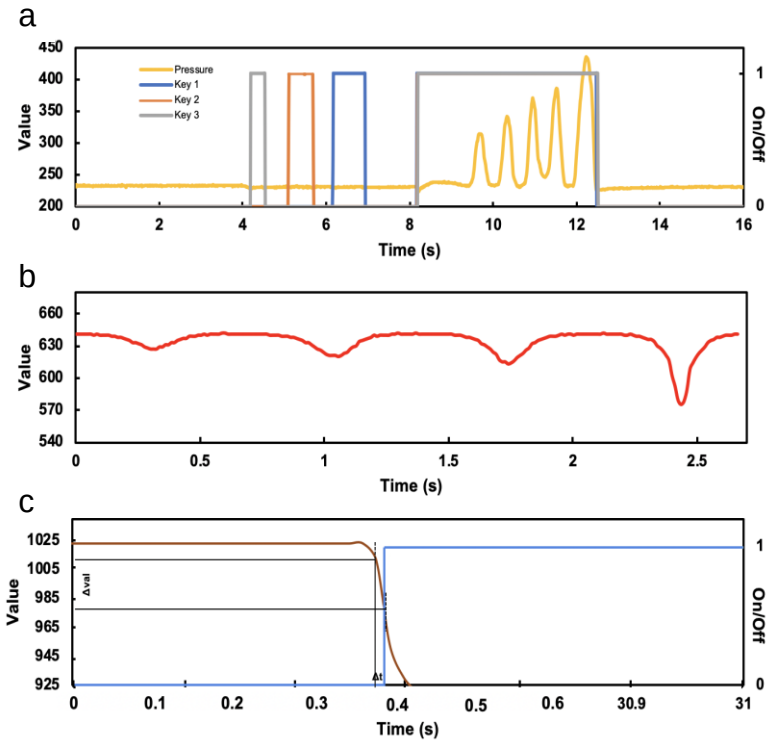

Figure 4.8: Signal response of a) touch events and pressure values from finger strikes and aftertouch, b) proximity values from hands approach, and c) touch event and capacitance value to determine note velocity

The pressure and stretch sensing circuits include a potential divider with a reference resistor tuned to optimal value and connected to the analog-digital converter (ADC) pin of the microcontroller through a voltage follower (TLV2374). The resistance of the piezo-resistive

pressure sensor ranges from 1 to 3 kΩ. The heating circuit consists of an n-channel Power MOSFET (IRLB8721, International Rectifier) with a load resistor, powered by a 6 V external supply. The thermochromic display change is activated in proximity sensing mode, requiring an actuation temperature of 40°C and taking around 5-10 seconds to appear and disappear. This visual feedback informs the user of different modes of play based on the color of the keys. With all touch, proximity, pressure, and heating channels activated, the *KnittedKeyboard* operates at a frequency of 83 Hz. The longest latency for a touch event, excluding serial and software delay, is 12 ms.

4.1.5: Functional Modes and Musical Mapping

The sensing mechanism is based on capacitive and piezo-resistive sensing. Every key acts as an electrode and is sequentially charged and discharged. This creates an electromagnetic field that can be disrupted by hand's approach, enabling us to detect not only contact touch, but also non-contact proxemic gesture such as hovering or waving on the air, contact touch, as well as to calculate strike velocity. The piezo-resistive layers underneath can measure pressure and stretch exerted on the knitted keyboard. All of the sensor data is converted to musical instrument digital interface (MIDI) messages by a central microprocessor, which will correspond to certain timbral, dynamic, and temporal variations (filter resonance, frequency, glide, reverb, amp, distortion, et cetera), as well as pitch-bend. Audio sequencing and generation software such as Ableton Live and Max/MSP map these MIDI messages to their corresponding channels, controls, notes, and effects.

Figure 4.8 shows the sensor outputs from various gestural inputs performed on the *KnittedKeyboard* before getting scaled and mapped into MIDI messages. As can be observed in Figure 4.8a, the keyboard can sense pressure exerted by the fingers, which is mapped to a MIDI channel expression (linked to an after-touch or a reverb for example) with a user-defined expression delay. The keyboard also has the ability to detect hand's approach or hover up to 10 cm above the fabric surface. The output value drops as the hand gets closer to the capacitive sensing area (Figure 4.8b). Finally, Figure 4.8c illustrates a technique to measure finger velocity by calculating the capacitance's slope of descent ($\Delta t/\Delta val$) in between a point where a touch event happens and the previous two proximity values. This technique requires a temporary array of variable in the program, that continuously stores capacitance values of each key before a touch event occurs.

To demonstrate the expressiveness of the *KnittedKeyboard* in a live performance, we collaborated with a pianist and composer. "Fabric of Time and Space" is a contemporary musical piece exclusively written for *KnittedKeyboard II* to illustrate its multi-dimensional expressiveness. The

piece metaphorically represents the expanding and contracting nature of the universe through melodic glissandi and the interplay between major and minor chords. The perturbations of space-time are expressed by the interaction between the performer and the fabric, shaping the sound envelope. The musical translation of these expressions was used to shape the envelope of the sound.

The underlying technology of the *KnittedKeyboard* enables further exploration of soft and malleable gestural interfaces, leveraging the unique mechanical structures of the materials and the intrinsic electrical properties of the knitted sensors. This opens up new possibilities for innovative musical expression and interactive experiences [164], [169].

4.1.6: Limitations and Future Work

There is substantial potential to extend this project in future work. First, we plan to continue our reliability tests, especially focusing on durability through washability tests on the fabric sensors, which will be crucial for ensuring the long-term functionality of the device in practical settings. An exciting next step is to extend the keyboard by adding trackpad and ribbon controllers, similar to the ones demonstrated in *FabricKeyboard,* that could enhance the range of interaction and expressiveness for the user. Additionally, we aim to enhance user interaction by incorporating fabric-based actuators that provide haptic feedback, allowing musicians to feel subtle vibrations or forces as they play, deepening the immersive experience.

A key limitation we've encountered is that the uniform color of the keys makes it difficult to differentiate between black and white keys, which may affect ease of use during performance. Additionally, capacitive sensing can behave differently for different users, so personalized calibration may be necessary to achieve consistent performance. Moreover, with so many sensing modalities at play (proximity, pressure, stretch, etc.), there is still much to explore regarding how to best alternate or combine them all for musical mapping, performance, and composition, ensuring that they enhance rather than complicate the user experience.

We plan to conduct in-depth user tests with different groups. For example, we aim to study expert and early-stage keyboardists to examine how each group interacts with the fabric keyboard, understanding the nuances of their use and how the device can be optimized for both professional musicians and novice users. We are also interested in collaborating with performers to brainstorm how this keyboard could be integrated into stage performances, either in its current form or through custom format, such as a wearable version. Creating these custom iterations could lead to novel performance techniques and foster more creative uses of the instrument in a live context.

Moreover, we aim to integrate visual elements into the fabric, using technologies such as electrochromic or electroluminescent fibers to create dynamic light patterns that respond to the player's actions. This would not only enhance the sensory experience for the performer but also create visually engaging performances for the audience. In summary, the potential for further developing this fabric-based musical controller is vast. Our goal is to contribute not only to the realm of fabric-based musical instruments but also to broader fields of physical interaction design, especially in the integration of electronic textiles for new interactive media.

4.2: 3DKnITS

4.2.1: Motivation and Related Work

We are motivated by the fact that most of our physical gestures and interactions involve contact between different parts of our body and a surface. During daily activities such as walking, sitting, exercising, or sleeping, characteristic spatiotemporal contact and pressure patterns can be monitored and identified through sensing fabrics in our apparel or upholstery (Figure 4.9a). As illustrated in Figure 4.9b, we propose a knitted piezo-resistive textile matrix for tracking and classifying activities. Monitoring biomechanical forces with high accuracy, repeatability, and comfort through wearables or sensing surfaces remains a research and practical challenge.

There are two common methods of pressure sensing in electronic textiles: capacitive and resistive-based. The capacitive approach consists of a spacer fabric between two conductive layers. Meyer et al. used a textile insulator between a bottom common electrode fabric and an embroidered array of electrodes as a top fabric for activity detection, specifically to recognize sitting postures [158]. The spacer was chosen to be squishy to improve the comfort of the pressure sensor. However, this method suffers from stray electromagnetic noise, requires shielding layers, and complex read-out circuits. Resistive sensing, on the other hand, leverages a piezo-resistive element in the form of yarn or fabric as a middle layer between two conductive elements [171]. The resistance of the piezo-resistive element changes as force is exerted due to the bridging of conductive particles. A cross-configuration of piezo-resistive sensing textile, with conductive top and bottom matrix lines, allows for distributed 2D pressure sensing across the fabric. Some efforts have also integrated piezoelectric materials in threads or textiles to detect vibration [172], [173]. However, this method does not measure pressure continuously and works only as a dynamic pressure or impact detector

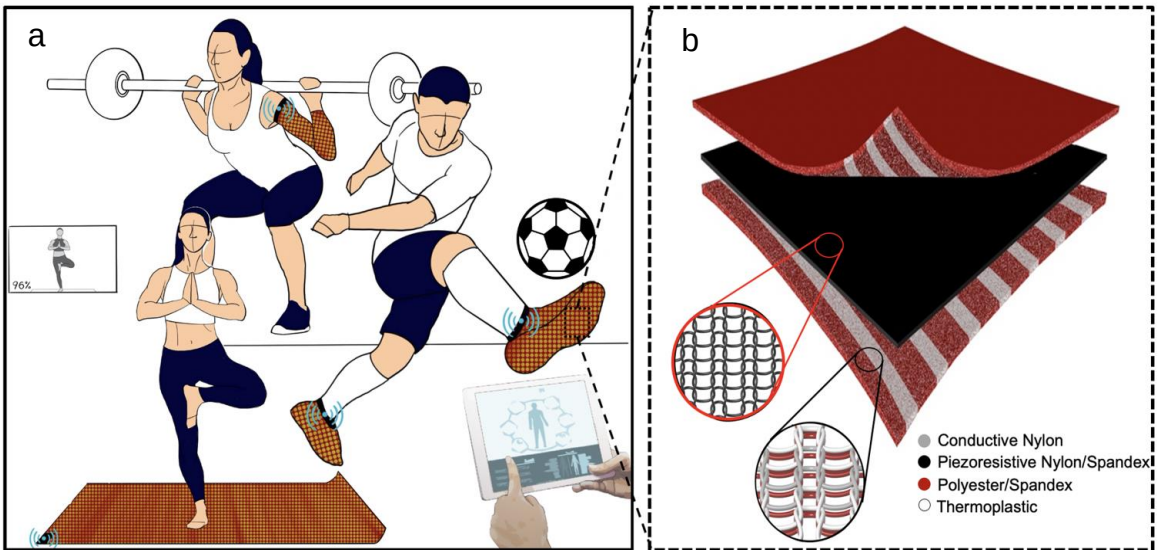

Figure 4.9: a) Illustration of 3D-knitted wireless intelligent textile for sport biomechanics. b) Multi-layer structure of pressure-sensitive textiles showing all the yarns used.

Piezo-resistivity in pressure-sensing textiles has been explored in many projects, particularly in human-computer interaction (HCI), sports, and medical science. In HCI, they have been used as 2D tactile inputs for musical or multimedia interfaces [28], as well as deformation sensors in the form of sleeves for fabric-based gestural interaction [174]. Several researchers have also explored the use of 2D pressure-sensing textiles integrated into mats, gloves, or clothing for object and human activity or posture recognition. Most of this work analyzed the subtle pressure distribution changes across the fabrics throughout the activity and applied machine learning principles for feature extraction and classification [90], [175]. Piezo-resistive textiles have also been widely used in rehabilitation and medical applications, such as gait analysis [176], respiration sensing [177], pressure ulcer monitoring and prevention [178], and compression therapy [179]. Due to their breathable, soft, and comfortable nature compared to flexible pressure sensing grids, these piezo-resistive sensing textiles can also be used to augment prosthetic covers, linings, or even robotic skin. Leong et al. presented a 2D piezo-resistive textile that covers a prosthetic foot for closed-loop, sensory-haptic feedback [180], while Data Glove provides a textile-based conformal pressure array for prosthetic and robotic hand applications [181].

Our approach to personalization ensures that textile wearables and structures are robust, form-fitting, and conformable, resulting in accurate and intimate sensing while maintaining comfort. Moreover, it allows for the rapid, large-scale manufacturing of electronic textiles with customizable looks and functions.

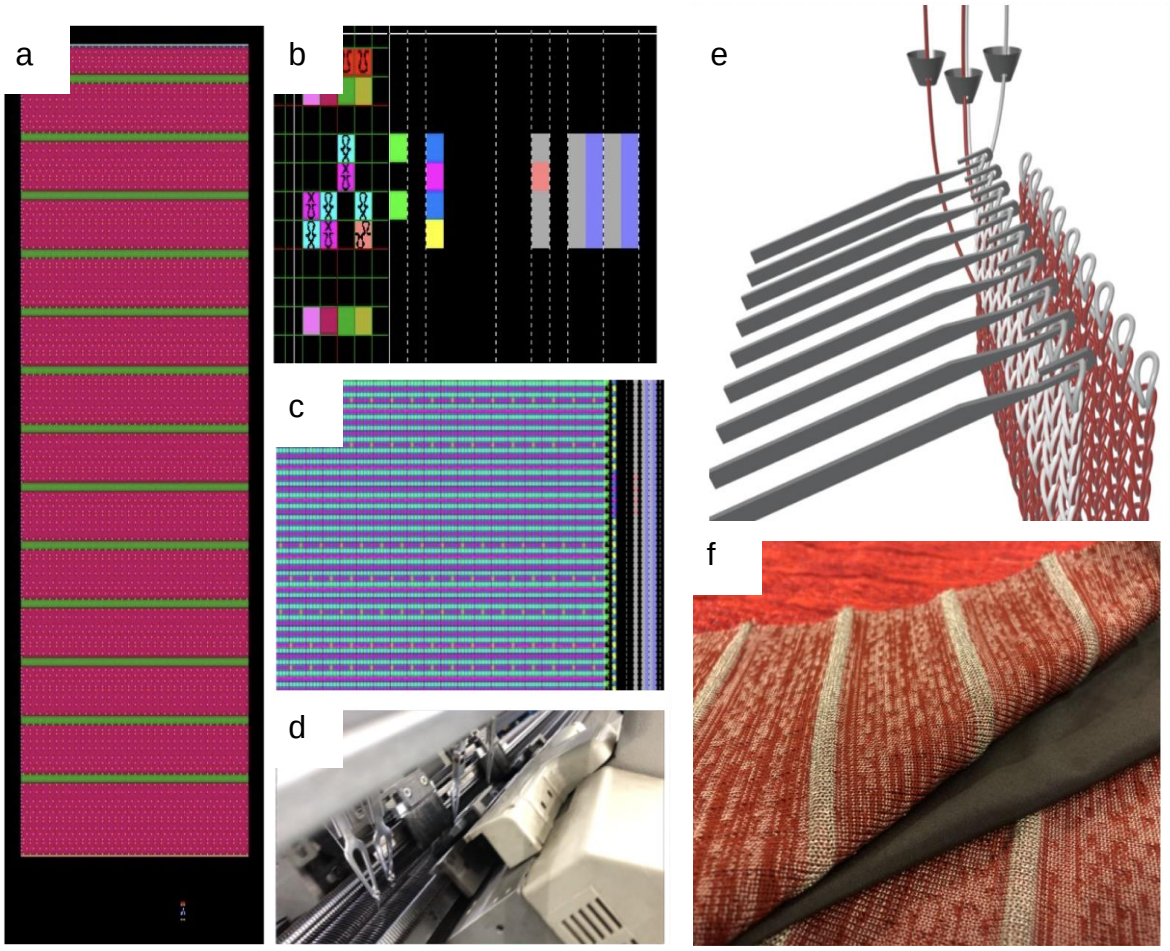

Figure 4.10: a) A knitting machine program with horizontal conductive interconnects design in green blocks and common, interlocked polyester yarns in maroon and pink blocks. b) Abstraction library that converts simple knitting program in (a) into line-by-line, machine-readable format in (c). d) Knitting machine in action showing all the yarn carriers being moved sideways by the slider. e) Flat-bed knitting structure with three yarn carriers (single polyester/conductive and twisted composite with melting yarn). f) Prototype of the pressure-sensitive textile with horizontal-vertical interconnects from knitted conductive yarns and PPy-coated knitted piezoresistive textile in the middle.

4.2.2: Digital Knitting Program and Fabrication

In this work, we leverage digital knitting techniques using flat-bed and circular knitting machines with thermoforming techniques to create 2D to 3D piezoresistive matrix textile mats and wearables capable of detecting multipoint pressure across their surfaces in real-time. This fabrication approach allows us to explore various parameters, including interconnect resistance, matrix resolution, pressure sensitivity, and the fabric's visual, mechanical, and electrical properties through functional and common fiber choices and knitting structures.

The knitting machine (Super-NJ 212, Matsuya) has two-layer beds, and we applied an interlock mechanism to blend two layers into one textile layer (Figure 4.10a-d). This insulation suppresses any possible parasitic impedance or shorts from the environment. By mixing polyester with melting yarns, we ensure strong adhesion between multiple layers and prevent sensor noise from motion artifacts due to fabric slippage (Figure 4.10e). One of our final prototypes is a piezoresistive mat with 1 cm width of knitted conductive lines (6 loops) and a 2.5 cm pitch, resulting in a total size of 45 x 45 cm with 16 x 16 knitted conductive lines.

The Three-dimensional Knitted Intelligent Textile Sensor (*3DKnITS*) comprises multi-layer knit textiles fused together through intrinsically-knitted bonding or melting fibers (Figure 4.10f). A piezoresistive knit textile (LTT-SLPA60k, Eeonyx Corporation) is sandwiched between two conductive knit textiles. The piezoresistive material is developed by coating polyester knit fabric with polypyrrole (PPy), an organic conducting polymer formed by the polymerization of pyrrole. This layer exhibits the piezoresistive effect that induces a change in its electrical properties when mechanical pressure is applied. This resistance change is constantly read by the outer transmission layers, which form a 2D conductive matrix. These layers are machine-knitted using a digital flat-bed knitting machine, combining polyester (270 denier, 2-ply, red), conductive (300 denier, Weiwei Line Industry, grey), and TPU as melting yarns (150 denier, 1-ply, white), as shown in Figure 4.10e. The outer layers (Figure 4.10f) are completely insulated on one side (all-polyester) and partly conductive on the other side (sequence of conductive lines in between the polyester base).

Figure 4.11a illustrates the *3DKnITS* shoe, sock, and sleeve fabrication and thermoforming process. To develop a tubular knit textile, we used a digital circular knitting machine with polyester, spandex, conductive, and TPU yarns (Figure 4.11b). This machine greatly increases productivity by replacing the relatively slow reciprocating motion of flat knit machines with a

continuous and faster circular motion. Circular knitting is primarily used to make various tubular garments such as socks, shoes, sleeves, underwear, or t-shirts. The result is a seamless *3DKnITS* with a customized orthogonal conductive stripes pattern in a tubular form-factor.

To create form-fitting apparel or prosthetic lining customized to the wearer, 3D-scanning of the human body can be performed to create 3D-printed models of the limbs, or in the case of footwear design, a shoe-last that best fits the user based on their size, as demonstrated in Figure 4.11d-e. Figure 4.11f shows a full prototype of the *3DKnITS* connected to the system hardware for sensor read-out and wireless communication. We sewed in TPU-insulated silver-conductive threads to connect each knitted conductive line on the skinner to its corresponding pin on the PCB. There is a total of 96 (8 x 12 matrix lines) pressure-points spread across the 3D surface of the skinner, with 1 cm width of knitted conductive lines and around 2.5 to 3 cm pitch (Figure 4.11c).

4.2.3: Textile Sensor Characterization

We performed mechanical and electrical characterization using a compression and tensile testing unit (Zwick BTC-EXMACRO, Roell) and a custom resistance sensing circuit (potential divider, buffer circuit, and 12-bit ADC) to study the relationship between force and resistance of the knitted textile sensors. For compression testing, we set the Zwick's crosshead speed to 10 mm/min with a 10 N preload on a piezo-resistive textile swatch with a 1 x 1 cm active area. For tensile testing, we set the crosshead speed to 10 mm/s with a 5 cm distance on 4 x 10 cm polyester-TPU textile swatches. As shown in Figure 4.12a, we compared two textile sensors: one with and one without TPU yarns and the thermoforming process.

Without thermoforming, the sensor exhibits non-linearity and significant hysteresis when compressed and relaxed due to volume gaps and discontinuities between layers, which can cause textile and sensor drifts. The untreated knitted sensor shows a large hysteresis gap of around 130% compared to a reduced gap of 27% in the thermoformed knitted textile sensor at a 100 N force. However, this improvement comes with a compromise in force-resistance sensitivity, which decreases from 58.7–2955 to 39.4 below a 500 N load. The thermoformed textile also demonstrates superior mechanical integrity due to strain (Figure 4.12b), making it much less sensitive than the untreated textile by approximately one-fourth, which enhances its robustness against secondary effects due to axial load. During cyclic compression tests (n = 100, crosshead speed = 30 mm/min, and cyclic min/max load = 10/1000 N), the thermoformed textile shows reliable performance with a steady response after the first 10 cycles (Figure 4.12e). Scanning electron microscopy (SEM) images in Figures 4.12c,d detail the yarn structures and surface texture of the knitted sensors before and after thermoforming

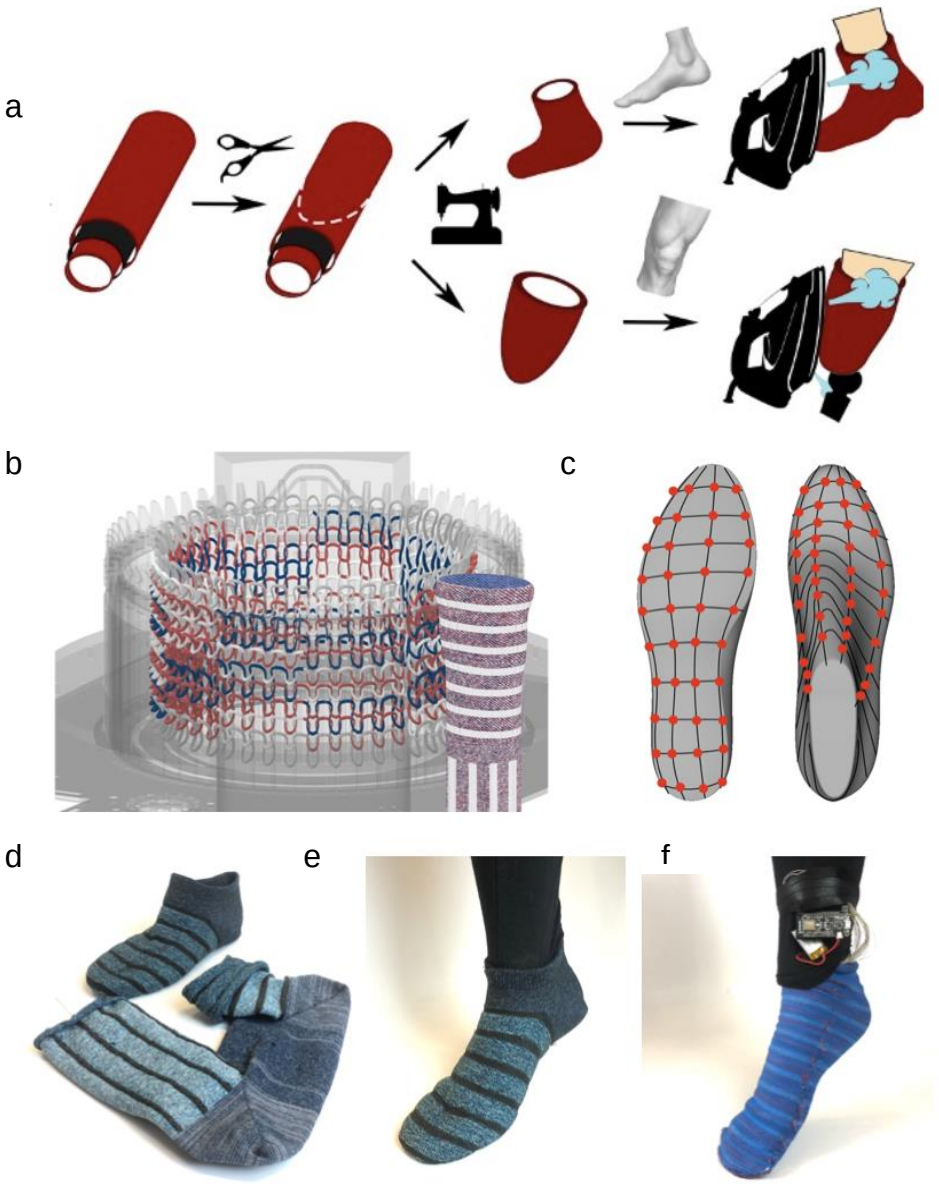

Figure 4.11: a) 3D shaping and thermoforming of tubular knitted e-textiles for intelligent shoe or prosthetic lining and socket. b) Illustration of a circular knitting machine with tubular knitted conductive textiles. c) Pressure sensor mapping across the 3D shoe. d-e) Knitted prototypes before and after thermoforming with shoe-last. f) Fully-functional prototype of custom 3D-KnITS smart skinner/shoe worn by the user and connected to its interface circuits with battery and wireless transmission.

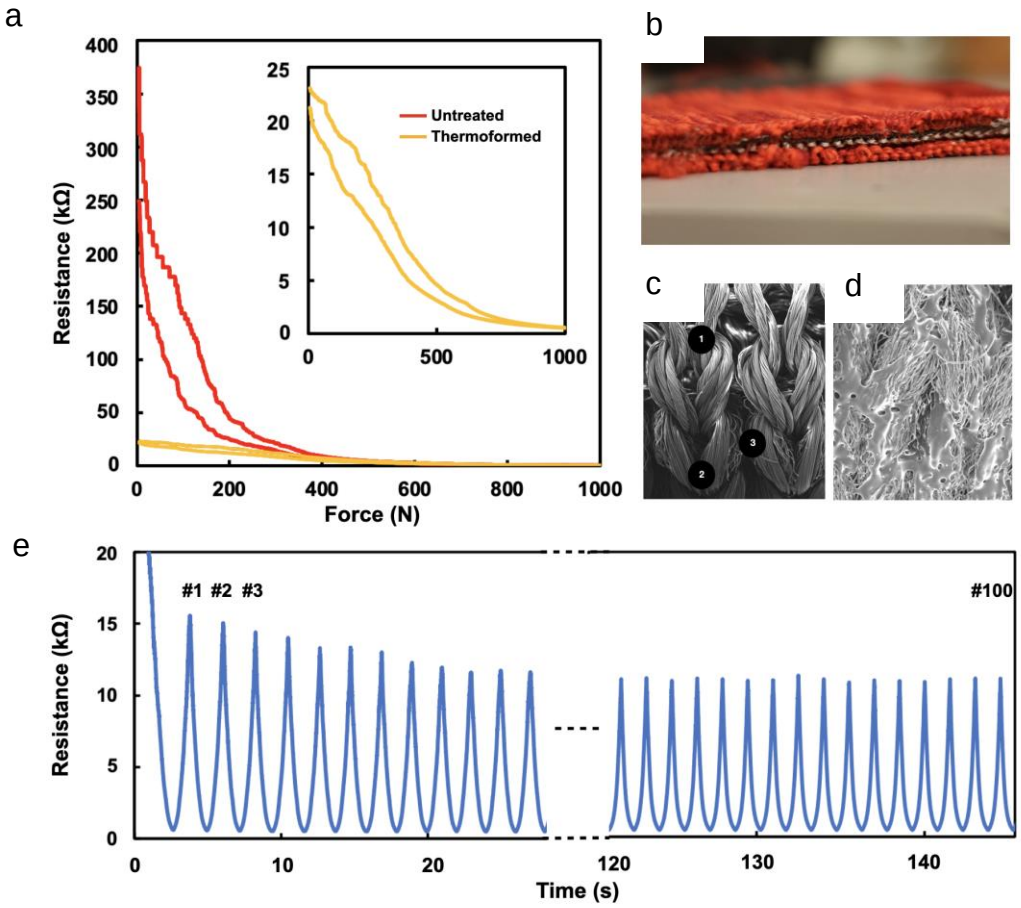

Figure 4.12: a) Force vs resistance characterization of both the untreated and melting-yarn, thermoformed multi-layer piezoresistive knit textiles. b) Close up picture of the cross-section of the thermoformed piezoresistive textile. c-d) SEM images of the knit structure and surface before and after thermoforming. e) Repeatability, cyclic test showing the robustness of the thermoformed piezoresistive knit textile.

4.2.4: Hardware Design and Development

Since we are working with a row-column resistive sensor matrix, we need to design a system that can scan through each line and read the entire 2D pressure points. Our system should also be robust against various sources of noise, including ghosting effects and neighboring crosstalk, which can affect the precision and accuracy of the readings. Figure 4.13a and Appendix A.8 and A.9 show our system's final PCB design, measuring 3 x 5 cm. The circuit consists of a 16-pin multiplexer (CD74HCT4067, Texas Instrument), two 8-pin shift registers (SN74LS595D, Texas Instrument), four 4-pin single-pole double-throw (SPDT) multiplexers (ADG734BRUZ, Analog Devices), and a potential divider with a buffer op-amp (TLV2371, Texas Instrument). The circuit enables scanning of 16 x 16 matrix lines for a total of 256 pressure sensing points. The board was

designed as an extension or a shield so users can choose the main microcontroller and wireless communication of their choice. Using an nRF5282 module with a 64 MHz ARM Cortex M4F (Nordic Semiconductor), we observed a scanning frequency of 15 Hz for the 16 x 16 matrix (which can reach up to 200 Hz using a Teensy 3.6 with a 180 MHz ARM Cortex-M4), 27 Hz for an 8 x 12 matrix with wired universal serial bus (Serial-USB), and approximately 20 Hz with wireless Bluetooth low energy (BLE) transfer.

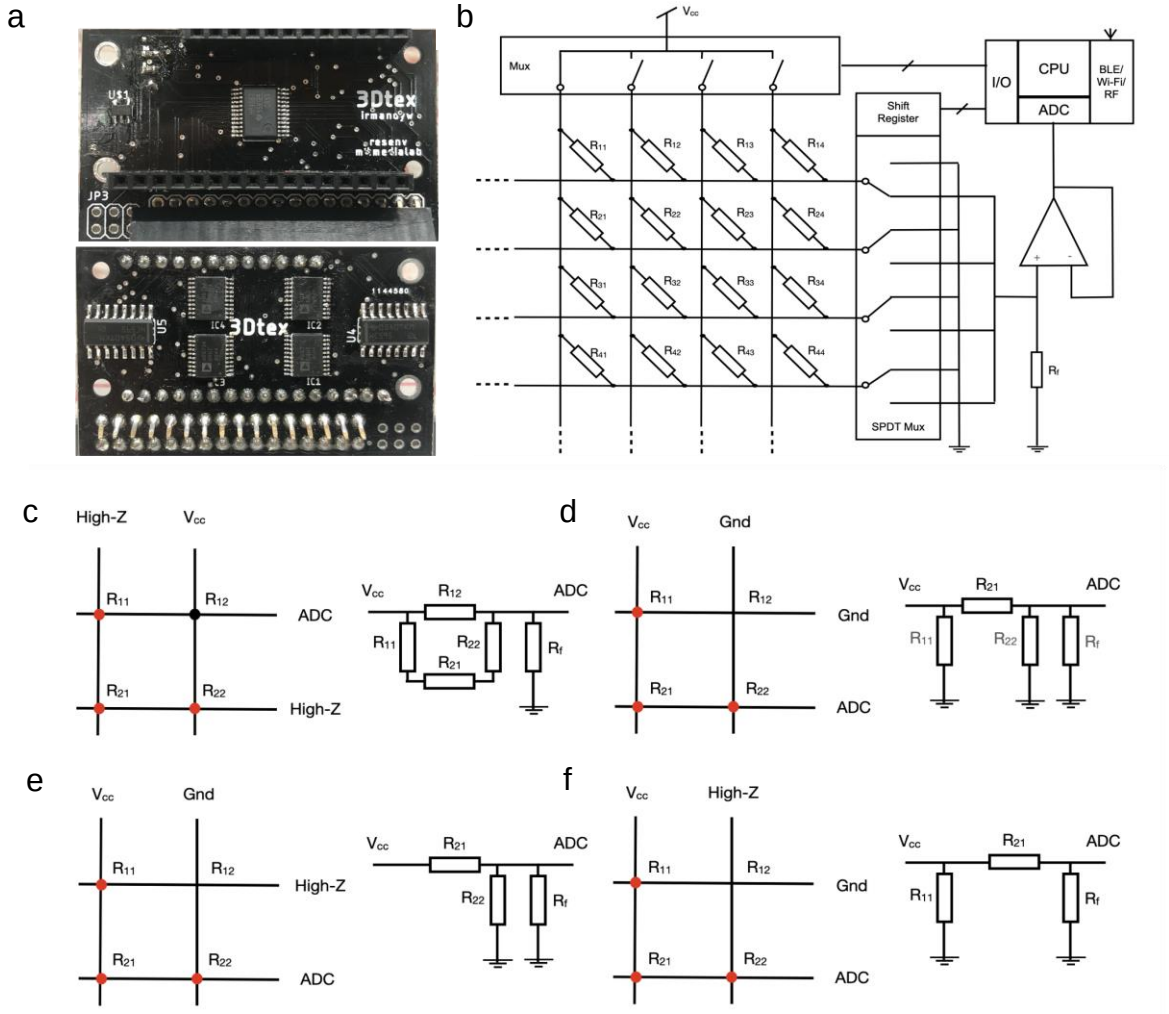

Figure 4.13: a) PCB design of the robust piezoresistive matrix array circuit consisting of b) a 16:1 multiplexer, 2 shift-registers, 4 single-pole double-throw (SPDT) muxes, and a buffer and potential-divider circuit that connects to the main micro-controller for wired-wireless control and data transfer. c-f) Studies of influence and intervention strategies for sensor ghosting and crosstalk from neighboring nodes and multi-pressure points (R_f meaning reference resistor for potential divider).

The vertical multiplexer periodically switches a 3.3 V voltage supply to each column while putting the rest on high-impedance. The horizontal SPDT multiplexers with shift registers connect the resistive sensing circuit to the ADC pin at the row of interest and ground the rest of the row lines, switching from one line to the next in sequence (Figure 4.13b). This mechanism solves ghosting and crosstalk issues common in most resistive sensing array read-out circuits [182], [183]. If we apply high-impedance to the rest of the row-column pins, as illustrated in Figure 4c, ghosting effects appear at the sensor point R12 due to the bridging connection between R11, R21, and R22. If we want to read sensor point R21, the switching configuration in Figures 4.13d and 4.13e shows that crosstalk from sensor points R11 + R22 and R22, respectively, will influence the R21 read-out. In our circuit configuration solution (Figure 4.13f), no connection exists from R22 or R12. R11 will also not interfere with the potential divider circuits and ADC readings as it is connected to the ground. Another possible approach is to use transimpedance amplifier on each row instead of the switching mux [184]. This hardware design ensures accurate and precise readings from the resistive sensor matrix, minimizing the effects of ghosting and crosstalk, and allowing for robust performance.

4.2.5: Sensor Data Processing and Deep-learning Algorithm

As a subset of machine learning, deep learning has flourished in solving complex image processing and speech recognition challenges. It provides an efficient way to learn high-level features from raw signals without complex feature extractions by training an end-to-end neural network [185]. In this work, we treat our spatiotemporal 2D pressure sensor data or heat-map similar to image frames. As a user balances and redirects their center of mass through their feet, they exert force on the ground. By detecting this pressure distribution through our intelligent mat, we can extract rich contextual information about posture and activities.

We conducted experimental testing on a healthy adult male volunteer, who provided signed consent and had no prior medical history of chronic disease or physical disability. This study complied with the guidelines of the Institutional Review Board of the Massachusetts Institute of Technology Committee on the Use of Humans as Experimental Subjects (COUHES Protocol 2009000229). We gathered training data for two types of recognition: seven common activities and exercises (Figure 4.14a), such as standing, walking, jumping, planking, and push-ups, and seven yoga poses (Figure 4.14b), including default position, tree, eagle, tree drishti, eagle drishti, warrior three, and balancing pigeon

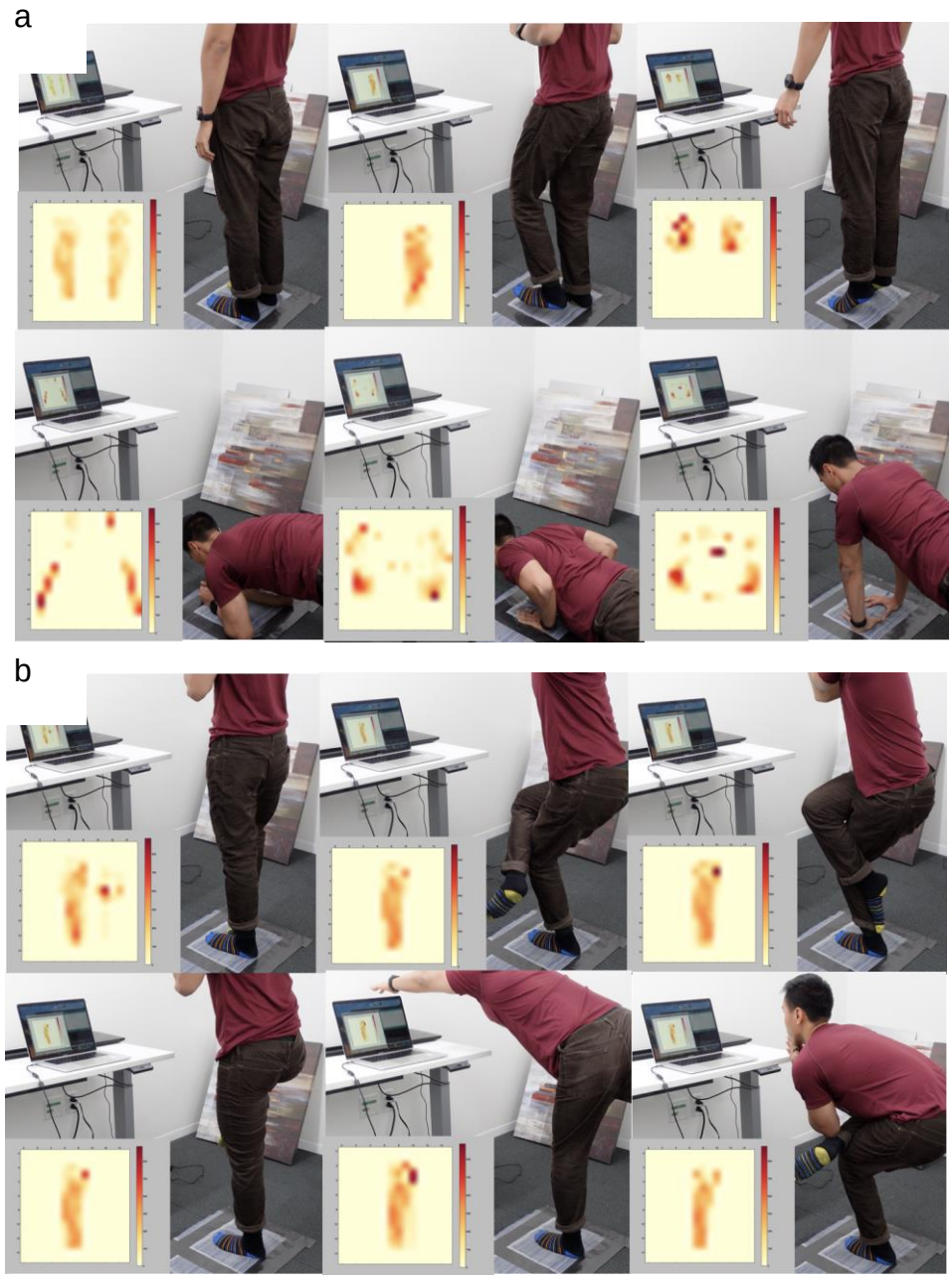

Figure 4.14: a) Pressure heat-maps of basic activities and exercise: standing, walking, tip-toe/jumping, planking, normal push-up, and diamond push-up. b) Pressure heat-maps of basic activities and exercise: standing, walking, tip-toe/jumping, planking, normal push-up, and diamond push-up.

The spatiotemporal pressure data were recorded and transmitted to a central processing unit. Each type of activity was performed and recorded sequentially for around one to two minutes. We collected a total of 7,160 pressure data frames for common activities and exercises and 13,040 data frames for yoga postures. This 22 minutes in total of training datasets were then randomized, segmented, labeled, and finally processed (80% for training, 20% for testing) in our personalized convolutional neural network (CNN) algorithm.

CNN has been demonstrated to achieve high accuracy for human activity recognition compared to other methodologies such as KNN, SVM, Extra Trees, or Random Forest [23,24]. The overall architecture of our 2D CNN model is depicted in Figure 4.15a. We utilized the layer-by-layer Sequential API of the Keras package with the sci-kit learn library.

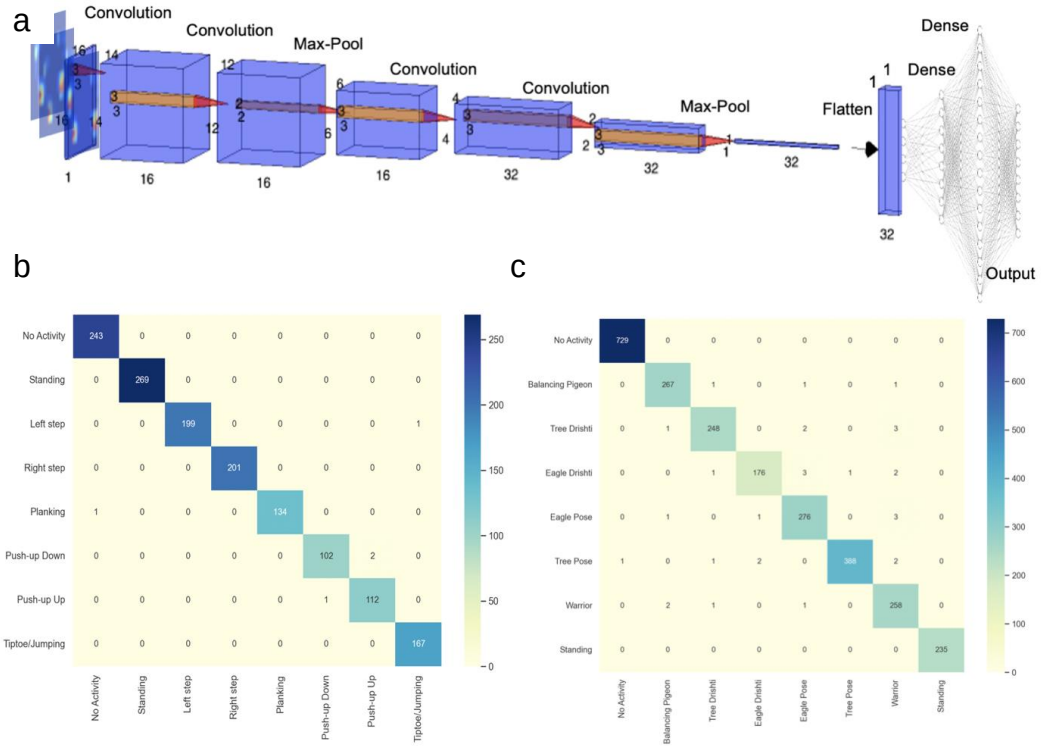

Figure 4.15: a) Convolutional neural network process and parameters schematic. b) Confusion matrix for classifying basic activities and exercises. c) Confusion matrix for classifying yoga poses.

The proposed network comprises four convolutional layers (Conv2D). We used nine weights on our 16 to 32 filters to evolve a pixel into a weighted average of itself and its eight neighbors for each convolutional layer. The network picks up valuable features as these weights are processed over the entire image. The Max-Pooling layers select the highest value from scanning the four neighboring pixels and reduce the image size by half. Combining convolutional and pooling

layers helps our network learn more high-level features of the image input. In our final classification process, we used the features in two fully-connected Dense layers based on previous output from the earlier layers. Batch Normalization allows us to optimize training time while Dropout randomly sets zero weights at each hidden layer in the training sample, driving the network to learn features in a distributed manner, reducing overfitting and generalization error.

In our final CNN model, we added 2 Conv2D layers with 16 filters and ReLU activation, 2 Conv2D layers with 32 filters and ReLU activation, 4 Batch Normalization layers, 2 Max-Pooling layers, 4 Dropout layers (3 with Dropout of 0.25, 1 with Dropout of 0.5), 2 Dense layers with ReLU activation, and a final Dense layer with soft-max activation. To improve accuracy, we used 50 epochs to train the CNN model and evaluated the accuracy using the 20% testing set. Figure 4.15b,c show the confusion matrices for both activity and yoga posture classification. The CNN models were able to classify all activities and poses with high accuracy of around 99.6% and 98.7%, respectively, offering great prospects for high-accuracy detection or recognition based on a deep-learning approach.

4.2.6: Applications

To demonstrate practical applications of our knitted intelligent textile mat, we developed a sliding window algorithm to infer transient activities such as walking, running, and jumping based on our classification results. For instance, by detecting the positions of the left and right feet on the mat, we can determine if a user is standing, walking, or running by analyzing alternating foot patterns within a specified time window, or sequences of standing, tiptoe, and no activity for jumping events. As shown in Figure 4.16a, we interfaced our recognition results to control a Minecraft video game in real-time, gamifying exercise. Additionally, by showing real-time yoga pose classification results, we could inform users if they have achieved the correct balance or pose, using training data reinforced by an expert.

As one of the world's most practice sports, a significant research effort has been conducted to study the science behind soccer [186]. We chose to explore the functionality of our 3D knitted sensing shoe or sock in this sport, which involves various biomechanical movements such as gait, balance, and muscle coordination when running, sliding, and kicking a ball. It also includes positioning the ball on the shoe to ensure the correct angle and trajectory.

In our preliminary test, shown in Figure 4.16b, we observed the responses of three pressure sensors: two plantar pressure points at the back and front of the foot, and one dorsal pressure point at the front of the foot. At heel strike, there is an increase in pressure at the corresponding sensor location. As the user prepares to kick the ball before toe-off, pressure gradually transitions

from the bottom to the upper region of the foot. After toe-off, and at the moment of kicking the ball, we observed a subtle pressure response on the surface of the shoe at the foot-ball interaction location. To better understand the spatiotemporal pressure data, we developed a real-time 3D visualization tool that represents the data as a heat map (Figure 4.16c).

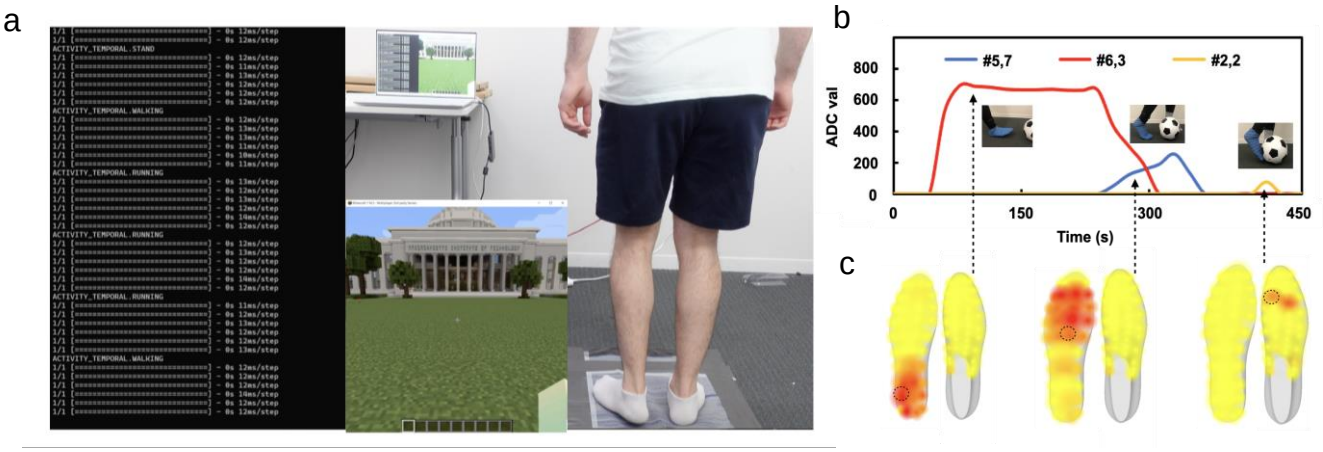

Figure 4.16: a) Example application of classifying movements (i.e. running or jumping) to control a Minecraft game. b) The smart skinner shoe for gait, biomechanics, and foot-ball interaction sensing. Transient sensor data of three points (row, column #5, 7, #6,3 , and #2,2) located in the shoe and (c) Plantar and dorsal pressure heat-maps of the entire 96 sensing points across the shoe before and during a kick event.

4.2.7: Limitations and Future Work

In summary, we have presented a set of 2D and 3D knitted pressure-sensitive textiles for various applications, including activity recognition and biomechanical monitoring, using industrial flat-bed and circular machine knitting techniques. We also designed a custom hardware circuit that enables accurate piezo-resistive matrix read-out while addressing ghosting and crosstalk issues, eliminating the need for sensor data post-processing. Our choice of materials and digital fabrication approach allows for tunable sensing resolution and customizable form factors based on the user's needs and requirements. This results in robust, scalable, low-cost, and sustainable interactive sensing textiles using knitting and thermoforming techniques. Compared to existing thin-film force-sensing and pressure-imaging technologies, our textile-based method is more seamless, breathable, comfortable, and intimate for the wearer, potentially improving interfacial contact and sensing accuracy [187].

We have fabricated prototypes of *3DKnITS* in the form of an intelligent mat and shoe, demonstrating several applications, including high-accuracy, deep-learning-assisted activity and posture recognition for real-time exercise and gaming interaction. Additionally, we proposed a smart soccer shoe that can track a player's movements and localize foot-ball interactions. Unlike camera-based systems, which can raise privacy concerns due to continuous, invasive sensing and recognition, our pressure-imaging approach is less intrusive and is not affected by line-of-sight or lighting levels.

However, the prototypes and applications of *3DKnITS* presented here are still in their infancy. To accommodate a larger-scale system, we need to modularize both the knitted textile sensor and hardware modules by applying distributed processing and networking principles [122]. This will enable the collection of larger datasets useful for applications such as room-scale sensing or crowd recognition. More subjects and labels will be needed to further validate the practicality of the knitted intelligent mat beyond our user-specific models. With the current labels, additional applications such as counting and timing exercises can be integrated into our real-time visualization and feedback system.

By increasing the resolution of our matrix and localizing interesting features, we could improve accuracy and eliminate the need for subjects to perform activities across the entire mat surface when gathering training data. Currently, there are separate models for common activities and yoga postures. Combining these models could make the classification process and applications more universal. Collaboration with physical therapists, orthopedics, and yoga experts for prototyping, study design, and data gathering will also benefit real testing, implementation, and identification of use cases for this technology. Finally, temperature and humidity or sweat tests could be conducted to study the effect of environmental factors on sensor properties.

The 3D knitted shoe or sock could be used to gather biomechanical and form-fitting data, which are useful not only for athletes and dancers but also for prosthetic designers and shoemakers. The same fabrication principles can be applied to develop other types of intelligent apparel, including sleeves, gloves, and shirts. Ultimately, since textiles are ubiquitous in our environments, the *3DKnITS* process and technology can spark intelligent textile and ubiquitous computing applications spanning activity tracking, biometrics, identification, sports and gait analysis, robotics, and human-computer interaction, creating new kinds of wearable technology and interactive environments.

4.3: Tapis Magique

4.3.1: Motivation and Related Work

"When the music and dance create with accord...
their magic captivates both the heart and the mind"
Jean-Georges Noverre

Body movements and gestures allow us to communicate, experience, and perceive each other and the world. Choreographers and dancers rely on these movements and gestures to create and express their art and intention. Dance and music have traditionally been two complementary art forms, with ballet tracing back to the Italian Renaissance in the 15th century [188]. However, their bi-directionality and seamless integration have been challenging and are a growing research topic in contemporary practices [189]. Choreography is often rehearsed to a musical piece, with dancers typically conforming to a predetermined routine, leaving limited space for agency and improvisation over both the visual and audio components. Integrating technology into interactive performances can introduce and augment new forms of expression, allowing dancers to gain more agency and become an integral part of music-making through the mediation of sensors and computers [190].

Ballets Russes by Diaghilev and Stravinsky in 1917 is an early demonstration of interactive performance that involves choreography, lighting, and objects played on a scenodynamic stage [191]. Another early example of a musical instrument exploring the direct relationship between movement and sound, particularly for dance is the *Terpsitone*, a system with similar working like the *Theremin* but with a base platform as capacitive-based control antenna instead. It was invented by Leon Theremin around the 1930s [192], [193]. The *Odyssey of Variations V* by Cage, Cunningham, and collaborators in 1965 is also a prominent example of the deep integration of music, dance, and technology, with dancers influencing the audio and visual elements directly through a dozen photoelectric cells and analog electronic sound mixing systems by Max Matthews and Bell Labs and five capacitive antennas for proximity sensing developed by Robert Moog [194]. At the time, the performance was a successful cross-pollination and collaborative effort between composers, dancers, visual artists, and hardware engineers.

As electronics became more miniaturized and new sensing modalities became available, there has been great interest in detecting human gestures for new kinds of performance or musical expressions. The *Digital Dance Project* used *the Big Eye*, a video camera with a software application that could recognize movement, acceleration, and position through image processing and send

standard MIDI messages to trigger sound and modulation [190]. *Palindrome Intermedia Performance Group* with their EyeCon, as well as David Rokeby with his *Very Nervous System* also developed a similar process, leveraging video and movement tracking, computer programs, synthesizers, and sound systems [195], [196]. The sound mapping and synthesis in their *Seine hohle Form* performance were done in real-time through a Max/MSP environment. Other work such as the SKIN project, have looked further at the physical activity of the dancers and the inner physiological signals or biometric data, such as heart rate, respiration, temperature, humidity, and muscle activity as input parameters [197]. Yamaha engineers with dancer Kaiji Moriyama have also applied back muscle sensing through distributed electromyography (EMG) and leveraged AI to convert the sensor data into MIDI messages to control a Disklavier piano and pedal in real-time, as demonstrated in their concert *Mai Hi Ten Yu* [198].

Figure 4.17: The geometrical patterns of the stars scattered around the brushstroke details on the tapis represent 1800 pressure-sensing pixels and are inspired by the galactic space. Parametric design transformed these patterns into a 3D spatial illusion to illustrate the multi-dimensionality of the sensor data.

In a softer, garment-based form-factor, Yamaha *Miburi* is a commercial wearable musical instrument consisting of a vest with capacitive displacement sensors, two hand-grips, a pressure sensor-embedded shoe, and a belt acting as a processing unit [199]. Researchers have also proposed with other methods, such as embedding suites of sensors (such as PVDF, force-sensitive resistors, inertial measurement units, bend sensors, and capacitive electrodes) into shoes [200], gloves [201], [202], and dance costumes [203], or embedding piezoelectric cables into a carpet [204]. As accelerometers and cameras have become more accessible, miniaturized, and advanced, we have seen many interactive performances and commercial products involving these technologies [205], [206].

Expanding the scale and application of *3DKnITS*, *Tapis Magique* is a pressure-sensitive, knitted electronic textile carpet that generates three-dimensional sensor data based on body postures and gestures, driving an immersive sonic environment in real-time (Figure 4.17). *Tapis Magique* demonstrates the interplay between art and technology, highlighting the deep emotional link between contemporary textiles, dance, and music through the physical-digital connection. It provides a canvas for dancers and sound artists to modulate sound, perform, and compose musical pieces based on choreography. It also creates an auditory-gestural synesthetic environment that invites and encourages audiences to interact and express themselves with the tapis, experiencing a magical connection that stimulates the body and mind (Figure 4.18).

A rollable, programmable interactive textile surface, rather than wearable devices, offers several advantages. It is less cumbersome and more versatile for dancers, allowing them to wear their typical performance costumes, and the active region or area, this is not typically a problem since performances are usually situated it can sense multiple dancers without adding complexity. Although sensing field is limited to on a surface or a stage, performances are usually situated it can sense multiple dancers without adding complexity. Although sensing field is limited to on a surface or a stage.

4.3.2: Textile Design and Structure

The most frequently applied approach to develop knit or weave patterns or motifs is through mathematical models (such as Boolean algebra) or parametric and generative methods [207], [208]. Multiple efforts have been conducted to connect music with textiles by mapping musical scores and notations into 2-D weave patterns [207] or vice versa, transforming traditional textile unique and meaningful patterns into a sonic experience [209].

Figure 4.18: Illustration of our vision. The *tapis* indeed not only serves for aesthetic, comfort, and insulation purposes, but is also augmented as a responsive skin that bridges the tactile-physical with the immersive-digital world. During stand-by, it can perform real-time context recognition (as demonstrated in *3DKnITS*). Then, it will react to user-intent and automatically transform the room into an immersive space with the surround system

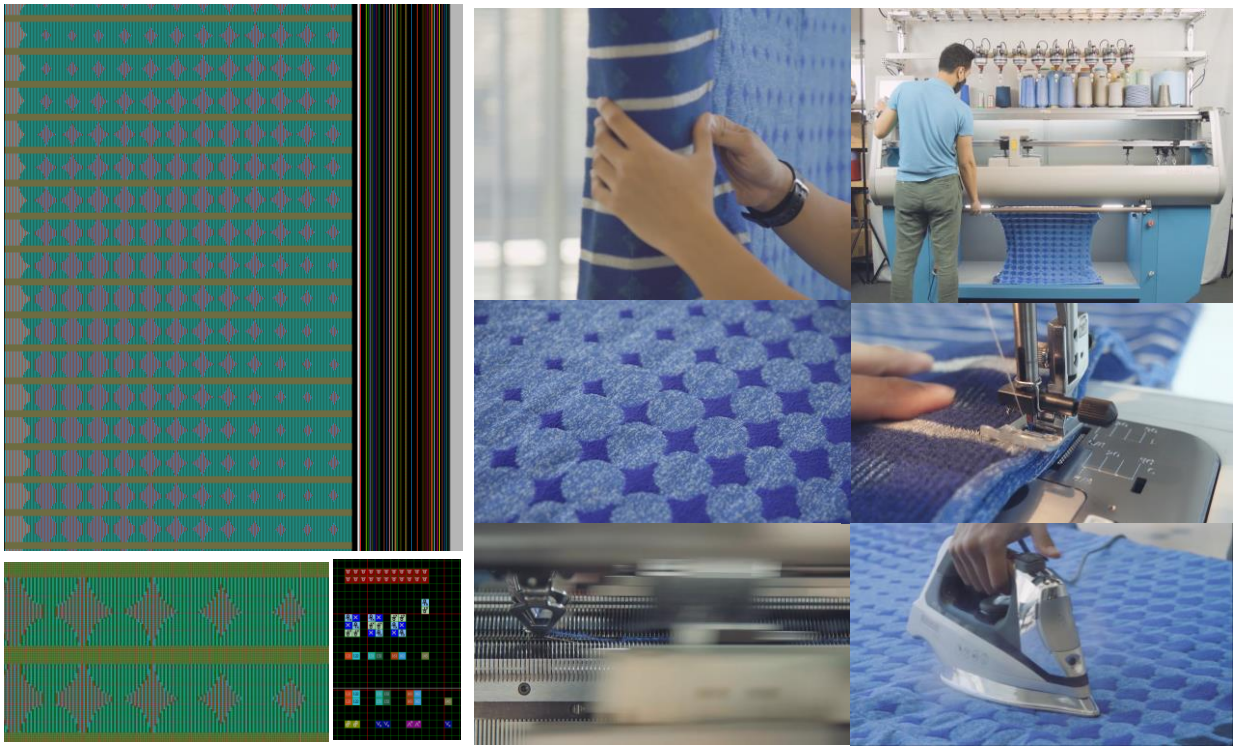

Figure 4.19: Knitting program of the *Tapis Magique* and its fabrication process from knitting to sewing two columns together and finally, thermoforming.

Other tangentially relevant textile designs touching the literal artistic inspiration of this work include the *Fabric of the Universe* [210] and *Listening Space: Satellite Ikat* [211]. In *The Fabric of the Universe*, a 3D astrophysical simulation was fed into a digital weaving machine to create a large-scale cosmic web textile installation. In *Listening Space*, real-time audio intercepts of satellite data were visually decoded and used as knitting patterns.

Cultural traditions have also been a source of inspiration for our textile development. Our design approach is inspired by various traditional cultures such as Javanese and Balinese gamelan [212], [213] and Maharashtra folk dance [214], which deeply connect their textile arts and traditional clothing to their dance and music. These cultures give personal value and a sense of shared identity to their textile patterns, which is currently lacking in technological textile design. The traditional textiles' symbols, patterns, and other visual metaphors represent deep and meaningful relationships between humans, nature, animals, and the universe. The visual aspects, particularly traditional textile pattern, proportion, balance (order and disorder), and irregularity, have also been argued to resemble typical musical structures and compositions [215].

Our artistic textile pattern is motivated by the overarching theme of our collective performance, which is *musica universalis* or the music of the spheres [216] through both *Venus Sunrise* and *Biotic-Abiotic Interactions* choreomusical pieces. The row-column matrix represents a space-time grid

that touches the principle of general relativity. Gravitational force is critical in the *Tapis Magique* workings. We are constantly sensing the exerted force due to our change of balance, gestures, and center of mass on the carpet amplified by gravity. On top of the grid that informs our sensor resolution, we applied geometrical patterns of the celestial stars and circles as planetary bodies to guide the dancers and choreographers regarding the sensor locations throughout the tapis (see Appendix A.2 for close-up details of *Tapis Magique*).

We leveraged parametric design to distribute the change of size of these circles and stars and create a swirl illusion. This multi-dimensional space also corresponds to the large spatiotemporal or 3-D sensor data that consist of x and y positions and z pressure values. Besides functioning as visual cues or coordinates, the dynamic textile pattern in *Tapis Magique* can also be individually mapped to challenge our cross-modal perception and explore the relationship between sound and visual signifiers [217]. Finally, the brushstroke details in the tapis background represent the universe's density and complexity.

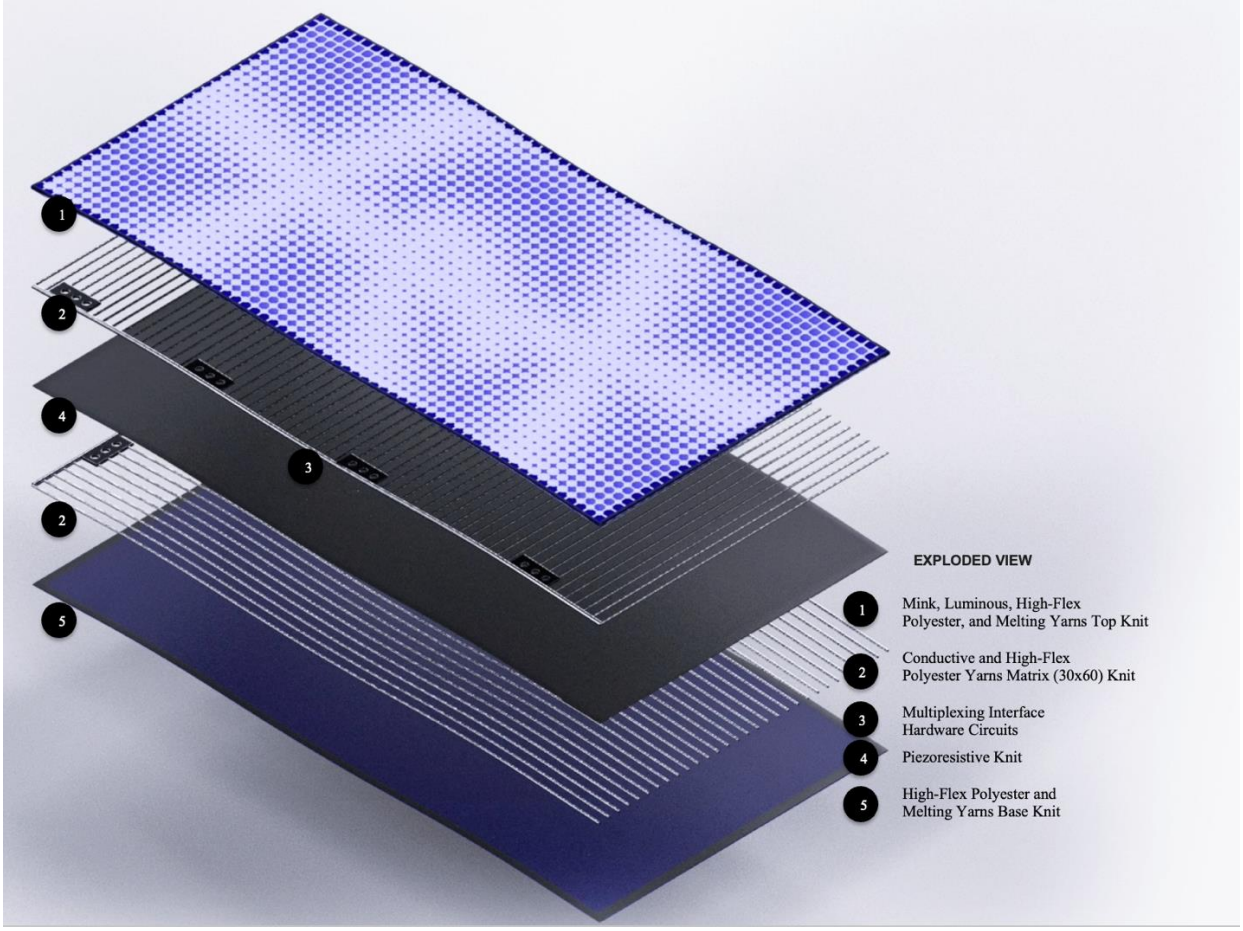

Figure 4.20: Exploded view of the multi-layer knit textiles in *Tapis Magique.*

The tapis design is composed of multi-layer knitted textiles (Figure 4.19 and 4.20). The top and bottom layers are orthogonal conductive line matrices knitted within a single operation using multi-material twisted yarns. The middle layer is a knitted piezo-resistive textile, a pressure-sensitive layer interfacing with the conductive matrices to create a 60 by 30 sensing grid. The outer skin of our carpet, spanning 3 meters in length and 1.5 meters in width (5 cm pitch between the matrix lines), was fabricated in two runs and sewn together in the middle due to the width limit of the knitting machine. The inward-facing conductive knitted lines, insulated by the outer layers, avoid possible shorts and parasitic impedance from the environment.

The furry textures from the synthetic mink yarns provide soft tactility for physical feedback and give an intimate and comforting feel to the tapis. The thermoplastic fibers were steamed to melt the multi-layer knitted textiles into one rigid surface, giving it structural reinforcement. Additionally, the outer-facing textile glows in the dark from the luminous yarns, creating starry effects for night performances.

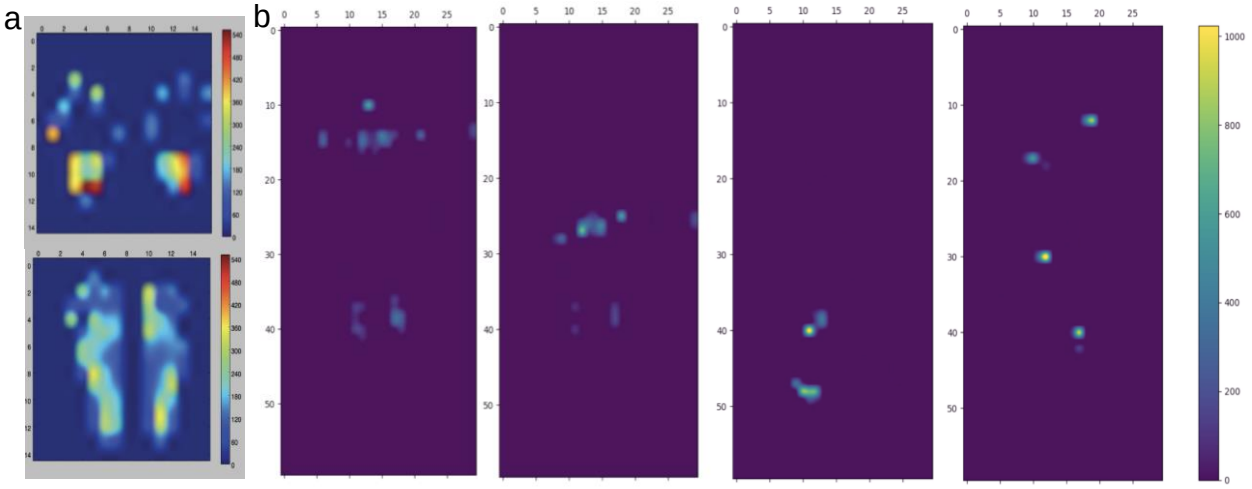

Figure 4.21: a) *3DKnITS* mat, a higher resolution version of the carpet (2.5 cm pitch). In this mat, we can see clearly the pressure distribution of the feet and hands to infer activities or interactions with the surface. b) Multiple pressure images of the carpet. It is also clear that the carpet, even though lower in resolution (5 cm pitch), can still detect the pressure gradient as the dancer (from right to left) laid down on its surface, tried to get up, stood on her feet, and crawled.

4.3.3: System Design and Sensor Data

The hardware system is an extended version of the *3DKnITS* system. We separated the shift registers, potential divider, and buffer from the multiplexers, resulting in four modules, as shown in Appendix A.10 and A.11, along with two modules of CD74HCT4067 analog multiplexers (each module accommodating 16 pins, one pin was left-out). The knitted conductive lines are connected

to this system hardware (Figure 4.20), which includes a microcontroller that sequentially reads each pressure-sensing pixel and sends the data to a computer. These pixels collectively generate continuous 3D spatiotemporal sensor data mapped into MIDI streams to trigger and control discrete notes, continuous effects, and immersive soundscapes through science-inspired musical tools. We used Teensy 3.6 as our main microcontroller, with a read-out frequency of 35ms or ~30 Hz, for sending 1800 pixels with each pixel having 12-bit pressure sensor data. We leveraged the in-built Teensy USB MIDI library to convert these sensor data to readable formats for musical mapping and sound synthesis through Max/MSP, Ableton Live, or VCV Rack.

As we balance and redirect our center of mass through our feet, we exert force on the ground. By detecting the pressure distribution of the feet through the e-textile carpet, we can extract rich contextual information about the dancer's location, gestures, or even postures [47, 48]. Our foot pressure distribution changes slightly as we move other body parts, allowing us to sense how hard the dancer hits or presses against the carpet.

Figure 4.21a shows a pressure distribution in the *3DKnITS* mat (2.5 cm pitch). In this mat, we can clearly see the pressure distribution of the feet and hands, allowing us to infer activities or interactions with the surface. To compare the resolution, Figure 4.21b presents multiple pressure images of the carpet as the dancer (from right to left) laid down on its surface, tried to get up, stood on her feet, and crawled. Even though the carpet has double the pitch of the mat (5 cm between pressure points), or half of the resolution, the heatmap result still effectively captures pressure distribution through various gestures and poses.

4.3.4: Musical Mapping and Live Performance

To create an emotionally engaging experience for both the dancer and audience, we adapted five interactive dance principles by Gonzalez, Carroll, and Latulipe [218]:

- The direct and indirect mapping should be done in such a way that the audience can intuitively understand that the dancer triggers the sound and modulation.
- The carpet should give the dancer a new degree of autonomy and musical expression.
- The music and the choreography should create a united, harmonious, and integrated experience.
- The intensity of the musical mapping or the sonic environment should be in sync with the choreography.
- The technologist and sound artist should be involved in the choreographic and musical mapping process and work side-by-side with the dancer and choreographer.

Curating a complex mapping for 1800 incoming MIDI notes (distributed equally into 15 MIDI Channels) in a 30x60 grid was made possible using the virtual modular synthesizer platform VCV Rack, as demonstrated in Figure 4.22. The incoming stream of MIDI data is first fed into quantizer modules that align the notes to major, minor, and pentatonic scales, as well as mystic chords. Several patches were designed to invoke various emotions while being demonstrated by our collaborator, contemporary dancer and choreographer Loni Landon (Figure 4.23). This created a sonic landscape ready to be explored by the dancers in an unreplicable experience. Using a virtual synthesizer provided by a flexible modular interface accommodates a much wider range of musical mapping [219].

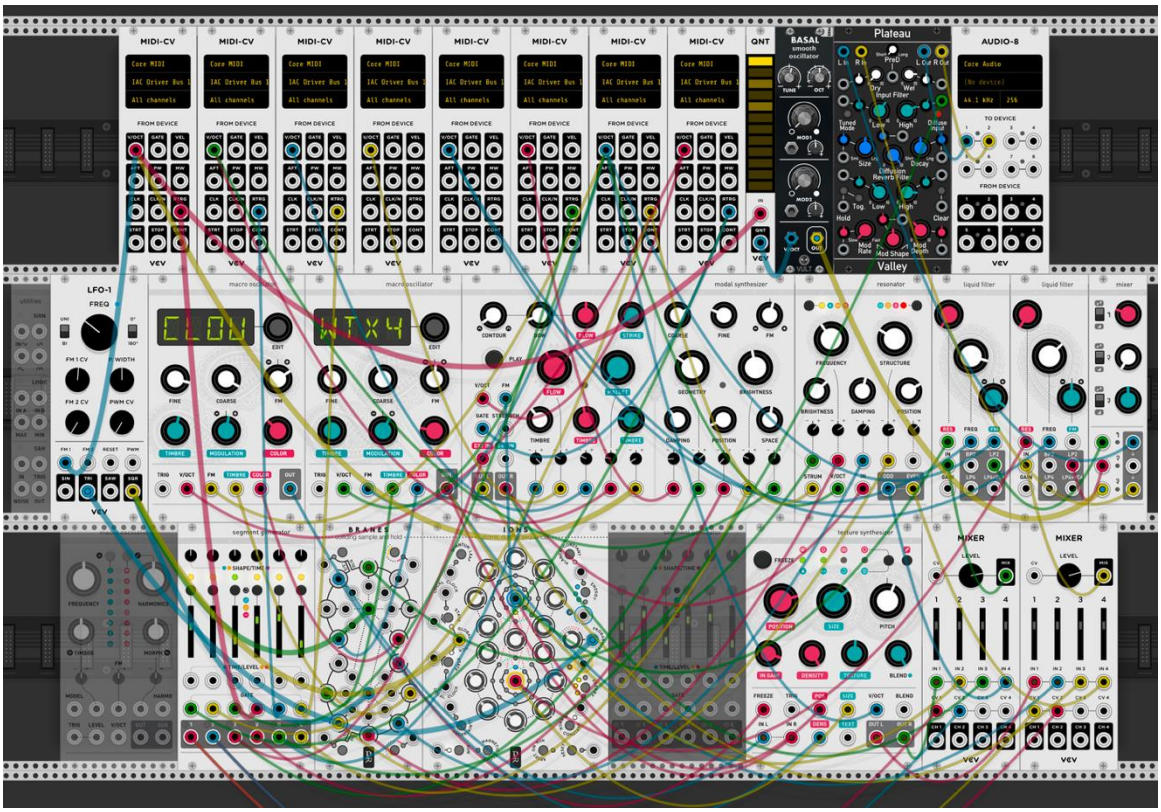

Figure 4.22: VCV Rack Synthesizer Modules/Patches for "Venus Sunrise" Performance.

Four different ideas were picked for this mapping, navigating themes ranging from space exploration, microorganisms and biological interactions, film noir and cinematic landscapes, and others. Depending on each theme, a quantizer module sets the musical scale of the overall patch accordingly. The patches also feature a finite state machine sequencer, complex oscillators, granular synthesis, physical modeling, as well as subtractive synthesis, all glued with stacks of digital spatiotemporal effects. The light intensity guides the brightness of the mapping in the room. For instance, major and pentatonic scales were selected in a patch called *Venus Sunrise* during the day (Figure 4.22). During the nighttime, darker themes were picked, governed by minor scales and the infamous mystic chord in a piece called *Biotic-Abiotic Interactions*.

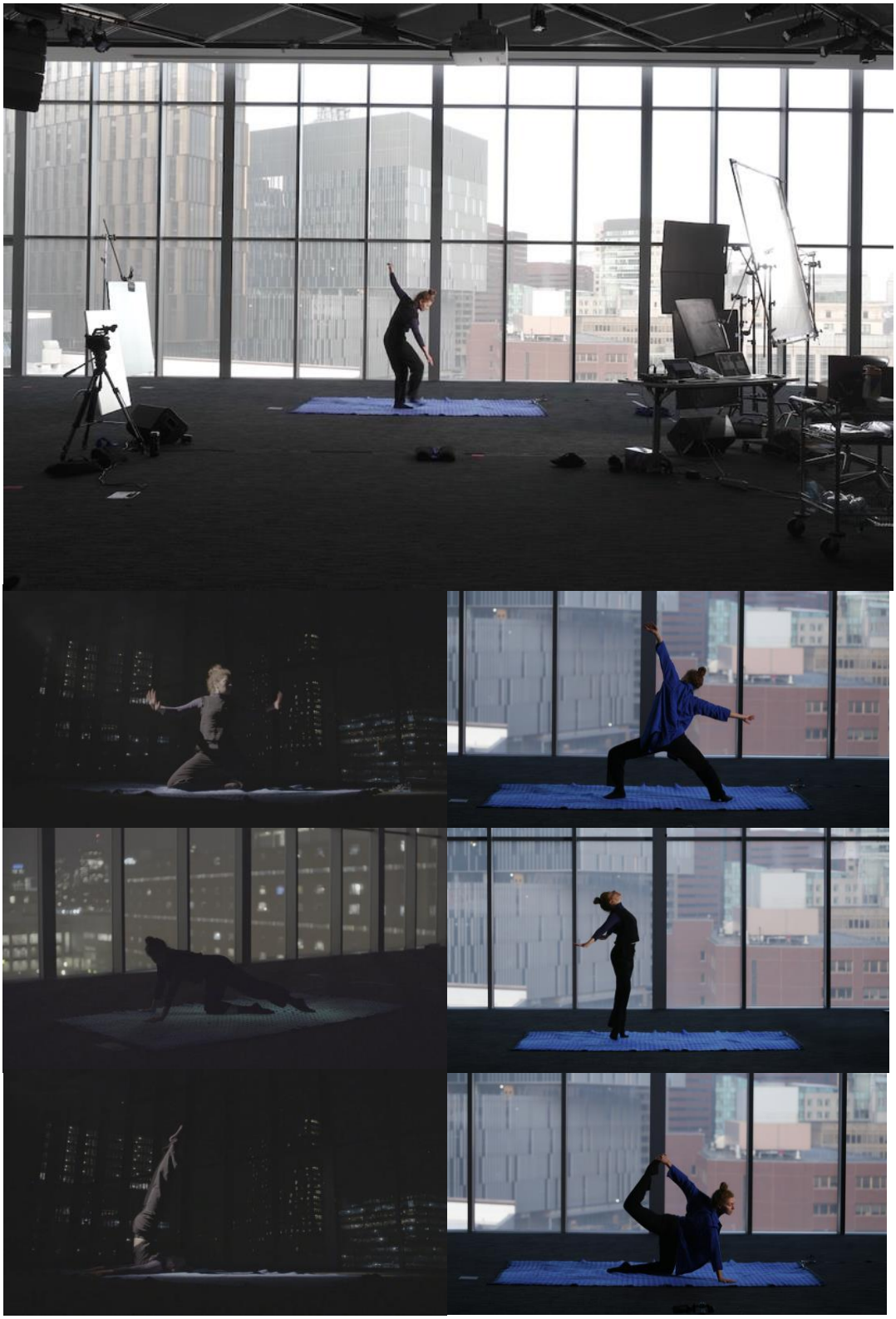

Figure 4.23: Excerpt images of the "Biotic-Abiotic Interactions" and "Venus Sunrise" performance with Loni Landon. (Photo Credit: Jimmy Day)

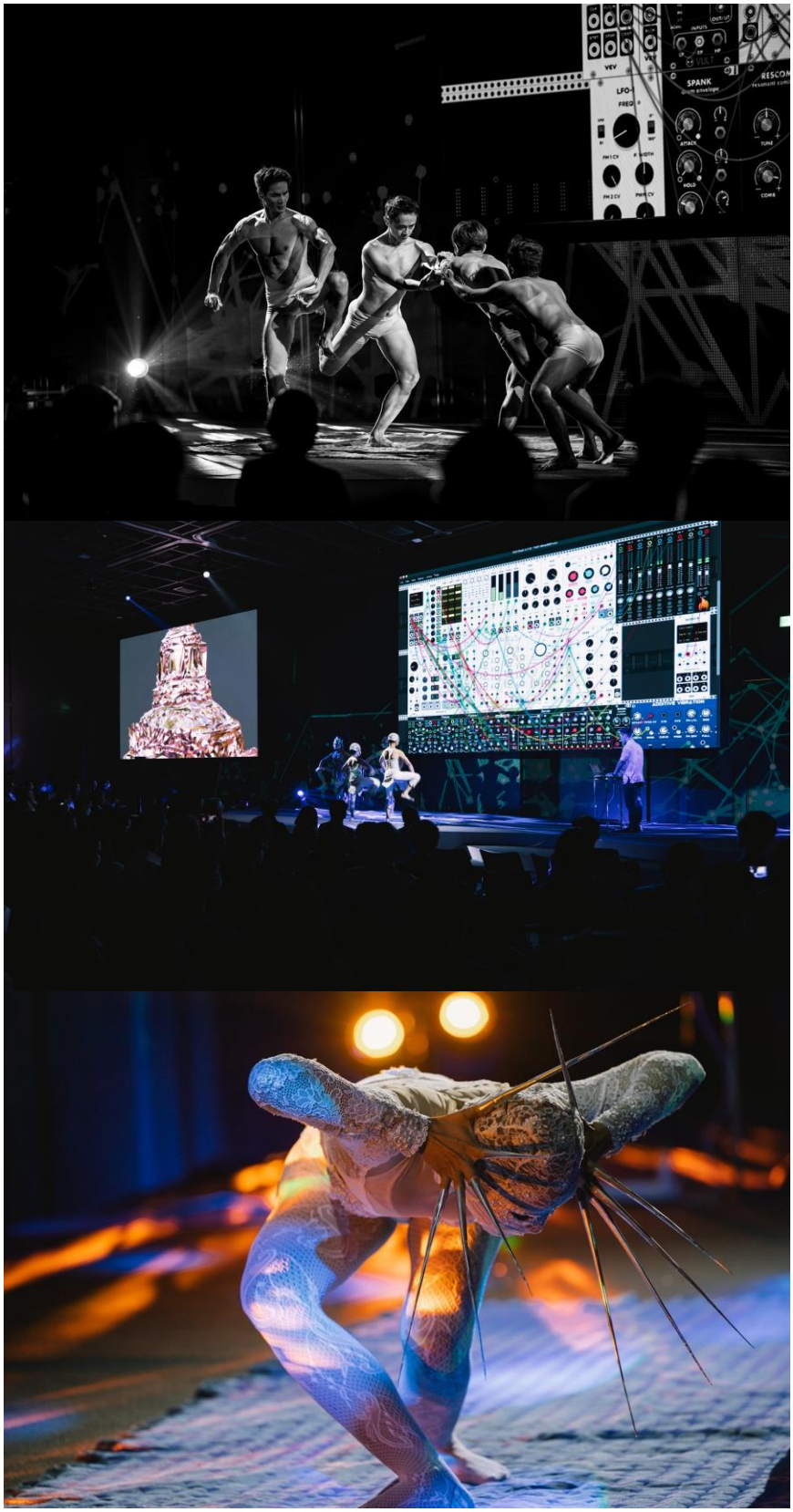

Figure 4.24: Excerpt images of live performance with Pichet Klunchun Dance Company (Photo Credit: Techsauce)

We also had an opportunity to collaborate with a group of contemporary dancers from the Pichet Klunchun Dance Company (Figure 4.24). Pichet Klunchun, a renowned avant-garde choreographer, and dancer, is known for his innovative approach that merges traditional Thai classical dance with contemporary techniques. His company has gained international acclaim for performances that challenge conventional boundaries and explore new artistic expressions [220]. The dancers' intricate movements, rooted in classical tradition yet boldly modern, were complemented by the electronic music driven by the textile surface and virtual synthesizers, resulting in a unique, immersive experience and compelling fusion of art, culture, and technology.

4.3.5: Limitations and Future Work

From the audience's point of view, seeing the dancer interacts with a carpet sparks questions and curiosities. "Does the dancer move because she wants to make that sound?" or instead, "does the dancer move in response to the sound made by the carpet and synthesizer?". "Was the performance choreographed? or was it organic and an improv?". There was an interesting discussion about whether the carpet or the dancer predominantly drives the sound or whether it is a constant feedback and conversation between the dancer and the carpet. These ambiguous yet stimulating experiences have challenged the perspective of liveness and virtuality argued by Auslander and Phelan [221].

This project is intended to spark discussions and explore the relationship between textiles, dance, and music. It is not in its final stage and, as such, will require further explorations in musical mapping and choreography. There is much more potential in leveraging the rich 3D data to not only control discrete sound and its velocity but also for continuous expression through pressure sensing. Incorporating other sensors into the performance to detect upper-body and micro-gestures using camera trackers or wearables, for example, will significantly improve the immersion and interaction between the movement and the music. Instead of one musical mapping per performance, we could also develop a dynamic musical mapping that gradually changes its ambiance and parameters throughout the performance. We are interested in exploring other musical mappings and different styles of dance.

By working side-by-side with a sound artist and a contemporary dancer and choreographer, this multi-disciplinary collaboration resulted in the demonstration of multiple performances and musical mapping, showing the capability of *Tapis Magique*. Since the *tapis* is programmable, we can fuse contemporary music with traditional dance and *vice versa*, allowing dancers and sound

artists to collaborate and experiment and push the boundaries between sound and movement, music and choreography. The *tapis* could also benefit other human-computer interaction and activity recognition applications such as kids' engagement in learning, musical therapy, elderly care, rehabilitation, sports science, robotics, and augmented and virtual reality (VR).

In the age of functional materials, digital fabrication, and immersive technologies, we are not only designing and developing textiles and other objects as material artifacts, but we are also beginning to redefine and reinvent their purpose as an intelligent-responsive skin, challenging the perceptions of materiality, their relationship with us as human, and the blurring dualities between material and immaterial; real and virtual [222]–[224].

4.4: Living Knitwork Pavilion

4.4.1: Motivation and Related Work

Textiles are an indispensable part of our daily lives, serving not only as clothing but also as large-scale coverings that protect us and shape our living spaces. They contribute significantly to human experience, expression, communication, and survival, offering qualities of fluidity, softness, and dynamism that influence our social function and interactions with the environment. Despite the prevalence of purpose-built textiles and soft materials in our surroundings—clothes, upholstery, lining, and formwork —they currently remain passive. The focus of textile design has traditionally prioritized attributes like strength, stability, protective capability, and surface characteristics. In the age of sensing, actuation, and computation, there is an immense potential in pushing architecture and textile function beyond the physical, through digitally-mediated interaction [225], [226].

The history of textiles in architecture spans millennia, with tents serving as early examples of portable shelters constructed by semi-nomadic and nomadic cultures [227]. Tents, utilizing textiles and animal skins as covers, represented the first type of soft shelter employing such materials, providing mobility and adaptability essential for survival in varying environmental conditions [228], [229]. Structures like yurts and teepees further exemplify the integration of textiles into architectural design, with woolen felt or canvas covers supported by wooden frames, offering weatherproof enclosures and functional versatility. The symbolic value of textile decorations within these skins and structures also reflects cultural beliefs and traditions, adding layers of significance beyond mere shelter [230].

In contemporary architecture, the principles of tensile architecture have also been embraced, harnessing the flexibility and efficiency of textile panels under tension to create structures, roofs, and canopies [231]. The O2 Millenium Dome, for example, utilizes a tensile fabric roof made from woven polyester fibers coated with polytetrafluoroethylene (PTFE). This fabric is then installed over a network of steel cables and masts, creating a vast enclosed space within the dome. Similarly, the hydraulically-operated retractable umbrellas at the Medina Haram Piazza features woven PTFE fabric with oriental motifs and special characteristics such as high tensile strength, wind and fire resistance, as well as reflectance to shade and protect occupants from the sun exposure, heat and rain.

Within the realm of architecture, digital knitting presents a unique design paradigm wherein material and pattern manipulation can be programmed in an abstraction, starting from a yarn as an input and a knitting loop as a unit [232]. In contrast to weaving techniques, knitting offers distinct advantages. Knitted textiles can be precisely tailored to achieve highly-customized tactile and visual patterns, multi-layer configuration, and three-dimensional shapes, facilitating automated and seamless integration of desired features without labor-intensive assembly.

KnitCandela showcases the versatility of large-scale 3D-knitted textiles to create 13ft tall curved shells that can be used as concrete formwork [233]. The ultra-lightweight fabric formwork, developed without generating textile waste through on-demand additive manufacturing and with less complex scaffolding, highlights the project's contribution to demonstrating minimal construction waste. Other architectural projects such as the *Sensory Playscape* [234], *Ada* [235], and *Lumen* [236] explore further the tactility and materiality of knitted textiles and tensile structures, and with the incorporation of an external system that sense and interact with human engagement, demonstrating multi-sensory responsive environments. These projects have demonstrated a new axis in designing architectural space and exemplified DeLanda's new materiality through the use of emerging technologies, such as projection mapping, gesture and camera-based sensing, and artificial intelligence [32].

As fibers and yarns become capable of accommodating more functionalities, new opportunities emerge to seamlessly integrate sensing, actuation, and computation directly into fabrics [101], [237]. Researchers have already explored the integration of functional yarns into fabrics with capabilities ranging from morphing and tactile sensing and feedback to display functionalities, catering to a wide range of applications from sensate wearables to room-scale environments [162], [238], [239].

.

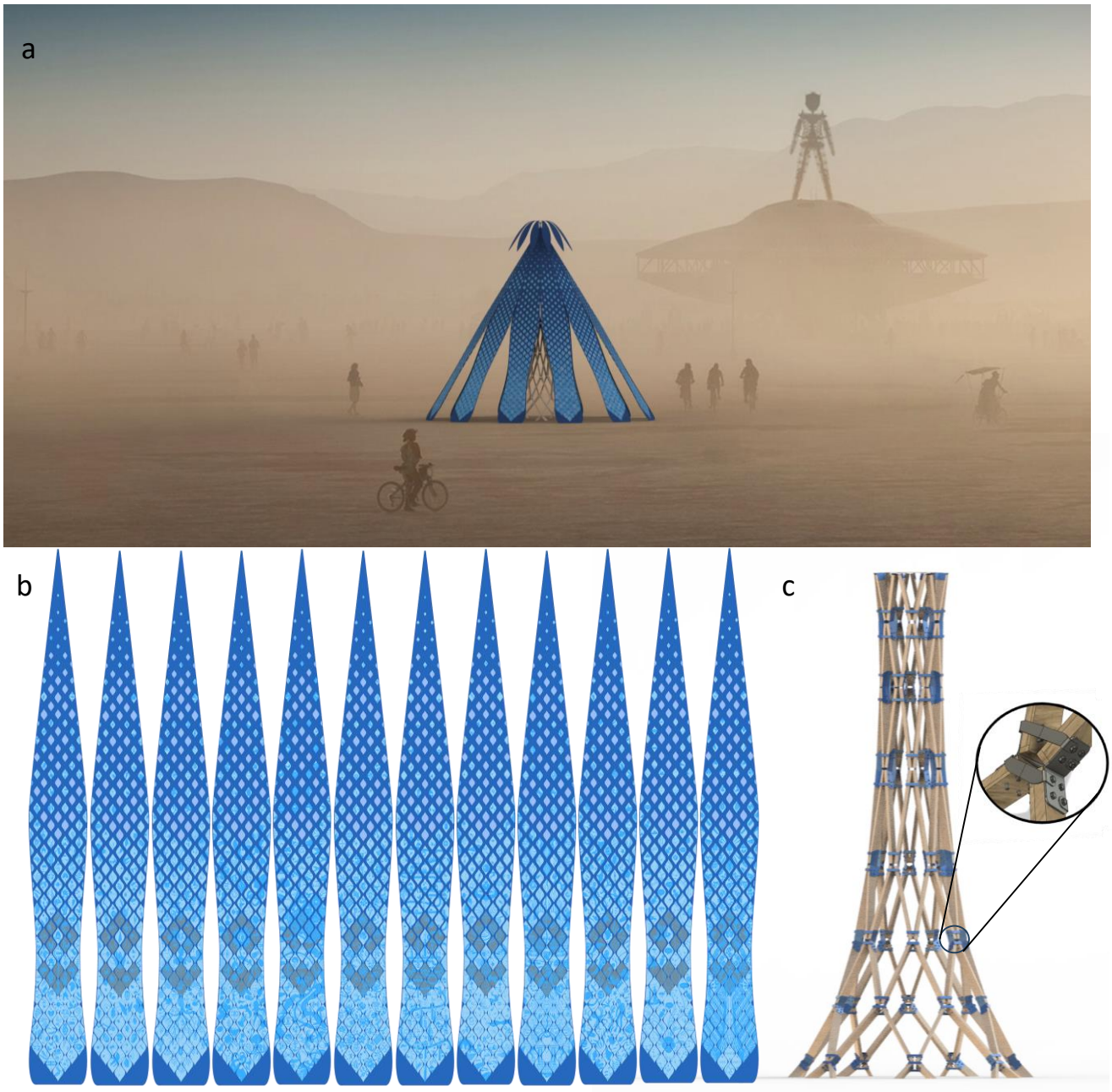

Figure 4.25: a) The *Living Knitwork Pavilion* was installed in a desert location in Nevada. b) Twelve of the Pavilion textile panels design. The popped-up textile patterns or reliefs, rich with symbols and illustrations, depict twelve stories of the future – from solarpunk cities and bio-machine interfaces to the deep ocean and space exploration. and c) 3D-model of the final discretized joint-beam robust design for the central structure of the Pavilion. The central structure consists of eight different levels, each with 14 beams and seven nodes, assembled from bottom to top.

In this work, we demonstrate a large-scale, textile-based electric-field or capacitive sensing system driven by knitted conductive textiles. The Pavilion is the largest electronic textile *tepee* and architectural *Theremin* or *Terpsitone* installation to date, extending the typical scale of such instrument's sensitivity from our fingers to our collective bodies, capable of sensing our gestures and locations to drive an integrated audio and lighting system in real-time [192], [240]. This concept was explored by multimedia artist Paul Earls during his tenure at MIT in the late 90s, utilizing the Fish system [241]. However, no records or traces of the installation have been found. *Living Knitwork Pavilion* offers a connected, immersive experience that engages multiple senses, including movement, sight, sound, and touch. Through our interdisciplinary effort, we also aim to demonstrate a portable and temporary soft architecture facilitated by an innovative large-scale 3D-knitted textiles.

The *Living Knitwork Pavilion* was installed in the desert environment of Black Rock City, Nevada, for Burning Man, a weeklong large-scale event focused on community, art, expression, and interactivity (Figure 4.25a). This aligns closely with our project goal of creating a textile sanctuary that offers shade and visual-tactile experiences during the day and transforms into an immersive space at night, fostering meditation, self-expression, and collective experiences. Given the event's location in the remote and harsh environment of the Black Rock Desert, known for severe wind, dust storms, and occasional rain, the *Living Knitwork Pavilion* structure has been designed prioritizing its suitability for extreme environment and public safety. Additionally, we have considered its modularity, portability, and ease of installation, requiring minimal equipment and work for setup. This section will delve into multiple facets of the *Living Knitwork Pavilion* project, encompassing textile design and fabrication, structural analysis and design, integration of sensing hardware, musical mapping, lighting design, and the logistics of transportation and construction at Burning Man.

4.4.2: Design Concept

Our design is driven by several constraints, primarily the need for the structure to function as a shade with distributed textile sensor networks. A conical or pyramidal shape is deemed most suitable as it allows the central meeting point at the top of the Pavilion connecting all integrated sensors within each textile panel to the main processor, as well as spatial audio and robotic lighting system. Additionally, the wooden-lattice tower at the center, besides offering structural support (Figure 4.25c), functions as a central transmitter and pathway for power and communication from the ground up.

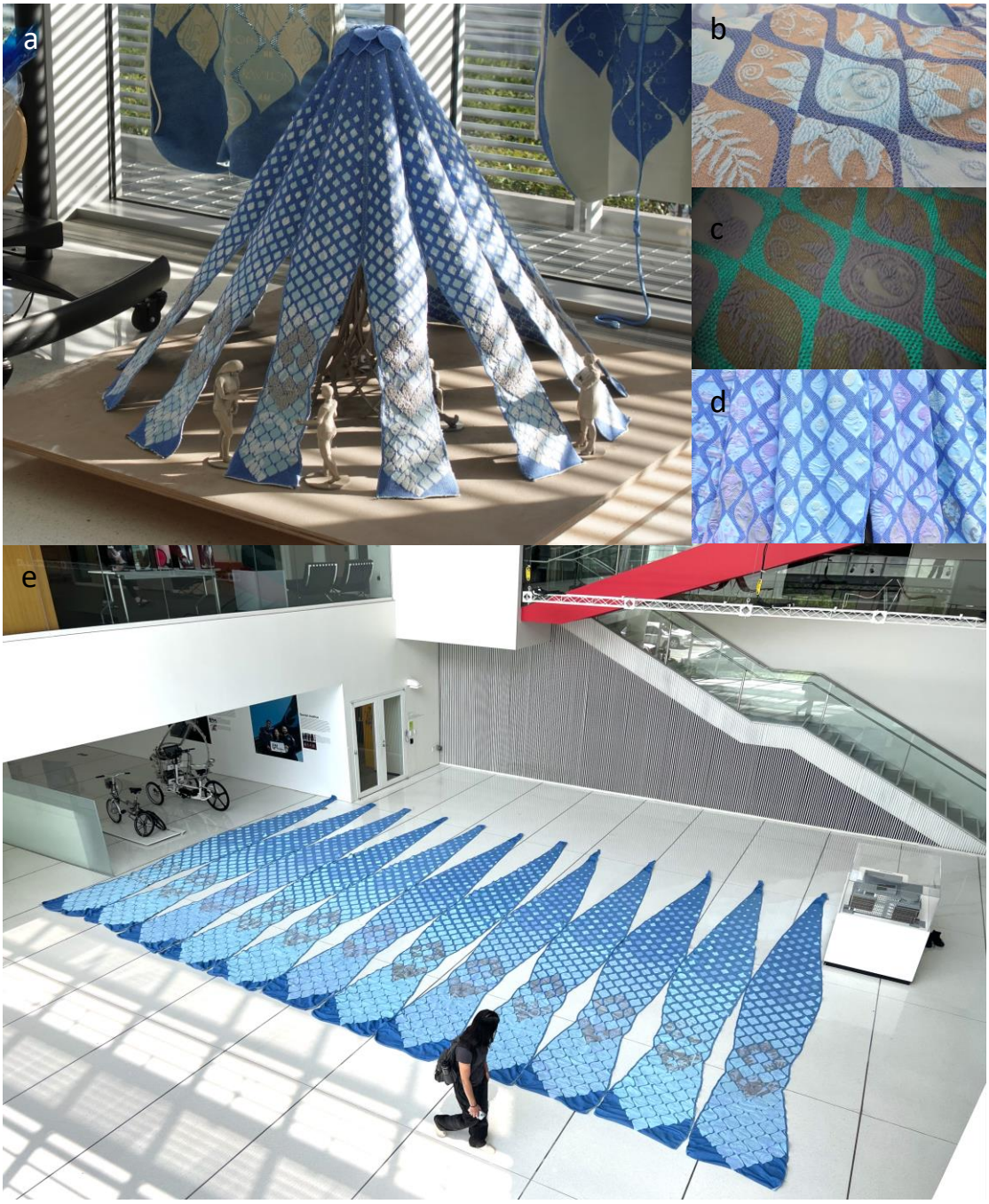

Figure 4.26: a) 1:8 diorama/model of the Living Knitwork Pavilion. In line with advances in knitting and functional yarns, our focus in creating an interactive architecture extends beyond utilizing functional yarns for their visual aesthetic appeal. b-d)We have knitted silver-plated conductive and optically-active yarns into the fabric of the *Living Knitwork Pavilion*, enabling the dynamic expression of colors and the intrinsic integration of transmit and receive antennas within its modular textile panels. Through photochromism, these reliefs change color with the shifting sun, harnessing sunlight energy to glow after dusk through photoluminescence. e) 12 modular knitted textile panels of Living Knitwork.

The final design of the *Living Knitwork Pavilion* takes the form of a dodecagonal pyramid measuring 18ft tall and 26ft wide, a configuration resembling *Umbrella Antenna*, which has a number of radial wires supported by a central lattice mast. Comprising twelve modular opto-electronic textiles resembling petals, each panel features 90 textile reliefs parametrically distributed across its surface (Figure 4.25b). Merging crafts with digital knitting technology, the *Living Knitwork Pavilion* is rooted in the reverence for artistry and wisdom found in Balinese Pura or temples, symbolizing sacred spaces adorned with stone carvings where communities gather and pray (Figure 4.26a,e). Each triangular Living Knitwork textile panel also resembles the Javanese Gunungan, a symbol synonymous with shadow-puppetry tapestry that signifies shifts in narratives. The fusion of parametric and hand-designed motifs transforms the Living Knitwork into a narrative artwork, reflecting both reverence for ancient artistry and a vision of the future (Appendix A.3 and A.4).

The popped-up textile reliefs, rich with symbols and illustrations, depict twelve stories of the future – from solarpunk cities and bio-machine interfaces to the deep ocean and space exploration. Through photochromism, these reliefs change color with the shifting sun, harnessing sunlight energy to glow after dusk through photoluminescence. Designed as a spiritual sanctuary, the Pavilion invites exploration and meditation by day, and metamorphoses at night with interactivity. The "Living" in the *Living Knitwork Pavilion* represents the computational and sensing-actuation response between the textile panels and audiovisual system, which continuously provide a constant dialogue between the individual and collective behaviors and the immersive spatial experience.

4.4.2: Digital Knitting and Fabrication

We used a flat, two-bed digital knitting machine (Super-NJ 212, Matsuya) and as shown in the knitting program in Figure 4.27, involved a total of five yarn carriers (Figure 4.28a): conductive yarns (3x 210D/Denier, Weiwei Line Industry), photochromic yarns (2x 300D, Endnus New Material), and high-flex base polyester yarns twisted with luminous yarns in 1:3 ratio (4x 150D, Energytech Inc.), and hyper-elastic polyester/spandex yarns (2x 75D). Both hyper-elastic and high-flex polyester yarns are also combined with low-melt yarns (150D, 1-ply). The knitting pattern results in 24,500 instruction lines and requires approximately 12 hours of knitting per panel. Each textile panel is approximately 4 kg in weight, 7.2 m in length, and has a maximum width of 1 m at the bottom and middle sections.

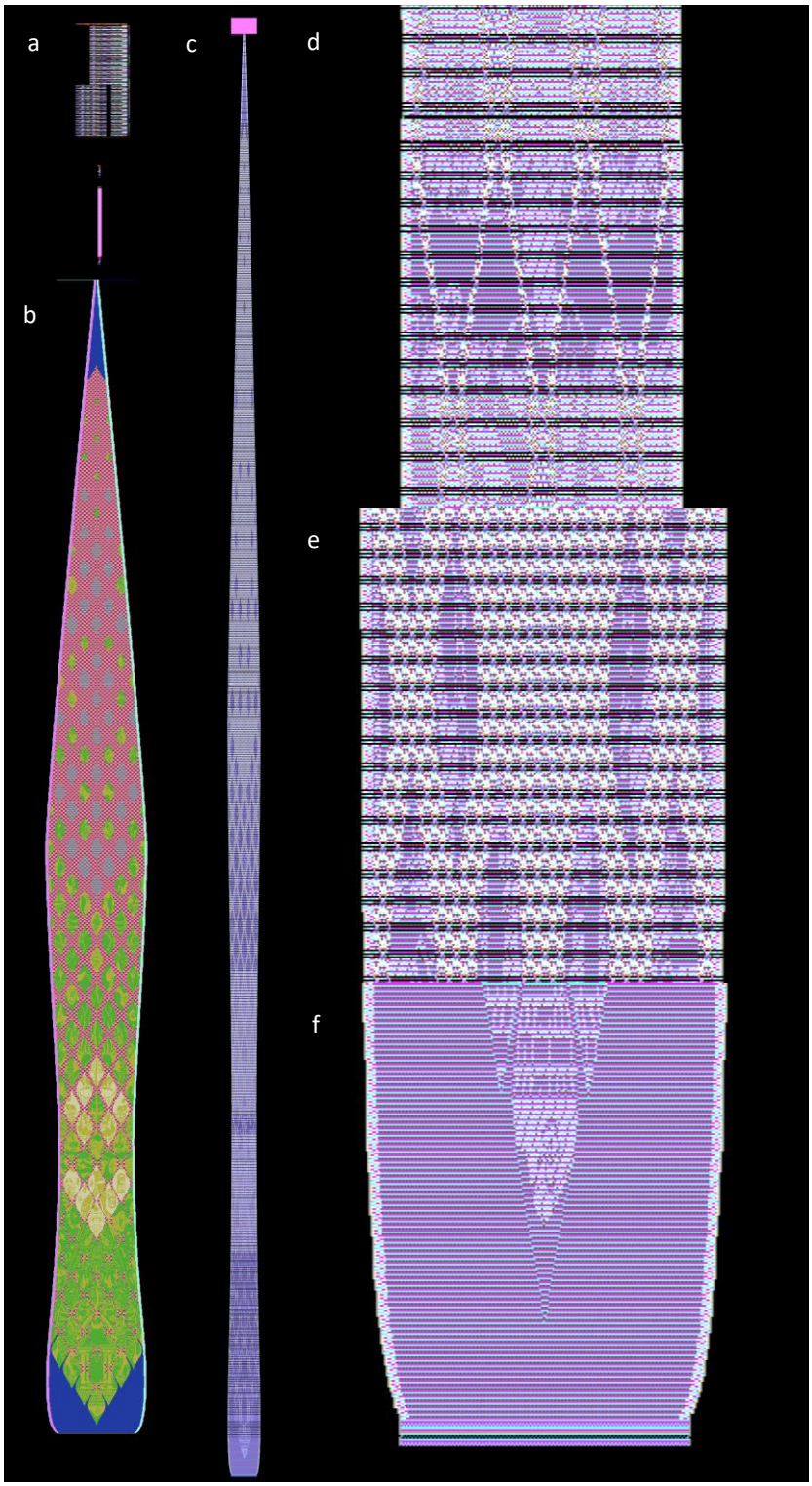

Figure 4.27: Digital knitting program of a Living Knitwork petal. To streamline the design and fabrication process, we have develop ped a) an abstraction library that can convert b) simpler, low-level patterns into c) more complex line-by-line front and back knitting machine instructions that the knitting machine program can interpret. d-f) Zoomed-in views of knitting machine program.

Figure 4.28: a) Various recycled polyester and functional yarns that make up five input spools used to fabricate the Living Knitwork petals. b) The knitting process. c) A custom large textile mold with wooden boards and nails were fabricated and used to stretch the panels. The textile panels are stretched by threading sailing ropes through both of the channels and securing them to designated nails before the thermoforming process. The low-melt yarns are activated through iron-steaming to fix the shape and size of all of the Knitwork petals. d) Dyneema ropes sewn with industrial sewing machines and heavy-duty yarns for central-line reinforcement.

Low-melt yarn, typically a thermoplastic polyurethane thread, melts at temperatures between 60°C and 85°C. Conductive yarn consists of silver fibers twisted together with polyester threads (Figure 4.26b). Solar-active or photochromic yarn is made by coating polyester yarns with pigments containing polymer microcapsules of photochromic compounds that change color (light blue to green and light blue to purple) in response to sunlight or ultraviolet light, while luminous yarns are coated with phosphorescent pigments that store and gradually release light energy (Figure 4.26c,d). By carefully controlling the yarn inputs and knitting patterns, each bespoke textile panel features both aesthetic and technical details (Figure 4.29):

Double-Layer Knit Textile Panels. Achieved through the use of two-bed flat knitting machines, the panels feature yarn reversal and interlocking of front and back patterns to create double-layer thickness, with each side showcasing unique color schemes. The front side highlights photochromic patterns within the grids, separated by luminous yarns, while the reverse side has the opposite configuration.

Figure 4.29: a-c) Front-side and d-f) back-side of a Living Knitwork panel. g-h) Channel openings that can be used to thread in electrical cabling and anchoring ropes. i) Multi-layer stranded wires are used to ground and shield every AC-transmission wire, protecting from external noise and pick-ups. Wires are crocheted to the knitted conductive textiles to ensure strong connection. j) First-stage transimpedance amplifier circuit beside the knitted receiver that can be slid into the channel.

Popped-Up Textile Reliefs. The combination of photochromic yarns in the patterns and spandex base yarns leads to popped-up tactile textile reliefs due to the buckling effect. To minimize differences in bump levels, particularly in larger patterns, and prevent yarn breakage, spandex-photochromic knitting loops were alternated every four rows.

Conductive Textile Electrodes. Each panel seamlessly integrated conductive yarns to form two separate conductive textile areas that function as transmitter and receiver electrodes. The upper transmitter has an active area of approximately 61 x 57 cm^2 with a resistance of 70 Ω, while the lower receiver has an active area of about 64 x 48 cm^2 with a resistance of 87 Ω. On the outer side, the conductive areas dominate the base grid with the photochromic patterns, while on the inner side, they are hidden by interlocking them in alternate with the other yarns.

Textile Meshes. Meshes or eyelet holes (3 x 5 mm) across the upper half of the panels allow wind and light to pass through and create unique shadow effects. The holes are formed by transferring stitches between needles on both beds, leaving empty needles to form eyelets.

Channels for Cabling, Rope, and Molding. Channels (16 mm wide) on both sides were created through tubular knit separation between the two textile layers, allowing space for cabling and rope insertion for sensing and anchoring systems. Openings distributed every 15 cm facilitate cable threading and textile stretching during thermoforming, as well as interlacing or connecting panels at the top half of the pavilion for roofing.

After knitting, each panel was sprayed with non-toxic, water-repellent, and fire-retardant liquids. Low-melt yarns were activated during thermoforming to provide rigidity and structural reinforcement. They also help resize the panels to their final shape.

The knitting process (Figure 4.28c) resulted in significant length deviations (about 30 cm) from the desired 7.2 m, due to unique patterns. More complex patterns cause greater shrinkage due to the buckling effects of spandex yarns. To resolve this, a large textile mold with wooden boards and nails were fabricated and used to stretch the panels. The textile panels were made roughly 10% smaller than the final size and then stretched by threading sailing ropes through both of the channels and securing them to designated nails before thermoforming. The low-melt yarns were activated through iron-steaming to fix the shape and size (Figure 4.28b). Finally, Dyneema ropes (3/16 inch hollow braid HMPE, SGT Knots) were sewn (Figure 4.28d) with industrial sewing machine and heavy-duty yarns for central-line reinforcement, cables with shielding were threaded for electrode connections, and sailing ropes (¼ inch dacron polyester rope, Quality Nylon) were also threaded to connect the top ring of the central structure to the ground anchors.

4.4.3: Structural Design, Simulation, and Analysis

The central tower is the only structural element of the installation, responsible for providing height for the top anchor of the textile panels, holding in place all electrical subsystems and holding the loads that the environment will subject the structure to. The harsh environment in which the tower will be displayed for several days necessitates careful consideration of material selection. The factors we had to take into account include a constant flow of alkaline dust, a wide temperature range, wind load of up to 90mph for the most extreme case and 70mph for temporary structure and recent case (Figure 4.30c), and the high probability of multiple climbers on the structure simultaneously.

The initial tower design (Figure 4.30a) featured a central structure characterized by a minimal surface linking the lower and upper rings via asymptotic curves forming a structural diagrid [242]. Such formulated multi-objective constrained optimization problem was solved with the bespoke Multi- Objective Constraint Multi-Swarm Particle Swarm Optimization Without Velocity (MOCMPSOWV) implemented in the GOLDFISH plug-in framework in Grasshopper3d [243]. The conceptual phase involved framing the design as a problem of optimizing multiple objectives with:

- **Three parameters**: top ring radius, bottom ring radius, number of interconnecting asymptotic curves,
- **Four objectives:** min. strain energy, min. displacement, min. the total length of laths, min. number of joints,
- **One constraint:** displacement < 4.0cm

The structurally promising continuous design concept (Figure 4.30b) had to be discretized for logistical, load, and manufacturing reasons. The grid can now be seen as multiple individual pine lumber beams converging at nodes composed of A36 steel plates and ⅜-inch steel bolts. The previous Figure 4.25c illustrates the aforementioned nodal architecture. To mitigate the threats posed by alkaline dust and temperature fluctuations, we utilized untreated dry two-by-four lumber that won't deform in situ. Additionally, we applied paint coating to all our A36 mid steel, and we utilized zinc-coated bolts, washers, and nuts.

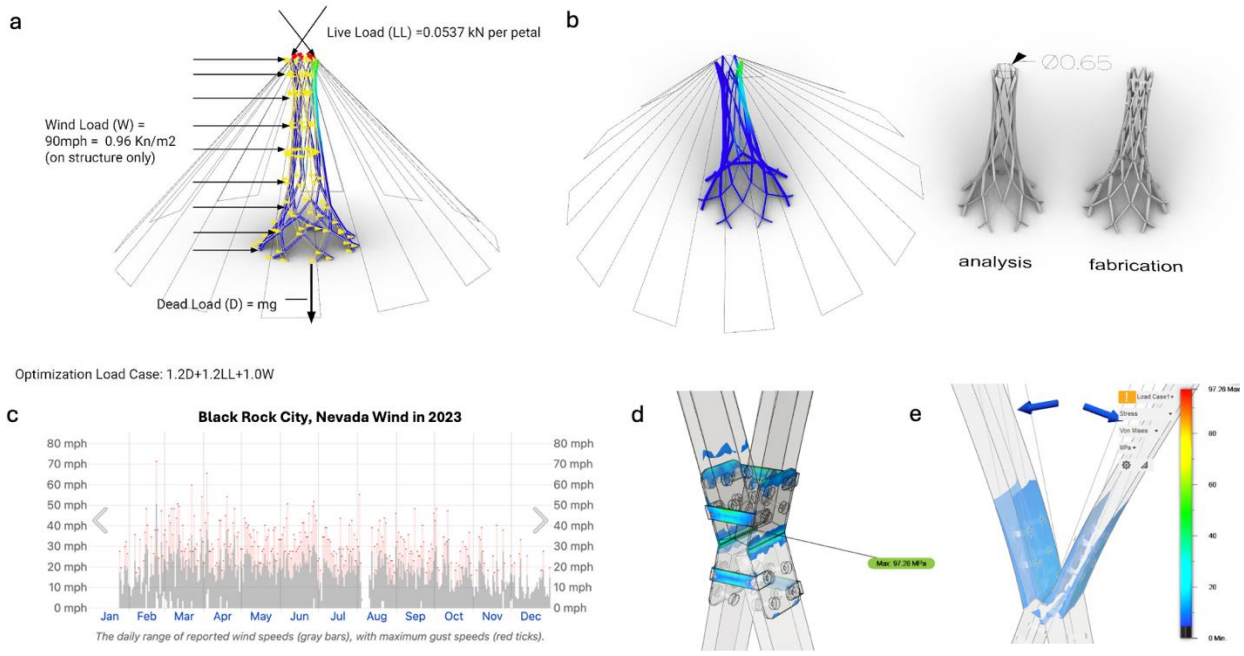

Figure 4.30: a) Final conceptual design as an optimization result. The design objectives and constraints were evaluated with the structural analysis. b) Continuous analysis model and the discretized model with linear members for fabrication. c) Black Rock City, Nevada wind and gust speed in 2023, showing © *WeatherSpark.com*, d-e) The continuum node exhibits a peak stress of 98 MPa concentrated in the wood joint, whereas in the discrete version, stress of equal magnitude is evenly distributed across the steel components, enabling them to withstand much higher stresses.

To validate the performance of the discrete tower model, we compared it against our continuum model used in Figure 4.30a-b, Figure 4.30d-e shows Fusion360 non-linear simulations of two equivalent nodes: continuum and discrete, both exhibiting the same displacement. The visualization highlights stress concentration areas and confirms the superiority of the discrete nodal geometry over the continuum global geometry. Consequently, we opt to conduct subsequent simulations using the continuum structure, as it is computationally less demanding and inherently provides an added safety margin.

The dynamic pressure as temporary structure resulting from 70mph wind speed acting over a 1 m^2 area is calculated as 588 N/m^2. Considering the 12 panels as a sheet of woven fabric with dimensions equivalent to an area of 5.5 m^2, we approximate that the fabric will expose an average of 25% of its area in high wind situations due to its deformation. Thus, the reduced wet area is calculated as 1.375 m^2. To determine the load experienced by a textile panel directly exposed to a

non-turbulent flow of 31.3 m/s, we multiply the dynamic pressure by the reduced wet area, yielding 808.5 N.

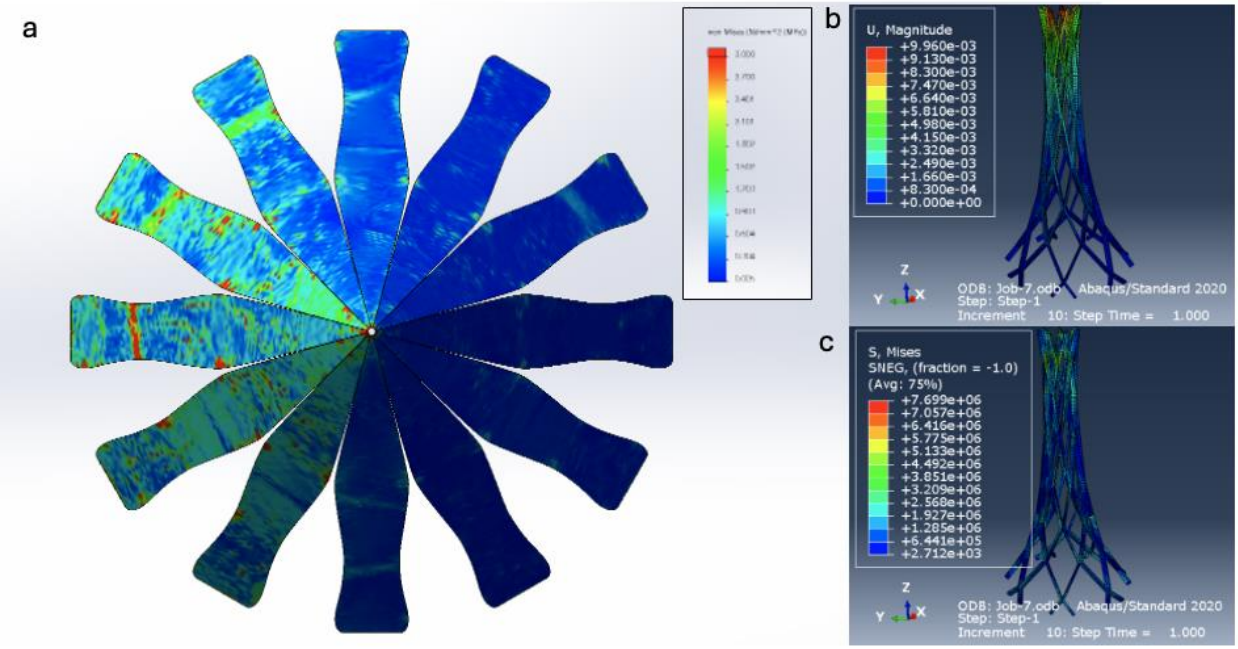

Figure 4.31: a) Solidworks 70mph wind simulation setup involved securing the bottom corners, mid-points, and top face of each petal. The material properties set for the simulation were an elastic modulus of 2 MPa, tensile strength of 20 MPa, shear modulus of 0.667 MPa, Poisson's ratio of 0.5, and a mass density of 1300 kg/m^3. Meshing was performed using tetrahedral elements to accurately conform to the complex geometrical configuration of the panels. b-c) Deformation and Von Mises stress simulation. Two primary load cases were applied: one involving people loads, 30mph wind, and gravity, and another incorporating 70mph winds alongside gravity. The latter load case proved to be the most severe.

As a safety factor, we do not consider the panels being held at an angle, which would further reduce the wet area. Applying a concentrated load at the centroid of our panel, the Wind Load Per Panel is distributed between the two anchor points to achieve equilibrium of forces. The natural radial arrangement of the panel ensures that regardless of wind direction, only five of them are directly exposed, as confirmed in our simulation in Figure 4.31a. These five panels generate turbulent flow, which benefits the rear panels by creating vortices, thus absorbing energy from the wind. As a conservative back of the envelope calculation, we can estimate that on average, a total of 8 panels will be exposed: five directly exposed and three compensating for the turbulent flow. Lastly, we will add ten people climbing the tower at random nodes. Each person will be quantified as a nodal load of 790N.

In Figure 4.31c, we present the von Mises stress map, highlighting its peaks. Additionally, we determined the reaction forces at the tower base under maximum wind loading—a crucial parameter for selecting appropriate ground penetrators. The simulation yielded a peak reaction force of 1500N at a single node. Given this value, we use anchors (PE26, American Earth Anchors) as we satisfy the allowable for any type of soil class. Concerning stresses, we observed a peak concentration stress of 7.7e6 Pa, which falls below the allowable limit for our wood type (UCS 1.2411e+7). Furthermore, a peak displacement of 10mm (Figure 4.31b) at the tower's top was recorded. These results validate the design and ensure safe performance under the specified conditions.

4.4.4: Constructing the Living Knitwork Pavilion

The modular textiles and discretized design of the central structure of the *Living Knitwork Pavilion* allow it to be packed and transported in six large storage boxes (57-gallon storage tote, HDX) measuring 38.44″ in length, 13.69″ in width, and 18.59″ in height. The installation sequence of the *Living Knitwork Pavilion* does not require scaffolding or heavy machinery and can be divided into five steps spread over two to three days: 1) wooden-lattice asymptotic tower construction, 2) top-ring and lighting fixture assembly, 3) textile panel fitting and connections, 4) audio system setup, and 5) firmware and hardware integration (Figure 4.32).

After mapping and drilling seven of the central structure's main anchors with an impact wrench, the base of the tower was secured into the ground. After completing the central structure, we connected the top steel ring for textile panels and lighting system fixtures (Figure 4.31a). The textile panels were attached to the holes in the top steel ring using heavy-duty carabiners (12 kN D-ring carabiner, Beifeng) and bowline sailing knots on each of the Dacron polyester and Dyneema ropes (two at the sides and one at the center of each panel).

The bottom anchors for the fabric include 12 1/2" x 18" lag bolts (hot-dipped galvanized steel, BoltDepot) and 24 1/2" x 24" lag bolts (three anchors for each textile panel), each with a galvanized chain link with an inner diameter of 5/16″ for bottom carabiner connections. All of the textile panels were then stretched and connected at their mid-way side points by joining the Dacron polyester ropes with heavy-duty zip-ties (0.5 kN zip-ties, Xingo). Electrical connections from each Tx-Rx unit on each textile panel were established and intersected at the top of the central structure for processing, communication, and power. A central transmitter electrode was applied by laminating copper tapes (6-inch copper foil, Bomei) onto the surface of the wooden tower. The power for the system is provided by a regulated and rechargeable Lithium Iron Phosphate battery with a 12V and 200Ah capacity (LiFePO4 battery, Goldenmate), and a solar panel situated nearby

for daily charging, with the unit capable of generating 1600W per day. Beside the sensing hardware, the battery is primarily used to power the interactive lighting and speaker system at night (Figure 4.33).

Figure 4.32: a) Two personnel climbed to the top and used climbing gear once the assembly reached the fifth level of the tower. b) The *Living Knitwork Pavilion* after construction completion. c) The central structure's joint-beam assembly during a sandstorm. d) The Living Knitwork panels hooked to the top ring. e) Morning community yoga after a night of intense sandstorm. f) The *Living Knitwork Pavilion* after two days of unusual rain in the desert.

Figure 4.33: Side and aerial view of *Living Knitwork Pavilion* illuminated at night.

4.4.5: Principles of Electric Field Sensing

Body-area electric field sensing, also known as body-area capacitive sensing, incorporates the innate conductivity of the human body into electrical systems, facilitating context perception in human-computer interaction and activity recognition fields [244]. By monitoring variations in the electric field, induced either directly or indirectly, this technology enables the deduction of body movements and environmental changes. Furthermore, when the human body intrudes into an existing electric field, it distorts the field, much like how the proximity of a musician's hands disrupts the electromagnetic fields around a theremin's antennas to produce sound or how species like the electric eel and rays generate electric fields to hunt, defend, or navigate their environment.

In active modes of body-area electric field sensing, an e-field transmitter and receiver (Tx-Rx) pair are employed, with the human body serving as an interference source [245]. The sensing process encompasses different modes: transmit, receive, shunt, and loading. In the transmit mode, the human body is becoming an extension of the transmitter electrodes. Conversely, in the receive mode, the system detects changes in the electric field induced by the human body interacting with the receiver electrodes. In the shunt and loading modes, our activities either disrupt or boost displacement current, thereby impacting sensor values based on our grounding. These allow proxemic applications ranging from detecting body position, collaborative interaction or activity, arm movements, to even finer finger adjustments.

4.4.6: Hardware Design and Development

The transmitter circuit consists of a microcontroller that outputs a square wave with a 50% duty cycle from its digital pin with pulse-width modulation, driving a resonant LC oscillator. When the square wave's frequency matches the oscillator's resonant frequency, the output is a high-amplitude sine wave, typically ranging from tens to a hundred volts. This output is connected to the transmit electrode, where the varying electric potential generates an electric field. The frequency and corresponding LC values necessary for operation can be determined using the equation $f = 1/2\pi\sqrt{LC}$, taking into account any parallel capacitance from the transmitter or receiver electrodes.

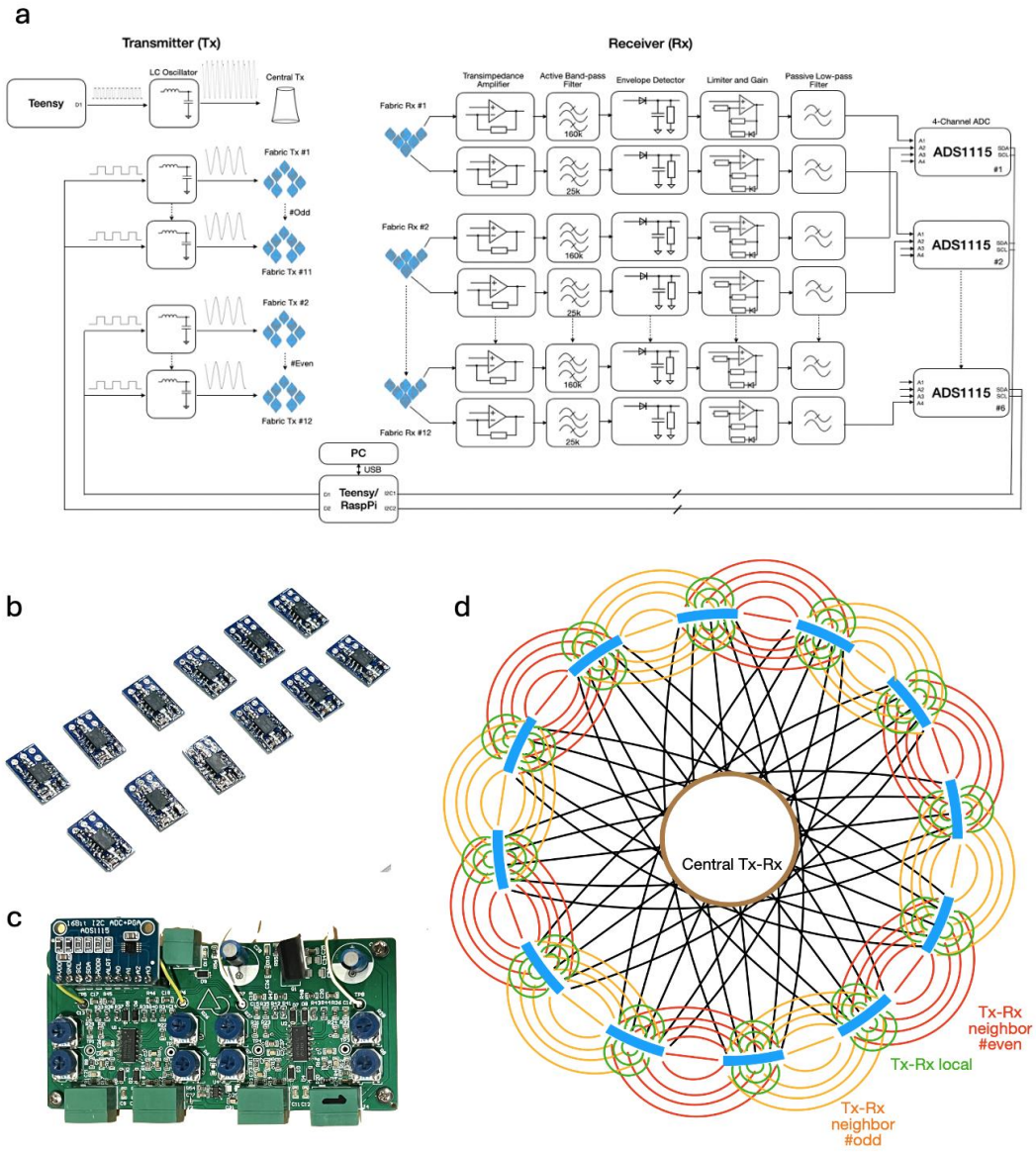

Figure 4.34: a) Transmitter and receiver hardware system, with its corresponding b) first and c) second stage receiver circuits. d) The two (central and fabric) transmitters and time-multiplexing configuration reduce neighboring field coupling and enable the spatialization inside the *Living Knitwork Pavilion* and differentiation of activity at specific fabric openings, aiding in identifying disturbances in the signal between the specific knitted transmitter and an adjacent knitted electrode receiver, especially for sensing entering or exiting activities.

We utilize two distinct frequencies across two circuits: the central transmitter operates at 180 kHz with an output of approximately 120 V, while the knitted transmitters operate at 25 kHz, with six knitted transmitter electrodes connected one at a time, each with an output of about 30 V. Time-multiplexing is employed to alternate the 25 kHz AC signals between these six knitted transmitter electrodes with a time delay of 30 ms. This multiplexing and configuration reduce neighboring field coupling and enable the differentiation of activity at specific fabric openings, aiding in identifying disturbances in the signal between the specific knitted transmitter and an adjacent knitted electrode receiver, especially for sensing entering or exiting activities.

The receiver circuit comprises two main stages (Figure 4.34 and Appendix A.12): the first stage is a transimpedance amplifier that converts current coupled with the transmitter into voltage with a gain of Rf, and the second stage is an integrated active narrow band-pass filter, envelope detector, and limiter.

- **First stage.** The transimpedance amplifier circuit (Figure 4.34b) in the first stage is embedded in the channel just beside each knitted receiver on every panel. This placement allows for immediate conversion of the coupled electric-field current into voltage, minimizing parasitic influence and current noise induced by electromagnetic waves and parasitic capacitance from the vicinity and the long cable leading to the central system at the top of the Pavilion. Multi-layer stranded wires (26 AWG) are used to ground and shield every AC-transmission wire, protecting from external noise and pick-ups.
- **Second stage.** The signals from the first stage (comprising two frequencies from the transmitters) are then filtered through band-pass filters with center frequencies of 25 kHz and 180 kHz and a quality factor of 10 (Figure 4.34c). These signals are transformed into DC signals with tunable gain through an envelope detector and limiter circuit, and then filtered again with a low-pass cut-off frequency of 15 Hz. Finally, the clean DC signals can be read by a 16-bit ADC module (ADS1115). The microcontroller or PC (such as Teensy or Raspberry Pi) scans through each ADC channel and converts the sensor data into MIDI signals for real-time audio and lighting controls.

4.4.7: Sensor Data and Analysis

Figure 4.34d illustrates the electric field distribution between the central transmitter and each knitted receiver electrode, as well as between the knitted transmitter electrode and the adjacent receiver electrodes. To demonstrate the different e-field sensing modes, Figure 4.35a provides an example. This figure shows the e-field signals of four knitted fabric receivers corresponding to the central transmitter, as well as the e-field signals between the first and second fabric panels' transmit-receive pair (Tx-Rx) and between the fifth and sixth fabric Tx-Rx pair. As a person enters

the pavilion, they act as a bridge, strengthening the coupling and resulting in an increase in the e-field signal. As the person walks through four of the fabric panels, the signal drops because the person acts in a shunt mode, acting as virtual ground and reducing the coupling between the central transmitter and the surrounding fabric receivers. The last Tx-Rx pair shows a peak signal as the person exits the pavilion.

In Figure 4.35b, the person positioned between each fabric panel and the central transmitter acts in a transmit mode. As the hand moves and extends, it transitions from a shunt to a transmit mode, becoming a bridge between the Tx-Rx pairs, resulting in an increase in the signal. Similarly, when the receiver (Figure 4.35c) or the transmitter (Figure 4.35d) is touched, the person essentially becomes an extension of the electrode, resulting in signal saturation, with touching the transmitter being an extreme case as the e-field is shared from the body through all of the neighboring knitted receivers.

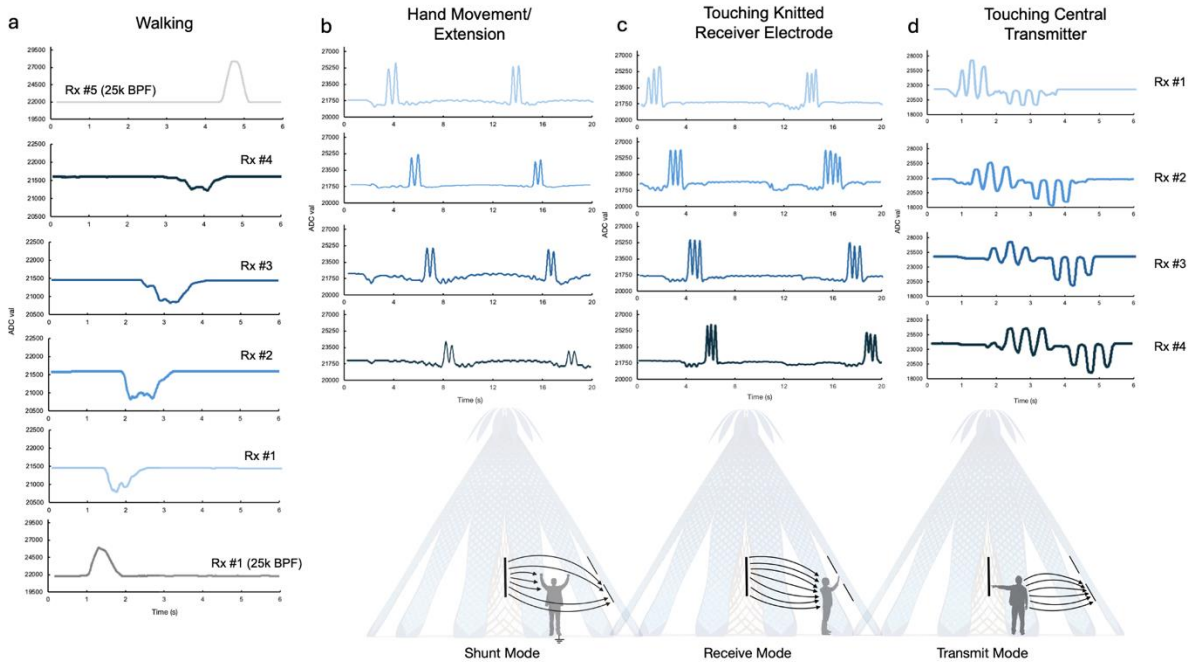

Figure 4.35: a) As a person enters the pavilion, they act as a bridge, strengthening the coupling and resulting in an increase in the e-field signal. As the person walks through four of the fabric panels, the signal drops because the person acts in a shunt mode, acting as virtual ground and reducing the coupling between the central transmitter and the surrounding fabric receivers. The last Tx-Rx pair shows a peak signal as the person exits the pavilion (first and last graphs are sensor data with 25kHz filtering, while the rest graphs are sensor data with 180kHz filtering). b-c) The increase in signal as a person extends their hand, bridging the central transmitter to the knitted receivers or touches the knitted receivers sequentially. d) Strong e-field that gets picked up by receivers in the vicinity as a person touches the central transmitter.

Analysis of this distribution allows for the detection of occupant movement, localization of their positions, and determination of approach, entry, or exit events based on the variations in the electric field sensor data (Figure 4.36). Furthermore, it can be used to evaluate the density of occupancy within the *Living Knitwork Pavilion*, providing insights into crowd and activity levels within the space.

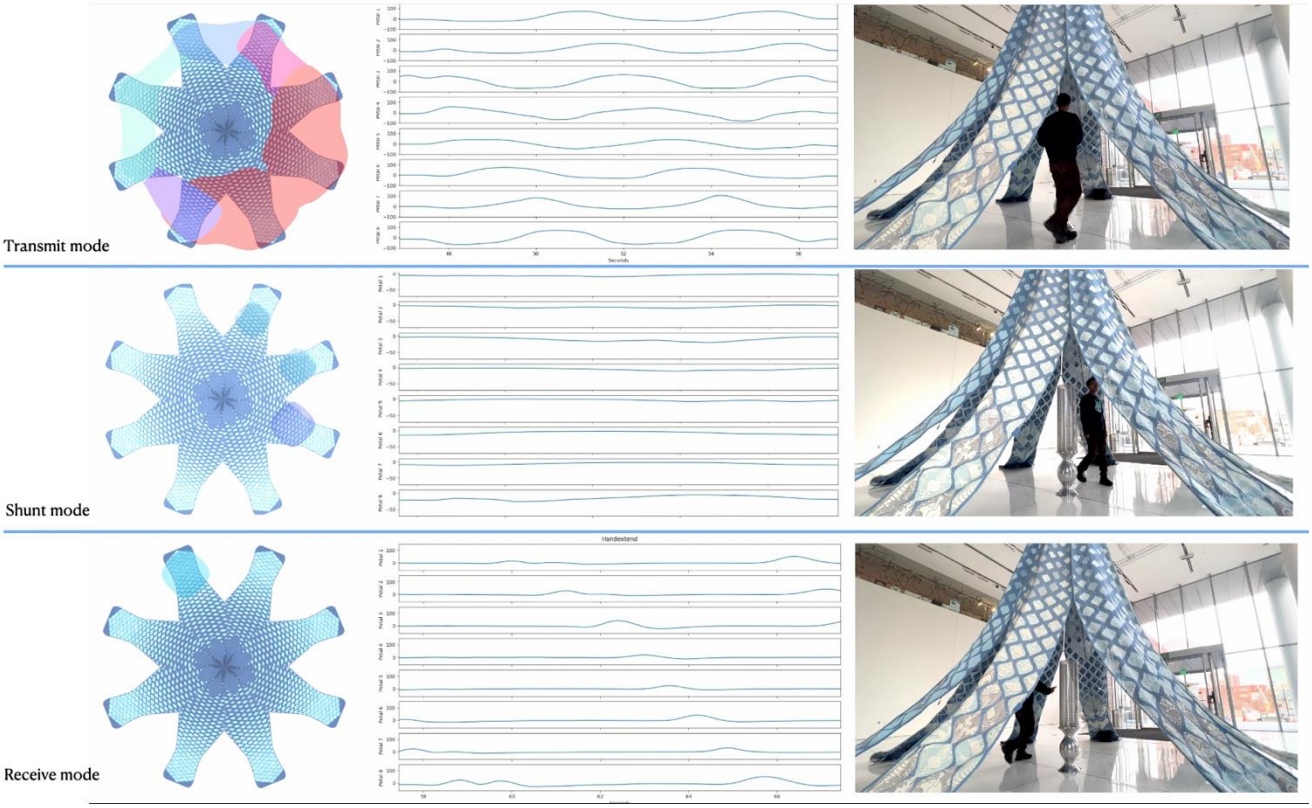

Figure 4.36: Sensor data and visualization as a person: a) touching the transmitter, amplifying its signal to neighboring electrodes and shunting/reducing the opposite, b) walking around and c) waving extending their hands without touching inside the Pavilion (all sensor data are with 180kHz filter, time-multiplexing with 25kHz filter was not activated in this case).

4.4.8: From Physical to the Digital: KnitworkVR

Motivated by projects in the *Responsive Environments Group*, such as *DoppelMarsh* and *DoppelLab*, where virtual environments generated from extensive sensor networks within buildings or environments [38], [246]. The rich information captured by these systems allows designers, musicians, and visual artists to animate sensor data in virtual environments through direct, artistic, or metaphorical mappings. Applying the concept of *Dual Reality*—where real and virtual worlds are distinct yet enhanced by their ability to reflect, influence, and merge via embedded sensor/actuator networks—*KnitworkVR* connects real-time sensor data streams and interactive systems in the *Living Knitwork Pavilion* into an immersive digital twin virtual environment and vice versa [247].

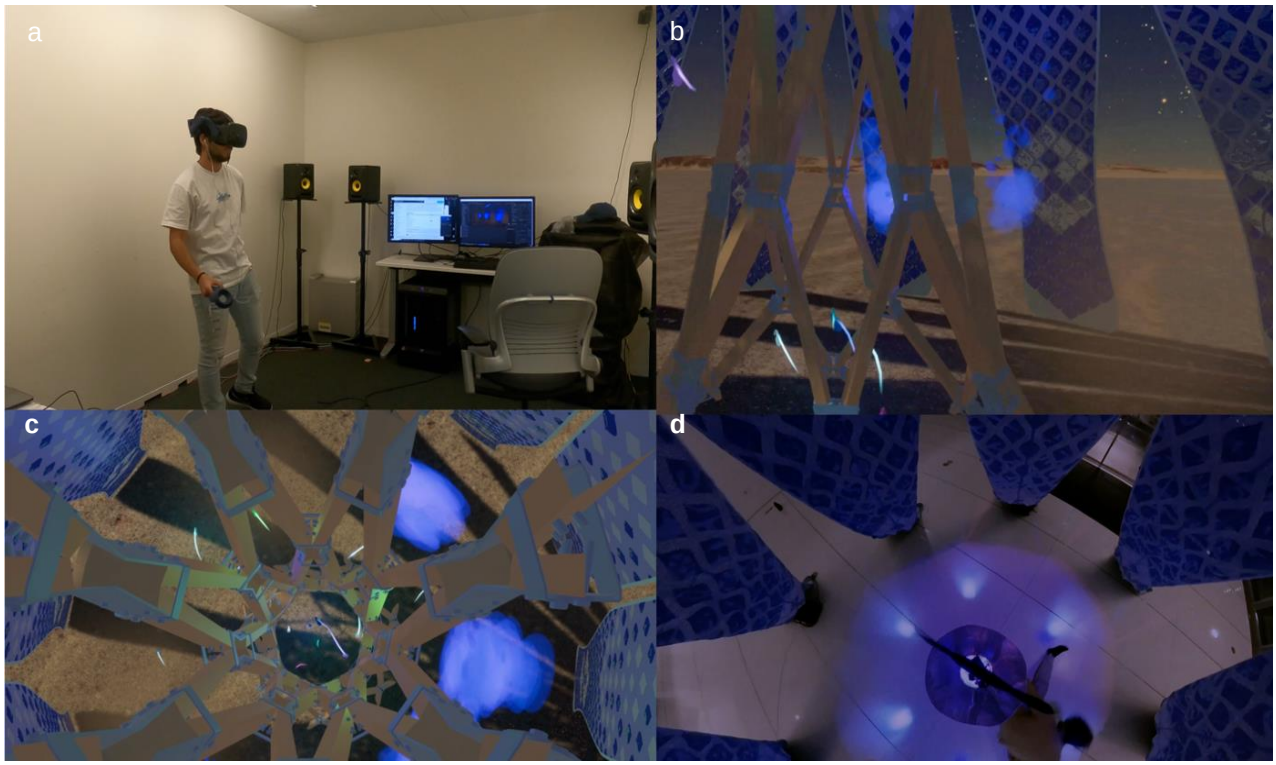

Figure 4.37: a) A user interacting in *KnitworkVR* and experiencing its rich b-c) immersive audiovisual landscape driven by d) interactive performance in real-time in the physical *Living Knitwork Pavilion* at another location

After its installation in Black Rock City, we installed the *Living Knitwork Pavilion* in a MIT Media Lab E14 lobby for a longer period of time. The installation offers audiences the opportunity to witness the intricacy of the textile as well as the immersive experience provided by the spatial

audio and visual systems, while the virtual reality correspondence offers an immersion into the *Living Knitwork Pavilion*'s original state in the Black Rock Desert landscape.

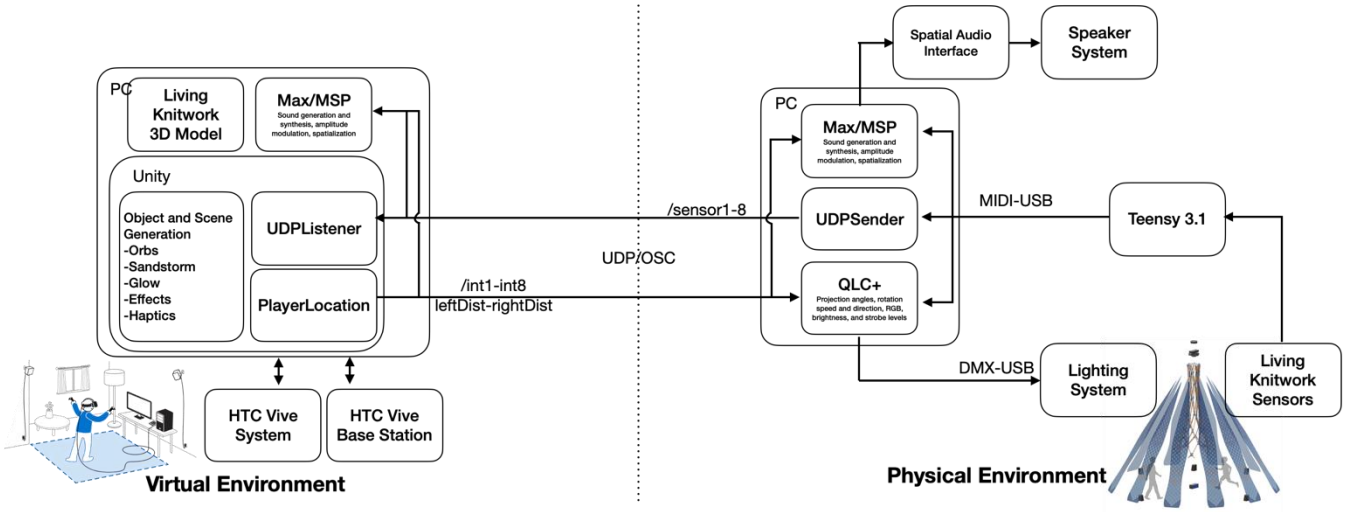

Figure 4.38: Sensor data and visualization as a person: a) touching the transmitter, amplifying its signal to neighboring electrodes and shunting/reducing the opposite, b) walking around and c) waving extending their hands without touching inside the Pavilion

Since the design is modular, in the lobby installation, we installed 8 of the textile panels (total area of 28.3 m^2) instead of the original 12 panels (50 m^2) due to space constraints. Finally, we have also developed a dual reality pipeline and environment where the sensors, audio, and visual experience of the *Living Knitwork Pavilion* in the physical reality interacts in real-time with the position trackers of the user, as well as the audio and animation of the virtual representation of the *Living Knitwork Pavilion* in Knitwork VR (Figure 4.36=8).

Sensor data in *KnitworkVR* is received via open-sound control/user datagram protocol (OSC/UDP) to the Unity environment connected to HTC Vive and SteamVR system with base trackers. Within Unity, a Listener *GameObject* receives this data, facilitating real-time updates and interactions within the virtual environment (Figure 4.39a-b)). The *PlayerLocation* script calculates the spatial position and orientation of a player's head in radial distance and angular orientation, as well as hand extension in the VR environment, transmitting this data via UDP. This fast, connectionless data transmission method ensures real-time updates crucial for immersive VR experiences. The Unity environment reacts to sensor data from the physical Pavilion through various visual and interactive elements. Additionally, we have incorporated haptic feedback action through our *SteamVR* plugin as the user hand reaches physical objects (i.e. fabric and structure) in the virtual environment (Figure 4.39c).

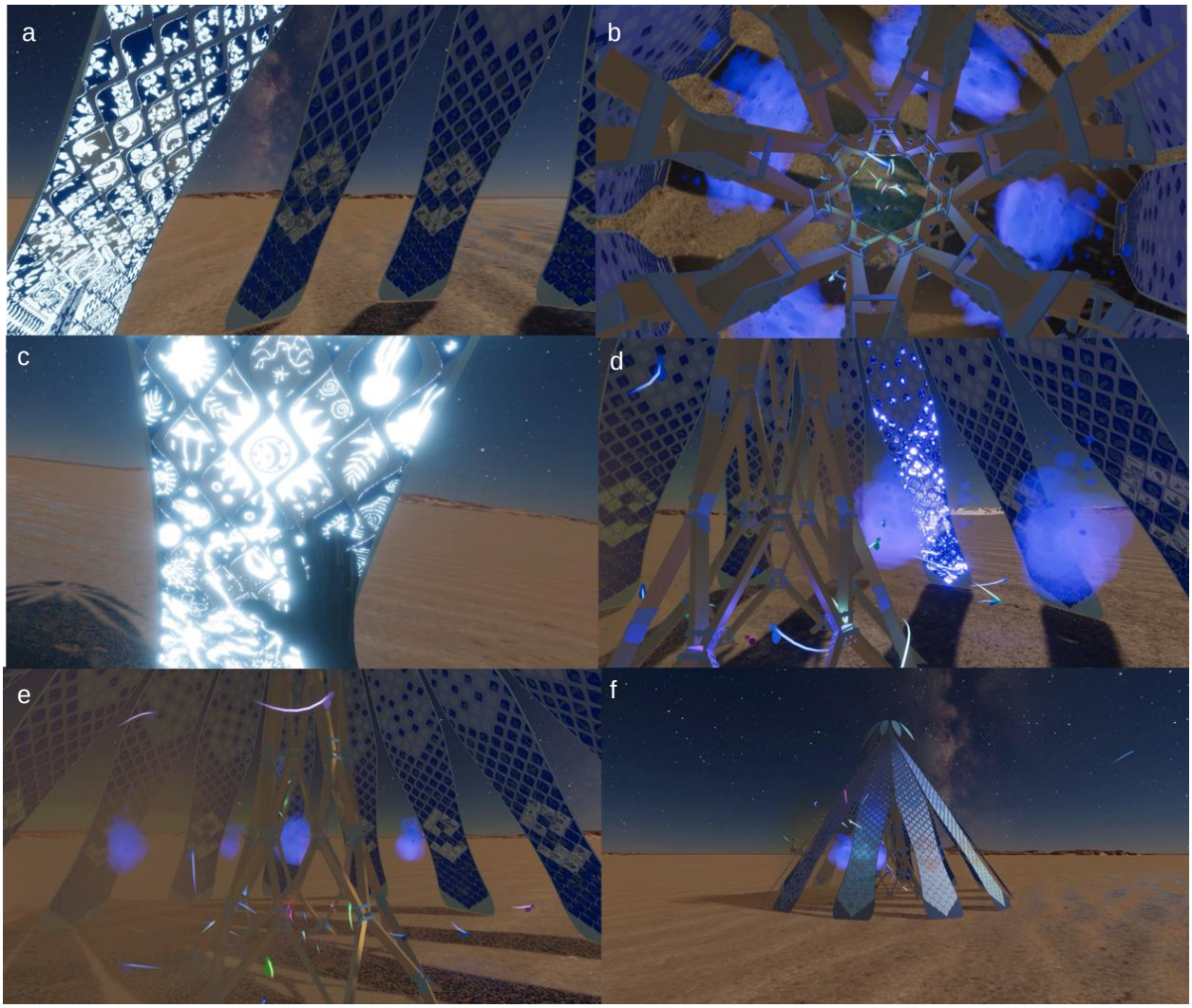

Figure 4.39: Virtual reality interaction and experience within the KnitworkVR including: a) white-glow on the fabric patterns as a user walking toward it, b) haptic sensation as the hand-tracker collides with the digital fabric, c-e) orbs/fireballs representing a presence of users in the physical Pavilion, with behavior and intensity of fireflies and sandstorm driven by the aggregate sensor data or collective movements, and bright blue-glow on the fabric patterns as users in the physical Pavilion touch the corresponding fabric. f) View of KnitworkVR from the outside

Our object and scene generation involves creating various animations with properties inputted from the sensor data. Orbs/Fireballs, handled by the *Fireball* script, vary in intensity and behavior depending on interaction levels, using a 5x5 matrix to adjust properties like size and lifespan (Figure 4.39c). The *GlowObserver* script controls the virtual fabric's glowing patterns, adjusting the intensity based on the player's proximity and touch interactions, using the *MeshRenderer*'s *MaterialPropertyBlock* to modify the *EmissiveColor* property (Figure 4.39d). Fireflies, managed by

the *Fireflies* script, represent the crowd density in the Pavilion, emitting particles based on the number of panels interacted with (Figure 4.39c-d). Sandstorms, controlled by the Sand script, emit particles when users interact with corresponding panels or when the VR player approaches, enhancing immersion by dynamically adjusting the *ParticleSystem*'s emission rate (Figure 4.39e). At the same time, Max/MSP system is run in the machine where both the OSC data from the player location in VR and the distributed sensors from the physical Pavilion create a sonic landscape driven by both performers. The VR component directly maps into the mellow version of the aforementioned 8 AI-generated musical loops.

4.4.9: Lighting System and Mapping

The Raspberry Pi or PC connected to the microcontroller interfaces with a rotating head light module (Figure 4.40a, YRZJ DMX Stage Light, Yuer Inc.) through a MIDI-DMX universal data transfer protocol mediated by QLC+ software. The rotating head light module consists of six individually motorized 30W RGB beam lights and a single motor controlling six 10W RGB beam lights. The module has 42 DMX channels that can control various parameters (Figure 4.40b) such as the movement of each of the six motorized lights, RGB levels, brightness levels, strobe levels, and rotation speed and direction (Figure 4.40c-e). We are exploring several light projection mappings:

Real-time Mode. MIDI sensor data corresponding to movements on each petal can be individually or spatially mapped to control the nearest motorized beam lights in real-time. This allows occupants to control the movement and intensity of the lights as they walk (green), dance (blue), and interact (movement of the light) within the space and each fabric panel of the *Living Knitwork Pavilion*. The aggregate sensor data corresponding to crowd and activity levels can also be represented by adjusting the total brightness and rotation speed, creating a collective immersive experience.

Playback Mode. By recording all MIDI activity sensor data and replaying it through the distributed lighting system, we can induce a novel lighting experience triggered by occupants' visits. This allows them to feel the presence of others and collaborate with past "living" souls, reliving the history of the *Living Knitwork Pavilion* and exploring the principles of *Teleexistence* and *Teleabsence* [248], [249].

Audio Mode. Using the in-built function of the DMX lighting system and its microphone to convert sound amplitude and frequency into pre-programmed lighting effects, we can set the lighting system to react to music driven by the spatial audio system.

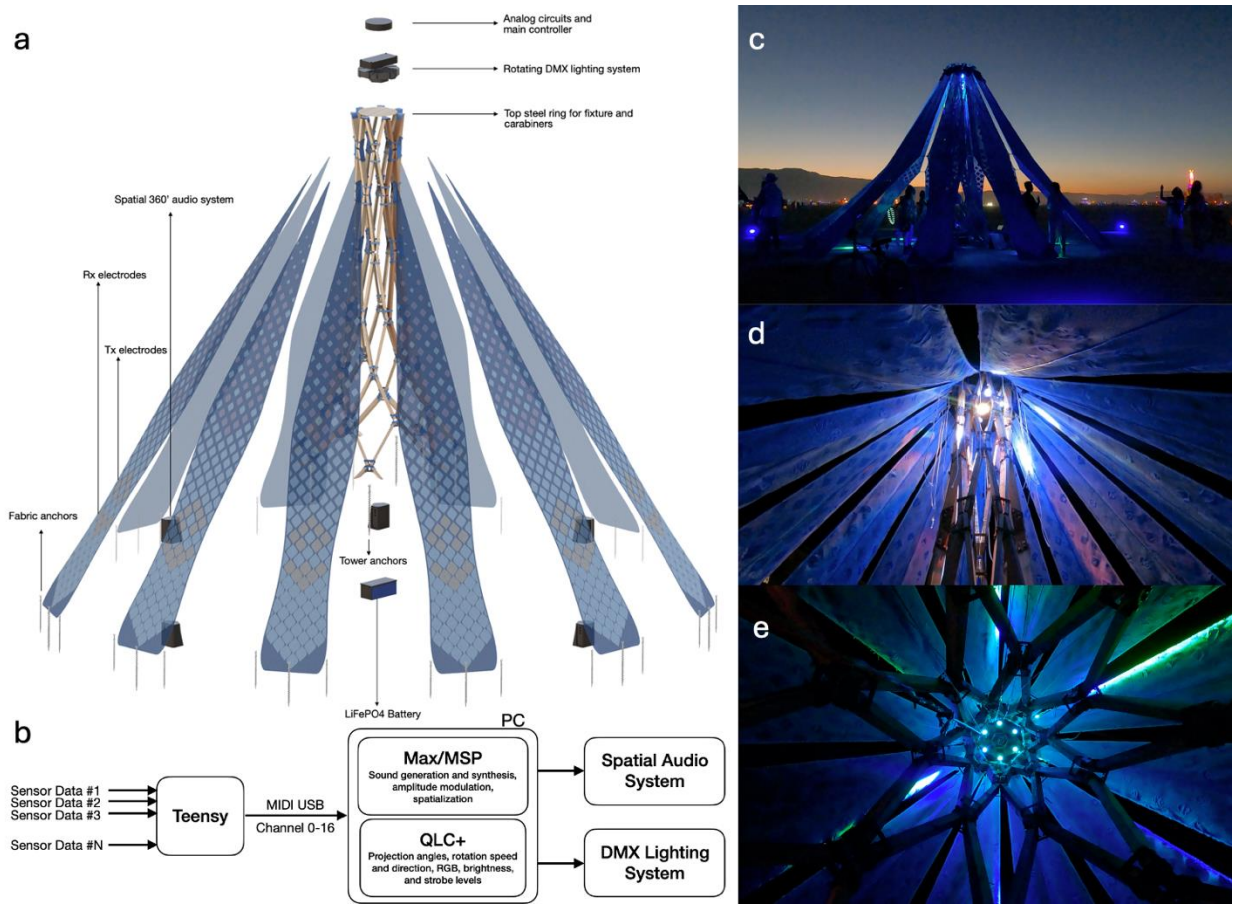

Figure 4.40: a) Exploded view of the *Living Knitwork Pavilion* integrated system featuring a distributed spatial audio system, as well as motorized rotating light beams. b) System diagram showing the interface between the Living Knitwork main hardware system and PC that sends sensor data as MIDI messages through USB to control both audio and lighting systems. c-e) *Living Knitwork Pavilion* interactivity at night.

For *KnitworkVR*, the QLC+ also accepts OSC data representative of the user location (int1/8) and hand extension (left/rightDist) in the VR environment. By connecting these values to the individual color of the RGB beam lights (physical/virtual location), as well as its strobe level (hand extension) we can demonstrate visual experience of dual reality co-presence by merging the green (physical) with purple light (virtual), as shown in Figure 4.41d-e.

4.4.10: Spatial Audio System, Sound Synthesis, and Mapping

As shown in Figure 4.40a, we have designed an immersive audio experience using a 4-channel distributed speaker system, and make use of state-of-the-art generative AI music models to allow users to engage in a full AI-generated 360-degree auditory environment both in the physical and virtual Pavilion (Figure 4.37). By using Max/MSP to interpret the live output of the sensors and through carefully-designed interactive modalities and specialization techniques, we enable users to explore the different sonic narratives of the installation. By leveraging sensor-driven modulation with AI-generated music and spatialization techniques in a Max/MSP patch, the system creates a truly interactive and immersive auditory environment and enables real-time audio synthesis. The patch consists of several key modules:

AI Music Module: This module employs machine learning algorithms to generate base musical compositions for each channel. The AI model, trained on a diverse dataset of musical pieces, produces intricate and harmonious loops inspired by the themes and patterns of the *Living Knitwork Pavilion*. We used the Transformer-based generative music system *MusicGen* [250] to generate musical loops–one for each of the panel's theme and patterns. The text conditioning modality of the model, together with additional curation, allowed us to generate 1-minute-long loops that were all in the same key and tempo, in order to create a harmonious and coherent mix during the experience.

Spatialization and Interactivity: We embed various modalities of interaction and spatialization methodologies inside a Max/MSP patch to create a fully immersive experience with or without KnitworkVR. Notably, we enable users in the physical and virtual Pavilion to both directly interact with each individual panel and explore the soundscapes created by the unison of multiple. Through the collection of 8/16 distinct sensor values, we can precisely locate the users within the structure and modulate the sound characteristic and volume of each loop accordingly to let them perceive the musical narrative associated with each panel. Additionally, using an ambisonic spatialization module, we distribute each musical component according to the physical location of each panel, creating a rich immersive experience in which the user can orchestrate the distribution of each musical element. By sensing the user's touch on individual panels, we can solo specific musical loops and let them surround the entire sonic space to let users explore specific details at their own pace.

4.4.11: Installation Experience and Future Work

The *Living Knitwork Pavilion* offered a unique opportunity to explore the interplay between architectural design, textile innovation, immersive environments, and social engagement in an extreme environment. Throughout the Burning Man event, the pavilion hosted a variety of pop-up events, including yoga sessions, dance performances, live music, and even a wedding ceremony (Figure 4.32e). These activities highlighted the pavilion's versatility and its ability to facilitate community gatherings.

However, during the event, unexpected challenges arose with extreme dust storms followed by a constant, heavy rainstorm (Figure 4.32f), an unusual occurrence in the desert location. Interestingly, this climatic twist benefited the pavilion by cleansing its textile surface of accumulated dust and revitalizing its vivid blue color. This unforeseen outcome highlighted the pavilion's resilience and adaptability, demonstrating its potential for long-term outdoor installations.

The initial installations provided valuable insights, yet the limited timeframe and unique conditions of the event constrained the scope of data collection and experimentation. During our MIT Media Lab E14 exhibition (Appendix A.5), the pavilion also hosted many events and performances, including an opening (Figure 4.41a), public demonstrations, a collaborative human-architecture live performance with experimental keyboardist Jordan Rudess (Figure 4.41b), and an interactive dance with contemporary dancer Treyden Chiavaralotti (Figure 4.41c-e). These activities further highlighted the pavilion's versatility and ability to facilitate various intimate performances and immersive experiences.

Due to the pavilion's high sensitivity in detecting subtle gestures and occupancy, we observed many interesting responses from the visitors. They experienced surprising and delightful reactions from their interactions with each other. For example, actions such as hand claps, body touches, or hugging created significant signal changes that were reflected in the audiovisual feedback, enhancing the collective experience and intimacy inside the pavilion.

Future work will involve further installations to gather more comprehensive data on occupant experiences and interactions with the pavilion. Advancements in various lighting, animations, and audio mappings, as well as interactivity and multi-user capabilities in the *KnitworkVR*, will be explored. Further collaborations for interactive performances will also demonstrate the pavilion's capabilities as a dynamic, responsive space that continues to evoke novel experiences and engage diverse audiences [251], [252].

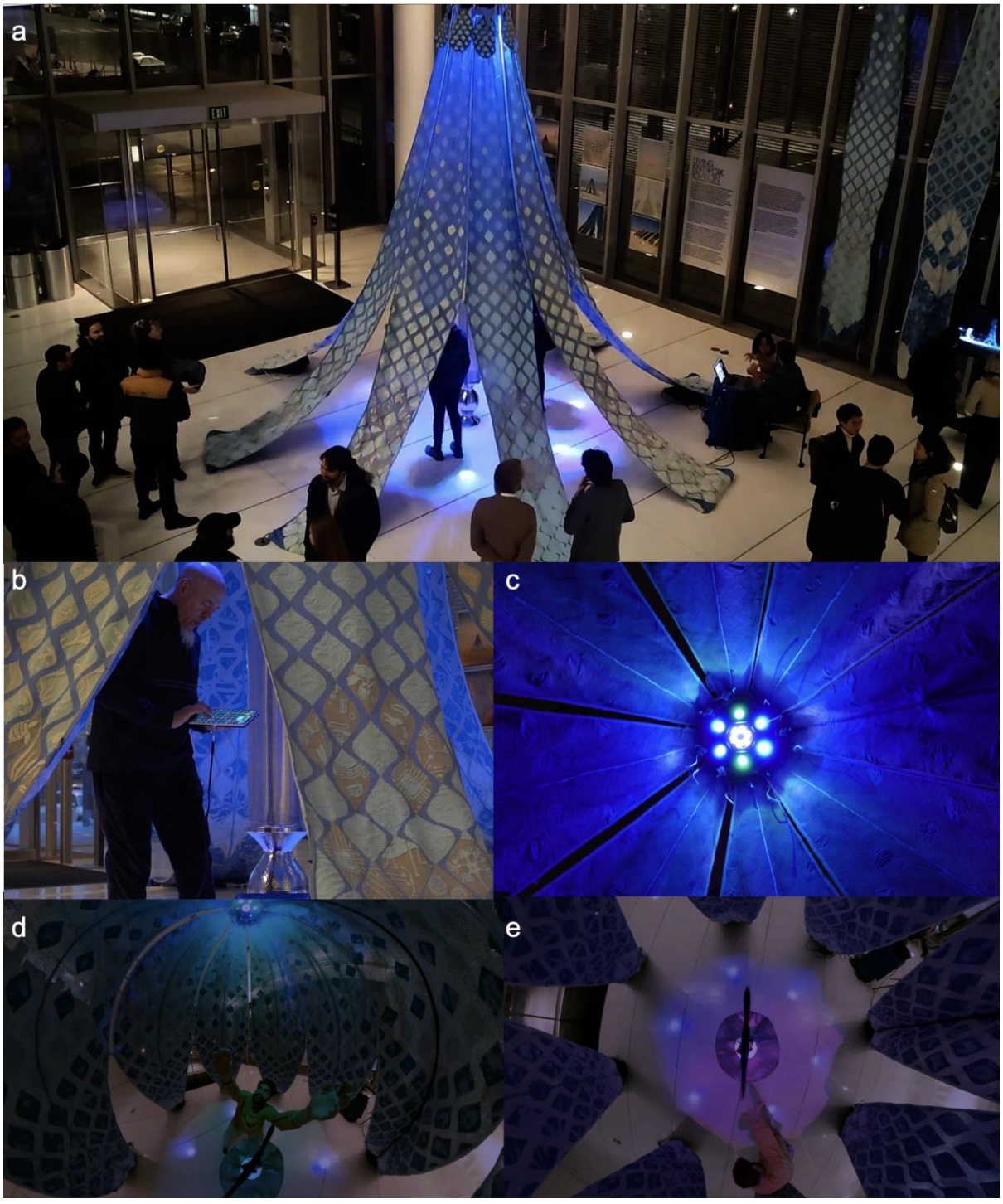

Figure 4.41: a) Public exhibition of the Living Knitwork showing people interacting with the immersive space. b) Keyboardist Jordan Rudess playing *GeoShred* inside the *Living Knitwork Pavilion* combining direct mapping from finger-strokes with the soundscape generated by his movement and location within Living Knitwork. c-d) Dancer Treyden Chiavaralotti interacting with DMX lighting and spatial audio system. e) The copresence of users in both *KnitworkVR* and physical Pavilion trigerring a purple projection from the RGB LED.

4.5: Summary of Contributions

This chapter advances the discourse on the seamless integration of functionalities within textiles, focusing on embedding sensors and electronics at a fundamental level—from individual fibers to complex multi-layer fabrics. By leveraging computational design and digital fabrication techniques, particularly digital knitting, I have achieved a fine-tuned control over the placement of sensors and interconnects within textile surfaces. This approach allows for a precise, scalable fabrication process, enabling the transition from 2D to 3D forms and from small-scale wearable objects to large-scale architectural installations.

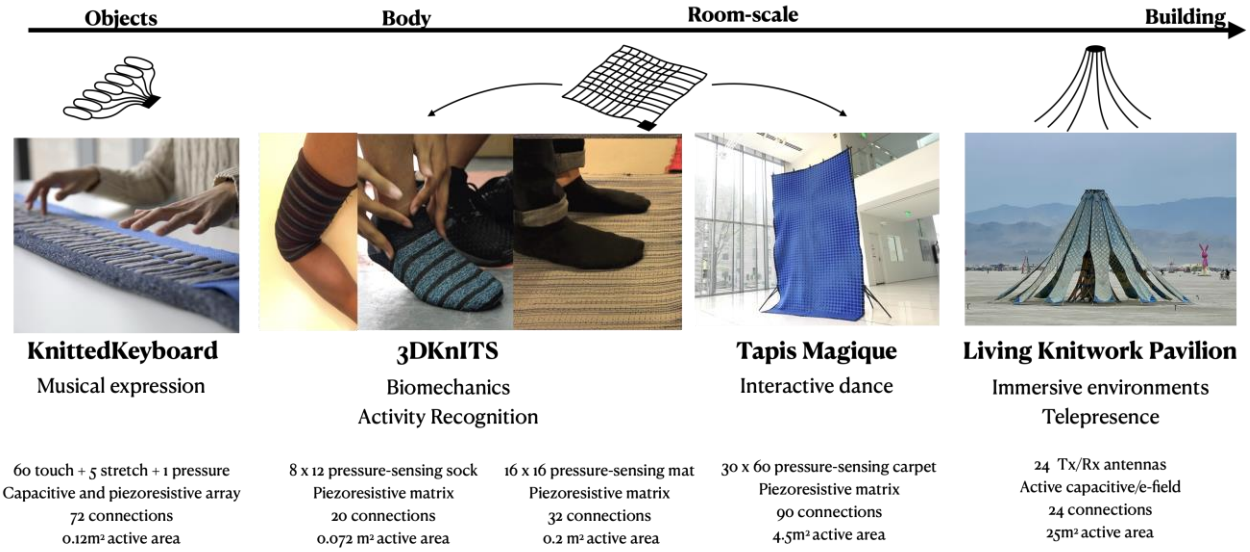

Figure 4.42: Digital knitting of sensate textiles across scales, showing differences in sensing modalities, from the scale of objects to the scale of buildings, showing the wiring architecture, modalities, number of sensor and connections, total active area, and applications of each project.

The work spans across multiple scales (Figure 4.42), demonstrating the versatility and adaptability of sensate textiles. I have demonstrated knitting across different orders of magnitude, beginning with small-scale applications like the *KnittedKeyboard*, which integrates single arrays of 60 capacitive touch-sensing keys along with pressure and stretch sensors, progressing to mid-scale projects like the *3DKnITS* and *Tapis Magique*, which utilize multiplexing configurations with 96, 256, to 1800 sensing pixels, and in the end, evolving into large-scale architectural implementations like the *Living Knitwork Pavilion*, a 25-square-meter immersive space structure that incorporates 24 knitted antennas for distributed active capacitive sensing.

These creations illustrate a continuum from intimate, single-user interfaces to expansive, multi-user environments. Each artifact showcases unique approaches: from the *KnittedKeyboard*'s multi-modal sensing, pressure-imaging surfaces, to the Pavilion's active capacitive sensing, combining elements of textile design, functional yarns, hardware systems, and structural engineering to create functional yet aesthetically rich fabrics.

Moreover, these collective projects delve into the dynamic relationship between movement and multi-sensory experiences that engage auditory, tactile, and visual modalities. Through these novel textile interfaces, the connection between gestures and sound, whether it's the delicate movement of our fingers, the hovering of our hands, or even our footwork, is explored in rich detail. In larger scale, full-body movements are mapped to collective experiences in immersive spaces, illustrating how textiles can mediate human interaction and augment sensory perception. The interplay between tactile feedback, gesture-based control, and sound in these artifacts not only emphasizes the technical capabilities of sensate textiles but also opens up new dimensions for intimate human-material and human-architecture interaction.

While the *KnittedKeyboard* and *Living Knitwork Pavilion* utilize a single array configuration, the *3DKnITS* and *Tapis Magique* projects employ more complex, multiplexed configurations to meet the increased sensing demands of larger surfaces or higher resolution. Both approaches—single arrays and multiplexed sensing systems—introduce significant challenges, particularly in managing the number of intricate wirings, dealing with bandwidth limitations, ensuring immunity and reliability against broken connections, and addressing the constraints of centralized processing. As shown in Figure 4.43, we have explored various mechanisms to connect the knitted sensate textiles to our circuits or main modules. These connections still involve manual stitching, looping, and tightening (Figure 4.43a,c-d) , or utilizing existing textile components such as snaps and fasteners for soft-hard interfaces (Figure 4.43b,f), as well as electronic components like headers and plugs (Figure 4.43e).

Textile-hardware interfacing, especially when dealing with a large number of sensors, remains a persistent challenge. The complexity increases as the scale of the textiles grows, demanding more efficient methods for managing sensor connections while maintaining the integrity and functionality of the system. Alternative methods to traditional manual tightening of connections have been investigated by several researchers to improve reliability and ease of assembly.

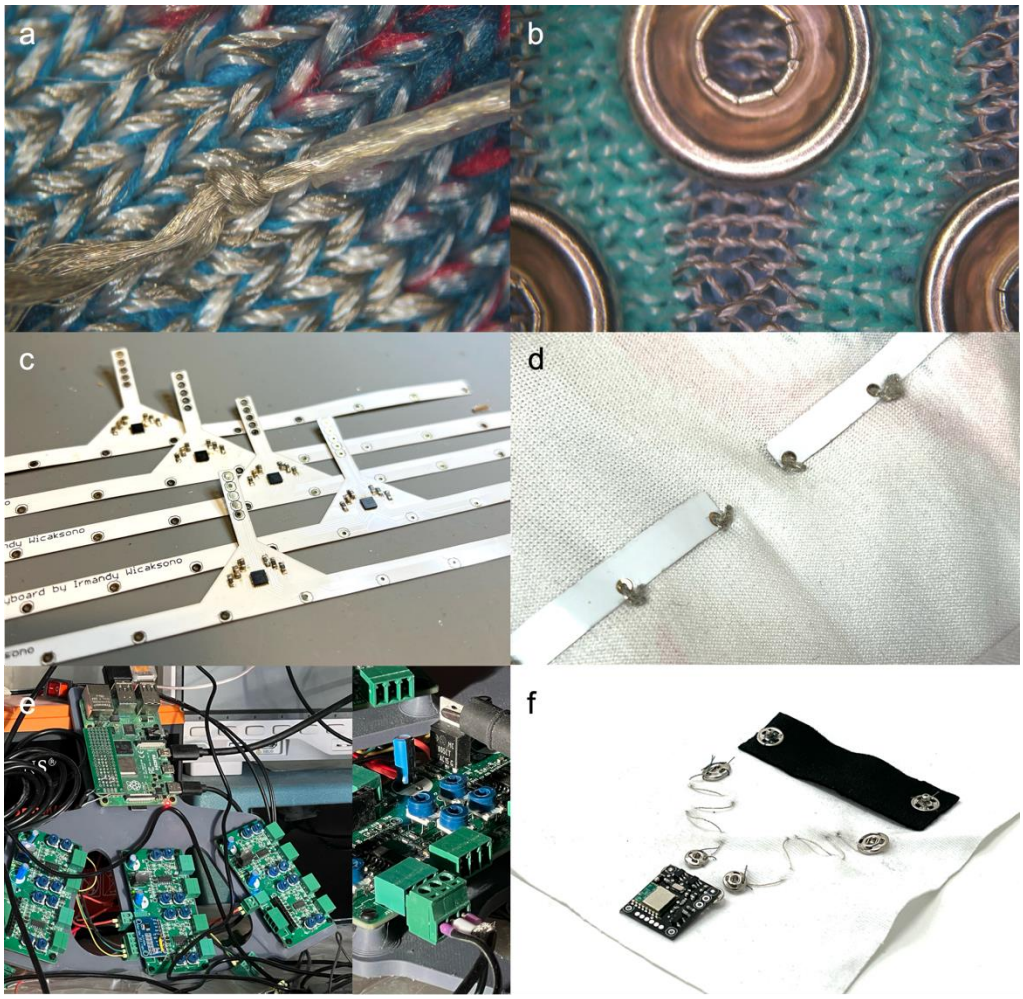

Figure 4.43: Connectorization or soft-hard interfacing in various e-textile projects from my work. a) Manual sewing, looping, and tightening using insulated conductive yarns (*Tapis Magique* and *KnittedKeyboard*). b) Leveraging heavy-duty stainless steel male-female snaps and fasteners to connect wiring and PCBs to knitted textile interconnects (*3DKnITS*). c-d) Flex PCB used to connect the keys in *KnittedKeyboard* to the MPR121 capacitive sensing module. Looping and tightening of conductive yarns were applied to both the PCB holes and the knitted sensor parts. e) *Living Knitwork Pavilion* hardware showing headers for connections. Crimped wires can be plugged into these headers, with the other ends connected to each electrode through crocheting (Figure 4.28). f) Carbonized textile sensor, which can be connected to a resistive sensing circuit integrated with a BLE System-on-Chip (SoC) module, both through snaps.

For instance, ultrasonic welding of wires to conductive textiles has been explored as a technique to create durable and consistent connections [253]. Additionally, other attachment mechanisms have been considered, such as magnetic or mechanical sockets that offer the benefit of being washable and reusable [254]. These may include sliding and snap mechanisms, belt-connectors, or bump designs that slide into tight pockets to ensure a secure electrical connection [255], [256]. Each of these approaches offers unique advantages in terms of durability, ease of use, and scalability, and they represent promising avenues for future development in textile-hardware interfacing. For these sensate textiles to become truly scalable, however, not only that they need robust textile-hardware interfacing, but they also require principles drawn from distributed systems and architectures, alongside advancements in circuit fabrication and modular designs. This will be explored in greater depth in Chapter 6, where I discuss potential solutions to these interfacing and scalability challenges to enable more robust, adaptive sensate textile and computational fabric systems.

Chapter 5: Design for Stretchability with Soft Printed Circuits

"What is strong and rigid is snapped and laid low.
What is flexible and soft will always prevail."
Lao Tzu

"When you want to know how things really work,
study them when they're coming apart."
William Gibson

In this chapter, we introduce a set of metrics or parameters to design interconnects for system-on-fabrics, supporting the development of networked electronic textile system (*NETS)* that will be outlined and discussed in Chapter 6. We propose an island-bridge configuration, where the islands represent miniaturized hardware nodes embedded within flexible PCBs (Figure 5.1). These islands, functioning as composite materials on the fabric, are designed as miniaturized, rigid, or moderately flexible hardware elements, each serving as processing centers with specific functions or housing a suite of components. To maintain the fabric's flexibility and stretchability, the interconnects between these islands must be highly stretchable. This design ensures that the electronic system can withstand mechanical deformations associated with fabric movement while maintaining reliable functionality.

In the development of stretchable electronics, a variety of materials and manufacturing techniques are available, including intrinsically stretchable conductors that can be screen-printed or deposited using specialized processes. However, I have chosen to utilize copper with gold-

plating for the fabrication of serpentine interconnects, despite these alternatives, primarily because its common use in printed circuit manufacturing technologies. This approach not only simplifies the fabrication process, but also ensures that the designs can be easily scaled for mass production. By leveraging established PCB manufacturing infrastructure, it becomes feasible to integrate stretchable interconnects into conventional electronics production lines, facilitating the transition from prototype to commercial product with minimal additional investment in new equipment or processes. In this chapter, I will explore the fabrication approaches for these soft and stretchable printed circuits. I will delve into the design strategies and considerations for creating stretchable interconnects and discuss the experimental methods and characterization studies conducted to evaluate the performance of these interconnects.

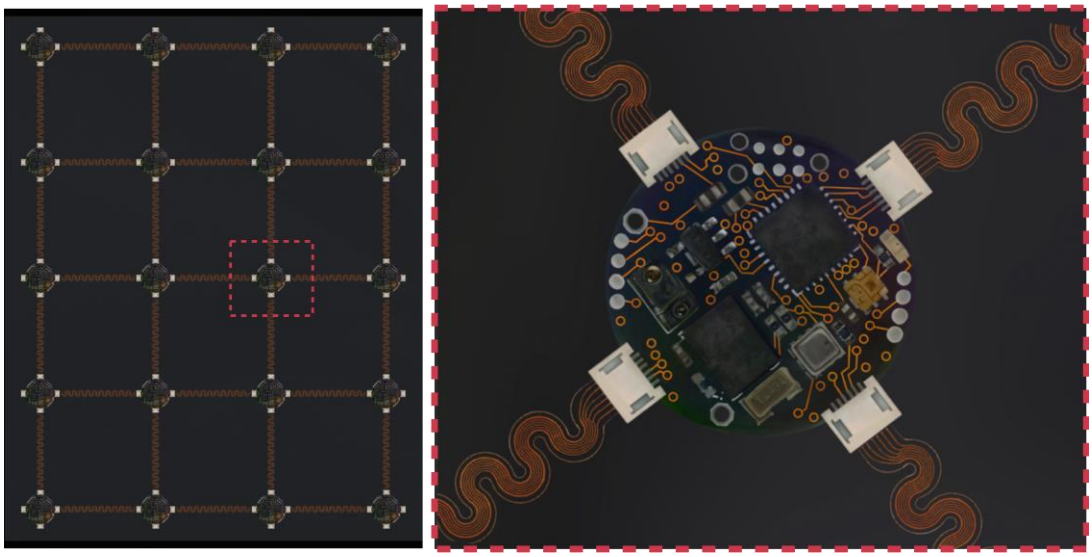

Figure 5.1: Node-interconnects or island-bridge configuration of *NETS* (Networked Electronic Textile Skin).

5.1: Soft Printed Circuits Fabrication

In the field of PCB manufacturing, two primary types of substrates are utilized: rigid and flexible. Both types exhibit similarities in their fabrication processes; however, they are distinguished by the substrate material used. Rigid PCBs typically employ materials such as FR4 (fiberglass reinforced epoxy laminate), while flexible and soft PCBs utilize a polyimide and polyurethane base substrate. This difference in material results in additional design constraints for soft PCBs.

5.1.1: Flexible Polyimide Printed Circuit Boards

The development of interconnects is achieved through a standard two-layer industrial process for flexible PCBs (as depicted in Figure 5.2). Initially, the process involves double-sided copper (5-35 μm thick) being deposited on a polyimide substrate (60 μm thick), which is then cut into sheets. Via holes, measuring 150 μm in diameter, are created using mechanical drilling to enable interlayer connections. Subsequently, an electroless plating process is employed to deposit a thin copper seed layer, approximately 0.3-0.5 μm thick, along the walls of the holes. This is followed by electroplating, which can increase the copper thickness to 5μm.

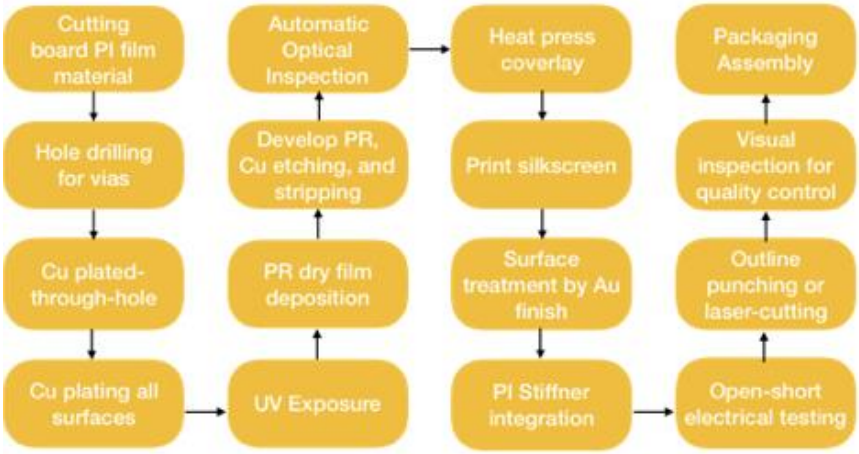

Figure 5.2: Flow diagram of flexible printed circuit board fabrication.

Next, a dry, photosensitive film is laminated onto the copper surface through pressing and prepared for image transfer. A photographic film serves as a selective mask for ultraviolet radiation, which polymerizes the exposed portions of the photosensitive film. The non-polymerized sections of the film are then removed using a sodium carbonate (Na_2CO_3) developer. The copper is etched through a chemical reaction involving copper chloride ($CuCl_2$), hydrochloric acid (HCl), and hydrogen peroxide (H_2O_2). The dry film on the copper foil is subsequently stripped off by submerging it in sodium hydroxide (NaOH). The fabricated circuit is then inspected using Automatic Optical Inspection (AOI) technology, which compares an image generated by a charged-coupled device (CCD) camera with the original design to identify any defects.

To protect the circuitry, a coverlay made of polyamide (28 μm thick) with an adhesive backing is patterned using drilling and laser cutting, and then bonded to the circuit through hot press lamination. Silkscreen printing is applied using a stainless-steel vacuum frame, and the circuit is then baked in an oven at 180°C. For the final surface finish, an electroless nickel immersion gold

(ENIG) process is conducted in a plating solution bath. To safeguard the IC contacts on the pads from potential damage, a polyamide stiffener (75 μm thick) is reinforced with a glue layer. The final step involves laser cutting to define the precise shape of the tracks and islands on the PCB.

The current capabilities of Flex PCB manufacturing provide significant flexibility and precision. The process supports panel sizes up to 234 × 490 mm and enables two-layer PCB designs. Utilizing a dry film process with LDI (laser direct image) exposure technology ensures high precision in pattern transfer, while the standard ENIG surface finish (1μ" or 2μ") offers excellent corrosion resistance and solderability. The manufacturing process allows for a minimum via hole size of 0.15 mm with a 0.35 mm diameter, supported by a minimum annular ring size of 0.1 mm and recommended via sizes of 0.3 mm (inner) and 0.55 mm (outer). Additionally, the minimum trace width and spacing for a 1 oz (35 μm) copper layer are 4 mils (0.1 mm), and can go down to 3 mils (0.07 mm) for 12 μm copper layer.

To enable reconfigurability of the spatial distribution and resolution of our serpentine interconnects or bridges using flexible polyimide PCB, we fabricated four PCB layouts (designed in AutoCAD and imported into Eagle PCB for Gerber file conversion) with different lengths (3, 7, 21, 47 cm corresponding to 5, 9, 23, and 49 pitch length between two nodes) as single-layer flexible PCB panels (Figure 5.3). Each design was carefully crafted with specific dimensions to meet varying application needs while maintaining a universal design approach.

Design 1:

- **Interconnect Dimensions:** 6.3 mm width x 3 cm length
- **Panel Size:** 20 x 8 cm
- **Configuration:** 6 rows x 13 columns (total of 78 interconnects per panel)

Design 2:

- **Interconnect Dimensions:** 6.3 mm width x 7 cm length
- **Panel Size:** 20 x 9 cm
- **Configuration:** 3 rows x 15 columns (total of 45 interconnects per panel)

Design 3:

- **Interconnect Dimensions:** 6.3 mm width x 21 cm length
- **Panel Size:** 42 x 9 cm
- **Configuration:** 2 rows x 15 columns (total of 30 interconnects per panel)

Design 4:

- **Interconnect Dimensions:** 6.3 mm width x 47 cm length
- **Panel Size:** 9 x 47 cm
- **Configuration:** 1 row x 15 columns (total of 15 interconnects per panel)

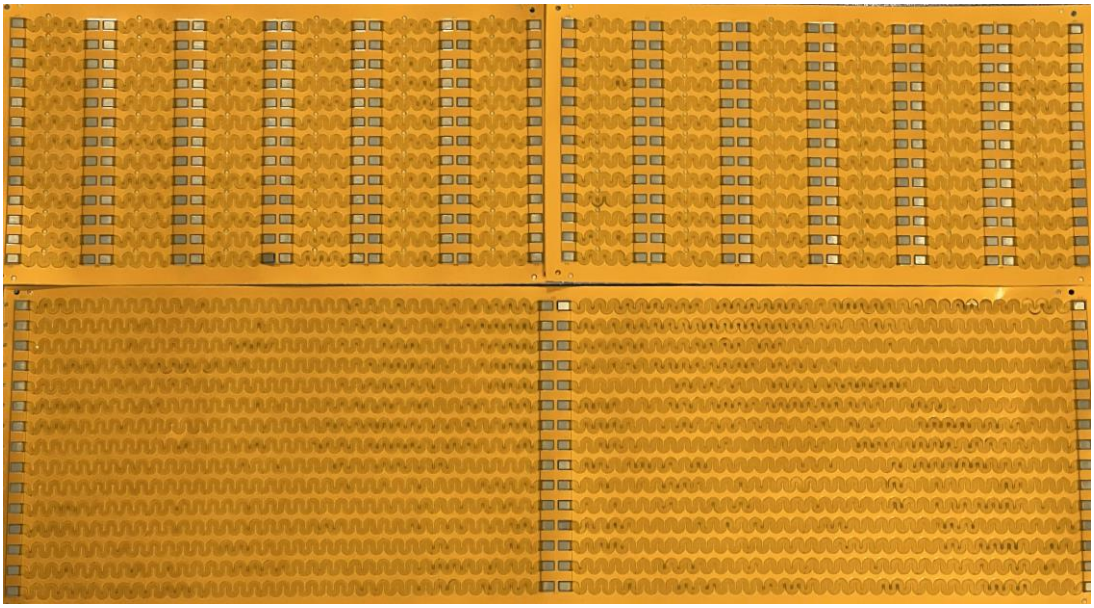

Figure 5.3: Serpentine interconnects fabricated through Flex PCB technology (Design 1 and 3).

Each of these designs was constructed and fabricated rapidly in multiple panels with a layered PCB structure, including a 200 μm Polyimide stiffener at both ends for interconnect plugs, a 25 μm Polyimide (PI) top coverlay, a 5 μm layer of 3M9077 adhesive at the bottom, and a 110 μm base Polyimide PCB thickness with a copper weight of 1 oz (35 μm). These materials ensure the panels are flexible yet durable, capable of withstanding mechanical stresses while maintaining electrical integrity and can be fused into fabrics through direct adhesion. Since the design is universal, we have the flexibility to tune the length and stretchability of the interconnects as needed, adapting them to a wide range of applications in flexible electronics. This versatility allows for precise control over the spatial distribution and resolution, ensuring optimal performance in various electronic systems.

5.1.2: Thermoplastic Polyurethane Printed Circuit Boards

The development of manufacturable stretchable circuits represents recent advances in the realm of PCB technologies. Two main approaches are currently used to build PCB-style stretchable circuits, both of which share similarities with flex PCB manufacturing [257]. The first approach involves using a stretchable carrier material, typically TPU laminated onto a copper sheet. The circuit is fabricated by patterning and wet etching the copper, followed by component assembly. This method closely mirrors traditional PCB fabrication but requires careful processing due to the stretchable carrier's limited resistance to chemicals and heat. For instance, low-melting-temperature solders, such as eutectic SnBi, are used instead of conventional lead-free solders that require higher process temperatures.

The second approach begins with the circuit being fabricated on a temporary carrier, which allows for the use of high-temperature processes and harsh chemicals before the stretchable carrier is introduced (Figure 5.4a). Once the circuit is complete, the stretchable carrier material is applied, and the temporary carrier is removed. Although this method diverges more from traditional PCB processing, it offers the advantage of completing all critical steps before the stretchable material is involved.

After the circuit is etched and printed, further steps such as encapsulation can also be applied using soft polymer materials such as PDMS, Ecoflex, or polyurethane (Figure 5.4b). Primarily, these materials act as mechanical buffers, effectively absorbing and distributing mechanical stresses during stretching events. This stress distribution mechanism is vital in preventing localized overstress that could lead to premature failure of the interconnects. The elastomeric properties of these materials allow them to deform in tandem with the underlying circuit, thereby maintaining the integrity of the electrical pathways even under significant strain.

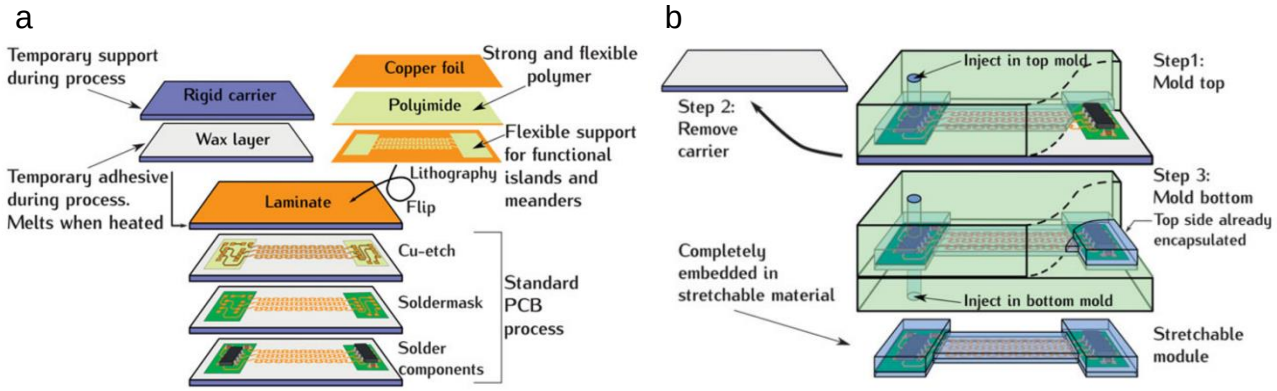

Figure 5.4: a) A stretchable circuit with flexible islands and interconnects is fabricated using PCB techniques on a temporary carrier with a removable adhesive. b) The circuit is partially encapsulated by polymer injection and curing, followed by removal of the carrier and a final molding step to fully encapsulate the circuit (reprinted from [258]).

The incorporation of these encapsulation layers significantly contributes to the overall durability and longevity of the interconnects. By enabling the circuit to withstand repeated mechanical deformations, these materials greatly enhance the cyclic reliability of the system. This is particularly crucial in applications that demand frequent flexing or stretching, such as wearable electronics or soft robotics. Moreover, these encapsulation layers provide a protective barrier against various environmental factors that could potentially compromise the circuit's functionality. They effectively shield the interconnects from moisture ingress, dust accumulation,

and abrasive forces, all of which can lead to degradation or failure of the electronic components over time.

The efficacy of such materials in stretchable substrates has been extensively studied and documented in the literature. Naserifar et al. conducted research on the use of elastomeric substrates and their material gradients in stretchable electronics, demonstrating their ability to significantly enhance the durability and performance of serpentine interconnects under mechanical stresses [259]. Similarly, Lacour et al. studied the mechanics of stretchable gold conductors on elastomeric substrates, elucidating the mechanisms by which these materials enable extreme stretchability while maintaining electrical conductivity [260].

The process of applying these encapsulation materials can vary depending on the specific requirements of the application and the properties of the chosen material. One notable method involves the use of liquid injection molding (LIM), a technique explored in depth by Vanfleteren et al. This process entails placing a top mold over the circuit, injecting a liquid two-component PDMS mixture, and subsequently curing the mixture at relatively low temperatures (ranging from room temperature to a maximum of 70°C for high-speed curing) [258].

The LIM process offers several advantages, including precise control over the encapsulation layer thickness, excellent conformity to complex geometries, and the ability to create large-area encapsulations efficiently. However, alternative methods for applying stretchable carrier materials exist and may be preferable in certain scenarios. These alternatives include cover lamination, which involves the application of pre-formed elastomeric sheets, and spraying, which allows for the deposition of thin, uniform coatings.

In our work, we utilized a TPU PCB fabricated through a precise and carefully controlled process to achieve high-performance stretchable electronics. The TPU PCB was supplied as a net panel with maximum design area of 264 x 459 mm and thickness of 100 μm. This TPU substrate exhibits a breaking tension of 60 MPa, dynamic stretchability ranging from 5% to 20% depending on the copper trace layout, and an elongation at break of 550%. The chosen Polyurethane material offers several advantageous properties: it is chemically stable against oils, ozone, tar, most solvents, and dilute acids; it has high tightness against liquid media while maintaining high vapor permeability; it is skin-safe and biocompatible and resistant to hydrolysis and microbial degradation; it also provides high UV and weather resistance, very good weldability and thermoformability, and excellent adhesive and printable characteristics.

The fabrication process begins with the lamination of the rough side of a PCB-grade copper foil, with a thickness ranging between 17 to 35 μm, onto the TPU sheet. The copper foil's rough surface,

characterized by a fractal topography of 3 to 5 μm, ensures robust adhesion to the TPU substrate. The copper is then patterned using a process similar to conventional PCB manufacturing. Specifically, an etch resist is applied, patterned, and developed, followed by copper etching to create the desired circuit layout. The process is constrained by parameters such as a trace-outline distance of 400 μm and a minimum trace linewidth of 100 μm.

To enhance the durability and functionality of the exposed copper traces, a second layer of TPU is laminated over the circuit. This covering TPU layer is pre-cut to include openings at the locations of solder mask patches, providing necessary access points while maintaining the circuit's integrity. The lamination of the TPU PCB onto a stretchable knit fabric is performed using either an iron or a heat-press, with separation foils (such as PET or PTFE) to protect the materials. The softening or fusing temperature is carefully controlled within the range of 150-180 °C to ensure optimal bonding without damaging the fabric or the TPU substrate.

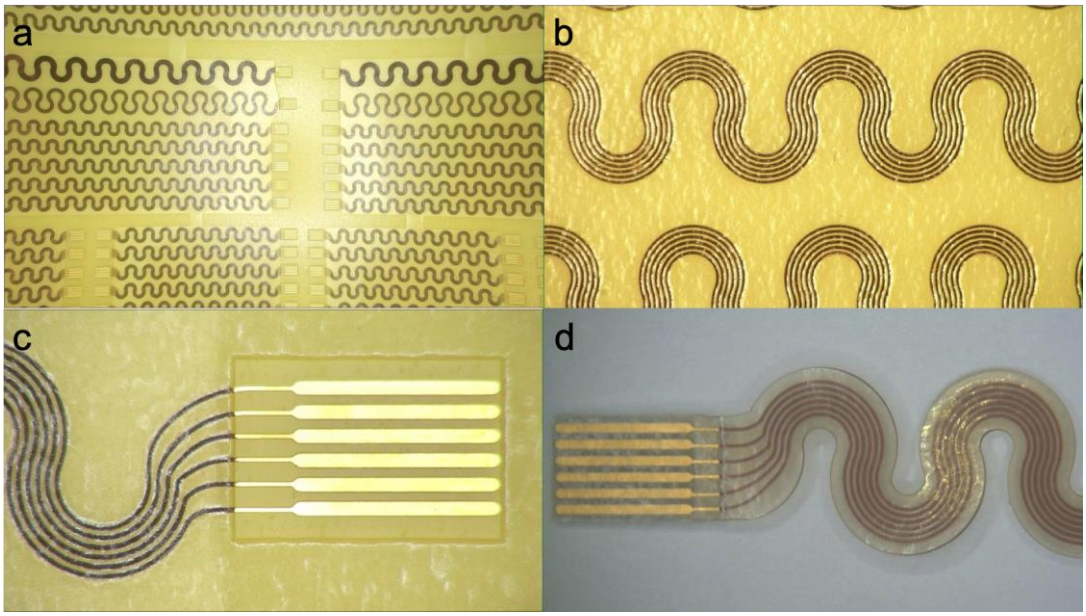

Figure 5.5: Thermoplastic polyurethane printed circuits before final laser-cutting showing a) zoomed-out view, b) zoomed-in view of the serpentine traces, c) exposed pads for further connection, and d) an interconnect after final laser-cutting.

To optimize the use of resources and minimize costs associated with the development of TPU PCBs—a relatively new technology—we strategically utilized the entire available panel area rather than fabricating separate panels for each design. This approach allowed us to incorporate all our interconnect designs into a single panel (refer to Appendix A.13), including interconnects with total lengths of 7 cm, 15 cm, 22 cm, and 47 cm, resulting in a total of 125 interconnect pieces. Additionally, we included extra designs to facilitate further experimental analyses. These

supplementary designs encompass various configurations of serpentine interconnects, including those with and without serpentine cut-outs on the base substrate. The implications and performance of these variations will be thoroughly analyzed and explained in the next section.

The mechanical properties of substrate materials play a crucial role in the performance and functionality of PCBs, particularly in applications requiring flexibility or stretchability. TPU and polyimide are two materials currently used in soft PCB manufacturing, but they exhibit markedly different mechanical characteristics, especially in terms of their Young's modulus. Thermoplastic polyurethane is known for its highly elastic and flexible nature. The Young's modulus of TPU is around 10 MPa [261]. This relatively low modulus allows TPU to stretch and deform significantly under stress without permanent deformation. The flexibility of TPU makes it an excellent choice for applications requiring high conformability and stretchability, such as wearable electronics or devices that need to adapt to complex contours.

In contrast, polyimide exhibits a much higher Young's modulus, typically around 1 to 3 GPa [262]. This higher modulus reflects polyimide's more rigid and strong nature. The substantial difference in modulus between TPU and polyimide - nearly two orders of magnitude - underscores the vast difference in their mechanical behavior. Polyimide's higher modulus provides greater stability and structural integrity, making it suitable for conventional flexible PCBs where significant mechanical strength is required. It's worth noting that these modulus values can vary depending on the specific formulation and manufacturing process of the materials. The stark difference in Young's modulus between TPU and polyimide highlights the important trade-offs between flexibility and strength in choosing a PCB base material. This understanding allows engineers to select the most appropriate material for their specific application, balancing factors such as conformability, stretchability, and mechanical robustness.

5.2: Serpentine Interconnects Design

5.2.1: Geometrical Parameters

The design of stretchable circuits presents unique challenges, particularly in the optimization of interconnects that can endure repeated mechanical deformation without failure. One of the most effective methods for achieving this is the use of a meander or serpentine structure for the interconnects. This design is widely recognized as an optimal approach for stretchable circuits due to its ability to distribute stress and strain more evenly across the structure, thereby enhancing the circuit’s durability under stretching. In our design, we utilized AutoCAD and

Eagle PCB to create the circuit schematic and layout (Appendix A.13). Within a 20 x 46 cm TPU flexible board, for example, we were able to incorporate 93 interconnection strips in different lengths, showcasing the high manufacturability and yield achievable with this approach.

The serpentine structure is particularly advantageous because it allows the interconnects to flex and stretch without concentrating stress at any single point. Specifically, using a horseshoe shape rather than a triangular, zigzag, square/rectangular or sinusoidal pattern helps to spread the stress more evenly, reducing the likelihood of breakage at the peak points of the serpentine under repeated mechanical deformation tests [263]. This horseshoe geometry is crucial for achieving optimal performance in stretchable circuits, as it minimizes localized strain concentrations that could lead to premature failure.

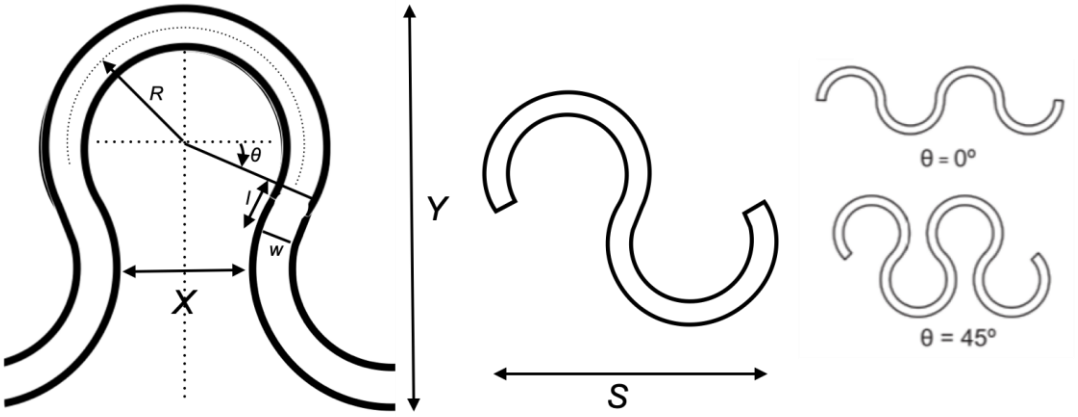

Figure 5.6*:* Horseshoe patterned stretchable interconnects geometrical parameters.

Our design decision process was guided by several key factors, including conformability, aesthetics, and spatial constraints. The need for optimal conformability to various surfaces necessitated a careful balance between flexibility and structural integrity. Additionally, we were constrained by the available space between nodes, with our smallest node and highest resolution being 15mm in diameter. This spatial limitation required that the width of the serpentine structure be smaller than 15mm to ensure proper functionality and avoid interference between adjacent components.

We determined that achieving a minimum elongation or strain level of 30%, would necessitate θ exceeding 20°C in the case of Polyimide PCB (Section 5.3). The most optimized Y is then a design with the smallest possible θ. For our chosen interconnect design parameters, the length of one serpentine period (S), as derived from Equation 5.1, is 5.45 mm. In an ideal scenario, extending a

serpentine period into a straight line will measure 11.14 mm, corresponding to 104% elongation. However, the actual maximum elongation is significantly lower due to the stress points in the serpentine interconnects, as well as the mechanical properties of the copper traces and base substrates.

In relation to Figure 5.6, our interconnects design parameters are Y = 6.3 mm, w = 1.9 mm, R = 1.45 mm, l = 0, and θ = 20 °C. These values were carefully chosen within the constraints of the Design-for-Manufacturing (DFM) tolerance for PCB and laser-cutting outlines to ensure high manufacturing yield. Additionally, we aimed to optimize conformability and aesthetics while being restricted by the available space between nodes. Our smallest node size and resolution are 15 mm, so we designed the width of the serpentine accordingly, ensuring that the serpentine thickness remains smaller than half of this value to avoid disrupting natural fabric movements.

To improve the stretchability and durability of these interconnects, an analytical solution of free-standing serpentine ribbon can be applied. Lu *et al.* demonstrated a 2D plane strain model of non-planar free-standing and elastomer-embedded serpentines using curved beam (CB) and elasticity theory [264]. We define the distance of one period of serpentine interconnects from end-to-end as:

$$S = 4(R\cos\theta - \frac{l}{2}\sin\theta) \quad (1)$$

Where $R = r$ as shown in Figure 4.3. Since there is no gap in between two arcs in the design, we can take $l = 0$. The effective applied strain (ε_{app}) due to tensile displacement (u_o) is given by:

$$\varepsilon_{\text{app}} = \frac{2u_0}{S}. \quad (2)$$

Due to its symmetry, one period unit of serpentines can be broken into a quarter cell with fixed boundary and displacement of $u_o/2$ at both ends. Assuming low energy deformation and linear elasticity, using the CB theory, normalized reaction force (P) and maximum strain (ε_{max}) around the serpentine can be expressed as:

$$\frac{P}{P'} = \frac{\frac{w}{R}\left(\cos\theta - \frac{l}{2R}\sin\theta\right)}{2\left[\begin{array}{c}\cos^2\theta\left(\frac{l^3}{2R^3} + 3\left(\frac{\pi}{2}+\theta\right)\frac{l^2}{R^2} + 12\frac{l}{R} - 12\left(\frac{\pi}{2}+\theta\right)\right) \\ +\sin 2\theta\left(6\left(\frac{\pi}{2}+\theta\right)\frac{l}{R} + 9\right) \\ +\frac{w^2}{R}\left[\left(\frac{\pi}{2}+\theta\right)\left(\frac{l}{2R}\cos\theta + \sin\theta\right)^2 + \frac{l}{2R}\left(\sin\theta + \frac{3\overline{E}}{2G}\cos\theta\right)\right] + 18\left(\frac{\pi}{2}+\theta\right)\end{array}\right]}, \quad (3)$$

$$P' = \frac{2\bar{E}wu_0}{S} \quad (4)$$

Where P′ is the force needed for the linear part of the serpentine to lengthen by $2u_o$, and E is the plane strain modulus.

$$\frac{\varepsilon_{\max}}{\varepsilon_{\text{app}}} = \frac{\frac{w}{R}\left[\frac{12}{2-\frac{w}{R}} + \left(\frac{12}{2-\frac{w}{R}} - \frac{w}{R}\right)\left(\sin\theta + \frac{l}{2R}\cos\theta\right)\right]\left(\cos\theta - \frac{l}{2R}\sin\theta\right)}{\left[\begin{array}{c}\cos^2\theta\left(\frac{l^3}{2R^3} + 3\left(\frac{\pi}{2}+\theta\right)\frac{l^2}{R^2} + 12\frac{l}{R} - 12\left(\frac{\pi}{2}+\theta\right)\right) \\ +\sin 2\theta\left(6\left(\frac{\pi}{2}+\theta\right)\frac{l}{R} + 9\right) \\ +\frac{w^2}{R}\left[\left(\frac{\pi}{2}+\theta\right)\left(\frac{l}{2R}\cos\theta + \sin\theta\right)^2 + \frac{l}{2R}\left(\sin\theta + \frac{3\bar{E}}{2G}\cos\theta\right)\right] + 18\left(\frac{\pi}{2}+\theta\right)\end{array}\right]}. \quad (5)$$

This analysis was found to have a good accuracy compared to FEM results when w/R < 0.5. When the maximum strain is plotted against w/R and θ, it can be concluded that the fracture always occurs around the inner region of the arc. Serpentines with low w/R exhibit small strain distribution, thus higher stretchability. However, this will be at the cost of higher interconnect resistance. Increasing θ could also boost interconnects stretchability, but since it could also increase the overall width (W_o), it will reduce the possible number of parallel meanders in one serpentine structure. Elasticity solution can be used in the case of wide serpentine (w/R > 0.5). In addition, experiments also confirmed that this analytical correlation can also be applied for serpentines embedded in elastomeric matrix (E_{matrix} < 100 MPa). To design the stretchability of interconnects under space and geometrical constraints, we can calculate the most optimal choice of *θ, w/R, and l/R*. For two arcs in the serpentine to not to overlap with each other, we can first define the distance between two arcs as

$$X = (R - \frac{W}{2})\cos\theta - l\sin\theta - (R + \frac{W}{2})(1 - \cos\theta) = 0 \quad (6)$$

Where *X* should be larger or equal to 0. By solving Equation 6, the most optimal *θ* for serpentine interconnects is then

$$\theta_{max} = 2\tan^{-1}\left(\frac{-2\frac{l}{R}}{6+\frac{w}{R}} + \sqrt{\frac{2\left(2\frac{l^2}{R}+\frac{w}{R}+6\right)}{\left(6+\frac{w}{R}\right)^2} - 1}\right) \quad (7)$$

Analytical results by Widlund et al. have demonstrated that CB theory and Finite Element Method (FEM) simulations validate each other, particularly in predicting the mechanical behavior of serpentine interconnects [265]. The analysis highlights that, due to symmetry and

bending effects, the maximum strains consistently occur at the center of the inner arc (Figure 5.7a-c). Among the three serpentine shapes analyzed, the modified horseshoe configuration exhibited the lowest normalized maximum strain (εmax/εapp = 0.042), making it the most stretchable and optimal design for applications requiring high flexibility.

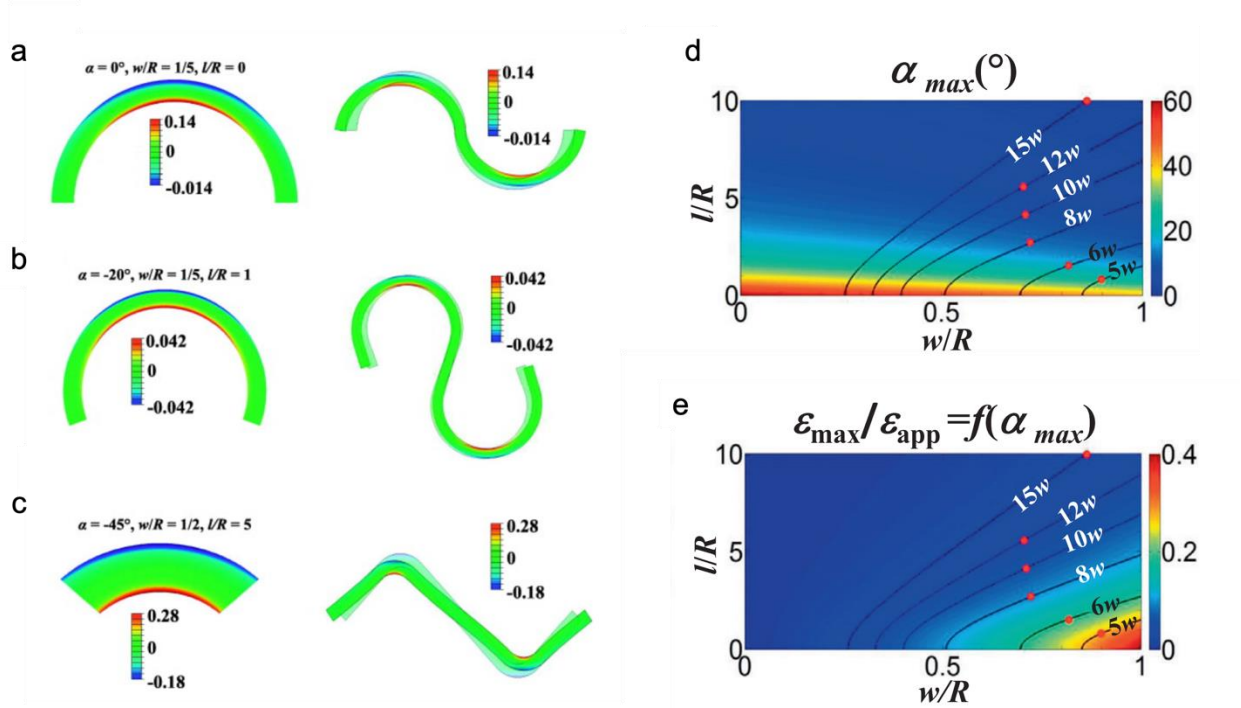

Figure 5.7: a-c) Strain fields obtained from CB theory and FEM with various geometric parameters and d-e) the maximum values of α, α_{max}, as a function of w/R and l/R considering the constraint that the trace do not overlap (reprinted from [265]).

Figure 5.7d-e plots the value of θ_{max} or α_{max} and $\varepsilon_{max}/\varepsilon_{app}$ as a function of w/R and l/R. By identifying the point on the constraint curve that yields the lowest εmax/εapp value, designers can find the optimal combination of w/R and l/R that maximizes stretchability within given parameters. Their dimensionless nature implies that the actual dimensions of the optimal serpentine can be scaled according to the ribbon width w. This scalability is essential in practical applications where different serpentine sizes may be required based on the specific design and space constraints of the circuit.

5.2.2: Additional Considerations

Serpentine interconnects are a fundamental design element in stretchable electronics, offering the flexibility needed to maintain electrical connectivity during mechanical deformations. To enhance the performance and longevity of serpentine interconnects, several advanced techniques can be employed.

In addition to manipulating these geometric parameters, we explored other avenues for improving the performance of our stretchable circuit. One key area of focus was the optimization of the interconnects' electrical resistance. While the width of traces and interconnect length play significant roles in determining resistance, two-layer PCBs can also be used as a means of further reducing resistance. This approach allows for the creation of wider effective trace widths without compromising the spatial constraints of our design. The use of two-layer PCBs offers several advantages in the context of stretchable circuits. Firstly, it allows for the distribution of current across multiple layers, effectively reducing the overall resistance of the interconnects. This can lead to improved power efficiency and reduced heat generation, both of which are critical factors in the performance and longevity of flexible electronic devices. Secondly, the additional layer provides greater design flexibility, allowing for more complex or miniaturized routing solutions that can further optimize the circuit's performance and stretchability.

Another of the critical challenges when using copper in stretchable electronics is managing the transition from rigid to stretchable regions. Copper or gold traces as stretchable interconnects, while highly conductive, are also prone to stress concentration and potential failure if the transition is not carefully designed. To address this, a gradual transition in geometry and material properties is recommended. Gradual geometric transitions can be achieved by tapering the width or curvature of the traces as they move from a rigid area, such as a PCB or sensor module, into the flexible serpentine pattern. This gradual change helps in evenly distributing mechanical stress across the interconnect, reducing the likelihood of localized failures [258].

The presence of sharp edges in the design of serpentine interconnects is also a critical issue, as these can lead to high-stress concentrations and subsequent failure. To enhance robustness, it is essential to design traces that gradually change direction and eliminate sharp edges. Curvilinear trace designs, which replace sharp corners with smooth, rounded paths, are particularly effective. These designs ensure that mechanical loads are distributed over a larger area, significantly reducing the risk of the interconnect tearing at stress points.

Moreover, using higher order and multi-directional fractals that smoothly change direction can further enhance flexibility and robustness. These patterns are designed to expand and contract in multiple directions, accommodating a range of deformations without focusing stress on any particular point. Fan et al. [266] and Ma et al. [267] demonstrated how fractal-inspired structures enable precise control of stress distribution, improving both mechanical stability and performance under dynamic loads. They developed a finite-deformation model validated by both FEA and experimental results, which precisely predicted the nonlinear stress–strain behavior and deformation configurations under axial stretching. Their findings highlight the benefit of fractal geometries over traditional designs in mechanically-adaptive soft systems.

Beyond the previously mentioned methods, other techniques can further enhance the robustness of serpentine interconnects. Pre-strain engineering, for instance, involves pre-stretching the substrate before applying the serpentine interconnects [268]. This introduces beneficial residual stresses, allowing the interconnects to accommodate more strain during actual use. Upon release from the pre-strain, the interconnects contract into a more relaxed state, enabling them to stretch further under load without reaching their failure point.

These studies and methods emphasize the importance of innovative structural and material design in achieving the desired mechanical performance in stretchable interconnects. The robustness of serpentine interconnects in stretchable electronics can be significantly enhanced through a combination of structural design optimization and protective strategies. Techniques such as gradual transitions between rigid and stretchable regions, elimination of sharp edges, multi-directional fractal-inspired design, and the use of encapsulation are crucial in improving the mechanical and electrical durability and repeatability of these systems for dynamic applications.

5.3: Electrical and Mechanical Characterization of Serpentine Interconnects

To assess the reliability and electromechanical performance of the serpentine interconnects, we performed three types of tests. The first test involved one-time uniaxial stretching until the substrate reached its breaking point. A commercial mechanical tester (Zwick BTC-EXMACRO, Roell) equipped with a 0.5 kN load cell was used. Load and extension data were recorded at a crosshead speed of 1 mm/s until the samples extended to 100% of their original length, with the test stopping when a sudden 10% jump in force measurement occurred. Three types of samples were prepared: (1) a raw base fabric substrate, (2) an interconnect without a serpentine base outline (referred to as TPU strip, Case 1), and (3) an interconnect with a cut-out serpentine base outline (Case 2). All samples had dimensions of 6.3 x 60 mm. The interconnects were fused into the knit fabric substrate by ironing at 150°C. The raw knit fabric substrate used in these experiments was a 4-way stretch fabric composed of 67% nylon and 33% spandex.

As shown in Figure 5.8a, the serpentine interconnect on a flat TPU base substrate— a design that has been widely studied in prior research—failed at 38% strain. In contrast, our proposed design, featuring a serpentine TPU base outline, exhibited significantly improved performance, withstanding up to 85% strain before failure. This superior performance of the serpentine TPU can be attributed to its ability to twist and conform more effectively, adapting its structure in response to the strain on the fabric substrate.

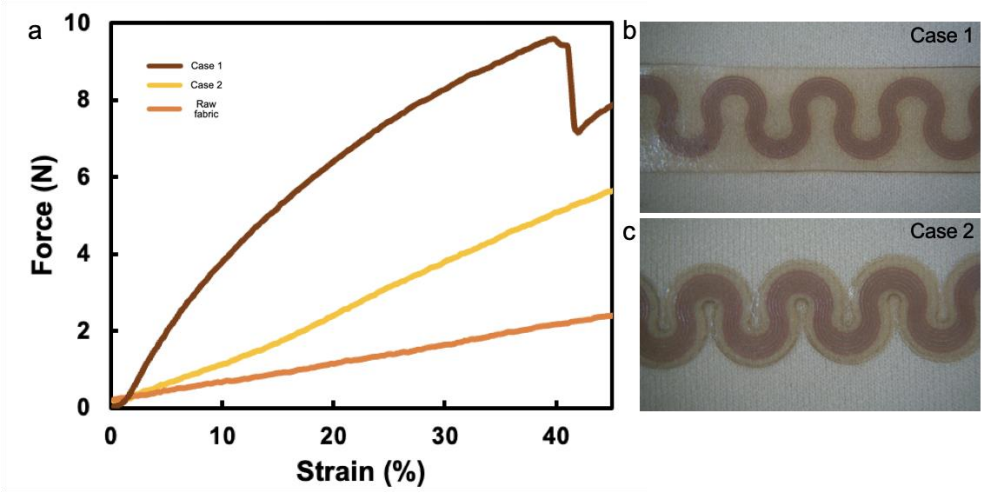

Figure 5.8: a) Strain-stress response of three tensile tests: raw fabric, b) serpentine interconnects without laser-cut outline (Case 1), and c) serpentine interconnects with laser-cut serpentine outline (Case 2).

Going into detail, Case 1 (Figure 5.8b and 5.9a), which uses a flat TPU substrate, demonstrated a much stiffer response due to the composite higher Young's modulus. This stiffness causes the interconnect to dominate the fabric's stress-strain behavior, essentially overriding the inherent stretchability of the knit fabric. In contrast, Case 2 (Figure 5.8c and 5.9b), with the serpentine base outline, required less than half the force to reach comparable strain levels, indicating a more synergistic strain interaction with the soft and stretchable base substrate. This improved integration between the interconnect and the fabric substrate in Case 2 results from the serpentine outline's ability to distribute mechanical loads more evenly and accommodate the complex deformations of the fabric. If you look at Figure 5.9b, for Case 2, even at a much higher strain of 150%, the TPU substrate remains intact with the fabric, showing excellent bonding between the TPU and base fabric.

In addition to assessing the breaking point, our second test focused on evaluating the electrical performance by examining conductor rupture in free-standing serpentine interconnects fabricated using flexible polyimide and TPU substrate technologies. During tensile testing, the resistance was measured using a constant current source (104 mA) constructed with an LM317 voltage regulator and a fixed resistor (12 Ω), which was connected to an ADC pin of a Teensy 4.0 microcontroller. The load, extension, and resistance data were synchronously obtained and logged for detailed analysis.

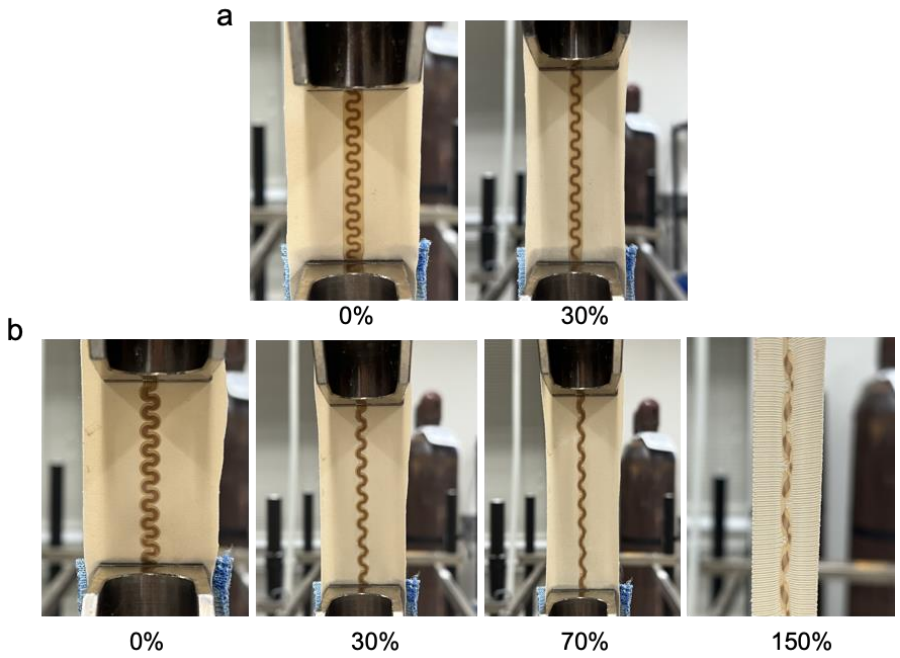

Figure 5.9: Images of serpentine interconnects of a) Case 1, without laser-cut outline and b) Case 2, with laser-cut serpentine outline under different strain levels.

As shown in Figure 5.10a, the extension of both free-standing stretchable interconnects did not significantly influence their resistance, which remained stable at approximately 7.4 Ω for the polyimide substrate and 9.8 Ω for the TPU substrate until rupture occurred. Rupture events were observed at strains of around 35% for the polyimide substrate and approximately 85% for the TPU substrate, indicating the superior stretchability of TPU interconnects. This observation is critical as it highlights the enhanced mechanical resilience and adaptability of TPU over polyimide when integrated into stretchable electronic systems.

The bonding characteristics of these materials with knit fabrics were also visually inspected. The polyimide PCB, which incorporates a 5 μm adhesive layer, exhibited significant dents due to its early stress in the viscoplastic region as it is being stretched and twisted and observable delamination after a few stretching cycles, particularly under high strain conditions (Figure 5.10b). In contrast, the TPU PCB, which requires fusing through ironing at temperatures around 150°C, formed a substantially stronger and more durable bond with the fabric substrate.

According to literature, the stretchability range for tailored garments is typically 15-25%, for sportswear 20-35%, and for form-fitting compression garments 30-40% [269], [270]. The tests demonstrated that both Polyimide and TPU-based stretchable PCBs can withstand strains exceeding 30%, making them suitable for integration into most wearable and dynamic textile applications. While the polyimide PCB offers advantages in prototyping due to its ease of

removal and reusability, it suffers from reduced adhesion after repeated use. Conversely, the TPU PCB, although more permanent in its application, provides a robust and reliable solution for final product development, where long-term durability is essential.

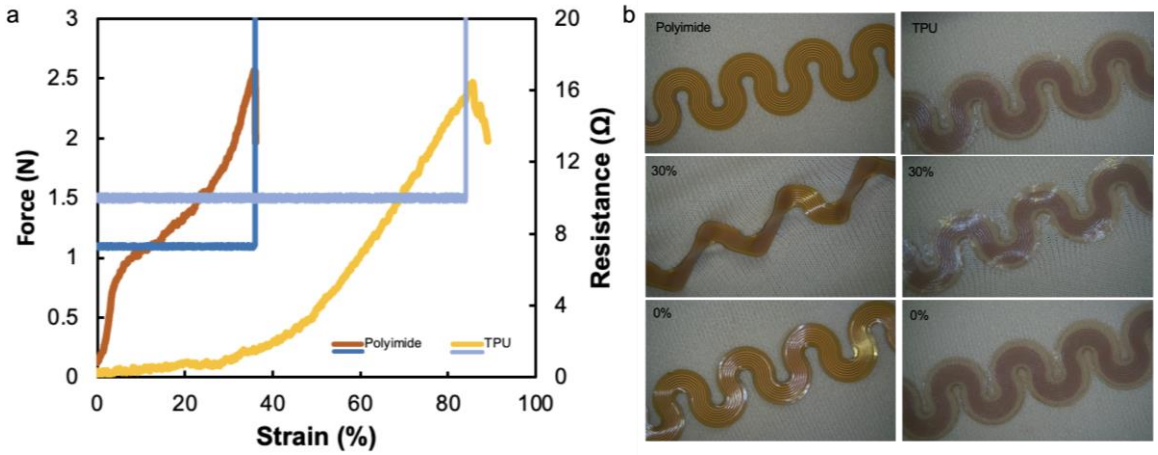

Figure 5.10: a) Electrical and mechanical characteristics of Polyimide and TPU-based interconnect under tensile breaking test, and b) stretching behaviors of both printed circuits under microscope.

The mechanical behavior of serpentine interconnects on serpentine soft substrate when subjected to tensile stress is complex and can be delineated into four stages based on the material properties and structural dynamics of both the interconnect and the substrate material. The strain response of serpentine interconnects begins with a structural reconfiguration, where the serpentine traces transition from a planar form to a more three-dimensional geometry. As the fabric substrate stretches, the serpentine traces bend, twist, and straighten, which dissipates some of the applied mechanical energy. During this phase, the mechanical behavior is largely dictated by the fabric, which absorbs and distributes the strain. The interaction between the fabric and the serpentine interconnect allows for gradual increases in stress while maintaining flexibility.

As the copper traces within the serpentine interconnect reach their maximum extension, they experience significant tensile stress, leading to rupture. After this, the TPU substrate takes over, accommodating further deformation with its viscoplastic and elastic properties. TPU's ability to undergo both permanent deformation and elastic recovery allows the system to continue stretching, even after the metallic components have failed. Eventually, the mechanical response may again be dominated by the fabric's characteristics, depending on its stretchability relative to the TPU. The fabric's tensile strength and elasticity play crucial roles in determining the overall performance and durability of the integrated system.

Our final electromechanical characterization and testing focused on the dynamic repeatability of the TPU-based interconnects under cyclic loading (Figure 5.11a-b). Samples with a single node connected to two interconnects via a Zero Insertion Force (ZIF) plug were subjected to 100 cycles in 500mm/min of stretching, with one interconnect experiencing 30% cyclic strain and the other 50%. During the first 20 cycles, we observed mechanical adaptation in the samples, primarily due to the interface between the TPU and the fabric. This adaptation likely results from microstructural adjustments within the materials and interfaces. Despite these initial adjustments, the interconnects and connections exhibited no signs of degradation throughout the entire testing process, consistently maintaining their electrical integrity (Figure 5.11c-d). This durability under cyclic loading is critical for applications in wearable electronics and dynamic substrates, where interconnects are subjected to repetitive stretching due to constant movement.

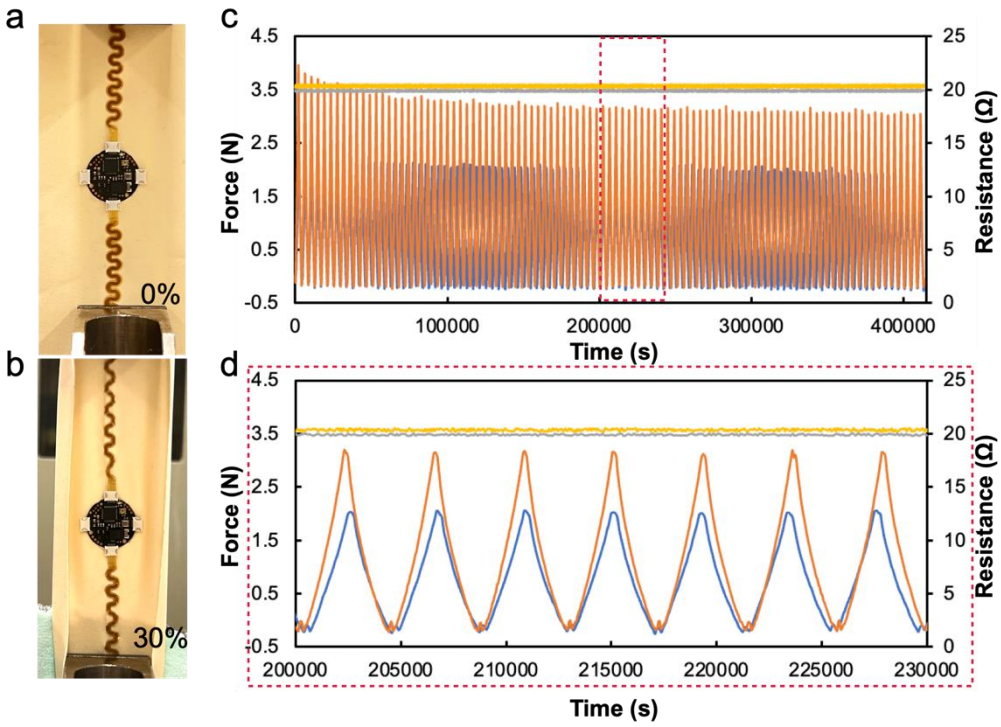

Figure 5.11: a-b) Node-interconnects undergoing cyclic loading tests, c) Resistance and force response due to repetitive strain of 30% and 50% (100 cycles), with d) a zoomed-in view.

Chapter 6: Distributed Computational Fabrics across Scales

"We are so engulfed by electronics that
we can scarcely gauge the impact of the art on society. "
John R. Pierce (1977)

In the past few decades, the exponential advancement in microelectronics, as encapsulated by Moore's Law, has continually doubled the number of transistors on a microchip, enabling the miniaturization of devices and pushing the boundaries of computational capabilities. Alongside, Bell's Law illustrates the evolution of computing classes that emerge as technologies advance, leading to new devices and systems. Today, we are witnessing a convergence of these trends with the concept of *Amorphous Computing, Paintable Computing* or the *Internet of Materials*, which envisions everyday materials embedded with computation and communication abilities [137], [138], [271]. This paradigm shift echoes Mark Weiser's vision of ubiquitous computing, where technology becomes so ingrained in our environment that it effectively disappears from our consciousness, blending seamlessly into the fabrics of our lives—quite literally in the case of sensate and computational fabrics [2].

The realization of sensate and computational fabrics necessitates a rethinking of both fabrication processes and the broader ecosystem that supports these technologies. This involves creating materials with integrated electronics that are scalable through industrial manufacturing processes. These materials must retain the flexibility and aesthetics of traditional textiles while

embedding sophisticated functionalities. The infrastructure supporting this new generation of materials must also address challenges in distributed processing and networking, power management, and wired and wireless communication, drawing on the principles of miniaturization and pervasive computing. As we continue to push the frontiers of what these materials can do, we must consider how they will interact with the environments they are part of, evolving from passive to active components in the Internet of Things, driving forward a future where our surroundings are as intelligent as they are responsive.

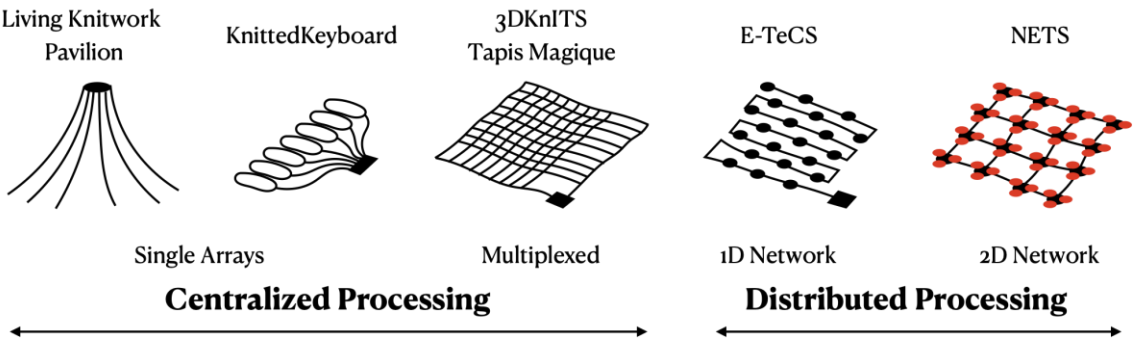

Figure 6.1: Interconnections and wiring architecture of various projects I have done in knitted sensate textiles and distributed computational fabrics.

Based on my previous explorations in developing and implementing sensate textiles across scales (Section 4.5, Figure 6.1), it is evident that current discrete sensing and multiplexed e-textiles with centralized processing face significant limitations in terms of scalability and application breadth. These systems often focus on a single modality or function and lack the scalability required for broader applications. As the demand for more complex and extensive sensor networks grows, several challenges become apparent. These include issues related to wiring complexity, node scalability, integration of multiple modalities, bandwidth constraints, robustness, and application-specific functions. Let's delve deeper into these challenges:

- **Wiring/Interconnects Complexity**: As sensor networks expand in size and function, the sheer number of connections needed to link these sensors becomes a formidable challenge. For example, a simple array sensing setup requires n∗2 or n+1 connections to the main processing module, while a multiplexed configuration with m rows and n columns necessitates m+n connections. As networks scale up, this can lead to a proliferation of wiring that not only complicates the physical design but also introduces higher risks of interference, signal degradation, and energy inefficiency.
- **Node Scalability**: Once sensate textiles have been produced, their size, resolution, and number of sensors are typically fixed, limiting their adaptability since their design is not

modular. As the number of sensor nodes increases, maintaining effective communication and data processing capabilities also becomes increasingly difficult. Each node in a distributed network requires power and communication channels, creating bottlenecks as the system scales.

- **Integration of Multiple Modalities**: The integration of various sensing modalities within a single node presents substantial difficulties. Different sensors may require varying power levels, read-out circuits, communication protocols, and physical configurations, making it challenging to integrate them without compromising the node's overall performance and reliability. For example, combining thermal, pressure, humidity and other sensors into a single node might necessitate distinct power management and signal processing strategies, complicating the design and potentially reducing the system's efficiency.
- **Bandwidth Constraints**: As the density and number of sensors increase, so too does the amount of data that needs to be transmitted and processed. Traditional communication protocols may not be sufficient to handle the high data throughput required by large-scale sensor networks. As mentioned earlier, in a mesh network, the maximum data throughput per node scales inversely with the square root of the number of nodes(n) as $1/\sqrt{n}$, highlighting how increased sensor density can significantly reduce data transmission efficiency. This can lead to potential latency, data loss, or bottlenecks, degrading the overall system performance.
- **Robustness and Fault Tolerance**: The distributed and multiplexed nature of these systems introduces the risk of cascading failures if a single node, line, or connection fails. The system needs to be self-aware and capable of self-organization to detect and compensate for faults autonomously, ensuring consistent performance even in the face of individual or group component failures.
- **Application-Specific Challenges**: Wearables and e-textiles are typically developed to serve specific users or purposes, which can limit their applicability across different domains. Each application imposes unique demands on the sensing elements and overall system architecture, including scalability, modularity, and the ability to integrate various modalities as discussed above. These challenges necessitate tailored solutions that address the specific needs of the users and environments while maintaining the flexibility and adaptability required for broader use.

These challenges are also true for research in flexible/stretchable devices and soft electronics. Despite the tremendous amount of research in these areas over the last two decades, the emphasis has primarily been on specific sensing modalities and novel fabrication technologies with limited spatial coverage. Applications of electronic skin have thus been limited to smaller-area wearable physiological and physical activity sensing. These studies, mostly applying row-column

addressing and centralized processing, have not yet sufficiently addressed the major challenge of realizing a scalable, customizable, and robust e-skin that could cover a large substrate and handle a significant amount of tactile and environmental information.

Distributed system architecture and integration with embedded processors dedicated to a local cluster of multi-modal sensors can be established to solve these challenges, as discussed in Section 2.4.2 and demonstrated in previous work such as the *Sensate Media* by Paradiso et al. and *Robot Skin* by Cheng et al. [127], [130] Though these distributed sensing systems are not soft and stretchable, a few relevant work as shown in Figure 6.2 are moving toward this direction.

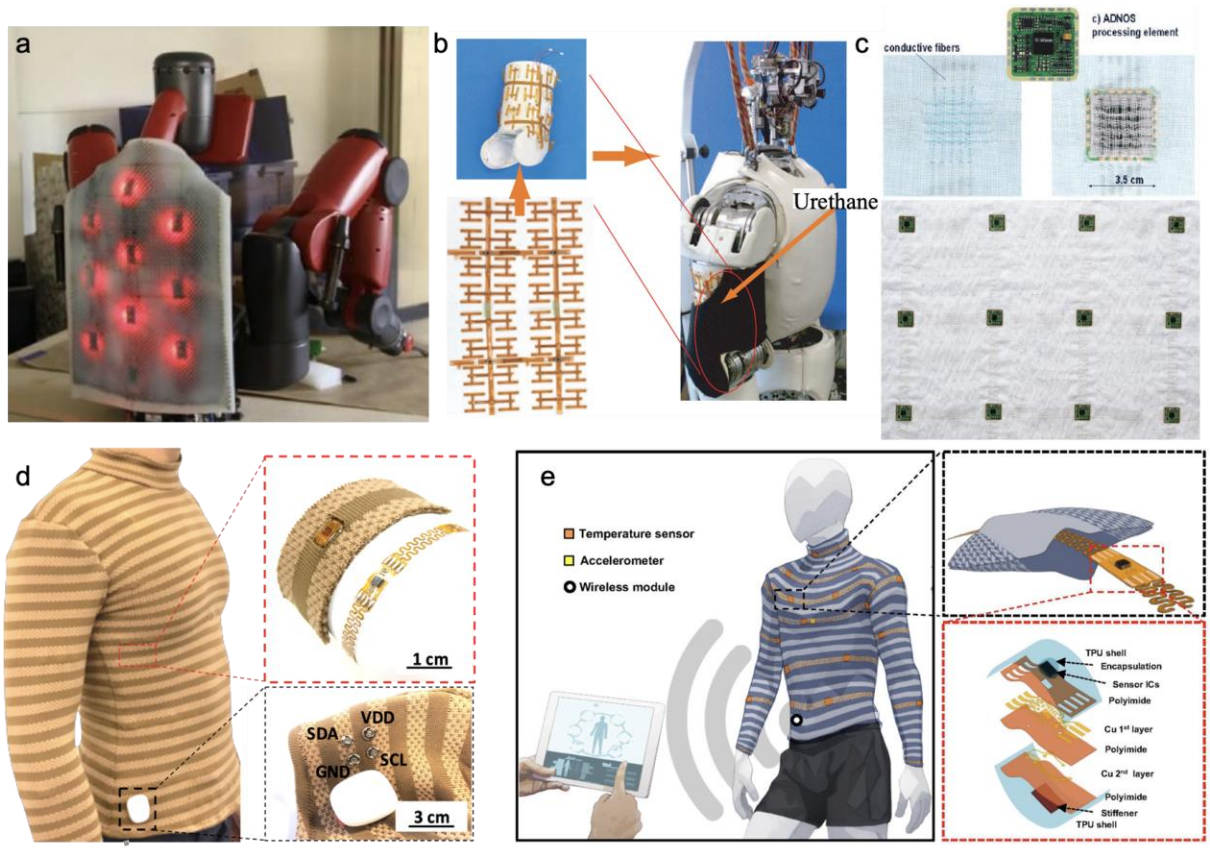

Figure 6.2: a) A soft, amorphous texture-sensitive skin from distributed microphones mounted on the back of a Baxter robot, b) Foldable tactile sensor network that can be embedded in deformable substrate for robotic skin, c) A large-area distributed embroidered capacitive sensing textile sensor, d-e) Electronic textile conformable suit (E-TeCS) with stretchable sensor network for large-scale spatiotemporal physiological sensing.

The concept of *Amorphous Skin*, which consists of rigid PCBs embedded within elastomers, demonstrates texture sensing and localization capabilities when wrapped around robotic surfaces [128]. This skin architecture networks its sensing and computing elements locally within a

neoprene lattice, utilizing sensor nodes embedded into an EcoFlex rubber substrate (Figure 6.2a). Each sensor node contains a microcontroller connected to a microphone, with nodes spaced 15 cm apart. The mesh, though not stretchable, measuring approximately 61 cm x 43 cm, enables distributed, collaborative processing of high-bandwidth sensor data, drastically reducing communication and central processing demands.

In another example of flexible PCB-based systems, Ohmura et al. developed a conformable and scalable tactile sensor skin utilizing discrete photo-reflectors (Figure 6.2b). These reflectors, which consist of an LED and photodetector, detect pressure changes by analyzing light distribution between a foam substrate and the reflectors. A single 120 mm x 200 mm unit contains a microcontroller with four serial-bus terminators, accessing up to 32 photo-reflectors. The array is modular, allowing the user to adjust the resolution by folding the network, offering flexibility in deployment.

SensorTape is another notable example of a flexible distributed sensor network. With its cut-and-rejoin design, *SensorTape* integrates multiple sensing modalities, including IMUs, proximity sensors, and ambient light sensors. Complementing this, *S.N.A.K.E.* extends the concept into a 2D network of flexible square tiles, each capable of sensing tactile pressure, stroke, proximity, ambient light, and temperature [272]. The nodes in both projects utilize peer-to-peer (P2P) communication over a shared I2C bus, enabling scalable and flexible sensate solutions for diverse applications.

In the realm of soft textiles, Lauterbach et al. developed woven, embroidered, and printed e-textile systems, with each module communicating with up to four neighbors via universal asynchronous receiver-transmitter (UART) in a P2P architecture (Figure 6.2c). These textiles can integrate electrodes that are embroidered or printed directly onto the fabric. The system's architecture supports reel-to-reel fabrication processes, enabling textiles to be cut into arbitrary shapes while maintaining low installation costs. Though the current pitch between microcontrollers is 20 cm, the density of four modules per square meter is sufficient for large-area applications, such as smart flooring. Additionally, they explored *Future-Shape*, a wireless attachable module for textile integration. This 3.5 x 3.5 cm^2 radio module operates at 868 MHz, featuring eight sensor pads, four voltage supply pads, and an integrated antenna.

A further example of distributed textile-based sensing is *E-TeCS*, which culminated during my Master thesis at the MIT Media Lab (Figure 6.2d-e) [84], [273]. *E-TeCS* is a stretchable, distributed sensing network that can be integrated into knit textiles. It enables the simultaneous, wireless monitoring of 30 skin temperature nodes across a 1500 cm^2 area, capturing seismocardiac events, respiration, and physical activity through inertial dynamics. While it demonstrates

spatiotemporal sensing capabilities, *E-TeCS* is limited to temperature sensing, relying on a specialized human body temperature chip (MAX30205) with a maximum of 32 I2C addresses. These nodes communicate via BLE with a common backbone, but the system lacks programmability—users cannot modify the microprocessor, design their own protocol and upload custom firmware.

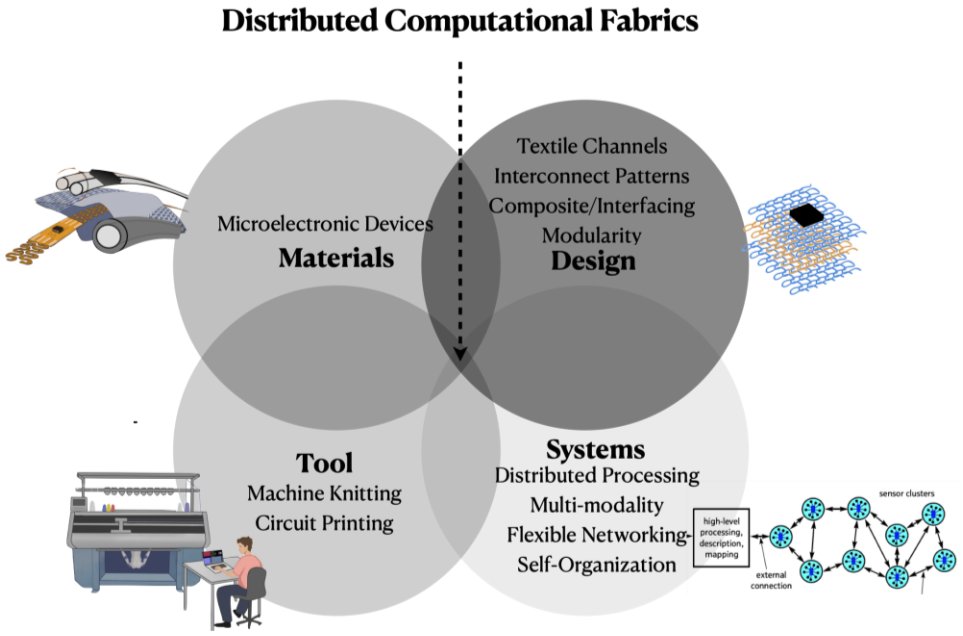

Figure 6.3: Design framework and methodology for architecting distributed computational fabrics

Building on prior work in distributed systems-on-materials and systems-on-textiles, this chapter will extend the discussion from Chapter 6 and leverage our approach on using soft and stretchable printed circuit technologies and manufacturing [83]. These circuits can be laminated or fused onto knit fabrics, forming a composite structure and mirroring the functional capabilities of biological skin and neural networks. The system is bioinspired by the intricate functionality of human skin, applying distributed networking, multi-modality sensing, adaptive networking, and self-organizing architectures within a network of nodes (Figure 6.3). The work presented here represents a step toward developing a high-density, multifunctional sensate textile network that is soft, stretchable, and miniaturized. It can be general-purpose computational fabrics that can conform to any surface, serving as a lining for electronic skin, interactive surfaces, or wearable computing systems. The two- and three-dimensional array of sensor nodes within this network also provides new opportunities for testing distributed communications, localization, scalability, and immersion in novel textile formats.

We envision a paradigm shift from application-specific e-textiles to a "generic" mass-producible e-textile platform that can be cut, tailored, and reconfigured for a wide variety of applications. This adaptability would enable designers and developers to construct smart garments or interior fabrics directly from raw computational fabrics, with the flexibility to program and customize their own applications. The goal of this general-purpose computational fabric is to democratize access to functional fabrics, moving them beyond niche research topics and into the realm of everyday materials. With this advancement, sensate and computational fabrics could become widely accessible commodities, transforming e-textiles into a default choice for interactive and functional clothing, interiors, and beyond.

6.1: Biological Skin and the Nervous System

Human skin (Figure 6.4) is not only a remarkable sensory organ capable of detecting a wide range of physical stimuli—including temperature, vibrations, pressure, and pain—but it is also inherently soft and deformable. These combined attributes enable skin to function as both an effective protective barrier and a highly responsive sensory interface. For instance, the human fingertip contains approximately 240 mechanoreceptors per cm^2, allowing for a highly sensitive tactile response [274]. In contrast, areas like the palm possess around 60 mechanoreceptors per cm^2, and the general body skin features about 30 mechanoreceptors per cm^2, reflecting lower sensitivity in less tactile-demanding regions [275]. Each mechanoreceptor in the skin plays a specialized role in how we perceive the world through touch [276]:

- **Meissner's corpuscles**: Located just beneath the surface of the skin, Meissner's corpuscles are highly concentrated in the fingertips and are responsible for detecting light touch and fine tactile details, such as texture and vibrations from surfaces. These receptors are particularly sensitive to low-frequency vibrations (around 40 Hz) and allow us to perceive small changes in textures when sliding our fingers across objects.
- **Merkel cells**: Found in the basal layer of the epidermis, Merkel cells provide high spatial resolution for detecting sustained pressure and texture. Unlike Meissner's corpuscles, which are more sensitive to light and brief touches, Merkel cells excel in detecting steady pressure and help us discern the shapes and edges of objects through touch. They are essential for tasks that require precise tactile feedback, such as typing or reading Braille.
- **Pacinian corpuscles**: These large, deep-seated mechanoreceptors are specialized for detecting high-frequency vibrations (40–500 Hz) and transient changes in mechanical pressure. Pacinian corpuscles are especially important for sensing rapid or strong vibrations, such as those produced when handling power tools or when a phone vibrates. They are less densely packed compared to other mechanoreceptors, but their sensitivity

to vibrations makes them critical for detecting subtle changes in pressure over a larger area.

- **Ruffini endings**: Located deeper within the skin and in connective tissues, Ruffini endings are responsible for detecting skin stretch and sustained pressure. These receptors play a vital role in proprioception, the ability to sense the position and movement of our body parts in space. Ruffini endings help us detect when our skin is stretched or when our joints are moving, contributing to our overall sense of body awareness and coordination.

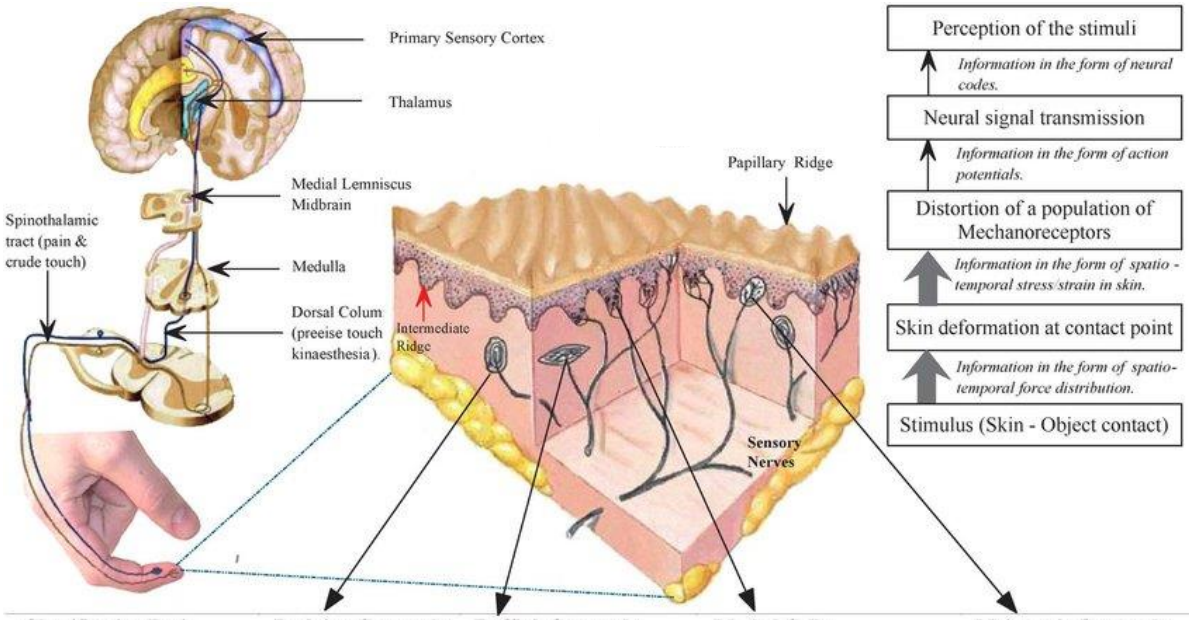

Classification Basis		Pacinian Corpuscle	Ruffini Corpuscle	Merkel Cells	Meissner's Corpuscle
Type		FA II	SA II	SA I	FA I
Adaptation Rate		Fast	Slow	Slow	Fast
Spatial Acuity (mm)		10+	7+	0.5	3-4
Vibration/rapid indent. threshold	Best(μm)	0.01	40	8	2
	Mean(μm)	0.08	300	30	6
Stimuli Frequency (Hz)		40-500+	100-500+	0.4-3	3-40
Conduction Velocity (m/s)		35-70	35-70	40-65	35-70
Effective Stimuli		Temporal changes in the skin deformation	Sustained downward Pressure; Lateral skin stretch; Skin slip.	Spatial deformation; Sustained pressure; Curvature, edge, corners.	Temporal changes in skin deformation
Sensory Function		High frequency vibration detection; Tool use.	Finger position; Stable grasp; Tangential Force; Motion direction	Pattern/form detection; texture perception; Tactile flow perception.	Low frequency vibration & motion detection; Grip control; Tactile flow perception.

Figure 6.4: Tactile signal transmission from the finger, to the spinal cord, and to somatosensory area of brain and *vice versa* (left). Location of various mechanoreceptors with their corresponding properties or classification (center). Functional events during sensory transmission from contact point to the brain. It is only shown in one way in this case (right, adapted from [276]).

Similarly, certain animals possess optical receptors embedded within their skin or use capacitive proximity sensing to detect changes in their environment. These animals offer inspiration for

advanced sensory systems . For instance, octopuses have light-sensitive cells in their skin, while some fish use electroreception to sense the electrical fields around them [277]. Creating sensate e-skin or fabrics that truly mimic the intricate functions of biological skin requires a comprehensive approach that integrates both sensory capabilities and mechanical properties, including varying receptor densities to match the functionality of different biological skin/body parts.

The human nervous system, particularly the somatosensory network, is a highly sophisticated system that processes a vast array of sensory inputs. The peripheral nervous system (PNS) serves as the first line of sensory data acquisition, where mechanoreceptors, thermoreceptors, nociceptors, and other specialized receptors convert physical stimuli into electrical signals. These signals are transmitted and processed at multiple levels through afferent nerve fibers to the spinal cord and ultimately to the central nervous system (CNS), where they are further processed, interpreted, and integrated to produce appropriate responses [278]. In contrast, electronic systems typically rely on centralized processing, which can become a bottleneck as sensor networks scale. By adopting distributed processing techniques inspired by biological systems, electronic skin and computational sensate fabrics could achieve greater scalability and efficiency. Localized and decentralized processing units embedded within the fabric could handle initial data filtering and noise reduction, transmitting only the most relevant information to centralized processors. This distributed processing approach would reduce the burden on central processing units and allow for more efficient and responsive systems.

In developing bioinspired soft systems like electronic skin, researchers have aimed to replicate these intricate processes within a synthetic medium. High-density sensors embedded within these deformable substrates mimic the distributed sensory receptors in human skin [279]. For example, Paradiso et al. estimated that an e-skin with fingertip-level sensor density could produce a data stream of approximately 12.5 MB/s for a 10 × 10 cm patch, assuming 8-bit digitized samples taken at 500 Hz [130]. To prevent data overload, these sensors could employ dynamic adaptation mechanisms, adjusting their sensitivity based on stimulus intensity and frequency, similar to biological receptors. Additionally, implementing lateral inhibition in electronic systems could involve designing circuits that suppress redundant signals and enhance contrast in sensor data, emulating inhibitory networks found in biological systems. These processes—including dynamic adaptation, which adjusts receptor sensitivity over time, lateral inhibition to enhance contrast in sensory input, and hierarchical processing that filters and refines data as it travels to higher cortical areas—are key to mimicking the functionality of biological sensory systems [280].

Additionally, the mechanical properties of human skin—its ability to stretch, compress, and recover—are crucial for both protection and sensory function. To replicate these properties, bioinspired systems can use soft, stretchable materials like fabrics and elastomers, which can be

embedded with stretchable electronics. These materials maintain their functionality under deformation, ensuring that the sensor networks within them remain responsive even during complex movements.

Biological systems are also inherently fault-tolerant, with redundancy built into their networks. If one pathway is damaged, alternative routes can often compensate, ensuring continued functionality. Developing similar fault-tolerant architectures in electronic systems, where failures in individual sensors or connections do not compromise the entire network, has long been a significant area of research and practice, especially in safety-critical applications like aerospace and autonomous vehicles [281], [282]. Furthermore, biological systems are naturally scalable, with the ability to grow and adapt over time. Advances in modular design and reconfigurable architectures could allow for more scalable and adaptable electronic systems, drawing inspiration from the growth and plasticity of biological networks [283], [284].

6.2: Hardware and Substrate Design

Based on the limitations of centralized systems discussed in Section 6.1, the remarkable functions and properties of biological skin and the nervous system in Section 6.2, and the concept of general-purpose sensing as platforms, I have proposed the following design principles in realizing distributed computational fabrics (Figure 6.3) for the development of ***NETS*:**

- **Scalability.** Scalability is essential for covering large surface areas efficiently, particularly when sensor nodes are miniaturized. The system must scale seamlessly as the number of nodes increases, maintaining high performance and adaptability.
- **Miniaturized Nodes and High Sensor Density.** Miniaturized nodes within N*ETS* increase sensor density, which improves the resolution for detecting environmental stimuli. Higher sensor density is critical for precision applications like tactile sensing, shape detection, and fine surface interactions, where detailed spatial information is required for effective processing.
- **Multi-modality.** *NETS* supports multi-modal sensing, allowing it to detect a wide range of physical stimuli. This flexibility makes *NETS* applicable to various domains, from healthcare monitoring, robotics, to environmental interaction. Multi-modal sensing also enables the discovery of unexpected, interesting events and optimization of resource usage based on specific demands.
- **Robustness and Fault-tolerant.** As a distributed sensor network, *NETS* is designed for robustness and fault tolerance. The mechanical and electrical systems ensure that failure

in individual nodes or wires does not affect the overall functionality, which is vital for applications in wearable electronics and smart textiles where mechanical stress or environmental factors may cause component failure.

- **Autonomous**. To reduce the need for frequent interventions, *NETS* is designed to operate as a generic event-driven system. By incorporating both local processing and a hybrid communication architecture—enabling centralized as well as decentralized communication between neighboring nodes—*NETS* can efficiently transfer information across its bus and peer-to-peer networks. This distributed architecture allows for autonomous decision-making at local nodes while still facilitating the sharing of critical data with centralized processors, optimizing system performance and reducing communication bottlenecks
- **Flexible Networking**: *NETS* supports a combination of wired and wireless communication, allowing for multiple data transfer methods. This flexibility makes the system highly adaptable to various infrastructures outside the nodes themselves. Whether integrating with existing wired networks or operating in environments where wireless communication is preferred, the flexible networking architecture ensures that *NETS* can function seamlessly across a range of conditions, further enhancing its versatility and resilience in different applications.
- **Low-power consumption**. To address the growing number of nodes in large networks, *NETS* is optimized for low power consumption. Efficient power management ensures that the system can operate over extended periods without excessive energy demands, particularly in scenarios where external power sources are not readily available.
- **Manufacturable at scale.** *NETS* leverages existing printed circuits and textile manufacturing technologies to produce scalable and cost-effective materials. By using established fabrication methods, the system can be mass-produced at scale.
- **Mechanical flexibility and stretchability.** Being soft, flexible, and stretchable are integral to the design of *NETS,* allowing it to bend, stretch, and conform to various shapes and surfaces without compromising performance. This flexibility is essential for applications across scales from dynamic wearables to static smart surfaces.
- **Modularity and Reconfigurability.** The modular design of *NETS* makes it adaptable and scalable for a wide variety of applications. Modular components can be easily expanded or reconfigured to meet specific requirements, providing flexibility for both large-scale industrial uses and personalized devices. One of the core features of *NETS* is its cuttable and reconfigurable design, enabling it to be customized into any size or shape. This versatility allows it to be integrated into various textile products or adapted to different surfaces. Reconfigurability supports rapid prototyping and customization, making it suitable for unique applications that require tailored solutions.

6.2.1: Node Hardware Design

Processing Module. The microprocessor device selected for our node design needed to support multiple clocks and power modes, while providing an adequate number of input and output pins for various interfacing requirements. We chose the ATSAMD21E18A microcontroller due to its rich feature set, which aligns perfectly with these needs. Its versatility, power efficiency, and scalability make it ideal for use in *NETS* (Figure 6.5).

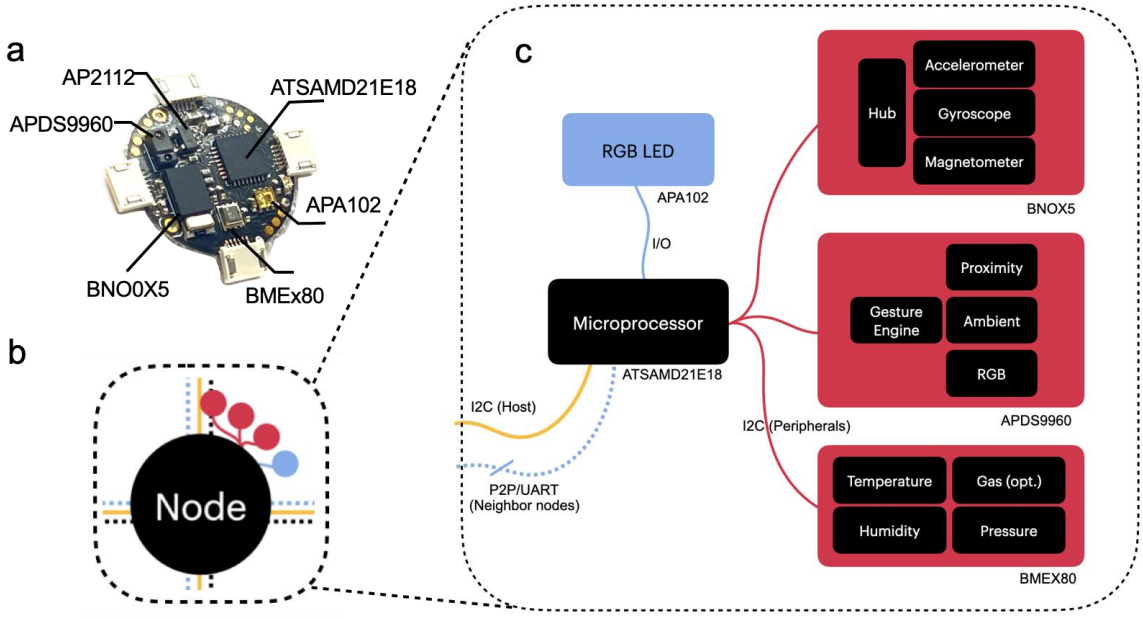

Figure 6.5: *NETS* node design and its system architecture block diagram.

- **Key Features.** The ATSAMD21E18A operates on a 1.62V to 3.63V power supply, offering a wide range of flexibility for various power conditions, and based on our sensor modules choice, we decided to operate at 3.3V. It features 256KB of Flash memory and 32KB of RAM, providing ample storage for program instructions and handling real-time data processing tasks efficiently. Powered by a 48 MHz, 32-bit ARM Cortex-M0+ core, this microcontroller ensures sufficient processing power for node operations within a distributed sensor network while maintaining energy efficiency. The ATSAMD21 MCU devices include several master clock source modules, each capable of producing a stabilized output frequency to drive the various peripherals and modules within the system. These clock source modules ensure accurate timing and synchronization for the sensor network, crucial for coordinated multi-node operations. The available clock sources include internal R/C oscillators such as OSC8M and OSC32K,
- **Communication Flexibility.** One of the key reasons for selecting the ATSAMD21 is its 6 SERCOM (Serial Communication) modules, which provide flexible communication

options. These modules can be configured for I2C, serial peripheral interface (SPI), or UART protocols, allowing seamless interfacing with various sensors and peripherals. This flexibility supports configurations like 3 UARTs and 3 SPIs, or 2 SPIs and 4 I2Cs, enabling a versatile communication infrastructure across the network, which is essential for efficient data exchange and hardware integration in distributed systems.

- **Real-time Counter.** The SAM D21 includes a Real-Time Counter (RTC), a 32-bit counter with a 10-bit programmable prescaler that operates continuously, even in low-power modes. This feature enables precise timekeeping, periodic events, interrupts, and time-based tasks such as system wake-ups. The RTC also supports multiple wake-up mechanisms, including alarm/compare wake-up, periodic wake-up, and overflow wake-up, ensuring the node can transition between sleep and active states without sacrificing power efficiency.
- **Power modes.** For optimized energy consumption, the SAMD21 microcontroller provides several power-saving modes. In STANDBY mode, system clocks are disabled, and voltage regulators switch to low-power operation, significantly reducing energy usage during idle periods. Additionally, there are three levels of IDLE mode, where the CPU clock is halted while peripherals remain active, allowing the system to continue processing essential data without unnecessary power drain. This ability to selectively manage clock signals helps optimize power consumption across the sensor network.
- **Native USB.** The ATSAMD21E18A also supports native USB, which is compatible with every major operating system. This feature is particularly important for applications requiring plug-and-play compatibility, enabling the microcontroller to be easily deployed in various environments. The native USB functionality ensures seamless communication between the microcontroller and external devices, simplifying tasks such as programming and debugging while removing the need for additional USB interface chips.

Pin Allocations. We utilized 28 of the 32 available pins for the ATSAMD21E18A microcontroller (Appendix A.16). The allocation of these pins was carefully structured to balance communication and peripheral needs across the node. Specifically:

- 8 pins were dedicated to communication, with 4 Tx and 4 Rx pins assigned to manage connections with the node's four neighboring nodes. For peripheral communication,
- 4 pins were allocated to two I2C channels: one channel was designated for the common-backbone connection to the host system, while the second I2C channel managed communication with various sensing peripherals. Additionally,
- 2 interrupt pins were reserved for the ambient light/proximity and IMU sensor modules, providing low-latency responses to changes in environmental conditions.

For maintenance and controls,

- 5 pins were dedicated to the joint testing action group (JTAG) port for debugging and programming purposes, ensuring efficient development and maintenance of the node's firmware through easy pogo-pin plugs/connections.
- 2 pins were assigned to the USB D+ and D- connections, enabling native USB support across operating systems if needed, and allowing any node to be a host device for data extraction through USB.
- 2 pins were designated for controlling the RGB LED, allowing visual feedback on node activity,
- 1 pin was reserved for an individual LED to serve as a system status indicator.

Power Regulation. To regulate power within the system, we used AP2112 linear voltage regulator. This component maintains a consistent 3.3V supply to the main processor, LEDs, and sensor peripherals, even when the input voltage reaches up to 6V. This regulation is critical for ensuring stable operation across the distributed network and plays a key role in expanding node coverage for large-area and dense arrays.

Sensing Modules. Sensor devices were selected based on several criteria to ensure optimal performance, efficiency, and integration within our distributed node system. These criteria included:

- Voltage compatibility with the 3.3V power supply used in the node system.
- Digital communication via I2C, avoiding the need for analog processing components, with distinct I2C addresses to prevent conflicts.
- Common packaging and easy integration into the node substrate, such as flexible PCBs, allowing for automated manufacturing (through pick and place).
- Miniaturized form-factors and footprint to ensure compactness on each node.
- Sensors that feature low-power modes and support interrupt pins, enabling switching between states to conserve energy.
- Functional equivalence to biological skin sensors for advanced multi-modal sensory capabilities.

Based on these requirements, we selected three multi-functional sensing modules: APDS9960**,** BME280/680**,** and BNO055/85**.**

- **APDS9960.** The APDS9960 is a versatile digital sensor that combines RGB color detection, ambient light sensing, proximity sensing, and gesture recognition. The device features an internal state machine that allows it to enter a low-power state between measurements, with a typical power consumption of 1.0 μA in sleep mode. The proximity detection is factory-calibrated to detect distances up to 100mm using a photodiode-based method of reflected IR intensity from an integrated LED. An interrupt can be generated with each new proximity result or whenever proximity results exceed or fall below threshold levels, enabling real-time event-driven operations, ideal for low-power applications.

  The sensor also includes advanced color and ambient light sensing using an array of photodiodes for red, green, and blue light detection, along with a clear channel for overall light intensity. This makes it suitable for lighting control and ambient environment monitoring. The gesture detection functionality relies on directional IR reflection sensing, enabling user interaction through gesture-based controls without physical contact.

- **BME280/680.** The BME280 sensor is designed to measure relative humidity, barometric pressure, and ambient temperature with high precision. It operates in a pressure range of 300 to 1100 hPa and a temperature range of -40°C to 85°C, with a 1-second response time for humidity and accuracy levels of ±3% for humidity and ±0.5°C for temperature. The BME680 variant offers additional functionality by incorporating volatile organic compounds (VOC) gas sensing for air quality monitoring. VOC gas sensing capabilities allow the sensor to detect VOCs, providing air quality data for applications like indoor pollution monitoring. The gas response time is 1 second, allowing for real-time monitoring of VOC levels.

  The sensor supports multiple power modes, including sleep, normal, and forced. The user can optimize data rate, noise, response time, and current consumption by adjusting sampling modes, filter settings, and operational frequency. The BME680 operates efficiently, with a current consumption of 2.1 μA for humidity and temperature, 3.1 μA for pressure and temperature, 3.7 μA for combined humidity, pressure, and temperature measurements, and 0.1 mA for full operation with gas sensing at 1 Hz for the lowest operation mode. This makes it highly suitable for energy-constrained applications requiring continuous environmental monitoring. In addition to its environmental sensing capabilities, we can transform this sensor and leverage the pressure readings to enable tactile pressure and strain sensing by encapsulating it in a deformable polymer matrix (Section 6.4).

- **BNO055/85.** The BNO055/85 is a system-in-package sensor hub that integrates a triaxial 12-bit accelerometer with a measurement range of ±8g, a triaxial 16-bit gyroscope with a range of ±2000 degrees per second, and a triaxial geomagnetic sensor with a resolution of 0.3 μT, along with a 32-bit ARM Cortex-M0+ microcontroller. The module runs a motion processing and power management firmware, and supports three operational power modes: Normal, Low Power, and Suspend. In Normal mode, all sensors are active, making it ideal for real-time motion sensing applications. In Suspend mode, both the sensors and microcontroller enter a low-power state, reducing energy consumption during inactivity.

  In Low Power Mode, only the accelerometer remains active, monitoring for motion events. When motion is detected, the system wakes up, returning to Normal mode for full operation. The built-in firmware also provides real-time 3D orientation, heading, calibrated acceleration, and angular velocity, alongside advanced features like step counting, stability detection, tap detection, and gesture recognition. As a **sensor hub**, the BNO055/85 offloads the data processing from the main microcontroller, reducing the computational load and improving power efficiency.

Display Module. The **APA102** LED module serves not only as a dynamic display tool but also as an integral part of the system's localization and AR interaction. It combines a driver IC with a RGB LED in a single package, allowing each LED to be individually addressable. the APA102 uses two data lines: data and clock. This means it is less prone to timing issues, as the clock line precisely synchronizes the data transmission between the controller and the LEDs. The ability to control brightness and color for each pixel with 8-bit PWM (Pulse Width Modulation), along with 5-bit global brightness control, enables smooth transitions and complex lighting patterns. In addition to visualizing sensor data, we utilize the APA102 LEDs for localization. By assigning unique colors to individual nodes, we can use a camera-based system to track the spatial positions of each node. The color of each APA102 LED relates to the node's ID, which enables precise tracking and AR-based localization of multiple nodes simultaneously.

Figure 6.6 shows the evolution of the sensor node from *SensorNETS* (Appendix A.14 and A.15) to *NETS* v3.0 (Appendix A.16 and A.17). As shown, for a single flexible PCB layer design, *NETS* has a diameter of 20 mm. However, by using a two-layer PCB design, with the microprocessor and voltage regulation on one side and the sensing peripherals on the other side, we can reduce the diameter to 15 mm, which also allows for the highest resolution possible. Additionally, it can be observed that on all four sides, there are traces for interconnects to neighboring nodes. These interconnects provide power (Vs and Gnd) and communication lines (P2P through RX and TX lines, and I2C through SDA and SCL lines).

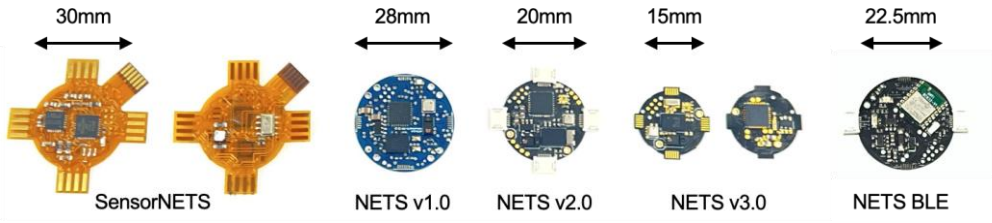

Figure 6.6: Evolution of *NETS* nodes throughout the time, including its first prototype, *SensorNETS* [83], latest design of *NETS* v3.0, and its wireless version of *NETS* BLE.

NETS BLE Module. For wireless applications, we have developed another node design (Appendix A.18 and A.19) using the BC832 module. This module integrates BLE 5.3 and an near-field communication (NFC) module with the Nordic nRF52832 SoC. The BC832 offers a line-of-sight communication range of up to 50 meters (150 feet). It is ideal for our system, as it includes two I2C interfaces that are crucial for managing the system's communication requirements. The BC832 also comes with a chip antenna, which is fully integrated into the module, creating an all-in-one package that simplifies the node design. In addition to the BLE SoC module, the node also includes a power regulation circuit that ensures voltage sharing across neighboring nodes. It supports communication through shared I2C SDA and SCL lines, as well as P2P communication through TX and RX lines to interact with the four neighboring nodes. The size of this node is 22.5 mm (Figure 6.6).

6.2.2: Substrate Design

Node Fabrication. For the sensor node, polyimide flex technology was chosen compared to other new or existing circuit fabrication techniques due to its durability and manufacturability (Figure 6.7a). Unlike rigid PCBs, polyimide flex technology is better suited to conform to irregular surfaces and can withstand continuous flexing without any degradation in performance. The material is highly stress-compliant, extremely thin, and capable of enduring high temperatures, making it ideal for environments where both flexibility and durability are critical requirements.

To protect the conductive traces on both sides of the node from environmental exposure and to provide a solder mask, we applied a coverlay as provided by the manufacturer. The polyimide base used has a thickness of 100 μm, which ensures structural integrity while maintaining flexibility. A stiffener (100 μm) was also used beneath surface-mount ICs to provide additional support and prevent pin breakage. Stiffeners are crucial in regions where stress from bending

could damage the pins or solder joints of the ICs, helping to relieve mechanical strain during flexing and bending.

Interconnect Fabrication. For the interconnects, besides the flex PCB based on Polyimide, we explore a newer PCB technology based on thermoplastic polyurethane (TPU), which offers enhanced softness and intrinsic stretchability compared to other base substrates. Although two-layer designs are feasible with TPU, fabricating vias and soldering IC components to TPU remains a challenge in terms of reliability and performance. Consequently, we implemented TPU for one-layer serpentine interconnects and compared their performance to flex PCBs, as discussed in Chapter 5. The TPU base used for the interconnects has a thickness of 100 μm, with 35 μm copper traces for both TPU and polyimide designs (Figure 6.7b). A 200 μm stiffener was used at both ends of the interconnects to aid in connectorization to plugs.

Substrate Options for Node and Interconnect Integration. We explored various substrate options for integrating the nodes and interconnects into fabrics. *NETS* are compatible with various surfaces (glass, plastic, walls, *etc*) and fabric types, including non-woven, woven, and knit fabrics, but we chose to use highly stretchable synthetic knit fabric (67% nylon, 33% spandex) to leverage the stretchability of the *NETS* for dynamic applications. When using flex PCBs, we experimented with a 5 μm sticking layer (3M9077 adhesive) applied during manufacturing to adhere the nodes to the fabric. However, we found that this adhesive was only suitable for one-time application; after being re-applied five times, it lost its adhesiveness, and over time, it showed signs of wearing off. As a result, we shifted to using a more robust adhesive, the 50 μm heavy-duty double-sided tape (YYXLIFE), which provided much better bonding over the long term.

For the TPU interconnects, we used a method of heat pressing or ironing to fuse the TPU directly to the fabric. This method was highly effective, as evaluated in Chapter 5, and demonstrated excellent bonding with long-term reliability. As discussed, polyimide PCB offers advantages during prototyping because of its ease of removal and reusability, supporting stretchability of up to 35%. However, for final product development, TPU interconnects provide a more robust and stretchable solution, particularly for applications where long-term bonding is essential. TPU interconnects offer stretchability of up to 85%, a significant improvement that is especially valuable in environments requiring frequent stretching or dynamic movement.

In addition to fabric-based substrates, we explored the use of polymers such as Ecoflex (Figure 6.12) or PDMS for embedding the sensor networks. In this method, we poured one layer of the polymer, placed the *NETS* on top, and submerged it in another layer of curable silicone. This encapsulation technique was particularly effective for two-layer node designs and for

applications involving tactile pressure and strain sensing, where the sensor network needed to be integrated into a stretchable, durable medium. Another potential polymer substrate is polyurethane, which will fuse and interface well with the TPU interconnects, given that they share similar base material and properties.

6.2.3: Mechanical Design

Connectors. Reconfigurable sensor networks provide significant advantages over fixed configurations, allowing nodes to be rearranged to meet varying application needs. However, this level of flexibility demands connectors that facilitate easy plugging and unplugging while ensuring the system remains mechanically and electrically stable. This is crucial for maintaining reliable power and communication even during reconfiguration. The connector needs to be compact and lightweight, so it does not contribute significantly to the overall system size or mass.

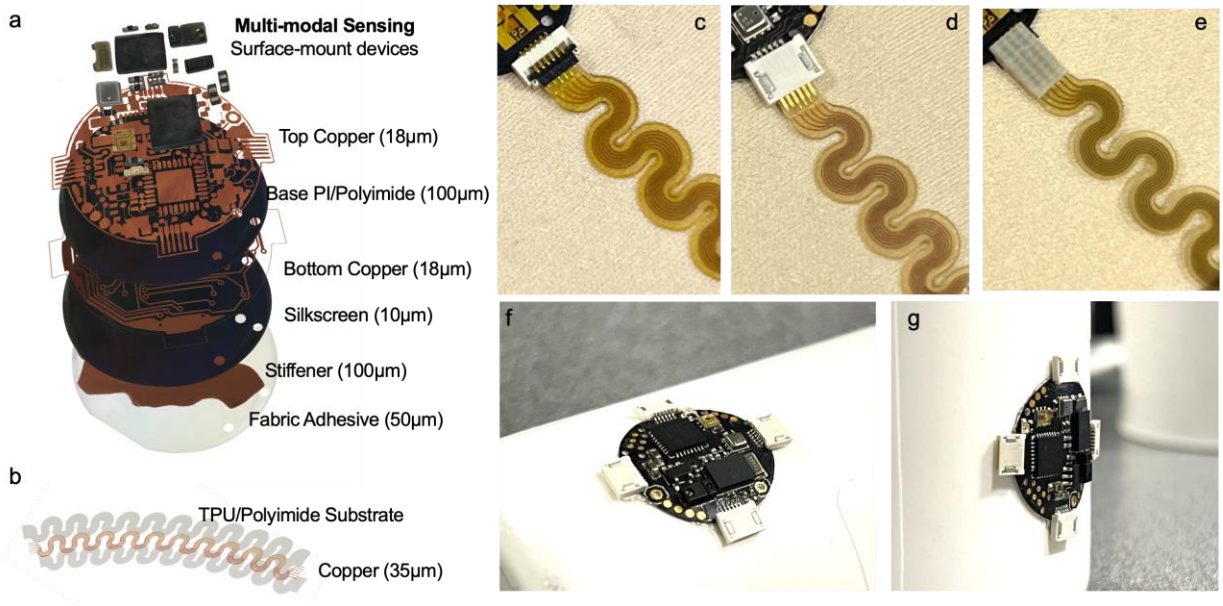

Figure 6.7: Exploded view of the a) flex PCB node layers and b) interconnect layers. Different ways to integrate nodes with their interconnects through temporary mechanism c) dual-contact easy-plug connector and d) standard snap ZIF connector, or e) permanent integration by fusing or heat-pressing them with conductive Z-tape. f-g) *NETS* nodes laminated onto a non-planar curvy surface to show its flexibility.

In designing the serpentine interconnects with TPU, and polyimide, we used a 6-pin configuration with a 0.5 mm pitch, similar to the industry-standard Flexible Flat Cable (FFC). This enabled compatibility with commonly available FFC and ZIF connectors. After evaluating several

options, we selected the Molex Easy-On FFC/FPC Connector (Non-ZIF, Dual Contact Style) for its ease of use and reliability (Figure 6.7d), allowing insertion from either side while maintaining stable connections. Extensive cyclic testing, as shown in Figure 5.11 in Chapter 5, demonstrated the durability of this connector when paired with our interconnects. Alternatively, a standard ZIF connector (Figure 6.7c) could be employed for a more secure and fixed connection, utilizing a sliding mechanism that snaps the end of interconnects into place. For a more streamlined and flexible integration, TPU interconnects can also be heat-pressed directly onto the side traces of the Flex PCB with conductive Z-tape (3M, 9703), resulting in a permanent, seamless bond (Figure 6.7e).

Size of nodes. Size considerations were also critical in the design of the node. The challenge was to balance the need for sufficient space to accommodate all components while maintaining a high sensor density within a compact area. For our design, the smallest node diameter achieved with single-sided PCB was 20 mm, with a bending radius of 3.25 cm (Figure 6.7f-g). The node design discussed can adapt to various body parts by considering their natural curvature [285]. For example, the finger joints exhibit tight curvatures, which might pose challenges for the node's flexibility, but it can perform well in less pronounced curves, such as the base of the finger or the palm. Moving to the arm, particularly around joints like the elbow, the curvature becomes moderate, making the design suitable for placement on areas like the forearm or upper arm.

Around the neck, the curvature is more gradual, and the node can comfortably conform to wearable devices or garments in this region. For broader body parts, such as the torso or back, the curvature is even less pronounced, making the node highly effective for applications in smart textiles or health monitoring systems that require coverage over larger areas. Future design improvements could focus on increasing flexibility for areas with tighter bends, like the fingers, by modifying the node's component layout, adjusting its shape, or minimizing its size. These adjustments would enhance the node's functionality and adaptability for a wider range of dynamic uses.

6.3: System Architecture

As illustrated in Figures 6.8, the proposed computational fabric system, or *NETS*, is composed of miniaturized, networked, flexible PCB nodes connected by stretchable interconnects. These nodes are laminated or embedded within a deformable substrate, such as fabric or rubber. The network architecture includes a single host that has communication access to all nodes through a common backbone using I2C channels. Any node in the system can also function as a host. In addition, nodes can communicate with neighboring nodes via peer-to-peer UART Tx and Rx channels. Each node includes a microcontroller (ATSAMD21E18A, Microchip) and various sensor and

actuator/display modules connected through a second I2C channel (BNOX5, APDS9960, and BMEX80). The interconnects between nodes consist of a 6-pin configuration that handles power, ground, and communication lines (I2C and P2P), allowing the entire network to operate cohesively.

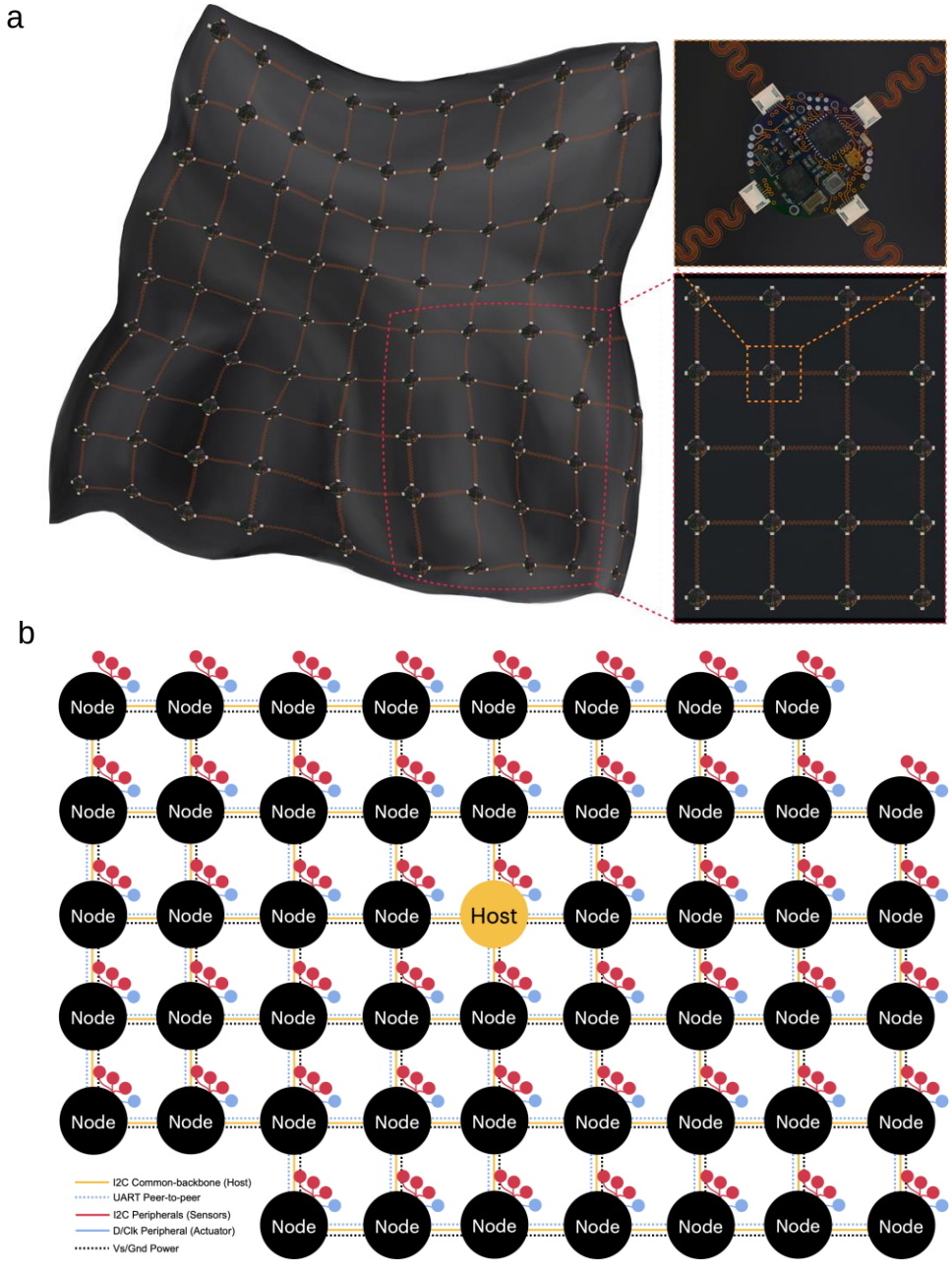

Figure 6.8: a) Illustration of *NETS* island-bridge stretchable configuration and b) its distributed system architecture with common backbone and peer-to-peer channels.

The sensor network is designed to support both wired and wireless communication with a PC (Figure 6.9), which serves as the primary data receiving and processing unit and provides connectivity to an extended reality (XR) environment for sensor visualization and immersion. Nodes can transition between peripheral devices and hosts using native USB functionality, allowing for direct connection to the PC. Alternatively, a custom-designed BLE node can function as another type of host, facilitating wireless applications such as wearables and mobile sensing. We envision that in stationary textile installations like curtains or carpets, the system will be connected and powered either via USB/wired or BLE/wireless nodes and power source, while mobile or wearable applications will use BLE nodes and batteries.

NETS operates as distributed sensors and processors utilizing a star topology, where each host node is responsible for coordinating a network of interconnected nodes arranged in a mesh structure. Each of these networks, composed of tens to hundreds of nodes, is supported by the I2C common backbone and P2P communication lines. Due to limitations such as the number of I2C addresses, parasitic capacitance, and voltage drops as the network scales (discussed in Section 6.6 and 6.7), each network can accommodate up to 100 nodes. *NETS* can also operate as a stand-alone device without a PC connection. In such cases, the in-built processing, sensing, and display modules can visualize stimuli and events, log relevant data, and respond to user or environmental interactions directly (Figure 6.10).

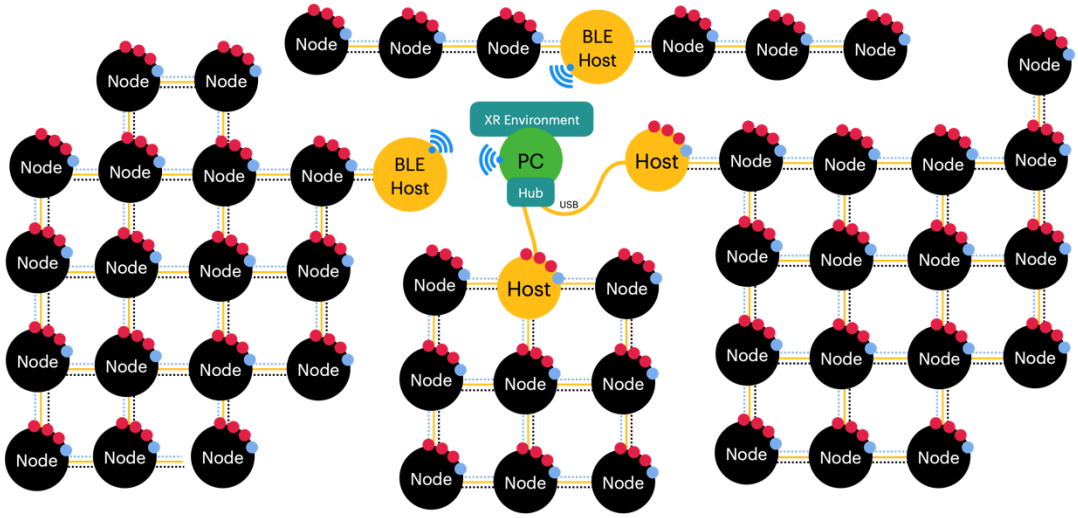

Figure 6.9: *NETS* peripheral nodes with wired and wireless BLE communication nodes as hosts connected to a PC as a hub

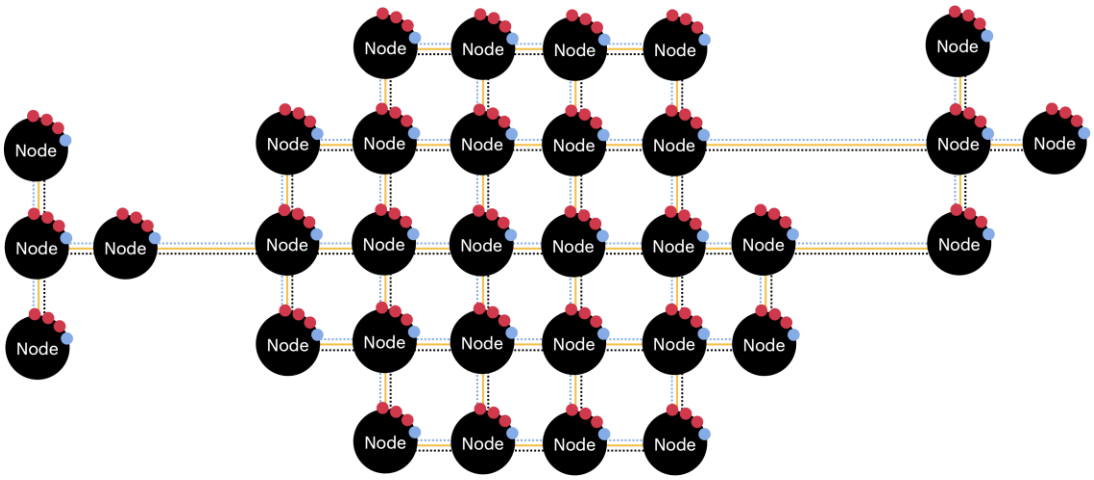

Figure 6.10: Reconfigurable *NETS* in stand-alone, independent mode

6.4: Sensor Characterization

Figure 6.11 displays sensor data from a 2 x 2 array of *NETS* nodes, tested under various stimuli and conditions. In this plot, we have specifically selected the sensor parameters relevant to each stimulus type. Figure 6.11a presents accelerometer data from all sensor nodes in response to finger taps, vibrations, and strikes. The results show the ability to localize the point of contact or impact based on the distance between the strike and each sensor node. This feature demonstrates the system's potential for tracking localized touch or pressure events across the fabric network.

The IMU, which includes the accelerometer and gyroscope on each sensor node, can also be used to detect tapping or vibrations (Figure 6.11a) and fabric deformations, such as bending, folding, twisting, and stretching. For example, bending, folding, and twisting can be detected by analyzing the angle or degree of the gyroscope readings (Figure 6.11b-c). Similarly, the relative strain on the fabric can be estimated by observing the direction and speed of the accelerometer signals, as illustrated in Figure 6.11d-e. The magnetometer in each sensor node can further be utilized to track the movements and locations of magnets in proximity, enabling interactive proxemic sensing (Figure 6.11f). In our tests, we observed that the magnetometer readings remained responsive to the presence of a magnet up to a distance of 20 cm. Incorporating the magnetometer enhances IMU readings by improving the system's ability to detect rotational movement and providing additional reference points for tracking orientation and motion in 3D space.

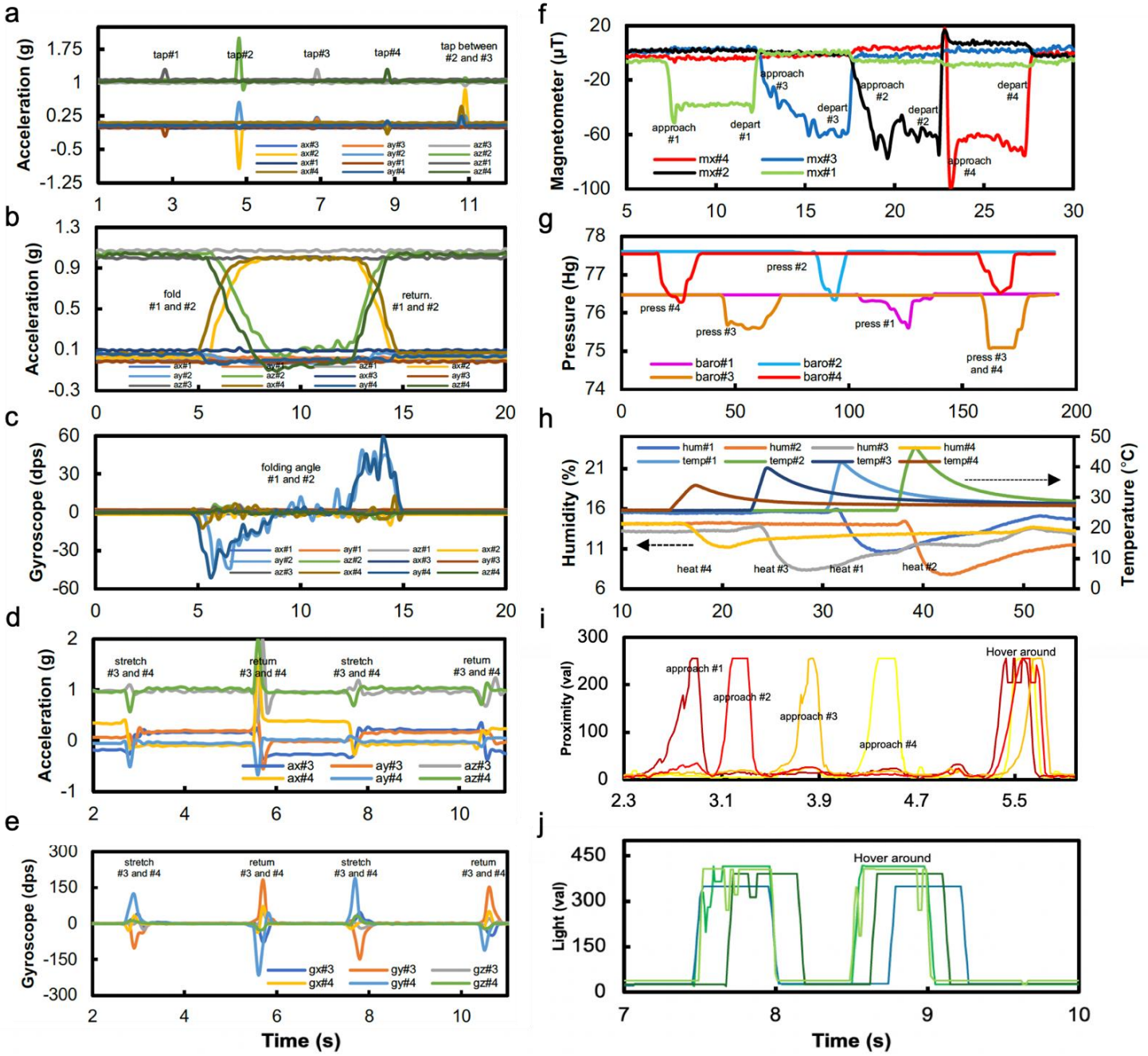

Figure 6.11: Large multi-modal sensor data of 4 *NETS* nodes based on various stimuli. a) Tapping, b-c) folding, d-e) stretching, f) magnet approach, g) tactile pressure, h) hot air flow, i-j) approach and hovering.

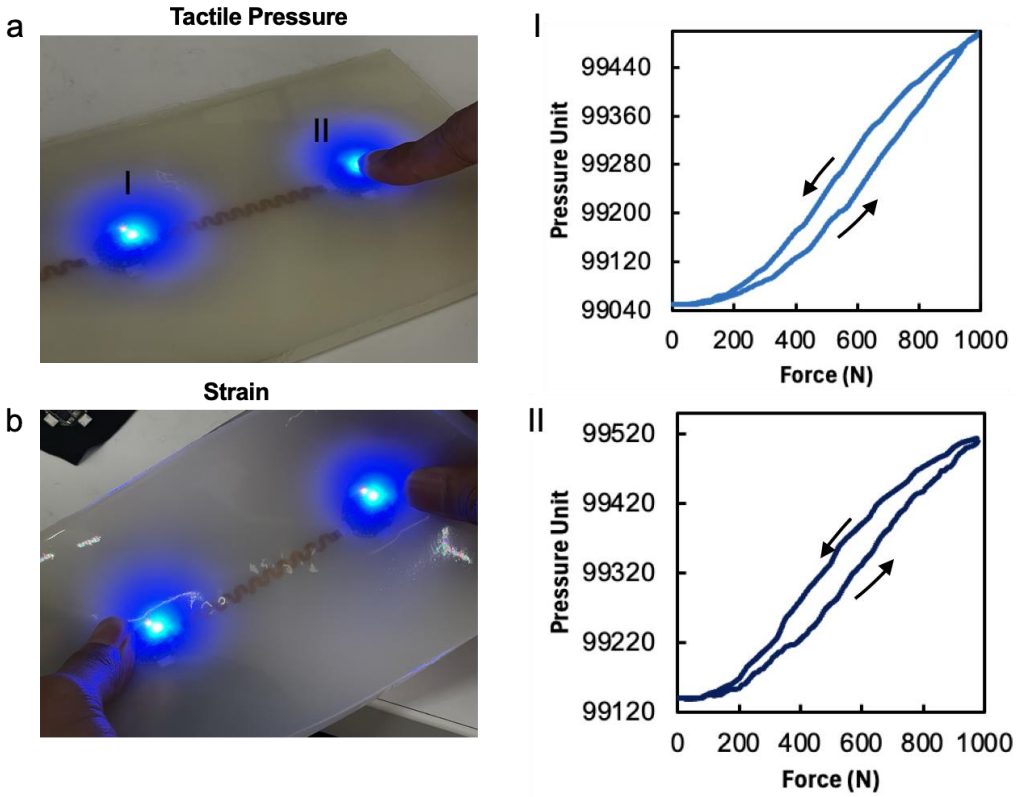

Figure 6.12: Encapsulated *NETS* nodes for a) tactile pressure and b) strain sensing, showing barometer pressure data of sensor I and II vs force exerted during a compression test.

To modify the barometer sensor's function from measuring atmospheric pressure to tactile pressure, we embedded the sensor nodes in polydimethylsiloxane (PDMS) through a process of casting and curing the soft rubber material. The interaction between the rubber and the barometer's strain gauge opening allows the sensor to detect tactile pressure by deforming in response to external forces [286]. This encapsulation enables each sensor node to detect not only light touches but also moderate and firm presses (Figure 6.11g). Figure 6.12 provides the characterization of the encapsulated barometer's response under compression, demonstrating a hysteresis effect due to the nature of the deformable substrate. Additionally, we have shown that the nodes can effectively sense changes in temperature and humidity by exposing them to heated air (Figure 6.11h) and skin contact during live demonstrations (Figure 6.38d). Finally, Figures 6.11i and 6.11j display the proximity and ambient light sensor responses as hands hovered over the sensor network, further showcasing the system's versatility in detecting environmental interactions.

Other stimuli can also be detected using different sensor modules integrated into the *NETS* nodes. Below is a summary of how various stimuli can be detected:

- **Tap/Vibration:** The accelerometer detects these events by capturing changes in motion and acceleration.
- **Touch/Proximity:** Proximity sensors can detect touch, especially when threshold levels are set. Ambient light sensors can also be used for proximity sensing, as they detect changes in light when a hand or object approaches, although this method works best in bright environments. Additionally, magnet tracking can be employed for proximity detection of objects embedded with magnets.
- **Magnet Localization**: The magnetometer can localize magnets in 3D space when the sensor network is sufficiently dense.
- **Light and RGB**: Ambient light and RGB sensors capture changes in light intensity and color, useful for visual or environmental monitoring.
- **Bending, Folding, Twisting:** These deformations are detected using a combination of IMU data from the accelerometer, gyroscope, and magnetometer, allowing for relative orientation tracking between different nodes.
- **Tactile Pressure:** The barometer, when encapsulated in a deformable material such as PDMS, is sensitive to tactile pressure. Another method for detecting pressure is to use proximity or ambient light sensors, as light trapping within the polymer substrate can indicate changes in surface deformation.
- **Strain:** Strain can be inferred from the difference in acceleration and direction between multiple accelerometers, especially during rapid movement. Pressure differences within a deformable material can also provide insight into strain due to the base substrate's Poisson effect.
- **Humidity**: Humidity changes are detected through the humidity sensor integrated into the nodes. It can also detect wind-flow, breathing patterns, and blowing activities.
- **Temperature:** The temperature sensor is sensitive enough to provide readings for both environmental and contact-based temperature changes.

In summary, our sensing modalities enable individual nodes and a collection of nodes in the computational fabrics to achieve somesthetic senses. The nodes are aware of their position (proprioception), can detect touch, pressure, and vibration (haptic perception), temperature (nociception), and even perform proxemic interaction. These capabilities are made possible through a range of sensors integrated into each node, including IMU with accelerometers and gyroscopes, as well as temperature, humidity, atmospheric and tactile pressure, and magnetic field sensors. This multimodal data capture and feedback system supports diverse wearable and smart surface applications, such as large-area tactile sensing, medical immersion, gaming interfaces, environmental sensing, and telepresence.

6.5: Communication Protocol and Networking

There are various serial protocols available for embedded systems, including 1-Wire, UART, RS-232, I2C, and SPI. Our system requires a protocol that balances bandwidth with a minimal hardware footprint. To develop a scalable, self-configuring, and self-organizing network, we needed a protocol capable of handling bus line communication without multiplexing. Therefore, UART and RS-232 were unsuitable. A bus supporting multi-master capability, allowing nodes to transition between host and peripheral roles, was also required, ruling out 1-Wire and SPI. As a result, I2C was chosen as the ideal solution due to its scalability (up to 128 addresses) and its support for communication speeds of up to 400 Kbps in fast mode and 3.4 Mbps in high-speed mode. Although I2C is slower than SPI, it only requires two additional lines (SDA and SCL), reducing hardware complexity and footprint.

The global I2C backbone allows for basic housekeeping tasks, such as address management, configuration checks, and direct access to sensor data, without needing to relay data through intermediary nodes. To address the limitations of the common backbone, we can implement multiple hosts with a sparsely connected I2C backbone alongside P2P communication. In a sparsely connected backbone, each host manages its own region, distributing the workload and bandwidth more efficiently, although at the cost of having multiple host nodes or networks. P2P communication allows for further scalability by enabling nodes to process data locally and communicate directly with one another without overloading the I2C backbone. P2P also provides a redundancy channel, ensuring the network remains operational even if parts of the I2C backbone become busy or fail. In this setup, neighboring nodes can communicate directly to identify issues, such as malfunctioning nodes, and remove them from the network without affecting overall system performance.

6.5.1: Initialization and Self-organizing Network

To create an autonomous, fault-tolerant, and reconfigurable sensor network, the *NETS* system implements self-organization and ad-hoc networking, as illustrated in Figure 6.13. This allows the network to dynamically assign addresses to nodes, update the topology in real-time, and maintain a global map of all connected nodes and sensors. Such capabilities are essential in environments where nodes can appear or disappear without manual intervention, ensuring uninterrupted operation of the network.

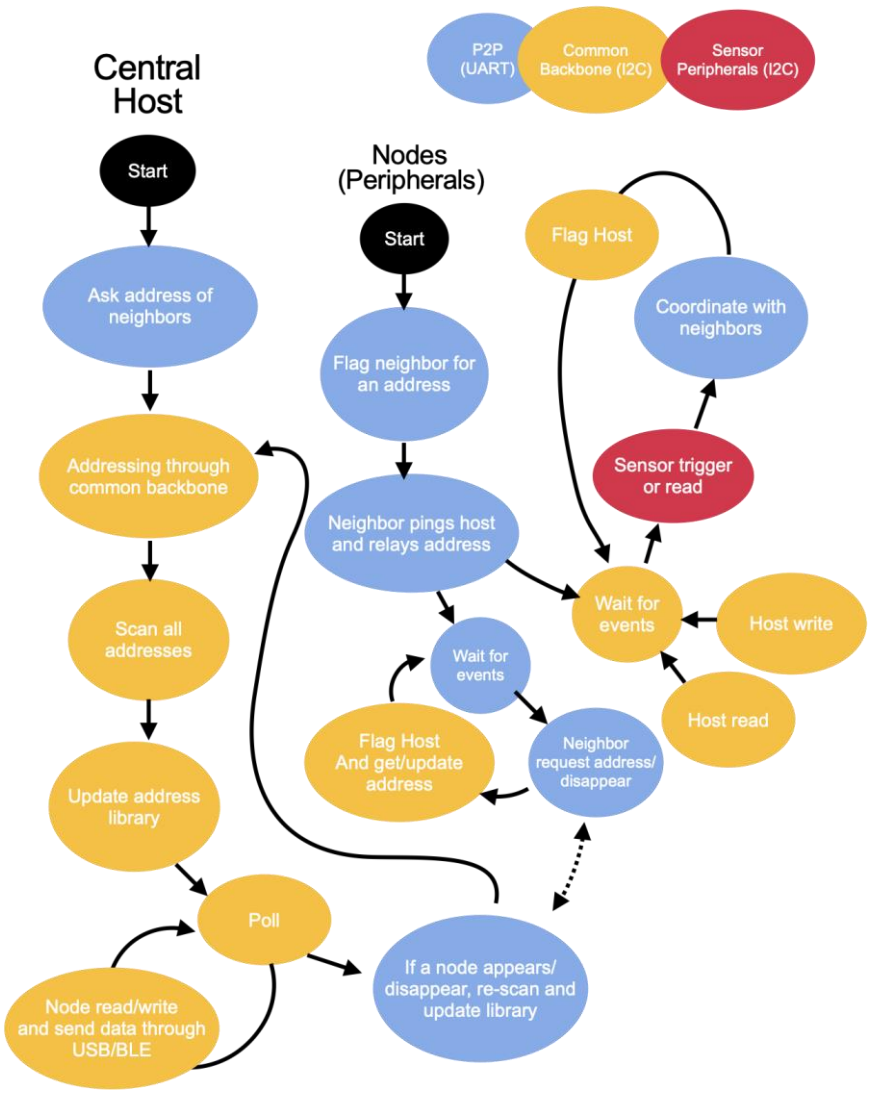

Figure 6.13: State-machine of *NETS* central host and peripheral nodes during system initialization and operation.

Address Assignment and Coordination Process. The central host manages the global state of the network, while peripheral nodes interact locally with their neighbors. When a peripheral node comes online, it flags its neighboring nodes to determine whether they already have assigned addresses. The peripheral node does not request an address directly but rather checks whether neighboring nodes have been integrated into the network.

- **Address Verification:** Peripheral nodes flag their neighbors to verify if they already have an address (P2P). If neighboring nodes already have addresses, the peripheral node relays this information to the host. If neighboring nodes do not have addresses, the neighbor pings the host, which then assigns unique addresses to both the new and disconnected nodes. This approach ensures there are no address conflicts and that all nodes in the network are properly integrated.
- **Host Assignment:** Once addresses are verified, the central host scans the network, ensuring all nodes have unique addresses. The host continuously updates its internal address library and regularly polls the nodes for status updates. This real-time scanning allows the host to keep track of changes in network topology, adding or removing nodes as necessary.

Since the peripheral nodes begin by flagging their neighbors, the central host must first trigger the address assignment process for its immediate neighbors. As shown in Figure 6.14, this address propagation will continue until the network is fully populated. If the fabric network is physically divided into multiple sections, such as being cut into three pieces, additional hosts can be assigned to manage each of the newly separated fabric sections, ensuring that all pieces continue to function independently and effectively (Figure 6.15).

Sensor Peripheral Triggers and Event Handling. Each node in the network has sensor peripherals (such as I2C-based sensors) which can trigger and communicate events. When a sensor peripheral is triggered at a node, the node handles the event locally and communicates the data to its neighbors and the host.

- **Coordination with Neighbors:** When a sensor peripheral is triggered, the node first coordinates with its neighbors through peer-to-peer network for different tasks, such as sleep/wake-up operation or data synchronization. This is especially important for systems requiring coordination between multiple sensors and nodes.
- **Host Communication:** After coordinating with neighboring nodes, the node sends the sensor trigger information to the central host through common backbone channel. The host processes this data and may perform additional actions, such as issuing commands or further aggregating the sensor data for analysis.

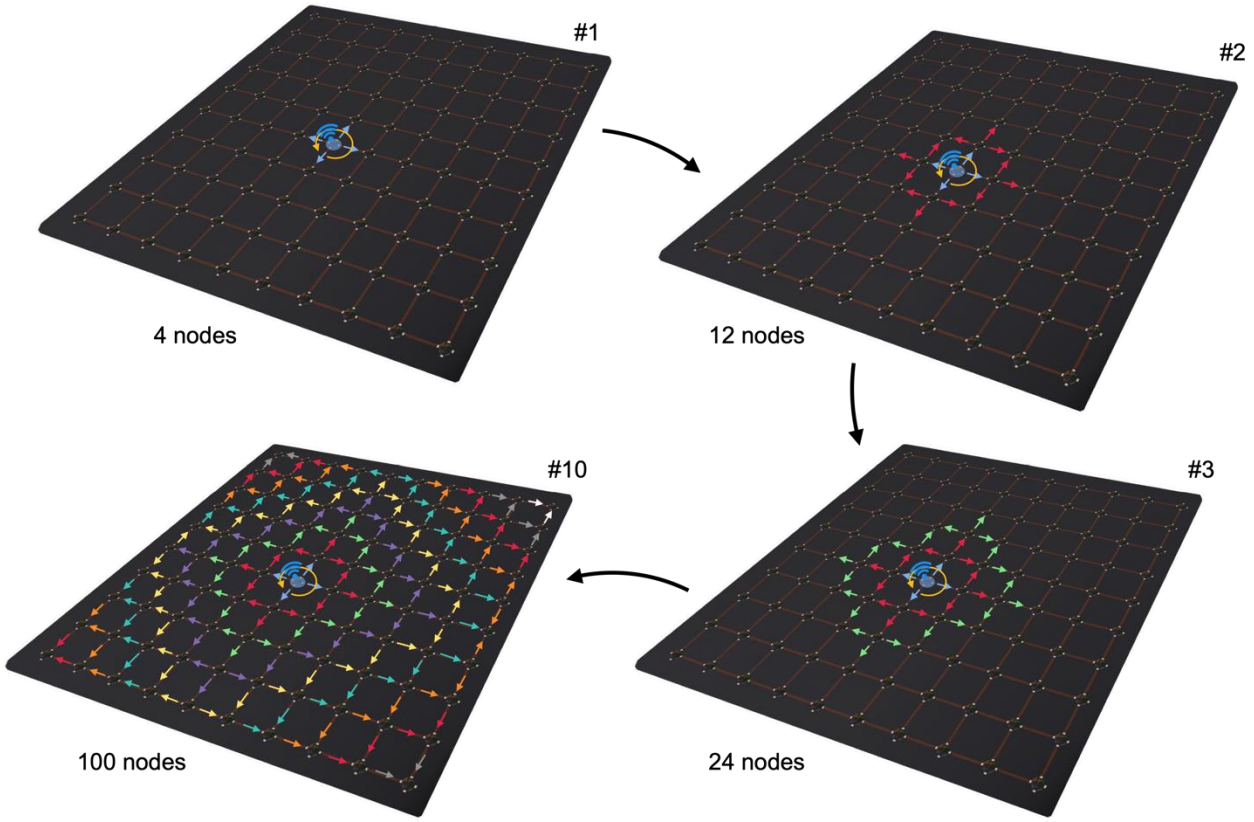

Figure 6.14: Address scanning and assignment through nodes peer-to-peer propagation.

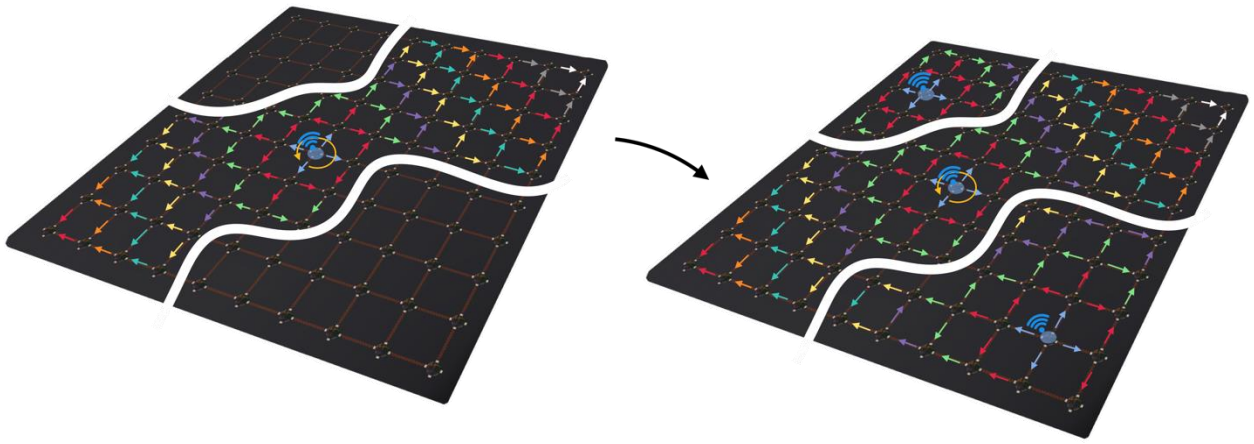

Figure 6.15: Cutting the fabric enables an operation with multiple hosts.

Handling Node Appearances and Disappearances The network is designed to be dynamic, automatically adjusting when nodes appear or disappear.

- **Node Appearance**: When a new node joins the network, it flags its neighbors to check if they have addresses. If the neighboring nodes have addresses, the new node relays this information to the host and requests its own address. If the neighbors do not have addresses, they collectively ping the host, initiating the address assignment process. The host then assigns new addresses, integrates the new node into the network, and updates its global address library.
- **Node Disappearance**: When a node disappears unexpectedly, neighboring nodes detect the absence and notify the host. The host triggers a re-scan of the network to remove the missing node from the address library and updates the network's topology. This ensures the network maintains a robust connection, even in the case of node failures, by dynamically rerouting communication paths and reconfiguring the topology.

Data Transmission and Host Role. The central host is responsible for continuously monitoring the network, polling the nodes, and transmitting sensor data.

- **Polling and Monitoring:** The host polls the nodes at regular intervals, reading sensor data and writing new commands when necessary. This polling ensures that all nodes remain synchronized and that the host has a complete view of the network's real-time state.
- **Data Aggregation and Transmission via USB/BLE:** Once the host has collected data from the various sensor nodes, it sends the aggregated information to an external system, such as a PC, via USB or BLE. This process ensures that sensor data is continuously available for logging, analysis, or further processing by the external system.

Global Coordinate Map of the Network. From the combination of node addresses and their sensor data, the host is capable of constructing a coordinate map of the entire network. This map represents the physical or logical layout of all nodes and their connections, enabling external systems to visualize the structure of the network. As new nodes are added or existing ones disappear, the host continuously updates the coordinate map to reflect the current state of the network. This global map can be shared with external systems via USB/BLE, allowing real-time monitoring and providing a complete view of the network's topology.

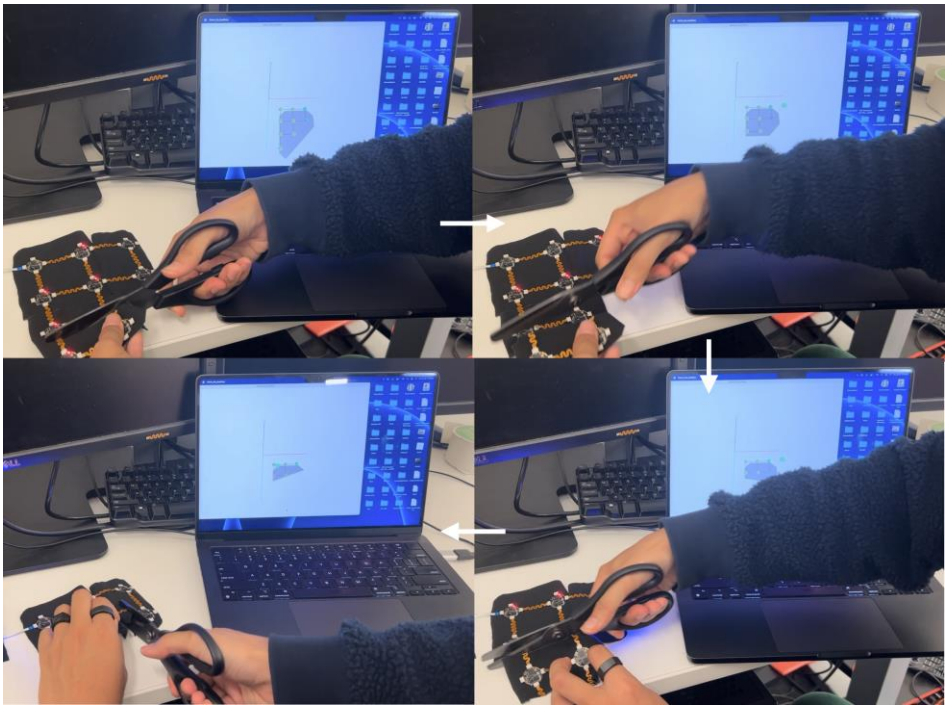

Figure 6.16: Real-time visualization of NETS while its being cut.

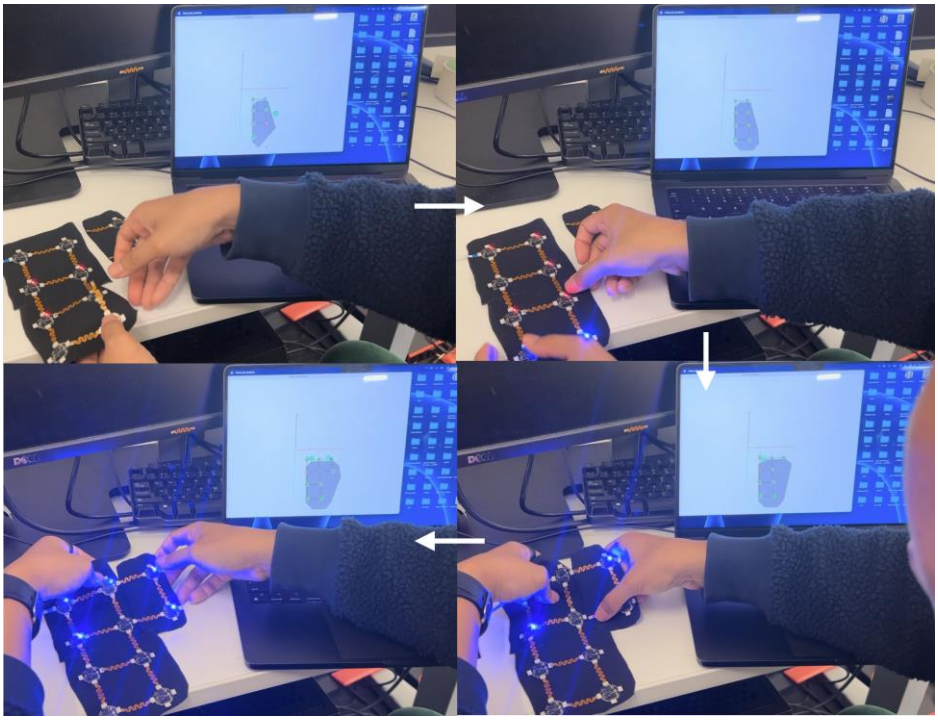

Figure 6.17: Real-time visualization of *NETS* while its being rejoined.

As shown in Figure 6.16 and 6.17, we have developed a visualization tool using Processing that receives real-time data via Serial communication from the sensor nodes and central host. This software processes the incoming data stream to generate a dynamic network map of the entire *NETS* network. The visualization provides a live representation of all nodes, their addresses, and the interconnections between them. As the *NETS* fabric is physically manipulated—such as when the fabric is cut, reconnected, or rearranged—the software detects these changes immediately and updates the network map in real-time, taking inspiration from projects such as *Z-Tiles* [122]and cuttable sensate sheets [126], [287].

This live updating process demonstrates the self-aware nature of the system, as it continuously monitors the status of all nodes and interconnects. The fault-tolerant aspect of *NETS* is thus visualized as the system adapts to changes without manual intervention, showing its ability to update and maintain connectivity. Moreover, the plug-and-play capability of the *NETS* network is emphasized as new nodes are seamlessly integrated into the network and visualized on the map.

6.5.2: I2C Communication and Data Structure

In theory, each host in the network can address a maximum of 128 peripheral nodes, with address values ranging from 0x00 to 0x7F. As previously discussed, while the allocation of addresses happens incrementally, the propagation of address assignment in all directions results in a somewhat random distribution of addresses across the sensor network. Additionally, these addresses are subject to complete reassignment whenever the network is reset. This dynamic operation ensures that each node maintains a unique address, with no risk of duplication, even as the network evolves.

In the event of an address collision—a scenario where two devices inadvertently attempt to use the same address—I2C arbitration mechanisms come into play. Specifically, when a collision is detected, an interrupt flag is generated in the losing device, signaling the host that arbitration has been lost. By processing this interrupt flag, the communication remains reliable, as the device that lost arbitration can retry the transmission. However, such collisions are rare, especially in networks with only one host managing address assignments.

One key factor influencing the performance of the I2C backbone bus is the speed at which it operates. This speed directly impacts the number of nodes that can be supported on a single patch. The bandwidth requirements of the I2C bus depend on several factors, including the number of nodes, sensor sampling rates, and the resolution at which each sensor is sampled.

Running the bus at a fast-speed mode of 3.4 Mbps would impose significant constraints on the length of the bus lines, as longer distances would cause signal degradation and timing issues. Conversely, running the bus at the standard speed of 100 Kbps would not provide enough bandwidth to support a large number of nodes, especially in networks with high sampling frequency.

As a compromise, the I2C bus in this system operates at high-speed mode of 400 Kbps. This speed allows the network to strike a balance between communication reliability and the number of nodes supported. The 400 Kbps speed provides sufficient bandwidth for handling data from a moderate number of sensor nodes while maintaining a stable communication link over typical interconnect lengths considering their load resistance and parasitic capacitance (Section 6.7).

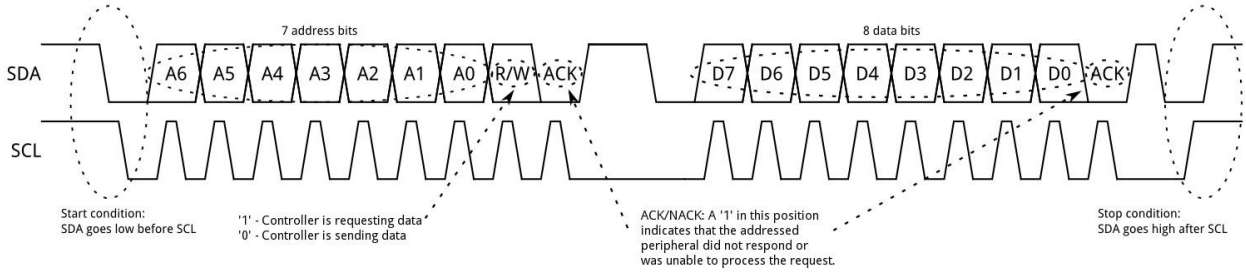

Figure 6.18: I2C messaging basic protocol (reprinted from [288]).

As shown in Figure 6.18, the I2C messaging protocol begins with a start condition, where the SDA transitions from high to low while the SCL remains high. This start condition signals the initiation of communication on the I2C bus. After the start condition, the next 7 bits represent the device address of the target node. These address bits are followed by an ACK/NACK (acknowledge/no acknowledge) bit. If the target device successfully receives the address, it will send an ACK by pulling the SDA line low; if it does not, a NACK is sent, and the SDA line remains high.

Following the ACK/NACK, the data bits are transmitted, which represent the actual payload being sent to or from the node. The behavior of the SDA and SCL lines continues to alternate as data bits are clocked out, with each byte being followed by an ACK/NACK to confirm receipt. The communication concludes with a stop condition, where the SDA transitions from low to high while SCL is held high. This signals the end of the transmission, allowing other devices on the I2C bus to initiate communication.

Although I2C protocol efficiently manages communication, it lacks a built-in mechanism for error checking. Given the growing complexity of multi-node networks and the potential for transmission errors, ensuring data integrity becomes essential. This limitation stems from the original purpose of I2C, which was designed for communication between components on a single

board, where the probability of error is relatively low. As the scale of communication increases, such as in multi-node networks, Packet Error Checking (PEC) becomes crucial to ensure data integrity. One method to enhance error checking in I2C communication is by implementing a Cyclic Redundancy Check (CRC), specifically CRC-8, to detect transmission errors [289].

The CRC-8 algorithm can be applied to the data packet, adding an 8-bit checksum at the end of the packet to verify its integrity. This checksum is calculated based on the transmitted data and is appended to the last byte of the packet. Upon receiving the packet, the receiving device performs the same CRC-8 calculation on the received data and compares the result with the transmitted checksum. If there is a mismatch, it indicates that an error occurred during transmission. By integrating CRC-8 at the last data packet, we can significantly improve the reliability of data communication in I2C, especially when dealing with long-distance or multi-node networks prone to transmission errors.

The interaction between the host and the peripheral nodes is managed using the *Wire* library. The host initiates communication by calling *Wire.requestFrom(address, bytes)* to request data from a specific peripheral node. Once the request is made, the peripheral node responds by sending the requested data packets. On the peripheral side, the function *onRequest()* is used to define what data the node should send when a request from the host is received. This function typically packages sensor data and other relevant parameters, such as deviceID into a format that the host can interpret and use. The communication is also bi-directional, meaning that not only can the host request data from the peripheral, but the peripheral can also send data packets to the host when needed. In this case, the host can define an *onReceive()* function, which is triggered whenever the peripheral sends data to the host. This allows the host to handle unsolicited data sent by the peripheral, such as sensor triggers or error states. The peripheral node sends the data using the *Wire.write().*

The *NETS* data packet contains comprehensive information about each node, including its own ID, neighboring addresses, and sensor data. The complete structure of this data packet is shown in Table 6.1, where each field contains critical data about the node's state and sensor readings.

Field	Description	Data Type	Value
deviceID	Node address	byte	c[0]
bottom_neighbor_addr	Bottom neighbor address	byte	c[1]
right_neighbor_addr	Right neighbor address	byte	c[2]
top_neighbor_addr	Top neighbor address	byte	c[3]
left_neighbor_addr	Left neighbor address	byte	c[4]

proximity	Proximity sensor reading	byte	c[5]
ambient	Ambient light sensor reading	int	c[6], c[7]
red	Red color sensor reading	int	c[8], c[9]
green	Green color sensor reading	int	c[10], c[11]
blue	Blue color sensor reading	int	c[12], c[13]
temp	Temperature sensor reading	float	c[14], c[15]
pres	Pressure sensor reading	float	c[16], c[17]
hum	Humidity sensor reading	float	c[18], c[19]
quat_w	Quaternion W (orientation)	float	c[20] - c[23]
quat_x	Quaternion X (orientation)	float	c[24] - c[27]
quat_y	Quaternion Y (orientation)	float	c[28] - c[31]
quat_z	Quaternion Z (orientation)	float	c[32] - c[35]
accel_x	Accelerometer X-axis reading	float	c[36] - c[39]
accel_y	Accelerometer Y-axis reading	float	c[40] - c[43]
accel_z	Accelerometer Z-axis reading	float	c[44] - c[47]
magnet_x	Magnetometer X-axis reading	float	c[48] - c[51]
magnet_y	Magnetometer Y-axis reading	float	c[52] - c[55]
magnet_z	Magnetometer Z-axis reading	float	c[56] - c[59]

Table 6.1: Complete data packet

deviceID	Starting address	Value

Table 6.2: Data packet format

Node Address (0-128)	1 (c[x])	4 bytes

Table 6.3: Self-initialization data packet

Node Address (0-128)	5 (c[x])	1 byte

Table 6.4: Proximity data packet

Node Address (0-128)	14 (c[x])	6 bytes

Table 6.5: Environmental (T,P,H) data packet

Node Address (0-128)	20 (c[x])	16 bytes

Table 6.6: IMU quaternion data packet

In the *NETS* network, peripheral nodes are capable of sending a complete data packet of 61 bytes (including one byte for CRC), doing so would significantly reduce the system's sampling rate, especially when multiple nodes are transmitting data concurrently. For instance, if a single node were to send its full 61-byte data packet, it would require transmitting 610 bits (accounting for 10 bits per byte, including overhead). At 400 Kbps, this would take approximately 1.525 ms, allowing a maximum sampling frequency of about 656 Hz. To address this issue, we developed a unique data packet format (Table 6.2) that allows peripheral nodes to send only relevant portions of the data, depending on the context. For instance, during initialization, a node only sends its neighboring addresses, which require just 4 bytes, as shown in Table 6.3.

When transmitting specific sensor data, the node sends only the starting data packet address and the associated byte values for that sensor (Table 6.4). For example, to transmit environmental sensor data (temperature, pressure, and humidity), the node starts at address 14 and sends 6 bytes—2 bytes each for temperature, pressure, and humidity, as outlined in Table 6.5. For IMU quaternion data, the packet starts at byte 20 and includes 16 bytes to cover all quaternion components (w, x, y, z), as detailed in Table 6.6. It is also worth noting that while gyroscope data are available, we omit them in our data packets since the quaternion values inherently contain the orientation information. This streamlined approach minimizes the data load, allowing for faster communication and higher sampling rates while still transmitting all necessary information. This data packet format ensures efficient use of bandwidth, particularly in efficient self-organizing and ad-hoc networks with high sensor density.

In the case of a network with 24 nodes, for example, which was tested in one of our prototypes, the total data transferred in one cycle would be 14,640 bits. This transmission would take around 36.6 ms, limiting the overall sampling frequency to about 27 Hz. Similarly, for a maximum I2C configuration of 128 nodes, the total data load would reach 78,080 bits, requiring approximately 195.2 ms to complete a transmission cycle. In this scenario, the sampling frequency would drop to about 5 Hz, which may be insufficient for real-time applications requiring frequent data updates.

However, it is important to note that these values only represent the time required for data transmission on the I2C bus and do not account for additional delays introduced by the host and peripheral nodes during computation. Both the host and peripheral nodes need to process the data before and after transmission. For instance, the peripheral node may require time to collect sensor data and package it into the data packet, while the host may experience delays while interpreting the incoming data and issuing further commands. Moreover, contention on the I2C bus can lead to further delays if multiple nodes attempt to transmit at the same time, necessitating arbitration and queuing, which can further reduce the sampling rate. As a result, the actual

sampling frequency in a real-world deployment of the *NETS* network is likely to be lower than the theoretical values calculated based solely on transmission times.

To optimize the bandwidth and sampling rates, the system can be designed to adapt based on specific sensor triggers or the importance of sensor data. For example, sensor nodes could be programmed to only send data when certain threshold values are exceeded, such as when a temperature sensor detects a significant change or an IMU sensor detects rapid movement. This approach ensures that only relevant data is transmitted, reducing unnecessary traffic on the I2C bus and freeing up bandwidth for other critical transmissions. For example, if only IMU sensors were used in the NETS network, each node would transmit a reduced data packet of 20 bytes instead of the full 61-byte packet, allowing the maximum sampling frequency for 128 nodes to increase to 18 Hz—an improvement of approximately 3.5 times compared to transmitting the full packet at 5 Hz.

Another effective adaptive strategy would involve prioritizing sensors based on the required frequency and resolution of data transmission, as well as the spatial resolution or the number of sensors needed. By considering both temporal and spatial demands, this approach ensures that the network efficiently allocates resources to the most critical sensors. For instance, IMU and proximity/touch sensors, which are vital for real-time orientation and movement and physical interaction tracking, might require higher transmission frequencies and finer spatial resolutions compared to environmental sensors like temperature or humidity, which typically operate at lower frequencies and may not need as many data points. An event-driven transmission could also be employed, where data is only transmitted when a significant change is detected or in response to specific events. When combined with compressive sensing techniques [290], [291], which allow for the recovery of sparse signals with fewer measurements than traditionally required, this adaptive strategy can lead to even greater improvements in data efficiency and scalability for large-scale sensor deployments.

6.5.3: Peer-to-Peer Networking

In the *NETS* network, peer-to-peer (P2P) communication was implemented in every node, allowing data to be exchanged directly between neighboring nodes without the need to utilize the common I2C backbone bus. This significantly enhances network efficiency by reducing data congestion on the shared I2C bus and enabling faster communication between neighbors. The *SoftwareSerial* library is used to configure 8 pins into 4 TX (transmit) and 4 RX (receive) pins, each representing a communication channel between a node and its four neighbors (top, bottom, left, and right). This method employs a software-based bit-banging technique to simulate serial communication on pins that are not typically hardware UART-compatible. Bit-banging allows

the transmission and reception of serial data on arbitrary GPIO pins, providing the flexibility to manage multiple communication lines simultaneously.

Bit-banging operates by manually toggling the GPIO pins to simulate the clock and data signals of serial communication. This allows the nodes to manage multiple connections without the need for dedicated hardware serial ports. However, while bit-banging is a versatile technique, it can introduce additional software overhead due to the need for the microcontroller to continuously manage the timing of the serial communication. In the case of *SoftwareSerial*, the library handles the timing and communication protocol in software, ensuring that each node can successfully send and receive data from its neighbors.

One of the key roles of P2P communication in *NETS* is to manage the addressing scheme for the I2C backbone. As new nodes are added to the network, P2P communication is used to determine whether neighboring nodes require an address to be assigned. When a node first powers on, it queries its neighbors to see if they have already been assigned an address. This is achieved through the P2P RX and TX lines, where the node sends out a message asking for the address status of its neighbors. If a neighbor responds that it does not have an address, the node initiates a request to the host to assign a new address for the unassigned node.

P2P communication enhances the network's resilience by ensuring that a failure in a single node does not incapacitate communication across the entire system. It also enables better scalability. The P2P protocol facilitates local data handling, allowing clusters of nodes (such as patches of the sensor network) to process stimuli at a local level without overloading the I2C backbone with unnecessary data transmissions. Additionally, P2P communication increases flexibility by providing mechanisms for event-based triggers and low-power operations. For example, a node can interrupt neighboring nodes when a sensor detects an important event, ensuring a timely response without overwhelming the I2C bus. Similarly, neighboring nodes can signal each other to enter sleep or wake-up modes, optimizing power usage in energy-constrained environments.

Moreover, the inclusion of the P2P protocol allows test-bed for information diffusion, agent-based control, and distributed networking algorithms [292]–[294], which would be challenging to implement using only the I2C bus. P2P can also act as a redundant communication channel if the I2C bus becomes overloaded or experiences failures. Nodes with broken I2C connections can still receive messages or be shut down if they are disrupting the common backbone network. If the entire I2C network is compromised, sensor data can also hop between nodes to reach the edge or host node before being transferred to an external system. By enabling these additional layers of functionality, P2P communication significantly improves the resilience and adaptability of the *NETS* network.

6.6: Power Consumption Analysis and Management

In our work, we conducted detailed current measurements to analyze the power consumption of each node during various operational modes. The primary objective was to understand the power demands of each component and identify opportunities for optimization. As shown in Figure 6.19a, the power consumption is broken down into various sensor components, including the IMU, microprocessor, environmental sensors (temperature, humidity, pressure), proximity/light sensor, and LEDs. Notably, the RGB LED emerged as the most power-hungry component when active, consuming the majority of current during operation.

We measured the power usage of the IMU, which draws 12 mA during active use, but can be reduced to 2 mA when placed in suspend mode. Similarly, through low-power management techniques, such as using a real-time clock (RTC) to schedule sensor activity, we can reduce the power consumption of the microprocessor to 1.76 mA by placing it in standby mode and turning off all sensors. This approach significantly reduces the node's overall power consumption, making it more suitable for long-term, low-energy applications.

We defined four distinct power modes based on the operational status of the sensors and microprocessor, as illustrated in the power modes chart:

- **Mode 1:** All sensors active, RGB LED on intermittently: In this mode, the IMU, environmental sensors, and proximity/light sensor are all operational, and the RGB LED is periodically activated. This mode consumes the most power, with current levels reaching up to 50 mA.
- **Mode 2:** All sensors active, RGB LED off: In this mode, the RGB LED is turned off, reducing overall power consumption to approximately 20-25 mA. This is a power-saving option when visual feedback is not required but sensor data is still necessary.
- **Mode 3:** IMU in suspend mode, microcontroller in idle, environmental and proximity sensors active: The IMU is placed in suspend mode, reducing its current draw to 2 mA. The microcontroller is set to idle mode, while the environmental and proximity sensors remain operational. This mode significantly reduces power consumption, drawing less than 10 mA in total.
- **Mode 4:** All sensors asleep, microcontroller on standby: This is the lowest-power mode. All sensors are powered down, and the microcontroller is placed in standby mode, consuming only 1.76 mA. This mode is suitable for situations where data collection can

be paused, allowing the system to poll over P2P or I2C channels and "wake up" when triggered by an external event, such as a sensor interrupt.

As illustrated in the power consumption over time graph (Figure 6.19b), the current fluctuates based on sensor activity and LED usage. Each peak corresponds to the activation of sensors or the LED, while valleys represent moments of inactivity or lower-power modes. These power management strategies allow for flexible, adaptive operation, ensuring that power-intensive components, such as the RGB LED, are only activated when necessary, while maintaining the functionality of critical sensors like the IMU and proxemic and environmental sensors.

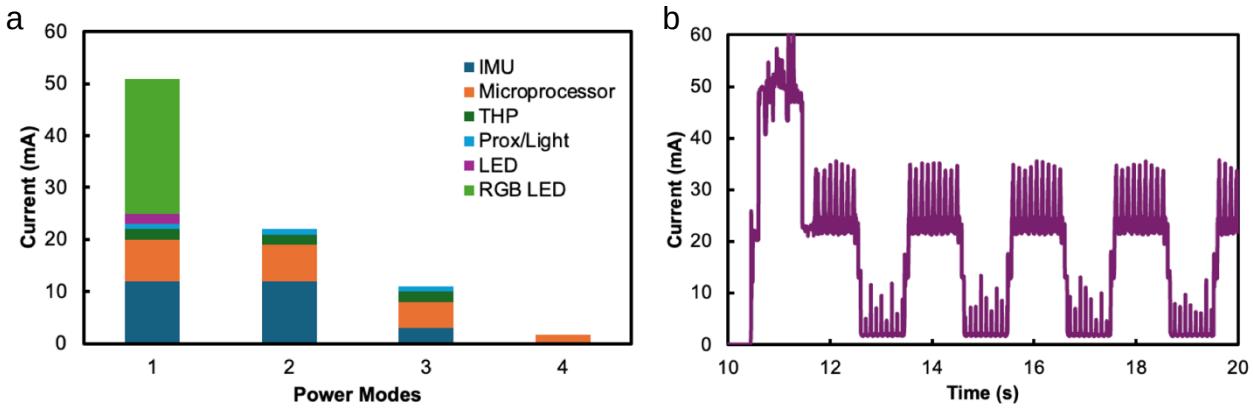

Figure 6.19: a) Distribution of current/power in a node during different modes shown in (b).

To derive an equation for the number of sensors N that can be supported by a battery based on the running time *t*, we start by defining the relevant parameters:

- *C* is the total battery capacity in mAh.
- *I* is the current consumption per sensor in mA.
- *t* is the running time in hours.

Given:

- Battery capacity *C* (mAh)
- Current consumption per sensor *I* (mA)
- Running time *t* (hours)

The total current consumption for N sensors over the running time *t* is given by,

$$N \times I \times t \qquad (6.1)$$

Since the total current consumption cannot exceed the battery capacity *C*, we have.

$$N \times I \times t \leq C \quad (6.2)$$

$$N \leq \frac{C}{I \times t} \quad (6.3)$$

The average current consumption I_{avg} is calculated as follows,

$$I_{\text{avg}} = I_{\text{active}} \times t_{\text{active}} + I_{\text{sleep}} \times t_{\text{sleep}} \quad (6.4)$$

Therefore, the equation for the number of sensors *N* based on the running time *t* is

$$N \leq \frac{C}{I_{\text{avg}} \times t} \quad (6.5)$$

To demonstrate the significance of switching between different power modes in reducing power consumption, refer to Figure 6.20. The figure illustrates the runtime of the *NETS* system with an increasing number of nodes across various power modes. For constant operation in Mode 2, which consumes approximately 22 mA, a network with 16 nodes (configured as 4x4) powered by a 6V, 1200 mAh battery (e.g., 4x AAA batteries) can operate for around 4 hours. This represents the worst-case scenario where all sensor peripherals are constantly active and the entire network continuously transmits data.

However, by adopting dynamic power management, the runtime can be significantly extended. For instance, if the IMU, the second most power-consuming component, is only used for one-third of the time, with the system switching to Mode 4 (where all sensors are asleep and the microcontroller is on standby, and the total average current is reduced) for the remaining time, the runtime can double to approximately 9 hours. If no significant dynamic activity is detected and the IMU remains in sleep mode, while only environmental and proximity sensing peripherals are active for one-third of the time, the system's lifetime can be extended even further, reaching up to 16 hours. This strategic use of different power modes highlights the importance of context-based power optimization in significantly extending the operational life of the *NETS* network while maintaining functionality.

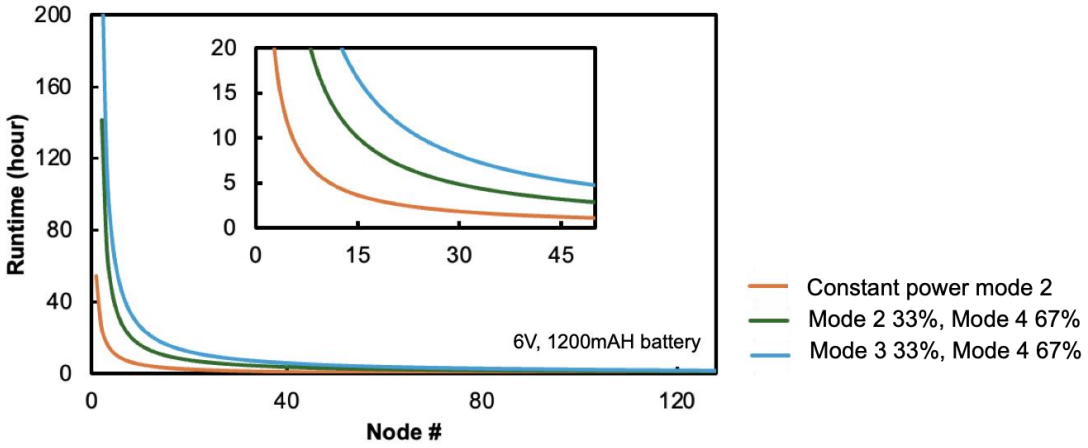

Figure 6.20: Battery usage vs number of nodes and power modes management.

There are even more advanced techniques we can apply to further improve power efficiency beyond the previously mentioned power modes. One approach is to have the node transition between power levels based on its context or detected stimuli. For example, a wake-on-approach feature could increase the sampling rates and initiate intensive sensing when a user is detected nearby through the proximity sensor or when subtle vibrations are picked up by the accelerometer. The node could wake up from stop mode to low-power sleep mode when a stimulus is detected, and if multiple stimuli are recognized, it could transition to standby mode or full-run mode for more intensive processing.

We can also design an attentive, self-organizing network by controlling spatiotemporal resolution (see Figure 6.21). When a node is triggered by a stimulus, it can wake up and execute an algorithm to ping neighboring nodes, prompting them to wake up from sleep and check for interesting events. This neighbor signaling should propagate through the network until the outermost nodes no longer detect any stimuli after their refractory period. This method minimizes power consumption by limiting processing to the nodes around the source of the stimulus.

A possible scenario for this low-power, self-organizing behavior for human interaction could include the following states or modes:

- **Default state:** Most nodes remain in low-power sleep mode, passively monitoring for minimal stimuli like proximity or vibrations.
- **Wake-on-approach** (<15 cm): As a user approaches the smart textile, the proximity sensors detect movement, triggering a wake-on-approach mode. The system responds by increasing the sampling rate and performing more detailed proximity and tactile sensing.
- **Closer proximity detection** (<5 cm): As the user gets closer, proximity sensing becomes more sensitive, increasing the sampling frequency further. Neighboring nodes are also

woken up through peer-to-peer communication, activating them to monitor the user's movements and check for additional stimuli.

- **Touchdown mode** (direct contact): When direct contact or pressure is detected, the system enters touchdown mode. All peripherals, including the IMU, are activated to gather detailed interaction data such as force, orientation, or movement.
- **Power optimization**: Throughout the process, power consumption is minimized by keeping most nodes in sleep mode until necessary, with only the nodes near the stimulus being activated, ensuring energy is used efficiently.

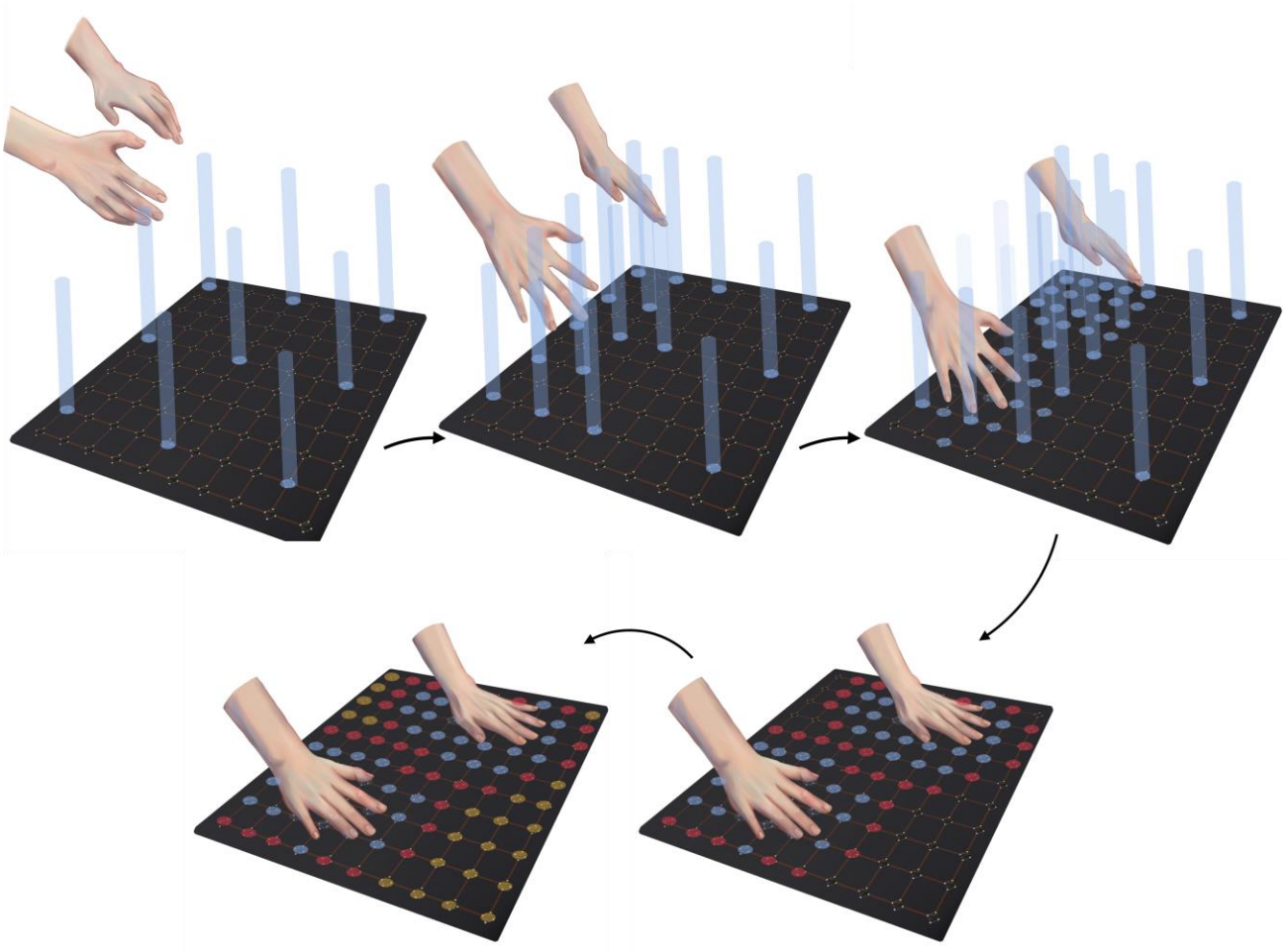

Figure 6.21: Illustration of *NETS* as a testbed for self-aware, attentive, and low-power resource management.

6.7: Voltage Distribution and Parasitic Effects

With the knowledge of current consumption, we can estimate the voltage drop on every node, allowing us to estimate how many nodes can be functional in each interconnect length. To find the maximum number of nodes *k* in a 1D network where each node consumes current, we need to consider the total voltage drop across the network and ensure that the voltage at the last node does not drop below a minimum threshold (Figure 6.22a). Given a supply voltage V_s of 6 V, current per node *I* of 22mA (all sensing peripherals running), serpentine interconnect resistance R (four different lengths), and minimum voltage required at each node $V_{min,}$ which is 3.5 V due to the minimum required supply voltage before regulation to power each *NETS* node (running in 3.3 V).

$$V_k = 6V - \sum_{i=1}^{k} V_{\text{drop},i} \qquad (6.6)$$

$$V_{\text{total\_drop}} = (k-1) \times (I \times R) \qquad (6.7)$$

$$V_s - V_{\text{total\_drop}} \geq V_{\min} \qquad (6.8)$$

Solving for k gives us,

$$V_s - V_{\min} \geq (k-1) \times (I \times R) \qquad (6.9)$$

$$\frac{V_s - V_{\min}}{I \times R} \geq k - 1 \qquad (6.10)$$

$$k \leq \frac{V_s - V_{\min}}{I \times R} + 1 \qquad (6.11)$$

As we know, the resistance of the interconnects with 125 μm width and 5, 10, 25, and 50 cm node-to-node pitch is 0.39, 0.8, 1.95, and 4 Ω, respectively. Using these resistances, we can calculate and plot the voltage drop as *k* scales (Figure 6.22b). Additionally, we also compare this with another interconnect cases with 1 mm width, as shown in Figure 6.21c. For 125 μm width interconnects, which we currently use, we can have up to 21 nodes with a distance of 5 cm from each other, or approximately 1 m in total, or 6 nodes with 50 cm pitch, corresponding to a total of 3 m line. This total length increases as we widen the interconnect width to 1 mm, to 66 nodes and 3.3 m, and 20 nodes and 10 m, respectively.

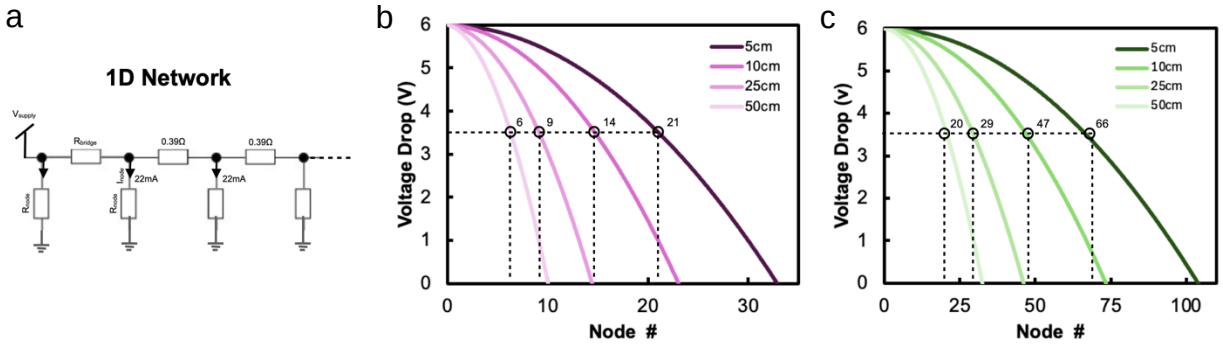

Figure 6.22: a) Equivalent circuit of 1D Network of *NETS*, b) voltage drop based on an increasing number of nodes for every interconnect length or node-to-node pitch and for b) 125µm and 1mm interconnect/trace width, with 3.5V set as the voltage supply threshold for a node to be operational.

In a 2D grid of *NETS*, the voltage at a node (i, j) depends on the cumulative current through the interconnects leading to that node. For simplicity, let's assume the power supply is at the top-left corner (0, 0). The worst-case voltage drop occurs at the farthest node, which is at position $(n-1, n-1)$ in an $n \times n$ grid. The total voltage drop to the node at (i, j) involves the sum of the voltage drops along the paths from the power supply to the node:

$$V_{\text{total\_drop}}(i,j) = \sum_{k=1}^{i+j} k \times V_{\text{drop}} \qquad (6.12)$$

So, the total voltage drop at node (i, j):

$$V_{\text{total\_drop}}(i,j) = \frac{(i+j)(i+j+1)}{2} \times V_{\text{drop}} \qquad (6.13)$$

$$V_{(i,j)} = V_0 - V_{\text{total\_drop}}(i,j) \qquad (6.14)$$

$$V_{(i,j)} = V_0 - \frac{(i+j)(i+j+1)}{2} \times (I \times R) \qquad (6.15)$$

To derive the relationship between the voltage drop and the grid number, we need to express the voltage at the farthest node in terms of the grid size n. For the farthest node in an $n \times n$grid:

$$i = n-1 \text{ and } j = n-1$$

The total distance to the farthest node is:

$$i + j = 2(n-1) \qquad (6.16)$$

The voltage at the farthest node $(n-1, n-1)$is:

$$V_{(n-1,n-1)} = V_0 - (n-1)(2n-1) \times (I \times R) \qquad (6.17)$$

To ensure each node receives at least $V_{\min}$:

$$V_0 - (n-1)(2n-1) \times (I \times R) \geq V_{\min} \qquad (6.18)$$

$$\frac{V_0 - V_{\min}}{I \times R} \geq (n-1)(2n-1), \qquad x = n-1 \qquad (6.19)$$

$$2x^2 + x - \frac{V_0 - V_{\min}}{I \times R} \leq 0 \qquad (6.20)$$

Using quadratic formula of $x = \frac{-b \pm \sqrt{b^2-4ac}}{2a}$:

$$x = \frac{-1 + \sqrt{1 + \frac{8(V_0 - V_{\min})}{I \times R}}}{4} \qquad (6.21)$$

$$n \leq \frac{-1 + \sqrt{1 + \frac{8(V_0 - V_{\min})}{I \times R}}}{4} + 1 \qquad (6.22)$$

As depicted in Figure 6.23a, the voltage drop calculation in 2D grid networks, such as *NETS,* becomes more complex due to the nature of voltage distribution across multiple interconnects. In a 1D network, voltage drops are linear and cumulative, but in 2D grids, current flows through multiple neighboring nodes, creating more intricate voltage drop patterns. To better understand this behavior, we examine two specific interconnect widths—125 μm and 1 mm—across different node-to-node pitch distances ranging from 5 cm to 50 cm. In each case, we calculate the total number of functional nodes while ensuring that the voltage remains above the minimum threshold.

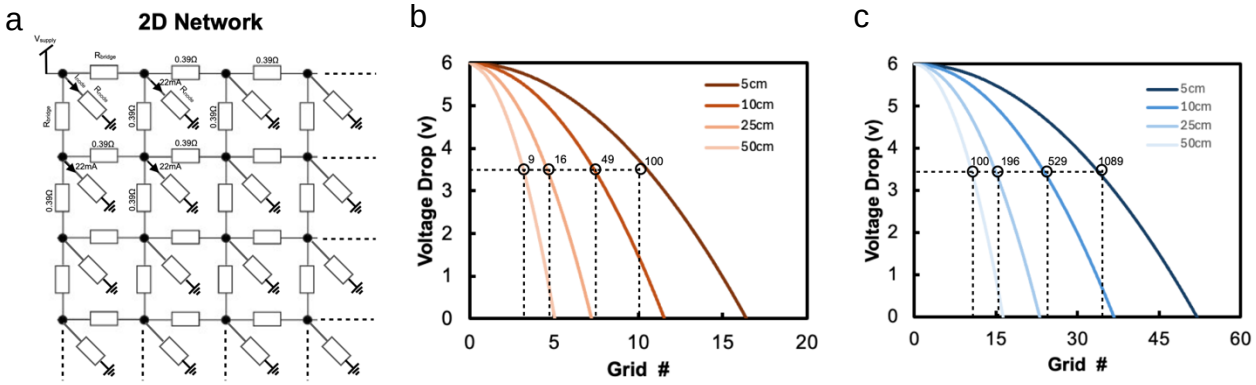

Figure 6.23: a) Equivalent circuit of 2D Network of *NETS*, b) voltage drop based on an increasing number of nodes for every interconnect length or node-to-node pitch and for b) 125µm and 1mm interconnect/trace width, with 3.5V set as the voltage supply threshold for a node to be operational.

For the 125 µm width (Figure 6.23b), the total number of nodes that can be supported in the network is determined by the pitch between nodes. For instance, when the node-to-node pitch is 5 cm, the maximum grid size is 10 x 10, allowing for 100 total nodes in a 50 cm x 50 cm area. This size is appropriate for wearable applications, such as covering the surface of a shirt. On the other hand, for a 50 cm node pitch, the maximum grid size is reduced to 3 x 3, which corresponds to 9 total nodes over a 1.5 m x 1.5 m area. Such configurations are better suited for larger surfaces, including walls or facades in smart environments or interactive displays.

When the interconnect width is increased to 1 mm (Figure 6.23c), we observe a significant improvement in the total possible number of nodes, due to reduced interconnect resistance. With a 5 cm node pitch, a 33 x 33 grid, or 1089 nodes, can theoretically be supported in the same 50 cm x 50 cm area. However, this setup is constrained by the I2C address limit, which allows only 128 nodes per host. Therefore, while this configuration demonstrates the potential for larger grids, it would require additional design solutions such as multiple hosts or hub systems to overcome the I2C limitation. For the 50 cm node pitch, using the 1 mm interconnect width allows us to achieve a 10 x 10 grid, totaling 100 nodes over a 5 m x 5 m area. This configuration is ideal for large-scale installations, such as a room-sized smart surface or a wall façade in a building. It provides an effective solution for integrating large numbers of functional nodes not only in wearables, but also large-scale architectural applications.

Another challenge that limits the number of possible nodes in an I2C network is parasitic capacitance on the communication lines. In an I2C bus operating at 400 kbps, the maximum allowable parasitic capacitance is typically 400 pF to ensure proper signal integrity and timing.

As the physical length of the wires increases, parasitic capacitance accumulates, further constraining the number of nodes that can be connected (Figure 6.24a). Parasitic capacitance in the I2C bus arises from the RC constant, where R represents the 1 kΩ I2C pull-up resistor, and C is the combined capacitance of two interconnects (5 cm pitch) and a node. The RC constant can be directly measured by probing the rise time of the I2C signals.

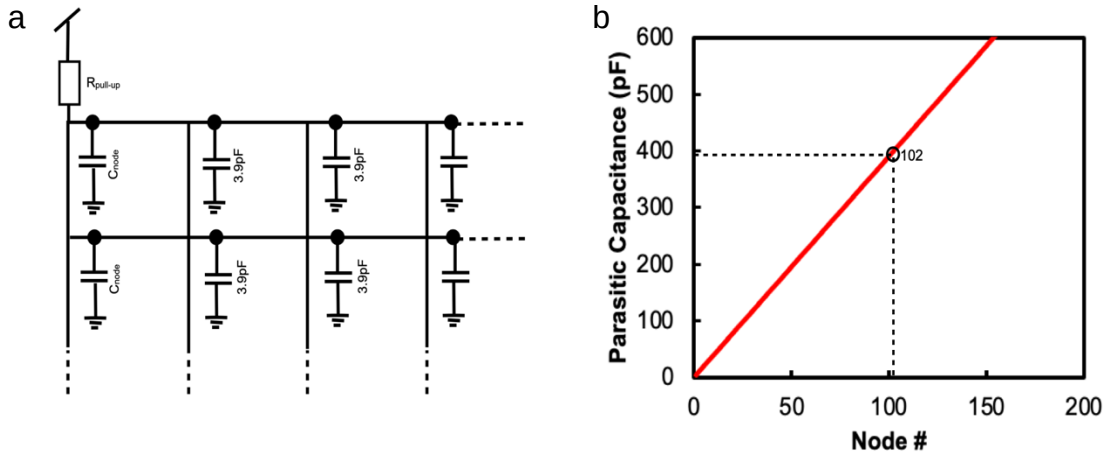

Figure 6.24: a) Equivalent parasitic capacitance in a 2D Network of *NETS*, and b) increasing value of total parasitic capacitance as the node scales, with I2C limit of 400pF.

Each node connected to the I2C bus contributes approximately 3.9 pF of capacitance. Therefore, the number of nodes is directly limited by the total capacitance of the bus. As shown in Figure 6.24b, we can calculate the maximum number of nodes that can be accommodated before the parasitic capacitance reaches its limit. The maximum allowable capacitance for a standard I2C bus at 400 kbps is 400 pF. Given that each node adds 3.9 pF, a maximum of 102 nodes (lower than the possible 128 number of I2C addresses) can therefore be connected to the I2C bus under these conditions. If the capacitance exceeds this threshold, the rise and fall times of the signals will degrade, disrupting the timing requirements of the I2C protocol and leading to potential communication failures.

As the length of the I2C lines increases, the parasitic capacitance also increases, which adds further constraints to the network. Longer wires pick up additional capacitance from the surrounding environment and the physical characteristics of the wiring, thereby reducing the number of nodes that can be connected to the bus. Therefore, we need to optimize both the node layout and interconnect lengths to minimize the total parasitic capacitance and ensure the I2C bus can operate reliably and optimally.

6.8: Prototype and Application Development

With the node and interconnect options available, we have developed *NETS* to scale across different domains—from objects, clothing, and upholstery to building-scale applications. These use cases span across wearables, smart objects, responsive surfaces, and even sensate linings or facades. By utilizing shorter interconnects, we can tune the resolution of *NETS* throughout a fabric surface, adjusting node amount and density based on application requirements.

6.8.1: Wearable and Mobile Sensing

We implemented peripheral nodes in 19 distinct locations on a long-sleeve shirt and connected a BLE-integrated host node in addition (running in 5 Hz) to demonstrate *NETS* robustness for dynamic wearable sensing. The configurability of the network enables *NETS* to function as a motion capture suit, with strategically placed nodes on critical body sections to capture upper-body movements. This setup ensures that at least one node is positioned on key sections such as the shoulders, elbows, and arms. As shown in Figures 6.25 and 6.26, we plotted the data from node #2 and node #6 in real-time as a person actively moved their arms and shoulders. The IMU data changed correspondingly with the body movements, accurately capturing the dynamic nature of the arm and shoulder movements. Additionally, as the room brightness increased, the ambient light sensor data showed a significant spike, demonstrating the system's ability to sense changes in environmental conditions.

In this demonstration, the IMU and proximity sensors' update rates are set at 50 Hz, while the other environmental sensors (including ambient light, RGB, humidity, temperature, and pressure) operated at 1 Hz. To signify low-frequency data transfer to the host, a red LED blinked with each 1 Hz timer event. The blue LED trigger (Figure 6.25a,c) indicated that the proximity sensor reached a certain threshold, reflecting in the sensor data when the user's other arm hovered over, tap, or touch it.

Figures 6.27 and 6.28 also show *NETS*' response in node #5 and node #8 as the user exited the building and performed exercises (such as jumping jacks). During the exercise, the IMU data reflected the dynamic physical movements, while the environmental sensors (humidity, temperature, and ambient light) recorded significant changes due to the transition from an indoor to an outdoor environment. The ability to maintain reliable connection and data communication, even while performing dynamic activities where interconnects were stretched frequently, demonstrates the reliability of the *NETS* platform in wearable and dynamic settings.

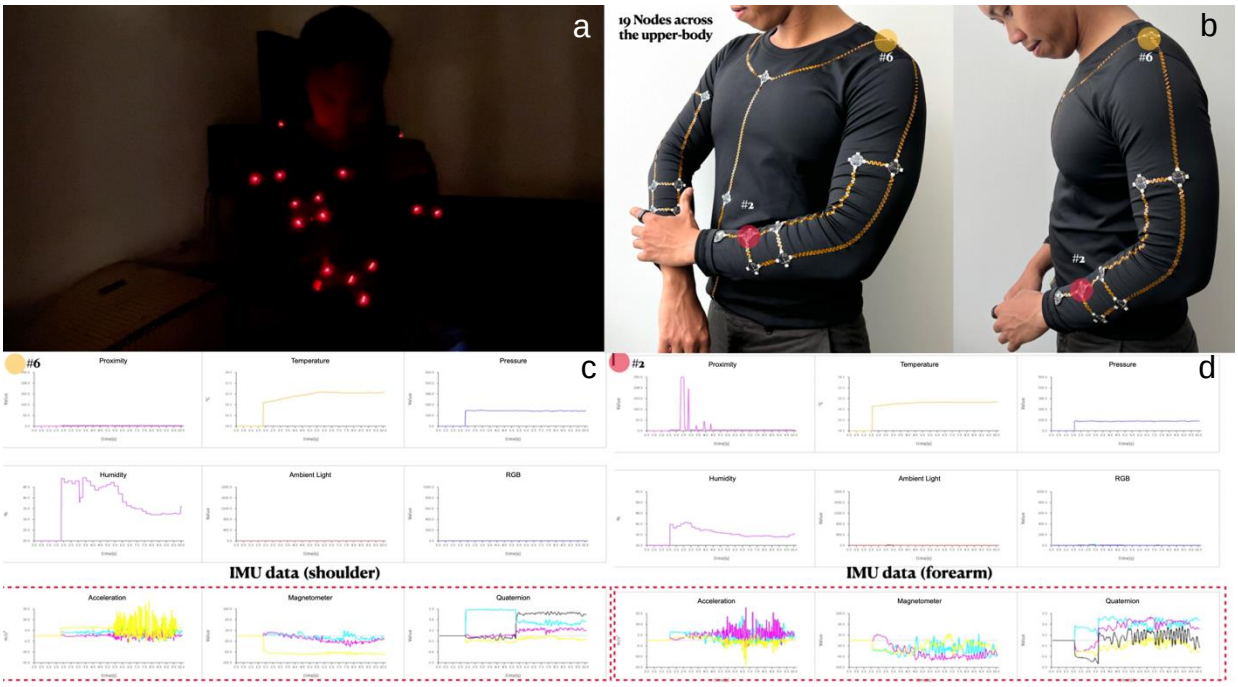

Figure 6.25: a-b) Real-time testing of 19 nodes of *NETS* during indoor activity showing c-d) the multi-modal sensor data in node #2 and #6 (active response shown in the IMU data).

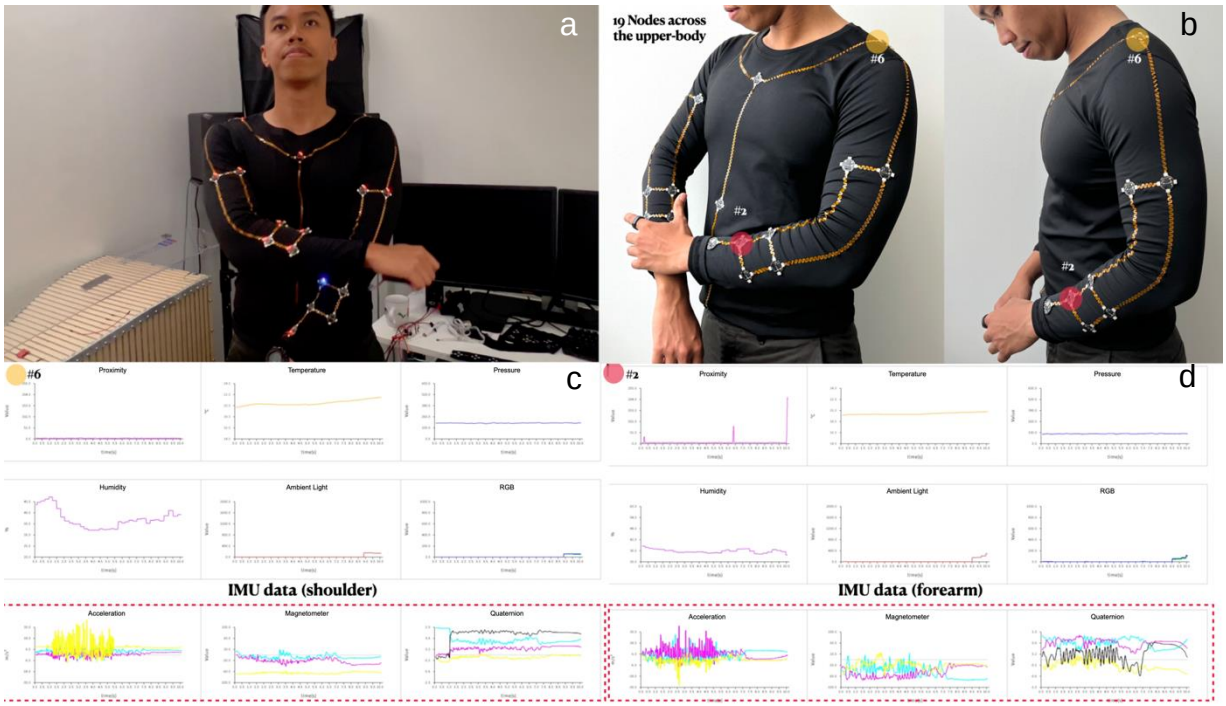

Figure 6.26: a-b) Real-time testing of 19 nodes of *NETS* during indoor activity showing c-d) the multi-modal sensor data in node #2 and #6. (active response shown in the IMU data).

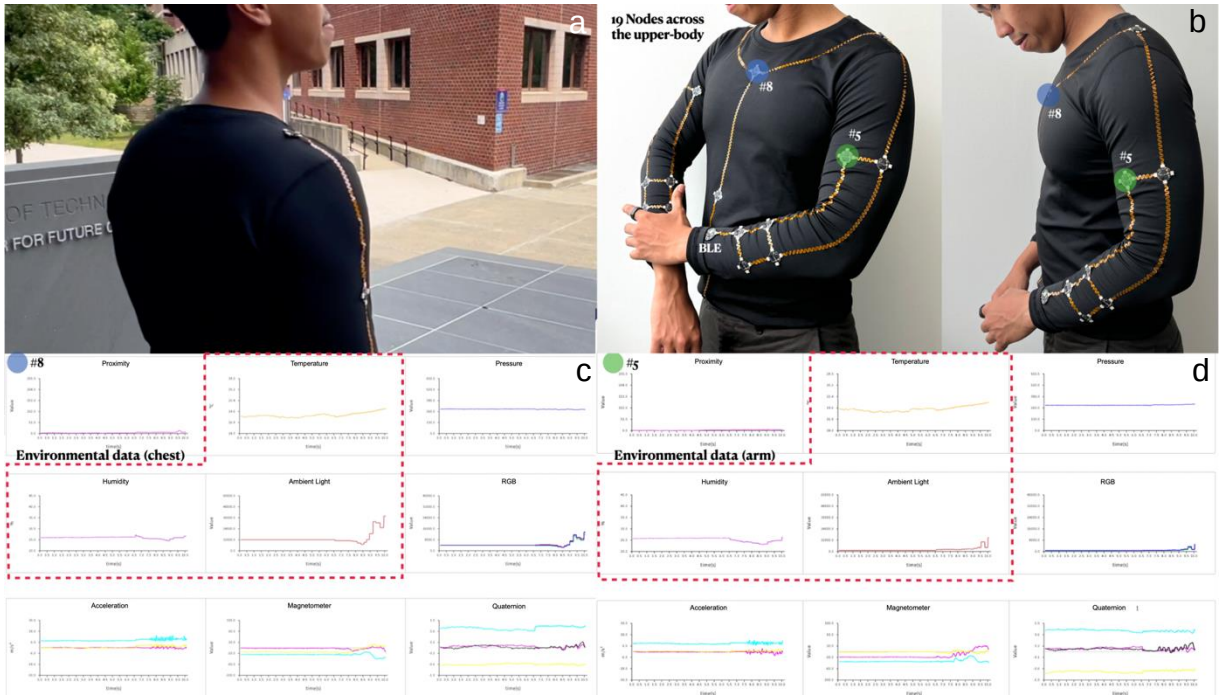

Figure 6.27: a-b) Real-time testing of 19 nodes of *NETS* during indoor activity showing c-d) the multi-modal sensor data in node #2 and #6. (active response shown in the IMU and environmental: humidity, light, and temperature data).

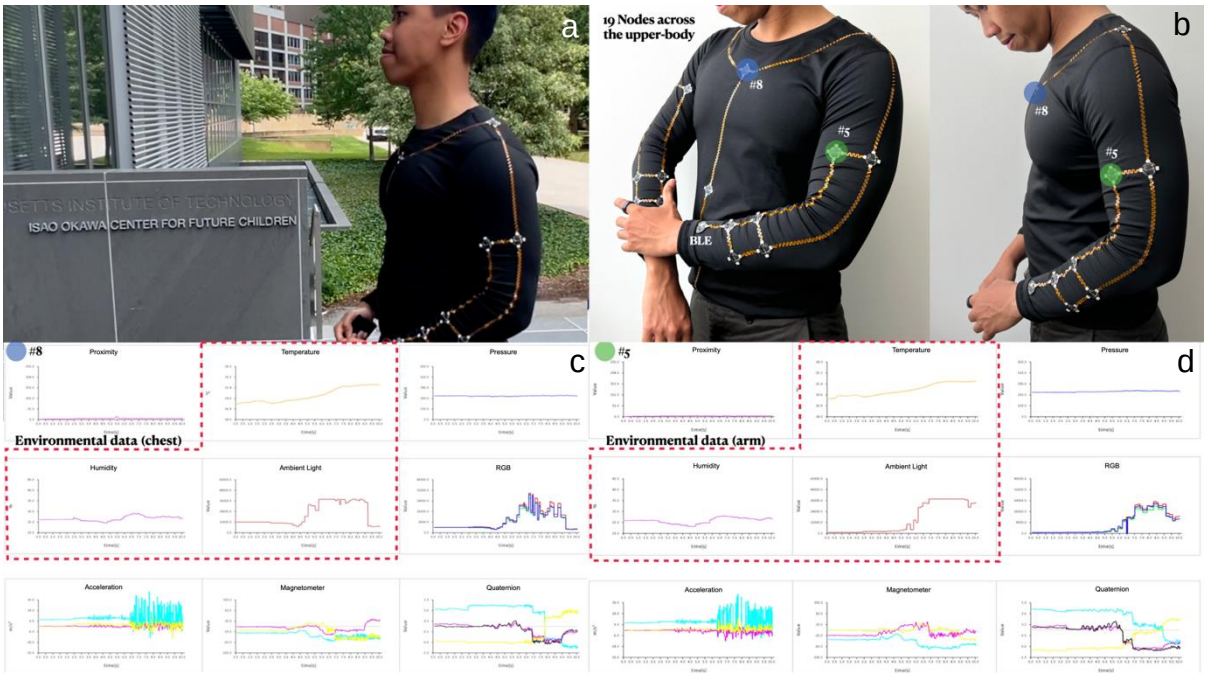

Figure 6.28: a-b) Real-time testing of 19 nodes of *NETS* during indoor activity showing c-d) the multi-modal sensor data in node #2 and #6. (active response shown in the IMU and environmental: humidity, light, and temperature data).

6.8.2: 3D Shape and Deformation Sensing

In shape sensing applications, IMU network can provide highly accurate positional and orientation data by leveraging each of the node's distribution and location relative to each other. These sensors, equipped with accelerometers, gyroscopes, and magnetometers, enable tracking the rotation and translation of connected nodes across predefined distances in both one-dimensional (1D) and two-dimensional (2D) configurations. IMUs have proven effective not only for detecting simple linear or planar shapes but also for capturing complex 3D shapes and deformations in real time. IMUs combine multiple sensing modalities:

- **Accelerometers**: Measure linear acceleration in the X, Y, and Z directions, giving a sense of the movement along different axes.
- **Gyroscopes**: Measure rotational velocity, providing data on how an object is rotating in space.
- **Magnetometers**: Measure the magnetic field, which helps to correct orientation drift that can occur in gyroscope measurements over time.

Together, these sensors enable the detection of both rotational and translational movements. The integration of the magnetometer is particularly important for correcting the orientation in 3D space, as it provides an absolute reference based on the Earth's magnetic field. In this work, we assume boundary conditions where each node is fixed within a certain distance and can only curve in one direction. This constraint means that the distribution of nodes also informs the resolution of the shape-sensing, ensuring that the network accurately captures the curvature and orientation of the surface it is sensing.

1D Network. The core idea behind a 1D network of IMUs is that each node's position and orientation are determined by its left neighbor and its own quaternion, as previously demonstrated by *SensorTape* [126]. A quaternion represents the orientation of the IMU in space, encompassing rotations around three axes: roll (rotation around the X-axis), pitch (Y-axis), and yaw (Z-axis). Each node is connected to its neighboring node by a fixed distance, forming a kinematic chain where the orientation and relative position of each node define the shape of the entire system.

In this context, quaternion algebra is crucial in computing the orientation of each node. The quaternion for each node is computed as:

$$q = [q_w \quad q_x \quad q_y \quad q_z] \qquad (6.23)$$

where q_w, q_x, q_y, and q_z represent the components of the quaternion corresponding to the node's orientation. The quaternion is then adjusted with an additional Euler rotation to ensure that the sensors or coins attached to the nodes are flat, which is achieved by applying a 90-degree rotation around the Z-axis:

$$\text{quat} *= \text{Quaternion.Euler}(0,0,90) \qquad (6.24)$$

Once the quaternion for a node is established, the next step is to decompose the quaternion into its roll, pitch, and yaw components using the following relations:

$$\text{yaw} = \text{atan2}(2 \cdot (q_y \cdot q_z + q_w \cdot q_x), q_w^2 - q_x^2 - q_y^2 + q_z^2) \qquad (6.25)$$

$$\text{pitch} = -\sin^{-1}(2 \cdot (q_x \cdot q_z - q_w \cdot q_y)) \qquad (6.26)$$

$$\text{roll} = \text{atan2}(2 \cdot (q_x \cdot q_y + q_w \cdot q_z), q_w^2 + q_x^2 - q_y^2 - q_z^2) \qquad (6.27)$$

These trigonometric relations enable us to determine the node's orientation in 3D space, which is essential for calculating its position relative to its neighboring node. Given the quaternion-derived roll, pitch, and yaw, we can calculate the new position of each node based on the direction vector between it and its left neighbor. The *direction* vector is defined by the following components:

$$X = \cos(\text{roll}) \cdot \cos(\text{pitch}) \qquad (6.28)$$

$$Y = -\sin(\text{roll}) \cdot \cos(\text{pitch}) \qquad (6.29)$$

$$Z = -\sin(\text{pitch}) \qquad (6.30)$$

This direction vector is normalized to maintain a constant distance between consecutive nodes, ensuring that the 1D network maintains physical consistency. The new position of a node n is computed by adding the direction vector to the position of its left neighbor, where there is a fixed distance between nodes in the network.

$$\text{newPos} = \text{leftPosition} + \text{direction} \times \text{constantDistance} \qquad (6.31)$$

Spline Generation. To create a smooth representation of the nodes' positions, a spline curve is generated using Catmull-Rom interpolation. This process ensures that the nodes' positions are not only determined based on their neighbors but are also interpolated to form a continuous curve. The spline generation process involves defining a series of knots at the nodes' positions,

with additional reference points to improve the smoothness of the curve. The steps to achieve the smooth spline are as follows:

- **Adjacent Pairs of Knots**: For each pair of adjacent knots (denoted as p_1 and p_2), two reference knots are used, $p_0$and p_3. Knot p_0 is the left neighbor of p_1, while p_3 is the right neighbor of p_2.
- **Handling Edge Cases**: If the left or right neighbor does not exist (as at the start or end of the spline), the position of the missing neighbor is replaced by the position of the existing knot. For instance, if p_0 does not exist, the leftmost knot will be used as p p_0.
- **Interpolation Process**: Between each pair of knots, 10 interpolated points are computed, following a cubic polynomial curve. This curve is derived from the positions of p_1, p_2, and their neighboring reference points p_0 and p_3 . The cubic polynomial is formed such that the curve passes through p_1 and p_2 , remaining tangent at the points:

$$\frac{p_2 - p_0}{2}, \frac{p_3 - p_1}{2} \qquad (6.32)$$

This ensures a smooth transition between the knots and reduces any sharp angles or discontinuities in the curve.

Figure 6.29: a-b) Shape-sensing and c-d) circumferential measurement based on 1D Network of *NETS*.

As shown in Figure 6.29, the 1D network can effectively perform line-based shape sensing in 3D, enabling the detection of bending, folding, and twisting in real-time. This capability arises from the network's ability to track the relative positions and orientations of its nodes, each equipped with IMUs. The network can sense curvature along a line or surface by detecting subtle changes in rotation (using quaternion data) and the positional offsets between adjacent nodes. *NETS* self-aware capability can also be extended and represented by its digital twin in a Unity VR environment. The construction of this digital twin is achieved by taking the real-time data from the IMUs—such as quaternion-based orientations, node positions, and shape transformations—and replicating these properties in a virtual model.

In addition to general shape sensing, the system can also perform cylindrical diameter and shape measurement. Cylindrical shapes can be detected by monitoring the proximity of nodes to each other. Specifically, if two nodes come within a threshold distance, this indicates the formation of a circular or cylindrical shape. When such proximity is detected, the cylinder measurement function is triggered, and a virtual model 3D cylindrical object with the corresponding diameter appears (Figure 6.29c,d).

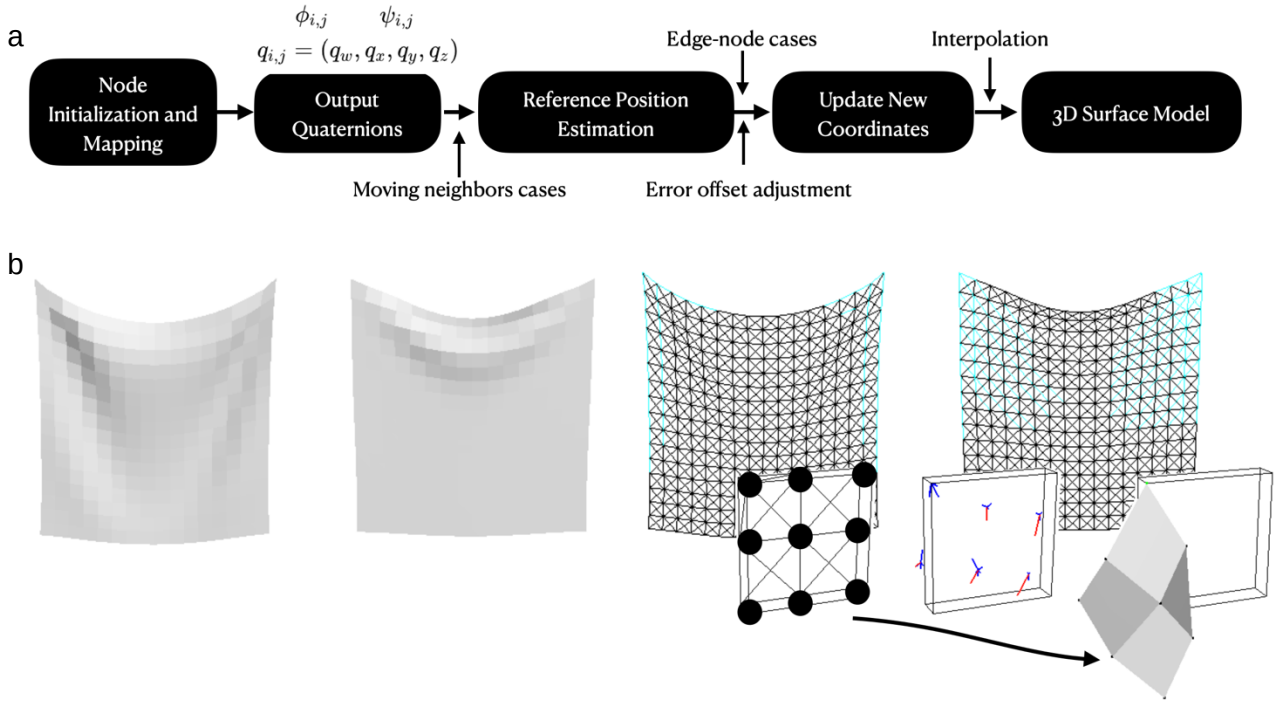

Figure 6.30: a) Block diagram of steps taken to convert *NETS* distributed IMU data into a dynamic 3D fabric model. b) Mass–spring model for cloth simulation/physics involving evenly spaced particles with flexion, spring, and shear connections (adapted from [295]).

2D Network. In more advanced applications, a 2D network of IMUs can be constructed to perform 3D shape sensing, which enables the detection of complex deformations across both planar and curved surfaces. A 2D network expands the capabilities of the 1D network by incorporating an additional dimension for shape detection, allowing for a richer and more detailed representation of how flexible surfaces bend, twist, or fold in 3D space. This section discusses how the 2D network is structured and how quaternion-based calculations are used to determine the relative positions and orientations of nodes in this network (Figure 6.30a).

We are motivated by how cloth is represented digitally in simulations such as those used in Unity [296]. In such systems, a spring-mass cloth system is employed to model the deformation of fabrics. In these simulations, a 2D grid of point masses is connected with structural, shear, and flexion/bend springs, which simulate the mechanical properties of the fabric and allow it to bend, fold, and stretch naturally in response to forces. In our case, the 2D grid of IMUs functions similarly, but instead of point masses connected with springs, we have a grid of points with flexion or bend springs modeled based on distributed IMU data (Figure 6.30b). The IMUs, through quaternion-based orientation and positional data, replace the bending dynamics by providing a continuous stream of data that reflects how the flexible surface behaves in 3D space.

In a 2D network, each node has neighbors in both the horizontal (left or right) and vertical (up or down) directions. The orientation and relative position of each node are computed based on quaternion-based calculations, similar to the 1D network but extended to handle interactions in both directions. Starting with the node network map from the self-initialization of *NETS*, as well as quaternion and direction vector as calculated in Equation 6.23-6.27, we can determine the position of each node based on its relative orientation and it's neighbor's position. This calculation differs depending on whether the node has neighbors to the left, above, or both.

- **If the node has no left neighbor** (i.e., it is on the edge of the 2D grid), the position is calculated relative to the node above. The direction vector is computed based on the pitch and roll angles, ensuring that the node maintains a constant distance from its vertical neighbor:

$$\text{direction} = \begin{bmatrix} -\sin(\text{pitch}) \\ \sin(\text{pitch}) \\ \cos(\text{roll}) \cdot \cos(\text{pitch}) \end{bmatrix} \tag{6.33}$$

  The new position is computed as:

$$\text{newPos} = \text{upPosition} + \text{direction} \times \text{constantDistance} \tag{6.34}$$

- **If the node has a left neighbor**, its position is computed relative to the left node. The direction vector in this case is calculated as:

$$\text{direction} = \begin{bmatrix} \cos(\text{roll}) \cdot \cos(\text{pitch}) \\ -\sin(\text{roll}) \cdot \cos(\text{pitch}) \\ -\sin(\text{pitch}) \end{bmatrix} \qquad (6.35)$$

  The new position is then given:

$$\text{newPos} = \text{leftPosition} + \text{direction} \times \text{constantDistance} \qquad (6.36)$$

- **If the node has both neighbors,** the node's position is influenced by both. The X position of the node is influenced by the left neighbor, the Z position is influenced by the up neighbor, and the Y position is computed as the average of the Y positions of both the left and up neighbors.

$$X_{\text{node}} = X_{\text{leftNeighbor}} \qquad (6.37)$$

$$Z_{\text{node}} = Z_{\text{upNeighbor}} \qquad (6.38)$$

$$Y_{\text{node}} = \frac{Y_{\text{upNeighbor}} + Y_{\text{leftNeighbor}}}{2} \qquad (6.39)$$

  This averaging ensures that the node maintains a balanced position between its neighbors in the Y direction, which helps smooth transitions across the grid.

The direction vector is normalized to ensure that the calculated new position maintains a consistent physical spacing between nodes. This guarantees that the network remains well-formed and accurately represents the real-world deformations being sensed. In all cases, the system also accounts for cases where either the left or up neighbor is moving and updates its position correspondingly.

To ensure the node's position and rotation remain accurate, the system tracks rotation errors and corrects them. If the rotation angles deviate from their expected values, these errors are subtracted from the node's computed angles, ensuring that the node's orientation remains consistent. The combination of quaternion-based orientation and relative position calculations enables the system to track complex as bending, folding, or twisting, across a grid of nodes. In addition, spline generation through 2D interpolation, as utilized in the 1D network, can also be employed to smoothen shape sensing in the 2D system.

In Figure 6.31, we see an experimental setup where each node embedded in the fabric (24 nodes, 4x6 grid) transmits data in ~20 Hz, which is processed through the system's host and sent to the PC through USB. These nodes form a sensor grid that collects distributed IMU data in real-time, feeding orientation and positional information to a 3D digital mesh in a Unity environment. The system allows the virtual mesh to precisely mirror the physical fabric's form, matching the manipulations applied by the user and as it is wrapped on an object.

The visual representation on the monitor shows a real-time synchronization between the fabric's movements and the corresponding virtual mesh, demonstrating how this sensor grid can track dynamic movements. One of the significant advantages of this system is that it enables fabric motion capture without the need for bulky or intrusive trackers. Unlike traditional motion capture systems that rely on cameras or physical markers confined to a specific space, this setup allows freeform movement in unbounded environments. It captures detailed deformations and motions in real-time, making it suitable for a wide range of applications.

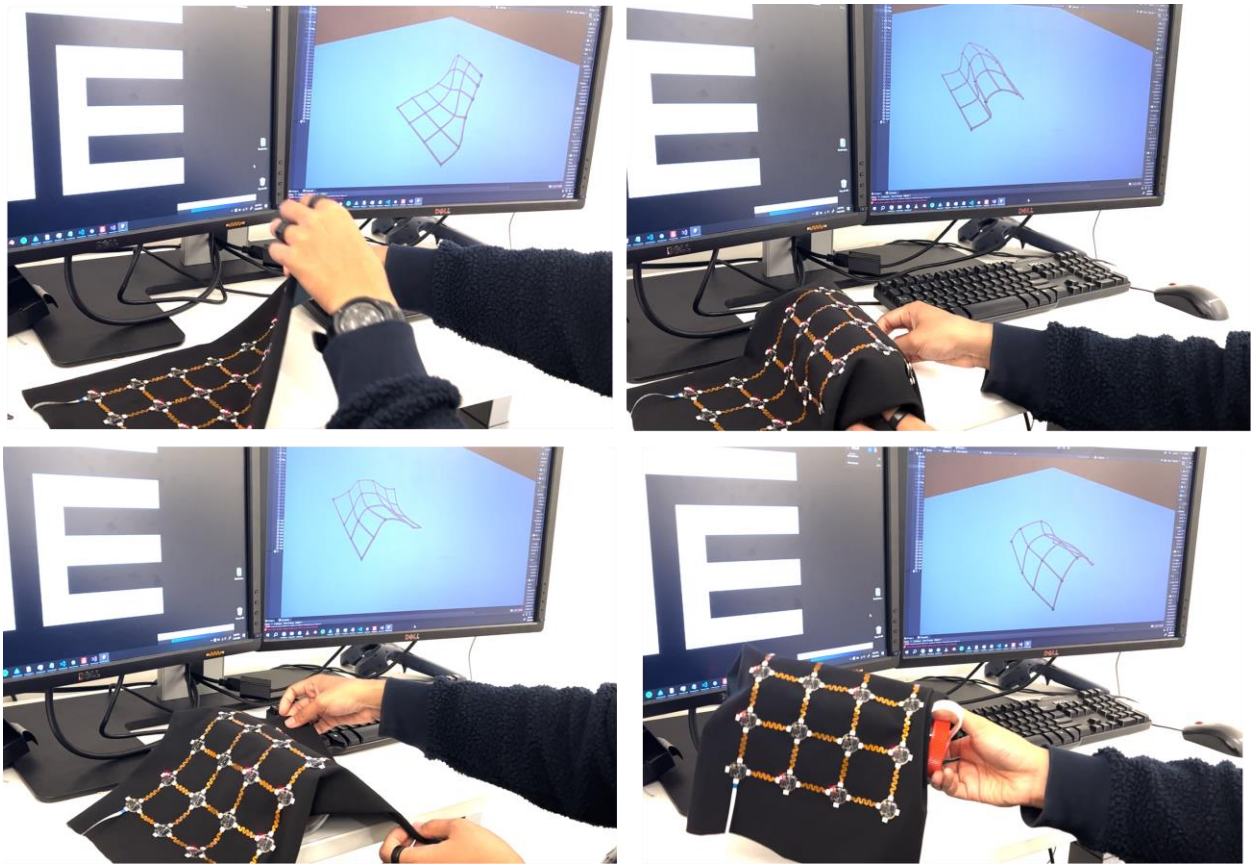

Figure 6.31: Real-time demonstration of 3D shape-sensing based on distributed IMUs.

Shape-sensing System Accuracy and Performance. In order to characterize the performance and accuracy of the shape-sensing system, we conducted a slope measurement using a grid of 24 nodes arranged in a 4x6 configuration, with 5 cm pitch between the nodes (Figure 6.32). This experiment was designed to assess the error across the network under various slope conditions. The goal was to quantify how well the distributed IMU network could detect and track deformations on a planar surface at different angles.

Experimental Setup. In this experiment, a plane object was set at various angles in Unity, and the physical nodes were aligned to match the plane's angle before the system was executed. The leftmost node, serving as the reference node, was anchored to the plane with zero error. The error for the remaining nodes was determined by calculating the shortest distance between each node's position and the plane. The system measured the performance across five different angles: 0°, 15°, 30°, 45°, and 60°. For each angle, the nodes were placed on a slab, and 2000 data points were collected for each node over a period of one minute. These data points were then averaged to calculate the 3D positions and distance errors for each node relative to the plane.

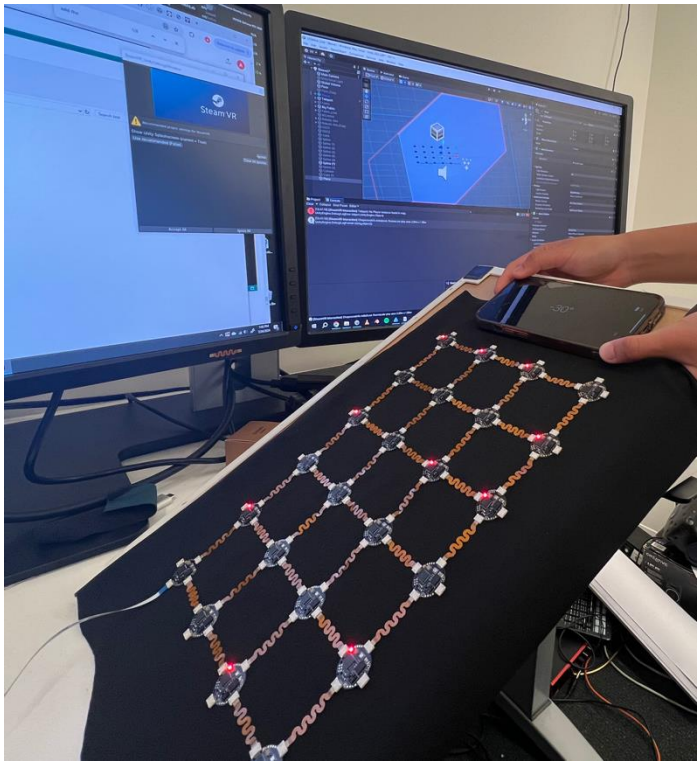

Figure 6.32: Experimental setup for the angle-error measurement tests.

Results and Analysis. Figure 6.33a-e illustrates the error for each row of nodes (with four nodes per row) as a function of the row number, for each of the angles tested. The rows are indexed from the leftmost reference node (Row 1) to the rightmost edge (Row 6). Each graph in the figure shows the distribution of error for the different angles tested—0°, 15°, 30°, 45°, and 60°.

From the data, we observe that the 0° angle produces the smallest error, which is expected due to the flat surface condition minimizing any deformation or angular deviation. On the other hand, the 30° angle shows the largest spread of error, likely due to inconsistencies in angular measurement or sensor calibration, despite not being the steepest slope. The errors for the 15°, 45°, and 60° angles fall between these extremes, indicating that the angle itself does not have a direct linear relationship with error magnitude. We did not experience any significant or noticeable IMU drift for an hour of continuous operation, as drift compensation is automatically managed on-chip.

Additionally, there is a clear linear increase in error as we move from the reference row (Row 1) to the farthest row (Row 6). This increase demonstrates how cumulative error builds up as nodes are positioned further from the reference node. Figure 6.33f highlights that the average error for the farthest row (Row 6) is approximately 12 mm, with a standard deviation of +/- 4 mm. This error translates to approximately 5 cm of average error per 1-meter-wide or long *NETS* fabric using the current system and algorithm. These results indicate that while the distributed IMU network is accurate for small deformations, cumulative error increases as the distance from the reference point grows.

To address this issue, incorporating calibration at initialization can help reduce errors. Each IMU may be in slightly different positions due to shifts in PCB fabrication and node interfacing with the fabric, which can lead to small discrepancies that accumulate over time. Initial calibration could prevent these discrepancies from propagating through the system. Given the linear relationship between distance and error, compensation techniques can also be applied. By recognizing this linearity, the system can compensate for the increasing error as nodes are positioned further away from the reference, effectively reducing the overall cumulative error. Finally, combining these methods with absolute localization on top of the existing relative positioning system could significantly enhance the accuracy of the IMU network and *NETS* global positioning, particularly for larger deformations and broader fabric surfaces.

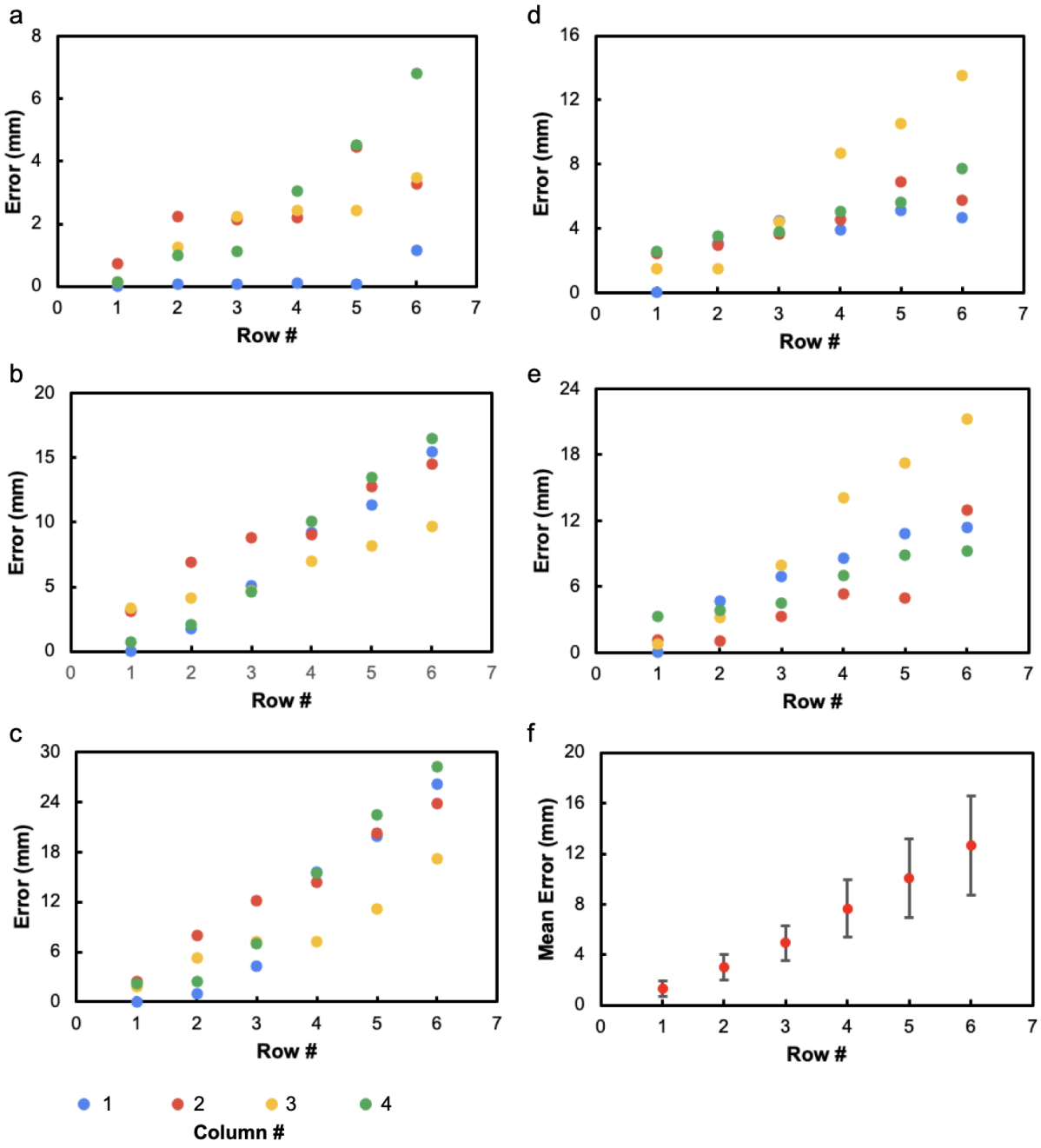

Figure 6.33: Distance error from each node to a reference plane on 2D Network of *NETS* with a) 0°, b) 15°, c) 30°,d) 45°, and e) 60° plane angle, and f) mean error and standard deviation as the number of row grows from all of the error data recorded in a-e).

6.8.3: VR Digital Skin and Smart Sleeve

Other prototypes and applications we have explored are to leverage Unity in mapping real-time sensor data collected from the fabric to corresponding visual effects in a virtual environment. Each sensor embedded in the fabric (24 nodes, 4x6 grid) transmits data in ~20 Hz, which is processed through the system's host and sent to the PC through USB. The data is parsed into various environmental parameters—proximity, humidity, light intensity, temperature, and motion—before being assigned to specific particle effects and visual animations in Unity.

Multi-nodal and multi-modal sensor data visualization in VR. Unity assigns each sensor node to an effect dictionary, where each node has a pre-defined set of animations (such as fog, lasers, auras, etc.) that are activated based on the real-time sensor readings (Figure 6.34a). The sensor data, including proximity, light, humidity, temperature, and IMU (inertial measurement unit) readings, are mapped onto 3D models in Unity, triggering real-time animations and dynamic changes in the visual environment. The animations used were selected from the Unity Asset Store, carefully chosen to correlate the behavior of the fabric with sensor parameters in a way that gives most analogous connection and enhances the interaction, ensuring that the physical actions on the fabric correlate intuitively with their digital counterparts.

Proximity data is among the most interactive aspects of the system. As the user's hand or another object approaches the fabric, proximity sensors detect the distance, triggering both physical and virtual feedback (Figure 6.34b). The proximity value is directly linked to the activation and the brightness of the blue LEDs on the physical fabric, indicating that an object or user is within range. Simultaneously, in the virtual environment, laser-like effects are generated from the node, projecting upward to visualize the distance between the object and the fabric. A key aspect of the proximity sensor is the use of a proximity threshold, which is also used to detect when the fabric is touched. Upon exceeding this threshold (i.e., when the user physically touches the fabric), the system triggers wave or ripple animations around the node, simulating the physical interaction in a visual manner (Figure 6.34c).

Humidity sensor data is mapped to a fog animation in the Unity environment (Figure 6.34d,e). As the fabric detects an increase in humidity around a node, the fog effect is activated. The density and intensity of the fog are directly proportional to the humidity values: higher humidity causes denser fog with more particles emitted from the node. The Particle System controlling this effect in Unity adjusts the fog’s emission rate and particle size in real-time, directly correlating the animation’s intensity to the sensor data.

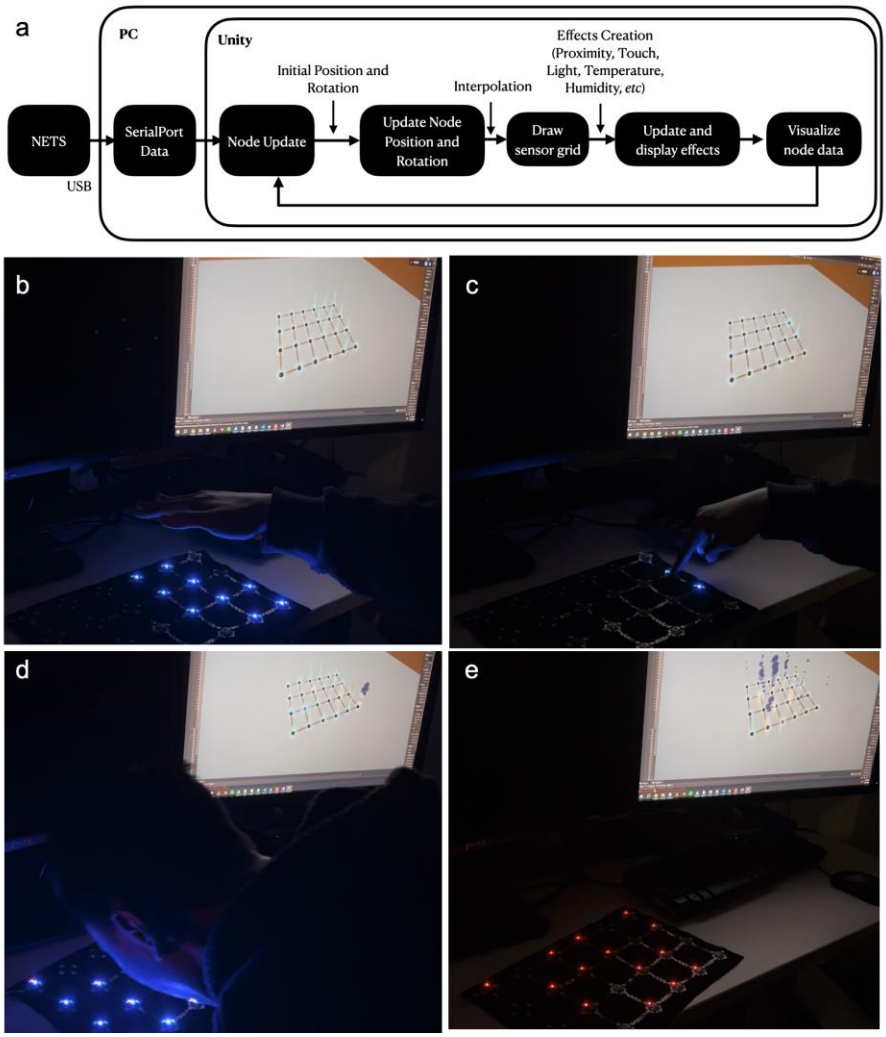

Figure 6.34: a) Flow diagram of multi-modal sensor data visualization using Unity. VR digital-twin of *NETS* with 24 nodes: Proximity sensors detecting b) hand approach and c) taps. d-e) Humidity sensors and their animation as someone blows onto the nodes, creating air flow.

Light intensity plays a crucial role in visualizing node interactions, particularly in dim environments. When a node detects a change in ambient light, a glow effect is triggered in Unity. This glow surrounds each node, becoming stronger as the light intensity increases. In low-light conditions, the glow effect becomes more pronounced, providing real-time feedback that reflects changes in the environment. The glow animation creates an aura around each node, pulsating with varying intensities depending on the light sensor's input, as shown in Figure 6.35a,b. This feedback is especially useful in darker rooms, as shown in the images, where the system becomes highly responsive to its surroundings, visually reflecting the interaction with external light sources.

Temperature data collected by the sensors modifies the aura color around each node, reflecting the environmental temperature. As the temperature increases, the color of the aura shifts from cool blues to warmer reds. This gradual change provides an intuitive visual representation of heat, offering users a clear indication of the ambient temperature based on the node's aura.

The integration of an IMU allows the fabric to detect changes in shape and motion, turning it into a shape-aware digital skin driven in real-time by dense and multi-modal sensor data. The IMU sensors monitor the orientation and movement of the fabric, with real-time data triggering corresponding animations in Unity. These sensors work in tandem with other modalities—proximity, light, humidity, and temperature—enabling a comprehensive multi-modal interaction model (Figure 6.35c,d).

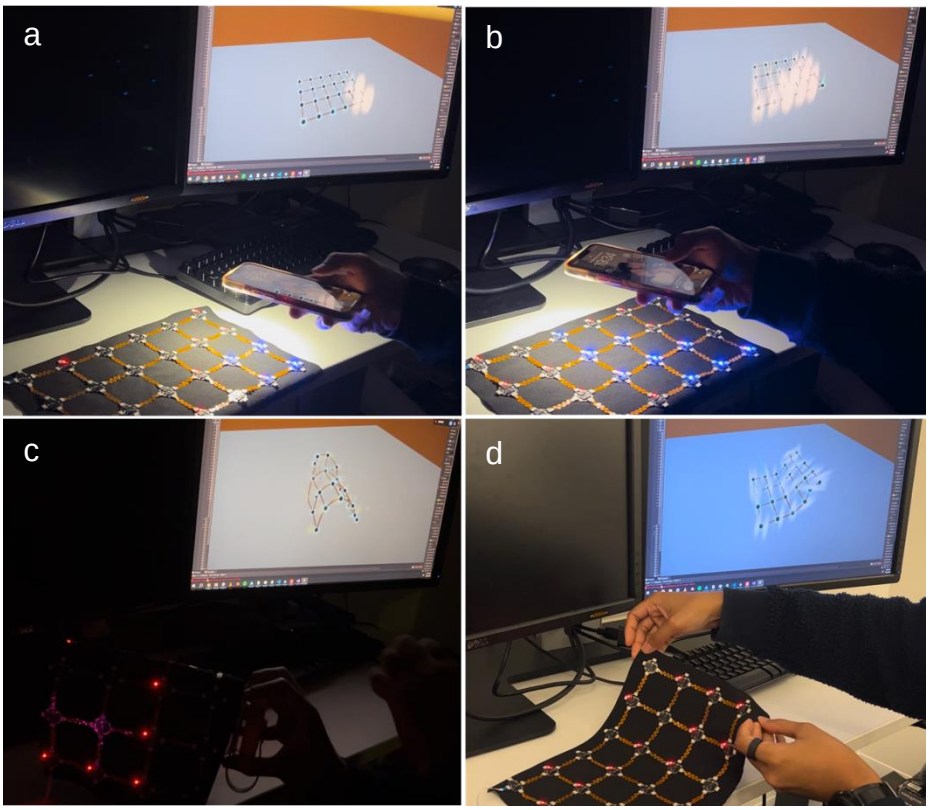

Figure 6.35: VR digital-twin of *NETS* with 24 nodes: a-b) the digital skin reacting to movements of lights, c-d) multi-modal visualization of 3D-shape and illumination sensing.

Shape-Aware Smart Sleeve. One of the key applications of this fabric is the smart sleeve, which utilizes the IMU's shape-awareness to detect when the fabric is wrapped around the user's arm (Figure 6.36a,b). In this cylindrical configuration, the nodes on the sleeve act as interactive buttons

that trigger animations or virtual effects within Unity. This smart fabric interface transforms the textile into a wearable user interface, where sensor data directly controls virtual interactions, as demonstrated in Figure 6.36c,d. By simply touching or moving the fabric, users can manipulate digital objects or trigger immersive animations, all driven by the real-time sensor data collected from the multi-modal sensor network.

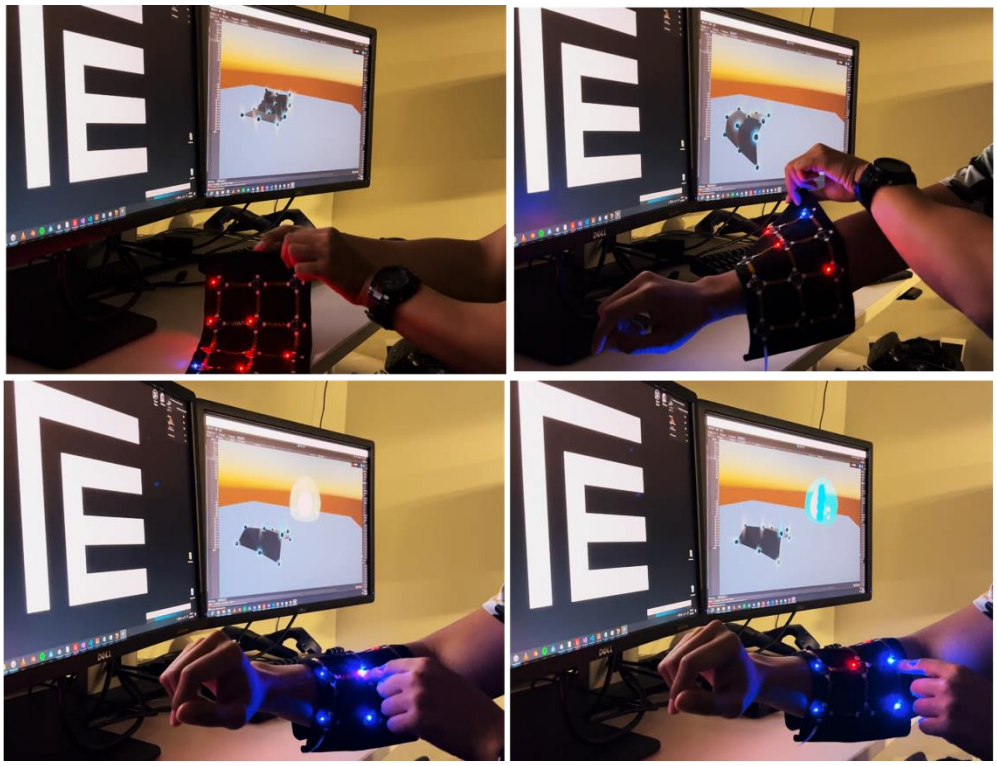

Figure 6.36: VR digital-twin of *NETS* with 12 nodes: a-b) the smart sleeve being wrapped onto an arm, c-d) the nodes can then be used as a controller.

6.8.4: Localization and AR-based Visualization

In the implementation of localization and AR-based visualization for *NETS*, we leveraged our network of RGB LEDs and combined BLE communication, LED tracking via OpenCV, and Apple's ARKit to visualize real-time distributed sensor data in a 3D augmented reality (AR) environment. This system enables spatial tracking of the sensor nodes, mapping the physical layout of the network to a digital twin in AR (Figure 6.37a).

Bluetooth Communication and Data Parsing. The system begins by establishing a connection between the iPhone and the BLE host nodes in the *NETS* network. BLE allows efficient, low-

power communication where the iPhone scans for and connects to the peripheral nodes. Once connected, the sensor data, which is transmitted in hexadecimal format, is parsed by the iPhone and converted into meaningful sensor readings.

We then decode this incoming data, transforming raw sensor readings (temperature, humidity, proximity, etc.) into a format that can be displayed in the AR environment. Each node is identified by a unique device ID, ensuring that the correct data is mapped to the correct virtual sensor in the AR space. BLE communication is processed on a separate thread to avoid interfering with the ARKit visualization, ensuring smooth and real-time updates.

LED Tracking and Color Differentiation using OpenCV. After data parsing, the next step involves LED tracking, which is used to visually locate and differentiate each sensor node in the real world. The camera, accessed via Apple's AVFoundation, captures the physical scene in real-time. The camera's exposure target is adjusted dynamically to handle various lighting conditions, ensuring consistent detection of the LEDs emitted by the sensor nodes (Figure 6.38b).

- **Exposure Target:** Exposure is decreased in bright environments to prevent over-saturation of the LEDs, while in dim conditions, exposure is increased to ensure that the LEDs remain clearly visible. This ensures consistent blob detection and accurate color capture, regardless of the environment.
- **OpenCV Blob Detection:** OpenCV is utilized to detect the LEDs by applying a thresholding technique that isolates bright blobs (the LEDs) from the rest of the image. Each detected blob is analyzed, and its average color is computed. The system then compares the detected RGB color to a set of pre-mapped colors for each sensor node, converting them to HSL (Hue, Saturation, Lightness) format to simplify the comparison process. The system minimizes color distance based on hue and identifies the corresponding node's device ID.

2D to 3D Mapping of *NETS*. After the LEDs are identified, the system maps the 2D image coordinates of each LED to the AR space using ARKit. ARKit relies on detecting distinct visual elements such as textures, edges, and corners to build a detailed world map, as well as adapting it to its navigation system. By placing the nodes in areas where there are abundant features—like patterned surfaces, well-lit areas, or textured backgrounds—ARKit can more reliably track the environment, reducing the chance of drift or inaccuracy in node placement. In this context, environments that are flat, smooth, or devoid of these features, such as blank walls, should be avoided when precision is required [297], [298]. The 2-3D mapping function is adapted from LightAnchors [299], a method that converts 2D points (LED positions in the camera frame) to 3D coordinates within the AR scene.

- **2D to 3D Translation:** ARKit leverages the iPhone's camera tracking to determine the current position and orientation of the device. Using this information, the mapping function computes the corresponding 3D position of each LED in the AR space. This process ensures the virtual objects in AR maintain correct spatial alignment with their real-world counterparts.
- **Tracking Spatial Relationships:** Once the 3D positions of the sensor nodes are established, ARKit places virtual objects (e.g., spheres or text labels) at these positions, and the objects are continuously updated as new sensor data is received. These virtual objects provide a real-time digital representation of the sensor network.

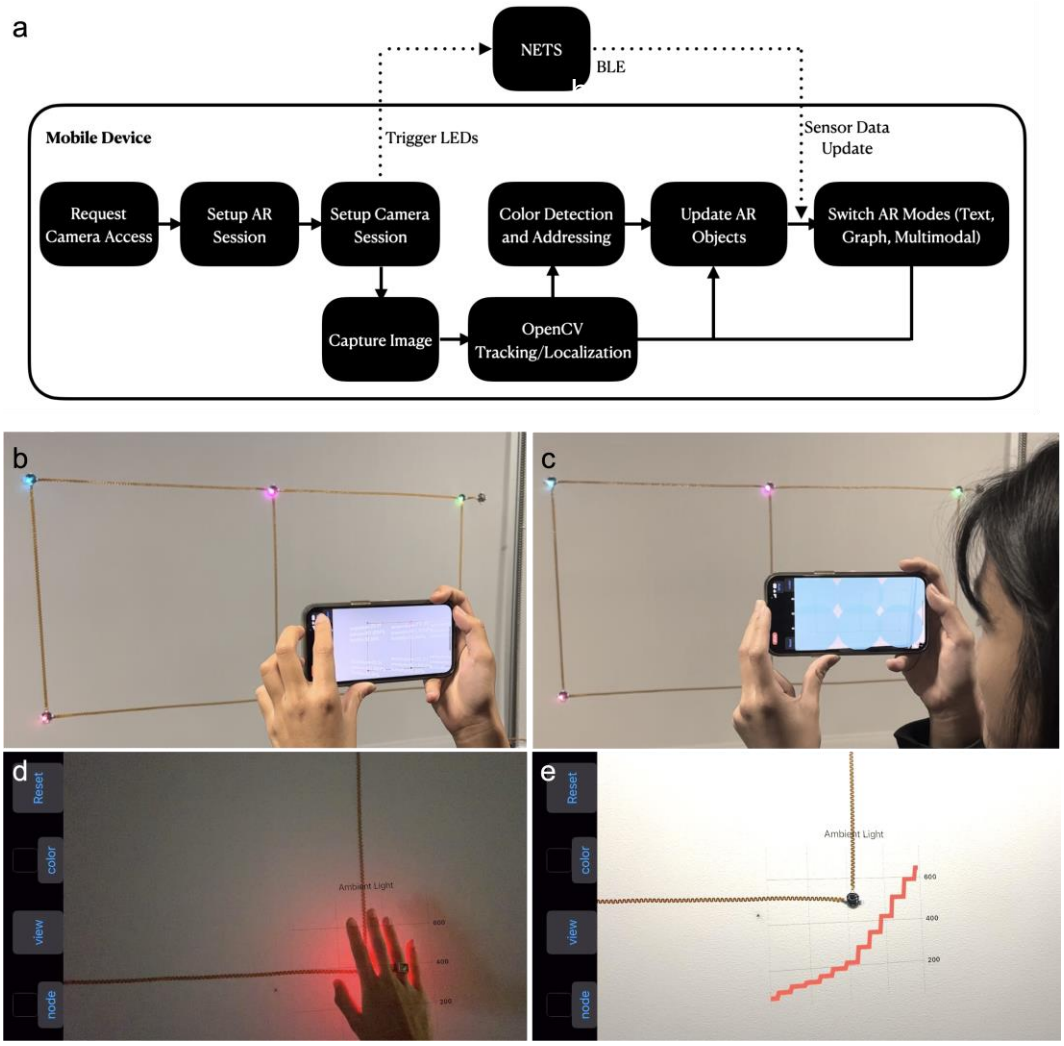

Figure 6.37: a) Flow diagram of AR-based localization and visualization using camera, OpenCV, and ARKit. a) Textual information of multi-modal sensor data on each node, b) blob color that corresponds to temperature, c-d) proximity detection that triggers a graph of the ambient light sensor updating in real-time (from dark to bright scene).

AR Visualization of Sensor Data. The final step involves visualizing the sensor data in ARKit through three distinct modes:

- **Text View:** Displays the sensor data in text format for detailed inspection, with each node's data accessible by tapping on the corresponding virtual object (Figure 6.37b).
- **Graph View:** Shows time-series graphs of sensor data (e.g., temperature trends) using Swift Charts, dynamically updating as new data comes in (Figure 6.37d-e).
- **Multimodal View**: This mode provides a more immersive representation, where sensor data is visualized through 3D objects and effects. For example, temperature is represented by colored spheres (red for warmer, blue for cooler temperatures, as shown in Figure 6.37c and 6.38c-d), and humidity is visualized using particle effects that intensify with higher moisture levels. This provides an intuitive, spatial understanding of the multi-modal sensor data (Figure 6.38e-f).

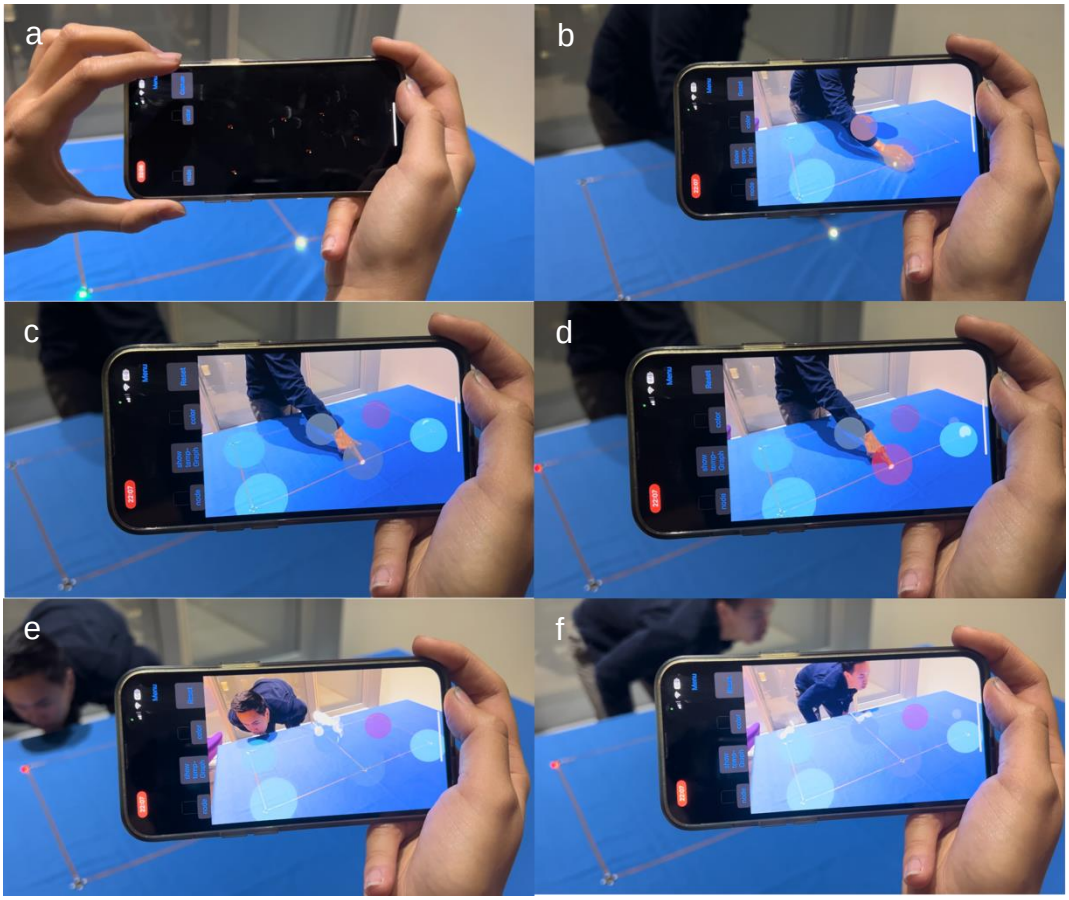

Figure 6.38: a) AR-based localization technique by detecting node LED illumination and mapping each LED's color in a 3D space. b) Proximity detection that triggers blobs animation (i.e. color change and bubbles drifting away) for visualizing c-d) temperature and e-f) humidity as the environments change or users interact with the nodes.

The system thus combines BLE data parsing, LED tracking, 2D-to-3D mapping, and multimodal visualization to create a seamless real-time sensor network representation in augmented reality. By using ARKit's 3D tracking capabilities, users can interact with sensor data in a more immersive, intuitive, and spatially aware manner, with each node represented in both position and data output.

LED Tracking Accuracy and Performance. To assess the accuracy and reliability of LED tracking for sensor nodes, a series of experiments were conducted using an iPhone 13 Pro equipped with a 12MP camera and a f/1.5 aperture wide-angle lens. The experiments were performed under consistent lighting conditions and on the same device to ensure repeatability. The tests focused on two primary metrics: color distance accuracy and distance from the camera, to evaluate how well the system tracks and differentiates sensor nodes in varying conditions.

In the color distance accuracy experiment, five colors were selected with varying degrees of hue difference from a chosen base color. The hue difference ranged from 5 to 35°, with snapshots taken from a 45° angle, 1 foot away, with the nodes connected with 10 cm pitch. The results showed that with a 35° hue difference, the system achieved a 100% success rate in tracking, allowing for up to 9 distinguishable nodes. When the hue difference decreased to 20°, the success rate dropped slightly to 90%, enabling the system to track up to 18 nodes. However, at 10 degrees, the success rate was 50%, and tracking became unreliable. Notably, even though the 5° difference was barely observable by the human eye, the system still achieved a 50% success rate. At 35°, the system proved consistent, making this setting the optimal choice for node tracking (Figure 6.39a).

As shown in Figure 6.39b, for the distance from camera experiment, four nodes with a 35° hue difference were arranged in a grid on a wall and connected 5 cm pitch interconnects. Snapshots were taken at intervals of 6 inches, starting from 1 foot away from the wall, with the camera positioned at a 90° angle. The system successfully tracked the nodes when the camera was within 4 feet. However, beyond this distance, the brightness of some LEDs, particularly those emitting light through the blue channel, diminished to the point where the camera struggled to detect them. By 5 feet, the tracking became inconsistent, highlighting the importance of LED brightness and saturation for effective long-range tracking.

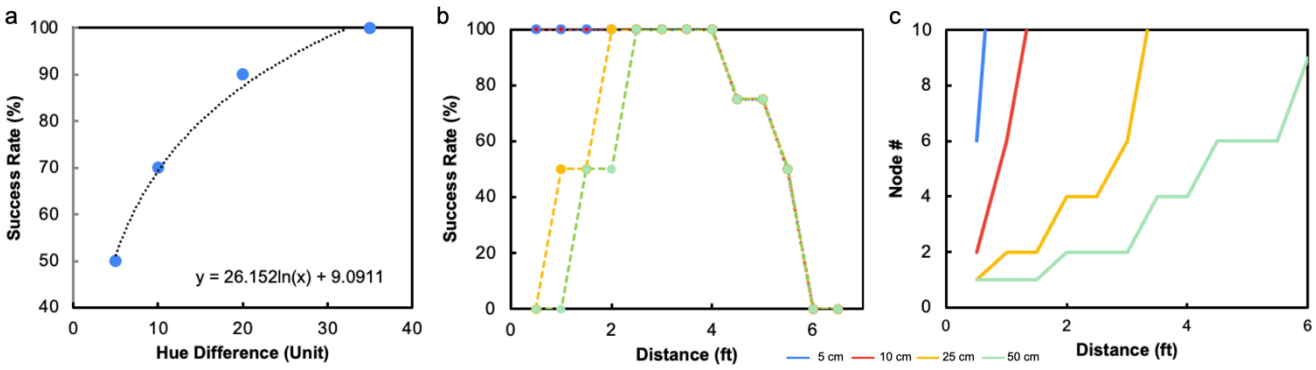

Figure 6.39: Success rate of the LED detection based on a) hue difference and b) camera distance. c) Node coverage with increasing camera distance.

Moreover, we extended these distance accuracy tests across four different pitch sizes between the nodes: 5 , 10, 25 , and 50 cm. We observed that for larger pitches, particularly the 25 cm and 50 cm configurations, the system became reliable between 2 to 4 feet. This range proved effective for all pitch sizes, making the 2 to 4 feet region a reliable zone for tracking regardless of node spacing. This flexibility across various pitch sizes is crucial for different *NETS* applications, as it ensures the system's robustness in configurations with flexible spacing between sensor nodes.

Due to the camera and screen coverage limitations (Figure 6.39c), we can observe that for the most densely packed nodes, the system can distinguish up to 9 nodes within a distance of less than 1 foot. In contrast, for the longest pitch, which works well between 2 to 4 feet from the camera, the system can capture a maximum of 2 to 4 nodes. This demonstrates the system's adaptability to various densities and distances, making it suitable for both close-range and large-scale tracking applications.

When considering systems with more than 9 distinct nodes, which is the maximum number that can be reliably tracked using the 35° hue difference, we can employ subsequent tracking and localization strategies. A promising approach involves the camera synchronizing with the *NETS* system to track the LEDs in groups. This method allows the system to divide the network into manageable sections, lighting up each group of nodes sequentially. The camera tracks these groups one at a time using time multiplexing, enabling the system to overcome the hue limitation and accurately track larger networks with many nodes. This approach significantly expands the number of nodes that can be tracked while maintaining the same level of accuracy.

6.8.5: Robotics Controller

We have also explored the integration of five *NETS* nodes to track joint and finger movements on a human arm and use this data to control both a robotic hand and its corresponding virtual reality (VR) digital twin in real time. The setup, as depicted in Figure 6.40, utilizes an Arduino Braccio robotic arm to replicate the movements detected by the nodes and their interconnects sticked along the arm. These distributed nodes provide quaternion data from the IMU, which is processed to calculate joint angles, allowing for synchronized control between the user's physical arm movements, the robotic hand, and the VR model.

System Overview. The system uses five distributed nodes attached directly to various points along the arm, specifically on the shoulder, upper arm, lower arm, and two fingers (as shown in Figure 6.40a). These sensors capture data in the form of quaternions, which represent the orientation of each segment in 3D space. The quaternion data is transmitted through a communication port to Unity, where it is processed to drive a digital model of the arm in real time. This digital model, serving as the VR digital twin, is mapped directly to the angles and rotations of the physical robotic arm.

For the physical robotic arm, the data relayed from Unity is transmitted through a separate communication port to the Arduino Braccio robotic arm. To calculate the angle between two quaternions, the data is first normalized to ensure the accuracy and eliminate any scaling distortions. A dot product is then calculated between the normalized quaternions to measure the angular difference between them. This value is passed through an inverse cosine function to extract the angle, which is then amplified (doubled) and converted into degrees to match the control requirements of the robotic arm.

The sensors are strategically placed along the arm such that the calculated angle between each quaternion corresponds to the physical joint angles of the human arm. This ensures that the robotic arm mimics the user's movements accurately. For example, the sensor data from the shoulder and elbow enables the system to calculate the flexion or extension of the arm, which is then mirrored by the robotic arm.

Real-Time Synchronization and Control. The real-time control of both the robotic hand and its VR twin requires precise synchronization between the sensor data and the control commands sent to the robotic arm. In this setup, quaternion data from the distributed sensor nodes is streamed continuously to Unity, which acts as an intermediary between the physical sensors and the robotic system. Unity processes the quaternion data in real time, updating the joint angles of

the virtual model in the VR space. These calculated angles are then sent through a second communication port to the physical Arduino Braccio arm, where the control commands are executed.

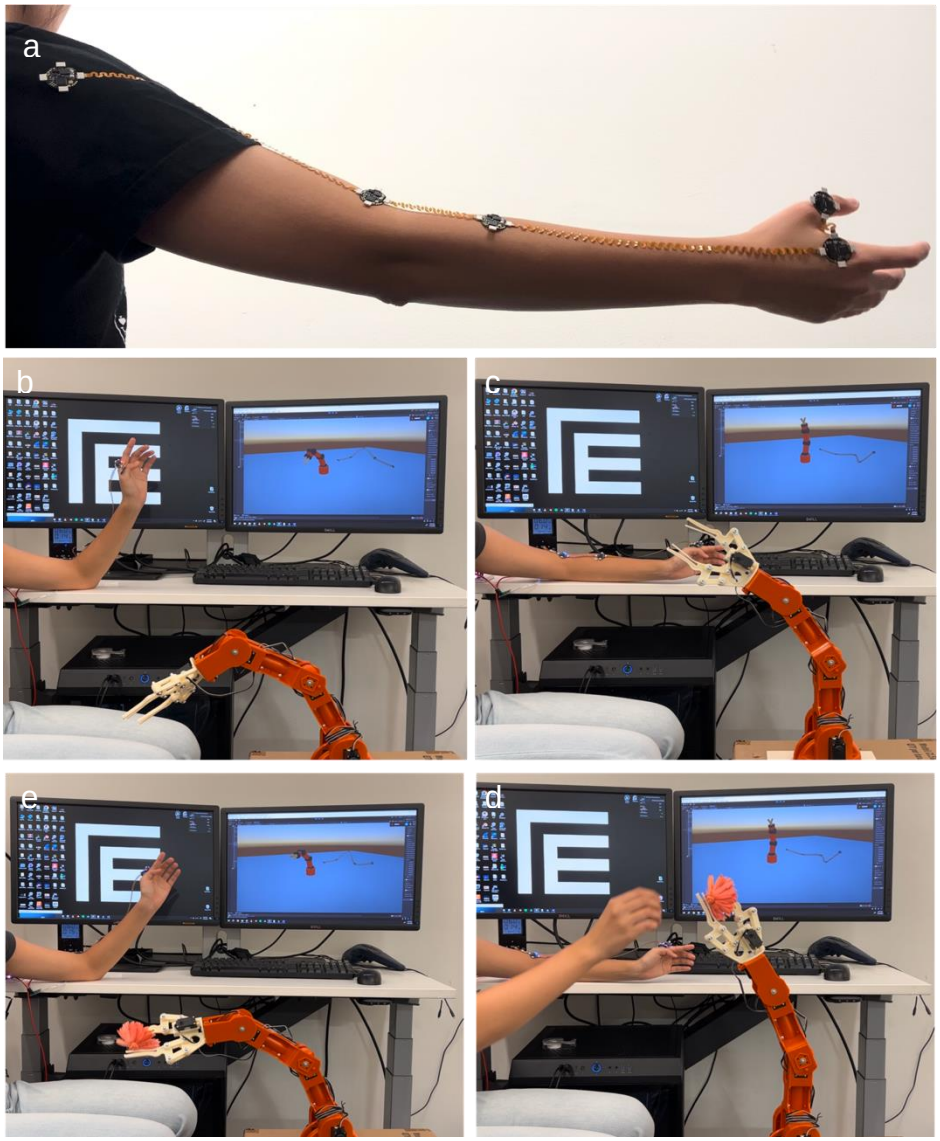

Figure 6.40: a) *NETS* nodes location around the shoulder, arm, and fingers attached directly on the skin. b-c) Real-time control of a robotic arm through the flexion of the arm, as well as d-e) robotic gripper through the pinching of the fingers.

As demonstrated in Figure 6.40b-e, during arm flexion or extension, the movements are captured by the sensors, and both the virtual and physical robotic hands follow the user's motion. It is important to note that both the virtual and physical robotic hands are rotated at a 90-degree angle and are not aligned with the same axis as the user's arm. Additionally, the system enables fine

motor control, such as finger pinching and releasing, to grasp objects—in this case, a flower. Nodes can also be wrapped on a robot as smart skins, capable of performing tactile and environmental sensing and enhancing the robot's ability to interact in the physical-digital worlds. This functionality highlights the system's capacity for dexterous manipulation, opening up possibilities for various applications, including remote robotic operation, assistive devices for individuals with mobility impairments, and immersive VR simulations for training and rehabilitation.

6.12 Future Work

The future directions for the development of *NETS* are vast, given its general-purpose nature as a computational fabric. Below are several key areas where future work can be focused to expand the capabilities of *NETS*.

Incorporation of Additional Sensing and Actuation Modalities. One of the most promising directions is the integration of additional sensing modalities into the *NETS* system. While the current focus is on motion and tactile sensing, incorporating sensors for electrophysiology could allow for advanced biofeedback and health monitoring applications. This would enable the real-time tracking of muscle and nerve activities, providing a richer dataset for applications in medical and sports sciences [300], [301]. Further, enhancing strain, shear, and pressure sensors could lead to more reliable and accurate measurements. The comparison between traditional microelectronic devices and printed or fabric-based sensors will be crucial in this development, ensuring that *NETS* can offer robust and consistent performance in various environments. Additionally, transitioning from purely sensing functionalities to actuation offers significant potential. For instance, integrating distributed haptics such as pneumatics, vibration, temperature control, and electrical stimulation would enable the fabric to provide real-time, interactive feedback, enhancing the user experience in applications like virtual reality or wearable technology [302], [303].

Miniaturization of Systems and Fabrication. A critical step forward is the further miniaturization of *NETS* components. The development of highly miniaturized chips and Application-Specific Integrated Circuits (ASICs) could reduce the number of discrete components, shrinking the overall system size to less than 10 mm^2 [304]. This would dramatically enhance the system's integration into fabrics, making it less obtrusive and more comfortable for wearable applications. Additionally, moving away from traditional flexible PCBs to a two-layer TPU or other soft PCBs could facilitate more seamless integration [112].

Power and Communication Distribution. As *NETS* scales in complexity and application, efficient power and communication distribution will become increasingly important. Utilizing the entire fabric substrate as a multi-layer power and communication substrate could reduce overall resistance and parasitic effects, ensuring more efficient energy use and data transmission [120]. Incorporating self-healing, deformable conductors could also enable *NETS* fabrics to recover from damage, akin to how biological skin heals [284]. This would enhance the durability and longevity of the fabric, particularly in harsh or dynamic environments.

Perhaps, each node in the *NETS* fabric might be equipped with wireless communication capabilities, individual batteries, and energy-harvesting technologies. These energy harvesters could capture ambient energy (e.g., solar, thermal, or mechanical vibrations) to recharge the nodes, reducing the need for external power sources and improving the system's autonomy in remote or dynamic environments [305], [306]. Wireless nodes would also allow for greater flexibility in the fabric's architecture, simplifying installation and reducing physical constraints posed by wiring [307]. In certain cases, such as for industrial textile applications, a mix between wireless and wired networking could prove beneficial, where more static or critical nodes maintain wired connections for guaranteed power and data stability, while other dynamic parts of the system leverage wireless communication to provide scalability and adaptability.

Computational Design and Configurability. Future work can also explore computational design strategies to optimize the distribution of nodes based on the specific requirements of the application and the properties of the substrate. Designing modular and reconfigurable interconnects would allow for varying node densities across the fabric, enabling customizable spatial resolution. This would be particularly useful in applications requiring high precision, such as spatiotemporal 3D deformation sensing.

Power-Efficient and Resource-Aware Networks. The development of power-efficient and resource-aware networks is another promising area for future research. Implementing context-aware power management strategies could significantly enhance the system's energy efficiency, extending the operational lifespan of *NETS* in portable and wearable applications [308]. Advanced techniques like sleep-wake cycles and intelligent power distribution can further optimize energy use, particularly in scenarios where the system experiences varying levels of activity. By allowing users to control the active resolution of the fabric, *NETS* could dynamically adjust its sensing capabilities depending on the task at hand, from sparse to dense sensing, optimizing power and computational resources through Bayesian estimation [309].

Advanced Networking Algorithms. *NETS* also presents an exciting platform for the exploration of advanced distributed computing and networking algorithms. The system's unique peer-to-

peer and global sensing and communication capabilities could be leveraged to investigate information diffusion, agent-based controls, and neuromorphic systems [292], [293], [310]. These advanced topics could enhance the fabric's adaptability and responsiveness, making it suitable for complex, large-scale deployments where decentralized decision-making is crucial.

3D Shape Sensing and Localization. Enhancing the system's capabilities in 3D shape sensing by incorporating not only IMUs, but also distributed strain and shear sensors would significantly improve its ability to measure detailed fabric deformations in real-time [311]. Moreover, advancing beyond the currently limited LED-based tracking, which assume fixed node locations to more sophisticated relative and absolute localization techniques is necessary for more practical applications. Techniques such as magnetic systems, active infrared (IR) tracking, and ultrasound could provide real-time 3D localization with sub-millimeter accuracy [312]. Active IR tracking, similar to that used in HTC Vive, could offer precise positioning by triangulating data from fixed IR transmitters and mobile nodes, potentially reaching sub-millimeter accuracy levels [313].

Ubiquitous Intelligence and Adaptive Systems. A particularly exciting avenue for future work is the integration of artificial intelligence (AI) and neural networks into the *NETS* platform. By processing the vast amounts of data generated by the distributed sensor nodes, AI systems can be trained to learn and adapt over time, continually improving based on both the environment and the users' needs [314], [315]. The incorporation of machine learning algorithms would enable *NETS* to become a self-optimizing system, predicting user behaviors and environmental changes to adjust its functions dynamically.

Platforms for Computational Fabrics across Scales. A critical aspect of making *NETS* more accessible to a broader audience is the development of user-friendly platforms for designers and researchers. Designing CAD tools specifically for the fabrication and programming of e-textiles would allow users to create and customize their own smart fabrics for a variety of applications. These platforms could enable users to design the structure, sensor placement, and interactivity of computational textiles, which could then be fabricated with embedded sensors and actuators. This would democratize the technology, allowing researchers, hobbyists, and industries to explore new applications. Designers could use *NETS* to create custom smart fabrics, such as from sleeve and clothing to robotic skin or interactive toys, upholstery, or other objects in the environment (Figure 6.41). The customizable nature of the system allows users to determine the distance between each sensor node, tailoring the fabric's resolution to suit their specific needs. This versatility means *NETS* fabrics could be wrapped around walls, surfaces, or even integrated into building formwork.

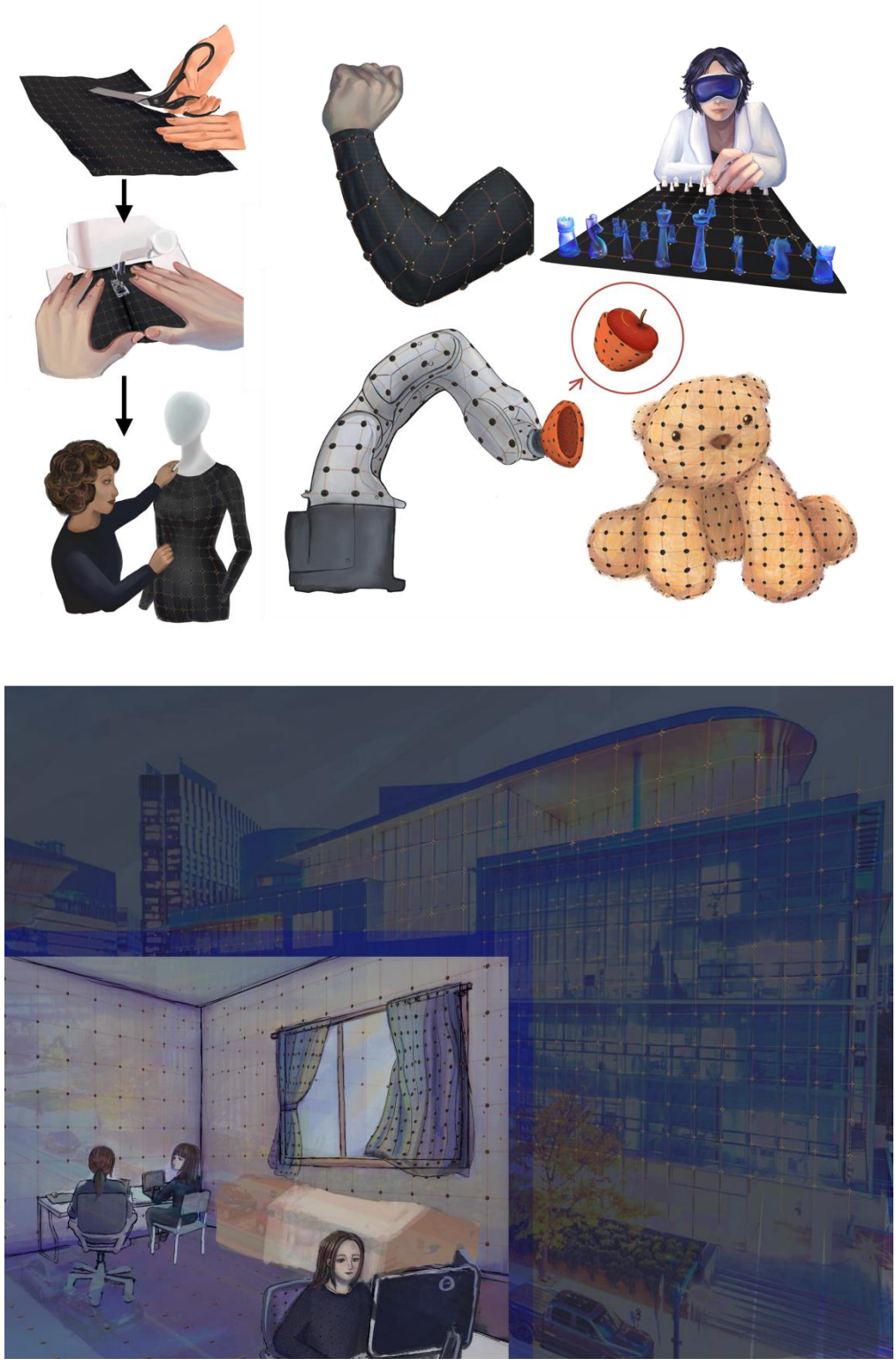

Figure 6.41: Customizability of *NETS*, treating it as general-purpose "raw" e-textiles or computational fabrics that can be cut, sewn, and programmed for various applications from wearables, smart objects, interactive surfaces, to building facades and formwork.

Expanding on the monumental scale of Christo and Jeanne-Claude's wrapping projects, *NETS* could extend beyond wearables and objects. The versatility means *NETS* fabrics could be wrapped around walls, surfaces, or even integrated into building facade or formworks and landscapes. Buildings equipped with sensors and actuators network that could communicate with the smart wearables, providing real-time data about environmental conditions, energy usage, and occupant health and behavior, and blurring the line between physical and digital infrastructure and ecosystems.

6.13 Summary of Contributions

One of the key contributions of this chapter is the development of *NETS*, computational fabrics that integrate multimodal sensing and distributed processing. This is achieved by leveraging soft, flexible, and stretchable printed circuit technologies, which enable the embedding of miniaturized sensors and processing nodes densely into textile substrates. Unlike previous approaches that focused on application-specific methodologies for sensate textiles, this research shifts towards creating a programmable, general-purpose computational fabric. By embedding microelectronics into soft materials, the system remains lightweight, flexible, and adaptable, ensuring that it can conform to different shapes and surfaces while maintaining its functionality. This development addresses the major challenge of integrating advanced computational systems into textiles without sacrificing the essential flexibility and stretchability required for wearable and large-scale applications.

We have also demonstrated nodes as islands and interconnects as bridges configuration. The node islands contain miniaturized sensor and processing elements and are capable of stretching up to 80%, ensuring high adaptability and conformability to complex surfaces. The interconnect bridges that connect these islands are based on a serpentine design, which allows for flexibility and stretch without breaking or affecting performance. This serpentine structure provides the interconnects with the necessary mechanical flexibility to adapt to deformations while maintaining electrical integrity. The serpentine design further enhances the ability of the fabric to stretch and bend, ensuring that the overall system remains robust even during dynamic activities and frequent wear.

Additionally, this node-island configuration is configurable, allowing the distribution of nodes to be customized depending on the specific application. For instance, in applications like wearable health monitoring or robotic skins, where high-resolution sensing is required, the node islands can be placed closer together. In contrast, for applications such as environmental

monitoring, where broader coverage is more important than detailed sensing, the node distribution can be sparser. This flexible architecture enables the fabric to support various use cases by simply adjusting the layout of the sensor nodes and their interconnections, making it highly adaptable to different domains.

Another important aspect of this work is the transition from centralized processing to a distributed architecture. Traditional centralized systems often suffer from bandwidth limitations and increased latency, particularly as the network scales. To overcome these challenges, the dissertation introduces a distributed processing model inspired by the human somatosensory system, where each sensor node is capable of processing data locally. This distributed approach not only improves bandwidth efficiency but also enhances scalability, fault tolerance, and resilience. The fabric can now handle multimodal sensing (temperature, pressure, motion, and environmental conditions) without overwhelming a central processor, as each node processes its data independently and communicates either via a common backbone or through peer-to-peer channels. By allowing nodes to process data locally, the system is better equipped to handle large-scale applications while ensuring that sensor data is processed in real-time, reducing latency and bandwidth demands. This architecture also enables fault tolerance, as the fabric can continue functioning even if some nodes fail, allowing for self-reconfiguration and adaptive behavior.

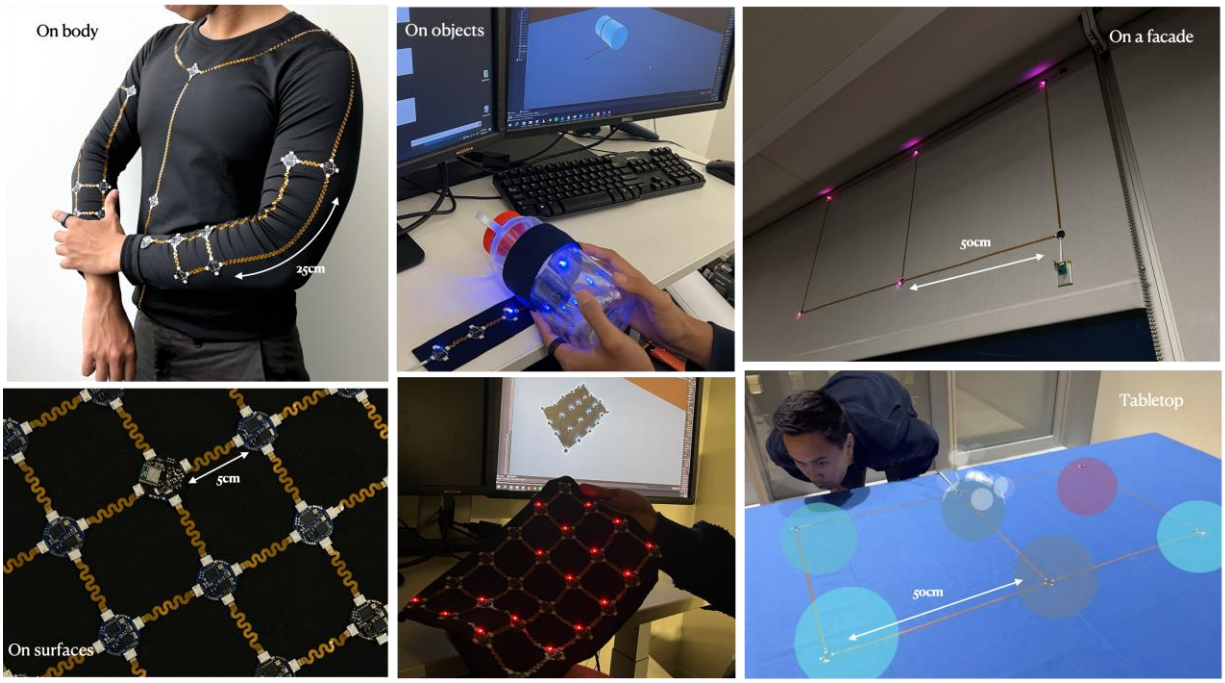

Figure 6.42: Designing and developing distributed computational fabrics across scales.

We have also demonstrated several prototypes and applications employing *NETS*. As demonstrated in Figure 6.42, we can distribute more nodes around the forearm for sleeve-based user interfaces and controllers. This configuration allows finer control and precision in sensing interactions in the forearm region, while nodes are more sparsely distributed across the rest of the shirt for joint sensing. This setup is ideal for creating a wireless motion capture shirt, which enables real-time tracking of body movements using a distributed network of nodes.

A 1D network of *NETS* can serve as a 2D-to-3D ruler that detects bending and twisting in real-time. This capability is particularly useful in bending and twisting sensors, where accurate deformation data is crucial. Alternatively, a 2D network of *NETS* can be used for 3D shape sensing on surfaces, employing a distributed IMU network to capture real-world physical interactions and synchronize them with virtual models, creating a type of digital skin. This network provides real-time data on deformations and environmental interactions, allowing the appearance and behavior of virtual models to be driven by multi-modal sensor data.

By choosing the largest feasible interconnect length or node-to-node pitch, we can also deploy a coarse version of *NETS* for large-scale applications. For instance, in building, room-scale, and environmental sensing, coarse *NETS* can be embedded into surfaces from mats to large-scale geotextiles. This enables the creation of responsive materials that interact with users and the environment, detecting motion, proximity, environmental changes, or other stimuli on everyday objects, indoor surfaces, building structures, to landscape architecture.

In conclusion, this chapter presents contributions to the design and development of computational fabrics with multimodal sensing and distributed processing capabilities. By utilizing flexible printed circuits, serpentine interconnects, and node-island configurations, this work addresses key challenges related to scalability, flexibility, and robustness. The integration of distributed architecture and fault tolerance into the design ensures that these fabrics can be robustly deployed across various scales and contexts. This research paves the way for a new generation of smart textiles that are not only highly programmable and multifunctional but also attentive, capable of dynamically self-organizing and self-configuring.

Chapter 7: Research Outlook

"Unbuilt as an antonym of built. These words invigorate our imagination…
The landscape of the unbuilt is a symbol of the present."
Tadao Ando

7.1 Textile Macroelectronics: Architecture, Technologies, and Environments

We have explored the foundational concepts of textiles and macroelectronics, merging them to establish a framework for advanced fabric-based systems that integrate sensing, computation, and eventually actuation, across scales. These contributions—knitted sensate textiles and distributed computational fabrics—are built on the understanding of textiles as hierarchical materials and macroelectronics as distributed, scalable, and adaptable substrate technologies. By bringing these two domains together, this chapter lays out how electronic capabilities embedded into fabrics will create a future where fabrics themselves become programmable, responsive, and

intelligent, from the scale of objects and wearables to room-scale systems and even architectural-scale environments.

Textiles, often misunderstood as a simple term and underestimated in their complexity, encompass the entire spectrum of materials and fabrication, from fiber to finished products; they are inherently hierarchical. The process begins at the fiber level, where individual strands are woven or knitted together to form fabrics, which are ultimately crafted into end products such as clothing, upholstery, or architectural materials. This hierarchical nature of textiles means that each level—from fiber to final product—can be customized to meet specific functional and aesthetic requirements. By leveraging the additive manufacturing process of digital knitting, we can harness the potential of large-scale industrial fabrication as a powerful tool for realizing electronic textile products from functional fibers. This approach allows for precise control over how fibers are interlaced to form complex structures. For instance, in the *KnittedKeyboard*, resistive and capacitive yarns are integrated during the knitting process to create a textile capable of sensing touch, pressure, strain, and proximity in a seamless and aesthetically pleasing form. Similarly, on a much larger scale, the *Living Knitwork Pavilion* incorporates knitted antennas and functional yarns into the fabric, demonstrating how textiles can serve as both functional and structural components in larger architectural systems.

Macroelectronics [14], on the other hand, is about scale. The development of large-area electronic systems, such as those found in the *Tapis Magique* carpet, Electronic Textile Conformable Suit (*E-TeCS*) and the Networked Electronic Textile System (*NETS*), showcases the potential of soft macroelectronics to transform entire environments into responsive, intelligent systems. By thinking of knitting or laminating electronics in a manner similar to roll-to-roll manufacturing, which allows for the continuous production of sensor-laden fabrics, macroelectronics can be seamlessly integrated into textiles at scale. The roll-to-roll process mirrors traditional textile production methods, allowing electronics to be woven or printed directly onto fibers, which can then be knitted, woven, or laminated into finished fabrics. This method not only ensures scalability but also enables the transformation of raw materials into functional fabrics with minimal manual intervention.

Multi-modality and spatiotemporality are crucial for creating sensate textiles that can be used across a wide range of applications, moving beyond application-specific functionality and making them more generalizable. However, as previously discussed, conventional sensor arrays and multiplexing architectures present significant challenges in terms of fabrication and integration, ultimately hindering the scalability of these systems. In response to these challenges, I have proposed a unique system architecture that includes novel power, communication, and networking protocols specifically designed for e-textiles.

As seen in Figure 7.1, the *NETS* architecture also integrates multiple sensing modalities, including those combined from all of the other projects and more. Unlike traditional e-textiles that are often constrained to a singular function, *NETS* combines diverse sensors along with the capacity for localized data processing. This diversity of modalities embedded within one system enhances its adaptability, allowing it to also serve across different environments and contexts, from wearables and personal health monitoring to large-scale architectural installations. For textiles to function as interactive systems at scale, they need to operate autonomously and in a decentralized manner. This is where the principles of distributed systems and self-organization become essential. By embedding sensor nodes and processing units throughout the textile, we create networks of autonomous components that communicate and collaborate seamlessly yet maintain the ability to operate independently. The *NETS* architecture ensures that each textile element can process data locally, reducing the reliance on central servers or hubs and increasing its robustness to physical damage or system failure.

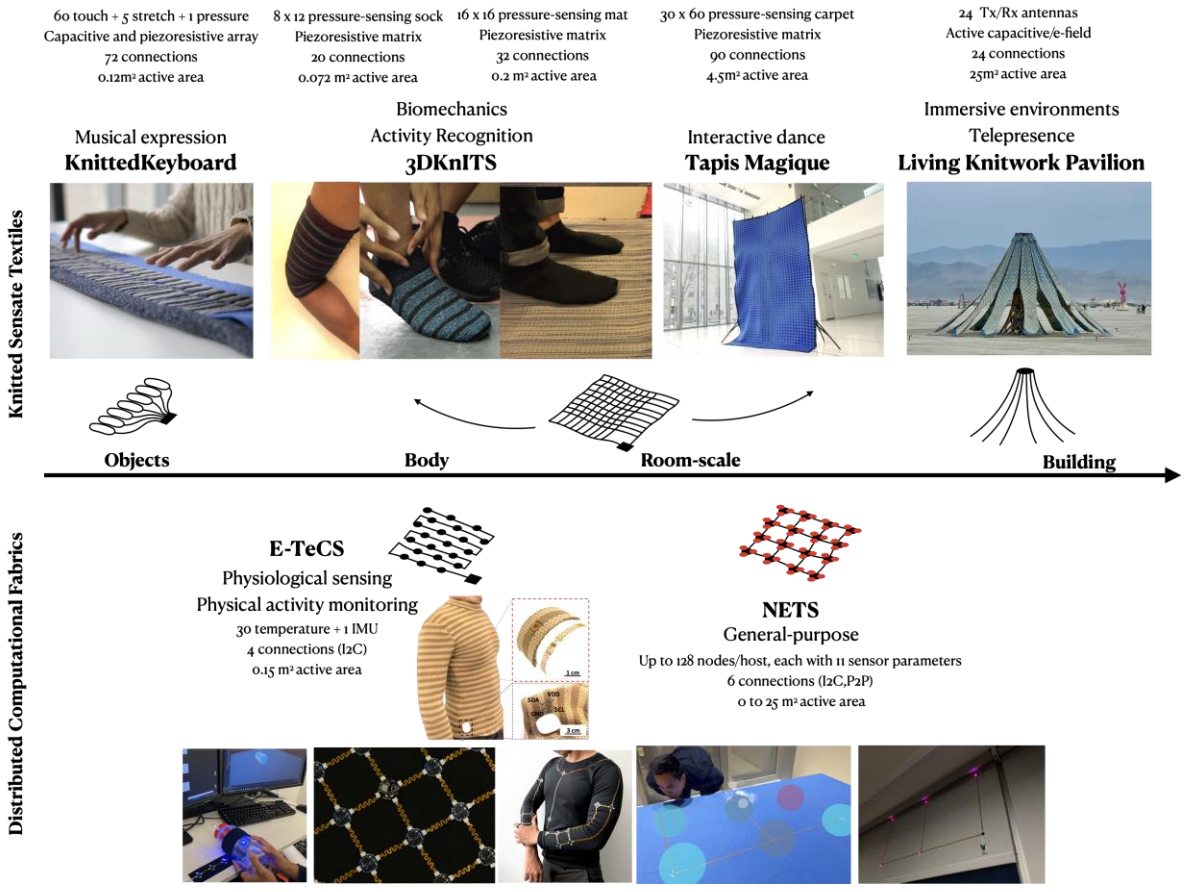

Figure 7.1: Knitted sensate textiles and distributed computational fabrics across scales, from the scale of objects to the scale of buildings, showing the wiring architecture, modalities, number of sensor and

connections, total active area, and applications of each project (E-TeCS is a prior work culminated from my MS thesis).

The potential applications that will be driven by *Textiles Macroelectronics* technologies are vast. Future textiles can function as *services*, providing users with real-time data about their environment or physical state. In *E-TeCS*, *NETS*, and *3DKnITS*, for instance, the intelligent clothing, shoes, and mats provide continuous feedback on physiology, posture, movement, and even specific exercises, making them valuable tools for rehabilitation and sports science. As a *physical-digital mesh*, these textiles bridge the gap between the physical and digital worlds, offering new interfaces for interaction. The *Tapis Magique* carpet and *Living Knitwork Pavilion* translates body movements into real-time audio, creating an immersive experience that combines physical movement with digital feedback. Finally, as *autonomous agents*, these textiles can make decisions and perform actions based on their sensing capabilities, such as in the *3DKnITS* system where neural network models enable the textiles to detect and infer user activities.

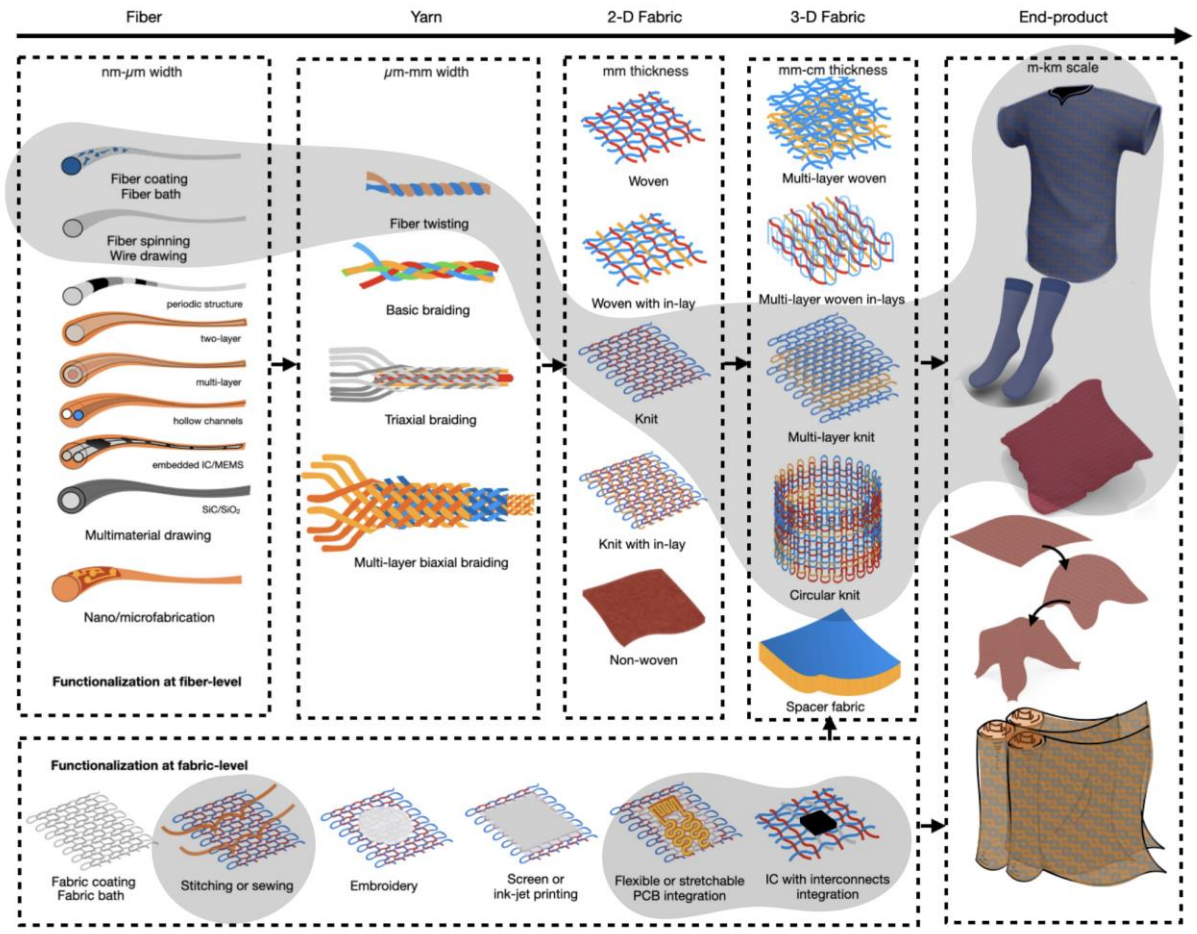

Figure 7.2: Hierarchical architecture and various structures of electronic textiles starting from fiber (1D),

yarn (1.5D), fabric (2D), fabric composite (3D), to the end-product. Besides structural functionalization, we also show the material functionalization stage at the fiber or fabric-level. Highlighted region shows yarn types, electronic devices, and textile integration techniques used in this dissertation.

In this dissertation, we have demonstrated only a subset of the existing fiber materials and textile integration techniques for the creation of electronic textile systems (Figure 7.2). The investigation focused on conductive and resistive yarns developed through fiber coating and drawing techniques, as well as fiber twisting to generate functional and aesthetic yarns. These yarns were subsequently integrated into multi-layer, circular, and tubular knitted structures using advanced digital knitting processes. Additionally, we explored the integration of printed circuits and miniaturized ICs onto textile substrates via fusing and adhesion techniques. However, this represents only a fraction of the existing knitting techniques and other textile integration technologies, and significant opportunities for future research remain.

Leveraging computational design, knitting structures, and machine parameters, we can begin exploring the creation of e-textile sensors with tunable mechanical and electrical properties. Further understanding the relationships between these properties opens a new dimension in the design of hybrid-computational materials. Through the incorporation of generative AI design, we move beyond traditional parametric methods, allowing for creative exploration of various e-textile forms and patterns inspired by both traditional and contemporary motifs, while optimizing their electromechanical properties, functionality, and spatial resolution. As illustrated in Figure 7.3, AI-driven digital fabrication provides the capability to fine-tune the properties of e-textiles by utilizing a vast range of parameter inputs and the expected output, including dynamic mechanical and electrical properties. Expanding the functional fiber library is a crucial next step, involving the exploration of fibers with magnetic, piezoelectric, optical, fluidic, pneumatic, and other interesting properties. Similarly, exploring a wider range of miniaturized integrated circuit devices, either off-the-shelf or microfabricated and custom-designed, could advance the form-factor and functionality of these textile systems.

In terms of integration techniques, there is considerable potential to extend beyond knitting. Braiding, for instance, could enable the creation of complex, multi-functional yarns that combine various properties in a single strand. Embroidery also offers a high degree of precision for localized functional zones, enabling the integration of specific sensors or circuits at defined locations on the textile surface [25]. Weaving, due to its structural density and ability to create ordered matrices, could allow for the development of highly compact and dense smart fabrics, as weaving allows for tighter control of fiber placement. For example, woven fabrics could incorporate matrix-based sensor arrays with higher resolution, allowing for the detection of more granular spatial data across large surfaces [61].

As we move forward, the distinction between *system-on-textile* and *system-in-textile* will dissolve, giving rise to programmable *super-substrates* where fibers themselves carry computation, sensing, and actuation capabilities. Advances in nano- and microfabrication technologies will enable the creation of dense, distributed sensor networks embedded within the fibers themselves, allowing for the development of highly intelligent, autonomous fabrics [67], [74]. We are also moving beyond sensate and computational fabrics to actuation fabrics, or robotic textiles that can both sense and respond, even with locomotive capabilities [238], [316]. These fabrics will not only be able to sense the environment but also actively engage with them, transforming from passive to active materials that can autonomously perform tasks.

Ultimately, the fusion of textiles and m276icroelectronics will result in fabrics that are not just passive materials, but active participants in our environments. Durable, adaptive fibers capable of surviving industrial knitting processes will make these fabrics commercially viable, while encapsulation techniques will ensure that they remain washable and resilient in everyday use. In this dissertation, I highlight why the scaling and infrastructure of computational fabrics are essential to realizing *Electronic Textile Gaia* and further driving the *Ubiquitous Computing* era. As computational fabrics scale, they will offer new forms of interaction by embedding intelligent systems into everyday objects, environments, and architectures. These systems will rely on the infrastructure of computational fabrics to manage and provide real-time data processing and interaction, forming a seamless interface between the physical and digital world.

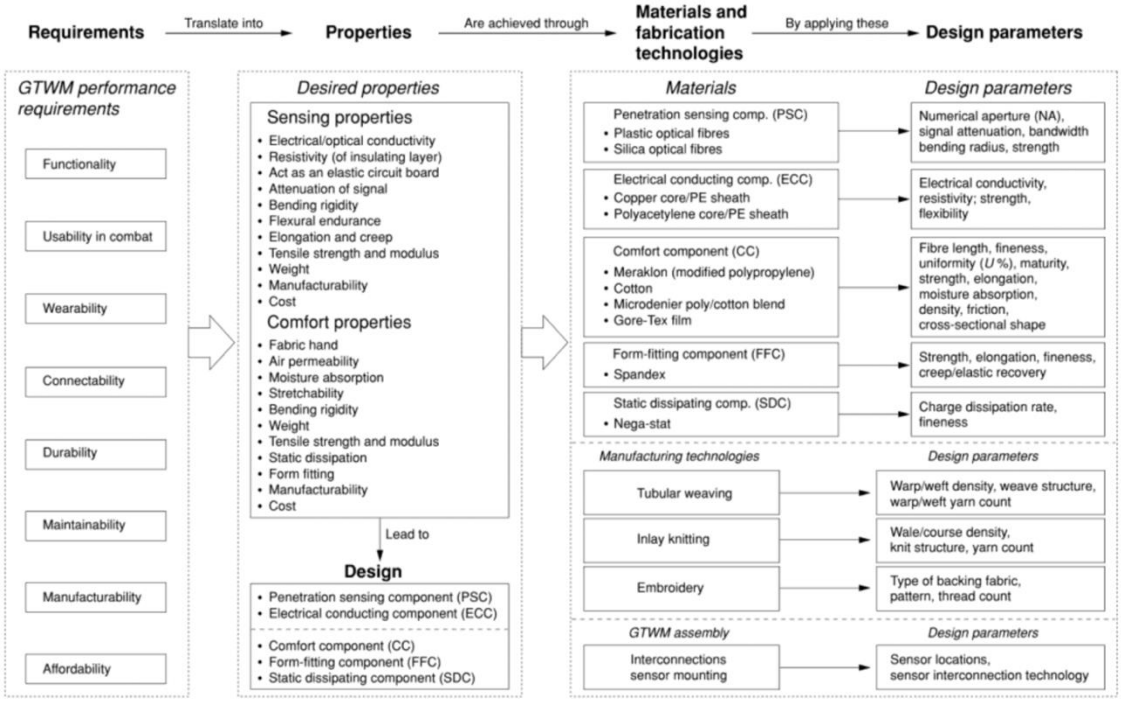

Figure 7.3: Design requirements and framework for adaptive and responsive textile structures (ARTS, reprinted from [317]).

Implication and Mitigation. Textiles and electronic products bring with them significant implications for sustainability, ethics, and privacy, all of which must be carefully considered as we move toward a future where intelligent textiles are deeply integrated into our lives. The textile industry currently contributes approximately 10% of worldwide carbon emissions [318], while electronic industry contributes to around 2% [319] (comparable to the airline industry), and this number will keep increasing if current practices continue.

To mitigate these concerns in the future e-textile industries, future work should focus on rethinking the entire lifecycle of e-textiles—from material selection and fabrication processes to usage and end-of-life considerations [320]. The first strategy is to adopt sustainable materials and fabrication techniques. Digital knitting, for instance, allows for the additive manufacturing and precise placement of functional components, minimizing raw material usage and waste and promoting resource efficiency [321]. Additionally, by using recyclable and environmentally-friendly materials in the construction of e-textiles, the overall impact on ecosystems can be reduced [322].

Another major aspect of sustainability lies in achieving higher utilization rates. E-textiles and computational fabrics should not merely be disposable products; they must be designed also for long-term and durability while enhancing their relationship with users and environments [323]. By augmenting textiles with computation, sensing, and communication capabilities, e-textiles can serve multiple functions over their lifetimes —thereby increasing their value and importance. As these textiles adapt and respond to both the user's needs and environmental conditions, their utility is maximized, which supports longer product lifetimes and reduces the demand for new products.

A third and vital aspect is considering the full lifecycle of the product from its initial fabrication to its eventual disposal [94]. Future research can also explore "design for disassembly" techniques, allowing for the recovery of valuable materials and components at the end of their life. One approach is to develop modular and reconfigurable systems where electronic components can be easily separated from the base textile, facilitating recycling or reuse [324], [325]. Additionally, low-power designs and energy-efficient mechanisms are essential to minimizing the power consumption during the product's operational phase [308].

Furthermore, integrating computation into clothing and other textiles presents novel opportunities for tracking product usage and supply chain logistics. With intelligent textiles, it becomes possible to trace the origins of materials, monitor the environmental impact of their

production, and track how products are used over time. This data could inform new strategies for reducing waste and adapting to climate change, giving designers, manufacturers, and policymakers the tools they need to make more informed decisions about the future of the textile industry.

We understand that sustainability is a complex issue that requires careful consideration across multiple dimensions, including material sourcing, energy costs, and how products are used and disposed of after production [326], [327]. Addressing these challenges requires a thorough life-cycle analysis to understand the environmental impact at each stage—from raw material extraction to manufacturing, usage, and end-of-life. A circular and holistic approach is essential, considering not only the energy costs involved in production, but also the environmental footprint of transportation, distribution, and disposal. The question of sustainability does not end with the production of an e-textile or computational fabric; it extends to how these products are integrated into daily life, how often they are replaced, and what happens to them once they are no longer needed.

Finally, the ethical implications of e-textiles go beyond environmental concerns to include issues of privacy and data security [328], [329]. As these fabrics become capable of collecting personal data, such as physiological metrics or location information, the risk of privacy violations increases. To address this, we must explore novel methods of local data processing. Distributed processing, where data is managed and encrypted and secure locally within the fabric, offers an opportunity to protect user privacy by minimizing the amount of data transmitted to external servers. This approach can also be enhanced by implementing hand-shaking and permission control protocols between source and sink or transmit and receive nodes—such as between wearables and environmental nodes—ensuring that data transmission is authorized and secure at every level. Local processing not only reduces the risk of data breaches but also allows for more efficient use of resources by limiting the need for high-bandwidth communication and centralized data storage. Additionally, secure communication protocols between textile networks can further protect sensitive data from unauthorized access or surveillance. By integrating such privacy measures, we can ensure that privacy is maintained even in highly connected, intelligent fabric networks.

7.2 Toward Electronic Textile Gaia

"Evolution is a tightly coupled dance, with life and the material environment as partners.

From the dance emerges the entity Gaia."
James Lovelock

In today's rapidly advancing world of semiconductor and industrial manufacturing technologies, we have developed deep-sea optical fibers stretching up to 39,000 kilometers, supporting communication across four continents. We've deployed 30-kilometer-long electrodynamic tethers in orbit to harvest power from Earth's magnetosphere, and we are now working on micron-scale multisensory neural probes and millimeter-scale sensory meshes that can be injected into the human body. These innovations span the full range of scales, from microns to kilometers, achieving functionality at the levels of fibers, yarns, fabrics, and systems. This broad spectrum of capability positions us at the cusp of realizing an *Electronic Textile Gaia*—an ecosystem where living, nonliving, and built environments operate as a single harmonious, self-regulating organism, as illustrated in Figure 7.4 [3].

The notion of *Electronic Textile Gaia* draws inspiration from the Gaia hypothesis. The hypothesis, which has sparked many discussions in the fields of environmental science, ecology, and planetary science, conceptualizes Earth as an integrated whole, where both living and non-living components work in concert to achieve a balance that supports life [330]. An example of this self-regulating system is Earth's climate. The Gaia hypothesis posits that life on Earth helps regulate the planet's temperature and atmospheric composition, creating conditions conducive to sustaining life. For instance, the presence of plants and algae contributes to the sequestration of carbon dioxide from the atmosphere, regulating global temperatures by reducing greenhouse gases. Simultaneously, these organisms produce oxygen, maintaining a breathable atmosphere for animals and other oxygen-dependent life forms. This process highlights a dynamic feedback loop between the biosphere and the atmosphere, where living organisms directly influence and stabilize the environmental conditions essential for their survival.

Extending this concept, *Electronic Textile Gaia* envisions the seamless integration of e-textiles into a wide range of environments—from human-scale wearables to large-scale architectural and infrastructural applications. In this framework, textiles serve as conduits for sensing, computation, and communication, forming a self-regulating, adaptive system much like Earth's biological feedback mechanisms. These textiles would autonomously respond to physiological and environmental inputs, providing continuous monitoring, feedback, and intervention. In addition, these e-textiles would communicate with surrounding IoT devices, wearable systems, and building infrastructures, forming a dynamic network that optimizes energy use, enhances health monitoring, and adapts environmental conditions.

Figure 7.4: Imagined *Electronic Textile Gaia*, in which fabrics and fibers take on electrically active functions in-body, on-body, across the built environment, submerged within landscapes, seascapes, and extending out to our orbital and even our interplanetary infrastructure.

As we walk through this dissertation, I hope we have come to respect and understand fiber and fabric in more architectural terms—as a line, a plane, and a surface—allowing us to imagine vast applications for e-textile substrates (Figure 7.5). Beyond homes and personal wearables, this approach scales to smart cities and even global systems. Imagine urban environments where textiles embedded in buildings and infrastructure continuously monitor air quality, temperature, and structural health, dynamically adjusting systems like heating, ventilation, and air conditioning (HVAC), lighting, or even the fabric of the buildings themselves. Such textiles could

enhance sustainability and energy efficiency, reducing a city's environmental footprint. In agriculture, fabric-based sensors embedded in fields as geotextiles could monitor soil health and crop conditions, enabling precise control over water usage and fertilization, ultimately reducing waste and improving yields. The principles of *Electronic Textile Gaia* allow the urban and rural fabric of human civilization to operate in harmony with the environment, responding to and interacting with nature as a single, interconnected system.

Expanding this vision beyond Earth, e-textiles could also play a critical role in space exploration and extraterrestrial habitats [331]. As we look to build sustainable human settlements beyond Earth, adaptive space suits made from smart fabrics could monitor and intervene with astronauts' vital signs and respond to environmental changes—adjusting their properties to compress, regulate temperature, or protect against harmful radiation [332], [333]. These textiles could form the basis of life-support systems that operate autonomously, providing a seamless interface between the astronaut's body and the harsh conditions of space. Similarly, fabric-based habitats could adapt to varying temperatures, radiation levels, and even self-repair when damaged, creating resilient off-Earth living environments.

The adaptability of these textiles also extends to their mechanical properties. E-textiles with tunable stiffness or texture could form the basis for a new generation of adaptive wearables, including braces that adjust their support based on movement or shoes that change their structure to provide optimal comfort and stability during different activities. In fashion, dynamic textiles could change color or texture based on the wearer's environment or mood, offering not just functional protection but also a new medium for collective experience and self-expression.

The healthcare implications of *Electronic Textile Gaia* are vast. Fabrics embedded with sensors that continuously monitor vital signs could form the basis of a proactive system, where real-time data is analyzed by AI to predict health issues and offer preventive measures. For example, wearable fabrics could detect early signs of cardiovascular stress or irregularities in blood pressure, alerting both the wearer and healthcare professionals before a serious problem arises. These fabrics could also adjust their properties to support the wearer's body during rehabilitation or physical activity, providing adaptive support based on the user's needs. Another frontier is the development of implantable fabric-net structures that combine mobility, sensing, and actuation [334], [335]. These implants, woven into delicate fibers, could autonomously navigate the body, sensing blockages or damage and intervening without the need for invasive surgery. Such systems would function much like biological organisms, where cells autonomously respond to injury or infection to maintain balance.

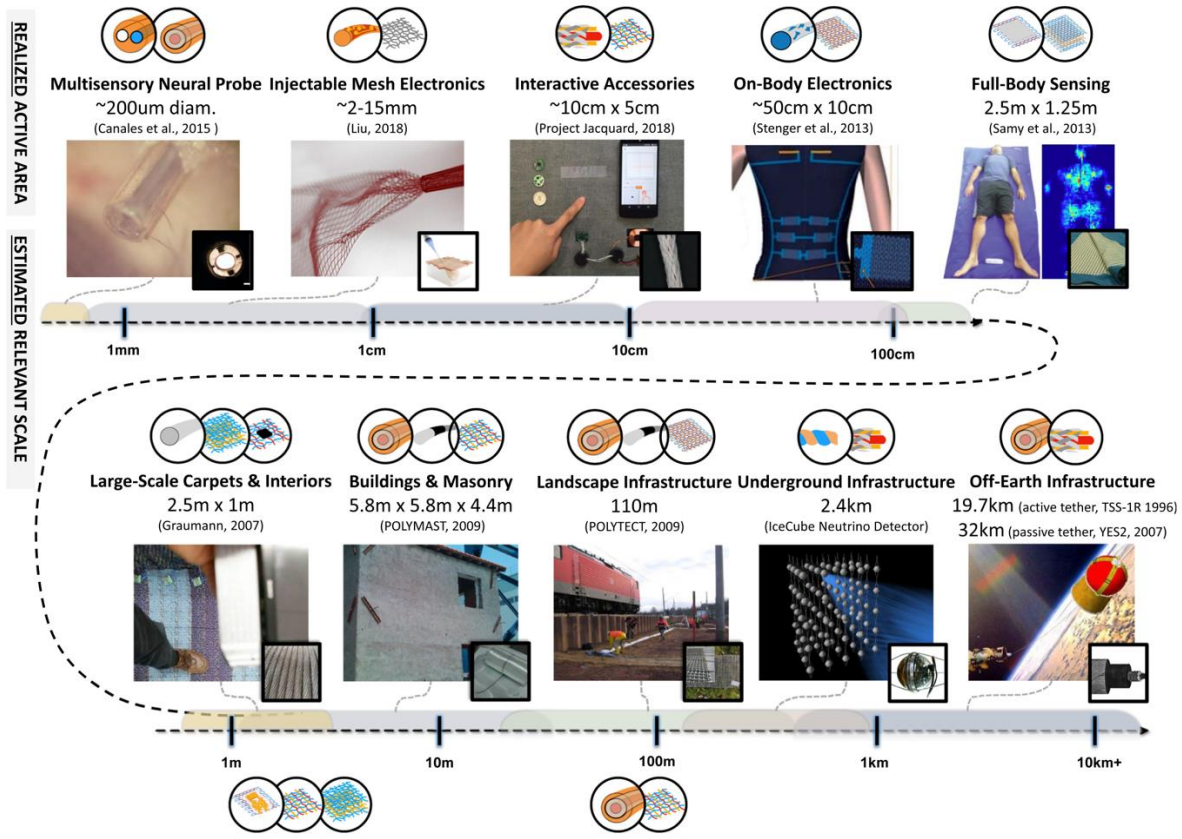

Figure 7.5: 3 A sampling of representative electronic fiber and textile application areas that have been realized across geometric scales ranging from sub-micron to 10 km. Each project is approximately categorized by its fabric/fiber functionalization mechanism, using symbols from Figure 7.2. (reprinted from [3], [69], [76], [334], [336]–[338])

As these fabrics become more integrated into the world around us, they will form a sort of *electronic nervous system*, sensing, processing, and responding to stimuli in real-time. By extending beyond the current scope of *Textile Macroelectronics* in the realm of wearable, object-based, and architectural textiles, *Electronic Textile Gaia* could encompass implants inside the body and large-scale structures in space, creating an ecosystem where every textile is intelligent and interconnected; no textiles function in isolation, they communicate with each other and an external ecosystem and contribute to the greater whole. Artificial intelligence will also be central to this transformation, enabling textiles to function autonomously and intelligently across these varied environments. Ultimately, this vision calls for a transformation in how we understand and utilize textiles—not merely as protective or decorative layers, but as dynamic, responsive systems that operate in concert with the Earth's natural and built ecosystems.

7.3 Beyond Textiles: Electronics as Raw Materials

"The future is already here – it's just not very evenly distributed."
William Gibson

In the *Amorphous Computing Manifesto* by Abelson et al., they predicted a future where microelectronics become so inexpensive and versatile that logic circuits, microsensors, actuators, and communication devices could be embedded in the very materials of our environment [137]. This vision extends to integrating electronics into everyday materials like paints, gels, polymers, and concrete, laying the groundwork for what is now being explored as large-scale embedded sensing. The potential for this transformation leads us to imagine new ways of utilizing electronics—not just as supplementary systems attached to objects, but as integral components of building materials, turning these materials into intelligent systems in their own right.

The principle of *Paintable Computing*, where electronic components could be mixed with bulk materials to create smart, responsive environments, moves us closer to a world where entire infrastructures could function as interconnected networks [138]. For instance, the integration of miniaturized MEMS And sensor networks into construction materials like concrete could transform how buildings interact with their surroundings, sensing temperature, structural integrity, and even vibrations. This shift could be seen as a tension between large-area screen-printed passive sensors and the miniaturized, embedded "raisins" within the material "pudding" [136]. It points toward a future where ubiquitous sensing is no longer bound by the limits of size, but is instead woven into the fabric of everyday life.

Instead of what was previously proposed in computational fabrics, where the nodes and networks, even though self-configuring and self-organizing, are still mapped in a distributed, *a priori* knowledge manner, future nodes and networks will be distributed not only densely but also randomly. This requires advanced strategies for handling dynamic configurations, optimizing communication, and managing redundancy across large-scale networks. These systems would need to incorporate adaptive algorithms that overcome current limitations in spatial mapping and fixed architectures. Exploring this concept demands further research in microelectronics, wireless communication, power management, self-organizing networks, and fabrication/integration technologies.

The potential for materials to become electronically functional presents a shift in how designers, architects, and engineers approach construction and product design. Traditionally, electronic systems are seen as additional tools or supplementary systems that enhance efficiency or

functionality. However, the challenge lies in incorporating these electronic systems as intrinsic elements in the design and fabrication processes. Future research aims to transcend beyond fibers and textiles as substrates for electronics, moving towards integrating them into other materials such as concrete, ceramics, elastomers, or even biological materials. In this framework, electronics become the "bricks within buildings," "clay within ceramics," or "cells within skins." This shift paves the way for a broader realization of *ubiquitous computational materials*—materials that are inherently capable of sensing, processing, actuating, and communicating. For those interested in exploring these ideas further, I highly recommend reading about other concepts like *Sensate Media* [130], *Smart Dust* [10], *Claytronics* [339], *Radical Atoms* [340], or *Fungal Computing* [341] .

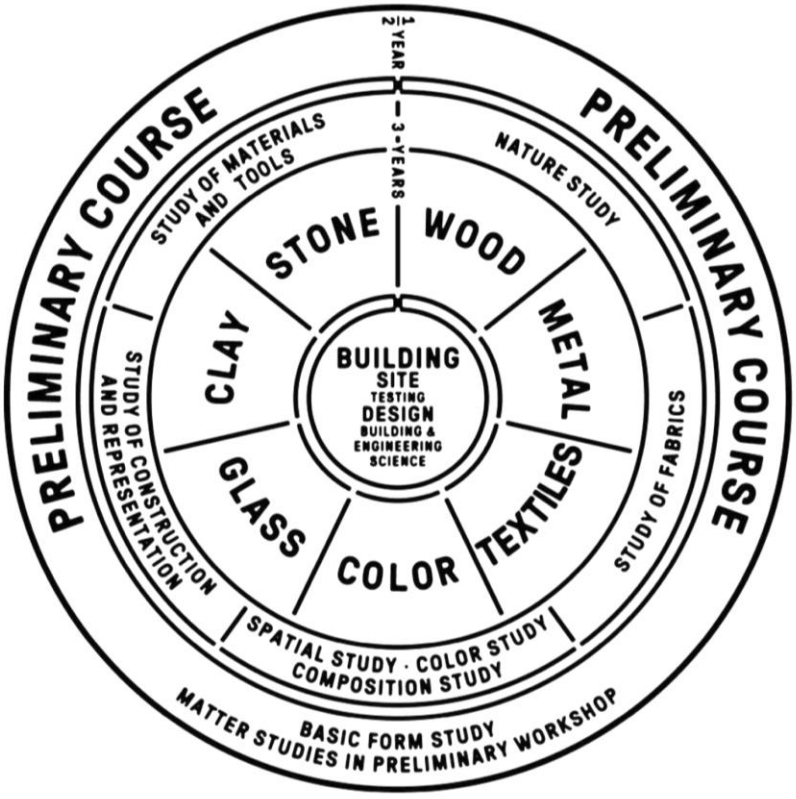

Figure 7.6: The Bauhaus wheel (principles and curriculum) diagram [342]. With the prevalence of new technologies, including digital fabrication and smart materials, how would we envision the future of objects and making?.

"New synthetic substances - steel, concrete, glass –
are actively superseding the traditional raw materials of construction."
Walter Gropius

The Bauhaus was one of the most influential art and design schools of the 20th century. Its revolutionary approach merged art, craftsmanship, and industrial production, reshaping design for the modern age [342]. The Bauhaus model emphasized functionality without sacrificing aesthetics, advocating for mass production to bring high-quality design to the wider public. The movement was cross-disciplinary at its core, blending art and technology and promoting a philosophy that form should follow function. However, as we move further into the 21st century, the emergence of computing devices, smart materials, digital fabrication techniques, and various forms of art and new media call for a reimagined model [343]—one that integrates the potential of electronic materials and digital technologies (*i.e*. advanced fabrication techniques, immersive systems, and artificial intelligence). Much like the original Bauhaus united artists, craftsmen, and architects, this new model would bring together architects, industrial designers, electrical engineers, material scientists, biomechanical engineers, mixed-media artists, and computer scientists, to develop a more holistic and integrated approach to design. This multidisciplinary effort is reminiscent of the approach that has been taken by the MIT Media Lab, which emerged alongside the rise of digital technologies [344].

Drawing inspiration from the original Bauhaus curriculum (Figure 7.6), this new approach would similarly foster the integration of functional, electronic materials into the design process. The study of electronic components and systems would not be treated as a separate discipline or practice, but instead, would become embedded in the core of design thinking and practice. Designers, architects, and engineers would approach electronic materials as integral components within the physical materials they work with, effectively blurring the lines between physical structure and digital intelligence. And *vice versa*—just as physical materials would be designed to incorporate electronic capabilities, digital systems would be designed with an understanding of their material and structural implications, ensuring that both the physical and digital realms inform each other in the design process.

By combining multiple and diverse expertise, practitioners can explore how electronic components—whether sensors, circuits, or processing units—can be seamlessly embedded into various materials, from ceramics and textiles to concrete and polymers. The practice would move beyond understanding basic circuits to conceptualizing how electronics can be fundamental to the design process, transforming everyday objects and structures. By experimenting across different scales, designers can develop a nuanced understanding of how electronic-ingrained materials behave in various contexts, leading to innovative applications of smart materials in architecture, civil engineering, product design, and beyond.

The integration of electronics into materials also raises important questions about the future of arts and crafts, the role of the designer, and the impact of mass production on the uniqueness of

design. Drawing on Walter Benjamin's essay *The Work of Art in the Age of Mechanical Reproduction* [345], we recognize that digital fabrication—while enabling precision and efficiency—risks diminishing the "aura" or unique presence of crafted works. In the context of e-textiles and computational materials, it is crucial to preserve the creative process, emphasizing the role of future artists and designers as both "digital" craftsmen and "physical" programmers.

The blurring dualities between material and immaterial are continuously evolving, as the design process no longer concludes with the completion of a material or product. Instead, it has become a dynamic interplay between digital and physical realms. Initially, materials are digitally designed and fabricated, then transitioned to the physical world for shaping and assembly. Subsequently, they return to the digital domain for programming and behavior modification, before being reintroduced into the physical environment, where their behavior is activated or adapted.

In this context, programmable fabrics, such as *NETS*, can be seen as a service to the user. The user has the ability to program the fabric's behavior, tailoring it to their specific needs or preferences. However, these fabrics also possess an inherent intelligence that allows them to act autonomously in their default mode. This means that even without direct input from the user, these programmable fabrics can adapt to environmental conditions, user interactions, or other stimuli, functioning as agents within the space they occupy. This iterative process, therefore, redefines how we conceptualize, design, and interact with everyday products. Rather than viewing materials and objects as static, finished entities, in this future, we will live with them and regard them as continuous, evolving systems.

This paradigm shift also creates new possibilities for material design and creative expression. For instance, as I have demonstrated in some of my work, e-textiles have the potential to revolutionize electronic media by embedding sensing within the fabric itself, enabling textiles that can control and modulate sound for musical expression. The textile itself becomes a canvas for sound artists and dancers to break new ground, creating immersive experiences that blend the physical and digital worlds. This approach not only enhances the expressive potential of the textile medium but also transforms it into a platform that allows new art forms to flourish. In the performing arts, for example, e-textiles can facilitate interactive performances where surface textiles dynamically respond to the movements of the performer. This interaction creates a feedback loop between physical gestures and sonic-synesthetic experience, allowing performers to explore new realms of creativity. The possibilities are limitless, as this medium opens doors to novel artistic expressions that were previously unimaginable.

As we move towards a future where electronic textiles and computational materials become more prevalent, it is essential to consider how these technologies intersect with human culture. Just as traditional crafts like *Batik* wax-patterning, *Ikat* weaving, and pottery have carried cultural and aesthetic significance for centuries, the future of computational materials must also reflect the richness of human creativity, while embracing the values that define our culture. The convergence of art, science, and technology, fostered through cross-disciplinary collaboration, ensures that these new materials are not only functional, but also deeply imbued with deep meaning and expression, even as they evolve in response to the ever-accelerating pace of technological change.

"We may say most aptly that the Analytical Engine weaves algebraic patterns just as the Jacquard loom weaves flowers and leaves."

Ada Lovelace

Chapter 8: Conclusion

In this dissertation, under the umbrella, methodology and framework of *Textile Macroelectronics*, I have explored the realization of *sensate textiles* and *computational fabrics* through the integrated perspectives of materials, fabrication processes, system architectures, and their applications. By demonstrating how we can integrate electronics into fabric substrates, my collective projects and complementary efforts reveal how e-textiles—across multiple scales, from fiber to fabric, objects to architecture—can be both highly functional and aesthetic. The ability to precisely tune patterns while embedding electronic devices enables the creation of e-textiles that are not only visually appealing but also capable of sensing, computing, and interacting with their environment.

Through advanced digital fabrication techniques such as 3D knitting and circuit printing, I have demonstrated how functional elements like sensors and processors can be seamlessly integrated into textiles, pushing the envelope of what is possible in the field of electronic fabrics. The *NETS* architecture, as proposed, exemplifies this vision by employing distributed local processing, self-organization, and multi-modality, allowing e-textiles to be treated as our current "raw" fabric materials, that we can source, design, and program for various applications. These principles are not limited to textiles alone. The methodologies and approaches outlined in this work—particularly the use of digital fabrication and the integration of distributed processing, multi-modality, and self-organization—can be applied to other material substrates as well. This dissertation, therefore, not only opens the door to innovation within e-textiles but also sets the stage for the broader realization of intelligent, computational materials across multiple domains.

Textiles as powerful media have truly been connecting people on multiple levels, from the personal, intimate scale to the collective, societal scale. This research also highlights the importance of multidisciplinary collaboration in the development and demonstration of computational textiles, involving multiple fields as diverse as material science, electrical engineering, computer science, interactive media, performing arts, industrial design and architecture. This approach enables the exploration of e-textiles across scales—from smart objects and wearable devices that monitor individual users to large-scale multi-sensory architectural installations that respond to crowd activity. The visual and tactile qualities of textiles are augmented, while the addition of sensing and computational capabilities transforms them into interactive media for musical expression, immersive experience, and telepresence.

Ultimately, this work highlights the potential of sensate textiles and computational fabrics to realize our vision of *Electronic Textile Gaia*. Future e-textiles will play multiple roles: as tools for creative expression, as mediums for interaction between the physical and digital realms, and as protective layers or "second skins" for enhancing health and well-being. Inspired by the deep cultural connection between humans and textiles, and drawing from the latest technological advances, I aim to demonstrate the importance of sensate and computational fabrics through the lens of new materials, innovative fabrication techniques, and human-computer interaction. These textiles will weave themselves into the very fabric of our lives, enriching our well-being, amplifying our expressions, and deepening our connections—transforming how we inhabit, experience, and interact with the world around us.

"We are called to be architects of the future, not its victims."
R. Buckminster Fuller

Research Contributions

Publications

Wicaksono, I., Colon, C., Chin, S., Bouchard, L., and Paradiso, J.A., 2024. KnitworkVR: Dual-reality Immersive Telepresence Experience through Distributed Sensor-Actuator Networks in the Living Knitwork Pavilion.(In review)

Wicaksono, I., Rubio, A. P., Cichoka, J., Advincula, G., Chin, S., Mishra, M., Yu, T.,and Paradiso, J.A., 2024. Living Knitwork Pavilion: Multi-sensory Responsive Architectural Space with Functional Textile Integrated System. (Accepted)

Wicaksono, I., Maheshwari, A., Haddad, D.D., Paradiso, J., and Danielescu, A., 2024. Design and Fabrication of Multifunctional E-Textiles by Upcycling Waste Cotton Fabrics through Carbonization. In *Proc. ACM Interactive, Mobile, Wearable, and Ubiquitous Technologies (IMWUT) 8, 2, Article 45 (June 2024), 31 pages.*

Wicaksono, I., Hwang, P. G., Droubi, S., Wu, F. X., Serio, A. N., Yan, W., and Paradiso, J.A., 2022. 3DKnITS: Three-dimensional Digital Knitting of Intelligent Textile Sensor for Activity Recognition and Biomechanical Monitoring. *IEEE in Medicine and Biology Society*.

Wicaksono, I., Haddad, D.D., and Paradiso, J.A., 2022. Tapis Magique: Machine-knitted Electronic Textile Carpet for Interactive Choreomusical Performance and Immersive Environments. *ACM Creativity and Cognition*.

Yan, W., Noel, G., Loke, G., Meiklejohn, E., Khiduyev, T., Marion, J., Rui, G., Lin, J., Cherston, J., Saharasbudhe, A., Wilbert, J., **Wicaksono, I.,** Hoyt, R.W., Missakian, A., Zhu, L., Ma, C., Joannopoulos, J., and Fink, Y., 2022. Single fibre enables acoustic fabrics via nanometre-scale vibrations. *Nature*, https://doi.org/10.1038/s41586-022-04476-9

Wicaksono, I.*, Cherston, J.* and Paradiso, J.A., 2021. Electronic Textile Gaia: Ubiquitous Computational Substrates Across Geometric Scales. *IEEE Pervasive Computing*. [Theme Article]

Wicaksono, I. and Paradiso, J.A., 2020. KnittedKeyboard: Digital Knitting of Electronic Textiles Musical Controller. In *New Interfaces for Musical Expression.*

Wicaksono, I., Kodama, E., Dementyev, A. and Paradiso, J.A., 2020, April. SensorNets: Towards Reconfigurable Multifunctional Fine-grained Soft and Stretchable Electronic Skins. In *Proceedings of the 2020 CHI Conference on Human Factors in Computing Systems* (pp. 1-8).

Wicaksono, I., Tucker, C.I., Sun, T., Guerrero, C.A., Liu, C., Woo, W.M., Pence, E.J. and Dagdeviren, C., 2020. A tailored, electronic textile conformable suit for large-scale spatiotemporal physiological sensing in vivo. *Nature Flexible Electronics*, *4*(1), pp.1-13.

In Spacesuit Technologies

Wicaksono, I., Shtarbanov, A., Slater, R., Ranade, E., Newman, D., and Paradiso, J., 2023. Design, Development, and Testing of Peristaltic Suit: Active-Dynamic Compression and Physiological Sensing Intra-vehicular Activity Spacesuit for Cardiovascular Deconditioning. In *International Conference on Environmental Systems (ICES) 2023*.

Ekblaw, A., Cherston, J., Liu, F., **Wicaksono, I.**, Haddad, D.D., Sumini, V. and Paradiso, J.A., 2023. From UbiComp to Universe—Moving Pervasive Computing Research Into Space Applications. *IEEE Pervasive Computing 2023*.

Wicaksono, I., Shtarbanov, A., Slater, R., Ranade, E. and Paradiso, J., 2022. Peristaltic (PS) Suit: Active Bioelectronic Sensing-Compression Spacesuit for Microgravity Adaptation and Cardiovascular Deconditioning. In *Accelerating Space Commerce, Exploration, and New Discovery (ASCEND) 2022* (p. 4208).

Payra, S.*, **Wicaksono, I.*,** Cherston, J., Honnet, C., Sumini, V. and Paradiso, J.A., 2021, March. Feeling Through Spacesuits: Application of Space-Resilient E-Textiles to Enable Haptic Feedback on Pressurized Extravehicular Suits. In *2021 IEEE Aerospace Conference (50100)* (pp. 1-12). IEEE.

Exhibitions

"The Living Knitwork Pavilion", Touch Me: Feeling Fashion, Ben Shahn Center for the Visual Arts, New Jersey, 2024.

"The Living Knitwork Pavilion", South by Southwest (SXSW) Innovation Showcase, Austin, Texas, 2024.

"The Living Knitwork Pavilion", Burning Man: ANIMALIA, Black Rock City, Nevada, 2023.

"The Living Knitwork Pavilion", MIT Saxon Lawn, Cambridge, Massachusetts, 2023.

"KnittedKeyboard and Tapis Magique", Knitting Beyond the Body, KSU Textile and Fashion Museum, Kent, Ohio 2023-2024.

"KnittedKeyboard and Tapis Magique", Labor of Life: Fibers + Textiles, Arlington Center for the Arts, Massachusetts, 2023.

"Tapis Magique", Annka Kultys Gallery: Phygital/Lumen Prize, London, United Kingdom, 2023.

"Tapis Magique: A Choreomusical Interactive Carpet", in collaboration with Pichet Klunchun Dance Company, MIT Media Lab Southeast Asia Forum, Bangkok, Thailand, 2022.

"Tapis Magique", Indonesian Contemporary Arts and Design (ICAD) 12, Jakarta, Indonesia, 2022.

"KnittedKeyboard and 3DKnITS", MIT Museum, Cambridge Science Festival + Boston Fashion Week, Cambridge, 2022.

"Tapis Magique: A Choreomusical Interactive Carpet", MIT Museum Lee Family Exchange, Cambridge Science Festival + Boston Fashion Week, Cambridge, 2022.

"The Tapis Magique", Phage/Institute Dome, 8.15 Esplanade, Burning Man, Black Rock City, Nevada, 2022.

"KnittedKeyboard and Tapis Magique", MIDI Innovation Awards, Los Angeles, California, 2022.

"KnittedKeyboard and Tapis Magique", Schnitzer Prize in the Visual Arts Exhibition, MIT Wiesner Art Gallery, Cambridge, 2022.

"Tapis Magique", in collaboration with Nina Gentile, South by Southwest (SXSW) Innovation Showcase, Austin, Texas, 2022.

"KnitX", Intersect by Lexus, Tokyo, Japan, 2021.

"Knitted Keyboard", ETH Zurich Rethinking Creativity Pavilion, World Economic Forum, Davos, Switzerland, 2020.

Grants

Lexus Design Award Grant '21
MIT Space Exploration Initiative-NASA TRISH Grant '21
Amazon-MIT Science Hub Gift Fund '22
Black Rock City Honoraria '22
MIT SAP Harold Horowitz Grant '23
Center for the Arts at MIT (CAMIT) Grant '23

References

[1] V. Postrel, *The fabric of civilization: how textiles made the world*. Hachette UK, 2020.

[2] M. Weiser, "The Computer for the 21st Century," *Sci. Am.*, vol. 265, no. 3, pp. 94–104, 1991.

[3] I. Wicaksono, J. Cherston, and J. A. Paradiso, "Electronic Textile Gaia: Ubiquitous Computational Substrates Across Geometric Scales," *IEEE Pervasive Comput.*, 2021.

[4] R. R. Schaller, "Moore's law: past, present and future," *IEEE Spectr.*, vol. 34, no. 6, pp. 52–59, 1997.

[5] H. Park and S. Kim, "Overviewing AI-Dedicated Hardware for On-Device AI in Smartphones," in *Artificial Intelligence and Hardware Accelerators*, Springer, 2023, pp. 127–150.

[6] K. Roy, B. Jung, D. Peroulis, and A. Raghunathan, "Integrated systems in the more-than-moore era: designing low-cost energy-efficient systems using heterogeneous components," *IEEE Des. Test*, vol. 33, no. 3, pp. 56–65, 2013.

[7] G. Bell, "Bell's law for the birth and death of computer classes," *Commun. ACM*, vol. 51, no. 1, pp. 86–94, 2008.

[8] J. Waring, "Number of devices to hit 4.3 per person by 2020 – report." [Online]. Available: https://www.mobileworldlive.com/featured-content/home-banner/connected-devices-to-hit-4-3-per-person-by-2020-report/. [Accessed: 01-Aug-2024].

[9] J. Morrish, "Where does the growth in connected devices come from?" [Online]. Available: https://transformainsights.com/blog/where-does-growth-in-connected-devices-come-from. [Accessed: 01-Aug-2024].

[10] B. Warneke, M. Last, B. Liebowitz, and K. S. J. Pister, "Smart dust: Communicating with a cubic-millimeter computer," *Computer (Long. Beach. Calif).*, vol. 34, no. 1, pp. 44–51, 2001.

[11] R. Spiegel, "Mouser Now Carries Bosch's Tiny Accelerometers," 2024.

[12] X. Wu *et al.*, "A 0.04 mm 3 16nW wireless and batteryless sensor system with integrated Cortex-M0+ processor and optical communication for cellular temperature measurement," in *2018 IEEE Symposium on VLSI Circuits*, 2018, pp. 191–192.

[13] J. Biggs *et al.*, "A natively flexible 32-bit Arm microprocessor," *Nature*, vol. 595, no. 7868, pp. 532–536, 2021.

[14] R. H. Reuss *et al.*, "Macroelectronics: Perspectives on technology and applications," *Proc.*

IEEE, vol. 93, no. 7, pp. 1239–1256, 2005.
[15] L. Wynand, S. Saurabh, P. Jaco, and A. Jassem, "The Economics of Semiconductor Scaling," in *Extending Moore's Law through Advanced Semiconductor Design and Processing Techniques*, CRC Press, 2018, pp. 33–66.
[16] C. Youtsey *et al.*, "Epitaxial lift-off of large-area GaAs thin-film multi-junction solar cells," in *CS Mantech Conference*, 2012, pp. 23–26.
[17] C. Cochrane, L. Meunier, F. M. Kelly, and V. Koncar, "Flexible displays for smart clothing: Part I—Overview," 2011.
[18] A. Furniturewalla, M. Chan, J. Sui, K. Ahuja, and M. Javanmard, "Fully integrated wearable impedance cytometry platform on flexible circuit board with online smartphone readout," *Microsystems Nanoeng.*, vol. 4, no. 1, p. 20, 2018.
[19] Y. Zou, "Materials selection in micro-or nano-mechanical design: Towards new Ashby plots for small-sized materials," *Mater. Sci. Eng. A*, vol. 680, pp. 421–425, 2017.
[20] D. U. Shah, "Natural fibre composites: Comprehensive Ashby-type materials selection charts," *Mater. Des.*, vol. 62, pp. 21–31, 2014.
[21] T. Ando and X.-A. Fu, "Materials: Silicon and beyond," *Sensors Actuators A Phys.*, vol. 296, pp. 340–351, 2019.
[22] W. D. Callister and D. Rethwisch, "Characteristics, applications, and processing of polymers," *Mater. Sci. Eng. an Introd.*, vol. 8, 2018.
[23] M. Ashby, "Designing architectured materials," *Scr. Mater.*, vol. 68, no. 1, pp. 4–7, 2013.
[24] L. Buechley and M. Eisenberg, "Fabric PCBs, electronic sequins, and socket buttons: Techniques for e-textile craft," *Pers. Ubiquitous Comput.*, 2009.
[25] E. R. Post, M. Orth, P. R. Russo, and N. Gershenfeld, "E-broidery: Design and fabrication of textile-based computing," *IBM Syst. J.*, 2010.
[26] Y. Wang *et al.*, "A highly stretchable, transparent, and conductive polymer," *Sci. Adv.*, vol. 3, no. 3, p. e1602076, 2017.
[27] A. Lund, N. M. van der Velden, N. K. Persson, M. M. Hamedi, and C. Müller, "Electrically conducting fibres for e-textiles: An open playground for conjugated polymers and carbon nanomaterials," *Materials Science and Engineering R: Reports*. 2018.
[28] I. Wicaksono and J. A. Paradiso, "FabricKeyboard : Multimodal Textile Sensate Media as an Expressive and Deformable Musical Interface," *Proc. Int. Conf. New Interfaces Music. Expr.*, 2017.
[29] P. P. Purslow, "The structure and growth of muscle," in *Lawrie's Meat Science*, Elsevier, 2023, pp. 51–103.
[30] F. Libonati and M. J. Buehler, "Advanced structural materials by bioinspiration," *Adv. Eng. Mater.*, vol. 19, no. 5, p. 1600787, 2017.
[31] P. Walters and D. McGoran, "Digital fabrication of 'smart' structures and mechanisms-creative applications in art and design," in *NIP & Digital Fabrication Conference*, 2011, vol. 27, pp. 185–188.
[32] M. DeLanda, "The new materiality," *Archit. Des.*, vol. 85, no. 5, pp. 16–21, 2015.
[33] E. Aarts and J. Encarnação, *True visions: The emergence of ambient intelligence*. 2006.
[34] P. Beesley and O. Khan, *Responsive architecture/performing instruments*. Architectural League of New York New York, NY, USA, 2009.

[35] C. Zheng, B. Han, X. Liu, L. Devendorf, H. Tan, and C. C. Yen, "Crafting interactive circuits on glazed ceramic ware," in *Proceedings of the 2023 CHI Conference on Human Factors in Computing Systems*, 2023, pp. 1–18.
[36] Y. Zhang, C. Yang, S. E. Hudson, C. Harrison, and A. Sample, "Wall++ room-scale interactive and context-aware sensing," in *Proceedings of the 2018 chi conference on human factors in computing systems*, 2018, pp. 1–15.
[37] G. Laput, Y. Zhang, and C. Harrison, "Synthetic sensors: Towards general-purpose sensing," in *Proceedings of the 2017 CHI Conference on Human Factors in Computing Systems*, 2017, pp. 3986–3999.
[38] G. Dublon *et al.*, "Doppellab: Tools for exploring and harnessing multimodal sensor network data," in *SENSORS, 2011 IEEE*, 2011, pp. 1612–1615.
[39] T. Heinzel, M. J. Tharakan, E. Kurbak, and R. Stewart, "Parallel industries," 2018.
[40] S. Monteiro, *The fabric of interface: Mobile media, design, and gender*. MIT Press, 2017.
[41] L. C. Aiello, "The multifaceted impact of Ada Lovelace in the digital age," *Artif. Intell.*, vol. 235, pp. 58–62, 2016.
[42] A. Tamar, "The Transition of Transistors: A Transistor History Timeline," 2017. .
[43] G. A. ans Culture, "Loom with Jacquard Mechanism." [Online]. Available: https://artsandculture.google.com/asset/loom-with-jacquard-mechanism-joseph-marie-jacquard. [Accessed: 01-Aug-2024].
[44] Cronatec, "How did the Analytical Engine work?"
[45] K. Patowary, "That Time When Computer Memory Was Handwoven by Women," 2020. [Online]. Available: https://www.amusingplanet.com/2020/02/that-time-when-computer-memory-was.html. [Accessed: 01-Aug-2024].
[46] T. Hongu, M. Takigami, and G. O. Phillips, *New millennium fibers*. Elsevier, 2005.
[47] A. Dwivedi and A. Dwivedi, "Role of computer and automation in design and manufacturing for mechanical and textile industries: CAD/CAM," *Int. J. Innov. Technol. Explor. Eng.*, vol. 3, no. 3, p. 8, 2013.
[48] S. Jiang, *The use of metallic effects in the innovative design of textile fabrics*. Hong Kong Polytechnic University (Hong Kong), 2005.
[49] T. Hughes-Riley, T. Dias, and C. Cork, "A historical review of the development of electronic textiles," *Fibers*, vol. 6, no. 2, p. 34, 2018.
[50] E. R. Post and M. Orth, "Smart fabric, or washable computing," *Dig. Pap. First Int. Symp. Wearable Comput.*, pp. 167–168, 1997.
[51] C. Gopalsamy, S. Park, R. Rajamanickam, and S. Jayaraman, "The Wearable Motherboard™: The first generation of adaptive and responsive textile structures (ARTS) for medical applications," *Virtual Real.*, vol. 4, pp. 152–168, 1999.
[52] M. Orth, J. R. Smith, E. R. Post, J. A. Strickon, and E. B. Cooper, "Musical jacket," in *ACM SIGGRAPH 1998 Electronic Art and Animation Catalog, SIGGRAPH 1998*, 1998.
[53] G. Weinberg, M. Orth, and P. Russo, "The embroidered musical ball: A squeezable instrument for expressive performance," in *Conference on Human Factors in Computing Systems - Proceedings*, 2000.
[54] E. P. Scilingo, F. Lorussi, A. Mazzoldi, and D. De Rossi, "Strain-sensing fabrics for wearable kinaesthetic-like systems," *IEEE Sens. J.*, vol. 3, no. 4, pp. 460–467, 2003.

[55] R. Paradiso, G. Loriga, N. Taccini, A. Gemignani, and B. Ghelarducci, "WEALTHY-a wearable healthcare system: new frontier on e-textile," *J. Telecommun. Inf. Technol.*, no. 4, pp. 105–113, 2005.
[56] T. Linz, C. Kallmayer, R. Aschenbrenner, and H. Reichl, "Fully integrated EKG shirt based on embroidered electrical interconnections with conductive yarn and miniaturized flexible electronics," in *Proceedings - BSN 2006: International Workshop on Wearable and Implantable Body Sensor Networks*, 2006.
[57] L. Buechley and M. Eisenberg, "Fabric PCBs, electronic sequins, and socket buttons: Techniques for e-textile craft," *Pers. Ubiquitous Comput.*, 2009.
[58] H. Perner-Wilson, L. Buechley, and M. Satomi, "Handcrafting textile interfaces from a kit-of-no-parts," in *Proceedings of the 5th International Conference on Tangible Embedded and Embodied Interaction, TEI'11*, 2011.
[59] L. Buechley and M. Eisenberg, "The LilyPad Arduino: Toward wearable engineering for everyone," *IEEE Pervasive Comput.*, vol. 7, no. 2, pp. 12–15, 2008.
[60] X. Tao, T. H. Huang, C. L. Shen, Y. C. Ko, G. T. Jou, and V. Koncar, "Bluetooth Low Energy-Based Washable Wearable Activity Motion and Electrocardiogram Textronic Monitoring and Communicating System," *Adv. Mater. Technol.*, 2018.
[61] I. Locher, T. Kirstein, and G. Tröster, "Routing Methods Adapted to e-Textiles," *Proc. 37th Int. Symp. Microelectron. (IMAPS 2004)*, 2004.
[62] S. Lee, B. Kim, T. Roh, S. Hong, and H. J. Yoo, "Arm-band type textile-MP3 player with multi-layer Planar Fashionable Circuit Board (P-FCB) techniques," in *Proceedings - International Symposium on Wearable Computers, ISWC*, 2010.
[63] K. Cherenack, C. Zysset, T. Kinkeldei, N. Münzenrieder, and G. Tröster, "Woven electronic fibers with sensing and display functions for smart textiles," *Adv. Mater.*, vol. 22, no. 45, pp. 5178–5182, 2010.
[64] A. Komolafe *et al.*, "Integrating flexible filament circuits for e-textile applications," *Adv. Mater. Technol.*, vol. 4, no. 7, p. 1900176, 2019.
[65] M.-N. Nashed, D. A. Hardy, T. Hughes-Riley, and T. Dias, "A novel method for embedding semiconductor dies within textile yarn to create electronic textiles," *Fibers*, vol. 7, no. 2, p. 12, 2019.
[66] M. Rein *et al.*, "Diode fibres for fabric-based optical communications," *Nature*. 2018.
[67] G. Loke *et al.*, "Digital electronics in fibres enable fabric-based machine-learning inference," *Nat. Commun.*, vol. 12, no. 1, pp. 1–9, 2021.
[68] M. Stoppa and A. Chiolerio, "Wearable electronics and smart textiles: A critical review," *Sensors (Switzerland)*, vol. 14, no. 7. pp. 11957–11992, 2014.
[69] N.-W. G. Ivan Poupyrev, M. E. K. Shiho Fukuhara, and Carsten, "Project Jacquard: Interactive Digital Textiles at Scale," in *Proceedings of the 2016 CHI Conference on Human Factors in Computing Systems*, 2016.
[70] A. Basu, "Smart electronic yarns and wearable fabrics for human biomonitoring," in *Nanosensors and Nanodevices for Smart Multifunctional Textiles*, 2021.
[71] F. Mokhtari, J. Foroughi, T. Zheng, Z. Cheng, and G. M. Spinks, "Triaxial braided piezo fiber energy harvesters for self-powered wearable technologies," *J. Mater. Chem. A*, vol. 7, no. 14, pp. 8245–8257, 2019.

[72] W. Yan *et al.*, "Thermally drawn advanced functional fibers: New frontier of flexible electronics," *Materials Today*. 2020.
[73] G. Mattana *et al.*, "Woven temperature and humidity sensors on flexible plastic substrates for e-textile applications," *IEEE Sens. J.*, 2013.
[74] F. Clemens *et al.*, "Computing Fibers: A Novel Fiber for Intelligent Fabrics?," *Adv. Eng. Mater.*, 2003.
[75] M. Hamedi, R. Forchheimer, and O. Inganäs, "Towards woven logic from organic electronic fibres," *Nat. Mater.*, vol. 6, no. 5, pp. 357–362, 2007.
[76] A. Canales *et al.*, "Multifunctional fibers for simultaneous optical, electrical and chemical interrogation of neural circuits in vivo," *Nat. Biotechnol.*, vol. 33, no. 3, pp. 277–284, 2015.
[77] S. Hwang *et al.*, "Chip on a fiber toward the e-textile computing platform," 2020.
[78] F. Mokhtari *et al.*, "Wearable electronic textiles from nanostructured piezoelectric fibers," *Adv. Mater. Technol.*, vol. 5, no. 4, p. 1900900, 2020.
[79] J. Mu *et al.*, "Sheath-run artificial muscles," *Science (80-.).*, 2019.
[80] S. H. Kim *et al.*, "Harvesting electrical energy from carbon nanotube yarn twist," *Science (80-.).*, 2017.
[81] J. Foroughi *et al.*, "Torsional carbon nanotube artificial muscles," *Science (80-.).*, vol. 334, no. 6055, pp. 494–497, 2011.
[82] R. Abbel, Y. Galagan, and P. Groen, "Roll-to-Roll Fabrication of Solution Processed Electronics," *Advanced Engineering Materials*. 2018.
[83] I. Wicaksono, E. Kodama, A. Dementyev, and J. A. Paradiso, "SensorNets: Towards reconfigurable multifunctional fine-grained soft and stretchable electronic skins," in *Conference on Human Factors in Computing Systems - Proceedings*, 2020.
[84] I. Wicaksono *et al.*, "A tailored, electronic textile conformable suit for large-scale spatiotemporal physiological sensing in vivo," *npj Flex. Electron.*, 2020.
[85] K. Chatterjee and T. K. Ghosh, "3D Printing of Textiles: Potential Roadmap to Printing with Fibers," *Advanced Materials*. 2020.
[86] A. Schwarz-Pfeiffer, M. Obermann, M. O. Weber, and A. Ehrmann, "Smarten up garments through knitting," in *IOP conference series: materials science and engineering*, 2016, vol. 141, no. 1, p. 12008.
[87] S. Anand, N. Soin, T. H. Shah, and E. Siores, "Energy harvesting '3-D knitted spacer' based piezoelectric textiles," in *IOP Conference Series: Materials Science and Engineering*, 2016, vol. 141, no. 1, p. 12001.
[88] S. Seyedin *et al.*, "Textile strain sensors: A review of the fabrication technologies, performance evaluation and applications," *Materials Horizons*. 2019.
[89] W. Fan *et al.*, "Machine-knitted washable sensor array textile for precise epidermal physiological signal monitoring," *Sci. Adv.*, vol. 6, no. 11, p. eaay2840, 2020.
[90] Y. Luo *et al.*, "Learning human--environment interactions using conformal tactile textiles," *Nat. Electron.*, vol. 4, no. 3, pp. 193–201, 2021.
[91] S. Seyedin, S. Moradi, C. Singh, and J. M. Razal, "Continuous production of stretchable conductive multifilaments in kilometer scale enables facile knitting of wearable strain sensing textiles," *Appl. Mater. today*, vol. 11, pp. 255–263, 2018.
[92] H. Wang *et al.*, "Downsized sheath--core conducting fibers for weavable superelastic

wires, biosensors, supercapacitors, and strain sensors," *Adv. Mater.*, vol. 28, no. 25, pp. 4998–5007, 2016.
[93] M. Zhang, C. Wang, H. Wang, M. Jian, X. Hao, and Y. Zhang, "Carbonized cotton fabric for high-performance wearable strain sensors," *Adv. Funct. Mater.*, vol. 27, no. 2, p. 1604795, 2017.
[94] I. Wicaksono, A. Maheshwari, D. D. Haddad, J. Paradiso, and A. Danielescu, "Design and Fabrication of Multifunctional E-Textiles by Upcycling Waste Cotton Fabrics through Carbonization," *Proc. ACM Interactive, Mobile, Wearable Ubiquitous Technol.*, vol. 8, no. 2, pp. 1–31, 2024.
[95] E. Kasaw, A. Haile, and M. Getnet, "Conductive coatings of cotton fabric consisting of carbonized charcoal for E-Textile," *Coatings*, vol. 10, no. 6, p. 579, 2020.
[96] A. Atalay *et al.*, "Batch fabrication of customizable silicone-textile composite capacitive strain sensors for human motion tracking," *Adv. Mater. Technol.*, vol. 2, no. 9, p. 1700136, 2017.
[97] R. Paradiso, G. Loriga, and N. Taccini, "A wearable health care system based on knitted integrated sensors," *IEEE Trans. Inf. Technol. Biomed.*, vol. 9, no. 3, pp. 337–344, 2005.
[98] C. Demolder, A. Molina, F. L. Hammond III, and W.-H. Yeo, "Recent advances in wearable biosensing gloves and sensory feedback biosystems for enhancing rehabilitation, prostheses, healthcare, and virtual reality," *Biosens. Bioelectron.*, vol. 190, p. 113443, 2021.
[99] R. Bloss, "Wearable sensors bring new benefits to continuous medical monitoring, real time physical activity assessment, baby monitoring and industrial applications," *Sens. Rev.*, vol. 35, no. 2, pp. 141–145, 2015.
[100] L. Eskandarian, E. Pajootan, A. Toossi, and H. E. Naguib, "Dry fiber-based electrodes for electrophysiology applications," *Adv. Fiber Mater.*, vol. 5, no. 3, pp. 819–846, 2023.
[101] J. Ou, D. Oran, D. D. Haddad, J. Paradiso, and H. Ishii, "SensorKnit: Architecting Textile Sensors with Machine Knitting," *3D Print. Addit. Manuf.*, 2019.
[102] A. Olwal, T. Starner, and G. Mainini, "E-Textile microinteractions: Augmenting twist with flick, slide and grasp gestures for soft electronics," in *Proceedings of the 2020 CHI Conference on Human Factors in Computing Systems*, 2020, pp. 1–13.
[103] J. A. Rogers, "Soft electronics for the human body," in *European Solid-State Device Research Conference*, 2016, vol. 2016-Octob, pp. 21–22.
[104] X. Liu, K. Vega, P. Maes, and J. A. Paradiso, "Wearability Factors for Skin Interfaces," *Proc. 7th Augment. Hum. Int. Conf. 2016 - AH '16*, pp. 1–8, 2016.
[105] S. Il Park *et al.*, "Soft, stretchable, fully implantable miniaturized optoelectronic systems for wireless optogenetics," *Nat. Biotechnol.*, vol. 33, no. 12, pp. 1280–1286, 2015.
[106] C. Dagdeviren *et al.*, "Conformal piezoelectric energy harvesting and storage from motions of the heart, lung, and diaphragm," *Proc. Natl. Acad. Sci.*, vol. 111, no. 5, pp. 1927–1932, 2014.
[107] S. Park, K. Chung, and S. Jayaraman, "Wearables: Fundamentals, Advancements, and a Roadmap for the Future," in *Wearable Sensors: Fundamentals, Implementation and Applications*, 2014, pp. 1–23.
[108] D.-H. Kim *et al.*, "Epidermal Electronics," *Science (80-.).*, vol. 333, no. 6044, pp. 838–843,

2011.
[109] K.-I. Jang *et al.*, "Rugged and breathable forms of stretchable electronics with adherent composite substrates for transcutaneous monitoring," *Nat. Commun.*, vol. 5, p. 4779, 2014.
[110] W. Gao *et al.*, "Fully integrated wearable sensor arrays for multiplexed in situ perspiration analysis," *Nature*, vol. 529, no. 7587, pp. 509–514, 2016.
[111] J. Kim *et al.*, "Stretchable silicon nanoribbon electronics for skin prosthesis," *Nat. Commun.*, vol. 5, p. 5747, 2014.
[112] Z. Huang *et al.*, "Three-dimensional integrated stretchable electronics," *Nat. Electron.*, vol. 1, no. 8, pp. 473–480, 2018.
[113] K.-I. Jang *et al.*, "Self-assembled three dimensional network designs for soft electronics," *Nat. Commun.*, vol. 8, no. 1, pp. 1–10, 2017.
[114] J. H. Ahn *et al.*, "High-speed mechanically flexible single-crystal silicon thin-film transistors on plastic substrates," *IEEE Electron Device Lett.*, vol. 27, no. 6, pp. 460–462, 2006.
[115] M. A. Meitl *et al.*, "Transfer printing by kinetic control of adhesion to an elastomeric stamp," *Nat. Mater.*, vol. 5, no. 1, pp. 33–38, 2006.
[116] M. Feil *et al.*, "Ultra thin ICs and MEMS elements: Techniques for wafer thinning, stress-free separation, assembly and interconnection," *Microsyst. Technol.*, vol. 9, no. 3, pp. 176–182, 2003.
[117] Y. Zhang *et al.*, "Mechanics of ultra-stretchable self-similar serpentine interconnects," *Acta Mater.*, vol. 61, no. 20, pp. 7816–7827, 2013.
[118] Y. Sun, W. M. Choi, H. Jiang, Y. Y. Huang, and J. A. Rogers, "Controlled buckling of semiconductor nanoribbons for stretchable electronics," *Nat. Nanotechnol.*, vol. 1, no. 3, pp. 201–207, 2006.
[119] Y. Wu *et al.*, "Thermoplastic Elastomers for Wireless, Skin-Interfaced Electronic, and Microfluidic Devices," *Adv. Mater. Technol.*, vol. 8, no. 19, p. 2300732, 2023.
[120] J. Lifton, D. Seetharam, M. Broxton, and J. Paradiso, "Pushpin computing system overview: A platform for distributed, embedded, ubiquitous sensor networks," in *Lecture Notes in Computer Science (including subseries Lecture Notes in Artificial Intelligence and Lecture Notes in Bioinformatics)*, 2002.
[121] J. Lifton, M. Broxton, and J. A. Paradiso, "Distributed sensor networks as sensate skin," 2004.
[122] B. Richardson, K. Leydon, M. Fernstrom, and J. A. Paradiso, "Z-Tiles: building blocks for modular, pressure-sensing floorspaces," in *CHI'04 extended abstracts on Human factors in computing systems*, 2004, pp. 1529–1532.
[123] B. F. T. Mistree and J. A. Paradiso, "ChainMail: a configurable multimodal lining to enable sensate surfaces and interactive objects," in *Proceedings of the fourth international conference on Tangible, embedded, and embodied interaction*, 2010, pp. 65–72.
[124] N.-W. Gong *et al.*, "PrintSense: a versatile sensing technique to support multimodal flexible surface interaction," *Proc. 32nd Annu. ACM Conf. Hum. factors Comput. Syst. - CHI '14*, pp. 1407–1410, 2014.
[125] N.-W. Gong, S. Hodges, and J. A. Paradiso, "Leveraging conductive inkjet technology to build a scalable and versatile surface for ubiquitous sensing," 2011.

[126] A. Dementyev and J. A. Paradiso, "SensorTape : Modular and Programmable 3D-Aware Dense Sensor Network on a Tape d," *Proc. 28th Annu. ACM Symp. User Interface Softw. Technol. - UIST '15*, 2015.
[127] G. Cheng, E. Dean-Leon, F. Bergner, J. R. G. Olvera, Q. Leboutet, and P. Mittendorfer, "A comprehensive realization of robot skin: Sensors, sensing, control, and applications," *Proc. IEEE*, vol. 107, no. 10, pp. 2034–2051, 2019.
[128] D. Hughes and N. Correll, "Texture recognition and localization in amorphous robotic skin," *Bioinspir. Biomim.*, vol. 10, no. 5, p. 55002, 2015.
[129] J. A. Paradiso, "The brain opera technology: New instruments and gestural sensors for musical interaction and performance," *J. New Music Res.*, vol. 28, no. 2, pp. 130–149, 1999.
[130] J. A. Paradiso, J. Lifton, and M. Broxton, "Sensate media - Multimodal electronic skins as dense sensor networks," *BT Technol. J.*, 2004.
[131] H. Harm, O. Amft, D. Roggen, and G. Tröster, "Smash: A distributed sensing and processing garment for the classification of upper body postures," in *3rd International ICST Conference on Body Area Networks*, 2010.
[132] X. Righetti and D. Thalmann, "Proposition of a modular I2C-based wearable architecture," in *Melecon 2010-2010 15th IEEE Mediterranean Electrotechnical Conference*, 2010, pp. 802–805.
[133] C. Lauterbach *et al.*, "A self-organizing and fault-tolerant wired peer-to-peer sensor network for textile applications," in *International Workshop on Engineering Self-Organising Applications*, 2004, pp. 256–266.
[134] Z. Zhou *et al.*, "3D deformation capture via a configurable self-sensing IMU sensor network," *Proc. ACM Interactive, Mobile, Wearable Ubiquitous Technol.*, vol. 7, no. 1, pp. 1–24, 2023.
[135] E. Rawn, "The Work and Vision of Ubiquitous Computing at Xerox PARC," *IEEE Ann. Hist. Comput.*, 2024.
[136] J. A. Paradiso, "Technical perspective: The future of large-scale embedded sensing," *Commun. ACM*, vol. 63, no. 12, p. 91, 2020.
[137] H. Abelson *et al.*, "Amorphous computing," *Commun. ACM*, vol. 43, no. 5, pp. 74–82, 2000.
[138] W. J. Butera, "Programming a paintable computer." Citeseer, 2002.
[139] D. J. Spencer, *Knitting technology: a comprehensive handbook and practical guide*, vol. 16. CRC press, 2001.
[140] G. A. V Leaf and A. Glaskin, "43—The geometry of a plain knitted loop," *J. Text. Inst. Trans.*, vol. 46, no. 9, pp. T587–T605, 1955.
[141] D. L. Munden, "26—The geometry and dimensional properties of plain-knit fabrics," *J. Text. Inst. Trans.*, vol. 50, no. 7, pp. T448–T471, 1959.
[142] A. Pavko-Cuden, A. Hladnik, and F. Sluga, "Loop length of plain single weft knitted structure with elastane," *J. Eng. Fiber. Fabr.*, vol. 8, no. 2, p. 155892501300800220, 2013.
[143] F. T. Peirce, "Geometrical principles applicable to the design of functional fabrics," *Text. Res. J.*, vol. 17, no. 3, pp. 123–147, 1947.
[144] E. Abd elzaher Eltahan, M. Sultan, and A.-B. Mito, "Determination of loop length, tightness factor and porosity of single jersey knitted fabric," *Alexandria Eng. J.*, vol. 55, no.

2, pp. 851–856, 2016.
[145] H. Zhang, X. Tao, S. Wang, and T. Yu, "Electro-mechanical properties of knitted fabric made from conductive multi-filament yarn under unidirectional extension," *Text. Res. J.*, vol. 75, no. 8, pp. 598–606, 2005.
[146] L. Li, W. M. Au, K. M. Wan, S. H. Wan, W. Y. Chung, and K. S. Wong, "A resistive network model for conductive knitting stitches," *Text. Res. J.*, vol. 80, no. 10, pp. 935–947, 2010.
[147] M. A. al Rumon *et al.*, "Textile knitted stretch sensors for wearable health monitoring: Design and performance evaluation," *Biosensors*, vol. 13, no. 1, p. 34, 2022.
[148] L. Li, S. Liu, F. Ding, T. Hua, W. M. Au, and K.-S. Wong, "Electromechanical analysis of length-related resistance and contact resistance of conductive knitted fabrics," *Text. Res. J.*, vol. 82, no. 20, pp. 2062–2070, 2012.
[149] K. M. B. Jansen, "Performance evaluation of knitted and stitched textile strain sensors," *Sensors*, vol. 20, no. 24, p. 7236, 2020.
[150] S. Palanisamy, V. Tunáková, J. Ornstová, M. Venkataraman, A. Ali, and J. Militký, "Flexible Textile Structures for Strain Sensing Applications," in *Advanced Multifunctional Materials from Fibrous Structures*, Springer, 2023, pp. 255–278.
[151] Y.-H. Kim *et al.*, "Assessing the Role of Yarn Placement in Plated Knit Strain Sensors: A Detailed Study of Their Electromechanical Properties and Applicability in Bending Cycle Monitoring," *Sensors*, vol. 24, no. 5, p. 1690, 2024.
[152] M. Li, H. Li, W. Zhong, Q. Zhao, and D. Wang, "Stretchable Conductive Polypyrrole / Polyurethane (PPy / PU) Strain Sensor with Netlike Microcracks for Human Breath Detection," *ACS Appl. Mater. Interfaces*, vol. 6, pp. 1313–1319, 2013.
[153] C. Honnet *et al.*, "PolySense: Augmenting Textiles with Electrical Functionality using In-Situ Polymerization," in *Proceedings of the 2020 CHI Conference on Human Factors in Computing Systems*, 2020, pp. 1–13.
[154] I. Wicaksono, "Design and Implementation of Multi-sensory Fabric as Deformable Musical Interface." ETH Zürich, 2016.
[155] O. Atalay, "Textile-based, interdigital, capacitive, soft-strain sensor for wearable applications," *Materials (Basel).*, vol. 11, no. 5, p. 768, 2018.
[156] M. Wang *et al.*, "A percolation model for piezoresistivity in conductor–polymer composites," *Adv. Theory Simulations*, vol. 2, no. 2, p. 1800125, 2019.
[157] J. Park, I. You, S. Shin, and U. Jeong, "Material approaches to stretchable strain sensors," *ChemPhysChem*, vol. 16, no. 6. pp. 1155–1163, 2015.
[158] J. Meyer, B. Arnrich, J. Schumm, and G. Troster, "Design and modeling of a textile pressure sensor for sitting posture classification," *IEEE Sens. J.*, 2010.
[159] O. Atalay, A. Atalay, J. Gafford, H. Wang, R. Wood, and C. Walsh, "A Highly Stretchable Capacitive-Based Strain Sensor Based on Metal Deposition and Laser Rastering," *Adv. Mater. Technol.*, vol. 1700081, p. 1700081, 2017.
[160] I. Wicaksono and J. Paradiso, "KnittedKeyboard: Digital Knitting of Electronic Textile Musical Controllers," *Proc. Int. Conf. New Interfaces Music. Expr.*, 2020.
[161] I. Wicaksono *et al.*, "3DKnITS: Three-dimensional Digital Knitting of Intelligent Textile Sensor for Activity Recognition and Biomechanical Monitoring," in *2022 44th Annual*

International Conference of the IEEE Engineering in Medicine & Biology Society (EMBC), 2022, pp. 2403–2409.
[162] I. Wicaksono, D. D. Haddad, and J. Paradiso, "Tapis Magique: Machine-knitted Electronic Textile Carpet for Interactive Choreomusical Performance and Immersive Environments," in *Creativity and Cognition*, 2022, pp. 262–274.
[163] I. Wicaksono *et al.*, "Living Knitwork Pavilion: Soft Responsive Architectural Space with Functional Textiles and Integrated System," *(to Appear.*, 2024.
[164] J. A. Paradiso, "Electronic music: new ways to play," *IEEE Spectr.*, 1997.
[165] T. Holmes, *Electronic and experimental music: technology, music, and culture*. Routledge, 2012.
[166] R. A. Moog and T. L. Rhea, "Evolution of the keyboard interface. The Bosendorfer 290 SE recording piano and the Moog Multiply-Touch-Sensitive keyboards," *Comput. Music J.*, 1990.
[167] A. McPherson, "Buttons, handles, and keys: Advances in continuous-control keyboard instruments," in *Computer Music Journal*, 2015.
[168] L. Stahlberg, "MusiCushions: Designing interactive cushions that integrate with the home environment," *Degree Proj. Comput. Sci. Eng.*, 2018.
[169] G. M. Troiano, E. W. Pedersen, and K. Hornbæk, "Deformable interfaces for performing music," in *Conference on Human Factors in Computing Systems - Proceedings*, 2015.
[170] J. Paradiso and L. Borque, "A Fabric Keyboard for Composing on the Road (Unpublished Proposal)."
[171] M. Parzer, P., Perteneder, F., Probst, K., Rendl, C., Leong, J., Schuetz, S., Vogl, A., Schwoediauer, R., Kaltenbrunner, M., Bauer, S. and Haller, "RESi: A Highly Flexible, Pressure-Sensitive, Imperceptible Textile Interface Based on Resistive Yarns," *Proc. 31st Annu. ACM Symp. User Interface Softw. Technol.*, pp. 745–756, 2018.
[172] J. Cherston and J. A. Paradiso, "SpaceSkin: development of aerospace-grade electronic textile for simultaneous protection and high velocity impact characterization," *Sensors Smart Struct. Technol. Civil, Mech. Aerosp. Syst.*, 2019.
[173] W. Yan *et al.*, "Single fibre enables acoustic fabrics via nanometre-scale vibrations," *Nature*, vol. 603, no. 7902, pp. 616–623, 2022.
[174] P. Parzer, A. Sharma, A. Vogl, J. Steimle, A. Olwal, and M. Haller, "SmartSleeve: Realtime sensing of surface and deformation gestures on flexible, interactive textiles, using a hybrid gesture detection pipeline," in *UIST 2017 - Proceedings of the 30th Annual ACM Symposium on User Interface Software and Technology*, 2017.
[175] B. Zhou, M. S. Singh, S. Doda, M. Yildirim, J. Cheng, and P. Lukowicz, "The carpet knows: Identifying people in a smart environment from a single step," in *2017 IEEE International Conference on Pervasive Computing and Communications Workshops, PerCom Workshops 2017*, 2017.
[176] P. Petz, F. Eibensteiner, and J. Langer, "Performance Evaluation of Conductive Textiles for Movement Pattern Recognition in Smart Socks," in *Proceedings of the International Conference on Information and Digital Technologies 2019, IDT 2019*, 2019.
[177] J. W. Jeong, Y. W. Jang, I. Lee, S. Shin, and S. Kim, "Wearable respiratory rate monitoring using piezo-resistive fabric sensor," in *IFMBE Proceedings*, 2009.

[178] P. Chung, A. Rowe, M. Etemadi, H. Lee, and S. Roy, "Fabric-based pressure sensor array for decubitus ulcer monitoring," in *Proceedings of the Annual International Conference of the IEEE Engineering in Medicine and Biology Society, EMBS*, 2013.
[179] I. Baldoli *et al.*, "Pressure mapping with textile sensors for compression therapy monitoring," *Proc. Inst. Mech. Eng. Part H J. Eng. Med.*, 2016.
[180] M. Leong, J., Parzer, P., Perteneder, F., Babic, T., Rendl, C., Vogl, A., Egger, H., Olwal, A. and Haller, "proCover: sensory augmentation of prosthetic limbs using smart textile covers," *Proc. 29th Annu. Symp. User Interface Softw. Technol.*, pp. 335–346, 2016.
[181] G. Buscher, R. Koiva, C. Schurmann, R. Haschke, and H. J. Ritter, "Tactile dataglove with fabric-based sensors," in *IEEE-RAS International Conference on Humanoid Robots*, 2012.
[182] J. Cheng, M. Sundholm, B. Zhou, M. Hirsch, and P. Lukowicz, "Smart-surface: Large scale textile pressure sensors arrays for activity recognition," *Pervasive Mob. Comput.*, 2016.
[183] M. Kim, H. Choi, K.-J. Cho, and S. Jo, "Single to Multi: Data-Driven High Resolution Calibration Method for Piezoresistive Sensor Array," *IEEE Robot. Autom. Lett.*, vol. 6, no. 3, pp. 4970–4977, 2021.
[184] D. Giovanelli and E. Farella, "Force sensing resistor and evaluation of technology for wearable body pressure sensing," *J. Sensors*, vol. 2016, no. 1, p. 9391850, 2016.
[185] A. S. Lundervold and A. Lundervold, "An overview of deep learning in medical imaging focusing on MRI," *Z. Med. Phys.*, vol. 29, no. 2, pp. 102–127, 2019.
[186] Y. Weizman and F. K. Fuss, "Sensor array design and development of smart sensing system for kick force visualization in soccer," *Procedia Technol.*, vol. 20, pp. 138–143, 2015.
[187] K. N. Bachus, A. L. DeMarco, K. T. Judd, D. S. Horwitz, and D. S. Brodke, "Measuring contact area, force, and pressure for bioengineering applications: using Fuji Film and TekScan systems," *Med. Eng. Phys.*, vol. 28, no. 5, pp. 483–488, 2006.
[188] B. Sparti, "The function and status of dance in the 15th-century Italian courts," *Danc. Res.*, vol. 14, no. 1, pp. 42–61, 1996.
[189] P. H. Mason, "Music, dance and the total art work: choreomusicology in theory and practice," *Res. Danc. Educ.*, vol. 13, no. 1, pp. 5–24, 2012.
[190] W. Siegel and J. Jacobsen, "The challenges of interactive dance: An overview and case study," *Comput. Music J.*, vol. 22, no. 4, pp. 29–43, 1998.
[191] C. Salter, *Entangled: technology and the transformation of performance*. MIT press, 2010.
[192] A. Glinsky, *Theremin: ether music and espionage*. University of Illinois Press, 2000.
[193] N. Collins, C. Kiefer, Z. Patoli, and M. White, "Musical Exoskeletons: Experiments with a Motion Capture Suit.," in *NIME*, 2010, pp. 455–458.
[194] L. E. Miller, "Cage, Cunningham, and Collaborators: The Odyssey of" Variations V"," *Music. Q.*, vol. 85, no. 3, pp. 545–567, 2001.
[195] J. B. Rovan, R. Wechsler, and F. Weiss, "Seine Hohle Form: artistic collaboration in an interactive dance and music performance environment," *Crossings eJournal Art Technol.*, vol. 1, no. 2, 2001.
[196] D. Rokeby, "The construction of experience: Interface as content," *Digit. Illusion Entertain. Futur. with high Technol.*, vol. 27, p. 47, 1998.
[197] S. Fdili Alaoui, "Making an interactive dance piece: Tensions in integrating technology in

art," in *Proceedings of the 2019 on designing interactive systems conference*, 2019, pp. 1195–1208.
[198] H. Zulić, "How AI can change/improve/influence music composition, performance and education: three case studies," *Insa. J. Contemp. Music. Art Technol.*, no. 2, pp. 100–114, 2019.
[199] L. R. Vickery, "The Yamaha MIBURI MIDI jump suit as a controller for STEIM's Interactive Video software Image/ine," in *Proceedings of the Australian Computer Music Conference, Melbourne, Australia*, 2002, pp. 181–188.
[200] J. Paradiso, K.-Y. Hsiao, and E. Hu, "Interactive music for instrumented dancing shoes," in *ICMC*, 1999.
[201] L. Sonami, "On my work," 2006.
[202] T. Mitchell, S. Madgwick, and I. Heap, "Musical Interaction with Hand Posture and Orientation: A Toolbox of Gestural Control Mechanisms.," in *NIME*, 2012.
[203] A. Martinez, M. Honauer, H. Sandhaus, and E. Hornecker, "Smart textiles in the performing arts," in *Textiles, Identity and Innovation: Design the Future*, CRC Press, 2018, pp. 311–318.
[204] J. Paradiso, C. Abler, K. Hsiao, and M. Reynolds, "The magic carpet: physical sensing for immersive environments," in *CHI'97 Extended Abstracts on Human Factors in Computing Systems*, 1997, pp. 277–278.
[205] R. Aylward and J. A. Paradiso, "Sensemble: A Wireless, Compact, Multi-User Sensor System for Interactive Dance.," in *NIME*, 2006, vol. 6, pp. 134–139.
[206] D. G. Rodrigues, E. Grenader, F. D. S. Nos, M. de S. Dall'Agnol, T. E. Hansen, and N. Weibel, "MotionDraw: a tool for enhancing art and performance using kinect," in *CHI'13 Extended Abstracts on Human Factors in Computing Systems*, 2013, pp. 1197–1202.
[207] R. A. Angelova, "Design of weave patterns: when engineering textiles meets music," *J. Text. Inst.*, vol. 108, no. 5, pp. 870–876, 2017.
[208] G. Smith, "Generative design for textiles: opportunities and challenges for entertainment AI," in *Proceedings of the AAAI Conference on Artificial Intelligence and Interactive Digital Entertainment*, 2017, vol. 13, no. 1, pp. 115–121.
[209] E. Medekšaitė, "Mapping Textile Patterns into Sonic Experience." PhD thesis, Durham University, 2016.
[210] B. Diemer and I. Facio, "The fabric of the universe: exploring the cosmic web in 3D prints and woven textiles," *Publ. Astron. Soc. Pacific*, vol. 129, no. 975, p. 58013, 2017.
[211] A. Psarra and A. Briot, "Listening space: Satellite ikats," in *Proceedings of the 2019 ACM International Symposium on Wearable Computers*, 2019, pp. 318–321.
[212] P. Kitley, "Ornamentation and originality: involution in Javanese batik," *Indonesia*, no. 53, pp. 1–19, 1992.
[213] U. Ramseyer, "Music, dance, and the textile craft in Bali," *Vis. Anthropol.*, vol. 1, no. 3, pp. 323–333, 1988.
[214] M. Sharma, *Musical Heritage of India*. APH Publishing, 2007.
[215] G. Pareyon, *On Musical Self-Similarity: Intersemiosis as Synecdoche and Analogy*. Gabriel Pareyon, 2011.
[216] J.-P. Birat, "Musica Universalis or the Music of the Spheres," *Matériaux Tech.*, vol. 105, no.

5–6, p. 509, 2017.
[217] I. Wicaksono *et al.*, "PerForm: Deformable Interface for Exploring Sound through Shapes," in *Extended Abstracts of the 2018 CHI Conference on Human Factors in Computing Systems*, 2018, pp. 1–6.
[218] B. Gonzalez, E. Carroll, and C. Latulipe, "Dance-inspired technology, technology-inspired dance," in *Proceedings of the 7th Nordic Conference on Human-Computer Interaction: Making Sense Through Design*, 2012, pp. 398–407.
[219] L. Gabrielli, *Developing Virtual Synthesizers with VCV Rack*. Focal Press, 2020.
[220] P. Damrhung and L. Skar, "Reinventing How We Move: The Pichet Klunchun Dance Company in the Context of Contemporary Thai Dance," in *The Routledge Companion to Dance in Asia and the Pacific*, Routledge India, 2021, pp. 201–213.
[221] I. Santana and F. Iazzetta, "Liveness in mediatized dance performance-an evolutionary and semiotic approach," *Np np, nd*, 2009.
[222] R. Grusin, "Radical mediation," *Crit. Inq.*, vol. 42, no. 1, pp. 124–148, 2015.
[223] M. Wiberg, J. Kaye, and P. Thomas, "PUC theme issue: material interactions," *Pers. Ubiquitous Comput.*, vol. 18, pp. 573–576, 2014.
[224] H. Ishii, "Tangible bits: beyond pixels," in *Proceedings of the 2nd international conference on Tangible and embedded interaction*, 2008, pp. xv–xxv.
[225] E. G. Özdamar, "A neuroarchitectural perspective to immersive architectural environments," *technoetic arts a J. Specul. Res.*, vol. 21, no. 1, pp. 35–51, 2023.
[226] B. Farahi and N. Leach, *Interactive Design: Towards a Responsive Environment*. Birkhäuser, 2023.
[227] R. Trisno, D. Husin, F. Lianto, and C. E. Hartoyo, "The Concept of Tent as a Temporary Architecture in the Millennium Era," *Sp. Cult.*, p. 12063312231159220, 2023.
[228] M. McQuaid and P. Beesley, *Extreme textiles: designing for high performance*. Princeton Architectural Press, 2005.
[229] H. Coch, "—Bioclimatism in vernacular architecture," *Renew. Sustain. energy Rev.*, vol. 2, no. 1–2, pp. 67–87, 1998.
[230] G. Doczi, "The power of limits: Proportional harmonies in nature, art, and architecture," 1981.
[231] M. A. Kamal, "An investigation into tensile structure system: construction morphology and architectural interventions," *J. Build. Mater. Struct.*, vol. 7, no. 2, pp. 236–254, 2020.
[232] S. Ahlquist and U. Planning, "Knit Architecture," in *Annual Conference of the Association for Computer Aided Design in Architecture Proceedings 2016 (ACADIA)*, 2016, pp. 254–259.
[233] M. Popescu *et al.*, "Structural design, digital fabrication and construction of the cable-net and knitted formwork of the KnitCandela concrete shell," in *Structures*, 2021, vol. 31, pp. 1287–1299.
[234] S. Ahlquist, "Sensory material architectures: Concepts and methodologies for spatial tectonics and tactile responsivity in knitted textile hybrid structures," *Int. J. Archit. Comput.*, vol. 14, no. 1, pp. 63–82, 2016.
[235] J. E. Sabin, J. Hilla, D. Pranger, C. Binkley, and J. Bilotti, "Embedded architecture: Ada, driven by humans, powered by AI," *Fabr. 2020*, pp. 246–255, 2020.
[236] K. M. Strobel, C. B. Binkley, and J. E. Sabin, "Lumen tensegrity towers," in *Proceedings of*

IASS Annual Symposia, 2018, vol. 2018, no. 5, pp. 1–8.
[237] Y. Luo, K. Wu, T. Palacios, and W. Matusik, "KnitUI: Fabricating Interactive and Sensing Textiles with Machine Knitting," in *Proceedings of the 2021 CHI Conference on Human Factors in Computing Systems*, 2021, pp. 1–12.
[238] J. Forman *et al.*, "FibeRobo: Fabricating 4D Fiber Interfaces by Continuous Drawing of Temperature Tunable Liquid Crystal Elastomers," in *Proceedings of the 36th Annual ACM Symposium on User Interface Software and Technology*, 2023, pp. 1–17.
[239] H. W. Choi *et al.*, "Smart textile lighting/display system with multifunctional fibre devices for large scale smart home and IoT applications," *Nat. Commun.*, vol. 13, no. 1, p. 814, 2022.
[240] B. Swedien, *Make mine music*. Hal Leonard Corporation, 2009.
[241] J. R. Smith, "Electric field imaging." Massachusetts Institute of Technology, 1999.
[242] E. Schling, H. Wang, S. Hoyer, and H. Pottmann, "Designing asymptotic geodesic hybrid gridshells," *Comput. Des.*, vol. 152, p. 103378, 2022.
[243] J. Cichocka and S. Łoj, "Multi-Objective Constraint Multi-Swarm Particle Swarm Optimization Without Velocity (MOCMPSOWV) and its implementation in the GOLDFISH framework.," 2024.
[244] S. Bian, M. Liu, B. Zhou, P. Lukowicz, and M. Magno, "Body-Area Capacitive or Electric Field Sensing for Human Activity Recognition and Human-Computer Interaction: A Comprehensive Survey," *Proc. ACM Interactive, Mobile, Wearable Ubiquitous Technol.*, vol. 8, no. 1, pp. 1–49, 2024.
[245] J. A. Paradiso and N. Gershenfeld, "Musical applications of electric field sensing," *Comput. Music J.*, vol. 21, no. 2, pp. 69–89, 1997.
[246] D. D. Haddad *et al.*, "Resynthesizing reality: Driving vivid virtual environments from sensor networks," in *ACM SIGGRAPH 2017 Talks*, 2017, pp. 1–2.
[247] J. Lifton and J. A. Paradiso, "Dual reality: Merging the real and virtual," in *Facets of Virtual Environments: First International Conference, FaVE 2009, Berlin, Germany, July 27-29, 2009, Revised Selected Papers 1*, 2010, pp. 12–28.
[248] H. ISHII *et al.*, "Human-Material Interaction for Expression, Performance, and Remembering," 2023.
[249] S. Tachi, "Telexistence: Past, present, and future," in *Virtual Realities: International Dagstuhl Seminar, Dagstuhl Castle, Germany, June 9-14, 2013, Revised Selected Papers*, 2015, pp. 229–259.
[250] J. Copet *et al.*, "Simple and controllable music generation," *Adv. Neural Inf. Process. Syst.*, vol. 36, 2024.
[251] F. Visi *et al.*, "Networking concert halls, musicians, and interactive textiles: Interwoven Sound Spaces," *Digit. Creat.*, vol. 35, no. 1, pp. 52–73, 2024.
[252] N. L'Huillier and T. Machover, "Spaces that perform themselves," *Editor. Coord. Rufus Adebayo, Ismail Farouk, Steve Jones, Maleshoane Rapeane-Mathonsi*, p. 170, 2018.
[253] S. Micus, S. G. Rostami, M. Haupt, G. T. Gresser, M. A. Meghrazi, and L. Eskandarian, "Integrating electronics to textiles by ultrasonic welding for cable-driven applications for smart textiles," *Materials (Basel).*, vol. 14, no. 19, p. 5735, 2021.
[254] A. Mehmann, M. Varga, and G. Tröster, "Reversible contacting for smart textiles," *Smart*

Text. Fundam. Des. Interact., pp. 185–198, 2017.
[255] A. Mehmann, M. Varga, K. Gönner, and G. Tröster, "A ball-grid-array-like electronics-to-textile pocket connector for wearable electronics," in *Proceedings of the 2015 ACM International Symposium on Wearable Computers*, 2015, pp. 57–60.
[256] J. Stanley, J. A. Hunt, P. Kunovski, and Y. Wei, "A review of connectors and joining technologies for electronic textiles," *Eng. Reports*, p. e12491, 2021.
[257] J. Vanfleteren *et al.*, "SCB and SMI: two stretchable circuit technologies, based on standard printed circuit board processes," *Circuit World*, vol. 38, no. 4, pp. 232–242, 2012.
[258] J. Vanfleteren *et al.*, "Printed circuit board technology inspired stretchable circuits," *MRS Bull.*, 2012.
[259] N. Naserifar, P. R. LeDuc, and G. K. Fedder, "Material Gradients in Stretchable Substrates toward Integrated Electronic Functionality.," *Adv. Mater.*, vol. 28, no. 18, pp. 3584–3591, 2016.
[260] S. P. Lacour, J. Jones, S. Wagner, T. Li, and Z. Suo, "Stretchable interconnects for elastic electronic surfaces," *Proc. IEEE*, vol. 93, no. 8, pp. 1459–1467, 2005.
[261] A. Vásquez Quintero, R. Verplancke, H. De Smet, and J. Vanfleteren, "Stretchable electronic platform for soft and smart contact lens applications," *Adv. Mater. Technol.*, vol. 2, no. 8, p. 1700073, 2017.
[262] M.-D. Damaceanu, "Polyimides: Past, present, and future," in *Polyimides*, Elsevier, 2024, pp. 1–50.
[263] Y. Lee, W. Guan, E. Y. Hsieh, and S. Nam, "Opportunities for Nanomaterials in Stretchable and Free-Form Displays," *Small Sci.*, vol. 4, no. 3, p. 2300143, 2024.
[264] S. Yang, S. Qiao, and N. Lu, "Elasticity solutions to nonbuckling serpentine ribbons," *J. Appl. Mech.*, vol. 84, no. 2, p. 21004, 2017.
[265] T. Widlund, S. Yang, Y. Y. Hsu, and N. Lu, "Stretchability and compliance of freestanding serpentine-shaped ribbons," *Int. J. Solids Struct.*, 2014.
[266] J. A. Fan *et al.*, "Fractal design concepts for stretchable electronics," *Nat. Commun.*, vol. 5, no. 1, p. 3266, 2014.
[267] Q. Ma and Y. Zhang, "Mechanics of fractal-inspired horseshoe microstructures for applications in stretchable electronics," *J. Appl. Mech.*, vol. 83, no. 11, p. 111008, 2016.
[268] Y. Huang, Y. Su, and S. Jiang, "Structural Engineering of Flexible Electronics," in *Flexible Electronics: Theory and Method of Structural Design*, Springer, 2023, pp. 1–26.
[269] Kathryn L. Hatch, *Textile Science*. Minneapolis: West Publishing, 1993.
[270] W. Aldrich, B. Smith, and Feng Dong, "Obtaining repeatability of natural extended upper body positions: its use in comparisons of the functional comfort of garments," *J. Fash. Mark. Manag.*, 1998.
[271] G. D. Abowd, "The Internet of materials: A vision for computational materials," *IEEE Pervasive Comput.*, vol. 19, no. 2, pp. 56–62, 2020.
[272] G. Barroeta Pérez, "SNAKE: a dynamically reconfigurable Artificial Sensate Skin." Massachusetts Institute of Technology, 2006.
[273] I. Wicaksono, "Flexible-stretchable woven electronic textile system: a tailored multi-modal bodysuit for spatiotemporal physiological and physical activity monitoring." Massachusetts Institute of Technology, 2019.

[274] R. S. Johansson and A. B. Vallbo, "Tactile sensibility in the human hand: relative and absolute densities of four types of mechanoreceptive units in glabrous skin.," *J. Physiol.*, vol. 286, no. 1, pp. 283–300, 1979.
[275] S. M. Mueller and M. Grunwald, "Anatomical and Physiological Basics," in *Human Touch in Healthcare: Textbook for Therapy, Care and Medicine*, Springer, 2023, pp. 43–81.
[276] R. S. Dahiya, G. Metta, M. Valle, and G. Sandini, "Tactile sensing—from humans to humanoids," *IEEE Trans. Robot.*, vol. 26, no. 1, pp. 1–20, 2009.
[277] T. Shigemitsu and S. Ueno, "The Coupling of Atmospheric Electromagnetic Fields with Biological Systems," in *Bioelectromagnetism*, CRC Press, 2022, pp. 105–143.
[278] M. Kandel and M. Tollet, "Anatomy of the Nervous System," *Brain–Computer Interfaces 1 Found. Methods*, pp. 1–24, 2016.
[279] M. L. Hammock, A. Chortos, B. C. K. Tee, J. B. H. Tok, and Z. Bao, "25th anniversary article: The evolution of electronic skin (E-Skin): A brief history, design considerations, and recent progress," *Adv. Mater.*, vol. 25, no. 42, pp. 5997–6038, 2013.
[280] A. Kohn, "Visual adaptation: physiology, mechanisms, and functional benefits," *J. Neurophysiol.*, vol. 97, no. 5, pp. 3155–3164, 2007.
[281] J. H. Lala, "History and Future Directions of Mission-and Safety-Critical Avionics," in *AIAA Guidance, Navigation, and Control (GNC) Conference*, 2013, p. 5206.
[282] M. Realpe, B. X. Vintimilla, and L. Vlacic, "A fault tolerant perception system for autonomous vehicles," in *2016 35th Chinese Control Conference (CCC)*, 2016, pp. 6531–6536.
[283] J. Yoon *et al.*, "Soft Modular Electronic Blocks (SMEBs): A Strategy for Tailored Wearable Health-Monitoring Systems," *Adv. Sci.*, 2019.
[284] S. J. Benight, C. Wang, J. B. H. Tok, and Z. Bao, "Stretchable and self-healing polymers and devices for electronic skin," *Progress in Polymer Science*, vol. 38, no. 12. pp. 1961–1977, 2013.
[285] S. Jian, "Industrial design of wearable intelligent devices based on wireless networks," *Meas. Sensors*, vol. 30, p. 100934, 2023.
[286] Y. Tenzer, L. P. Jentoft, and R. D. Howe, "The feel of MEMS barometers: Inexpensive and easily customized tactile array sensors," *IEEE Robot. Autom. Mag.*, vol. 21, no. 3, pp. 89–95, 2014.
[287] S. Olberding, N.-W. Gong, J. Tiab, J. A. Paradiso, and J. Steimle, "A cuttable multi-touch sensor," in *Proceedings of the 26th annual ACM symposium on User interface software and technology*, 2013, pp. 245–254.
[288] SparkFun, "I2C." [Online]. Available: https://learn.sparkfun.com/tutorials/i2c/all. [Accessed: 08-Jan-2024].
[289] L. Miliani, "CRC8 Dallas/Maxim." [Online]. Available: https://www.leonardomiliani.com/?p=849&lang=en. [Accessed: 08-Jan-2024].
[290] R. Adelsberger and G. Tröster, "Enabling High-Speed Data Acquisition with Compressive Sampling," in *International Conference on Wearable and Implantable Body Sensor Networks (BSN 2014)*, 2014.
[291] H. Zheng, J. Li, X. Feng, W. Guo, Z. Chen, and N. Xiong, "Spatial-temporal data collection with compressive sensing in mobile sensor networks," *Sensors*, vol. 17, no. 11, p. 2575, 2017.

[292] R. Giordanelli, C. Mastroianni, and M. Meo, “Bio-inspired P2P systems: The case of multidimensional overlay,” *ACM Trans. Auton. Adapt. Syst.*, vol. 7, no. 4, pp. 1–28, 2012.
[293] R. K. Ghosh and H. Ghosh, *Distributed Systems: Theory and Applications*. John Wiley & Sons, 2023.
[294] R. S. Carbajo and C. Mc Goldrick, “Decentralised peer-to-peer data dissemination in wireless sensor networks,” *Pervasive Mob. Comput.*, vol. 40, pp. 242–266, 2017.
[295] C. Rensselaer, “Cloth & Fluid Simulation: Advanced Computer Graphics.” [Online]. Available: https://www.cs.rpi.edu/~cutler/classes/advancedgraphics/S11/hw2_simulation.html. [Accessed: 08-Jan-2024].
[296] H. Va, M.-H. Choi, and M. Hong, “Real-time cloth simulation using compute shader in Unity3D for AR/VR contents,” *Appl. Sci.*, vol. 11, no. 17, p. 8255, 2021.
[297] L. Nissen *et al.*, “Towards preventing gaps in health care systems through smartphone use: Analysis of arkit for accurate measurement of facial distances in different angles,” *Sensors*, vol. 23, no. 9, p. 4486, 2023.
[298] I. Mutis and A. Ambekar, “Challenges and enablers of augmented reality technology for in situ walkthrough applications.,” *J. Inf. Technol. Constr.*, vol. 25, 2020.
[299] K. Ahuja, S. Pareddy, R. Xiao, M. Goel, and C. Harrison, “Lightanchors: Appropriating point lights for spatially-anchored augmented reality interfaces,” in *Proceedings of the 32nd Annual ACM Symposium on User Interface Software and Technology*, 2019, pp. 189–196.
[300] N. Tacca *et al.*, “Wearable high-density EMG sleeve for complex hand gesture classification and continuous joint angle estimation,” *Sci. Rep.*, vol. 14, no. 1, p. 18564, 2024.
[301] I. Wicaksono, A. Shtarbanov, E. Ranade, R. Slater, D. Newman, and J. Paradiso, “Design, Development, and Testing of Peristaltic Suit: Active-Dynamic Compression and Physiological Sensing Intra-vehicular Activity Spacesuit for Cardiovascular Deconditioning,” 2023.
[302] Y. H. Jung *et al.*, “A wireless haptic interface for programmable patterns of touch across large areas of the skin,” *Nat. Electron.*, vol. 5, no. 6, pp. 374–385, 2022.
[303] S. Payra, I. Wicaksono, J. Cherston, C. Honnet, V. Sumini, and J. A. Paradiso, “Feeling Through Spacesuits: Application of Space-Resilient E-Textiles to Enable Haptic Feedback on Pressurized Extravehicular Suits,” in *2021 IEEE Aerospace Conference (50100)*, 2021, pp. 1–12.
[304] Y. Wang, F. Miao, Q. An, Z. Liu, C. Chen, and Y. Li, “Wearable multimodal vital sign monitoring sensor with fully integrated analog front end,” *IEEE Sens. J.*, vol. 22, no. 13, pp. 13462–13471, 2022.
[305] N. Arora, T. Starner, and G. D. Abowd, “SATURN: An introduction to the Internet of Materials,” *Commun. ACM*, vol. 63, no. 12, pp. 92–99, 2020.
[306] M. Magno *et al.*, “InfiniTime: Multi-sensor wearable bracelet with human body harvesting,” *Sustain. Comput. Informatics Syst.*, vol. 11, pp. 38–49, 2016.
[307] A. Dementyev, T. Vega Gálvez, and A. Olwal, “SensorSnaps: Integrating wireless sensor nodes into fabric snap fasteners for textile interfaces,” in *Proceedings of the 32nd Annual ACM Symposium on User Interface Software and Technology*, 2019, pp. 17–28.

[308] A. Y. Benbasat and J. A. Paradiso, "Groggy wakeup-automated generation of power-efficient detection hierarchies for wearable sensors," in *4th International Workshop on Wearable and Implantable Body Sensor Networks (BSN 2007) March 26–28, 2007 RWTH Aachen University, Germany*, 2007, pp. 59–64.
[309] S. Barbarossa, S. Sardellitti, and P. Di Lorenzo, "Distributed detection and estimation in wireless sensor networks," in *Academic Press Library in Signal Processing*, vol. 2, Elsevier, 2014, pp. 329–408.
[310] F. Liu, S. Deswal, A. Christou, Y. Sandamirskaya, M. Kaboli, and R. Dahiya, "Neuro-inspired electronic skin for robots," *Sci. Robot.*, vol. 7, no. 67, p. eabl7344, 2022.
[311] O. Glauser, D. Panozzo, O. Hilliges, and O. Sorkine-Hornung, "Deformation capture via soft and stretchable sensor arrays," *ACM Trans. Graph.*, vol. 38, no. 2, pp. 1–16, 2019.
[312] R. F. Brena, J. P. García-Vázquez, C. E. Galván-Tejada, D. Muñoz-Rodriguez, C. Vargas-Rosales, and J. Fangmeyer Jr, "Evolution of indoor positioning technologies: A survey," *J. Sensors*, vol. 2017, no. 1, p. 2630413, 2017.
[313] M. Borges, A. Symington, B. Coltin, T. Smith, and R. Ventura, "HTC vive: Analysis and accuracy improvement," in *2018 IEEE/RSJ International Conference on Intelligent Robots and Systems (IROS)*, 2018, pp. 2610–2615.
[314] A. N. Balaji and L.-S. Peh, "AI-On-Skin: Towards Enabling Fast and Scalable On-body AI Inference for Wearable On-Skin Interfaces," *Proc. ACM Human-Computer Interact.*, vol. 7, no. EICS, pp. 1–34, 2023.
[315] C. Xu, S. A. Solomon, and W. Gao, "Artificial intelligence-powered electronic skin," *Nat. Mach. Intell.*, vol. 5, no. 12, pp. 1344–1355, 2023.
[316] T. L. Buckner, R. A. Bilodeau, S. Y. Kim, and R. Kramer-Bottiglio, "Roboticizing fabric by integrating functional fibers," *Proc. Natl. Acad. Sci. U. S. A.*, 2020.
[317] S. Park and S. Jayaraman, "Adaptive and responsive textile structures (ARTS)," in *Smart Fibres, Fabrics and Clothing*, 2010.
[318] J. Conca, "Making climate change fashionable-the garment industry takes on global warming. Forbes." 2015.
[319] A. Vasan, B. Sood, and M. Pecht, "Carbon footprinting of electronic products," *Appl. Energy*, vol. 136, pp. 636–648, 2014.
[320] M. N. Pervez *et al.*, "Sustainable e-textiles—development and importance," in *Smart Textiles from Natural Resources*, Elsevier, 2024, pp. 343–365.
[321] A. K. Pattanayak, "Sustainability in fabric manufacturing," in *Sustainable Technologies for Fashion and Textiles*, Elsevier, 2020, pp. 57–72.
[322] S. Maity, K. Singha, and P. Pandit, "Advanced applications of green materials in wearable e-textiles," in *Applications of Advanced Green Materials*, Elsevier, 2021, pp. 239–263.
[323] E. MacArthur, "Towards the circular economy," *J. Ind. Ecol.*, vol. 2, no. 1, pp. 23–44, 2013.
[324] S. Wu and L. Devendorf, "Unfabricate: designing smart textiles for disassembly," in *Proceedings of the 2020 CHI Conference on Human Factors in Computing Systems*, 2020, pp. 1–14.
[325] J. Kang *et al.*, "Modular and Reconfigurable Stretchable Electronic Systems," *Advanced Materials Technologies*, 2018.

[326] L. Smith and P. Ball, "Steps towards sustainable manufacturing through modelling material, energy and waste flows," *Int. J. Prod. Econ.*, vol. 140, no. 1, pp. 227–238, 2012.
[327] V. Arroyos *et al.*, "A Tale of Two Mice: Sustainable Electronics Design and Prototyping," in *CHI Conference on Human Factors in Computing Systems Extended Abstracts*, 2022, pp. 1–10.
[328] S. P. Ramalingam and P. K. Shanmugam, "A comprehensive review on wired and wireless communication technologies and challenges in smart residential buildings," *Recent Adv. Comput. Sci. Commun. (Formerly Recent Patents Comput. Sci.*, vol. 15, no. 9, pp. 1140–1167, 2022.
[329] H. Wang and Q. Li, "Distributed user access control in sensor networks," in *International Conference on Distributed Computing in Sensor Systems*, 2006, pp. 305–320.
[330] J. E. Lovelock and L. Margulis, "Atmospheric homeostasis by and for the biosphere: the Gaia hypothesis," *Tellus*, vol. 26, no. 1–2, pp. 2–10, 1974.
[331] A. Ekblaw *et al.*, "From UbiComp to Universe—Moving Pervasive Computing Research Into Space Applications," *IEEE Pervasive Comput.*, 2023.
[332] L. Tessmer *et al.*, "3D Knit Spacesuit Sleeve with Multifunctional Fibers and Tunable Compression," 2022.
[333] I. Wicaksono, A. Shtarbanov, R. Slater, E. Ranade, and J. Paradiso, "Peristaltic (PS) Suit: Active Bioelectronic Sensing-Compression Spacesuit for Microgravity Adaptation and Cardiovascular Deconditioning," in *ASCEND 2022*, 2022, p. 4208.
[334] J. Liu *et al.*, "Syringe-injectable electronics," *Nat. Nanotechnol.*, vol. 10, no. 7, pp. 629–635, 2015.
[335] D. H. Kim *et al.*, "Thin, flexible sensors and actuators as 'instrumented' surgical sutures for targeted wound monitoring and therapy," *Small*, vol. 8, no. 21, pp. 3263–3268, 2012.
[336] L. Samy, M. C. Huang, J. J. Liu, W. Xu, and M. Sarrafzadeh, "Unobtrusive sleep stage identification using a pressure-sensitive bed sheet," *IEEE Sens. J.*, 2014.
[337] D. Graumann *et al.*, "Large surface area electronic textiles for ubiquitous computing: A system approach," in *2007 Fourth Annual International Conference on Mobile and Ubiquitous Systems: Networking & Services (MobiQuitous)*, 2007, pp. 1–8.
[338] K. Jost *et al.*, "Knitted and screen printed carbon-fiber supercapacitors for applications in wearable electronics," *Energy Environ. Sci.*, vol. 6, no. 9, pp. 2698–2705, 2013.
[339] S. C. Goldstein and T. C. Mowry, "Claytronics: A scalable basis for future robots," 2004.
[340] H. Ishii, D. Lakatos, L. Bonanni, and J.-B. Labrune, "Radical atoms: beyond tangible bits, toward transformable materials," *interactions*, vol. 19, no. 1, pp. 38–51, 2012.
[341] A. Adamatzky, *Fungal machines: Sensing and computing with fungi*, vol. 47. Springer Nature, 2023.
[342] E. Lupton and J. A. Miller, *ABC's of the Bauhaus:: The Bauhaus and Design Theory*, vol. 5. Princeton Architectural Press, 1991.
[343] L. Forlano, M. W. Steenson, and M. Ananny, *Bauhaus futures*. MIT Press, 2019.
[344] S. Brand and R. E. Crandall, "The media lab: Inventing the future at MIT," *New York*, p. 211, 1987.
[345] W. Benjamin, "The work of art in the age of mechanical reproduction," in *A museum studies approach to heritage*, Routledge, 2018, pp. 226–243.

Appendix

This appendix includes close-up images of the *KnittedKeyboard, Tapis Magique,* and *Living Knitwork Pavilion,* as well as PCB schematics and layouts for the *KnittedKeyboard, 3DKnITS, Tapis Magique, Living Knitwork,* and *NETS* in various versions.

Figure A.1: Close-up images of *KnittedKeyboard*.

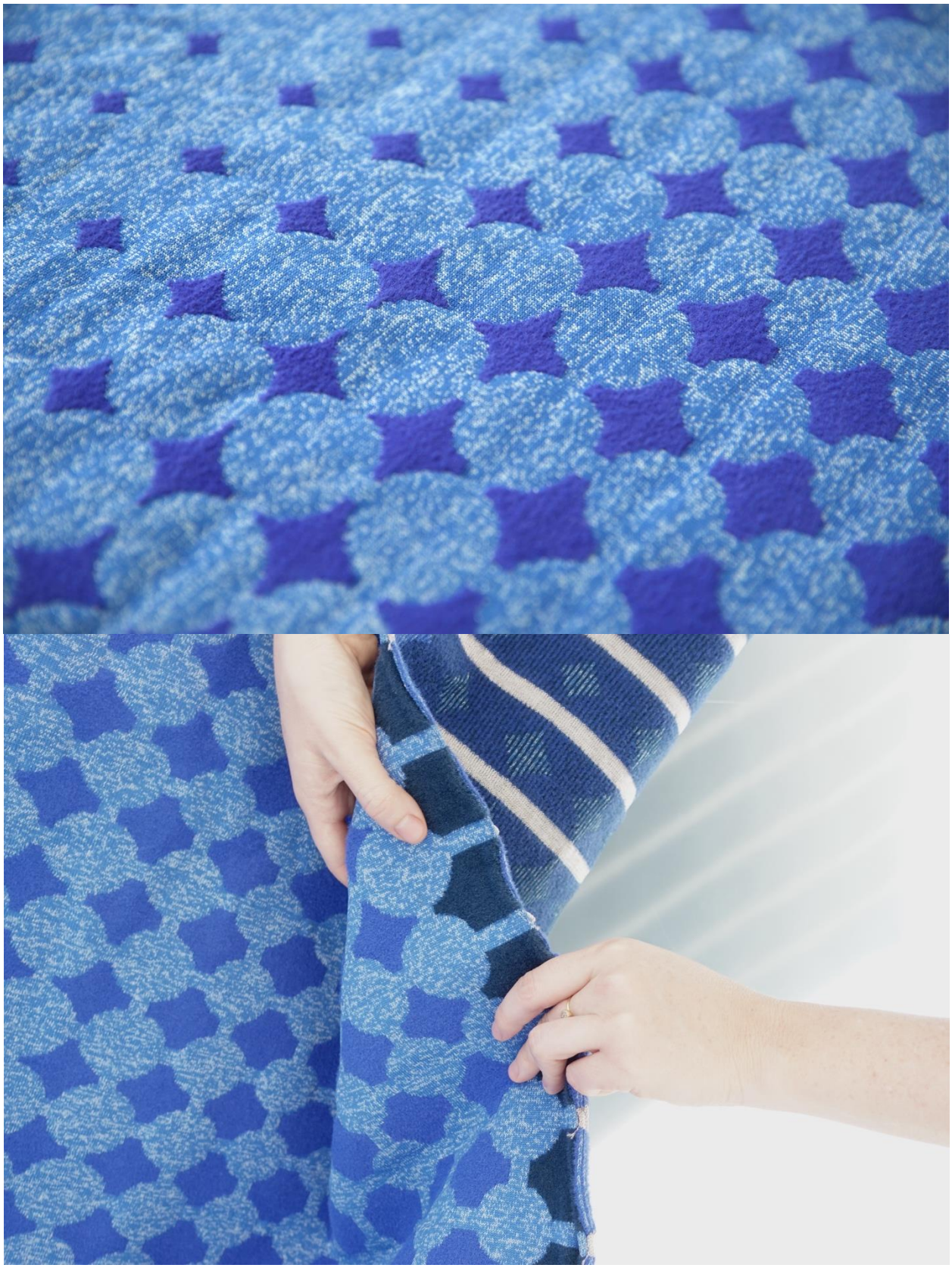

Figure A.2: Close-up images of *Tapis Magique.*

Figure A.3: Close-up images of *Living Knitwork Pavilion* petals.

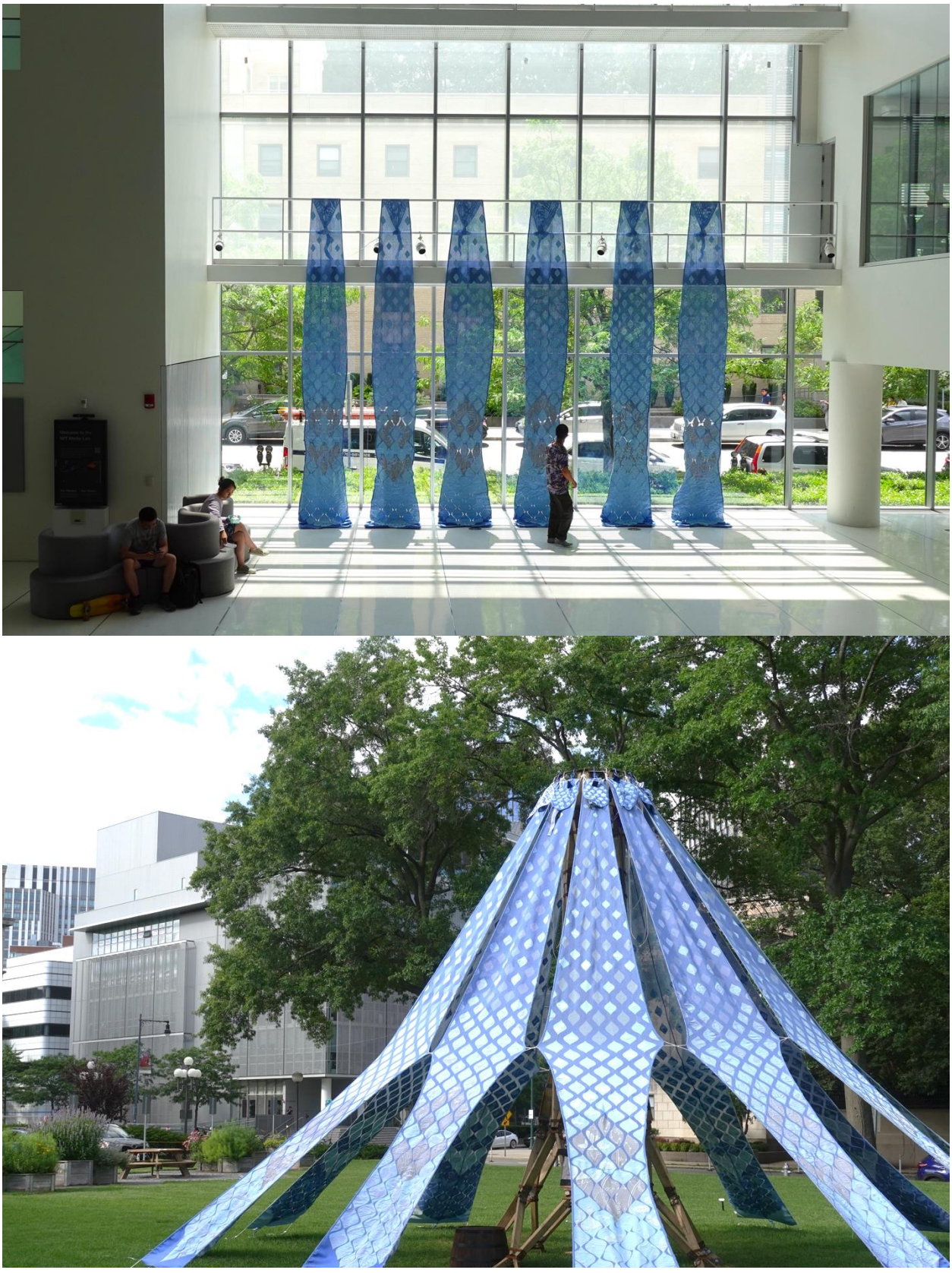

Figure A.4: *Living Knitwork* as tapestry and its installation at the MIT Saxon Lawn.

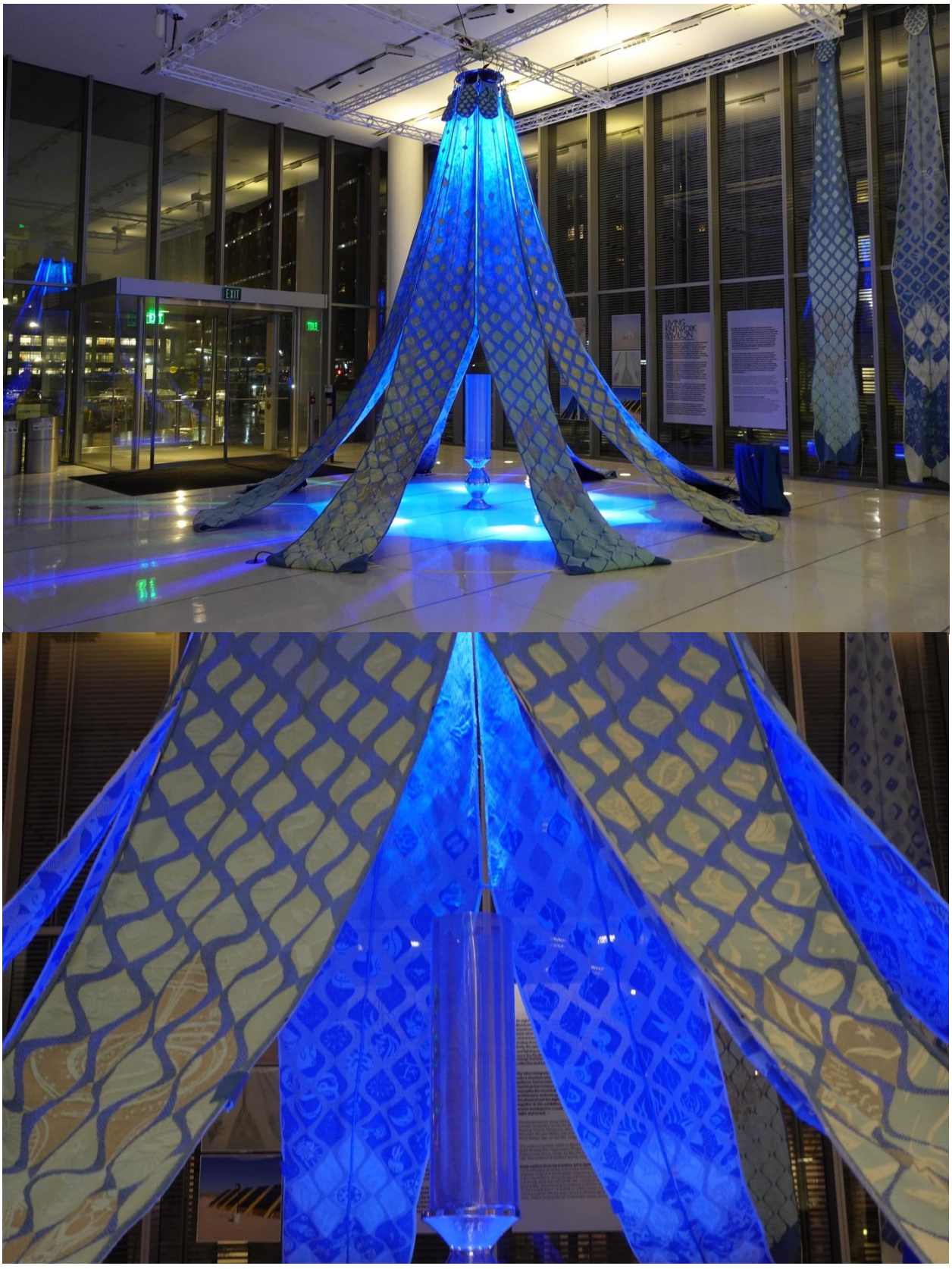

Figure A.5: *Living Knitwork Pavilion* at the E14 MIT Media Lab lobby during the night.

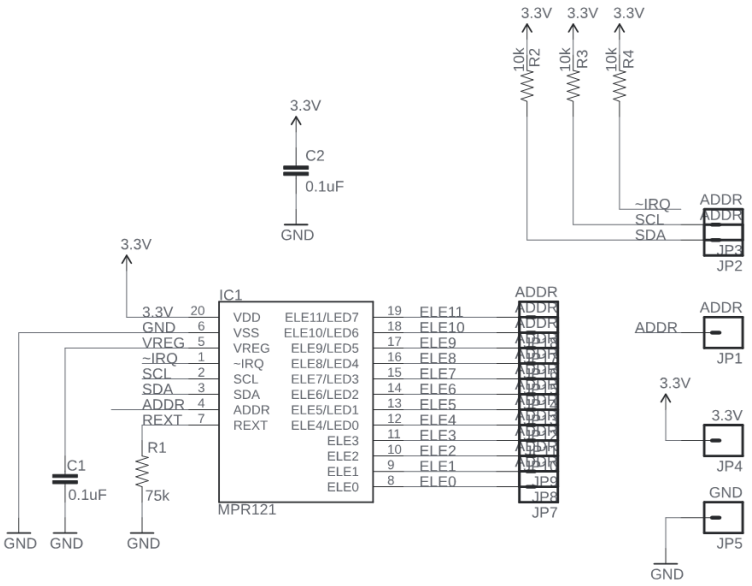

Figure A.6: Flex PCB schematic of the capacitive sensing module for the *KnittedKeyboard* II.

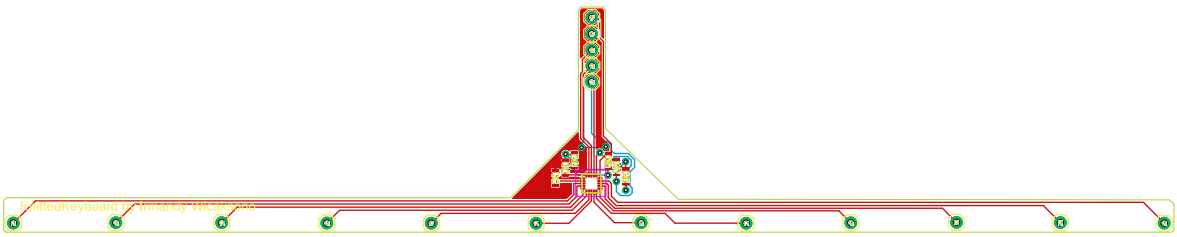

Figure A.7: Flex PCB lay-out of the capacitive sensing module for the *KnittedKeyboard* II.

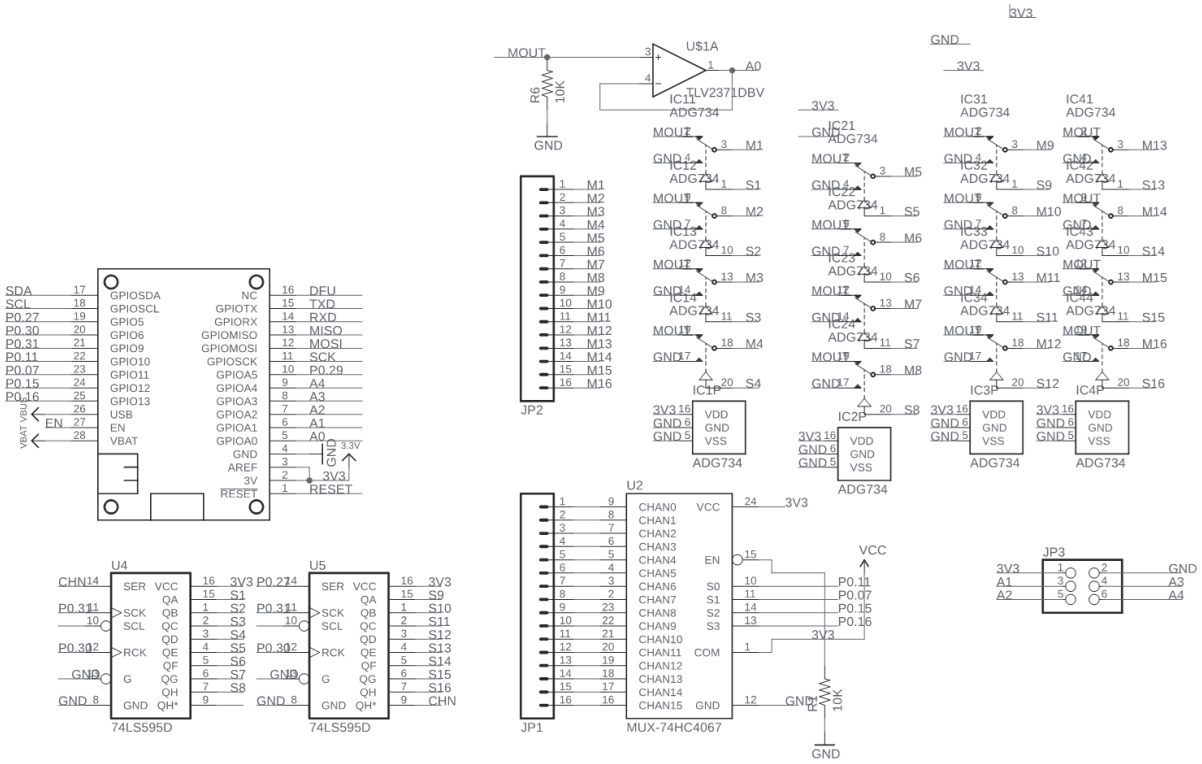

Figure A.8: PCB schematic/break-out of the 16x16 resistive sensing circuit matrix for *3DKnITS*.

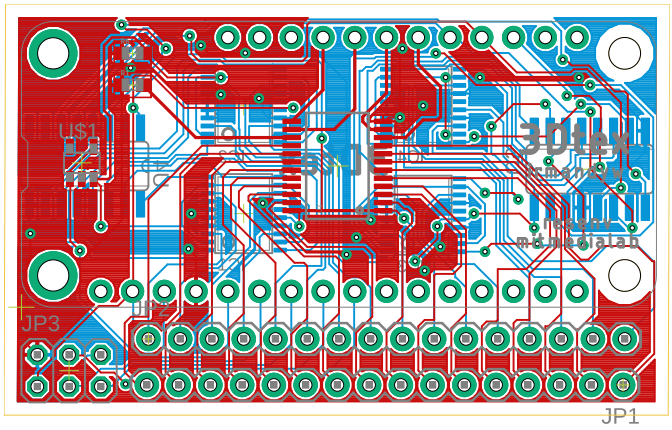

Figure A.9: PCB layout of the 16x16 resistive sensing circuit matrix for *3DKnITS*.

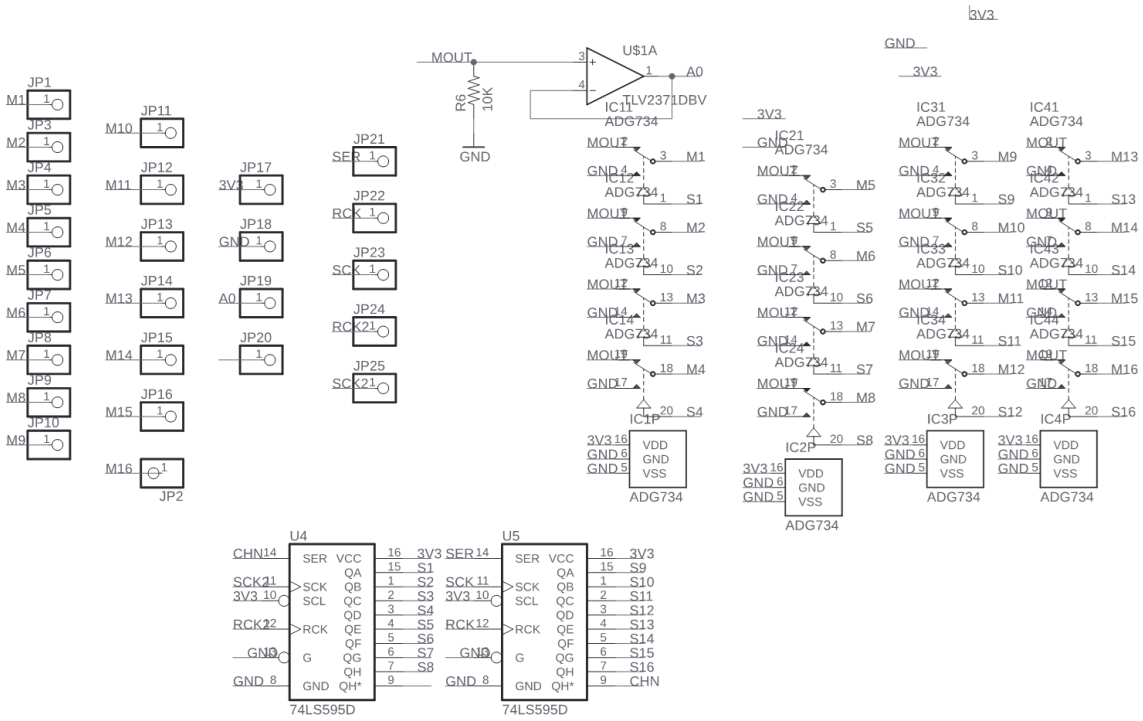

Figure A.10: PCB extension schematic of the n x 16 row array in the resistive sensing circuit matrix for *Tapis Magique.*

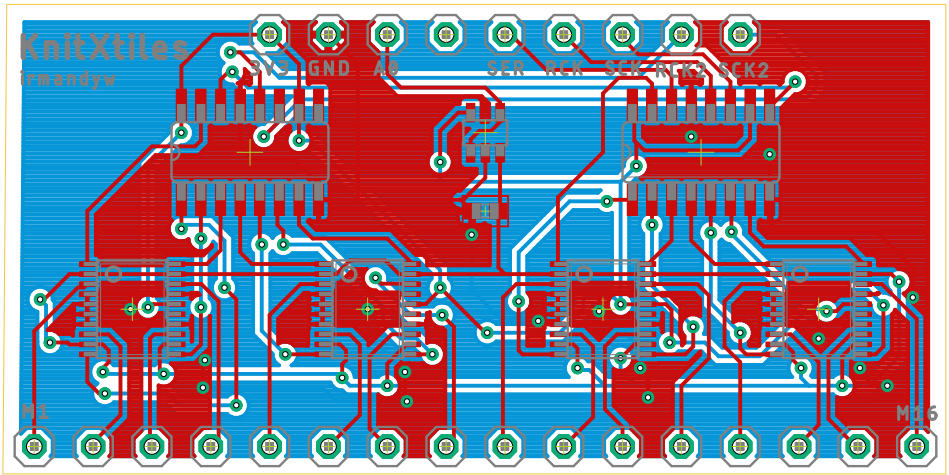

Figure A.11: PCB layout of the n x 16 row array in the resistive sensing circuit matrix for *Tapis Magique.*

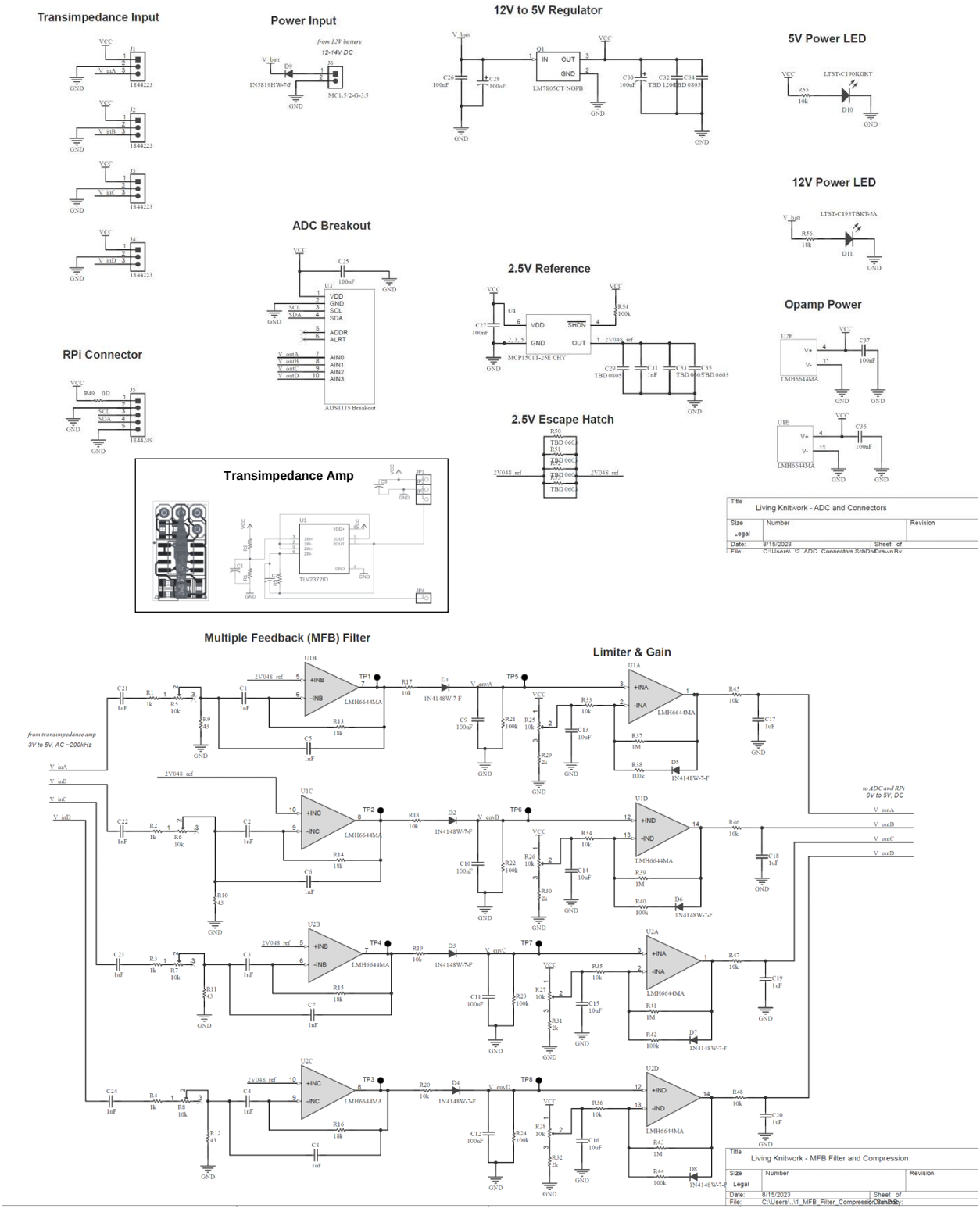

Figure A.12: Analog PCB schematic of the Rx circuit for the *Living Knitwork Pavilion*

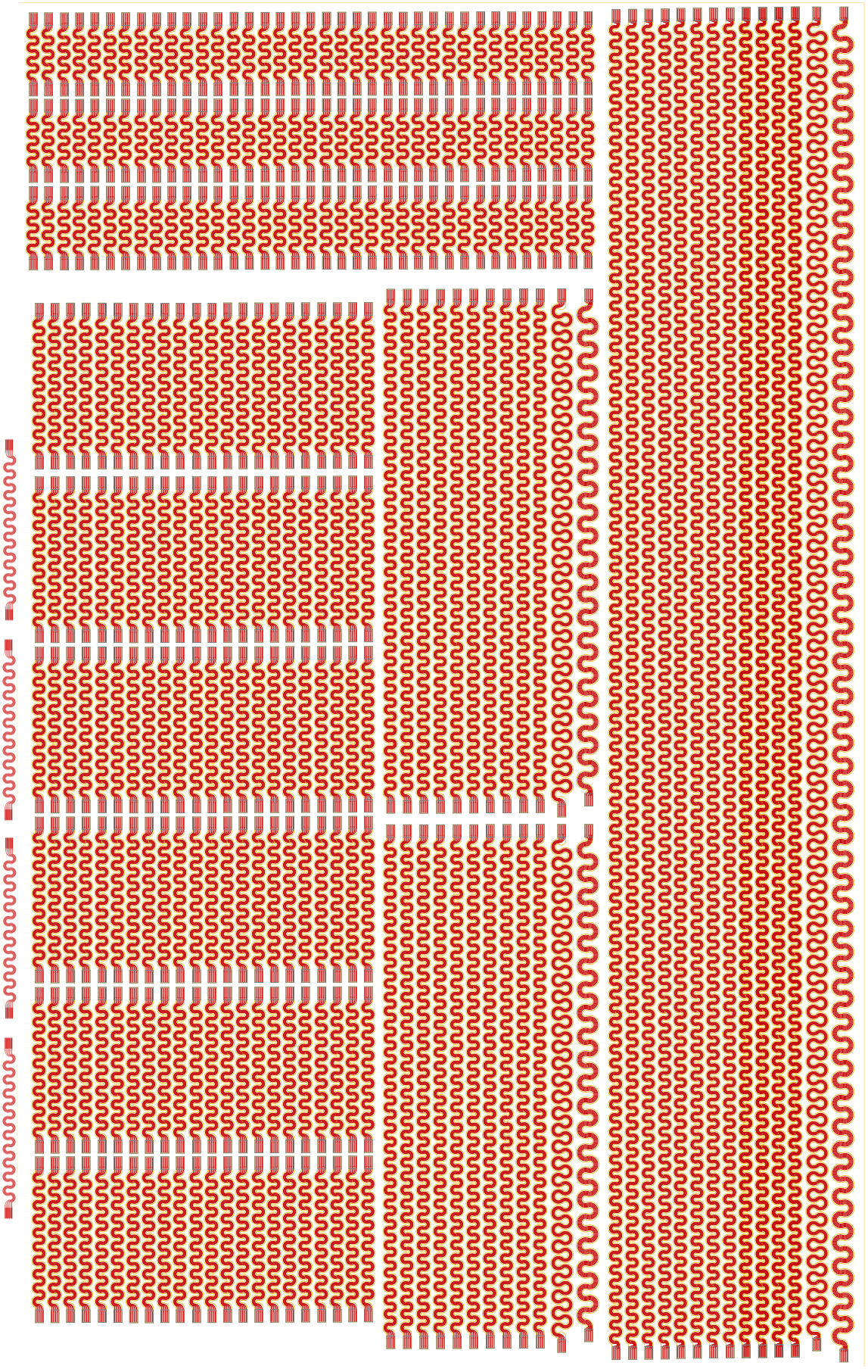

Figure A.13: Serpentine interconnects design in four different lengths for *NETS*.

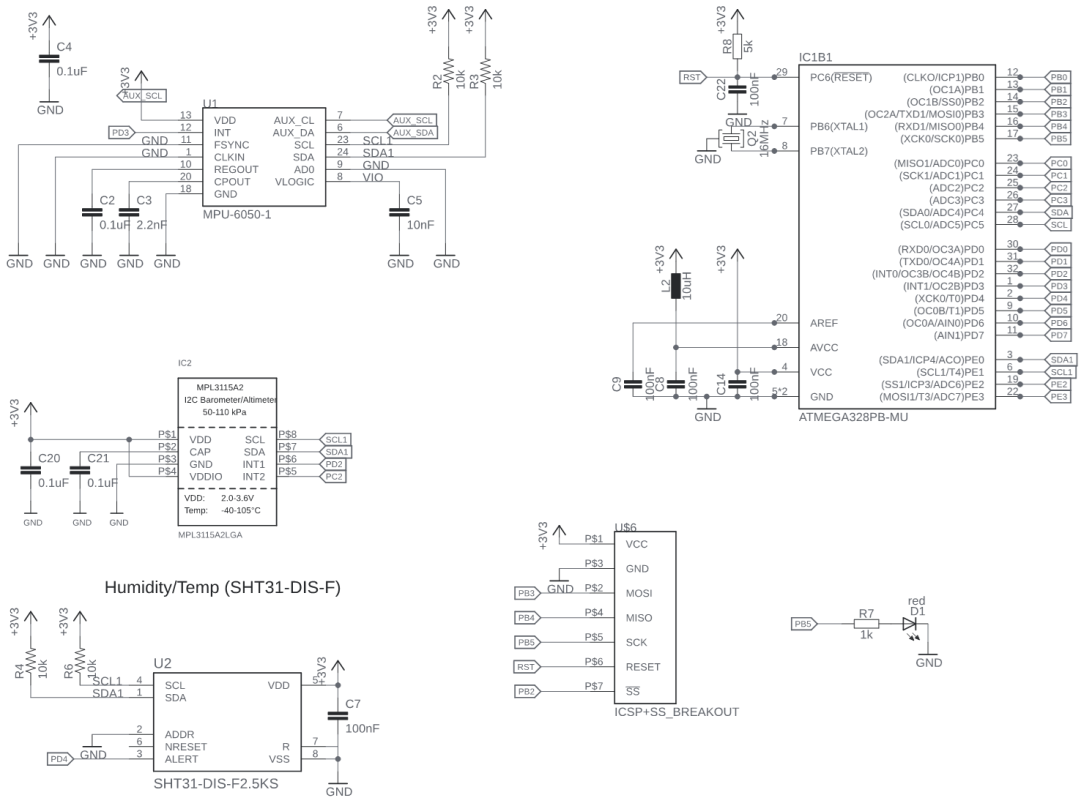

Figure A.14: Flex PCB schematic for *SensorNETS*.

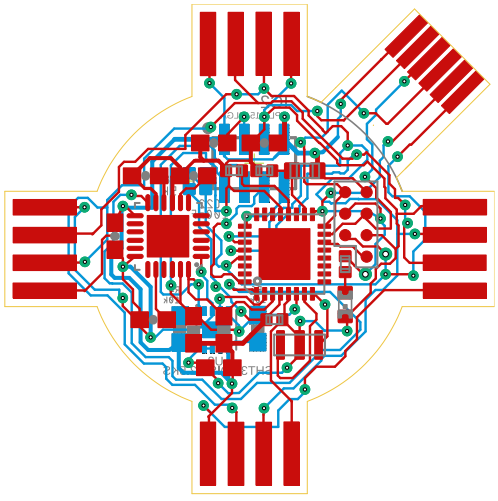

Figure A.15: Flex PCB schematic for *SensorNETS*.

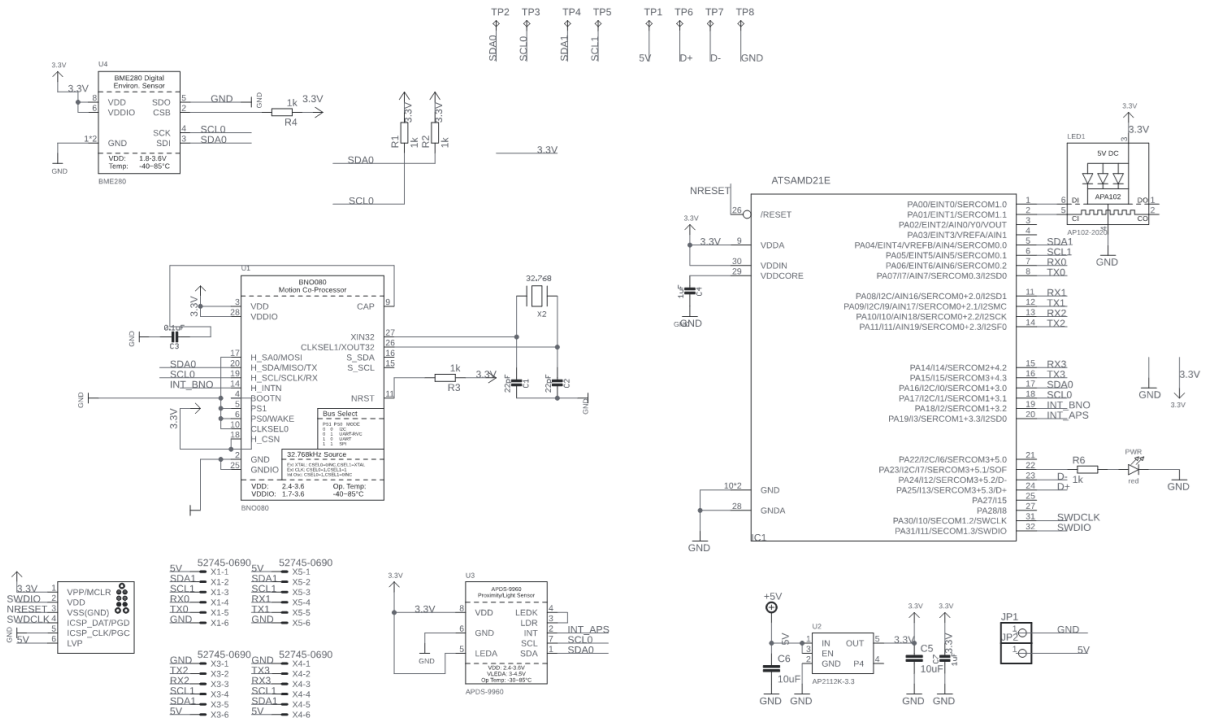

Figure A.16: Flex PCB schematic for *NETS v2.0/3.0*.

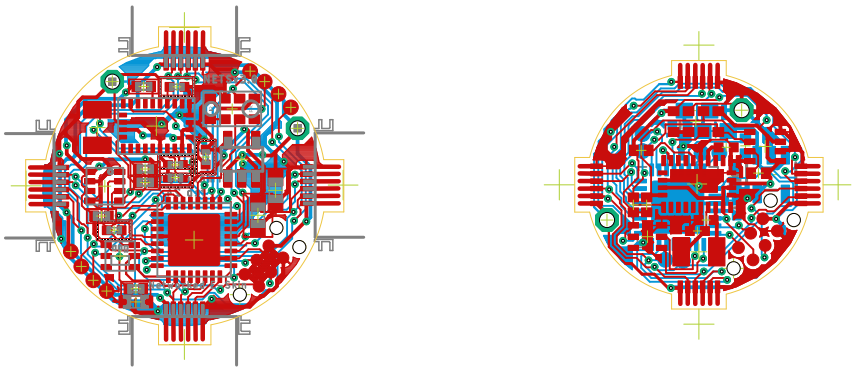

Figure A.17: Flex PCB lay-out for *NETS v2.0* (left) and *NETS v3.0* (right).

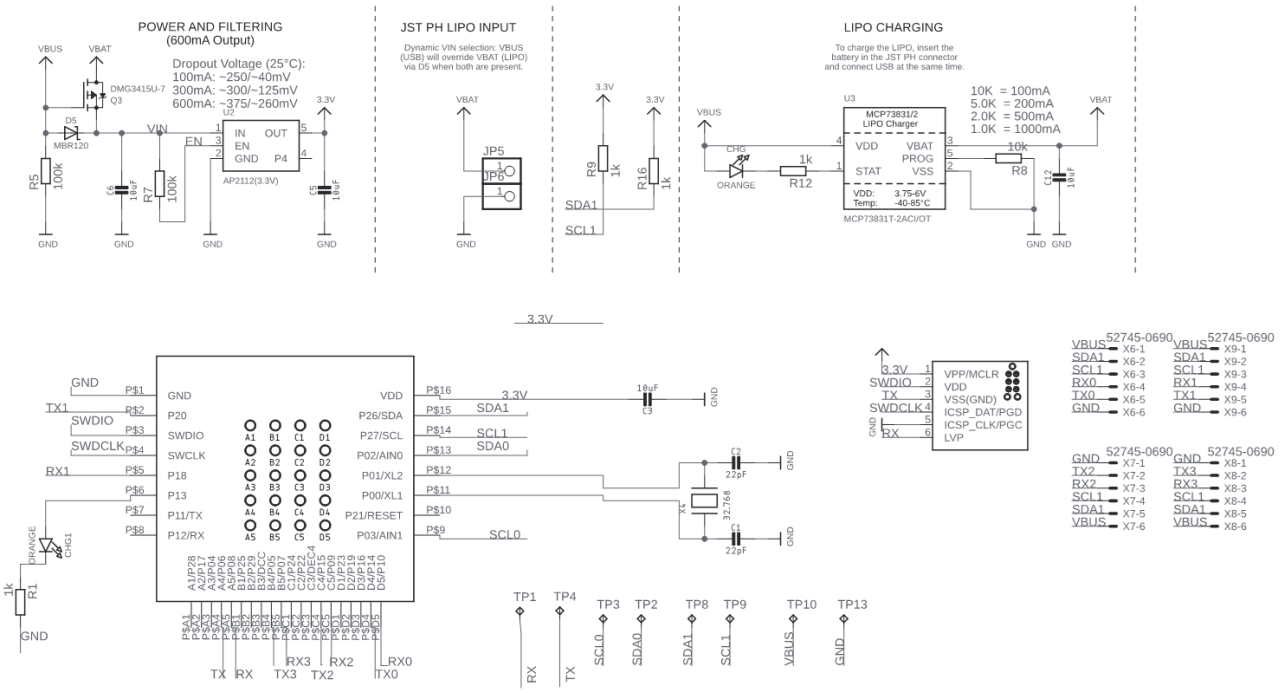

Figure A.18: Flex PCB schematic for *NETS BLE*.

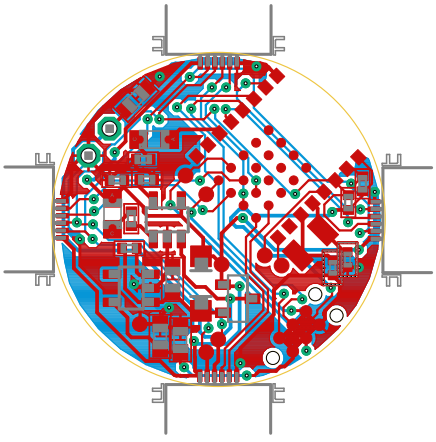

Figure A.19: Flex PCB lay-out for *NETS BLE*.